

# Niobium-Mediated Synthesis of Phosphorus-Rich Molecules

by

Brandi M. Cossairt

B.S., Chemistry (2006)  
California Institute of Technology

Submitted to the Department of Chemistry  
in partial fulfillment of the requirements for the degree of

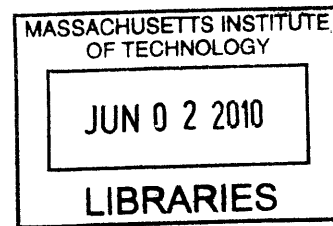
Doctor of Philosophy

at the

MASSACHUSETTS INSTITUTE OF TECHNOLOGY

June 2010

© Massachusetts Institute of Technology 2010. All rights reserved.



**ARCHIVES**

Author .....  
Department of Chemistry  
May 4, 2010

Certified by .....  
Christopher C. Cummins  
Professor of Chemistry  
Thesis Supervisor

Accepted by .....  
Robert W. Field  
Chairman, Department Committee on Graduate Studies



This Doctoral Thesis has been examined by a Committee of the Department of Chemistry as follows:



Professor Richard R. Schrock .....

Frederick G. Keyes Professor of Chemistry  
Chairman



Professor Christopher C. Cummins .....

Professor of Chemistry  
Thesis Supervisor

^

Professor Stephen J. Lippard .....

Arthur Amos Noyes Professor of Chemistry  
Committee Member



# Niobium-Mediated Synthesis of Phosphorus-Rich Molecules

by

Brandi M. Cossairt

Submitted to the Department of Chemistry  
on May 4, 2010, in partial fulfillment of the  
requirements for the degree of  
Doctor of Philosophy in Inorganic Chemistry

## Abstract

The use of a sterically demanding enolate ligand  $-\text{OC}[\text{}^2\text{Ad}]\text{Mes}$  supported by niobium has allowed for the synthesis of  $(\text{Mes}[\text{}^2\text{Ad}]\text{CO})_3\text{Nb}=\text{PP}_7\text{Nb}(\text{OC}[\text{}^2\text{Ad}]\text{Mes})_3$  through  $\text{P}_4$  coupling by a low-valent niobium intermediate. This asymmetric phosphorus-rich cluster harbors a niobium phosphinidene unit bound to a niobium-supported  $\text{P}_7$  cluster. The phosphinidene terminus was found to react with a range of ketones to give phosphalkene complexes  $\text{R}_2\text{C}=\text{PP}_7\text{Nb}(\text{OC}[\text{}^2\text{Ad}]\text{Mes})_3$ . These phosphalkenes are unstable towards intramolecular rearrangement to give  $\text{R}_2\text{CP}_8\text{Nb}(\text{OC}[\text{}^2\text{Ad}]\text{Mes})_3$  in which the carbene unit has been internalized into the  $\text{P}_8$  cage. This rearrangement was studied through both Eyring and Hammett analyses. Structurally the new  $\text{R}_2\text{CP}_8\text{Nb}(\text{OC}[\text{}^2\text{Ad}]\text{Mes})_3$  are viewed as coordinated-diphosphenes and it was found that the diphosphene unit could be liberated and trapped by reaction with pyridine-*N*-oxide in the presence of excess 1,3-cyclohexadiene, generating niobium oxo and  $\text{R}_2\text{CP}_8(\text{C}_6\text{H}_8)$ .

Searching for new platforms to investigate niobium-phosphorus chemistry led to the synthesis of  $[\text{Na}(\text{THF})_3][\text{P}_3\text{Nb}(\text{ODipp})_3]$ , an anionic *cyclo*- $\text{P}_3$  complex that is accessible in two steps from commercially available reagents. It was discovered that  $[\text{Na}(\text{THF})_3][\text{P}_3\text{Nb}(\text{ODipp})_3]$  could function as a source of  $\text{P}_3^{3-}$ , which has allowed for the synthesis of the tetraatomic molecule  $\text{AsP}_3$  as a pure substance for the first time.  $\text{AsP}_3$  has been studied by gas-phase electron diffraction, photoelectron spectroscopy, solid-state NMR spectroscopy, raman spectroscopy, as well as high resolution mass spectrometry, and a variety of quantum chemical calculations. Further, a wide array of  $\text{AsP}_3$  reaction chemistry has been probed including the synthesis and structural characterization of two metal complexes with a coordinated, intact  $\text{AsP}_3$  ligand.

Motivated to explore the chemistry of  $[\text{Na}(\text{THF})_3][\text{P}_3\text{Nb}(\text{ODipp})_3]$  further, a series of investigations were carried out to generate substituted triphosphirene ligands complexed to niobium. In particular  $\text{Ph}_3\text{SnP}_3\text{Nb}(\text{ODipp})_3$  was prepared and was found to react cleanly and efficiently with pyridine-*N*-oxide in the presence of an excess of 1,3-cyclohexadiene to generate the niobium oxo complex and  $\text{Ph}_3\text{SnP}_3(\text{C}_6\text{H}_8)$ , the product of a Diels-Alder reaction between the liberated triphosphirene and 1,3-cyclohexadiene. This unusual phosphorus-rich molecule was exploited in a number of transformations. One reaction of particular interest was the synthesis of  $\text{P}_3\text{Rh}(\text{PPh}_3)_3$  from  $\text{Ph}_3\text{SnP}_3(\text{C}_6\text{H}_8)$  and Wilkinson's catalyst ( $\text{ClRh}(\text{PPh}_3)_3$ ) with loss of 1,3-cyclohexadiene and  $\text{ClSnPh}_3$ . This transformation is an illustrative example of the ability of  $\text{Ph}_3\text{SnP}_3(\text{C}_6\text{H}_8)$  to act as a  $\text{P}_3^-$  transfer agent.

Thesis Supervisor: Christopher C. Cummins

Title: Professor of Chemistry



## Framing the Story: A Prelude

The answer is never the answer. What's really interesting is the mystery. If you seek the mystery instead of the answer, you'll always be seeking. I've never seen anybody really find the answer – they think they have, so they stop thinking.

–Ken Kesey

Like all good stories, there is a frame, and a context, and a flow, to what is written herein. This work was not produced in a vacuum and I thought it might be nice to provide some of the background. When I joined the Cummins lab, Josh Figueroa had recently discovered a niobium diphosphaazide complex (the “eliminator”), which Nick Piro showed was able to liberate diatomic P<sub>2</sub> in solution. I was tasked to find a new niobium-based system that was capable of generating P<sub>2</sub> under mild conditions and compare it with the “eliminator” complex. I turned to a ligand that had been previously synthesized but little explored in our group and with it developed a new niobium enolate platform. Once phosphorus was introduced to this system, my project goal took an abrupt turn... we did not obtain a Nb<sub>2</sub>(μ-P<sub>2</sub>) (a precursor to the eliminator complex) or any “sensible” P<sub>4</sub> activation product. Instead, two molecules of P<sub>4</sub> became asymmetrically coupled between two niobium centers. This unexpected result led to a wide array of interesting reactivity investigations that resulted in the synthesis of several niobium-supported polyphosphorus clusters incorporating organic fragments. The highlight of this chemistry, I think, was the discovery of pyridine-*N*-oxide as an oxygen-atom transfer agent that would liberate niobium oxo from the phosphorus cluster without oxidizing the phosphorus atoms themselves. This led to the synthesis of my first phosphorus-rich main-group molecule, Ph<sub>2</sub>CP<sub>8</sub>(C<sub>6</sub>H<sub>8</sub>).

After about a year and a half, it became obvious that having a simpler system (one that didn't require a six step ligand synthesis or several synthetic steps to enter into interesting phosphorus chemistry) would be highly desirable and would allow us to expand the number of niobium-phosphorus systems available for comparison. A few undergraduates and visiting students began to explore different commercially available aryloxide based ligands. Things were looking a little grim until Mariam Diawara (a visiting graduate student from France) arrived. Mariam was given 2,6-diisopropylphenoxide, a ligand made famous by Ian Rothwell, to investigate. We tried several strategies to enter quickly into phosphorus chemistry with this platform, but it wasn't until I suggested trying an *in situ* reduction of the niobium(V) dichloride in the presence of P<sub>4</sub> that positive results were obtained. Mariam quickly discovered a potential route to access an anionic niobium *cyclo*-P<sub>3</sub> complex, but shortly thereafter her time at MIT was up, and I turned to work out a procedure to produce this *cyclo*-P<sub>3</sub> anion on a preparative scale. After some time, a robust, reproducible synthesis was devised. We quickly realized that this special *cyclo*-P<sub>3</sub> anion was capable of complete P<sub>3</sub><sup>3-</sup> transfer, which led to the synthesis of AsP<sub>3</sub> as a pure and isolable substance. The discovery of AsP<sub>3</sub> was a milestone in my PhD research and it opened the doors to a number of fun reactivity studies and, more importantly, to a number of productive collaborations with several groups around the world. I think AsP<sub>3</sub> is probably now one of the best characterized molecules in the Cummins group arsenal and it was my second phosphorus-rich main-group molecule.

While trying to devise a way to functionalize  $\text{AsP}_3$  directly using organic radicals, I discovered that the tetrahedron was completely breaking down giving rise to, mainly, trisubstituted phosphines. Given the long standing interest in phosphorus chemistry to develop methods to go directly to phosphines from  $\text{P}_4$ , I took a short diversion to pursue this line of thought. The radical synthesis of trisubstituted phosphines from  $\text{P}_4$  is developed in Appendix A of this document.

The niobium *cyclo*- $\text{P}_3$  anion became a workhorse molecule for reactivity studies extending beyond simple  $\text{P}_3^{3-}$  transfer. It was readily functionalized by a range of electrophiles to produce interesting new types of triphosphirene complexes. It wasn't long before I realized the structural connection between these niobium triphosphirene complexes and some of the monometallic  $\text{P}_8$  complexes I had seen years earlier. Pyridine-*N*-oxide, again, provided a method to release these triphosphirene fragments from the niobium metal center and this reactivity led to my third phosphorus-rich main group molecule,  $\text{Ph}_3\text{SnP}_3(\text{C}_6\text{H}_8)$ . This diene-protected, tin-substituted *cyclo*- $\text{P}_3$  molecule was quite intriguing because it could be made in one pot from the starting niobium *cyclo*- $\text{P}_3$  anion complex and was extremely easy to isolate due to convenient solubility properties. This molecule, then, became the starting material for a series of reactivity studies all their own.

I will stop now, but I hope you enjoy reading about this chemistry, and I hope you see all the mysteries that were uncovered along the way. Have fun.



# Table of Contents

<b>1</b>	<b>Synthesis and Reactivity of <math>(\text{Mes}[\text{}^2\text{Ad}]\text{CO})_3\text{Nb}=\text{PP}_7\text{Nb}(\text{OC}[\text{}^2\text{Ad}]\text{Mes})_3</math></b>	<b>21</b>
1.1	Introduction . . . . .	23
1.2	Metallation of the Enolate Ligand with Niobium . . . . .	29
1.3	Reduction and Disproportionation of the Niobium Diiodide Complex . . . . .	32
1.4	$\text{P}_4$ Activation . . . . .	34
1.5	Phosphinidene Reactivity . . . . .	36
1.6	Rearrangement of the Phosphaalkene Complex . . . . .	40
1.7	Liberation of $\text{R}_2\text{CP}_8$ from the Niobium Metal Center . . . . .	51
1.8	Conclusions . . . . .	58
1.9	Experimental Details . . . . .	59
1.10	References . . . . .	81
<b>2</b>	<b>Synthesis, Physical Properties, and Reactivity Patterns of <math>\text{AsP}_3</math></b>	<b>85</b>
2.1	Introduction . . . . .	87
2.2	Facile Synthesis of a <i>Cyclo</i> - $\text{P}_3$ Anion Complex . . . . .	91
2.3	Synthesis of $\text{AsP}_3$ . . . . .	93
2.4	Physical and Electronic Properties of $\text{AsP}_3$ . . . . .	98
2.5	Reactivity Patterns of $\text{AsP}_3$ . . . . .	114
2.6	Reaction of the <i>Cyclo</i> - $\text{P}_3$ Anion Complex with Other Tripositive Electrophiles . . . . .	133
2.7	Towards Arsenic-Rich Tetrahedra . . . . .	136
2.8	Conclusions . . . . .	140
2.9	Experimental Details . . . . .	140
2.10	References . . . . .	159
<b>3</b>	<b>The Development of New <math>\text{P}_3</math> Transfer Reagents: <math>\text{Ph}_3\text{SnP}_3(\text{C}_6\text{H}_8)</math> and Related Compounds</b>	<b>169</b>
3.1	Introduction . . . . .	170
3.2	Synthesis of Substituted <i>Cyclo</i> - $\text{P}_3$ Complexes . . . . .	171
3.3	$\text{P}_3$ Transfer Chemistry of a Triphosphirene Complex . . . . .	172
3.4	The Diverse Reactivity of $\text{Ph}_3\text{SnP}_3(\text{C}_6\text{H}_8)$ . . . . .	176
3.5	Preparation and Reaction Chemistry of $\text{LiP}_3(\text{C}_6\text{H}_8)$ . . . . .	182

3.6	Conclusions . . . . .	189
3.7	Experimental Details . . . . .	189
3.8	References . . . . .	203
<b>A</b>	<b>Radical Synthesis of Trisubstituted Phosphines from P<sub>4</sub></b>	<b>205</b>
A.1	Introduction . . . . .	205
A.2	Synthesis of Homoleptic Trisubstituted Phosphines . . . . .	207
A.3	Synthesis of Heteroleptic Trisubstituted Phosphines . . . . .	209
A.4	Conclusions . . . . .	209
A.5	Experimental Details . . . . .	210
A.6	References . . . . .	217
	<b>Acknowledgments</b>	<b>219</b>
	<b>Curriculum Vitae</b>	<b>221</b>

## List of Figures

1.1	Polyphosphorus ligands. . . . .	24
1.2	Polyphosphorus molecules as free and complexed entities. . . . .	26
1.3	The enolate ligand system. . . . .	28
1.4	Crystal Structure of $\text{ONb}(\text{OC}[\text{}^2\text{Ad}]\text{Mes})_3$ . . . . .	30
1.5	$^1\text{H}$ NMR spectra of $\text{INb}(\text{OC}[\text{}^2\text{Ad}]\text{Mes})_3(\text{THF})$ and $[(\text{Mes}[\text{}^2\text{Ad}]\text{CO})_3\text{Nb}]_2(\mu\text{-I})$ . . . . .	33
1.6	$^{31}\text{P}$ NMR spectrum of $(\text{Mes}[\text{}^2\text{Ad}]\text{CO})_3\text{Nb}=\text{PP}_7\text{Nb}(\text{OC}[\text{}^2\text{Ad}]\text{Mes})_3$ . . . . .	35
1.7	Variable temperature NMR spectrum of $(\text{Mes}[\text{}^2\text{Ad}]\text{CO})_3\text{Nb}=\text{PP}_7\text{Nb}(\text{OC}[\text{}^2\text{Ad}]\text{Mes})_3$ . . . . .	36
1.8	NMR shielding tensor calculations for $(\text{Mes}[\text{}^2\text{Ad}]\text{CO})_3\text{Nb}=\text{PP}_7\text{Nb}(\text{OC}[\text{}^2\text{Ad}]\text{Mes})_3$ . . . . .	37
1.9	Crystal Structure of $\text{H}_2\text{PP}_7\text{Nb}(\text{OC}[\text{}^2\text{Ad}]\text{Mes})_3$ . . . . .	39
1.10	$^{31}\text{P}$ NMR spectrum of $\text{H}_2\text{PP}_7\text{Nb}(\text{OC}[\text{}^2\text{Ad}]\text{Mes})_3$ . . . . .	39
1.11	$^{31}\text{P}$ NMR spectrum of $\text{Ph}_2\text{C}=\text{PP}_7\text{Nb}(\text{OC}[\text{}^2\text{Ad}]\text{Mes})_3$ . . . . .	41
1.12	$^{31}\text{P}$ NMR spectrum of $\text{Ph}_2\text{CP}_8\text{Nb}(\text{OC}[\text{}^2\text{Ad}]\text{Mes})_3$ . . . . .	42
1.13	Crystal Structure of $\text{Ph}_2\text{CP}_8\text{Nb}(\text{OC}[\text{}^2\text{Ad}]\text{Mes})_3$ . . . . .	43
1.14	Eyring analysis of the rearrangement of $\text{Ph}_2\text{C}=\text{PP}_7\text{Nb}(\text{OC}[\text{}^2\text{Ad}]\text{Mes})_3$ . . . . .	44
1.15	Hammett analysis. . . . .	45
1.16	Details of the formation of $((\text{Me}_2\text{N})\text{C}_6\text{H}_4)_2\text{CP}_8\text{Nb}(\text{OC}[\text{}^2\text{Ad}]\text{Mes})_3$ . . . . .	46
1.17	Alternative Hammett analysis. . . . .	47
1.18	Kinetic data for rearrangement of $\text{Ph}_2\text{C}=\text{PP}_7\text{Nb}(\text{OC}[\text{}^2\text{Ad}]\text{Mes})_3$ in THF. . . . .	48
1.19	$^{31}\text{P}$ NMR spectrum of $\text{Ph}_2\text{SnP}_8\text{Nb}(\text{OC}[\text{}^2\text{Ad}]\text{Mes})_3$ . . . . .	50
1.20	$^{31}\text{P}$ NMR spectrum of $\text{dmpPP}_8\text{Nb}(\text{OC}[\text{}^2\text{Ad}]\text{Mes})_3$ . . . . .	51
1.21	$^{31}\text{P}$ NMR spectrum of $\text{Ph}_2\text{CP}_8(\text{C}_6\text{H}_8)$ . . . . .	52
1.22	Crystal Structure of $\text{Ph}_2\text{CP}_8(\text{C}_6\text{H}_8)$ . . . . .	53
1.23	The $\text{Ph}_2\text{CP}_8(\text{R})$ family. . . . .	54
1.24	Cyclic voltammogram of $\text{Ph}_2\text{CP}_8(\text{C}_6\text{H}_8)$ . . . . .	56
1.25	Computed HOMO for $\text{Ph}_2\text{CP}_8(\text{C}_6\text{H}_8)$ . . . . .	57
1.26	Computed LUMO for $\text{Ph}_2\text{CP}_8(\text{C}_6\text{H}_8)$ . . . . .	57
1.27	Treatment of $\text{Ph}_2\text{CP}_8(\text{C}_6\text{H}_8)$ with $\text{I}_2$ . . . . .	58
2.1	Group 15 elemental molecules. . . . .	88
2.2	Previously reported <i>cyclo</i> - $\text{P}_3$ complexes. . . . .	89
2.3	Two structural forms of the <i>cyclo</i> - $\text{P}_3$ anion. . . . .	93

2.4	High-resolution electron-impact mass spectrum of AsP <sub>3</sub> .	95
2.5	Raman spectrum of AsP <sub>3</sub> .	96
2.6	Raman polarization experiment for AsP <sub>3</sub> .	96
2.7	Gas-phase electron diffraction data for AsP <sub>3</sub> and P <sub>4</sub> .	100
2.8	Photoelectron spectra of AsP <sub>3</sub> and P <sub>4</sub> .	101
2.9	Vibrational fine structure in the PES spectrum.	102
2.10	Experimental energy level diagrams for P <sub>4</sub> and AsP <sub>3</sub> .	103
2.11	He I and He II photoelectron spectra for P <sub>4</sub> and AsP <sub>3</sub> .	104
2.12	Solid-state <sup>75</sup> As and <sup>31</sup> P NMR data for AsP <sub>3</sub> .	105
2.13	Variable-temperature <sup>75</sup> As and <sup>31</sup> P spin-lattice relaxation data obtained for solid AsP <sub>3</sub> .	106
2.14	Cyclic voltammogram of AsP <sub>3</sub> and P <sub>4</sub> .	107
2.15	Molecular orbital diagram of AsP <sub>3</sub> and P <sub>4</sub> .	108
2.16	UV-Vis absorption spectrum of AsP <sub>3</sub> .	109
2.17	Orientation of the magnetic field and the molecules in the GIMIC calculations.	110
2.18	Current densities in AsP <sub>3</sub> and P <sub>4</sub> .	111
2.19	Laplacian plot of AsP <sub>3</sub> .	112
2.20	Plot of $\Delta_f H^{\circ}_0$ vs $n$ for As <sub><i>n</i></sub> P <sub>4-<i>n</i></sub> .	114
2.21	AsP <sub>3</sub> thermolysis data.	115
2.22	AsP <sub>3</sub> photolysis; before and after.	116
2.23	Crystal structure of (AsP <sub>3</sub> )Mo(CO) <sub>3</sub> (P <sup><i>i</i></sup> Pr) <sub>2</sub> .	118
2.24	Variable temperature <sup>31</sup> P NMR spectrum of (AsP <sub>3</sub> )Mo(CO) <sub>3</sub> (P <sup><i>i</i></sup> Pr) <sub>2</sub> .	118
2.25	Crystal structure of [(AsP <sub>3</sub> )Fe(Cp*)(dppe)][BPh <sub>4</sub> ].	120
2.26	<sup>31</sup> P NMR spectrum of [(AsP <sub>3</sub> )Fe(Cp*)(dppe)][BPh <sub>4</sub> ].	120
2.27	Charge analysis of [(AsP <sub>3</sub> )Fe(Cp*)(dppe)][BPh <sub>4</sub> ].	121
2.28	<sup>31</sup> P NMR spectrum of [P(N <sup><i>i</i></sup> Pr) <sub>2</sub> (N(SiMe <sub>3</sub> ) <sub>2</sub> ) <sub>2</sub> ](AsP <sub>3</sub> ).	122
2.29	Crystal structure of [P(N <sup><i>i</i></sup> Pr) <sub>2</sub> (N(SiMe <sub>3</sub> ) <sub>2</sub> ) <sub>2</sub> ](AsP <sub>3</sub> ).	122
2.30	<sup>31</sup> P NMR spectrum of (Ar[CH <sub>2</sub> <sup><i>t</i></sup> Bu]N) <sub>3</sub> Nb(PE)Nb(N[CH <sub>2</sub> <sup><i>t</i></sup> Bu]Ar) <sub>3</sub> .	124
2.31	<sup>31</sup> P NMR spectrum of As[GaC(SiMe <sub>3</sub> ) <sub>3</sub> ] <sub>3</sub> P <sub>3</sub> and P[GaC(SiMe <sub>3</sub> ) <sub>3</sub> ] <sub>3</sub> AsP <sub>2</sub> .	126
2.32	Crystal structure of As[GaC(SiMe <sub>3</sub> ) <sub>3</sub> ] <sub>3</sub> P <sub>3</sub> .	127
2.33	<sup>31</sup> P NMR spectrum of AsP <sub>3</sub> [GaC(SiMe <sub>3</sub> ) <sub>3</sub> ] <sub>4</sub> .	128
2.34	DFT geometry optimization of a model complex (AsP <sub>3</sub> [GaCH <sub>3</sub> ] <sub>4</sub> ) of the quadruple insertion product.	128
2.35	<sup>31</sup> P NMR spectrum of [Na(THF) <sub>3</sub> ][E <sub>3</sub> Nb(ODipp) <sub>3</sub> ].	130
2.36	<sup>31</sup> P NMR spectrum of AsP <sub>3</sub> , As <sub>2</sub> P <sub>2</sub> , As <sub>3</sub> P.	131
2.37	GC chromatograph of tetrahedra mixture.	131
2.38	Fragmentation patterns for the tetrahedra.	132
2.39	Generation and <sup>31</sup> P NMR spectrum of SbP <sub>3</sub> .	133
2.40	<sup>31</sup> P NMR spectrum of [(SbP <sub>3</sub> )Fe(Cp*)(dppe)][BPh <sub>4</sub> ].	135
2.41	DFT calculations for [(SbP <sub>3</sub> )Fe(Cp*)(dppe)][BPh <sub>4</sub> ].	135

2.42	$^{31}\text{P}$ NMR spectrum of $(\text{SbP}_3)[\text{Re}(\text{CO})_2(\text{triphos})]_2$ and $(\text{SbP}_3)\text{Re}(\text{CO})_2(\text{triphos})$ . . .	136
2.43	Crystal structure of $[\text{Na}(\text{THF})_6][\text{As}_3\text{Nb}(\text{ODipp})_3]$ . . . . .	138
2.44	$^{31}\text{P}$ NMR spectrum and GC-mass spectrum of $\text{As}_3\text{P}$ . . . . .	139
3.1	Substituted niobium <i>cyclo</i> - $\text{P}_3$ complexes. . . . .	171
3.2	$^{31}\text{P}$ NMR spectrum of $\text{Ph}_3\text{SnP}_3\text{Nb}(\text{ODipp})_3$ . . . . .	172
3.3	Variable temperature $^{31}\text{P}$ NMR spectra of $\text{Ph}_3\text{SnP}_3\text{Nb}(\text{ODipp})_3$ . . . . .	173
3.4	$^{31}\text{P}$ NMR spectrum of $\text{Ph}_3\text{SnP}_3(\text{C}_6\text{H}_8)$ . . . . .	174
3.5	$^{119}\text{Sn}$ NMR spectrum of $\text{Ph}_3\text{SnP}_3(\text{C}_6\text{H}_8)$ . . . . .	174
3.6	Crystal structure of $\text{Ph}_3\text{SnP}_3(\text{C}_6\text{H}_8)$ . . . . .	175
3.7	Conversion of $\text{Ph}_3\text{SnP}_3(\text{C}_6\text{H}_8)$ to $\text{Ph}_3\text{SnP}_3(\text{C}_6\text{H}_{10})$ by a retro-Diels-Alder reaction. . . . .	177
3.8	Literature examples of diene-exchange reactions of substituted diphosphenes. . . . .	178
3.9	Crystal structure of $\text{Ph}_3\text{SnP}_3(\text{C}_6\text{H}_8)(\text{C}_2\text{N}_2(\text{NC}_5\text{H}_4)_2)$ . . . . .	180
3.10	$^{31}\text{P}$ NMR spectrum of $\text{P}_3\text{Rh}(\text{PPh}_3)_3$ . . . . .	181
3.11	Crystal structure of $\text{P}_3\text{Rh}(\text{PPh}_3)_3$ . . . . .	181
3.12	$^{31}\text{P}$ NMR spectrum of $\text{LiP}_3(\text{C}_6\text{H}_8)$ . . . . .	183
3.13	$^{31}\text{P}$ and $^1\text{H}$ NMR spectra of $\text{HP}_3(\text{C}_6\text{H}_8)$ . . . . .	185
3.14	Geometry optimization and calculated chemical shifts of $\text{HP}_3(\text{C}_6\text{H}_8)$ . . . . .	186
3.15	$^{31}\text{P}$ NMR spectra of $\text{P}_3\text{H}_3$ . . . . .	187
3.16	Geometry optimization and calculated/observed chemical shifts of $\text{P}_3\text{H}_3$ . . . . .	188
3.17	Crystal structure of $[\text{Na}][\text{Nb}(\text{OC}_6\text{F}_5)_2(\text{ODipp})]$ . . . . .	188
3.18	$^{31}\text{P}$ NMR spectrum of putative $[\text{Ph}_3\text{SnP}_3]_x$ . . . . .	194
A.1	$\text{Ti}(\text{N}[\text{t-Bu}]\text{Ar})_3$ together with various $\text{P}_4$ -derived phosphanes and polyphosphorus products. . . . .	207
A.2	$^{31}\text{P}\{^1\text{H}\}$ NMR spectrum of $\text{P}(\text{SiMe}_3)_3$ . . . . .	213
A.3	$^{31}\text{P}\{^1\text{H}\}$ NMR spectrum of $\text{P}(\text{SnPh}_3)_3$ . . . . .	213
A.4	$^{31}\text{P}\{^1\text{H}\}$ NMR spectrum of $\text{P}_3\text{Mes}_3$ . . . . .	214
A.5	$^{31}\text{P}\{^1\text{H}\}$ NMR spectrum of <i>cis,trans</i> - $\text{DmpP}_4\text{Dmp}$ . . . . .	214



## List of Schemes

1.1	Niobium-phosphorus chemistry in the Cummins lab. . . . .	27
1.2	First reports of the OC[ <sup>2</sup> Ad]Ar ligand system. . . . .	29
1.3	Metallation of the enolate ligand system. . . . .	30
1.4	Metallation of the enolate ligand system: 2. . . . .	31
1.5	Reduction of I <sub>2</sub> Nb(OC[ <sup>2</sup> Ad]Mes) <sub>3</sub> . . . . .	32
1.6	Preparation of (Mes[ <sup>2</sup> Ad]CO) <sub>3</sub> Nb=PP <sub>7</sub> Nb(OC[ <sup>2</sup> Ad]Mes) <sub>3</sub> . . . . .	35
1.7	Preparation of H <sub>2</sub> PP <sub>7</sub> Nb(OC[ <sup>2</sup> Ad]Mes) <sub>3</sub> . . . . .	38
1.8	Preparation of Ph <sub>2</sub> C=PP <sub>7</sub> Nb(OC[ <sup>2</sup> Ad]Mes) <sub>3</sub> . . . . .	40
1.9	Preparation of Ph <sub>2</sub> CP <sub>8</sub> Nb(OC[ <sup>2</sup> Ad]Mes) <sub>3</sub> . . . . .	41
1.10	Proposed mechanism for rearrangement of Ph <sub>2</sub> C=PP <sub>7</sub> Nb(OC[ <sup>2</sup> Ad]Mes) <sub>3</sub> . . . . .	48
1.11	Synthesis of Ph <sub>2</sub> SnP <sub>8</sub> Nb(OC[ <sup>2</sup> Ad]Mes) <sub>3</sub> and dmpPP <sub>8</sub> Nb(OC[ <sup>2</sup> Ad]Mes) <sub>3</sub> . . . . .	50
1.12	Synthesis of Ph <sub>2</sub> CP <sub>8</sub> (C <sub>6</sub> H <sub>8</sub> ). . . . .	53
1.13	Energetics for possible pathways in the formation of Ph <sub>2</sub> CP <sub>8</sub> (C <sub>6</sub> H <sub>8</sub> ). . . . .	55
2.1	Previously observed reactivity of a niobium <i>cyclo</i> -P <sub>3</sub> anion complex. . . . .	90
2.2	P <sub>4</sub> addition to [Na][P≡Nb(N[CH <sub>2</sub> <sup>t</sup> Bu]Ar) <sub>3</sub> ]. . . . .	91
2.3	Two methods for preparing P <sub>3</sub> Nb(ODipp) <sub>3</sub> anion. . . . .	92
2.4	Preparation of AsP <sub>3</sub> . . . . .	94
2.5	Preparation of S <sub>7</sub> . . . . .	94
2.6	Proposed mechanism for the formation of AsP <sub>3</sub> . . . . .	97
2.7	Preparation of (AsP <sub>3</sub> )Mo(CO) <sub>3</sub> (P <sup>i</sup> Pr <sub>3</sub> ) <sub>2</sub> . . . . .	117
2.8	Preparation of [(AsP <sub>3</sub> )Fe(Cp*)(dppe)][BPh <sub>4</sub> ]. . . . .	119
2.9	Preparation of [P(N <sup>i</sup> Pr <sub>2</sub> )(N(SiMe <sub>3</sub> ) <sub>2</sub> ) <sub>2</sub> ](AsP <sub>3</sub> ). . . . .	121
2.10	Preparation of (Ar[ <sup>t</sup> Bu]N) <sub>3</sub> Ti[P(P <sub>2</sub> )As]Ti(N[ <sup>t</sup> Bu]Ar) <sub>3</sub> . . . . .	123
2.11	Preparation of (Ar[CH <sub>2</sub> <sup>t</sup> Bu]N) <sub>3</sub> Nb(PE)Nb(N[CH <sub>2</sub> <sup>t</sup> Bu]Ar) <sub>3</sub> . . . . .	124
2.12	Preparation of As≡Mo(N[ <sup>t</sup> Bu]Ar) <sub>3</sub> and P≡Mo(N[ <sup>t</sup> Bu]Ar) <sub>3</sub> . . . . .	125
2.13	Preparation of As[GaC(SiMe <sub>3</sub> ) <sub>3</sub> ] <sub>3</sub> P <sub>3</sub> and P[GaC(SiMe <sub>3</sub> ) <sub>3</sub> ] <sub>3</sub> AsP <sub>2</sub> . . . . .	126
2.14	Preparation of AsP <sub>3</sub> , As <sub>2</sub> P <sub>2</sub> , As <sub>3</sub> P, and As <sub>4</sub> . . . . .	130
2.15	Preparation of [Na(THF) <sub>3</sub> ][As <sub>3</sub> Nb(ODipp) <sub>3</sub> ] from As <sub>4</sub> . . . . .	137
2.16	Preparation of As <sub>3</sub> P. . . . .	139

3.1	Synthesis of $\text{Ph}_3\text{SnP}_3\text{Nb}(\text{ODipp})_3$ . . . . .	172
3.2	Synthesis of $\text{Ph}_3\text{SnP}_3(\text{C}_6\text{H}_8)$ . . . . .	173
3.3	Proposed mechanism for formation of $\text{Ph}_3\text{SnP}_3$ from $\text{Ph}_3\text{SnP}_3\text{Nb}(\text{ODipp})_3$ and $\text{ONC}_5\text{H}_5$ . . . . .	176
3.4	Treatment of $\text{Ph}_3\text{SnP}_3(\text{C}_6\text{H}_8)$ with 2,6-di-4-pyridyl tetrazine. . . . .	179
3.5	Synthesis of $\text{P}_3\text{Rh}(\text{PPh}_3)_3$ . . . . .	180
3.6	Synthesis of $\text{LiP}_3(\text{C}_6\text{H}_8)$ . . . . .	183
3.7	Synthesis of $\text{HP}_3(\text{C}_6\text{H}_8)$ . . . . .	184
3.8	Synthesis of $\text{P}_3\text{H}_3$ . . . . .	187
A.1	Idealized scheme for the sythesis of phosphines from $\text{P}_4$ using $\text{Ti}(\text{N}[\text{tBu}]\text{Ar})_3$ . . . . .	206



## List of Tables

1.1	Rate Constants for Degradation of $\text{Ph}_2\text{C}=\text{PP}_7\text{Nb}(\text{OC}[\text{}^2\text{Ad}]\text{Mes})_3$ . . . . .	44
1.2	Rate Constants for Growth of $\text{Ar}_2\text{CP}_8\text{Nb}(\text{OC}[\text{}^2\text{Ad}]\text{Mes})_3$ : Hammett Analysis . . .	45
1.3	Optimized atomic coordinates of $(\text{MeO})_3\text{Nb}=\text{PP}_7\text{Nb}(\text{OMe})_3$ . . . . .	71
1.4	Optimized atomic coordinates of $\text{Ph}_2\text{CP}_8\text{NbCl}_3$ (bisoradamantane type-structure). . . . .	71
1.5	Optimized atomic coordinates of $\text{Ph}_2\text{CP}_8\text{Nb}(\text{OC}[\text{}^i\text{Pr}]\text{Mes})_3$ . . . . .	72
1.6	Optimized atomic coordinates of $\text{Ph}_2\text{CP}_8\text{Nb}(\text{OC}[\text{}^i\text{Pr}]\text{Mes})_3(\text{ONC}_5\text{H}_5)$ . . . . .	73
1.7	Optimized atomic coordinates of $\text{ONb}(\text{OC}[\text{}^i\text{Pr}]\text{Mes})_3(\text{ONC}_5\text{H}_5)$ . . . . .	75
1.8	Optimized atomic coordinates of $\text{Ph}_2\text{CP}_8\text{ONb}(\text{OC}[\text{}^i\text{Pr}]\text{Mes})_3$ (metallacycle). . . . .	76
1.9	Optimized atomic coordinates of $\text{Ph}_2\text{CP}_8(\text{C}_6\text{H}_8)$ . . . . .	77
1.10	Optimized atomic coordinates of $\text{Ph}_2\text{CP}_8$ (diphosphene). . . . .	78
1.11	Crystallographic data for $\text{ONb}(\text{OC}[\text{}^2\text{Ad}]\text{Mes})_3(\text{Et}_2\text{O})$ and $\text{H}_2\text{PP}_7\text{Nb}(\text{OC}[\text{}^2\text{Ad}]\text{Mes})_3$ . . . . .	79
1.12	Crystallographic data for $\text{Ph}_2\text{CP}_8\text{Nb}(\text{OC}[\text{}^2\text{Ad}]\text{Mes})_3$ and $\text{Ph}_2\text{CP}_8(\text{C}_6\text{H}_8)$ . . . . .	80
2.1	Vertical ionization energies of $\text{P}_4$ and $\text{AsP}_3$ . . . . .	102
2.2	The ratios of the peak areas from the He I and the He II photoelectron spectra of $\text{AsP}_3$ and $\text{P}_4$ . . . . .	104
2.3	A comparison of the isotropic $^{31}\text{P}$ chemical shifts between $\text{P}_4$ and $\text{AsP}_3$ in different environments. . . . .	105
2.4	Computed NMR Chemical Shifts for $\text{AsP}_3$ and $\text{P}_4$ . . . . .	108
2.5	Calculated Atomic Charges for $\text{AsP}_3$ . . . . .	112
2.6	Calculated heats of atomization, bond energies, and standard heats of formation for $\text{As}_n\text{P}_{4-n}$ . . . . .	113
2.7	NMR and GC-MS data for the generation of $\text{AsP}_3$ , $\text{As}_2\text{P}_2$ , $\text{As}_3\text{P}$ , and $\text{As}_4$ . . . . .	130
2.8	Comparison of chemical shift and HOMO-LUMO gaps in $\text{EP}_3$ tetrahedra ( $\text{E} = \text{P}, \text{As}, \text{Sb}$ ). . . . .	134
2.9	Optimized atomic coordinates of $\text{AsP}_3$ . . . . .	152
2.10	Optimized atomic coordinates of $\text{P}_4$ . . . . .	152
2.11	Optimized atomic coordinates of $\text{As}_2\text{P}_2$ . . . . .	153
2.12	Optimized atomic coordinates of $\text{As}_3\text{P}$ . . . . .	153
2.13	Optimized atomic coordinates of $[(\text{AsP}_3)\text{Fe}(\text{Cp}^*)(\text{dppe})]^+$ . . . . .	153
2.14	Optimized atomic coordinates of $(\text{Ph}[\text{Me}]\text{N})_3\text{Ti}[\text{P}(\text{P}_2)\text{As}]\text{Ti}(\text{N}[\text{Me}]\text{Ph})_3$ . . . . .	154

2.15	Optimized atomic coordinates of $\text{AsP}_3(\text{GaCH}_3)_4$ . . . . .	155
2.16	Optimized atomic coordinates of $[(\text{SbP}_3)\text{Fe}(\text{Cp}^*)(\text{dppe})]^+$ . . . . .	155
2.17	Refinement Details for the Gas-Phase Electron Diffraction Structure Determination of $\text{P}_4$ . . . . .	157
2.18	Refinement Details for the Gas-Phase Electron Diffraction Structure Determination of $\text{AsP}_3$ . . . . .	158
2.19	Crystallographic data for $[\text{Na}][\text{P}_3\text{Nb}(\text{ODipp})_3]$ and $[\text{Na}][\text{P}_3\text{Nb}(\text{ODipp})_3]$ . . . . .	160
2.20	Crystallographic data for $(\text{AsP}_3)\text{Mo}(\text{CO})_3(\text{P}^i\text{Pr}_3)_2$ and $[(\text{AsP}_3)\text{Fe}(\text{Cp}^*)(\text{dppe})][\text{BPh}_4]$ . . . . .	161
2.21	Crystallographic data for $[\text{P}(\text{N}^i\text{Pr}_2)(\text{N}(\text{SiMe}_3)_2)]_2(\text{AsP}_3)$ and $[\text{Na}][\text{As}_3\text{Nb}(\text{ODipp})_3]$ . . . . .	162
2.22	Crystallographic data for $\text{As}[\text{GaC}(\text{SiMe}_3)_3]_3\text{P}_3$ . . . . .	163
3.1	Optimized atomic coordinates of $\text{P}_3\text{Rh}(\text{PPh}_3)_3$ . . . . .	198
3.2	Optimized atomic coordinates of $\text{Ph}_3\text{SnP}_3$ (free triphosphirene). . . . .	200
3.3	Crystallographic data for $\text{Ph}_3\text{SnP}_3(\text{C}_6\text{H}_8)$ and $\text{Ph}_3\text{SnP}_3(\text{C}_6\text{H}_8)(\text{C}_2\text{N}_2(\text{NC}_5\text{H}_4)_2)$ . . . . .	201
3.4	Crystallographic data for $\text{P}_3\text{Rh}(\text{PPh}_3)_3$ and $[\text{Na}][\text{P}_3\text{Nb}(\text{ODipp})(\text{OC}_6\text{F}_5)_2]$ . . . . .	202
A.1	Synthesis of $\text{PR}_3$ from $n(\text{RX} + \text{Ti}(\text{N}^i\text{Bu}]\text{Ar})_3)$ and $0.25 \text{ P}_4$ in benzene solvent at $20^\circ\text{C}$ . . . . .	208
A.2	Attempt to generate $\text{PR}_3$ from $\text{P}_4$ using other halogen atom abstractors. . . . .	216
A.3	Effect of stoichiometry on reaction of $\text{V}(\text{N}[\text{Np}]\text{Ar})_3$ with $\text{P}_4$ and $\text{CyBr}$ . . . . .	216

## List of Compounds

- 1  $\text{ONb}(\text{OC}[\text{}^2\text{Ad}]\text{Mes})_3$
- 2  $(\text{F}_3\text{C}(\text{O})\text{CO})_2\text{Nb}(\text{OC}[\text{}^2\text{Ad}]\text{Mes})_3$
- 3  $\text{I}_2\text{Nb}(\text{OC}[\text{}^2\text{Ad}]\text{Mes})_3$
- 4  $(\text{PhC}\equiv\text{CPh})\text{Nb}(\text{OC}[\text{}^2\text{Ad}]\text{Mes})_3$
- 5  $\text{INb}(\text{OC}[\text{}^2\text{Ad}]\text{Mes})_3(\text{THF})$
- 6  $[(\text{Mes}[\text{}^2\text{Ad}]\text{CO})_3\text{Nb}]_2(\mu\text{-I})$
- 7  $(\text{Mes}[\text{}^2\text{Ad}]\text{CO})_3\text{Nb}=\text{PP}_7\text{Nb}(\text{OC}[\text{}^2\text{Ad}]\text{Mes})_3$
- 8  $\text{H}_2\text{PP}_7\text{Nb}(\text{OC}[\text{}^2\text{Ad}]\text{Mes})_3$
- 9  $\text{Ph}_2\text{C}=\text{PP}_7\text{Nb}(\text{OC}[\text{}^2\text{Ad}]\text{Mes})_3$
- 10  $\text{Ph}_2\text{CP}_8\text{Nb}(\text{OC}[\text{}^2\text{Ad}]\text{Mes})_3$
- 11  $((\text{Me}_2\text{N})\text{C}_6\text{H}_4)_2\text{C}=\text{PP}_7\text{Nb}(\text{OC}[\text{}^2\text{Ad}]\text{Mes})_3$
- 12  $((\text{MeO})\text{C}_6\text{H}_4)_2\text{C}=\text{PP}_7\text{Nb}(\text{OC}[\text{}^2\text{Ad}]\text{Mes})_3$
- 13  $(\text{MeC}_6\text{H}_4)_2\text{C}=\text{PP}_7\text{Nb}(\text{OC}[\text{}^2\text{Ad}]\text{Mes})_3$
- 14  $(\text{ClC}_6\text{H}_4)_2\text{C}=\text{PP}_7\text{Nb}(\text{OC}[\text{}^2\text{Ad}]\text{Mes})_3$
- 15  $((\text{F}_3\text{C})\text{C}_6\text{H}_4)_2\text{C}=\text{PP}_7\text{Nb}(\text{OC}[\text{}^2\text{Ad}]\text{Mes})_3$
- 16  $\text{Cl}_2\text{Nb}(\text{OC}[\text{}^2\text{Ad}]\text{Mes})_3$
- 17  $\text{Cy}_2\text{C}=\text{PP}_7\text{Nb}(\text{OC}[\text{}^2\text{Ad}]\text{Mes})_3$
- 18  ${}^i\text{Pr}_2\text{C}=\text{PP}_7\text{Nb}(\text{OC}[\text{}^2\text{Ad}]\text{Mes})_3$
- 19  $\text{Ph}_2\text{SnP}_8\text{Nb}(\text{OC}[\text{}^2\text{Ad}]\text{Mes})_3$
- 20  $\text{dmpPP}_8\text{Nb}(\text{OC}[\text{}^2\text{Ad}]\text{Mes})_3$
- 21  $\text{Ph}_2\text{CP}_8(\text{C}_6\text{H}_8)$
- 22  $\text{ONb}(\text{OC}[\text{}^2\text{Ad}]\text{Mes})_3(\text{ONC}_5\text{H}_5)$
- 23  $\text{Ph}_2\text{CP}_8(\text{C}_6\text{H}_{10})$
- 24  $\text{Ph}_2\text{CP}_8(\text{C}_7\text{H}_8)$
- 25  $[\text{Na}(\text{THF})_3][\text{P}_3\text{Nb}(\text{ODipp})_3]$
- 26  $[\text{CoCp}_2][\text{P}_3\text{Nb}(\text{ODipp})_3]$
- 27  $\text{AsP}_3$
- 28  $(\text{AsP}_3)\text{Mo}(\text{CO})_3(\text{P}^i\text{Pr}_3)_2$
- 29  $[(\text{AsP}_3)\text{Fe}(\text{Cp}^*)(\text{dppe})][\text{BPh}_4]$
- 30  $[\text{P}(\text{N}^i\text{Pr}_2)(\text{N}(\text{SiMe}_3)_2)]_2(\text{AsP}_3)$
- 31  $(\text{Ar}[\text{}^t\text{Bu}]\text{N})_3\text{Ti}[\text{P}(\text{P}_2)\text{As}]\text{Ti}(\text{N}[\text{}^t\text{Bu}]\text{Ar})_3$
- 32  $(\text{Ar}[\text{}^t\text{Bu}]\text{N})_3\text{Ti}[\text{P}(\text{P}_2)\text{P}]\text{Ti}(\text{N}[\text{}^t\text{Bu}]\text{Ar})_3$
- 33  $(\text{Ar}[\text{CH}_2{}^t\text{Bu}]\text{N})_3\text{Nb}(\text{PAs})\text{Nb}(\text{N}[\text{CH}_2{}^t\text{Bu}]\text{Ar})_3$
- 34  $(\text{Ar}[\text{CH}_2{}^t\text{Bu}]\text{N})_3\text{Nb}(\text{P}_2)\text{Nb}(\text{N}[\text{CH}_2{}^t\text{Bu}]\text{Ar})_3$
- 35  $\text{E}\equiv\text{Mo}(\text{N}[\text{}^t\text{Bu}]\text{Ar})_3$  (E = As, P)
- 36  $\text{As}[\text{GaC}(\text{SiMe}_3)_3]_3\text{P}_3$
- 37  $[\text{Na}(\text{THF})_3][\text{P}_2\text{AsNb}(\text{ODipp})_3]$
- 38  $[\text{Na}(\text{THF})_3][\text{PAs}_2\text{Nb}(\text{ODipp})_3]$
- 39  $[\text{Na}(\text{THF})_3][\text{As}_3\text{Nb}(\text{ODipp})_3]$
- 40  $\text{As}_2\text{P}_2$
- 41  $\text{As}_3\text{P}$
- 42  $\text{As}_4$
- 43  $\text{SbP}_3$
- 44  $[(\text{SbP}_3)\text{Fe}(\text{Cp}^*)(\text{dppe})][\text{BPh}_4]$
- 45  $\text{Ph}_3\text{SnP}_3\text{Nb}(\text{ODipp})_3$
- 46  $\text{Bu}_3\text{SnP}_3\text{Nb}(\text{ODipp})_3$
- 47  $\text{Me}_3\text{SiP}_3\text{Nb}(\text{ODipp})_3$
- 48  $\text{Ph}_3\text{SiP}_3\text{Nb}(\text{ODipp})_3$
- 49  $\text{Ph}_3\text{CP}_3\text{Nb}(\text{ODipp})_3$
- 50  $(\text{Ar}[\text{}^t\text{Bu}]\text{N})_3\text{TiP}_3\text{Nb}(\text{ODipp})_3$
- 51  $\text{Cp}_2\text{ClZrP}_3\text{Nb}(\text{ODipp})_3$
- 52  $\text{Ph}_3\text{SnP}_3(\text{C}_6\text{H}_8)$
- 53  $[\text{ONb}(\text{ODipp})_3]_2$
- 54  $\text{Ph}_3\text{SnP}_3(\text{C}_6\text{H}_{10})$
- 55  $\text{Ph}_3\text{SnP}_3(\text{C}_6\text{H}_8)(\text{C}_2\text{N}_2(\text{NC}_5\text{H}_4)_2)$
- 56  $\text{P}_3\text{Rh}(\text{PPh}_3)_3$
- 57  $\text{LiP}_3(\text{C}_6\text{H}_8)$
- 58  $\text{HP}_3(\text{C}_6\text{H}_8)$
- 59  $\text{P}_3\text{H}_3$
- 60  $[\text{Na}(12\text{-crown-4})_2][\text{P}_3\text{Nb}(\text{ODipp})(\text{OC}_6\text{F}_5)_2]$

# List of Abbreviations

<sup>2</sup> Ad	2-adamantyl	K	Kelvin
Å	angstrom (10 <sup>-10</sup> m)	LUMO	lowest unoccupied molecular orbital
Ar	3,5-Me <sub>2</sub> C <sub>6</sub> H <sub>3</sub>	m	multiplet or meter
br	broad	<i>m</i>	<i>meta</i>
Bu	butyl	Me	methyl
°C	degree Celsius	Mes	mesityl (2,4,6-Me <sub>3</sub> C <sub>6</sub> H <sub>2</sub> )
cal	calories	mg	milligram
calcd.	calculated	mL	milliliter
CCD	charge-coupled device	min	minutes
cm <sup>-1</sup>	wavenumbers	mol	moles
COSY	correlation spectroscopy	m.p.	melting point
Cp	cyclopentadienyl ([C <sub>5</sub> H <sub>5</sub> ] <sup>-1</sup> )	MS	mass spectrometry
Cp*	[C <sub>5</sub> Me <sub>5</sub> ] <sup>-1</sup>	NMR	nuclear magnetic resonance
Cp''	[1,3- <sup>t</sup> Bu <sub>2</sub> -2,4,5-Me <sub>3</sub> C <sub>5</sub> ] <sup>-1</sup>	<i>o</i>	<i>ortho</i>
Cy	cyclohexyl ( <i>cyclo</i> -C <sub>6</sub> H <sub>11</sub> )	OTf	trifluoromethylsulfonate (O <sub>3</sub> SCF <sub>3</sub> )
d	days or doublet	<i>p</i>	<i>para</i>
dec	decomposes	Ph	phenyl (C <sub>6</sub> H <sub>5</sub> )
DFT	density functional theory	ppm	parts per million
Dipp	diisopropylphenyl (2,6- <sup>i</sup> Pr <sub>2</sub> C <sub>6</sub> H <sub>3</sub> )	py	pyridine
DME	1,2-dimethoxyethane	q	quartet
e	electron	<i>r<sub>e</sub></i>	equilibrium bond length
equiv	equivalent(s)	<i>r<sub>g</sub></i>	thermally averaged bond length
eV	electron volt	s	singlet
Et <sub>2</sub> O	diethyl ether	t	triplet
Fc	ferrocene	<sup>t</sup> Bu	<i>tert</i> -butyl (C(CH <sub>3</sub> ) <sub>3</sub> )
G	gauss	T	temperature
g	grams	TBA	tetrabutyl ammonium
h	hour	THF	tetrahydrofuran
<i>H</i>	enthalpy	UV	ultra violet
<sup>1</sup> H	proton	vis	visible
HOMO	highest occupied molecular orbital	VT	variable temperature
Hz	hertz (s <sup>-1</sup> )	δ	chemical shift
<sup>i</sup> Pr	<i>iso</i> -propyl (CH(CH <sub>3</sub> ) <sub>2</sub> )	ε	extinction coefficient
IR	infra red	μ <sub>eff</sub>	effective magnetic moment
<i>J</i>	coupling constant	μ <sub>L</sub>	micro liters

# CHAPTER 1

## Synthesis and Reactivity of (Mes[<sup>2</sup>Ad]CO)<sub>3</sub>Nb=PP<sub>7</sub>Nb(OC[<sup>2</sup>Ad]Mes)<sub>3</sub>

### Contents

<b>1.1 Introduction</b>	<b>23</b>
1.1.1 Polyphosphorus Ligands	24
1.1.2 A Foundation for Niobium-Phosphorus Chemistry	26
1.1.3 The Enolate Ligand System	27
<b>1.2 Metallation of the Enolate Ligand with Niobium</b>	<b>29</b>
1.2.1 Synthesis and Subsequent Activation of ONb(OC[ <sup>2</sup> Ad]Mes) <sub>3</sub>	29
1.2.2 Direct synthesis of I <sub>2</sub> Nb(OC[ <sup>2</sup> Ad]Mes) <sub>3</sub>	31
<b>1.3 Reduction and Disproportionation of the Niobium Diiodide Complex</b>	<b>32</b>
1.3.1 Synthesis of INb(OC[ <sup>2</sup> Ad]Mes) <sub>3</sub> (THF)	32
1.3.2 Disproportionation	34
<b>1.4 P<sub>4</sub> Activation</b>	<b>34</b>
<b>1.5 Phosphinidene Reactivity</b>	<b>36</b>
1.5.1 Reaction with H <sub>2</sub> O	37
1.5.2 Reaction with Ketones	38
<b>1.6 Rearrangement of the Phosphaalkene Complex</b>	<b>40</b>
1.6.1 Eyring Analysis	43
1.6.2 Hammett Study	44
1.6.3 Stable Phosphaalkene Complexes	49

Reproduced in part with permission from:

Cossairt, B. M.; Cummins, C. C. *Angew. Chem. Int. Ed.*, **2008**, *46*, 169–172; Copyright 2008 Wiley-VCH.

Cossairt, B. M.; Cummins, C. C. *Inorg. Chem.*, **2008**, *47*, 9363–9371; Copyright 2008 American Chemical Society, License 2380430856627.

Cossairt, B. M.; Cummins, C. C. *Angew. Chem. Int. Ed.*, **2008**, *47*, 8863–8866; Copyright 2008 Wiley-VCH.

Cossairt, B. M.; Piro, N. A.; Cummins, C. C. *Chem. Rev.*, **2010**, DOI: 10.1021/cr9003709; Copyright 2010 American Chemical Society, License 2380440884613.

1.6.4	Putting Other Elements in the Cluster: Preparation of $\text{Ph}_2\text{SnP}_8\text{Nb}(\text{OC}[\text{}^2\text{Ad}]\text{Mes})_3$ and $\text{DmpPP}_8\text{Nb}(\text{OC}[\text{}^2\text{Ad}]\text{Mes})_3$ . . . . .	49
<b>1.7</b>	<b>Liberation of <math>\text{R}_2\text{CP}_8</math> from the Niobium Metal Center</b> . . . . .	<b>51</b>
1.7.1	Reaction of $\text{Ph}_2\text{CP}_8\text{Nb}(\text{OC}[\text{}^2\text{Ad}]\text{Mes})_3$ with $\text{ONC}_5\text{H}_5$ in the Presence of 1,3-Cyclohexadiene . . . . .	52
1.7.2	Pathways for the Formation of $\text{Ph}_2\text{CP}_8(\text{C}_6\text{H}_8)$ . . . . .	54
1.7.3	Properties and Reactivity Patterns of $\text{Ph}_2\text{CP}_8(\text{C}_6\text{H}_8)$ . . . . .	56
<b>1.8</b>	<b>Conclusions</b> . . . . .	<b>58</b>
<b>1.9</b>	<b>Experimental Details</b> . . . . .	<b>59</b>
1.9.1	General Considerations . . . . .	59
1.9.2	Preparation of $\text{ONb}(\text{OC}[\text{}^2\text{Ad}]\text{Mes})_3(\text{OEt}_2)$ , <b>1</b> . . . . .	59
1.9.3	Preparation of $(\text{F}_3\text{CC}(\text{O})\text{O})_2\text{Nb}(\text{OC}[\text{}^2\text{Ad}]\text{Mes})_3$ , <b>2</b> . . . . .	60
1.9.4	Preparation of $\text{I}_2\text{Nb}(\text{OC}[\text{}^2\text{Ad}]\text{Mes})_3$ from <b>2</b> , <b>3</b> . . . . .	60
1.9.5	Preparation of $(\text{PhC}\equiv\text{CPh})\text{Nb}(\text{OC}[\text{}^2\text{Ad}]\text{Mes})_3$ , <b>4</b> . . . . .	61
1.9.6	Preparation of $\text{I}_2\text{Nb}(\text{OC}[\text{}^2\text{Ad}]\text{Mes})_3$ , <b>3</b> ; One-pot Procedure . . . . .	61
1.9.7	Preparation of $\text{INb}(\text{OC}[\text{}^2\text{Ad}]\text{Mes})_3(\text{THF})$ , <b>5</b> . . . . .	61
1.9.8	Disproportionation of $\text{INb}(\text{OC}[\text{}^2\text{Ad}]\text{Mes})_3(\text{THF})$ in the absence of a trap . . . . .	62
1.9.9	Preparation of $(\text{Mes}[\text{}^2\text{Ad}]\text{CO})_3\text{Nb}=\text{PP}_7\text{Nb}(\text{OC}[\text{}^2\text{Ad}]\text{Mes})_3$ , <b>7</b> . . . . .	62
1.9.10	Preparation of $\text{H}_2\text{PP}_7\text{Nb}(\text{OC}[\text{}^2\text{Ad}]\text{Mes})_3$ , <b>8</b> . . . . .	63
1.9.11	Preparation of $\text{Ph}_2\text{CP}_8\text{Nb}(\text{OC}[\text{}^2\text{Ad}]\text{Mes})_3$ , <b>10</b> . . . . .	64
1.9.12	Preparation of $((\text{Me}_2\text{N})\text{C}_6\text{H}_4)_2\text{C}=\text{PP}_7\text{Nb}(\text{OC}[\text{}^2\text{Ad}]\text{Mes})_3$ , <b>11</b> . . . . .	64
1.9.13	Preparation of $((\text{MeO})\text{C}_6\text{H}_4)_2\text{C}=\text{PP}_7\text{Nb}(\text{OC}[\text{}^2\text{Ad}]\text{Mes})_3$ , <b>12</b> . . . . .	65
1.9.14	Preparation of $(\text{MeC}_6\text{H}_4)_2\text{C}=\text{PP}_7\text{Nb}(\text{OC}[\text{}^2\text{Ad}]\text{Mes})_3$ , <b>13</b> . . . . .	65
1.9.15	Preparation of $(\text{ClC}_6\text{H}_4)_2\text{C}=\text{PP}_7\text{Nb}(\text{OC}[\text{}^2\text{Ad}]\text{Mes})_3$ , <b>14</b> . . . . .	65
1.9.16	Preparation of $((\text{F}_3\text{C})\text{C}_6\text{H}_4)_2\text{C}=\text{PP}_7\text{Nb}(\text{OC}[\text{}^2\text{Ad}]\text{Mes})_3$ , <b>15</b> . . . . .	65
1.9.17	Preparation of $\text{C}_7\text{H}_7\text{C}=\text{PP}_7\text{Nb}(\text{OC}[\text{}^2\text{Ad}]\text{Mes})_3$ , <b>17</b> . . . . .	66
1.9.18	Preparation of ${}^i\text{Pr}_2\text{C}=\text{PP}_7\text{Nb}(\text{OC}[\text{}^2\text{Ad}]\text{Mes})_3$ , <b>18</b> . . . . .	66
1.9.19	Kinetic Investigations of the Rearrangement of $\text{Ph}_2\text{C}=\text{PP}_7\text{Nb}(\text{OC}[\text{}^2\text{Ad}]\text{Mes})_3$ : Eyring Analysis and Hammett Trend Analysis . . . . .	66
1.9.20	Preparation of $\text{Ph}_2\text{SnP}_8\text{Nb}(\text{OC}[\text{}^2\text{Ad}]\text{Mes})_3$ , <b>19</b> . . . . .	67
1.9.21	Preparation of $\text{dmpPP}_8\text{Nb}(\text{OC}[\text{}^2\text{Ad}]\text{Mes})_3$ , <b>20</b> . . . . .	68
1.9.22	Preparation of $\text{Ph}_2\text{CP}_8(\text{C}_6\text{H}_8)$ , <b>21</b> . . . . .	68
1.9.23	Preparation of $\text{Ph}_2\text{CP}_8(\text{C}_6\text{H}_{10})$ , <b>23</b> . . . . .	69
1.9.24	Preparation of $\text{Ph}_2\text{CP}_8(\text{C}_7\text{H}_8)$ , <b>24</b> . . . . .	69
1.9.25	X-Ray Structure Determinations . . . . .	70
1.9.26	Computational Studies . . . . .	70
<b>1.10</b>	<b>References</b> . . . . .	<b>81</b>

## 1.1 INTRODUCTION

Phosphorus-containing molecules are ubiquitous in the world around us and the synthetic and industrial utilization of phosphorus has prospered for over a century.<sup>1,2</sup> The industrial reduction of phosphate rock (apatite,  $\text{Ca}_{10}(\text{PO}_4)_6(\text{X})_2$ ,  $\text{X} = \text{OH}, \text{F}, \text{Cl}, \text{or Br}$ ) to white phosphorus,  $\text{P}_4$ , exceeds 500,000 tons annually as  $\text{P}_4$  still represents the major commercial P-atom source for the production of organophosphorus compounds utilized by the food, detergent, specialty chemical, and pharmaceutical industries.<sup>3</sup> The present day synthesis of organophosphorus compounds is a multi-step process in which  $\text{P}_4$  is first chlorinated to generate  $\text{PCl}_3$ , which in turn is functionalized by reaction with an appropriate Grignard or organolithium reagent, or by treatment with a halogenated organic compound and a powerful reducing agent.<sup>4,5</sup> For example, the industrial method for triphenylphosphine preparation is based on the high temperature reaction of chlorobenzene with phosphorus trichloride in the presence of molten sodium.<sup>4,6</sup> From both a safety and a sustainability standpoint, the need for  $\text{PCl}_3$  as an intermediate for the production of organophosphorus compounds is unpalatable and methods that circumvent its use are of great interest. This has provoked intensive investigations into the mild and controlled activation of  $\text{P}_4$ , a clear objective being the development of catalytic methods for phosphorus incorporation into organic molecules.

Sustained interest in the chemistry of low-valent, early-transition-metal complexes arises from their propensity to reductively activate a wide variety of small molecule substrates.<sup>7</sup> A combination of coordinative unsaturation, inherent Lewis acidity, and availability of chemically accessible *d* electrons endows low-valent, early-transition-metal fragments with a rich reaction chemistry. The ability to apply the reductive power of such reactive metal systems is therefore of great interest for applications ranging from organic catalysis to dinitrogen fixation and it comes as no surprise that low-valent, early-transition-metal complexes have received considerable attention as agents for  $\text{P}_4$  activation. The use of early-transition-metal complexes to study  $\text{P}_4$  activation and functionalization is motivated by the wide array of P-containing ligands that can be obtained.  $\text{P}_1$  through  $\text{P}_8$  ligands have been isolated and studied from  $\text{P}_4$  activation reactions of early-transition-metal complexes, and many of these metal-phosphorus systems have proven to be themselves reactive due to the hard-soft mismatch of early-transition-metal-phosphorus bonds. This bonding mismatch provides an underlying thermodynamic driving force by which assembled phosphorus ligands can be liberated from the metal center by exchange with preferred hard, anionic ligands, such as  $\text{O}^{2-}$  and  $\text{X}^-$  ( $\text{X} = \text{Cl}, \text{Br}, \text{I}$ ).

In this dissertation, several strategies for  $\text{P}_4$  activation with complexes of an early-transition metal (niobium) are developed with an emphasis placed on subsequent transformation of the phosphorus-containing metal complexes and an eye towards the synthesis of phosphorus-rich main group molecules. In this chapter, a novel  $\text{P}_4$  coupling reaction is identified and the reaction chemistry of this product is developed. The generation of a  $\text{P}_8$ -containing polyphosphorus ligand from  $\text{P}_4$  coupling is not, itself, a new reaction type, but the structure of the  $\text{P}_8$  complex developed

herein and its abundant chemistry is certainly noteworthy in the context of polyphosphorus chemistry.

### 1.1.1 Polyphosphorus Ligands

#### From P<sub>4</sub>

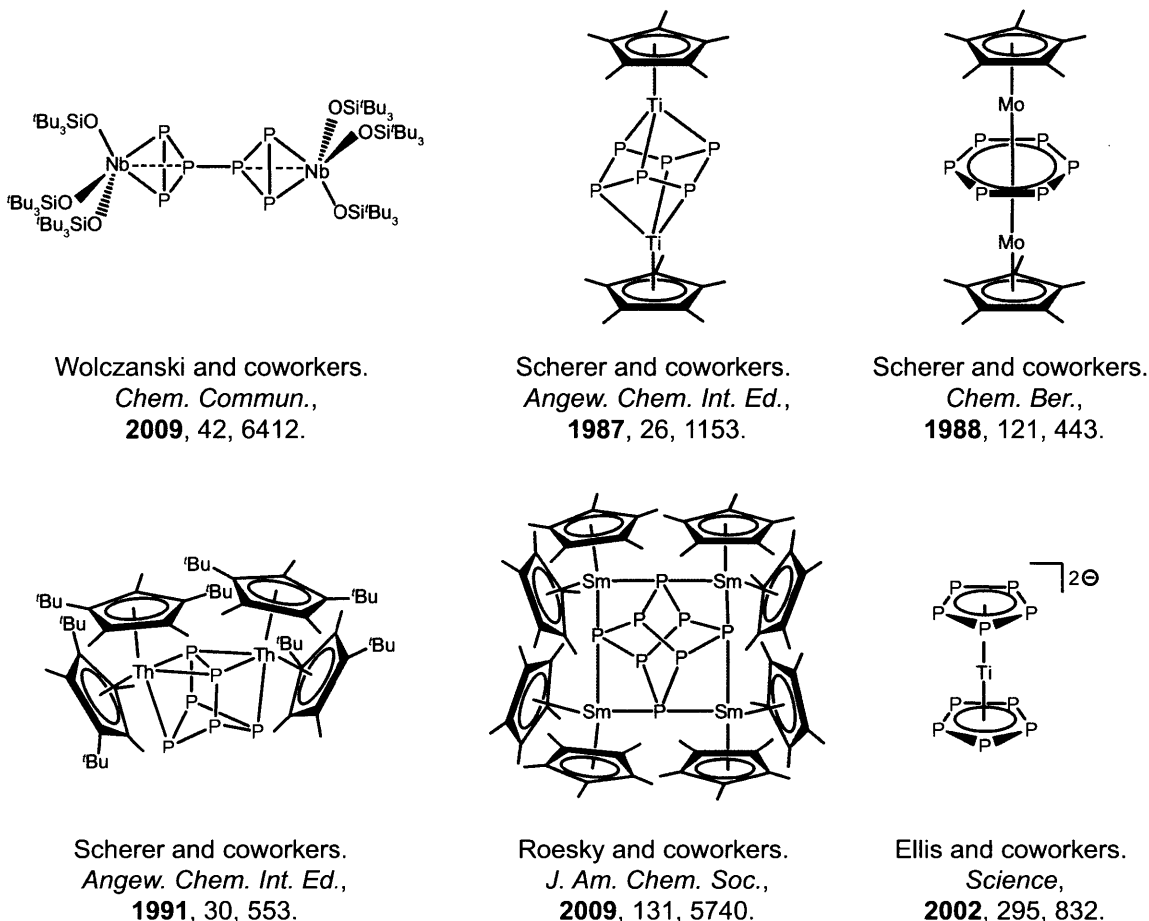


**Figure 1.1.** P<sub>4</sub>-derived polyphosphorus ligands supported by early-transition-metal complexes.

The divergent and fascinating reactivity of P<sub>4</sub> with early-transition-metal systems is highlighted particularly well by the cases in which polyphosphorus ligands with greater than four P atoms are formed, Figure 1.1.<sup>8–13</sup> Instances of such aggregation are common in P<sub>4</sub> activation chemistry and these reactions are important to developing a thorough understanding of structure and bonding in phosphorus chemistry. Perhaps one of the most intriguing examples of P<sub>4</sub> activation by an early-transition metal was provided by Ellis and coworkers in 2002.<sup>14</sup> A highly reactive naphthalene-stabilized titanate complex was first formed by reduction of TiCl<sub>4</sub>(THF)<sub>2</sub> with six equivalents of potassium naphthalenide in THF at –60 °C, followed by addition of 2 equiv of 18-crown-6. The complex so obtained was found to react with 2.5 equiv of P<sub>4</sub> to give [K(18-crown-6)]<sub>2</sub>[Ti(η<sup>5</sup>-P<sub>5</sub>)<sub>2</sub>],



an all-inorganic analogue of the titanocene dianion, Figure 1.1.<sup>14</sup> Despite being isovalent with the group 6 metallocenes,  $[\text{K}(\text{18-crown-6})]_2[\text{Ti}(\eta^5\text{-P}_5)_2]$  is both surprisingly air and moisture stable and chemically inert. This decaphosphametallocene remains the only such molecule and is a prime example of the isolobal analogy between P atoms and CH fragments.<sup>8</sup>

Both monocyclic and bicyclic  $\text{P}_6$  ligands have been isolated when sandwiched between early transition metals. The first example of the *cyclo*- $\text{P}_6$  ligand was provided by Scherer and coworkers while exploring the chemistry of  $[\text{Cp}^*(\text{CO})_2\text{Mo}]_2$  ( $\text{Cp}^* = \text{C}_5\text{Me}_5$ ) with  $\text{P}_4$ . Treatment of  $[\text{Cp}^*(\text{CO})_2\text{Mo}]_2$  with  $\text{P}_4$  in xylene at 140 °C results in formation of a mixture of products including  $\text{Mo}_2(\text{CO})_4\text{Cp}^*_2(\mu_2 : \eta^2, \eta^2\text{-P}_2)$  and  $(\eta^3\text{-P}_3)\text{Mo}(\text{CO})_2\text{Cp}^*$ , as well as the triple-decker complex  $[\text{Cp}^*\text{Mo}]_2(\mu_2 : \eta^6, \eta^6\text{-P}_6)$ , Figure 1.1.<sup>15</sup> As the all-phosphorus analogue of benzene, *cyclo*- $\text{P}_6$  has been stabilized by a variety of triple-decker complexes of early transition metals including those of W, V, Nb, and Ti by thermolysis of a half-sandwich precursor (usually a cyclopentadienyl/carbonyl complex) with  $\text{P}_4$  in a hydrocarbon solvent.<sup>10,12,16-18</sup> Several of the  $\text{P}_6$  triple-decker complexes adopt the expected  $D_{6h}$  configuration with a planar  $\text{P}_6$  unit, but in the case of  $[\text{Cp}^*\text{Ti}]_2(\mu_2 : \eta^6, \eta^6\text{-P}_6)$  a distortion to a chair-like *cyclo*-hexaphosphido form occurs, and the  $\text{P}_6$  ligand binds in a  $\mu_2 : \kappa^3, \kappa^3$  fashion as a  $\text{P}_6^{6-}$  ligand, Figure 1.1.

Additional geometries can be obtained for  $\text{P}_6$  ligands as illustrated by the activation of  $\text{P}_4$  by  $\text{Cp}''_2\text{Th}(\eta^4\text{-C}_4\text{H}_6)$  ( $\text{Cp}'' = 1,3\text{-}i\text{Bu}_2\text{-2,4,5-Me}_3\text{C}_5$ ) in toluene at 100 °C. The resultant  $(\text{Cp}''_2\text{Th})_2(\mu_2 : \eta^3, \eta^3\text{-P}_6)$  complex contains a bicyclic  $\text{P}_6^{4-}$  ligand, which resembles a reduced hexaphosphabenzvalene ligand sandwiched between two thorium metal centers, Figure 1.1.<sup>11</sup> Yet another unique  $\text{P}_6$  ligand geometry has been provided by Wolczanski and coworkers who found that if a reaction mixture containing  $(i\text{Bu}_3\text{SiO})_3\text{NbPMe}_3$  and  $\text{P}_4$  was allowed to incubate at -78 °C for 7 h, followed by slow warming to 23 °C, then the red  $\text{P}_6$ -complex,  $((i\text{Bu}_3\text{SiO})_3\text{Nb})_2(\mu_2 : \eta^2, \eta^2\text{-}^c\text{P}_3\text{-}^c\text{P}_3)$  could be isolated in 77% yield, Figure 1.1.<sup>9</sup> In  $((i\text{Bu}_3\text{SiO})_3\text{Nb})_2(\mu_2 : \eta^2, \eta^2\text{-}^c\text{P}_3\text{-}^c\text{P}_3)$ , two of the niobium-phosphorus distances of 2.559(8) and 2.576(5) Å are significantly shorter than the third (2.784(7) Å). The average P-P interatomic distance within each of the  $^c\text{P}_3$  rings is 2.172(2) Å, and the two  $^c\text{P}_3$  rings are linked via a 2.217(7) Å diphosphorus bond. As such, the structural parameters may be best represented by considering the metal-ligand interaction as that of a niobium center interacting with a triphosphirene ring and benefiting from substantial backbonding.

Polyphosphorus ligands up through  $\text{P}_{12}$  have been isolated by activation of white phosphorus by late transition-metal fragments, but early-transition-metal systems to date have given ligands containing only up to as many as eight phosphorus atoms.<sup>19</sup> One interesting example of ostensible  $\text{P}_4$  dimerization comes from the lab of Roesky and coworkers who found that diffusion of  $\text{P}_4$  vapor into a toluene solution of solvate-free permethyl samarocene,  $\text{Cp}^*_2\text{Sm}$ , over a period of several days resulted in the formation of  $(\text{Cp}^*_2\text{Sm})_4\text{P}_8$  as red crystals, Figure 1.1.<sup>13</sup>  $(\text{Cp}^*_2\text{Sm})_4\text{P}_8$  can be described as containing a  $\text{P}_8^{4-}$  ligand in a realgar-type homoatomic conformation supported by four Sm(III) metal centers and represents the first example of a lanthanide-supported polyphosphide.

## From Phosphorus Polyanions

In contrast to the numerous known and often technically important main-group mono- and diphosphorus compounds, polyphosphorus compounds and coordination complexes have remained largely unexplored until relatively recently. Research on this “element-near” chemistry of phosphorus has produced further impressive advances with the result that a surprisingly large variety of compounds with skeletons consisting of chains or rings of phosphorus atoms are known today. This is thanks largely in part to the efforts of Marianne Baudler and coworkers who pioneered the synthesis of mono and polycyclic phosphorus hydrides and other “lightly-substituted” phosphorus-rich species, Figure 1.2.<sup>20,21</sup> Significant advances in the study of the reactivity of such phosphorus-rich clusters with transition metals were provided by Fenske and Eichhorn, to name a few.<sup>22-25</sup> These zintl-ion chemists realized that great opportunity lay in the development of the molecular chemistry of the group 15 polyanions as counterparts to the traditional field of P<sub>4</sub> activation chemistry and have shown that many new structural motifs have been left unexplored, Figure 1.2.

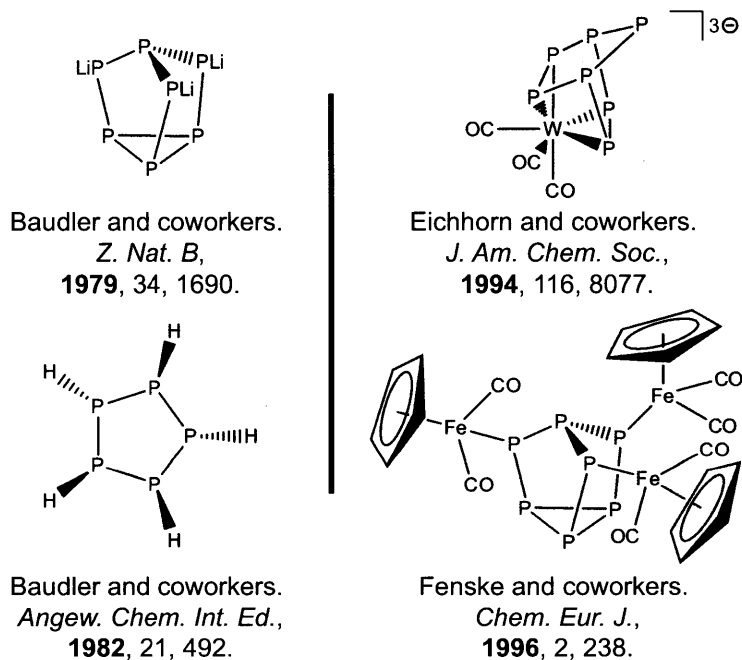
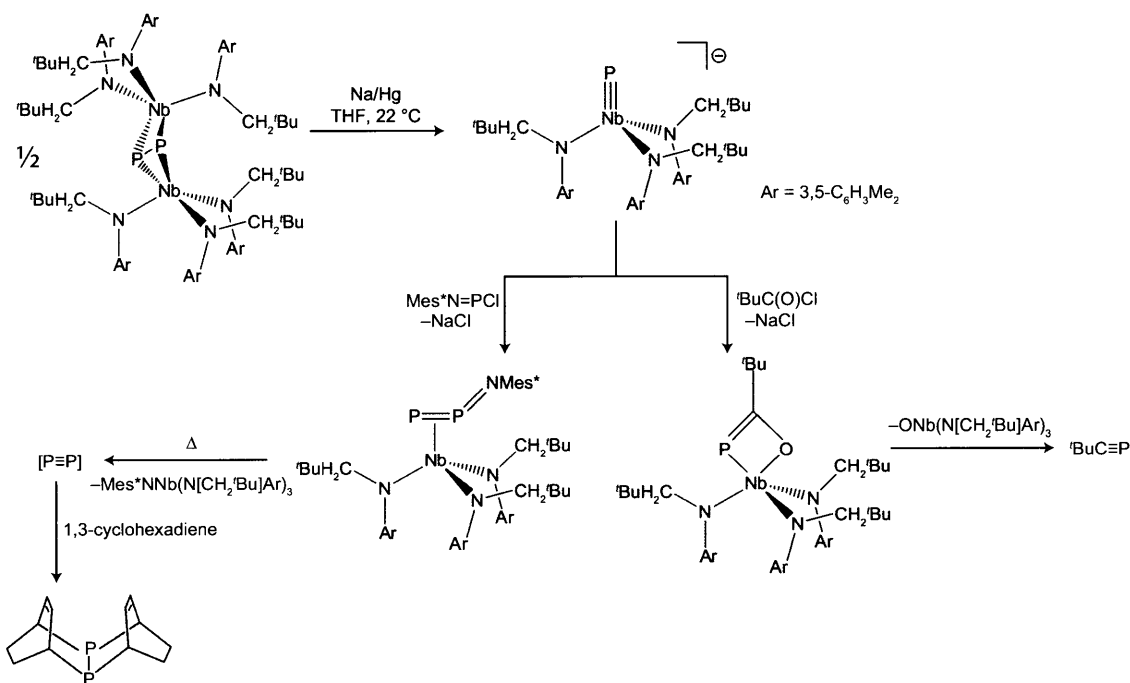


**Figure 1.2.** Polyphosphorus molecules as free and complexed entities.

### 1.1.2 A Foundation for Niobium-Phosphorus Chemistry

In the ensuing work, it was our desire to assemble phosphorus-rich ligands atop early-transition-metal platforms and to use those newly created complexes in the synthesis of phosphorus-rich main-group molecules. This strategy would represent a new motif in the synthesis of phosphorus-rich species and would allow access to structures unobtainable by more traditional methods. An early foundation for these studies had been provided by several reports out of the Cummins lab. The

first of these was the synthesis of  $(\mu_2\text{-}\eta^2, \eta^2\text{-P}_2)[\text{Nb}(\text{N}[\text{CH}_2^t\text{Bu}]\text{Ar})_3]_2$  ( $\text{Ar} = 3,5\text{-Me}_2\text{C}_6\text{H}_3$ ) through  $\text{P}_4$  activation by the niobaziridine hydride complex,  $\text{Nb}(\text{H})(\eta^2\text{-}^t\text{Bu}(\text{H})\text{C}=\text{NAr})(\text{N}[\text{CH}_2^t\text{Bu}]\text{Ar})_2$ .<sup>26</sup> Reduction of this intriguing dimeric diphosphide provided access to  $[\text{Na}][\text{P}\equiv\text{Nb}(\text{N}[\text{CH}_2^t\text{Bu}]\text{Ar})_3]$ , which in turn led to the eventual synthesis of the diphosphaazide complex  $(\eta^2\text{-Mes}^*\text{N}=\text{P}=\text{P})\text{-Nb}(\text{N}[\text{CH}_2^t\text{Bu}]\text{Ar})_3$ , Scheme 1.1.<sup>27</sup> This diphosphaazide complex, termed “the eliminator”, led to the generation of  $\text{P}\equiv\text{P}$  as a reactive transient, which was used with great success in the assembly of a wide array of new main-group and transition-metal-containing molecules, Scheme 1.1.<sup>27-29</sup> The phosphide anion complex  $[\text{Na}][\text{P}\equiv\text{Nb}(\text{N}[\text{CH}_2^t\text{Bu}]\text{Ar})_3]$  also led to a phosphalkyne generating system which proceeded through an intriguing NbPCO metallacycle intermediate, Scheme 1.1. It was our hope to enter into a new type of phosphorus-activation chemistry by tuning the ancillary ligands on the niobium metal center. Two criteria led us to the choice of a sterically demanding enolate ligand; first, it was thought that using more electronegative oxygen-donor ligands would make the niobium-center more Lewis acidic (and hence more reactive at higher oxidation states) and second, was the notion that the enolate functionality would push the steric bulk further away from the immediacy of the metal center and thereby allow for higher coordination numbers and potentially interesting new structural types.



**Scheme 1.1.** Niobium-phosphorus chemistry in the Cummins lab.

### 1.1.3 The Enolate Ligand System

While related to alkoxide, siloxide, and aryloxy supporting ligands, oxygen-bound enolates constitute an ancillary ligand class that has been largely overlooked in the context of stabilizing

low-coordinate early-metal complexes.<sup>30</sup> It was suspected that enolate ligation would impart certain benefits to early transition metal complexes, particularly minimizing unwanted side-reactions stemming from ancillary ligand vulnerability.<sup>30-34</sup> Accordingly, this new ligand system was designed to include an enolate essentially incapable (for steric reasons) of coordination to a metal through the enolate carbon, and that included one round adamantylidene cage and one flat aryl substituent. The latter requirement produces a class of enolate ligands “-OC[<sup>2</sup>Ad]Mes” (<sup>2</sup>Ad = 2-adamantylidene, Mes = 2,4,6-Me<sub>3</sub>C<sub>6</sub>H<sub>2</sub>), as illustrated in Figure 1.3, that is reminiscent topologically of the *N*-tert-hydrocarbonyl anilide ligands, which have been demonstrated to be versatile ligands for a variety of metals.<sup>35-37</sup> This ligand was used with great success by Han Sen Soo (a former Cummins group undergraduate) in the synthesis of both tantalum and molybdenum-enolate complexes.<sup>38,39</sup>

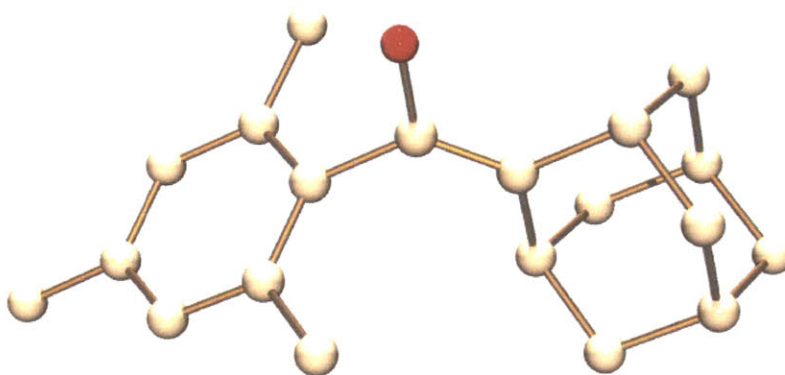
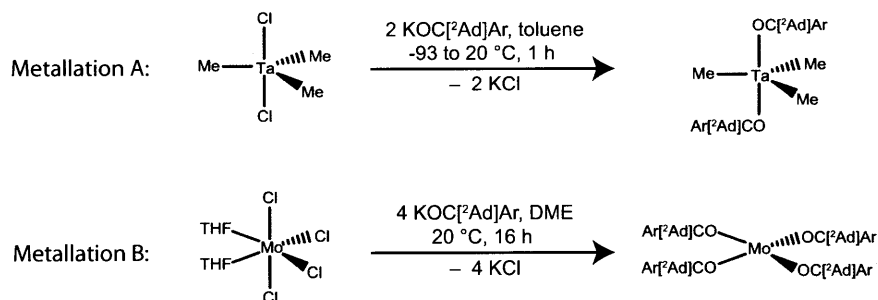


**Figure 1.3.** An enolate ligand designed to support electrophilic early transition metals.

The first metallation of these sterically demanding enolate ligands was with tantalum to generate trimethyltantalum bis-enolate complexes TaMe<sub>3</sub>(OC[<sup>2</sup>Ad]Ar)<sub>2</sub> (Ar = 3,5-C<sub>6</sub>H<sub>3</sub>Me<sub>2</sub> and 2,4,6-C<sub>6</sub>H<sub>2</sub>Me<sub>3</sub>) from a salt metathesis reaction between TaMe<sub>3</sub>Cl<sub>2</sub> and 2 equiv of the corresponding potassium enolate.<sup>38</sup> It was found that these complexes reacted with pyridine in the presence of dihydrogen, resulting in an unanticipated pyridine coupling with formation of the bipyridine complex TaMe(OC[<sup>2</sup>Ad]Ar)<sub>2</sub>(py)(bpy) (py = pyridyl and bpy = 2,2'-bipyridyl), Scheme 1.2. The second metallation of these unique enolate ligands was with molybdenum. While a Mo(OC[<sup>2</sup>Ad]Ar)<sub>3</sub> species was sought, a homoleptic molybdenum(IV) tetrakis enolate complex Mo(OC[<sup>2</sup>Ad]Mes)<sub>4</sub>, was instead obtained and characterized as the first structurally characterized example of an Mo(OR)<sub>4</sub> species.<sup>39</sup> Prior to the ensuing work, no tris-enolate complexes of any metal had been prepared.



**Scheme 1.2.** First explorations of the OC[<sup>2</sup>Ad]Ar ligand system (Ar = 3,5-C<sub>6</sub>H<sub>3</sub>Me<sub>2</sub> and 2,4,6-C<sub>6</sub>H<sub>2</sub>Me<sub>3</sub>).

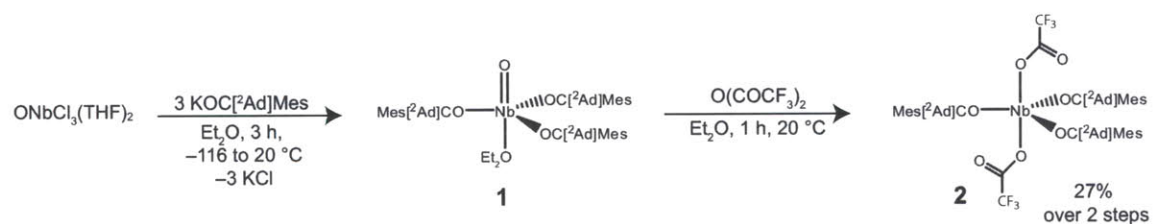
## 1.2 METALLATION OF THE ENOLATE LIGAND WITH NIOBIUM

Several strategies have been used within the Cummins group for the niobium-metallation of the anilide ligand LiN[CH<sub>2</sub><sup>t</sup>Bu]Ar. One fruitful method involved the use of Pedersen's (PhCCPh)NbCl<sub>3</sub>(THF)<sub>2</sub> precursor with 3 equiv of LiN[CH<sub>2</sub><sup>t</sup>Bu]Ar. This afforded the corresponding diphenylacetylene complex (PhCCPh)Nb(N[CH<sub>2</sub><sup>t</sup>Bu]Ar)<sub>3</sub> in 35% yield. Diphenylacetylene deprotection with 1 equiv of I<sub>2</sub> gave the diiodide complex I<sub>2</sub>Nb(N[CH<sub>2</sub><sup>t</sup>Bu]Ar)<sub>3</sub> in 65% yield.<sup>26</sup> This strategy was usurped when it was found that LiN[CH<sub>2</sub><sup>t</sup>Bu]Ar could be easily metallated with ONbCl<sub>3</sub>(THF)<sub>2</sub> to give ONb(N[CH<sub>2</sub><sup>t</sup>Bu]Ar)<sub>3</sub> in good yield. In a remarkable oxo-activation transformation, ONb(N[CH<sub>2</sub><sup>t</sup>Bu]Ar)<sub>3</sub> could be treated, in the same pot, with 1 equiv of triflic anhydride to give (OTf)<sub>2</sub>Nb(N[CH<sub>2</sub><sup>t</sup>Bu]Ar)<sub>3</sub>, which serves as a reduction precursor, in an overall yield of 68%.<sup>40,41</sup>

### 1.2.1 Synthesis and Subsequent Activation of ONb(OC[<sup>2</sup>Ad]Mes)<sub>3</sub>

Due to the convenience previously observed in starting with the ONbCl<sub>3</sub>(THF)<sub>2</sub> precursor, ONb(OC[<sup>2</sup>Ad]Mes)<sub>3</sub> was targeted as a first entry point into niobium-enolate chemistry. Treatment of ONbCl<sub>3</sub>(THF)<sub>2</sub> with 3 equiv KOC[<sup>2</sup>Ad]Mes in thawing Et<sub>2</sub>O results in a color progression from white to gray/green to blue and finally to yellow-brown over 30 minutes. Allowing the reaction mixture to warm to room temperature and stirring for an additional 2 h results in complete consumption of the KOC[<sup>2</sup>Ad]Mes. Removal of the salts and crystallization from Et<sub>2</sub>O at -35 °C resulted in a 30% yield of ONb(OC[<sup>2</sup>Ad]Mes)<sub>3</sub>(Et<sub>2</sub>O), **1**, Scheme 1.3. Analysis of the crude reaction mixture showed the presence of a significant amount of a previously observed enolate coupling product<sup>42</sup> that presumably resulted from oxidation of the enolate ligand with ONbCl<sub>3</sub>(THF)<sub>2</sub>.

A single crystal X-ray diffraction study was carried out on a yellow crystal of complex **1**. Complex **1** crystallizes in the space group *P* $\bar{1}$  and exhibits a short Nb≡O interaction of 1.703(3)



**Scheme 1.3.** Metallation of  $\text{KOC}[\text{Ad}]\text{Mes}$  with  $\text{ONbCl}_3(\text{THF})_2$ .

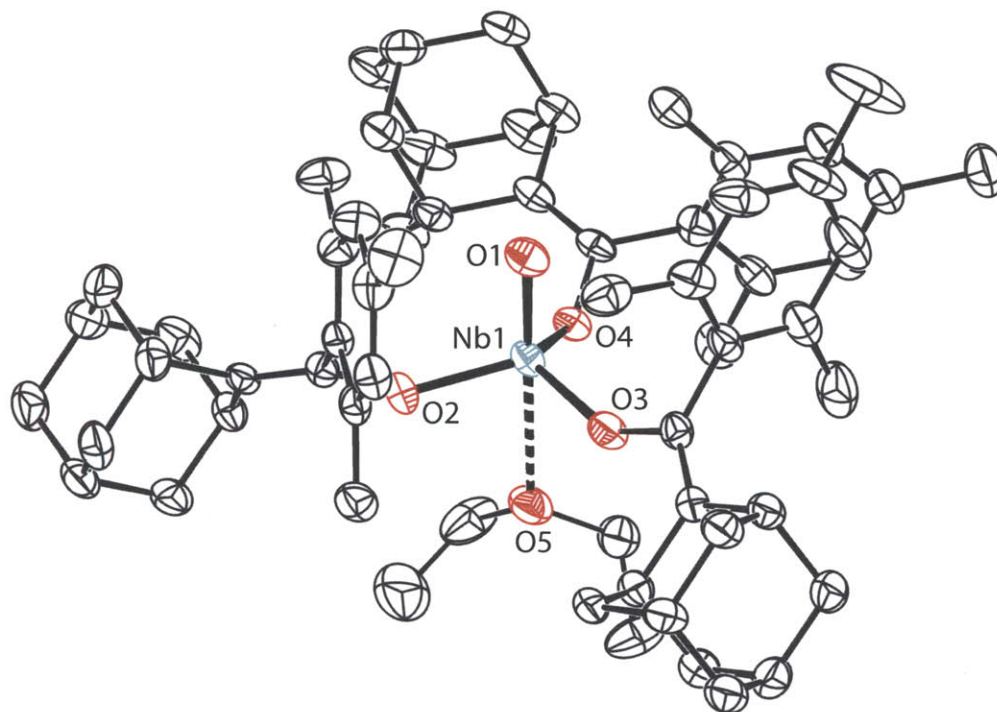
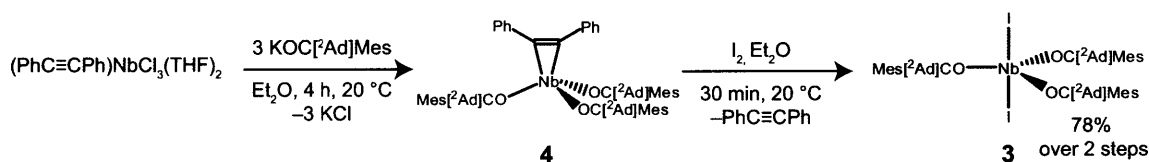


**Figure 1.4.** Thermal ellipsoid plot (50% probability) of  $\text{ONb}(\text{OC}[\text{Ad}]\text{Mes})_3$  with hydrogen atoms omitted for clarity.

Å and average Nb–enolate interaction of 1.908(3) Å. Interestingly, and in contrast with the anilide ligand sets, the niobium metal center in **1** binds even weak Lewis bases like diethyl ether. In the crystal structure, the Nb–OEt<sub>2</sub> distance is 2.494(3) Å. This may be suggestive that the niobium center supported by more electron withdrawing oxygen donor ligands is indeed more Lewis acidic than its anilide analogues. Furthermore, it supports the notion that there is less steric congestion directly at the metal center, easily allowing for penta-coordination.

Treatment of **1** with 1 equiv of triflic anhydride in thawing Et<sub>2</sub>O results in a mixture of unidentifiable products, which was discouraging in light of the ease with which ONb(N[CH<sub>2</sub><sup>t</sup>Bu]Ar)<sub>3</sub> is activated under identical conditions. It was found, however, that treatment of **1** with 1 equiv of trifluoroacetic anhydride in Et<sub>2</sub>O allowed for facile access to (F<sub>3</sub>CC(O)O)<sub>2</sub>Nb(OC[<sup>2</sup>Ad]Mes)<sub>3</sub>, **2**, Scheme 1.3, in 90% isolated yield. While it was possible to reduce **2** with 0.5 equiv magnesium anthracene in order to access a Nb(IV)-monoacetate species, this reduction led to many undesired byproducts. Instead, a method for conversion of **2** to the corresponding dihalide was sought. Treatment of **2** with 2 equiv of TMSI (TMS = Me<sub>3</sub>Si) in Et<sub>2</sub>O was found to result in precipitation of the desired I<sub>2</sub>Nb(OC[<sup>2</sup>Ad]Mes)<sub>3</sub>, **3**, in good yield over several hours. It was believed that **3** would allow easy access to a reduced niobium species to carry out P<sub>4</sub> activation chemistry. The main drawback of this sequence of reactions leading to **3** is the very low yield of the initial metallation product **1**. It was therefore desirable to have a more direct procedure for accessing the diiodide complex.

### 1.2.2 Direct synthesis of I<sub>2</sub>Nb(OC[<sup>2</sup>Ad]Mes)<sub>3</sub>



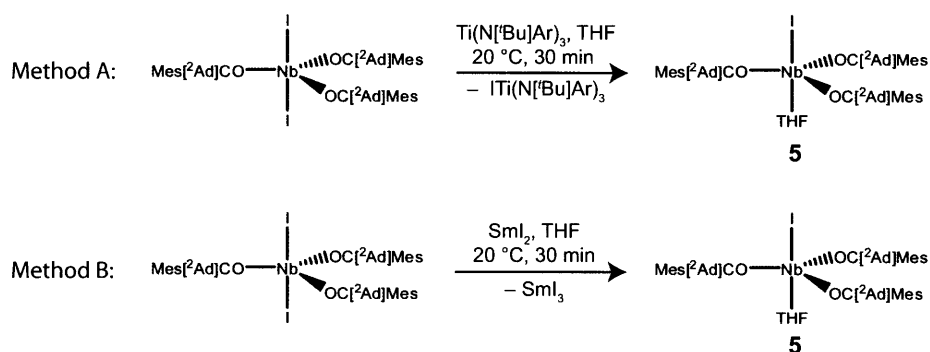
**Scheme 1.4.** Metallation of KOC[<sup>2</sup>Ad]Mes with (PhC≡CPh)NbCl<sub>3</sub>(THF)<sub>2</sub>.

It was hoped that the model provided by the earlier metallation protocol for LiN[CH<sub>2</sub><sup>t</sup>Bu]Ar would provide a cleaner entry into the chemistry of the niobium-trisenolate system.<sup>26</sup> Treatment of 3 equiv KOC[<sup>2</sup>Ad]Mes with (PhCCPh)NbCl<sub>3</sub>(THF)<sub>2</sub> in Et<sub>2</sub>O results in a gradual darkening of the mixture from tan to light brown over 4 h. After removal of KCl, (PhC≡CPh)Nb(OC[<sup>2</sup>Ad]Mes)<sub>3</sub>, **4**, is present as the only product and is obtained spectroscopically and analytically pure in 68% isolated yield. Given the clean metallation of KOC[<sup>2</sup>Ad]Mes with (PhCCPh)NbCl<sub>3</sub>(THF)<sub>2</sub>, it is actually unnecessary to isolate **4** from the reaction mixture. Filtration into a clean flask and addition of 1 equiv of I<sub>2</sub> to the filtrate results rapidly in a bright-red precipitate with full consumption of **4** observed after 20 minutes of stirring at 20 °C. The bright-red precipitate was identified as the desired product, I<sub>2</sub>Nb(OC[<sup>2</sup>Ad]Mes)<sub>3</sub>, **3** and is isolated by filtration in 80% yield over the two steps from (PhCCPh)NbCl<sub>3</sub>(THF)<sub>2</sub>, Scheme 1.4. Once isolated, **3** is virtually insoluble in pentane,

hexane, Et<sub>2</sub>O, benzene, toluene, and acetonitrile, however it has sparing solubility in pyridine and THF making those the solvents of choice for subsequent reaction chemistry.

### 1.3 REDUCTION AND DISPROPORTIONATION OF THE NIOBIUM DIIODIDE COMPLEX

#### 1.3.1 Synthesis of INb(OC[<sup>2</sup>Ad]Mes)<sub>3</sub>(THF)



**Scheme 1.5.** Reduction of I<sub>2</sub>Nb(OC[<sup>2</sup>Ad]Mes)<sub>3</sub>. Method A: 1 equiv Ti(N[<sup>t</sup>Bu]Ar)<sub>3</sub>; Method B: 1 equiv SmI<sub>2</sub>.

The selective one electron reduction of **3** was initially carried out with Ti(N[<sup>t</sup>Bu]Ar)<sub>3</sub>, which selectively abstracts one iodine atom in THF to give INb(OC[<sup>2</sup>Ad]Mes)<sub>3</sub>(THF), **5**, as an off-white solid, Scheme 1.5.<sup>43,44</sup> While Ti(N[<sup>t</sup>Bu]Ar)<sub>3</sub> is an interesting halogen atom abstracting agent,<sup>43–46</sup> the use of Ti(N[<sup>t</sup>Bu]Ar)<sub>3</sub> as a stoichiometric reductant is suboptimal for several reasons. First, separation of the ITi(N[<sup>t</sup>Bu]Ar)<sub>3</sub> byproduct is required and it has similar solubility properties with respect to **5**. Second, preparation of Ti(N[<sup>t</sup>Bu]Ar)<sub>3</sub> is required and when anilide ligand synthesis is factored in, this procedure is quite time consuming and costly. Alternative reducing agents were sought, however an initial scan showed that Na/Hg amalgam, Na metal, KC<sub>8</sub>, and magnesium anthracene all gave complex product mixtures when used for the generation of **5**. It was eventually discovered that blue solutions of SmI<sub>2</sub> in THF were an excellent surrogate for the costly Ti(N[<sup>t</sup>Bu]Ar)<sub>3</sub>. The inner-sphere reduction of **3** by SmI<sub>2</sub> leads to SmI<sub>3</sub> as the byproduct which precipitates from THF as a pale yellow powder, Scheme 1.5. With this synthetic advance came the ability to prepare and study the chemistry of **5** on large scales. The monoiodide complex **5** is readily isolated as the THF adduct, Scheme 1.5 and Figure 1.5 (top). EPR spectroscopy (10 line pattern at  $g_{iso} = 1.97$ ) and solution Evans' method magnetic moment (1.93  $\mu_B$ ) determination were consistent with the assignment of this species as a  $d^1$  paramagnetic molecule.



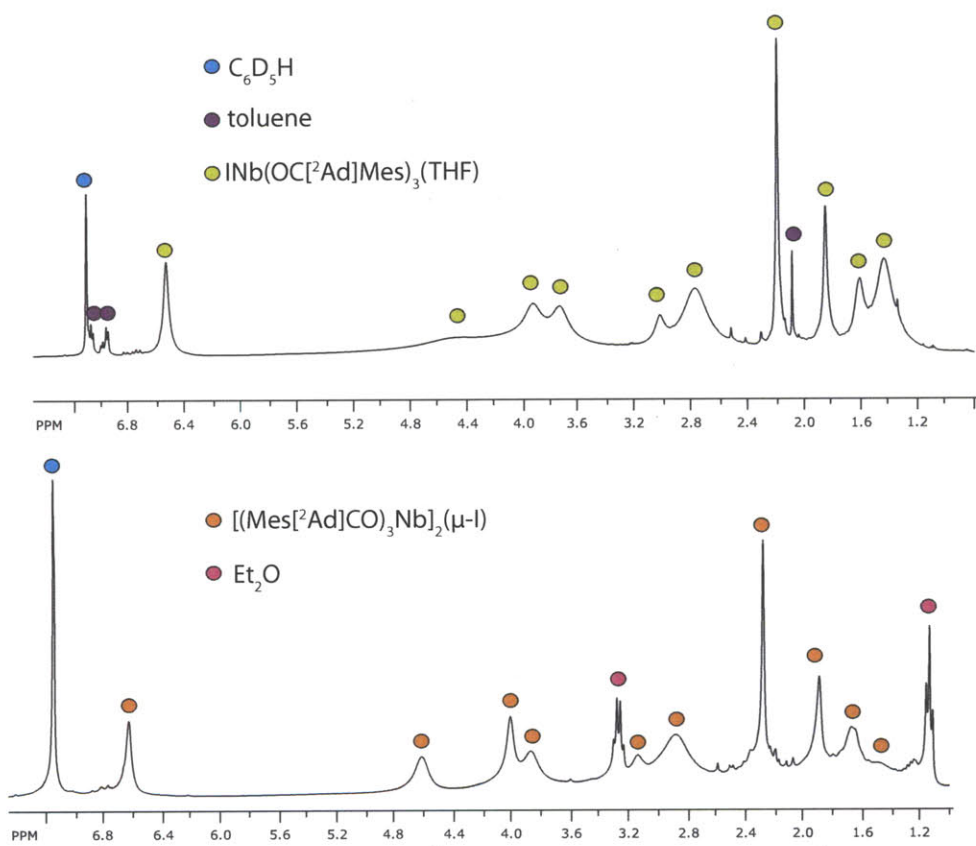


**Figure 1.5.**  $^1\text{H}$  NMR spectra of  $\text{INb}(\text{OC}[\text{2Ad}]\text{Mes})_3(\text{THF})$  (top) and  $[(\text{Mes}[\text{2Ad}]\text{CO})_3\text{Nb}]_2(\mu\text{-I})$  (bottom).

### 1.3.2 Disproportionation

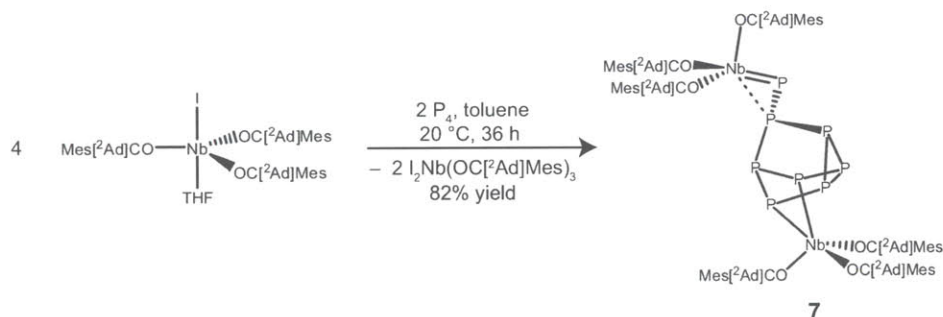
It was discovered that base stabilization of the niobium(IV)-iodide species was essential because in the absence of a donor, such as THF, **5** readily disproportionates to give 0.34 equiv of diiodide **3** and 0.67 equiv of what has been tentatively assigned from the amassed data as  $[(\text{Mes}[\text{Ad}]\text{CO})_3\text{Nb}]_2(\mu\text{-I})$ , **6**, Figure 1.5 (bottom). A precedent for this disproportionation comes from Wolczanski and co-workers' tris(siloxy)tantalum system.<sup>47</sup> In that work, Wolczanski showed that reduction of various siloxide supported Ta(V) dichlorides affords the bridging dichloride Ta(IV) dimer, which is stable when the smallest siloxide of their study is utilized, that is,  $[(\text{Pr}_3\text{SiO})_3\text{Ta}]_2(\mu\text{-Cl})_2$ . For all other cases, significant steric interactions of the adjacent metal centers encourage disproportionation to the respective Ta(V) dichlorides ( $\text{Cl}_2\text{Ta}(\text{OSiR})_3$  and Ta(III) ( $\text{Ta}(\text{OSiR})_3$ ) species.<sup>47</sup>

In the hopes of shedding light on the implications of the disproportionation reaction described above, **5** was treated with 0.5 equiv of  $\text{PhC}\equiv\text{CPh}$  in toluene. Over the course of 24 h, 0.5 equiv of bright red **3** precipitated from the reaction mixture and 0.5 equiv of  $(\text{PhC}\equiv\text{CPh})\text{Nb}(\text{OC}[\text{Ad}]\text{Mes})_3$  remained in solution. Thus, 1 equiv of  $\text{INb}(\text{OC}[\text{Ad}]\text{Mes})_3(\text{THF})$  disproportionates to give 0.5 equiv of the Nb(V)-diiodide species and, presumably, 0.5 equiv of a “ $\text{Nb}(\text{OC}[\text{Ad}]\text{Mes})_3$ ” which can react with substrates of interest. This remarkable disproportionation reaction formed the basis for the  $\text{P}_4$  activation chemistry that follows.

## 1.4 $\text{P}_4$ ACTIVATION

Introduction of two equivalents of  $\text{P}_4$  to four equivalents of monoiodide **5** in toluene leads to the slow formation of two equivalents of diiodide **3** and one equivalent of  $(\text{Mes}[\text{Ad}]\text{CO})_3\text{Nb}=\text{PP}_7\text{Nb}(\text{OC}[\text{Ad}]\text{Mes})_3$ , **7**, over the course of 24-36 hours, Scheme 1.6. This reaction proceeds by disproportionation of two equivalents of niobium(IV) into one equivalent of niobium(V) and one of “niobium(III)”, the latter presumably effecting the  $\text{P}_4$  reductive coupling. A solvent screen showed toluene to give the highest conversion to compound **7**. Diiodide **3** can be recovered quantitatively as it precipitates out of solution; three cycles of drying the filtrate, stirring the resulting residue in pentane, and filtering through Celite results in pure **7** in 82% yield as an orange powder.

The  $\text{P}_8$  core of **7** is of great interest as it evidently originates from the asymmetric coupling of two molecules of  $\text{P}_4$ . <sup>31</sup>P NMR spectroscopy assists in understanding the covalent structure of the  $\text{P}_8$  cage in **7**. There are five distinct phosphorus environments spanning the –122 to 380 ppm range. From the NMR data, the structure shown in Figure 1.6 was proposed. Assuming a rigid bonding model, one may expect eight inequivalent phosphorus atoms. However, the resonances arising from phosphorus C1/C2, D1/D2, and E1/E2 are time averaged in solution owing to rapid reductive elimination of the C1/E1 bond and concomitant oxidative addition of the C2/E2 bond at the niobium. This process generates a virtual mirror plane that bisects the phosphorus C1/2 and



**Scheme 1.6.** Disproportionation of  $\text{INb}(\text{OC}[\text{2Ad}]\text{Mes})_3(\text{THF})$  to give  $(\text{Mes}[\text{2Ad}]\text{CO})_3\text{Nb}=\text{PP}_7\text{Nb}(\text{OC}[\text{2Ad}]\text{Mes})_3$ .

E1/2 bonds making phosphorus atoms C1 and E1 chemically equivalent to C2 and E2, respectively, in turn equating D1 and D2 on the NMR time scale at 20 °C.

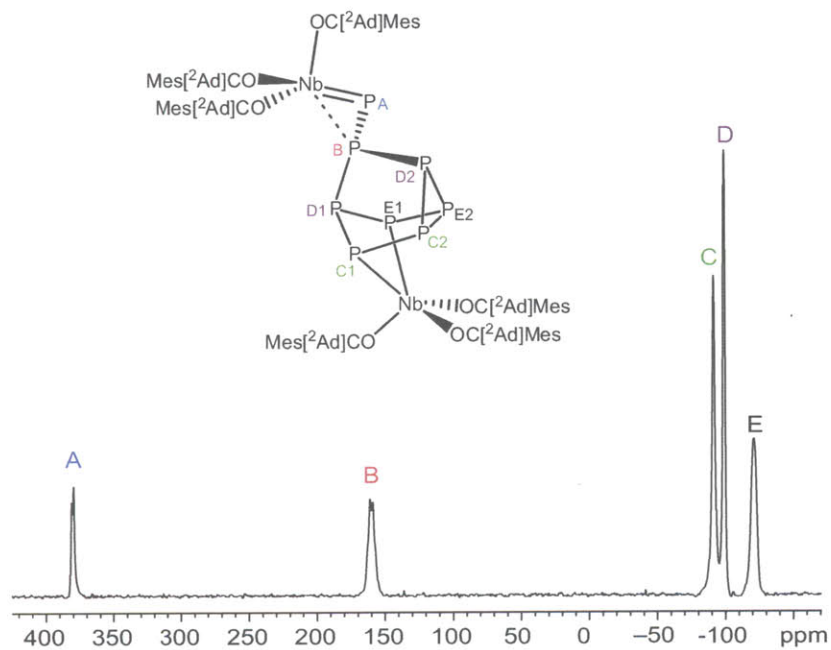


**Figure 1.6.**  $^{31}\text{P}$  NMR spectrum of  $(\text{Mes}[\text{2Ad}]\text{CO})_3\text{Nb}=\text{PP}_7\text{Nb}(\text{OC}[\text{2Ad}]\text{Mes})_3$  in  $\text{C}_6\text{D}_6$ , referenced externally to 85%  $\text{H}_3\text{PO}_4$ .

To understand better the bonding in the phosphorus cluster, a variable temperature (VT) NMR experiment was carried out, Figure 1.7. There are two points of interest in the VT study: as the temperature is increased from 10 to 70 °C, the peaks corresponding to phosphorus C1/2 and E1/2 broaden and eventually coalesce, and the peak corresponding to phosphorus B broadens significantly and is barely visible above the baseline by 70 °C. This is interpreted to be the result of the fluxional process described above at room temperature, coupled with an inversion at phosphorus B. When this inversion is rapid, an additional virtual mirror plane is generated making phosphorus C1/2 chemically equivalent to phosphorus E1/2. The two processes operating in unison make all

the phosphorus atoms C and E equivalent, and is responsible for the coalescence observed at 70 °C in the  $^{31}\text{P}$  NMR spectrum. The downfield resonances at  $\delta = 380$  and 160 ppm are characteristic of a niobium-bound phosphinophosphinidene.<sup>48</sup> The NMR data, then, are consistent with a model based on a  $\text{P}_7$  nortricyclic core with a phosphinophosphinidene moiety connected to one of the three bridges.

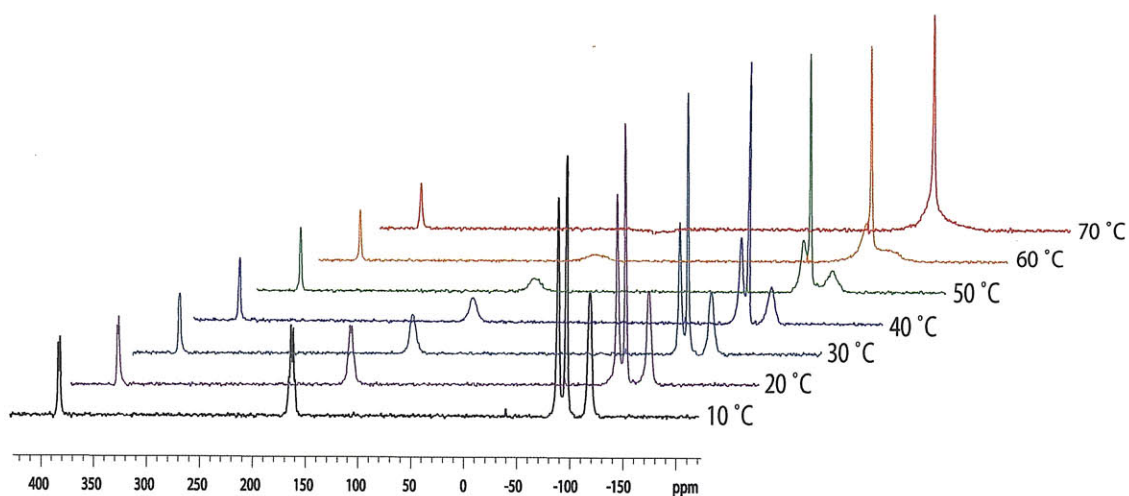


**Figure 1.7.** Variable temperature  $^{31}\text{P}$  NMR spectrum of  $(\text{Mes}[\text{}^2\text{Ad}]\text{CO})_3\text{Nb}=\text{PP}_7\text{Nb}(\text{OC}[\text{}^2\text{Ad}]\text{Mes})_3$  from 20 °C to 70 °C.

This structure and the NMR data described above are quite reminiscent of those reported for related  $\text{P}_7$  complexes synthesized by Eichhorn and co-workers, Figure 1.2.<sup>23–25</sup> To add further support to our structural assignment, the results of NMR shielding calculations performed using DFT methods on a model system are in agreement with the observed data and chemical-shift assignments, Figure 1.8. Recently, the first example of such a  $\text{P}_8$  core was established by Wright and co-workers.<sup>49</sup> They discovered that two equivalents of  $[(\text{Me}_3\text{Si})_3\text{Si}][\text{K}(\text{[18]crown-6})]$  treated with two equivalents of  $\text{P}_4$  gave rise to a  $[\text{P}_8\text{R}_2]^{2-}$  species with a  $\text{P}_8$  core that is structurally similar to 7. The distinguishing features of 7, however, are that the  $\text{P}_8$  architecture is bare apart from niobium coordination, providing a potentially useful unit for functionalization and elaboration; furthermore there exists a metal phosphinidene moiety (an  $\text{Nb}=\text{P}$  double bond), providing easy inroads to reaction chemistry, as discussed below.

## 1.5 PHOSPHINIDENE REACTIVITY

Since Mathey showed that terminal phosphinidene complexes  $\text{RPM}(\text{CO})_5$  ( $\text{M} = \text{W}, \text{Cr}, \text{Mo}$ ) can be generated *in situ* from phosphanorbornadienes,<sup>50</sup> the carbene-like reactivity of these electrophilic species toward various functional groups has been scrutinized.<sup>8</sup> 1,2-additions across the  $\text{M}=\text{P}$

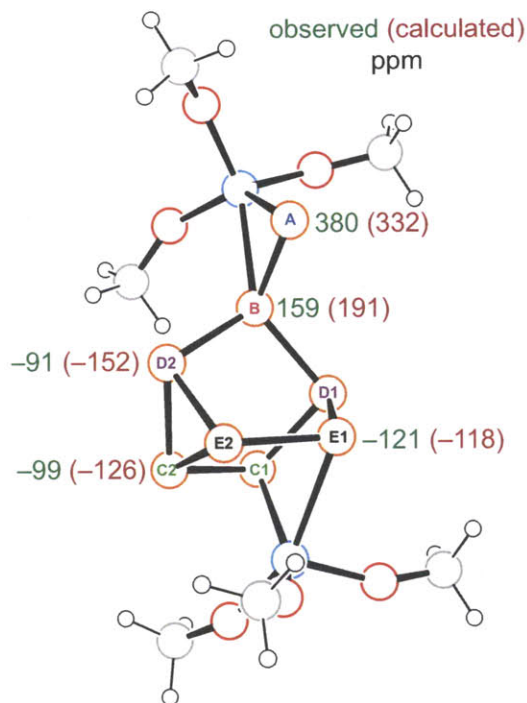
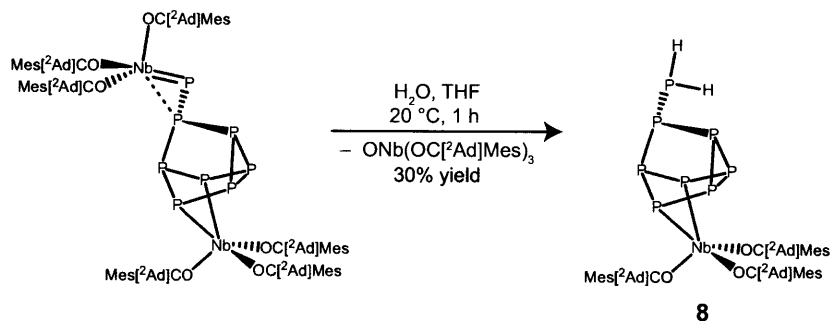


**Figure 1.8.** NMR shielding tensor calculations on a model structure of  $(\text{Mes}[\text{}^2\text{Ad}]\text{CO})_3\text{Nb}=\text{PP}_7\text{Nb}(\text{OC}[\text{}^2\text{Ad}]\text{Mes})_3$  with the enolate ligand set truncated to methoxide.

bond occur with simple  $\text{C}=\text{C}$  and  $\text{C}\equiv\text{C}$  bonds; while treatment with dienes results in larger five-membered ring structures from a subsequent 1,3-sigmatropic shift or by direct 1,4-addition.<sup>51</sup> Bond insertions into the  $\text{P}=\text{W}$  bond of  $\text{PhPW}(\text{CO})_5$  are also well established. They have been shown to occur for OH, NH, and CH bonds and even for selected CC and CP bonds, giving a broad spectrum of phosphine derivatives.<sup>8,51</sup> Coordination of the phosphinidene complex to the P-atom of phosphines  $\text{PR}_3$  ( $\text{R} = \text{alkyl, phenyl}$ ) gives metal phosphino-phosphinidene complexes  $(\text{R}_3\text{PP}(\text{Ph})\text{W}(\text{CO})_5)$  which can be applied as phospho-Wittig reagents to generate  $\text{P}=\text{C}$  bonds.<sup>52-54</sup> Terminal metal phosphinidenes have also been shown, themselves, to be competent phospho-Wittig reagents.<sup>55</sup> Interested in exploiting the potential reactivity of the niobium-phosphinidene unit in **7**, various nucleophiles have been investigated, as delineated below.

### 1.5.1 Reaction with $\text{H}_2\text{O}$

Treatment of **7** with one equivalent of  $\text{H}_2\text{O}$  in THF at  $20\text{ }^\circ\text{C}$  results in formation of  $\text{H}_2\text{PP}_7\text{Nb}(\text{OC}[\text{}^2\text{Ad}]\text{Mes})_3$ , **8**, Scheme 1.7. This species was isolated in 30% yield as a yellow-orange solid from the reaction mixture; however, it should be noted that the reaction is not quantitative. It was shown by  $^1\text{H}$  NMR spectroscopy that  $\text{ONb}(\text{OC}[\text{}^2\text{Ad}]\text{Mes})_3$ , **1**, forms as the reaction coproduct; however, it gets scavenged by the water present, and the final mixture contains **8**, a small amount



**Scheme 1.7.** Reaction of  $(\text{Mes}[\text{Ad}]_2\text{CO})_3\text{Nb}=\text{PP}_7\text{Nb}(\text{OC}[\text{Ad}]_2\text{Mes})_3$  with water to give **8**.

of oxo **1**, and significant amounts of the free ligand  $\text{MesC}(\text{O})[\text{Ad}]$ . Despite these complications, **8** crystallizes from a benzene solution (slow evaporation) over the course of several days.

A low-temperature X-ray crystallography study shows that **8** contains a  $\text{P}_8$  core much like that described above for complex **7**, Figure 1.9. It should be noted that, as expected for such a structure, there are two short and two long P–Nb contacts at 2.624(14) Å, 2.706(12) Å and 2.849(4) Å, 2.921(5) Å, respectively. Despite this asymmetry in the solid state, the  $^{31}\text{P}$  NMR spectrum for this molecule shows a 2:2:2:1:1 pattern similar to that described for **7**, further corroborating our hypothesis for the molecular structure of **7**, Figure 1.10. It is noteworthy that in the  $^1\text{H}$  coupled  $^{31}\text{P}$  NMR spectrum, the doublet at –205 ppm, which corresponds to the  $\text{PH}_2$  phosphorus atom, splits into an apparent quartet (two overlapping triplets) as a result of direct coupling to the two protons. In searching for a quantitative synthesis of **8**, other proton sources were investigated. The most successful alternative synthesis involves treatment of **7** with two equivalents of 2,6-lutidinium iodide, which results in cleaner conversion into one equivalent of **8** and one equivalent of diiodide **3**. Diiodide **3** precipitates cleanly out of solution in 90% yield and **8** may be recrystallized from toluene/ $\text{Et}_2\text{O}$  in 30% yield. This procedure is more synthetically useful, as diiodide **3** may be reintroduced into our reaction cycle without further workup.

### 1.5.2 Reaction with Ketones

Incorporation of  $\text{P}_4$ -derived phosphorus atoms into organic molecules post transition metal activation of white phosphorus has been accomplished in select instances, but this area is developing and there is much room for exploration.<sup>27,56</sup> The first clear example of metal-mediated P–C bond formation originating from the direct transfer of an organic group to a metal-activated tetraphosphorus molecule was recently reported by Peruzzini and co-workers with their  $(\text{triphos})\text{Rh}(\eta^2\text{:}\eta^1\text{-P}_4\text{R})$  ( $\text{R} = \text{Me}, \text{Et}, \text{Ph}$ ) complexes.<sup>57</sup> Direct reaction of the  $\text{P}_4$  molecule with certain organic reagents, sans intervention by a transition-metal complex, is also contributing to the goal of direct functionalization of  $\text{P}_4$ . Bertrand and co-workers reported on the activation of  $\text{P}_4$  by their cyclic alkyl(amino)carbenes, which resulted in reactive products envisioned as synthons for

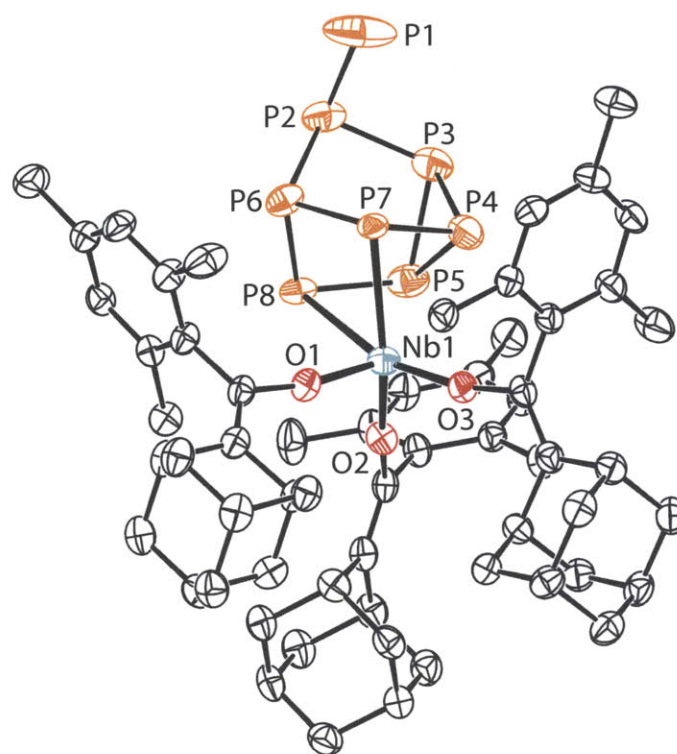


**Figure 1.9.** Thermal ellipsoid plot (50% probability) of  $\text{H}_2\text{PP}_7\text{Nb}(\text{OC}[\text{Ad}]\text{Mes})_3$  with hydrogen atoms omitted for clarity.

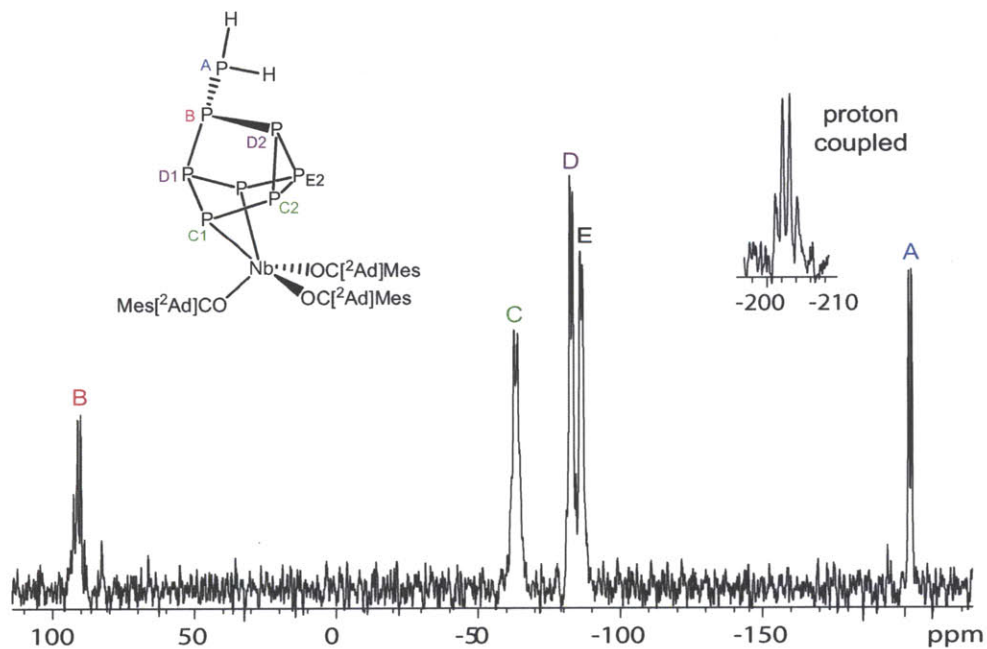
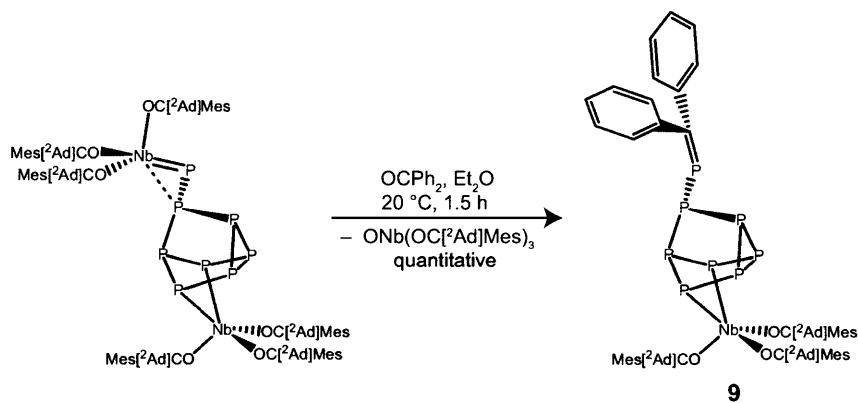


**Figure 1.10.**  $^{31}\text{P}$  NMR spectrum of  $\text{H}_2\text{PP}_7\text{Nb}(\text{OC}[\text{Ad}]\text{Mes})_3$  in  $\text{C}_6\text{D}_6$ , referenced externally to 85%  $\text{H}_3\text{PO}_4$ .

the construction of P<sub>4</sub> containing molecules harboring P–C bonds.<sup>58</sup> Research in this general area of phosphorus activation continues apace with strides being made toward the synthesis of new and unusual phosphorus-containing molecules.<sup>27,56,59–65</sup>

As previously mentioned, it is known that metal phosphinidenes (M=PR) behave as phosphawittig reagents, reacting with aldehydes to yield the corresponding metal oxo complex and phosphalkenes.<sup>55</sup> This transformation is analogous to the olefination of carbonyl compounds by tantalum alkylidene complexes, a reaction thought to proceed *via* four-membered metallacyclic intermediates.<sup>66</sup> The presence of a metal phosphinidene in **7** led us to investigate its reactivity with organic carbonyl compounds. Upon treating a stirring solution of complex **7** in diethyl ether with benzophenone, the orange color of the solution gradually increased in intensity over the course of 1.5 h at 20 °C. Probing the reaction mixture by <sup>31</sup>P NMR spectroscopy revealed the complete consumption of **7** with formation of a new product having four resonances at 231.1, 136.0, –64.0, and –79.8 (2 overlapping peaks) ppm, Scheme 1.8 and Figure 1.11. The doublet at 231.1 ppm provided evidence that a phosphalkene moiety was formed during the reaction, as phosphalkenes have characteristic low field <sup>31</sup>P and <sup>13</sup>C NMR resonances.<sup>67–69</sup> The phosphalkene carbon resonates at 230 ppm in the <sup>13</sup>C NMR spectrum and has a characteristic one-bond, carbon-phosphorus *J*-coupling (<sup>1</sup>*J*<sub>C/P</sub> = 70 Hz).<sup>67,68</sup>



**Scheme 1.8.** Reaction of (Mes[<sup>2</sup>Ad]CO)<sub>3</sub>Nb=PP<sub>7</sub>Nb(OC[<sup>2</sup>Ad]Mes)<sub>3</sub> with benzophenone to give Ph<sub>2</sub>C=PP<sub>7</sub>Nb(OC[<sup>2</sup>Ad]Mes)<sub>3</sub>.

## 1.6 REARRANGEMENT OF THE PHOSPHAALKENE COMPLEX

The phosphalkene complex Ph<sub>2</sub>C=PP<sub>7</sub>Nb(OC[<sup>2</sup>Ad]Mes)<sub>3</sub>, **9**, was not the final product of this phosphalkene-generating reaction. Over the course of 6 h, **9** converted to a new species with a unique set of resonances in the <sup>31</sup>P NMR spectrum, Figure 1.12. This observation is consistent with the well-established propensity of phosphalkenes to undergo rearrangement or oligomerization reactions when not sterically protected.<sup>67,68</sup> The <sup>1</sup>H NMR spectrum of the final reaction mixture



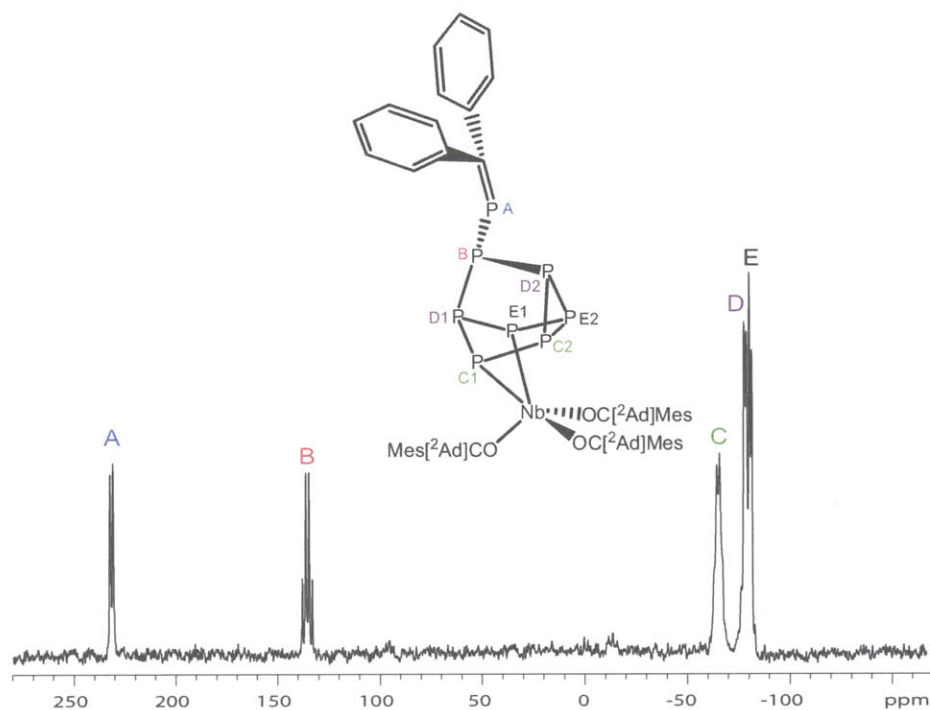
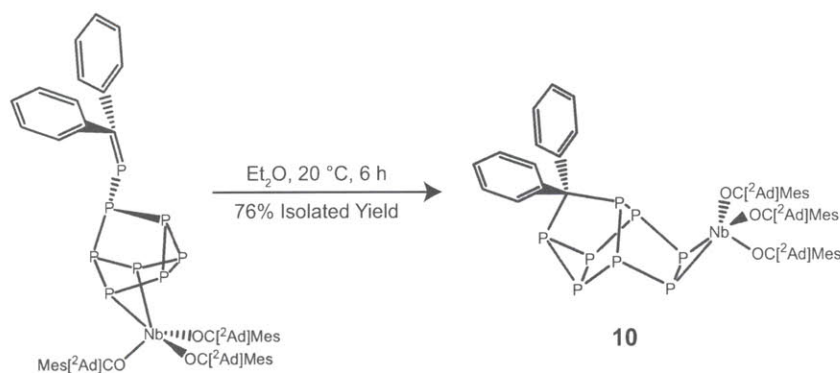


**Figure 1.11.**  $^{31}\text{P}$  NMR spectrum of  $\text{Ph}_2\text{C}=\text{PP}_7\text{Nb}(\text{OC}[\text{2Ad}]\text{Mes})_3$  in  $\text{C}_6\text{D}_6$ , referenced externally to 85%  $\text{H}_3\text{PO}_4$ .

revealed two enolate environments corresponding to  $\text{ONb}(\text{OC}[\text{2Ad}]\text{Mes})_3(\text{OEt}_2)$  and one new species. The new species selectively precipitated from a  $\text{Et}_2\text{O}$ /pentane solution over 10 h at  $-35^\circ\text{C}$ , in 76% yield. The resulting tan colored precipitate was isolated and  $^{31}\text{P}$  NMR spectroscopic analysis revealed it to be the phosphorus-containing product,  $\text{Ph}_2\text{CP}_8\text{Nb}(\text{OC}[\text{2Ad}]\text{Mes})_3$  (**10**), Scheme 1.9. Coproduct **1** may be isolated from the filtrate by crystallizing from  $\text{Et}_2\text{O}$  in 65% yield and can be recycled back to the starting material  $\text{I}_2\text{Nb}(\text{OC}[\text{2Ad}]\text{Mes})_3$  (**3**) in 72% yield by treatment with 1 equiv of trifluoroacetic anhydride and subsequent treatment with 2 equiv of  $\text{ISiMe}_3$ .



**Scheme 1.9.** Rearrangement of  $\text{Ph}_2\text{C}=\text{PP}_7\text{Nb}(\text{OC}[\text{2Ad}]\text{Mes})_3$  to give  $\text{Ph}_2\text{CP}_8\text{Nb}(\text{OC}[\text{2Ad}]\text{Mes})_3$ .

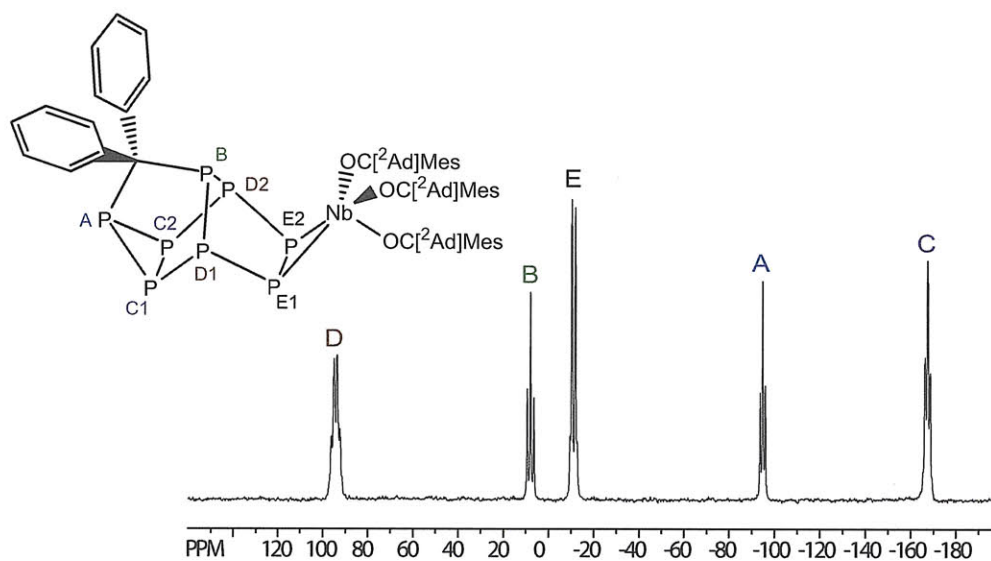


**Figure 1.12.**  $^{31}\text{P}$  NMR spectrum of  $\text{Ph}_2\text{CP}_8\text{Nb}(\text{OC}[\text{}^2\text{Ad}]\text{Mes})_3$  in  $\text{C}_6\text{D}_6$ , referenced externally to 85%  $\text{H}_3\text{PO}_4$ .

The structure of **10** was first elucidated through data obtained from a  $^{31}\text{P}$  *g*COSY 2D NMR experiment and was later corroborated by crystallographic studies, revealing an unusual  $\text{CP}_8$  cluster that incorporates the benzophenone-derived  $\text{CPh}_2$  moiety into the cluster framework, Figure 1.13. As alluded to previously, Bertrand and coworkers described activation of white phosphorus by cyclic (alkyl)aminocarbenes to generate phosphorus chains and clusters with carbene substituents.<sup>58,70</sup> The synthesis of **10** is unique in that the organic carbene moiety is incorporated directly into the cluster framework in a post- $\text{P}_4$ -activation step. As a result, the organic fragment can be varied through ketone selection, giving rise to a large number of possible product clusters.

In **10**, the  $\text{Nb}(\text{OC}[\text{}^2\text{Ad}]\text{Mes})_3$  unit binds to atoms P1 and P2 at distances of 2.5404(8) and 2.5685(8) Å, respectively, with a P1–Nb–P2 angle of 51.03°, Figure 1.13. The complex adopts the exo configuration relative to the P7 bridge, structurally hinting at a least-motion mechanism for the formation of the rearranged cluster (*vide infra*). The niobium-phosphorus interaction may be regarded as side-on coordination of a diphosphene ( $\text{RP}=\text{PR}$ ) to a strongly  $\pi$ -donating  $d^2$  niobium center, a viewpoint that may be fruitful when considering potential reactivity studies involving this complex.<sup>26,28,61,71–73</sup> This interpretation also highlights the formal exchange of the C–P  $\pi$  bond in **9** for a complexed P–P  $\pi$  bond in **10**.<sup>67</sup> The driving force for the **9** to **10** rearrangement can be traced tentatively to this extinguishing of P-unsaturation. All of the P–P distances in the new cluster are consistent with P–P single bonds and range between 2.180(1) Å and 2.229(1) Å. The P–C distances of 1.923(3) and 1.887(3) Å are as expected for P–C single bonds, and the P–C–P angle is near-tetrahedral at 111.45 °C.

The chemistry of polycyclic phosphanes and their substituted derivatives is a relatively well-established field that came into its own with the pioneering work of Baudler, as mentioned

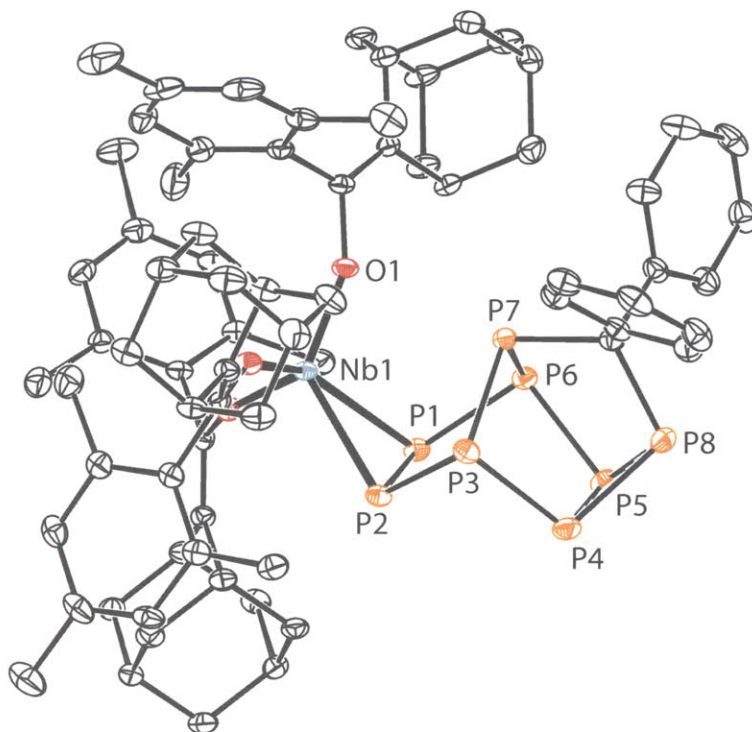


**Figure 1.13.** Thermal ellipsoid plot (50% probability) of  $\text{Ph}_2\text{CP}_8\text{Nb}(\text{OC}[\text{}^2\text{Ad}]\text{Mes})_3$  with hydrogen atoms omitted for clarity.

previously.<sup>20,21</sup> Phosphorus cluster chemistry is rich with examples of  $\text{P}_9$  clusters with a core similar to that of **10** except with a ninth phosphorus atom in place of the carbene fragment, but inclusion of heteroatoms (such as carbon) into such cages is, to our knowledge, a new motif. The addition of the phosphalkene  $\text{P}=\text{C}$  unit to the  $\text{P}_7$  core leads to the formation of a previously unknown  $\text{CP}_8$  cluster, and understanding the mechanism of such an addition reaction will aid in the design of similar transformations.

### 1.6.1 Eyring Analysis

The reaction that generates **10** from **9** was found to follow a strict first-order kinetic profile, consistent with an intramolecular process. The decay of **9** was monitored by  $^{31}\text{P}$  NMR spectroscopy at 10 °C, 25 °C, 40 °C, and 55 °C. The first-order rate constants obtained over this temperature range varied from  $2.6(4) \times 10^{-5} \text{ s}^{-1}$  to  $1.7(5) \times 10^{-3} \text{ s}^{-1}$  and are summarized in Table 1.1.

The enthalpy of activation,  $\Delta H^\ddagger$ , and the entropy of activation,  $\Delta S^\ddagger$ , were estimated from an Eyring analysis and were found to be 16.7(1) kcal/mol and  $-20.4(3)$  eu, respectively, Figure 1.14.<sup>74</sup> Given that the rearrangement of **9** to **10** exhibited first-order kinetics, a mechanism involving an electrocyclic rearrangement in which the phosphalkene  $\text{P}=\text{C}$  unit folds itself into the  $\text{P}_7$  cluster seemed most likely. The process is not unlike an intramolecular Diels-Alder reaction, in which the

**Table 1.1.** Rate constants<sup>a</sup> for degradation of Ph<sub>2</sub>C=PP<sub>7</sub>Nb(OC[<sup>2</sup>Ad]Mes)<sub>3</sub> at various temperatures.

T	10 °C	25 °C	40 °C	55 °C
Run 1	2.73	10.3	49.4	106
Run 2	2.41	13.3	51.0	188
Run 3	2.58	12.4	52.8	145
Average	2.57	12.0	51.1	146
Std Dev	0.16	3.82	1.70	41

<sup>a</sup> Values are in units of 10<sup>-5</sup> sec<sup>-1</sup>

diene and dienophile must preorganize prior to a 6e rearrangement. Given this interpretation, it is gratifying that the values for  $\Delta H^\ddagger$  and  $\Delta S^\ddagger$  are in accord with those of intramolecular Diels-Alder reactions.<sup>75</sup>

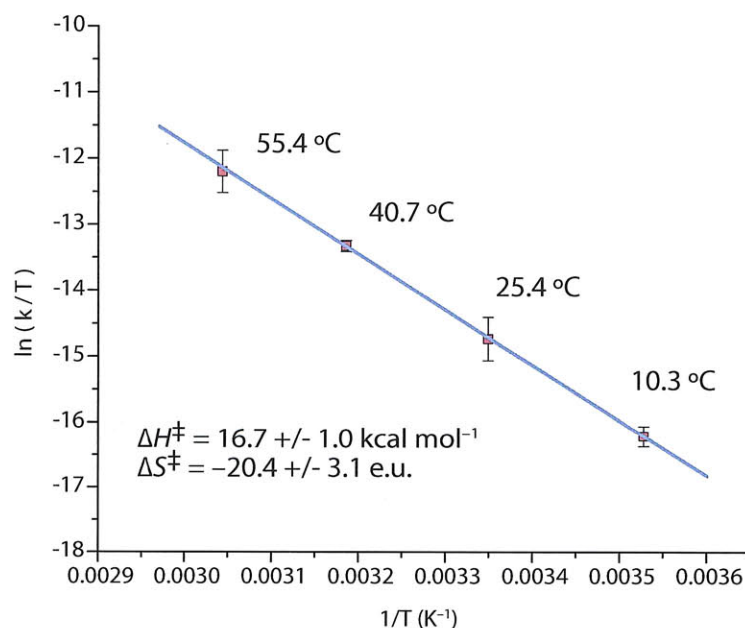


**Figure 1.14.** Eyring analysis plot of the rearrangement of Ph<sub>2</sub>C=PP<sub>7</sub>Nb(OC[<sup>2</sup>Ad]Mes)<sub>3</sub> to give Ph<sub>2</sub>CP<sub>8</sub>Nb(OC[<sup>2</sup>Ad]Mes)<sub>3</sub>.

## 1.6.2 Hammett Study

To probe further the mechanism of rearrangement, a linear free energy relationship was assessed by exploring various di-para-substituted benzophenones as substrates for reaction with (Mes[<sup>2</sup>Ad]CO)<sub>3</sub>Nb=PP<sub>7</sub>Nb(OC[<sup>2</sup>Ad]Mes)<sub>3</sub>.<sup>76,77</sup> Such a survey would also determine the tolerance of the system toward different functional groups. In all, six different benzophenones were

**Table 1.2.** Rate constants<sup>a</sup> for growth of  $\text{Ar}_2\text{CP}_8\text{Nb}(\text{OC}[\text{}^2\text{Ad}]\text{Mes})_3$  for  $\text{Ar} = 4\text{-MeC}_6\text{H}_4$ ,  $4\text{-(MeO)C}_6\text{H}_4$ ,  $4\text{-(Me}_2\text{N)C}_6\text{H}_4$ ,  $\text{C}_6\text{H}_5$ ,  $4\text{-ClC}_6\text{H}_4$ , and  $4\text{-(CF}_3\text{)C}_6\text{H}_4$ .

Run	1	2	3	Average	Std Dev
4-(CF <sub>3</sub> )C <sub>6</sub> H <sub>4</sub>	40.6	40.5	38.7	39.9	1.07
4-ClC <sub>6</sub> H <sub>4</sub>	23.8	20.0	22.9	22.2	1.99
Ph	12.7	12.0	14.1	12.9	1.07
4-MeC <sub>6</sub> H <sub>4</sub>	10.2	11.8	10.0	10.7	0.99
4-(OMe)C <sub>6</sub> H <sub>4</sub>	8.74	9.02	8.29	8.68	0.37
4-(NMe <sub>2</sub> )C <sub>6</sub> H <sub>4</sub>	2.62	2.81	2.44	2.62	0.19

<sup>a</sup> Values are in units of  $10^{-5} \text{ sec}^{-1}$

investigated: parent benzophenone, 4,4'-dichlorobenzophenone, 4,4'-dimethylbenzophenone, 4,4'-dimethoxybenzophenone, 4,4'-bis(dimethylamino)benzophenone, and 4,4'-bis(trifluoromethyl)benzophenone. The rate of rearrangement of  $\text{Ar}_2\text{C}=\text{PP}_7\text{Nb}(\text{OC}[\text{}^2\text{Ad}]\text{Mes})_3$  to  $\text{Ar}_2\text{CP}_8\text{Nb}(\text{OC}[\text{}^2\text{Ad}]\text{Mes})_3$  was measured at 25 °C, and the concentration of  $\text{Ar}_2\text{CP}_8\text{Nb}(\text{OC}[\text{}^2\text{Ad}]\text{Mes})_3$  plotted versus time and fit to an exponential equation of the form  $I(t) = Ae^{-kt} + b$ . The first-order rate constants,  $k$ , so obtained, varied from  $2.6(2) \times 10^{-5} \text{ s}^{-1}$  to  $4.0(1) \times 10^{-4} \text{ s}^{-1}$  and are summarized in Table 1.2 and as a Hammett plot in Figure 1.15.

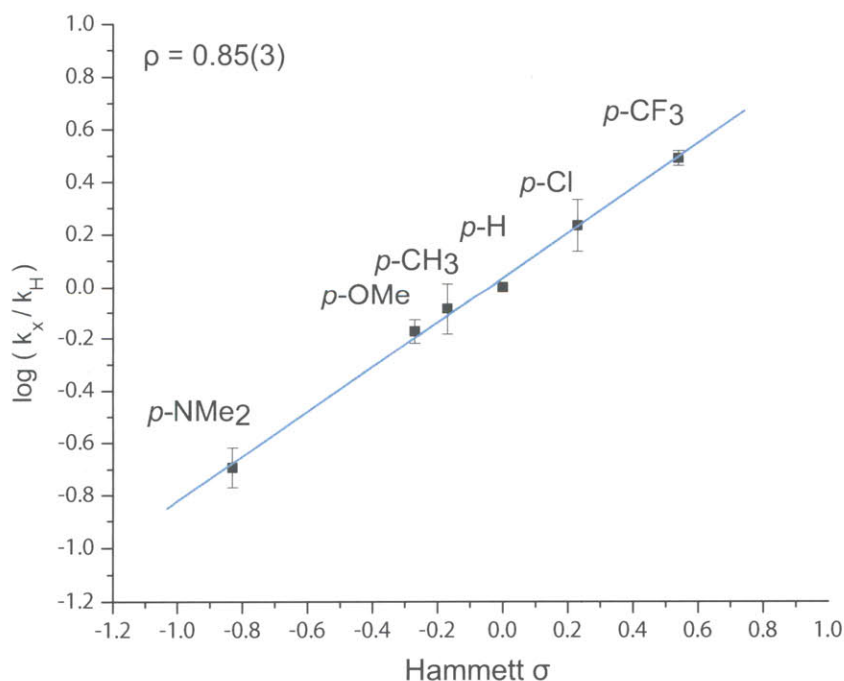


**Figure 1.15.** Hammett analysis plot of the rearrangement of  $\text{Ar}_2\text{C}=\text{PP}_7\text{Nb}(\text{OC}[\text{}^2\text{Ad}]\text{Mes})_3$  ( $\text{Ar} = \text{MeC}_6\text{H}_4$ ,  $(\text{MeO})\text{C}_6\text{H}_4$ ,  $(\text{Me}_2\text{N})\text{C}_6\text{H}_4$ ,  $\text{C}_6\text{H}_5$ ,  $\text{ClC}_6\text{H}_4$ , and  $(\text{CF}_3)\text{C}_6\text{H}_4$ ). Rates of formation used.

It should be noted that there is double substitution in these molecules, and the actual Hammett effect (given by  $\rho$  and generally thought of as additive) will be half of the observed effect since the Hammett constants only account for single substitution.<sup>76</sup> When moving to the more electron releasing substituents in the Hammett series we observe the effects of a divergent process for loss of the phosphalkenes  $(\text{MeC}_6\text{H}_4)_2\text{C}=\text{PP}_7\text{Nb}(\text{OC}[\text{Ad}]\text{Mes})_3$  (**13**),  $((\text{MeO})\text{C}_6\text{H}_4)_2\text{C}=\text{PP}_7\text{Nb}(\text{OC}[\text{Ad}]\text{Mes})_3$  (**12**), and  $((\text{Me}_2\text{N})\text{C}_6\text{H}_4)_2\text{C}=\text{PP}_7\text{Nb}(\text{OC}[\text{Ad}]\text{Mes})_3$  (**11**). In fact, during the kinetics experiment probing the rearrangement of **11**, a new species was observed, Figure 1.16. This new species is associated with phosphalkene decay and is interpreted as an intermediate along an alternate, competing pathway for overall **11** to  $((\text{Me}_2\text{N})\text{C}_6\text{H}_4)_2\text{CP}_8\text{Nb}(\text{OC}[\text{Ad}]\text{Mes})_3$  conversion. This species was observed to increase in concentration with concomitant consumption of **11** and then to slowly convert to the final product  $((\text{Me}_2\text{N})\text{C}_6\text{H}_4)_2\text{CP}_8\text{Nb}(\text{OC}[\text{Ad}]\text{Mes})_3$ . This confounding factor leads to a nonlinear Hammett plot if rates of disappearance of  $\text{Ar}_2\text{C}=\text{PP}_7\text{Nb}(\text{OC}[\text{Ad}]\text{Mes})_3$  are compared, Figure 1.17. However, since the rate for conversion of this new intermediate to  $\text{Ar}_2\text{CP}_8\text{Nb}(\text{OC}[\text{Ad}]\text{Mes})_3$  is much slower than the competing, direct  $\text{Ar}_2\text{C}=\text{PP}_7\text{Nb}(\text{OC}[\text{Ad}]\text{Mes})_3$  to  $\text{Ar}_2\text{CP}_8\text{Nb}(\text{OC}[\text{Ad}]\text{Mes})_3$  process, we can easily extract first-order rate information for the direct conversion of  $\text{Ar}_2\text{C}=\text{PP}_7\text{Nb}(\text{OC}[\text{Ad}]\text{Mes})_3$  to  $\text{Ar}_2\text{CP}_8\text{Nb}(\text{OC}[\text{Ad}]\text{Mes})_3$  by plotting the growth of  $\text{Ar}_2\text{CP}_8\text{Nb}(\text{OC}[\text{Ad}]\text{Mes})_3$  only for the reaction time period wherein this intermediate species has not yet appreciably begun to decay.

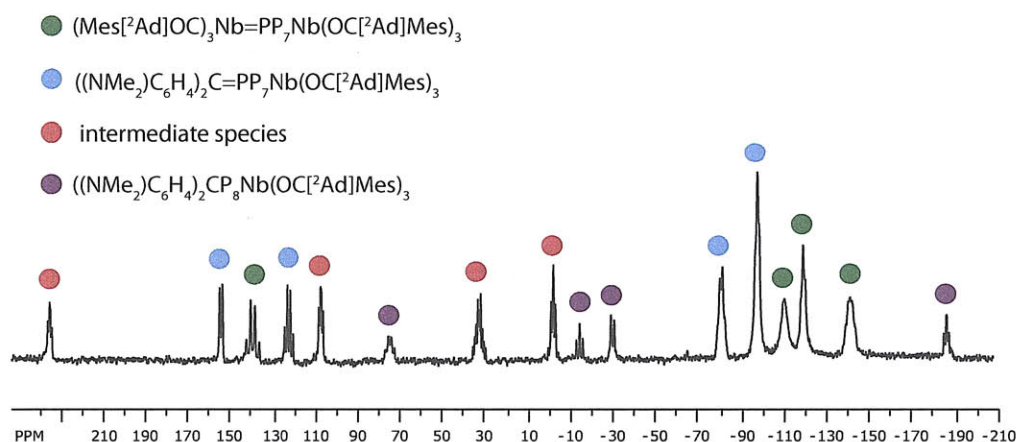


**Figure 1.16.** NMR spectrum of product mixture observed en route to formation of  $((\text{Me}_2\text{N})\text{C}_6\text{H}_4)_2\text{CP}_8\text{Nb}(\text{OC}[\text{Ad}]\text{Mes})_3$ , spectrum obtained after 1.5 h of reaction time at  $-15^\circ\text{C}$ .

The Hammett analysis of the kinetic data reveals a positive value for  $\rho$ , indicating more rapid rearrangement with more electron-withdrawing substituents. A 6e, asynchronous, concerted electrocyclic rearrangement initiated by nucleophilic attack on the phosphalkene carbon is shown in Scheme 1.10 and represents a plausible least-motion mechanism for the observed transformation. Density-functional theory calculations suggest that such a pathway involves very little molecular

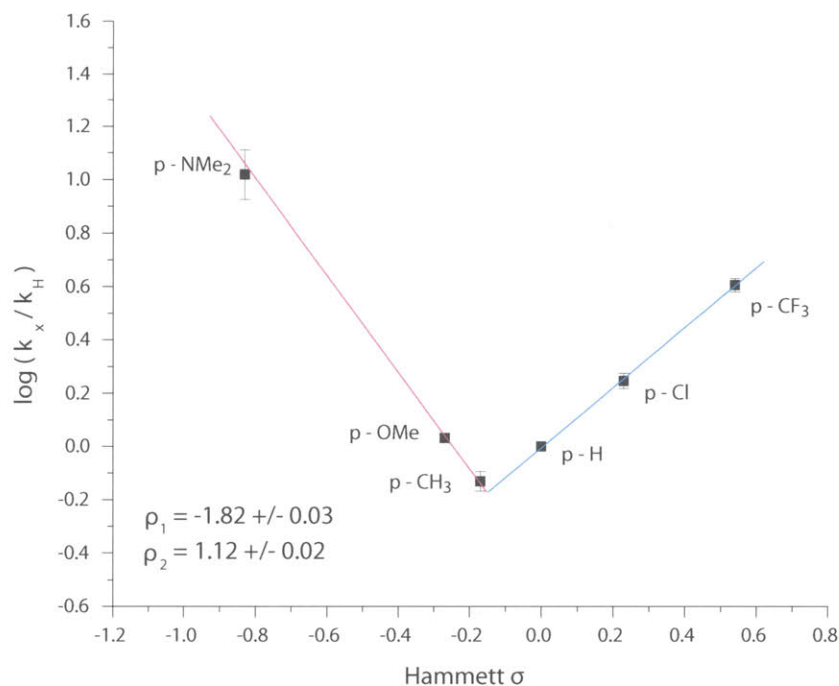
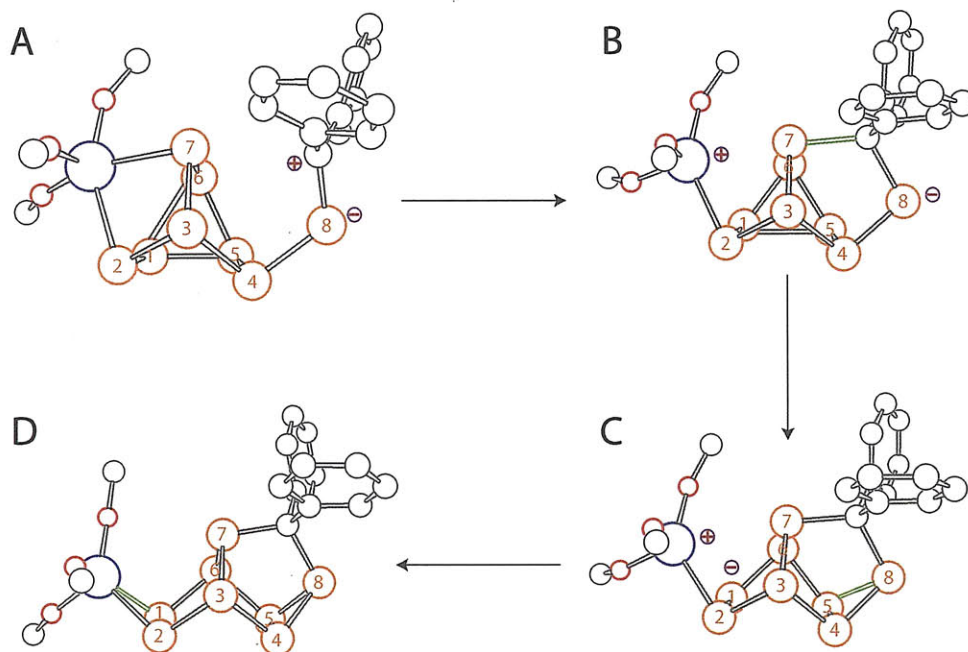


**Figure 1.17.** Hammett plot for rates of disappearance of  $\text{Ar}_2\text{C}=\text{PP}_7\text{Nb}(\text{OC}[\text{Ad}]\text{Mes})_3$ .

motion, except for swinging the  $\text{P}=\text{C}$  moiety into proximity of the  $\text{P}_7$  cluster, and would be energetically quite feasible.

All of the rate constants discussed above were obtained in  $\text{C}_6\text{D}_6$  (dielectric constant of 2.28). To address the effect of solvent polarity on the transformation rate, we conducted one set of kinetic measurements in THF (dielectric constant of 7.568) at 25 °C. When  $\text{Ph}_2\text{C}=\text{PP}_7\text{Nb}(\text{OC}[\text{Ad}]\text{Mes})_3$  is allowed to form in THF, a new species is observed in addition to  $\text{Ph}_2\text{CP}_8\text{Nb}(\text{OC}[\text{Ad}]\text{Mes})_3$ . This new species harbors very similar spectral features to those observed with the  $\text{NMe}_2$  substituted benzophenone. This intermediate species slowly decays with growth of  $\text{Ph}_2\text{CP}_8\text{Nb}(\text{OC}[\text{Ad}]\text{Mes})_3$ . It is possible to fit the kinetic data obtained in THF to a model of two consecutive first order reactions with  $k_1 = 2.4(2) \times 10^{-4} \text{ s}^{-1}$  and  $k_2 = 3.0(1) \times 10^{-5} \text{ s}^{-1}$ ; however, this does not rule out a more complicated process, Figure 1.18. On the basis of the NMR data and DFT calculations, a tricyclooctaphosphine structure with a  $\text{P}_8$  skeleton analogous to that of bisnoradamantane is proposed for this intermediate species, Figure 1.18. A retrosynthetic analysis from this bisnoradamantane species to the phosphalkene involves a four electron rearrangement in which the  $\text{C}-\text{P}_7$  bond is disconnected with formation of a  $\text{C}=\text{P}_8$  double bond, followed by a disconnection of the  $\text{P}_8-\text{P}_5$  bond and closing of the  $\text{P}_5-\text{P}_7$  bond.



**Scheme 1.10.** Proposed mechanism for rearrangement of  $\text{Ph}_2\text{C}=\text{PP}_7\text{Nb}(\text{OC}[\text{}^2\text{Ad}]\text{Mes})_3$  to give  $\text{Ph}_2\text{CP}_8\text{Nb}(\text{OC}[\text{}^2\text{Ad}]\text{Mes})_3$ . The mechanism is proposed to be a 6e concerted, asynchronous rearrangement, and is shown stepwise here for clarity.

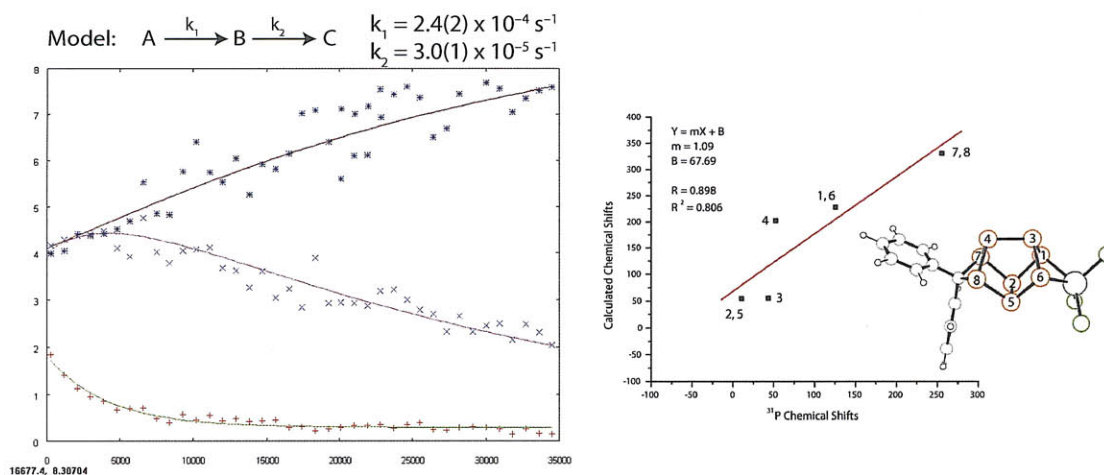


**Figure 1.18.** Kinetic data for rearrangement of  $\text{Ph}_2\text{C}=\text{PP}_7\text{Nb}(\text{OC}[\text{}^2\text{Ad}]\text{Mes})_3$  in THF. The proposed structure for the intermediate is shown on the right and the observed chemical shifts are plotted versus those calculated for a model complex ( $\text{Ph}_2\text{CP}_8\text{Nb}(\text{OH})_3$ ) in ADF.



### 1.6.3 Stable Phosphaalkene Complexes

Metathetical generation of phosphaalkene-substituted clusters by treating **7** with ketones is not limited to the benzophenone class. When using diisopropyl or dicyclohexyl ketone as the Nb=P clipping reagent, the rate of niobium oxo formation is quite slow, taking 3 days at 22 °C to go to completion when carried out with 1 equiv of such a sterically crowded ketone. This process is greatly accelerated to 5 hours by using 20 equiv of ketone in the reaction mixture. Interestingly, the new cluster phosphaalkenes,  $\text{C}_y\text{C}=\text{PP}_7\text{Nb}(\text{OC}[\text{}^2\text{Ad}]\text{Mes})_3$ , **17**, and  ${}^i\text{Pr}_2\text{C}=\text{PP}_7\text{Nb}(\text{OC}[\text{}^2\text{Ad}]\text{Mes})_3$ , **18**, are stable for as long as 5 days at 20 °C and for upward of 2 months at -35 °C. The stability of these alkyl-substituted phosphaalkenes may be a result of the electron-donating nature of the alkyl groups, in line with the notion that the first step in the mechanism of rearrangement involves a nucleophilic attack at the phosphaalkene, as discussed above. On the other hand, for these systems the phosphaalkene carbon is also more sterically shielded than is the case for the benzophenone-derived  $\text{Ph}_2\text{C}=\text{PP}_7\text{Nb}(\text{OC}[\text{}^2\text{Ad}]\text{Mes})_3$  system. Phosphaalkenes **17** and **18** were isolated from  $\text{Et}_2\text{O}/(\text{SiMe}_3)_2\text{O}$  in 58% and 62% yield, respectively, as bright-orange powders. The appreciable solubility of both **17** and **18** in hydrocarbon solvents has thus far limited the isolated yields of these products from otherwise clean reaction mixtures.

### 1.6.4 Putting Other Elements in the Cluster: Preparation of $\text{Ph}_2\text{SnP}_8\text{Nb}(\text{OC}[\text{}^2\text{Ad}]\text{Mes})_3$ and $\text{DmpPP}_8\text{Nb}(\text{OC}[\text{}^2\text{Ad}]\text{Mes})_3$

The synthesis of phosphorus-rich clusters with internalized heavy main-group heteroatom fragments presented an intriguing target for the extension of the observed ketone reactivity. While loss of  $\text{ONb}(\text{OC}[\text{}^2\text{Ad}]\text{Mes})_3$  is a great driving force for this chemistry by virtue of its strong niobium-oxo interaction, it was hypothesized that targeting  $\text{Cl}_2\text{Nb}(\text{OC}[\text{}^2\text{Ad}]\text{Mes})_3$  as a coproduct might also be sufficient. As such, treatment of **7** with  $\text{Ph}_2\text{SnCl}_2$  in  $\text{Et}_2\text{O}$  was found to result in immediate precipitation of a bright orange powder. After 2.5 h of stirring at 20 °C the reaction mixture was found to contain no starting material. The precipitate,  $\text{Cl}_2\text{Nb}(\text{OC}[\text{}^2\text{Ad}]\text{Mes})_3$  (**16**), was isolated atop a frit. Concentration and cooling of the ethereal filtrate to -35 °C for 2 days resulted in precipitation of a deep orange precipitate. This material was isolated, giving the product  $\text{Ph}_2\text{SnP}_8\text{Nb}(\text{OC}[\text{}^2\text{Ad}]\text{Mes})_3$ , **19**, in 35% yield, Scheme 1.11. The phosphorus NMR of **19** is quite similar to that of **10**, with the exception that the two Sn-bound phosphorus atoms (PA and PB) are shifted quite upfield and are flanked by tin satellites with  ${}^1J_{117/119\text{Sn}/\text{P}} = 1267$  Hz for PA and  ${}^1J_{117/119\text{Sn}/\text{P}} = 997$  Hz for PB, Figure 1.19.

This internalization of heteroatom fragments with ejection of  $\text{Cl}_2\text{Nb}(\text{OC}[\text{}^2\text{Ad}]\text{Mes})_3$  is not limited to group 14 dihalides. It was found that the bulky  $\text{dmpPCl}_2$  ( $\text{dmp} = 2,6\text{-Mes}_2\text{C}_6\text{H}_3$ ) molecule was competent at promoting this mode of reactivity as well. The reaction between  $\text{dmpPCl}_2$  and **7** was found to be quite slow, requiring a full 24 h to go to completion in  $\text{Et}_2\text{O}$

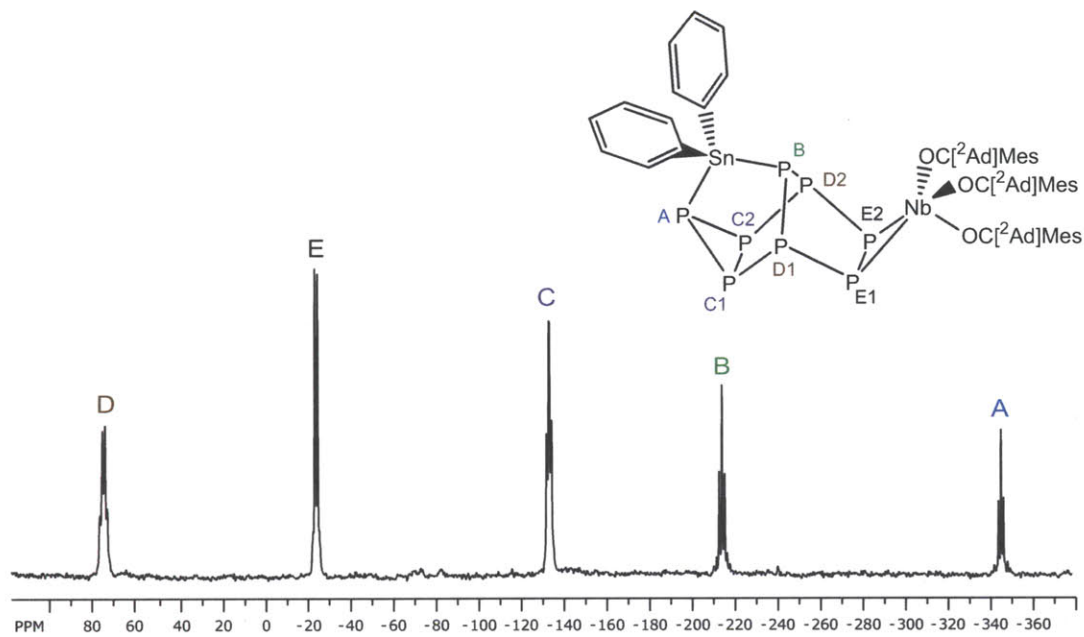
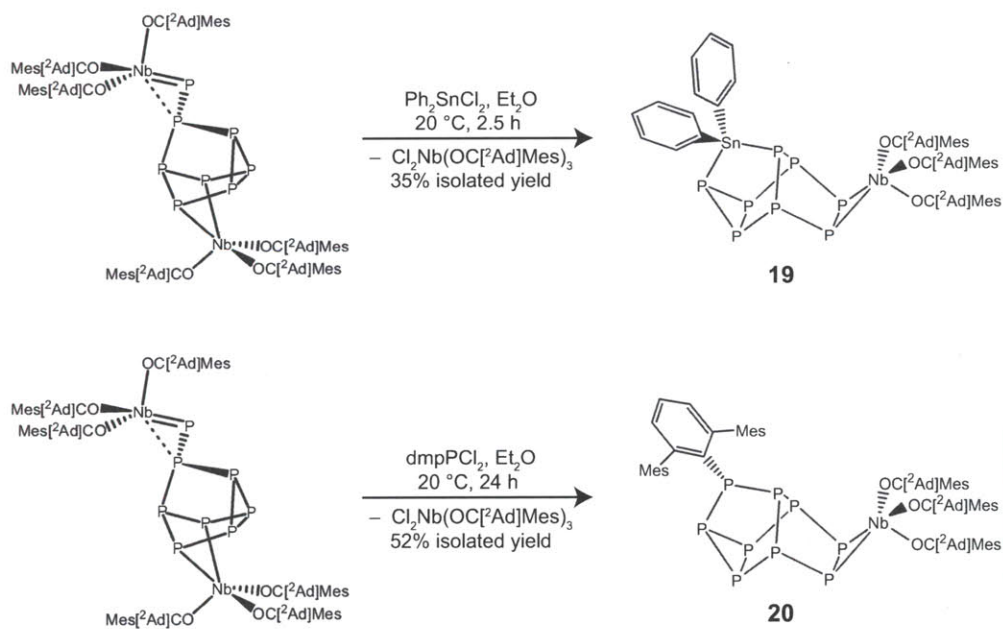


**Figure 1.19.**  $^{31}\text{P}$  NMR spectrum of  $\text{Ph}_2\text{SnP}_8\text{Nb}(\text{OC}[\text{2Ad}]\text{Mes})_3$  in  $\text{C}_6\text{D}_6$ , referenced externally to 85%  $\text{H}_3\text{PO}_4$ .



**Scheme 1.11.** Synthesis of  $\text{Ph}_2\text{SnP}_8\text{Nb}(\text{OC}[\text{2Ad}]\text{Mes})_3$  and  $\text{dmpPP}_8\text{Nb}(\text{OC}[\text{2Ad}]\text{Mes})_3$  from **7**.

solution. After 24 h of stirring, bright orange **16** can be removed by filtration. Concentration and cooling of the ethereal solution to  $-35\text{ }^{\circ}\text{C}$  for 2 days resulted in precipitation of orange-brown  $\text{dmpPP}_8\text{Nb}(\text{OC}[\text{Ad}]\text{Mes})_3$ , **20**, in 52% yield, Scheme 1.11. The  $^{31}\text{P}$  NMR spectrum of **20** is quite fascinating as the presence of the  $\text{dmpP}$  functional group breaks the symmetry of the cluster rendering all nine phosphorus atoms inequivalent, Figure 1.20. Despite this loss of symmetry, the phosphorus NMR spectrum bears a striking resemblance to that observed for **10** and is readily assigned by  $^{31}\text{P}$  2D gCOSY NMR spectroscopy.

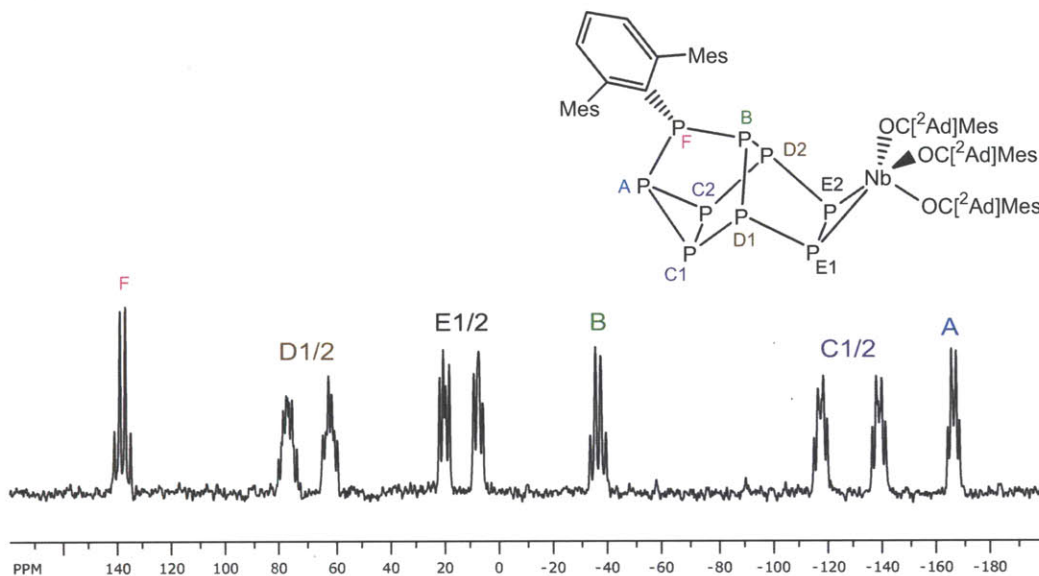


**Figure 1.20.**  $^{31}\text{P}$  NMR spectrum of  $\text{dmpPP}_8\text{Nb}(\text{OC}[\text{Ad}]\text{Mes})_3$  in  $\text{C}_6\text{D}_6$ , referenced externally to 85%  $\text{H}_3\text{PO}_4$ .

## 1.7 LIBERATION OF $\text{R}_2\text{CP}_8$ FROM THE NIOBIUM METAL CENTER

The ultimate goal of this chemistry is to produce phosphorus-rich molecules free of any transition metal interactions. Such main-group species could prove interesting in and of themselves, not to mention the fact that the methodologies developed to form them could prove versatile. The metal-P interaction of  $\text{Ph}_2\text{CP}_8\text{Nb}(\text{OC}[\text{Ad}]\text{Mes})_3$  is not one for which there is direct group transfer precedent. One example of metal to metal diphosphene transfer has been provided by Fenske and coworkers in an attempt to prepare heterobimetallic clusters.<sup>78</sup> They found that treatment of a nickel diphenyl diphosphene adduct with  $[\text{CpMo}(\text{CO})_3]_2$  resulted in precipitation of nickel and formation of  $[\text{CpMo}(\text{CO})_3]_2(\text{PhPPPh})$ .<sup>78</sup> This reaction, though interesting, does not provide us with the framework needed to do transfer in our case. It was thought that if we could take advantage of the propensity of Nb to make a very strong  $\text{Nb}\equiv\text{O}$  bond, we could release the diphosphene from **10** and then trap it with a suitable cycloaddition substrate. This new methodology is developed herein.

### 1.7.1 Reaction of $\text{Ph}_2\text{CP}_8\text{Nb}(\text{OC}[\text{}^2\text{Ad}]\text{Mes})_3$ with $\text{ONC}_5\text{H}_5$ in the Presence of 1,3-Cyclohexadiene

Compound **10** has previously been described as having a niobium-phosphorus interaction that may be regarded as side-on coordination of a diphosphene ( $\text{RP}=\text{PR}$ ) to a strongly  $\pi$ -donating  $d^2$  niobium center. This leads to the notion that when the  $\text{Nb}(\text{OC}[\text{}^2\text{Ad}]\text{Mes})_3$  fragment is removed what remains is a diphosphene, a P–P unsaturated species that would react with an appropriate substrate. It was found that treatment of **10** with two equivalents of pyridine-*N*-oxide as a suspension in  $\text{Et}_2\text{O}$  containing 20 equivalents of 1,3-cyclohexadiene led rapidly to a yellowing of the solution as  $\text{ONb}(\text{OC}[\text{}^2\text{Ad}]\text{Mes})_3(\text{ONC}_5\text{H}_5)$ , **22**, is formed. Formation of **22** was confirmed by the characteristic peaks in the  $^1\text{H}$  NMR spectrum. The fate of the phosphorus cluster was initially determined by a combination of  $^1\text{H}$  and  $^{31}\text{P}$  NMR analysis of the crude reaction mixture. The  $^1\text{H}$  NMR spectrum reveals a single olefinic resonance at  $\delta = 5.80$  ppm as well as three aliphatic and three aromatic resonances. The  $^{31}\text{P}$  NMR spectrum clearly indicates retention of the core structure of the starting material as shown in Figure 1.21. This led us to postulate the formation of the Diels-Alder cycloaddition product that would form upon reaction of the liberated (*Z*)-diphosphene with 1,3-cyclohexadiene,  $\text{Ph}_2\text{CP}_8(\text{C}_6\text{H}_8)$ , **21**, Scheme 1.12. This reaction is a rare instance of reactive diphosphene liberation from a transition-metal complex and the first instance of the use of pyridine-*N*-oxide to effect such a transformation.<sup>78–80</sup>

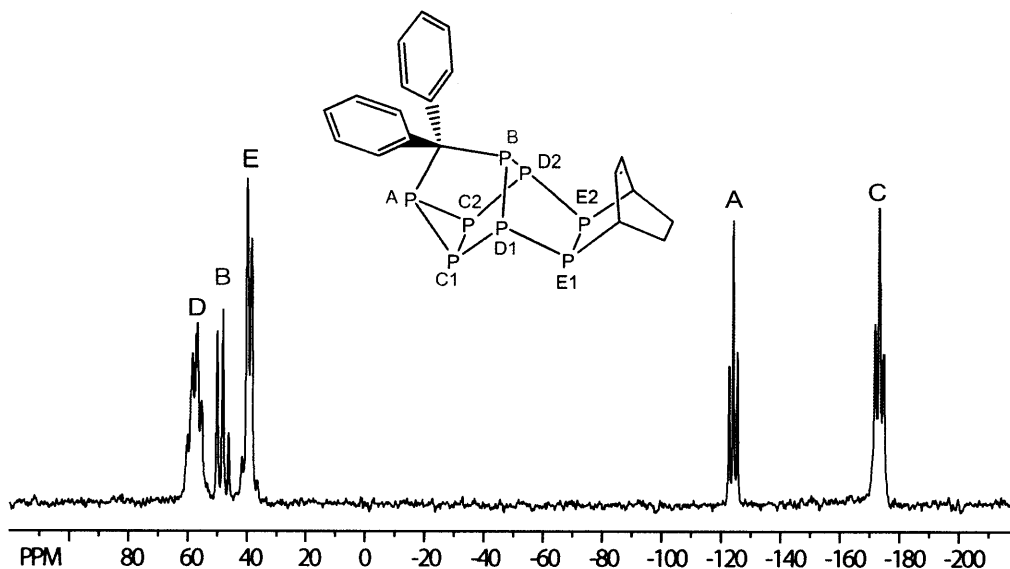
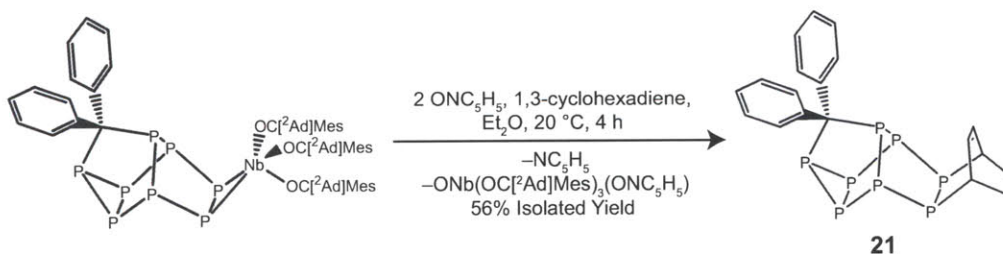


Figure 1.21.  $^{31}\text{P}$  NMR spectrum of  $\text{Ph}_2\text{CP}_8(\text{C}_6\text{H}_8)$  in  $\text{C}_6\text{D}_6$ , referenced externally to 85%  $\text{H}_3\text{PO}_4$ .

Separation of **22** from the phosphorus-containing product is achieved by precipitation from an  $\text{Et}_2\text{O}$  solution, affording **21** as a white powder in 40 to 50% yield. Complex **22** is isolated in subsequent crystallizations as a fine yellow powder, which is recycled back to  $\text{I}_2\text{Nb}(\text{OC}[\text{}^2\text{Ad}]\text{Mes})_3$  as discussed previously to close the synthetic cycle. X-ray diffraction quality crystals of **21** were



**Scheme 1.12.** Synthesis of  $\text{Ph}_2\text{CP}_8(\text{C}_6\text{H}_8)$  from **10**.

grown from toluene/hexane (3:1) at  $-35^\circ\text{C}$  for two days. The crystal structure shows that the  $\text{C}_6\text{H}_8$  unit binds exo to the phosphorus cluster with the double bond between C104 and C105 (with a C–C distance of  $1.330(3) \text{ \AA}$ ), which is likely the result of secondary orbital interactions (directed by the lone pair on P6), a common feature of Diels-Alder chemistry, Figure 1.22.<sup>74</sup> The remainder of the  $\text{CP}_8$  core deviates little from that described previously for **10**. The yield of isolated **21** is limited due to the inefficient trapping of the transient diphosphene by cyclohexadiene. By NMR analysis, the best trapping yield observed is 72% by the procedure described above. Increasing the diene concentration did not improve the yield, and a solvent screening showed  $\text{Et}_2\text{O}$  to be the best choice for this experiment. The fate of the untrapped diphosphene cluster was not determined.

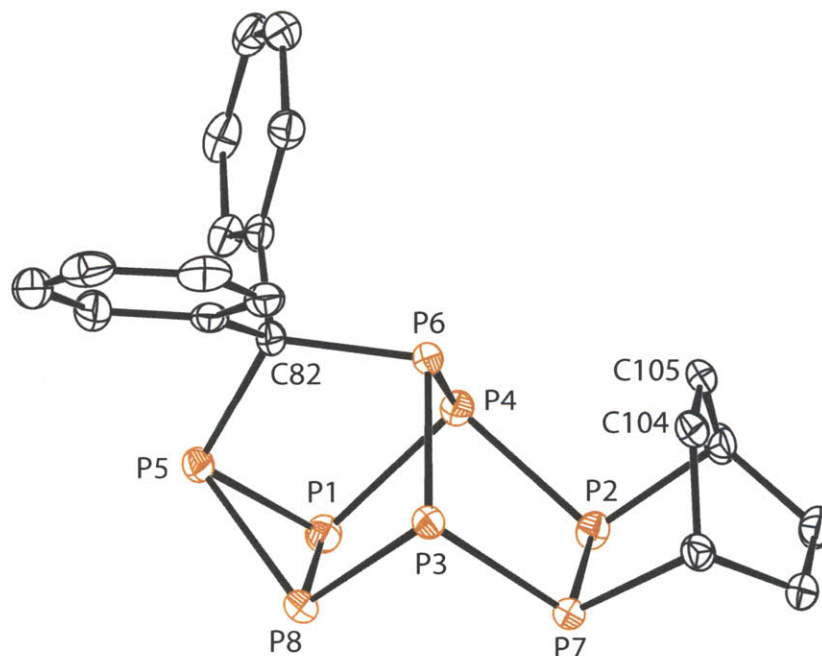


**Figure 1.22.** Thermal ellipsoid plot (50% probability) of  $\text{Ph}_2\text{CP}_8(\text{C}_6\text{H}_8)$  with hydrogen atoms omitted for clarity.

In addition to 1,3-cyclohexadiene, 2,3-dimethylbutadiene was also found to be capable of trapping the liberated carbophosphorus cluster with approximately equal efficiency to yield  $\text{Ph}_2\text{CP}_8(\text{C}_6\text{H}_{10})$ , **23**. The yield of the diene-trapped phosphorus cluster is, however, significantly

improved by moving to spiro[2.4]hepta-1,6-diene, a more reactive Diels-Alder diene, Figure 1.23.<sup>81</sup> By referencing to an internal standard of PPh<sub>3</sub> at a known concentration, we confirm formation in excess of 95% yield of the diene-trapping product, Ph<sub>2</sub>CP<sub>8</sub>(C<sub>7</sub>H<sub>8</sub>), **24**. This phosphorus-rich organic molecule has very similar <sup>31</sup>P NMR features to compound **21** and the <sup>1</sup>H NMR spectrum clearly indicates the presence of the intact cyclopropane group with the methylene protons resonating at  $\delta = -0.08$  ppm. Unfortunately, the increased solubility of **24** in hydrocarbon solvents hinders its clean separation from **22**.

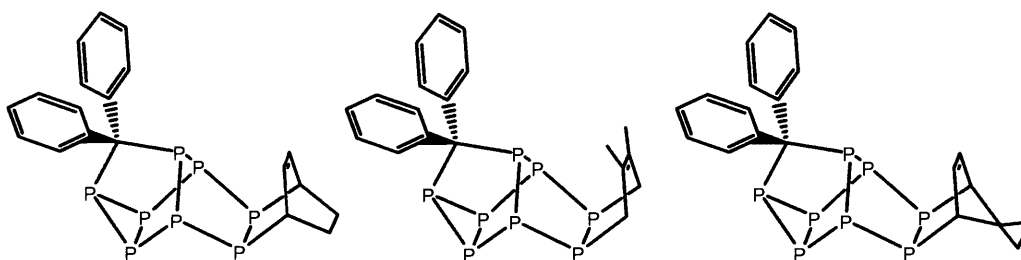
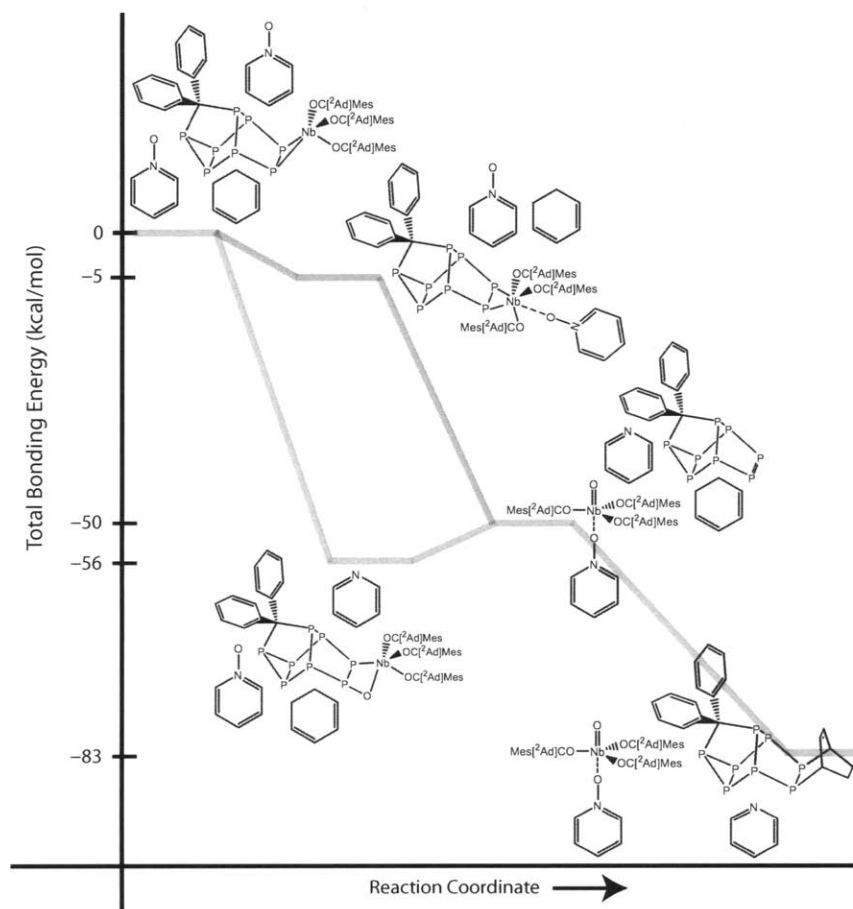


**Figure 1.23.** The family of Ph<sub>2</sub>CP<sub>8</sub> diene trapping products.

### 1.7.2 Pathways for the Formation of Ph<sub>2</sub>CP<sub>8</sub>(C<sub>6</sub>H<sub>8</sub>)

Two possible pathways for the formation of the (*Z*)-diphosphene precursor from phosphorus cluster **21** have been investigated by DFT methods, Scheme 1.13. Pathway A involves formation of an NbPPO metallacyclic intermediate,<sup>40</sup> following deoxygenation of an equivalent of pyridine-*N*-oxide, whereas pathway B assumes loss of niobium-oxo without going through a metallacyclic species (oxygen atom transfer from pyridine to niobium followed by Nb≡O triple bond formation and diphosphene release). The total bonding energies of the reactants, the proposed intermediates, and the final products (all relative to restricted spherical-atom fragments) were calculated and have shown both pathways to be viable. Formation of the NbPPO metallacycle was calculated to be 50 kcal mol<sup>-1</sup> downhill of the starting materials and only a very small (6 kcal mol<sup>-1</sup>) uphill progression for the breakup of the metallacycle to give niobium-oxo was found. The final products (**22**, **21**, and pyridine) were overall 83 kcal mol<sup>-1</sup> downhill from the starting materials supporting the notion that this is a very thermodynamically favorable process. Given the electrophilic nature of the niobium metal center in these complexes, a pathway in which ONC<sub>5</sub>H<sub>5</sub> precoordinates to the niobium metal center prior to O-atom transfer is favored. We have seen OEt<sub>2</sub> coordination in the niobium-oxo species **1** and pyridine-*N*-oxide coordination in the niobium-oxo species **22**, suggestive that such an interaction is possible. Furthermore, this hypothesis is circumstantially corroborated in a related niobium system that is engaged in a diphosphene interaction (see Chapter 3).



**Scheme 1.13.** Energetics for possible pathways in the formation of  $\text{Ph}_2\text{CP}_8(\text{C}_6\text{H}_8)$ .

### 1.7.3 Properties and Reactivity Patterns of $\text{Ph}_2\text{CP}_8(\text{C}_6\text{H}_8)$

The physical and electronic properties of **21** have been investigated. Compound **21** is thermally stable, showing no signs of decomposition in solution up to 120 °C as assessed by NMR spectroscopy and in the solid state it has a decomposition point of 165 °C. Compound **21** also displays considerable air stability. In a stirring solution of THF at 22 °C under an atmosphere of air, **21** persists with a half life of approximately 36 h as assessed by phosphorus NMR spectroscopy. The cyclic voltammogram of **21** was obtained in THF, Figure 1.24. Sweeping cathodically reveals two irreversible reduction events at  $-3.0$  V and  $-3.5$  V vs  $\text{Fc}/\text{Fc}^+$ . The anodic return wave gives two oxidation events at  $-1.1$  V and  $-0.8$  V. The event at  $-1.1$  V appears to be the result of formation of a new species during the initial reduction event at  $-3.0$  V. This is confirmed by sweeping anodically between  $-2.0$  V and 0 V where only one oxidation wave at  $-0.8$  V is observed. This observed electrochemical behavior is consistent with the calculated molecular-orbital picture which shows a large HOMO-LUMO ( $\pi \rightarrow \pi^*$ ) gap of 3.2 eV, Figure 1.25 and 1.26.

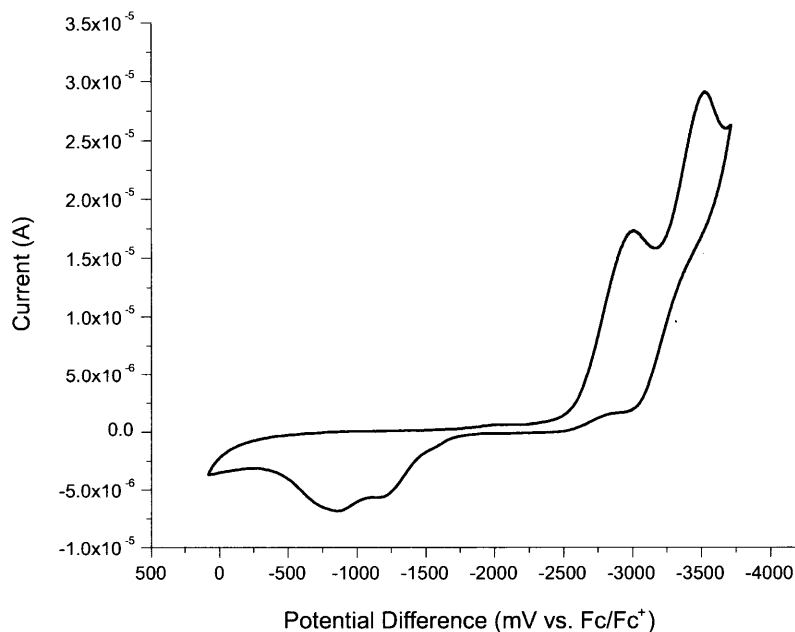


**Figure 1.24.** Cyclic voltammogram of  $\text{Ph}_2\text{CP}_8(\text{C}_6\text{H}_8)$  at  $300 \text{ mV s}^{-1}$  with  $0.20 \text{ M } [\text{TBA}][\text{PF}_6]$  in THF.

Preliminary reactivity studies of **21** suggest that its reactivity is similar to that of  $\text{P}_4$ . For example, treatment of **21** with ten equivalents of  $\text{I}_2$  at  $-116$  °C gives, upon warming, clean formation of four equivalents of  $\text{PI}_3$  ( $\delta^{31}\text{P} = 174.2$  ppm in  $\text{C}_6\text{D}_6$ ) and what we have assigned (by  $^1\text{H}$  and  $^{31}\text{P}$  NMR spectroscopy as well as MALDI-MS) as one equivalent of  $(\text{I}_2\text{P})_2(\text{C}_6\text{H}_8)$  and one equivalent of  $(\text{I}_2\text{P})_2\text{CPh}_2$  ( $\delta^{31}\text{P} = 138.34$  and  $133.95$  ppm in  $\text{C}_6\text{D}_6$ , Figure 1.27).<sup>6,69</sup> This reactivity mimics that which might be expected for a functionalized  $\text{P}_4$  molecule.<sup>82</sup> Consistent with the electrochemistry data, we were unable to effect cluster reduction of **21** using a variety of



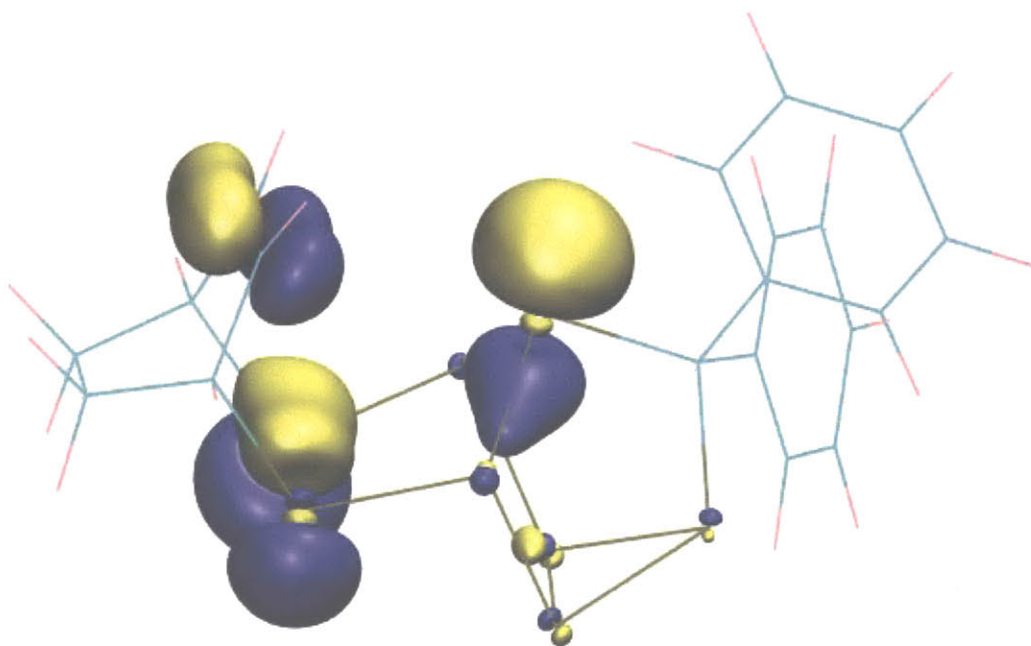


**Figure 1.25.** Computed highest occupied molecular orbital (HOMO) for Ph<sub>2</sub>CP<sub>8</sub>(C<sub>6</sub>H<sub>8</sub>).

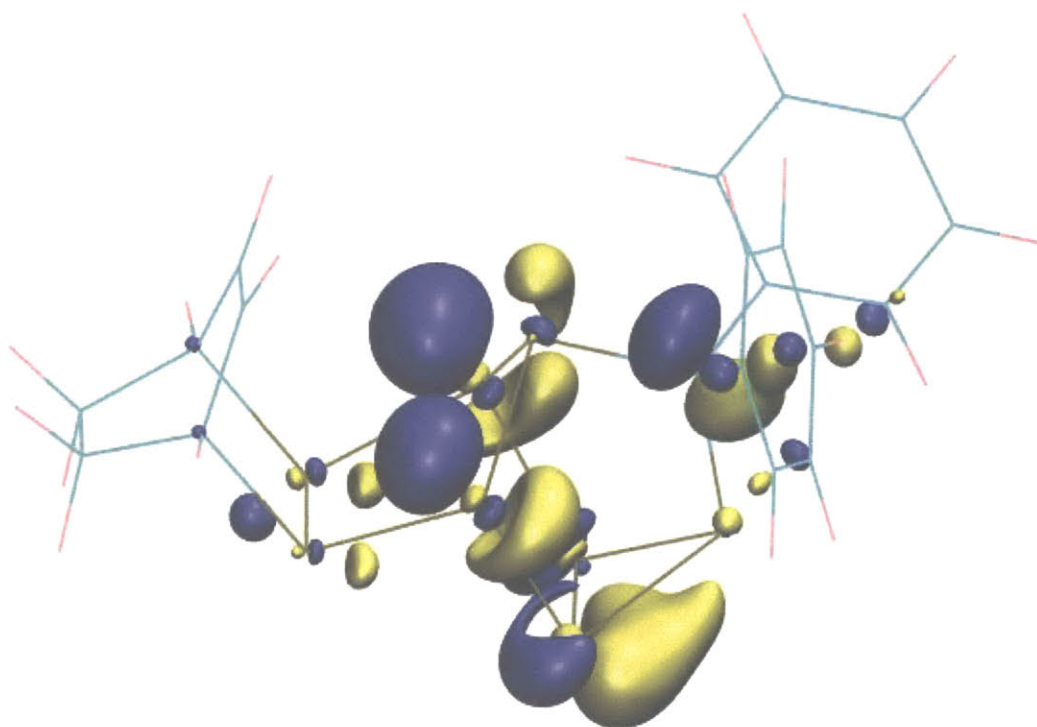


**Figure 1.26.** Computed lowest unoccupied molecular orbital (LUMO) for Ph<sub>2</sub>CP<sub>8</sub>(C<sub>6</sub>H<sub>8</sub>).

reducing agents, and all of the observed oxidation chemistry resulted in fragmentation as described for  $I_2$ .

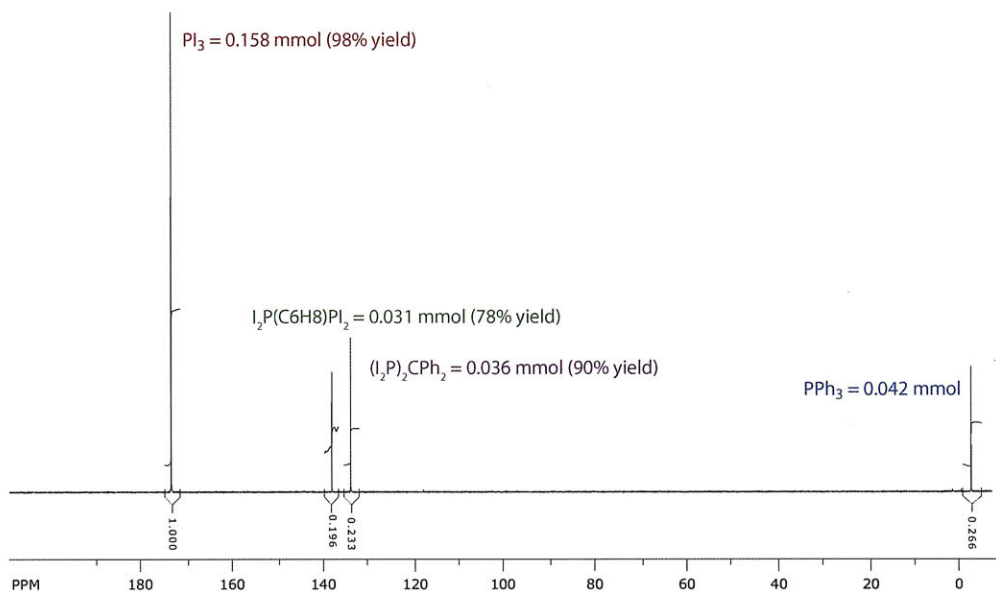


**Figure 1.27.** Treatment of  $\text{Ph}_2\text{CP}_8(\text{C}_6\text{H}_8)$  with  $\text{I}_2$ .  $\text{PPh}_3$  is present as an internal standard.

## 1.8 CONCLUSIONS

In this work,  $\text{P}_4$  aggregation led to the synthesis, isolation, and characterization of a number of phosphorus-rich transition metal complexes and main-group molecules. In particular, disproportionation of  $\text{INb}(\text{OC}[\text{Ad}]\text{Mes})_3(\text{THF})$  in the presence of  $\text{P}_4$  has led to a synthesis of the interesting octaphosphorus cluster  $(\text{Mes}[\text{Ad}]\text{CO})_3\text{Nb}=\text{PP}_7\text{Nb}(\text{OC}[\text{Ad}]\text{Mes})_3$ . This metallo-phosphorus cluster bears a unit of niobium-phosphorus unsaturation and has led to the synthesis of phosphorus-rich metallo-phosphaalkene complexes  $\text{R}_2\text{C}=\text{PP}_7\text{Nb}(\text{OC}[\text{Ad}]\text{Mes})_3$ . When  $\text{R} = \text{Ar}$ , it was found that complexes  $\text{R}_2\text{C}=\text{PP}_7\text{Nb}(\text{OC}[\text{Ad}]\text{Mes})_3$  rearrange to internalize the diaryl-carbene fragment into the  $\text{P}_8$  cluster-core. In a remarkable final transformation, the niobium metal center of  $\text{Ph}_2\text{CP}_8\text{Nb}(\text{OC}[\text{Ad}]\text{Mes})_3$  was ejected by treatment with pyridine-*N*-oxide, and the resultant  $\text{Ph}_2\text{CP}_8$  reactive transient was trapped in a Diels-Alder cycloaddition reaction with various dienes. These phosphorus-rich organic molecules were found to exhibit interesting structural and chemical properties. It is hoped that their potential applications in synthesis will be explored further by others. Another area that has great potential, yet was only lightly touched on here, are the reactivity properties of  $\text{INb}(\text{OC}[\text{Ad}]\text{Mes})_3(\text{THF})$  and the related  $\text{I}[\text{Nb}(\text{OC}[\text{Ad}]\text{Mes})_3]_2$  species. The interesting disproportionation chemistry of these two species certainly merits a full exploration.

By tailoring the steric bulk and electrophilicity of the niobium metal center, we have uncovered a range of new structural motifs in polyphosphorus chemistry. While the outcome of the  $\text{P}_4$  activation

chemistry reported herein could not have been anticipated, it does shed light on the promiscuity of P<sub>4</sub> and on its ability to continually surprise. Moreover, the transformations reported above represent rare examples of polyphosphorus-ligand reactivity and will hopefully encourage others to further study the reactivity of P<sub>4</sub> derived polyphosphorus-ligands. In an effort to determine the variability of P<sub>4</sub> activation chemistry by reduced niobium species, a more streamlined approach in gaining access to such reactivity was sought and is the subject of the following chapter.

## 1.9 EXPERIMENTAL DETAILS

### 1.9.1 General Considerations

All manipulations were performed in a Vacuum Atmospheres model MO-40M glove box under an atmosphere of purified dinitrogen. Solvents were obtained anhydrous and oxygen-free from a Contour Glass Solvent Purification System, or by analogous methods.<sup>83</sup> Celite 435 (EM Science), 4 Å molecular sieves (Aldrich), and alumina (EM Science) were dried by heating at 200 °C under dynamic vacuum for at least 24 hours prior to use. All glassware was oven-dried at temperatures greater than 170 °C prior to use. Deuterated solvents for NMR spectroscopy were purchased from Cambridge Isotope Labs. Benzene-*d*<sub>6</sub> and toluene-*d*<sub>8</sub> were degassed and stored over molecular sieves for at least 2 days prior to use. CDCl<sub>3</sub> was distilled off of CaH<sub>2</sub> and stored over molecular sieves. The compounds ONbCl<sub>3</sub>(THF)<sub>2</sub>, (PhCCPh)NbCl<sub>3</sub>(THF)<sub>2</sub>, KOC[<sup>2</sup>Ad]Mes, and spiro[2,4]hepta-1,6-diene were prepared according to literature procedures.<sup>38,81,84,85</sup> 4,4'-Bis(trifluoromethyl)benzophenone was prepared according to literature procedures using a CEM Explorer Series microwave reactor.<sup>86</sup> All other ketones were purchased from Aldrich chemical company and recrystallized once from THF or toluene prior to use. Pyridine-*N*-oxide and iodine were purchased from Aldrich chemical company and were sublimed prior to use. Trifluoroacetic anhydride was purchased from Oakwood chemical company and was used as received. Trimethylsilyl iodide and samarium(II) Iodide were purchased from Aldrich chemical company and used as received. NMR spectra were obtained on Varian Mercury 300 or Varian Inova 500 instruments equipped with Oxford Instruments superconducting magnets or on Bruker Avance 400 instruments equipped with Magnex Scientific superconducting magnets. <sup>1</sup>H NMR spectra were referenced to residual C<sub>6</sub>D<sub>5</sub>H (7.16 ppm), CHCl<sub>3</sub> (7.27 ppm) or C<sub>5</sub>D<sub>4</sub>HN (8.74 ppm). <sup>13</sup>C NMR spectra were referenced to C<sub>6</sub>D<sub>6</sub> (128.39 ppm), CDCl<sub>3</sub> (77.23 ppm), or C<sub>5</sub>D<sub>5</sub>N (150.35 ppm). <sup>31</sup>P NMR spectra were referenced externally to 85% H<sub>3</sub>PO<sub>4</sub> (0 ppm). Elemental analyses were performed by Midwest Microlab, LLC (Indianapolis, Indiana).

### 1.9.2 Preparation of ONb(OC[<sup>2</sup>Ad]Mes)<sub>3</sub>(OEt<sub>2</sub>), **1**

A suspension of ONbCl<sub>3</sub>(THF)<sub>2</sub> (1.81 g, 5.04 mmol) in 140 mL of Et<sub>2</sub>O was chilled to –116 °C in the glovebox cold well. Upon removal from the cold well, solid KOC[<sup>2</sup>Ad]Mes (5.0 g, 15.6

mmol) was added gradually in several portions. Upon warming, the color of the reaction mixture proceeded from white to gray/green to blue and finally to yellow-brown. After returning to 20 °C the solution was stirred an additional 2 h. The mixture was then concentrated and pentane added to help precipitate KCl. The solution was filtered through Celite to remove KCl resulting in an amber colored solution. The filtrate was then dried, slurried once with cold pentane, concentrated and stored at -35 °C to encourage crystallization of the reaction product. After 16 h, a bright yellow crystalline material had formed. This material was isolated atop a sintered-glass frit and dried to constant mass (1.55 g, 1.51 mmol, 30% yield). X-ray quality crystals were grown from an Et<sub>2</sub>O solution at -35 °C. <sup>1</sup>H NMR (20 °C, benzene-d<sub>6</sub>, 500 MHz): δ = 1.43 (4 H, broad, Et<sub>2</sub>O), 1.60-2.19 (39 H, multiple overlapping peaks, <sup>2</sup>Ad-H), 2.23 (9 H, s, *p*-Me), 2.35 (18 H, s, *o*-Me), 3.32 (3 H, s, allylic H), 3.65 (6 H, broad, Et<sub>2</sub>O), 6.83 (6 H, s, Ar-H); <sup>13</sup>C{<sup>1</sup>H} NMR (20 °C, 126 MHz, C<sub>6</sub>D<sub>6</sub>): δ = 14.64 (Et<sub>2</sub>O), 20.50 (CH<sub>3</sub>), 21.39 (CH<sub>3</sub>), 29.26 (CH), 33.55 (CH), 37.91 (CH<sub>2</sub>), 39.45 (CH<sub>2</sub>), 39.68 (CH<sub>2</sub>), 68.76 (Et<sub>2</sub>O), 125.05 (O-C=C), 128.82 (Ar), 135.28 (Ar), 136.99 (Ar), 137.31 (Ar), 145.36 (O-C=C). Elemental analysis calculated for C<sub>64</sub>H<sub>85</sub>NbO<sub>5</sub>: C 74.83, H 8.34; Found: C 75.04, H 8.34.

### 1.9.3 Preparation of (F<sub>3</sub>CC(O)O)<sub>2</sub>Nb(OC[<sup>2</sup>Ad]Mes)<sub>3</sub>, **2**

ONb(OC[<sup>2</sup>Ad]Mes)<sub>3</sub>(Et<sub>2</sub>O) (1.4 g, 1.36 mmol) was suspended in 50 mL of diethyl ether and placed in the cold well. A thawing ether solution of 350 mg (1.66 mmol) of O(CF<sub>3</sub>CO)<sub>2</sub> was added in a dropwise fashion with vigorous stirring to the cold ONb(OC[<sup>2</sup>Ad]Mes)<sub>3</sub>(Et<sub>2</sub>O). There was gradual color change from golden yellow to yellow-orange. As the solution warmed to room temperature dissolution of the material was observed with formation of a bright luminescent orange solution. The solution was allowed to stir at room temperature for an additional 1 hour at which time the solution was taken to dryness under reduced pressure. Addition of 7 mL of pentane to the resulting orange residue and chilling to -35 °C for 2 days resulted in 1.2 g (1.03 mmol, 76% yield) of pure material. <sup>1</sup>H NMR (20 °C, benzene-d<sub>6</sub>, 500 MHz): δ = 1.40-1.95 (39 H, multiple overlapping peaks, <sup>2</sup>Ad-H), 2.123 (9 H, s, *p*-Me), 2.226 (18 H, s, *o*-Me), 2.298 (3 H, s, allylic H), 6.708 (6 H, s, Ar-H); <sup>13</sup>C{<sup>1</sup>H} NMR (20 °C, 126 MHz, C<sub>6</sub>D<sub>6</sub>): δ = 19.81 (CH<sub>3</sub>), 21.05 (CH<sub>3</sub>), 28.34 (CH), 33.23 (CH), 38.89 (CH<sub>2</sub>), 39.03 (CH<sub>2</sub>), 39.14 (CH<sub>2</sub>), 128.52 (O-C=C), 129.12 (Ar), 133.97 (Ar), 136.97 (Ar), 137.72 (Ar), 148.76 (O-C=C); <sup>19</sup>F{<sup>1</sup>H} NMR (20 °C, 470 MHz, C<sub>6</sub>D<sub>6</sub>): δ = -75.66 ppm. Elemental analysis calculated for C<sub>64</sub>H<sub>75</sub>NbO<sub>7</sub>F<sub>6</sub>: C 66.08, H 6.50; Found: C 65.24, H 6.78.

### 1.9.4 Preparation of I<sub>2</sub>Nb(OC[<sup>2</sup>Ad]Mes)<sub>3</sub> from **2**, **3**

(F<sub>3</sub>CC(O)O)<sub>2</sub>Nb(OC[<sup>2</sup>Ad]Mes)<sub>3</sub> (250 mg, 0.215 mmol) was dissolved in 20 mL of Et<sub>2</sub>O. This solution was frozen in the cold well and upon thawing, TMSI (300 mg, 1.5 mmol) was added dropwise to the stirring solution. There was a noticeable darkening of the solution color to a more red-orange color upon addition and after 15 minutes a red precipitate began to form. The reaction

mixture was allowed to stir for 3 h after which time the red precipitate was isolated atop a glass frit, washed with 10 mL of Et<sub>2</sub>O, and dried to constant mass resulting in 184 mg (0.154 mmol, 72% yield) of I<sub>2</sub>Nb(OC[<sup>2</sup>Ad]Mes)<sub>3</sub>. See characterization data below.

#### 1.9.5 Preparation of (PhC≡CPh)Nb(OC[<sup>2</sup>Ad]Mes)<sub>3</sub>, **4**

KOC[<sup>2</sup>Ad]Mes (2.17 g, 6.77 mmol) was dissolved in 60 mL of Et<sub>2</sub>O. Solid (PhCCPh)NbCl<sub>3</sub>(THF)<sub>2</sub> (1.17 g, 2.24 mmol) was added in portions over the course of 10 min. The solution gradually darkened from tan to a light brown color. The solution was allowed to stir for 4 h. At this time the solution volume was concentrated to 30 mL and 30 mL of pentane was added to help precipitate the salts. The solution was then filtered over a pad of Celite to remove the salts and the filtrate was taken to dryness under reduced pressure. The resulting tan-colored powder was found to be spectroscopically and analytically pure once dried to constant mass (1.70 g, 1.43 mmol, 64% yield). Note: Isolation of this complex is not necessary en route to the diiodide (see below). <sup>1</sup>H NMR (20 °C, C<sub>6</sub>D<sub>6</sub>): δ = 1.60-1.90 (36 H, multiple overlapping peaks, <sup>2</sup>Ad-H), 2.097 (9 H, s, *p*-Me), 2.188 (18 H, s, *o*-Me), 2.292 (3 H, s, allylic H), 3.478 (3 H, s, allylic H), 6.706 (6 H, s, Ar-H), 7.010 (2 H, t, PhCCPh), 7.125 (4 H, t, PhCCPh), 7.185 (4 H, d, PhCCPh). Elemental analysis calculated for C<sub>74</sub>H<sub>85</sub>NbO<sub>3</sub>: C 79.68, H 7.68; Found: C 79.31, H 7.95.

#### 1.9.6 Preparation of I<sub>2</sub>Nb(OC[<sup>2</sup>Ad]Mes)<sub>3</sub>, **3**; One-pot Procedure

KOC[<sup>2</sup>Ad]Mes (16.34 g, 0.051 mol) was dissolved in 450 mL of Et<sub>2</sub>O. Solid (PhCCPh)NbCl<sub>3</sub>(THF)<sub>2</sub> (8.87 g, 0.017 mol) was added to the vigorously stirred solution at 20 °C. The solution slowly proceeded from an orange-brown color to a tan color over the course of 4 h. After this time the solution was filtered through a pad of Celite into a fresh round bottom flask removing the KCl generated in the reaction. To this new flask was added a solution of I<sub>2</sub> (4.32 g, 0.017 mol) in Et<sub>2</sub>O. The solution was allowed to stir at 20 °C for 1 h during which time **3** precipitated cleanly out of solution as a bright red powder. **3** was collected on a medium porosity frit and washed three times with 150 mL of Et<sub>2</sub>O to ensure complete removal of any excess I<sub>2</sub>. Yield: 16.27 g (80% yield over two steps). <sup>1</sup>H NMR (20 °C, C<sub>6</sub>D<sub>6</sub>): δ = 1.55-2.15 (36 H, multiple overlapping peaks, <sup>2</sup>Ad-H), 2.17 (9 H, s, *p*-Me), 2.35 (18 H, s, *o*-Me), 2.57 (3 H, s, allylic H), 3.47 (3 H, s, allylic H), 6.73 (6H, s, Ar-H); the low solubility of **3** precluded <sup>13</sup>C NMR analysis. Elemental analysis calculated for C<sub>60</sub>H<sub>75</sub>I<sub>2</sub>NbO<sub>3</sub>: C 60.51, H 6.35; Found: C 61.12, H 6.54.

#### 1.9.7 Preparation of INb(OC[<sup>2</sup>Ad]Mes)<sub>3</sub>(THF), **5**

I<sub>2</sub>Nb(OC[<sup>2</sup>Ad]Mes)<sub>3</sub> (6.0g, 5.04 mmol) was suspended in 50 mL of THF. SmI<sub>2</sub> (50 mL as a 0.1 M solution in THF) was added portionwise to the stirring suspension of I<sub>2</sub>Nb(OC[<sup>2</sup>Ad]Mes)<sub>3</sub>. Over the course of 20 min I<sub>2</sub>Nb(OC[<sup>2</sup>Ad]Mes)<sub>3</sub> was observed to solubilize and a yellow precipitate (SmI<sub>3</sub>)

formed. The mixture was allowed to stir for a total of 1 h at which time the solution was filtered through a pad of Celite removing the  $\text{SmI}_3$  byproduct as a bright yellow powder. The filtrate was concentrated to 50 mL, 20 mL of pentane were added, and the solution was placed in the glovebox freezer at  $-35^\circ$  to encourage crystallization of the reaction product. It should be noted that this reaction proceeds cleanly and quantitatively and as such the material can be generated and used *in situ* if desired. Yield: 4.00 g (70% yield);  $^1\text{H NMR}$  ( $20^\circ\text{C}$ ,  $\text{C}_6\text{D}_6$ ): broadened resonances occur at  $\delta = 1.46, 1.64, 1.88, 2.23, 2.82, 3.06, 3.78, 3.97, 4.48$  (very broad), and 6.59 ppm. EPR  $g_{iso} = 1.97$  in benzene at  $20^\circ\text{C}$  has a 10 line pattern characteristic of  $d^1$  Nb ( $I = 9/2$ ). Evans' method solution magnetic moment:  $1.93 \mu_B$ . Elemental analysis calculated for  $\text{C}_{64}\text{H}_{83}\text{I}_1\text{NbO}_4$ : C 67.65, H 7.36; Found: C 67.34, H 8.05.

### 1.9.8 Disproportionation of $\text{INb}(\text{OC}[\text{}^2\text{Ad}]\text{Mes})_3(\text{THF})$ in the absence of a trap

$\text{I}_2\text{Nb}(\text{OC}[\text{}^2\text{Ad}]\text{Mes})_3$  (900 mg, 0.756 mmol) was suspended in 30 mL of THF.  $\text{SmI}_2$  (7.2 mL as a 0.1 M THF solution, 0.75 mmol) was added in portions over 2 minutes. The solution was allowed to stir for 1 h. At this point the solution volume was concentrated to 10 mL and was filtered to remove the  $\text{SmI}_3$  byproduct and any unreacted  $\text{I}_2\text{Nb}(\text{OC}[\text{}^2\text{Ad}]\text{Mes})_3$ . Toluene (20 mL) was added to the filtrate and the filtrate was taken to dryness to remove all THF. The resulting residue was then taken up in 20 mL of  $\text{Et}_2\text{O}$  and allowed to stir at room temperature. Over the course of the next hour a copious red precipitate began to form indicating that the disproportionation reaction was proceeding. An aliquot was taken for NMR analysis indicating the presence of a small amount of remaining  $\text{INb}(\text{OC}[\text{}^2\text{Ad}]\text{Mes})_3(\text{THF})$  and a new paramagnetic product. The solution was again taken to dryness to remove all THF formed during the reaction. An additional 20 mL of  $\text{Et}_2\text{O}$  were added and the solution was allowed to stir for an additional hour. At this point an aliquot revealed by NMR that the reaction had gone to completion.  $\text{I}_2\text{Nb}(\text{OC}[\text{}^2\text{Ad}]\text{Mes})_3$  (257 mg isolated) was filtered away and the remaining material was taken to dryness leaving an amber colored solid. This amber solid was recrystallized from 5 mL of  $\text{Et}_2\text{O}$  yielding 575 mg of amber powder. Evans' method analysis: assuming  $[\text{Nb}(\text{OC}[\text{}^2\text{Ad}]\text{Mes})_3]_2\text{I}(\text{THF})_2 : \mu_{eff} = 2.61 \mu_B$ . EPR silent at  $20^\circ\text{C}$ .  $^1\text{H NMR}$  (500 MHz,  $\text{C}_6\text{D}_6$ ): very broad peaks in the diamagnetic region at 1.6, 1.7, 2.21, 2.82, 3.12, 3.72, 4.0, 4.6, and 6.6 ppm. This species is stable in solution; however if a substrate is added, it will further disproportionate. For instance, when 100 mg of this material as isolated above is combined with 13 mg  $\text{P}_4$  in toluene, after 36 h, full conversion to  $(\text{Mes}[\text{}^2\text{Ad}]\text{CO})_3\text{Nb}=\text{PP}_7\text{Nb}(\text{OC}[\text{}^2\text{Ad}]\text{Mes})_3$  and  $\text{I}_2\text{Nb}(\text{OC}[\text{}^2\text{Ad}]\text{Mes})_3$  is observed. Elemental analysis calculated for  $\text{C}_{128}\text{H}_{166}\text{I}_1\text{Nb}_2\text{O}_8$ : C 71.66, H 7.80; Found: C 71.42, H 7.61.

### 1.9.9 Preparation of $(\text{Mes}[\text{}^2\text{Ad}]\text{CO})_3\text{Nb}=\text{PP}_7\text{Nb}(\text{OC}[\text{}^2\text{Ad}]\text{Mes})_3$ , 7

A THF solution of  $\text{INb}(\text{OC}[\text{}^2\text{Ad}]\text{Mes})_3(\text{THF})$  (5.72 g, 5.04 mmol), prepared *in situ*, was added to a solution of  $\text{P}_4$  (335 mg, 2.52 mmol) in toluene (50 mL). THF was removed from the solution

under reduced pressure. As solvent evaporated it was replaced by additional toluene. This process of evaporation and solvent replacement was continued for 8 h. After this time significant red precipitate ( $\text{I}_2\text{Nb}(\text{OC}[\text{}^2\text{Ad}]\text{Mes})_3$ ) had begun to form, indicating that the disproportionation was proceeding. The flask was sealed with a rubber stopper and stirring was continued for 36 h. After this time, the solution was taken to dryness under reduced pressure. Diethyl ether (50 mL) was added and the bright red solid  $\text{I}_2\text{Nb}(\text{OC}[\text{}^2\text{Ad}]\text{Mes})_3$  was collected on a frit in quantitative yield (3.0 g). The filtrate was taken to dryness, and the resulting residue redissolved in 50 mL of pentane. The solution was then filtered through a pad of Celite. This process was repeated twice to remove any insoluble material. The final pentane solution was concentrated to 15 mL and placed in a glove-box freezer to induce precipitation. Yield: 2.2 g (82%).  $^1\text{H}$  NMR (20 °C, 500 MHz,  $\text{C}_6\text{D}_6$ ):  $\delta$  = 1.62.2 (78 H, multiple overlapping peaks,  $^2\text{Ad-H}$ ), 2.22 and 2.27 (18 H, s, *p*-Me), 2.37 and 2.47 (36H, s, *o*-Me), 3.34 and 3.43 (6H, s, allylic H), 6.82 and 6.88 ppm (12 H, s, Ar-H);  $^{13}\text{C}\{^1\text{H}\}$  NMR (20 °C, 126 MHz,  $\text{C}_6\text{D}_6$ ):  $\delta$  = 147.61, 137.44, 137.27, 136.94, 136.85, 134.61, 133.84, 131.66, 129.29, 128.87, 128.63, 128.37, 127.45, 39.77, 39.49, 39.32, 39.22, 39.04, 37.70, 37.38, 34.48, 30.87, 30.58, 29.14, 28.87, 21.39, 20.58 ppm;  $^{31}\text{P}\{^1\text{H}\}$  NMR (20 °C, 202 MHz,  $\text{C}_6\text{D}_6$ ):  $\delta$  = 379 (1 P, d,  $^1J_{\text{P/P}} = 356$  Hz, PA), 161 (1 P, m, PB), -92 (2 P, br, PC1/2), -100 (2 P, br, PD1/2), -122 ppm (2 P, br, PE1/2). Elemental analysis (%) calcd for  $\text{C}_{120}\text{H}_{175}\text{Nb}_2\text{P}_8$  : C 67.92, H 7.12, P 11.67; found: C 67.04, H 7.09, P 11.61.

### 1.9.10 Preparation of $\text{H}_2\text{PP}_7\text{Nb}(\text{OC}[\text{}^2\text{Ad}]\text{Mes})_3$ , **8**

Method 1 (with  $\text{H}_2\text{O}$ ): **7** (500 mg, 0.235 mmol) was dissolved in 150 mL of  $\text{Et}_2\text{O}$  in a 300 mL Schlenk flask. The flask was removed from the glove box and placed under a positive pressure of argon on the Schlenk line. The flask was chilled in an ice water bath.  $\text{H}_2\text{O}$  (4.14 mg, 0.236 mmol) was syringed into the flask as a stock solution in THF. The solution was allowed to stir for 2 h during which time the solution progressed from a bright orange homogeneous state to a yellow-orange inhomogeneous mixture. After 2 h, the volatiles were removed under reduced pressure and the flask was brought back into the glovebox. The residue was slurried with  $\text{Et}_2\text{O}$  and the solids were collected on a frit. The solids were washed three times with pentane (20 mL) and were then dried. Dissolution of the material in benzene and allowing a slow evaporation over several days afforded X-ray quality crystals. Yield: 83 mg (30%);  $^1\text{H}$  NMR (20 °C, 500 MHz,  $\text{C}_6\text{D}_6$ ):  $\delta$  = 1.552.15 (38 H, multiple overlapping peaks,  $^2\text{Ad-H}$ , P-H), 2.19 (9 H, s, *p*-Me), 2.49 (18 H, s, *o*-Me), 3.45 (3 H, s, allylic H), 6.89 ppm (6 H, s, Ar-H);  $^{31}\text{P}$  NMR (20 °C, 126 MHz,  $\text{C}_6\text{D}_6$ ):  $\delta$  = 89 (1 P, q, PB), -65 (2P, br, PE), -84 (2P, br, PD), -87.5 (2P, br, PC), -203 ppm (1P, d, PA,  $^1J_{\text{P/H}} = 196$  Hz).

Method 2 (with 2,6-lutidinium iodide): **7** (500 mg, 0.235 mmol) was dissolved in  $\text{Et}_2\text{O}$  (10 mL) and was added to solid 2,6-lutidinium iodide (111 mg, 0.471 mmol). The mixture was allowed to stir for 4 h during which time there was copious precipitation of  $\text{I}_2\text{Nb}(\text{OC}[\text{}^2\text{Ad}]\text{Mes})_3$  and  $\text{H}_2\text{PP}_7\text{Nb}(\text{OC}[\text{}^2\text{Ad}]\text{Mes})_3$ . The mixture was filtered through a medium-porosity frit and the solids were collected and washed with  $\text{Et}_2\text{O}$  (20 mL). The solids were then washed with toluene (40

mL) and Et<sub>2</sub>O (10 mL) into a fresh filtration flask, leaving I<sub>2</sub>Nb(OC[<sup>2</sup>Ad]Mes)<sub>3</sub> (249 mg, 89% yield) on the frit as a bright red solid. The filtrate was then concentrated to a volume of 5 mL and was stored at –35 °C, allowing H<sub>2</sub>PP<sub>7</sub>Nb(OC[<sup>2</sup>Ad]Mes)<sub>3</sub> to crystallize as a pumpkin-orange solid. X-ray quality crystals were grown from a benzene solution (slow evaporation) and a unit-cell determination confirmed the identity of this material. Yield 87 mg (30%).

### 1.9.11 Preparation of Ph<sub>2</sub>CP<sub>8</sub>Nb(OC[<sup>2</sup>Ad]Mes)<sub>3</sub>, 10

(Representative procedure for compounds **10** through **18**). To a 20 °C, bright orange Et<sub>2</sub>O solution (15 mL) of **7** (600 mg, 0.28 mmol) was added an Et<sub>2</sub>O solution (5 mL) of benzophenone (52 mg, 0.28 mmol, 1 equiv) with stirring. Over the course of 1 h there was a brightening of the solution to a more vibrant red-orange color. This solution was allowed to stir for an additional 6 h during which time the solution darkened to yellow-brown. After this time the solvent was removed *in vacuo* and the residue was slurried in pentane (2 mL) and diethyl ether (10 mL) and placed in the glovebox freezer at –35 °C. After 10 h a copious tan colored precipitate formed. This material was collected by filtration on a glass frit and was washed with cold pentane (15 mL). The tan powder was then dried to constant mass (290 mg, 0.21 mmol, 76% yield). <sup>31</sup>P{<sup>1</sup>H} NMR (20 °C, benzene-d<sub>6</sub>, 202.5 MHz): δ = 94.75 (m, 2 P), 7.81 (t, <sup>1</sup>J<sub>P/P</sub> = 297 Hz, 1 P), –11.75 (apparent d, <sup>1</sup>J<sub>P/P</sub> = 316 Hz, 2 P), –93.00 (t, <sup>1</sup>J<sub>P/P</sub> = 228 Hz, 1 P), –167.95 (t, <sup>1</sup>J<sub>P/P</sub> = 238 Hz, 2 P). <sup>1</sup>H NMR (20 °C, benzene-d<sub>6</sub>, 500 MHz): δ = 1.59-1.94 (multiple overlapping peaks, 36 H, <sup>2</sup>Ad-H), 2.02 (s, 3 H, allylic H), 2.18 (s, 9 H, *p*-Me), 2.34 (s, 18 H, *o*-Me), 3.48 (s, 3 H, allylic H), 6.78 (s, 6 H, aryl H enolate), 6.91 (t, 2 H, <sup>1</sup>J<sub>H/H</sub> = 7 Hz, Ar-H CPh<sub>2</sub>), 6.99 (t, 4 H, <sup>1</sup>J<sub>H/H</sub> = 7 Hz, Ar-H CPh<sub>2</sub>), 7.56 (d, 4H, <sup>1</sup>J<sub>H/H</sub> = 7 Hz, Ar-H CPh<sub>2</sub>). <sup>13</sup>C{<sup>1</sup>H} NMR (20 °C, benzene-d<sub>6</sub>, 125.8 MHz): δ = 20.68 (CH<sub>3</sub>), 21.29 (CH<sub>3</sub>), 28.82 (CH), 31.00 (CH), 33.35 (CH<sub>2</sub>), 37.28 (CH<sub>2</sub>), 39.36 (m, CPh<sub>2</sub>), 100.18 (O-C=C), 127.83 (Ar), 127.52 (Ar), 128.35 (Ar), 129.17 (m, Ar), 129.96 (Ar), 133.52 (Ar), 137.01 (Ar), 137.64 (Ar), 148.83 (O-C=C). Elemental analysis calculated for C<sub>73</sub>H<sub>85</sub>NbO<sub>3</sub>P<sub>8</sub>: C, 64.89; H, 6.34; P, 18.34. Found: C, 64.68; H, 6.15; P, 18.48.

### 1.9.12 Preparation of ((Me<sub>2</sub>N)C<sub>6</sub>H<sub>4</sub>)<sub>2</sub>C=PP<sub>7</sub>Nb(OC[<sup>2</sup>Ad]Mes)<sub>3</sub>, 11

The reaction mixture, prepared as described above, was stirred for 16 h prior to workup. The phosphorus containing material was separated from the niobium oxo by precipitation from 1:2 C<sub>5</sub>H<sub>12</sub>/Et<sub>2</sub>O at –35 °C at an isolated yield of 42%. <sup>31</sup>P{<sup>1</sup>H} NMR (20 °C, benzene-d<sub>6</sub>, 202.5 MHz): δ = 93.08 (m, 2 P), 4.66 (t, <sup>1</sup>J<sub>P/P</sub> = 296 Hz, 1 P), –9.39 (apparent d, <sup>1</sup>J<sub>P/P</sub> = 320 Hz, 2 P), –99.96 (t, <sup>1</sup>J<sub>P/P</sub> = 230 Hz, 1 P), –168.24 (t, <sup>1</sup>J<sub>P/P</sub> = 226 Hz, 2 P). <sup>1</sup>H NMR (20 °C, benzene-d<sub>6</sub>, 500 MHz): δ = 1.60-2.00 (multiple overlapping peaks, 36 H), 2.05 (s, 3 H), 2.19 (s, 9 H), 2.39 (s, 18 H), 2.48 (s, 12 H), 3.55 (s, 3 H), 6.42 (d, <sup>1</sup>J<sub>H/H</sub> = 8.8 Hz, 4 H), 6.80 (s, 6 H), 7.57 (d, <sup>1</sup>J<sub>H/H</sub> = 8.5 Hz, 4 H).



### 1.9.13 Preparation of ((MeO)C<sub>6</sub>H<sub>4</sub>)<sub>2</sub>C=PP<sub>7</sub>Nb(OC[<sup>2</sup>Ad]Mes)<sub>3</sub>, 12

The reaction mixture, prepared as described above, was stirred for 12 h prior to workup. The phosphorus containing material was separated from the niobium oxo by precipitation from 1:2 C<sub>5</sub>H<sub>12</sub>/Et<sub>2</sub>O at -35 °C at an isolated yield of 73%. <sup>31</sup>P{<sup>1</sup>H} NMR (20 °C, benzene-d<sub>6</sub>, 202.5 MHz): δ = 94.28 (m, 2 P), 7.85 (t, <sup>1</sup>J<sub>P/P</sub> = 297 Hz, 1 P), -11.20 (apparent d, <sup>1</sup>J<sub>P/P</sub> = 318 Hz, 2 P), -94.84 (t, <sup>1</sup>J<sub>P/P</sub> = 229 Hz, 1 P), -167.53 (t, <sup>1</sup>J<sub>P/P</sub> = 234 Hz, 2 P). <sup>1</sup>H NMR (20 °C, benzene-d<sub>6</sub>, 500 MHz): δ = 1.50-2.05 (multiple overlapping peaks, 39 H), 2.18 (s, 9 H), 2.35 (s, 18 H), 3.27 (s, 6 H), 3.49 (s, 3 H), 6.64 (d, <sup>1</sup>J<sub>H/H</sub> = 8.5 Hz, 4 H), 6.79 (s, 6 H), 7.53 (d, <sup>1</sup>J<sub>H/H</sub> = 8.5 Hz, 4H).

### 1.9.14 Preparation of (MeC<sub>6</sub>H<sub>4</sub>)<sub>2</sub>C=PP<sub>7</sub>Nb(OC[<sup>2</sup>Ad]Mes)<sub>3</sub>, 13

The reaction mixture, prepared as described above, was stirred for 16 h prior to workup. The phosphorus containing material was separated from the niobium oxo by precipitation from 1:2 C<sub>5</sub>H<sub>12</sub>/Et<sub>2</sub>O at -35 °C at an isolated yield of 68%. <sup>31</sup>P{<sup>1</sup>H} NMR (20 °C, benzene-d<sub>6</sub>, 202.5 MHz): δ = 94.82 (m, 2 P), 7.23 (t, <sup>1</sup>J<sub>P/P</sub> = 293 Hz, 1 P), -10.80 (apparent d, <sup>1</sup>J<sub>P/P</sub> = 318 Hz, 2 P), -94.26 (t, <sup>1</sup>J<sub>P/P</sub> = 228 Hz, 1 P), -167.92 (t, <sup>1</sup>J<sub>P/P</sub> = 228 Hz, 2 P). <sup>1</sup>H NMR (20 °C, benzene-d<sub>6</sub>, 500 MHz): δ = 1.58-1.95 (multiple overlapping peaks, 39 H), 2.03 (s, 6 H), 2.18 (s, 9 H), 2.36 (s, 18 H), 3.50 (s, 3 H), 6.79 (s, 6 H), 6.79 (s, 6 H), 6.89 (d, <sup>1</sup>J<sub>H/H</sub> = 8 Hz, 4 H), 7.53 (d, <sup>1</sup>J<sub>H/H</sub> = 8 Hz, 4 H). Elemental analysis calculated for C<sub>74</sub>H<sub>89</sub>NbO<sub>3</sub>P<sub>8</sub>: C, 65.29; H, 6.51; P, 17.98. Found: C, 64.96; H, 6.57; P, 18.11.

### 1.9.15 Preparation of (ClC<sub>6</sub>H<sub>4</sub>)<sub>2</sub>C=PP<sub>7</sub>Nb(OC[<sup>2</sup>Ad]Mes)<sub>3</sub>, 14

The reaction mixture, prepared as described above, was stirred for 5 h prior to workup. The phosphorus containing material was separated from the niobium oxo by precipitation from 1:2 C<sub>5</sub>H<sub>12</sub>/Et<sub>2</sub>O at -35 °C at an isolated yield of 70%. <sup>31</sup>P{<sup>1</sup>H} NMR (20 °C, benzene-d<sub>6</sub>, 202.5 MHz): δ = 95.70 (m, 2 P), 10.41 (t, <sup>1</sup>J<sub>P/P</sub> = 296 Hz, 1 P), -13.62 (apparent d, <sup>1</sup>J<sub>P/P</sub> = 311 Hz, 2 P), -90.46 (t, <sup>1</sup>J<sub>P/P</sub> = 221 Hz, 1 P), -165.10 (t, <sup>1</sup>J<sub>P/P</sub> = 202 Hz, 2 P). <sup>1</sup>H NMR (20 °C, benzene-d<sub>6</sub>, 500 MHz): δ = 1.53-2.05 (multiple overlapping peaks, 39 H), 2.18 (s, 9 H), 2.31 (s, 18 H), 3.43 (s, 3 H), 6.77 (s, 6 H), 7.02 (d, <sup>1</sup>J<sub>H/H</sub> = 8.5 Hz, 4 H), 7.29 (d, <sup>1</sup>J<sub>H/H</sub> = 8.5 Hz, 4 H).

### 1.9.16 Preparation of ((F<sub>3</sub>C)C<sub>6</sub>H<sub>4</sub>)<sub>2</sub>C=PP<sub>7</sub>Nb(OC[<sup>2</sup>Ad]Mes)<sub>3</sub>, 15

The reaction mixture, prepared as described above, was stirred for 3.5 h prior to workup. The phosphorus containing material was separated from the niobium oxo by precipitation from 1:2 O(SiMe<sub>3</sub>)<sub>2</sub>/Et<sub>2</sub>O at -35 °C at an isolated yield of 43%. The appreciable solubility of this species in hydrocarbon solvents prevents isolation of more material free of niobium oxo. <sup>31</sup>P{<sup>1</sup>H} NMR (20 °C, benzene-d<sub>6</sub>, 202.5 MHz): δ = 95.05 (m, 2 P), 13.15 (t, <sup>1</sup>J<sub>P/P</sub> = 303 Hz, 1 P), -14.52 (apparent

d,  $^1J_{P/P} = 323$  Hz, 2 P),  $-88.14$  (t,  $^1J_{P/P} = 227$  Hz, 1 P),  $-166.33$  (t,  $^1J_{P/P} = 246$  Hz, 2 P).  $^1H$  NMR (20 °C, benzene- $d_6$ , 500 MHz):  $\delta = 1.50$ -2.05 (multiple overlapping peaks, 39 H), 2.16 (s, 9 H), 2.30 (s, 18 H), 3.41 (s, 3 H), 6.76 (s, 6 H), 7.27 (d,  $^1J_{H/H} = 8.4$  Hz, 4 H), 7.40 (d,  $^1J_{H/H} = 8.5$  Hz, 4 H) ppm.  $^{19}F\{^1H\}$  NMR (20 °C, benzene- $d_6$ , 282.4 MHz):  $\delta = -62.7$  ppm (s, 6 F).

### 1.9.17 Preparation of $Cy_2C=PP_7Nb(OC[{}^2Ad]Mes)_3$ , 17

The reaction mixture was prepared using 20 equiv of dicyclohexyl ketone and was stirred for a total reaction time of 5 h. The phosphorus containing material was separated from the niobium oxo by precipitation from 1:2 O(SiMe $_3$ ) $_2$ /Et $_2$ O at  $-35$  °C in 62% yield.  $^{31}P\{^1H\}$  NMR (20 °C, benzene- $d_6$ , 202.5 MHz):  $\delta = 201.70$  (d,  $^1J_{P/P} = 260$  Hz, 1 P), 115.44 (q,  $^1J_{P/P} = 260$  Hz, 1 P),  $-67.50$  (m, 2 P),  $-82.80$  (m, 4 P).  $^1H$  NMR (20 °C, benzene- $d_6$ , 500 MHz):  $\delta = 0.77$ -2.15 (multiple overlapping peaks, 53 H,  $^iPr$  and  ${}^2Ad$ -H), 2.20 (s, 9 H, *p*-Me), 2.47 (s, 18 H, *o*-Me), 3.44 (s, 3 H, allylic H), 6.88 (s, 6 H, Ar-H).  $^{13}C\{^1H\}$  NMR (20 °C, benzene- $d_6$ , 125.8 MHz):  $\delta = 231.0$  (d,  $^1J_{C/P} = 69$  Hz). Elemental analysis calculated for C $_73$ H $_95$ NbO $_3$ P $_8$ : C, 64.39; H, 7.04; P, 18.21. Found: C, 64.92; H, 7.05; P, 18.42.

### 1.9.18 Preparation of ${}^iPr_2C=PP_7Nb(OC[{}^2Ad]Mes)_3$ , 18

The reaction mixture, prepared as described above, was stirred for 3 d prior to workup. The phosphorus containing material was separated from the niobium oxo by precipitation from 1:2 O(SiMe $_3$ ) $_2$ /Et $_2$ O at  $-35$  °C at an isolated yield of 43%. The appreciable solubility of this species in hydrocarbon solvents prevents isolation of more material free of niobium oxo. To effect a more rapid conversion to the phosphalkene, 20 equiv of diisopropyl ketone may be used and the reaction mixture may be worked up after 5 h of stirring at 22 °C. Precipitation as described above results in 58% isolated yield of the bright orange phosphalkene when the reaction is effected in this manner.  $^{31}P\{^1H\}$  NMR (20 °C, benzene- $d_6$ , 202.5 MHz):  $\delta = 199.7$  (d,  $^1J_{P/P} = 237$  Hz, 1 P), 114.98 (q,  $^1J_{P/P} = 266$  Hz, 1 P),  $-68.40$  (m, 2 P),  $-81.50$  (m, 4 P).  $^1H$  NMR (20 °C, benzene- $d_6$ , 500 MHz):  $\delta = 0.89$  (m, 12 H), 1.48-2.14 (multiple overlapping peaks, 42 H), 2.22 (s, 9 H), 2.47 (s, 18 H), 3.43 (s, 3 H), 6.87 (s, 6 H).

### 1.9.19 Kinetic Investigations of the Rearrangement of $Ph_2C=PP_7Nb(OC[{}^2Ad]Mes)_3$ : Eyring Analysis and Hammett Trend Analysis

A solution (2 mL) of **7** (100 mg, 0.047 mmol, 1 equiv) in C $_6$ D $_6$  was added to solid benzophenone (10 mg, 0.056 mmol, 1.2 equiv). This solution was stirred for 30 s and placed in a sealable NMR tube equipped with a capillary containing PPh $_3$  in C $_6$ D $_6$  or  $d_8$ -toluene as reference and was then chilled for transport to an NMR probe preset to the appropriate temperature as measured by a methanol or ethylene glycol NMR thermometer.  $^{31}P$  NMR spectra (64 scans) were collected every

300 s for 3-14 h depending on temperature on a Bruker Avance 400 spectrometer (162 MHz  $^{31}\text{P}$ ). The integrals of the phosphalkene resonances were monitored following complete consumption of the starting  $(\text{Mes}[\text{Ad}]\text{CO})_3\text{Nb}=\text{PP}_7\text{Nb}(\text{OC}[\text{Ad}]\text{Mes})_3$ . The integrals of the phosphalkene molecule as a function of time, corrected versus the  $\text{PPh}_3$  standard, were fit to the first-order rate equation,  $I(t) = Ae^{-kt} + b$ , using the automated routine of *Gnuplot* to extract  $k$ , Table 1.1. Three runs were performed at each temperature and the error bars were calculated at the 95% confidence level. The Eyring fit was performed using the error-weighted least squares regression analysis of *Gnuplot*.<sup>87</sup>

For the Hammett analysis, the same operational procedures were followed. The integrals of the forming  $\text{Ar}_2\text{CP}_8\text{Nb}(\text{OC}[\text{Ad}]\text{Mes})_3$  resonances were monitored following complete consumption of the starting  $(\text{Mes}[\text{Ad}]\text{CO})_3\text{Nb}=\text{PP}_7\text{Nb}(\text{OC}[\text{Ad}]\text{Mes})_3$ . The integrals of the  $\text{Ar}_2\text{CP}_8\text{Nb}(\text{OC}[\text{Ad}]\text{Mes})_3$  molecules as a function of time, corrected versus the  $\text{PPh}_3$  standard, were fit to the first-order rate equation,  $I(t) = Ae^{-kt} + b$ , using the automated routine of *Gnuplot* to extract  $k$ , Table 1.2. Three runs were performed for each molecule at 25 °C and the error bars were calculated at the 95% confidence level. The Hammett fit was performed using the error-weighted least squares regression analysis of *Gnuplot*.<sup>87</sup>

### 1.9.20 Preparation of $\text{Ph}_2\text{SnP}_8\text{Nb}(\text{OC}[\text{Ad}]\text{Mes})_3$ , 19

$(\text{Mes}[\text{Ad}]\text{CO})_3\text{Nb}=\text{PP}_7\text{Nb}(\text{OC}[\text{Ad}]\text{Mes})_3$  (1.508 g, 0.71 mmol) was dissolved in 50 mL of  $\text{Et}_2\text{O}$  in a round bottom flask. In a separate vessel,  $\text{Ph}_2\text{SnCl}_2$  (244 mg, 0.71 mmol) was likewise dissolved in 30 mL of  $\text{Et}_2\text{O}$ . The  $\text{Ph}_2\text{SnCl}_2$  was added to a stirring solution of  $(\text{Mes}[\text{Ad}]\text{CO})_3\text{Nb}=\text{PP}_7\text{Nb}(\text{OC}[\text{Ad}]\text{Mes})_3$  slowly over 10 minutes. Immediately upon addition a bright orange precipitate formed. The reaction mixture was allowed to stir for 2.5 h. After 2.5 h had elapsed an aliquot was removed for NMR analysis indicating that all of the starting material had been consumed. The precipitate ( $\text{Cl}_2\text{Nb}(\text{OC}[\text{Ad}]\text{Mes})_3$ ) was isolated atop a frit, resulting in 608 mg (0.60 mmol) of bright white solid. The filtrate was concentrated to 20 mL and placed in the glove box freezer. After 20 h a small amount of light colored (off-white) precipitate had formed; this precipitate was removed by filtration and the remaining red-orange filtrate was concentrated to 10 mL and left in the freezer for 2 days. After this time a copious orange precipitate formed. This material was isolated atop a frit and dried to constant mass yielding 300 mg (0.21 mmol, 30% yield) of  $\text{Ph}_2\text{SnP}_8\text{Nb}(\text{OC}[\text{Ad}]\text{Mes})_3$ .  $^1\text{H}$  NMR ( $\text{C}_6\text{D}_6$ , 400 MHz): 7.51 (d,  $^1J_{\text{H}/\text{H}} = 7$  Hz, 4 H), 7.13 (t,  $^1J_{\text{H}/\text{H}} = 7$  Hz, 4 H), 7.11 (t,  $^1J_{\text{H}/\text{H}} = 7$  Hz, 2 H), 6.72 (s, 6 H), 3.55 (s, 3 H), 2.36 (s, 18 H), 2.14 (s, 9 H), 2.05–1.50 ppm (multiple overlapping peaks, 39 H);  $^{31}\text{P}\{^1\text{H}\}$  NMR ( $\text{C}_6\text{D}_6$ , 162 MHz): 76.47 (m, 2 P), -24.87 (apparent doublet, 261 Hz, 2 P), -133.02 (t,  $^1J_{\text{P}/\text{P}} = 210$  Hz, 2 P), -214.06 (t,  $^1J_{\text{P}/\text{P}} = 260$  Hz, 1 P,  $^1J_{\text{Sn}/\text{P}} = 989$  Hz), -345.25 ppm (t,  $^1J_{\text{P}/\text{P}} = 230$  Hz, 1 P,  $^1J_{\text{Sn}/\text{P}} = 1257$  Hz);  $^{13}\text{C}\{^1\text{H}\}$  NMR ( $\text{C}_6\text{D}_6$ , 100 MHz): 20.93, 21.23, 28.73, 33.25, 37.24, 39.35, 39.24, 108.31, 128.73, 129.26, 129.90, 133.58, 136.58, 136.74, 137.33, 148.62 ppm. Elemental analysis calculated for  $\text{C}_{72}\text{H}_{85}\text{NbO}_3\text{P}_8\text{Sn}$ : C, 59.32; H, 5.88; P, 17.00. Found: C, 60.87; H, 6.30; P,

17.28. Elemental analysis on the coproduct  $\text{Cl}_2\text{Nb}(\text{OC}[\text{}^2\text{Ad}]\text{Mes})_3$ ; calculated for  $\text{C}_{60}\text{H}_{75}\text{Cl}_2\text{NbO}_3$ : C, 71.54; H, 7.51; Cl, 6.95. Found: C, 71.60; H, 7.28; Cl, 6.75.

### 1.9.21 Preparation of $\text{dmpPP}_8\text{Nb}(\text{OC}[\text{}^2\text{Ad}]\text{Mes})_3$ , 20

$(\text{Mes}[\text{}^2\text{Ad}]\text{CO})_3\text{Nb}=\text{PP}_7\text{Nb}(\text{OC}[\text{}^2\text{Ad}]\text{Mes})_3$  (1.5 g, 0.71 mmol) was dissolved in 15 mL of  $\text{Et}_2\text{O}$ . In a separate vial,  $\text{dmpPCl}_2$  (294 mg, 0.71 mmol) was likewise dissolved in 15 mL of  $\text{Et}_2\text{O}$ . Both vials were cooled at  $-35\text{ }^\circ\text{C}$ . After 15 minutes of cooling, the  $\text{dmpPCl}_2$  was added to a stirring solution of  $(\text{Mes}[\text{}^2\text{Ad}]\text{CO})_3\text{Nb}=\text{PP}_7\text{Nb}(\text{OC}[\text{}^2\text{Ad}]\text{Mes})_3$  in a 100 mL round bottom flask. The reaction mixture was allowed to stir for 6 h during which time a significant amount of bright orange precipitate formed. After 6 h had elapsed an aliquot was removed for NMR analysis indicating that approximately 15% of the two starting reagents still were present. The solution was allowed to stir for an additional 3 h after which time an aliquot was removed for NMR analysis indicating that approximately 8% of the two starting reagents still were present. The reaction mixture was allowed to stir overnight in order to complete the conversion. In the morning, the precipitated dichloride was collected on a frit and washed with 20 mL of pentane resulting in 474 mg of bright orange powder (0.47 mmol, 67% yield). The brown colored filtrate was taken to dryness under reduced pressure resulting in 900 mg of brown powder. This powder was recrystallized from  $\text{Et}_2\text{O}$  for 2 days at  $-35\text{ }^\circ\text{C}$  resulting in 562 mg (0.367 mmol, 52% yield) of  $\text{dmpPP}_8\text{Nb}(\text{OC}[\text{}^2\text{Ad}]\text{Mes})_3$ .  $^1\text{H}$  NMR ( $\text{C}_6\text{D}_6$ , 400 MHz): 7.02 (br, 2 H), 6.98 (br, 1 H), 6.84 (br, 4 H), 6.78 (br, 6 H), 3.61 (s, 3 H), 2.47 (s, 6 H), 2.39 (s, 6 H), 2.35 (s, 9 H), 2.31 (s, 3 H), 2.26 (s, 3 H), 2.16 (s, 18 H), 2.141.62 ppm (multiple overlapping peaks, 39 H);  $^{31}\text{P}\{^1\text{H}\}$  NMR ( $\text{C}_6\text{D}_6$ , 162 MHz): 138.71 (apparent q, 1 P), 77.48 (m, 1 P), 61.88 (m, 1 P), 20.43 (m, 1 P), 7.88 (m, 1 P),  $-36.24$  (apparent q, 1 P),  $-117.63$  (m, 1 P),  $-139.31$  (m, 1 P),  $-16.69$  (apparent q, 1 P).

### 1.9.22 Preparation of $\text{Ph}_2\text{CP}_8(\text{C}_6\text{H}_8)$ , 21

$\text{Ph}_2\text{CP}_8\text{Nb}(\text{OC}[\text{}^2\text{Ad}]\text{Mes})_3$  (1.448 g, 1.07 mmol, 1 equiv) was suspended in  $\text{Et}_2\text{O}$  (60 mL). Excess 1,3-cyclohexadiene (1.72 g, 21.4 mmol, 20 equiv) was added to the stirred suspension. To this mixture was added pyridine-*N*-oxide (305 mg, 3.2 mmol, 3 equiv) as a solid. The mixture was allowed to stir for 10 h. After this time there was a gray-white precipitate that had formed. The precipitate, a gray solid (presumably the untrapped material) was removed by filtering the reaction mixture through a pad of Celite. An aliquot from the reaction filtrate was taken for  $^1\text{H}$  NMR analysis and revealed only two species, the oxo-niobium complex  $\text{ONb}(\text{OC}[\text{}^2\text{Ad}]\text{Mes})_3(\text{ONC}_5\text{H}_5)$  and compound  $\text{Ph}_2\text{CP}_8(\text{C}_6\text{H}_8)$ . The filtrate was dried and then slurried in  $\text{Et}_2\text{O}$  (20 mL), resulting in formation of an off-white precipitate. This precipitate was isolated on a frit, washed with  $\text{Et}_2\text{O}$  (50 mL) and pentane (20 mL) and dried under reduced pressure resulting in 203 mg (38% yield). The filtrate was concentrated and placed in the glovebox freezer for additional crops resulting in an additional 51 mg of white powder. Yield: 254 mg (0.51 mmol, 48% yield).  $^1\text{H}$  NMR (20  $^\circ\text{C}$ , 500

MHz, C<sub>6</sub>D<sub>6</sub>):  $\delta$  = 0.78 (br, 2 H), 1.06 (br, 2 H), 2.54 (br, 2 H), 5.80 (apparent q, 2 H), 6.89 (m, 6 H), 7.55 (d,  $^1J_{\text{H/H}} = 7.53$  Hz, 4 H).  $^{13}\text{C}\{^1\text{H}\}$  NMR (20 °C, 126 MHz C<sub>6</sub>D<sub>6</sub>):  $\delta$  = 24.6 (m, CH<sub>2</sub>), 30.8 (m, CH), 39.4 (m, PCP), 128.7 (s, Ar), 128.9 (s, Ar), 128.9 (s, Ar), 132.1 (br, C=C), 145.0 (s, Ar).  $^{31}\text{P}\{^1\text{H}\}$  NMR (20 °C, 202 MHz, C<sub>6</sub>D<sub>6</sub>):  $\delta$  = -173.2 (t,  $^1J_{\text{P/P}} = 230$  Hz, 2 P), -124.0 (t,  $^1J_{\text{P/P}} = 245$  Hz, 1 P), 39.3 (pseudo d,  $^1J_{\text{P/P}} = 220$  Hz, 2 P), 48.3 (t,  $^1J_{\text{P/P}} = 327$  Hz, 1 P), 57.2 ppm (m, 2 P). Elemental analysis calcd. for C<sub>19</sub>H<sub>18</sub>P<sub>8</sub> : C 46.16, H 3.67; found: C 46.88, H 4.05. m.p.: 165-168 °C (dec).

### Characterization of ONb(OC[<sup>2</sup>Ad]Mes)<sub>3</sub>(ONC<sub>5</sub>H<sub>5</sub>) byproduct, 22

Best isolated yield: 86% by two rounds of Et<sub>2</sub>O crystallization of the reaction mixture following separation of complex 21 as discussed in the main text. NMR Spectral features:  $^1\text{H}$  NMR (C<sub>6</sub>D<sub>6</sub>, 500 MHz): 1.71-2.05 (multiple overlapping peaks, AdH, 36 H), 2.07 (s, *p*-Me, 9 H), 2.21 (s, al H, 3 H), 2.58 (s, *o*-Me, 18 H), 3.97 (s, al H, 3 H), 6.10 (br, pyNO, 2 H), 6.21 (br, pyNO, 1 H), 6.64 (s, ArH, 6 H), 8.08 (br, pyNO, 2 H).  $^{13}\text{C}\{^1\text{H}\}$  NMR (C<sub>6</sub>D<sub>6</sub>, 126 MHz): 21.11 (CH<sub>3</sub>), 21.51 (CH<sub>3</sub>), 29.73 (CH), 33.67 (CH), 39.85 (CH<sub>2</sub>), 40.22 (CH<sub>2</sub>), 121.51 (O-C=C), 123.54 (Ar), 125.07 (Ar), 135.28 (Ar), 136.44 (Ar), 137.32 (Ar), 139.12 (Ar), 145.82 (O-C=C), 150.80 (Ar). Elemental analysis calculated for C<sub>65</sub>H<sub>80</sub>NbO<sub>5</sub>N: C 74.47, H 7.69, N 1.33; found: C 74.41, H 7.22, N 1.17.

ONb(OC[<sup>2</sup>Ad]Mes)<sub>3</sub>(ONC<sub>5</sub>H<sub>5</sub>) may also be independently prepared quantitatively by treatment of ONb(OC[<sup>2</sup>Ad]Mes)<sub>3</sub>(OEt<sub>2</sub>) with one equivalent of pyridine-*N*-oxide in toluene.

### 1.9.23 Preparation of Ph<sub>2</sub>CP<sub>8</sub>(C<sub>6</sub>H<sub>10</sub>), 23

Ph<sub>2</sub>CP<sub>8</sub>Nb(OC[<sup>2</sup>Ad]Mes)<sub>3</sub> (148 mg, 0.11 mmol) was suspended in 10 mL of toluene. 2,3-dimethylbutadiene (0.5 mL) was added. To this solution was added pyridine-*N*-oxide (31 mg, 0.32 mmol) as a solid. After 30 minutes, the solution became homogeneous and began to lighten in color. The mixture was allowed to stir for 2 hours at which time the solution was observed to have taken on a much more yellow hue. The volatiles were removed from the solution. The solution was triturated twice with hexane and fully dried again leaving behind a yellow powder. This residue was slurried in Et<sub>2</sub>O (10 mL), resulting in formation of an off-white precipitate. This precipitate was isolated on a frit, washed with Et<sub>2</sub>O (5 mL) and pentane (5 mL) and dried under reduced pressure resulting in 19 mg (0.038 mmol, 35% yield).  $^{31}\text{P}\{^1\text{H}\}$  NMR (20 °C, 202 MHz, C<sub>6</sub>D<sub>6</sub>):  $\delta$  = -182 (t,  $^1J_{\text{P/P}} = 244$  Hz, 2 P), -116 (t,  $^1J_{\text{P/P}} = 244$  Hz, 1 P), 1.10 (pseudo d,  $^1J_{\text{P/P}} = 260$  Hz, 2 P), 135 (t,  $^1J_{\text{P/P}} = 320$  Hz, 1 P), 251 ppm (m, 2 P).

### 1.9.24 Preparation of Ph<sub>2</sub>CP<sub>8</sub>(C<sub>7</sub>H<sub>8</sub>), 24

Ph<sub>2</sub>CP<sub>8</sub>Nb(OC[<sup>2</sup>Ad]Mes)<sub>3</sub> (360 mg, 0.266 mmol) was dissolved in 30 mL of THF. To this stirring solution was added spiro[2,4]hepta-4,6-diene (3.54 g of 14% stock solution). Pyridine-*N*-oxide (78

mg, 0.82 mmol) was then added as a solution in 15 mL of THF. After 5 minutes of stirring the solution became bright yellow in color. The mixture was allowed to stir an additional 45 minutes after which time the volatile components of the mixture were removed under reduced pressure resulting in a pale yellow residue. This residue was slurried in Et<sub>2</sub>O (10 mL), resulting in formation of an off-white precipitate. This precipitate was isolated on a frit, washed with Et<sub>2</sub>O (5 mL) and pentane (5 mL) and dried under reduced pressure resulting in 98 mg (73% yield of 85% pure material). <sup>1</sup>H NMR (20 °C, 500 MHz, C<sub>6</sub>D<sub>6</sub>): δ = -0.08 (s, 4 H), 2.04 (m, 4 H), 5.56 (m, 2 H), 6.91 (m, 6 H), 7.56 (d, <sup>1</sup>J<sub>H/H</sub> = 8 Hz, 4 H). <sup>31</sup>P{<sup>1</sup>H} NMR (20 °C, 202 MHz, C<sub>6</sub>D<sub>6</sub>): δ = -164 (t, <sup>1</sup>J<sub>P/P</sub> = 230 Hz, 2 P), -97 (t, <sup>1</sup>J<sub>P/P</sub> = 230 Hz, 1 P), 42 (m, 2 P), 47 (d, <sup>1</sup>J<sub>P/P</sub> = 284 Hz, 2 P), 51 ppm (t, <sup>1</sup>J<sub>P/P</sub> = 308 Hz, 1 P).

### 1.9.25 X-Ray Structure Determinations

Diffraction quality crystals of ONb(OC[<sup>2</sup>Ad]Mes)<sub>3</sub>(OEt<sub>2</sub>) were grown from Et<sub>2</sub>O/*n*-pentane at -35 °C. Crystals of H<sub>2</sub>PP<sub>7</sub>Nb(OC[<sup>2</sup>Ad]Mes)<sub>3</sub> were grown by slow evaporation of a benzene solution at 20 °C over 1 week. Crystals of Ph<sub>2</sub>CP<sub>8</sub>Nb(OC[<sup>2</sup>Ad]Mes)<sub>3</sub> were grown from slow cooling of a warm benzene solution over 2 days. Crystals of Ph<sub>2</sub>CP<sub>8</sub>(C<sub>6</sub>H<sub>8</sub>) were grown from toluene/hexane (3:1) at -35 °C for two days. All crystals were mounted in hydrocarbon oil on a nylon loop or a glass fiber. Low-temperature (100 K) data were collected on a Siemens Platform three-circle diffractometer coupled to a Bruker-AXS Smart Apex CCD detector with graphite-monochromated Mo Kα radiation (λ = 0.71073 Å) performing φ- and ω-scans. A semi-empirical absorption correction was applied to the diffraction data using SADABS.<sup>88</sup> All structures were solved by direct or Patterson methods using SHELXS<sup>89,90</sup> and refined against *F*<sup>2</sup> on all data by full-matrix least squares with SHELXL-97.<sup>90,91</sup> All non-hydrogen atoms were refined anisotropically. All hydrogen atoms were included in the model at geometrically calculated positions and refined using a riding model. The isotropic displacement parameters of all hydrogen atoms were fixed to 1.2 times the *U*<sub>eq</sub> value of the atoms they are linked to (1.5 times for methyl groups). In structures where disorders were present, the disorders were refined within SHELXL with the help of rigid bond restraints as well as similarity restraints on the anisotropic displacement parameters for neighboring atoms and on 1,2- and 1,3-distances throughout the disordered components.<sup>92</sup> The relative occupancies of disordered components were refined freely within SHELXL. Further details are provided in Tables 1.11 and 1.12, on Reciprocal Net,<sup>93</sup> and in the form of cif files available from the CCDC.<sup>94</sup>

### 1.9.26 Computational Studies

All calculations were carried out using ADF 2007.01 or ADF 2008.01 from Scientific Computing and Modeling (<http://www.scm.com>) on an eight or 32-processor Quantum Cube workstation from Parallel Quantum Solutions (<http://www.pqschem.com>).<sup>95,96</sup> In all cases, the LDA functional employed was that of Vosko, Wilk, and Nusair (VWN),<sup>97</sup> while the GGA part was handled using

the functionals of Baker and Pulay (OLYP).<sup>98</sup> In addition, all calculations were carried out using the zero-order regular approximation (ZORA) for relativistic effects.<sup>99–101</sup> For phosphorus, the basis sets were quadruple- $\zeta$  with four polarization functions (QZ4P) as supplied with ADF and frozen-core approximations were not made. In all other cases, the basis sets were triple- $\zeta$  with two polarization functions (TZ2P) as supplied with ADF and again, frozen-core approximations were not made. Chemical-shielding tensors were calculated for the <sup>31</sup>P nuclei in the optimized structures by the GIAO method using the ADF package.<sup>102–105</sup> The functionals, basis sets, and relativistic approximations used were the same as those described above. The isotropic value of the absolute chemical shielding was converted to a chemical shift downfield of 85% phosphoric acid using PH<sub>3</sub> or P<sub>4</sub> as a computational reference; its computed absolute shielding value was associated with a chemical shift equal to its experimental value in the gas phase.<sup>106,107</sup> Geometries were optimized to default convergence criteria and energies are uncorrected for zero-point energies.

**Table 1.3.** Optimized atomic coordinates of (MeO)<sub>3</sub>Nb=PP<sub>7</sub>Nb(OMe)<sub>3</sub>.

Atom	x	y	z	Atom	x	y	z
Nb	0.241870	0.097287	-0.005388	P	0.015636	-0.764135	4.734481
P	1.417012	-0.338198	3.123372	P	-1.915649	-0.676972	3.673566
P	0.465890	1.372100	2.250786	P	-1.606371	0.759626	2.080691
P	0.717538	-1.805116	1.718269	P	-1.414029	-1.527100	1.754732
P	0.195943	-2.561514	5.734907	O	-0.479265	1.725718	-0.661911
O	-0.603493	-1.185246	-1.118727	O	2.033197	0.182629	-0.498470
C	-1.162662	2.930182	-0.649924	C	3.408285	0.152219	-0.331631
C	-1.502020	-2.187945	-1.449927	H	-1.310032	3.259247	-1.675246
H	-2.134809	2.830967	-0.176820	H	-0.596240	3.692760	-0.123163
H	-1.580393	-2.244780	-2.531644	H	-1.161735	-3.149569	-1.078707
H	-2.486043	-1.991260	-1.037248	H	3.888775	0.194314	-1.303988
H	3.737376	1.002088	0.257734	H	3.711862	-0.760928	0.169224
Nb	0.171918	-0.702371	7.243373	O	-0.671220	1.022983	7.252487
O	-0.792287	-1.709015	8.522716	O	1.959487	-0.466814	7.776910
C	-1.252650	2.031928	6.498965	C	3.248920	-1.021639	7.906916
C	-1.587250	-2.817057	8.774452	H	-1.411701	2.897405	7.137725
H	-0.615021	2.335867	5.674088	H	-2.216225	1.731431	6.095264
H	3.724945	-0.596433	8.784967	H	3.205066	-2.098342	8.015195
H	3.842238	-0.777352	7.032517	H	-1.981563	-2.753953	9.784421
H	-2.421634	-2.868737	8.081587	H	-1.012618	-3.734612	8.683925

**Table 1.4.** Optimized atomic coordinates of Ph<sub>2</sub>CP<sub>8</sub>NbCl<sub>3</sub> (bisoradamantane type-structure).

Atom	x	y	z	Atom	x	y	z
P	-4.951360	-8.293899	-0.247892	P	-3.308021	-6.834959	-0.446275
P	-6.170242	-7.373319	1.399466	Nb	-6.544705	-7.148817	-1.918180
P	-4.559625	-6.566974	2.776815	P	-4.477621	-4.846870	-0.233819
P	-6.544208	-5.568587	0.132037	P	-2.653231	-7.059828	1.683605
Cl	-6.996907	-5.132252	-2.994580	C	-2.273596	-5.191148	2.001672
Cl	-4.990623	-7.848687	-3.491483	P	-4.087028	-4.513953	1.943081
Cl	-8.406452	-8.436659	-1.677225	C	-1.333276	-4.588723	0.964899
C	-1.709745	-4.990894	3.416678	C	-1.448959	-3.246951	0.571644

**Table 1.4.** Optimized atomic coordinates of Ph<sub>2</sub>CP<sub>8</sub>NbCl<sub>3</sub> (bisnoradamantane type-structure), continued.

C	-0.547187	-2.690631	-0.337810	C	0.485641	-3.465886	-0.868531
C	-0.859478	-5.945389	3.998051	C	-0.285092	-5.724684	5.250937
C	-0.546387	-4.543351	5.947104	C	0.610564	-4.802763	-0.485102
C	-0.289885	-5.357335	0.425200	C	-1.388269	-3.584904	5.380001
C	-1.963655	-3.805561	4.127799	H	-2.252352	-2.629109	0.977128
H	-0.655243	-1.647599	-0.632959	H	1.187062	-3.032362	-1.580396
H	-0.643009	-6.871699	3.464725	H	0.371129	-6.480380	5.681352
H	-0.096375	-4.370613	6.924446	H	1.409783	-5.419123	-0.894814
H	-0.180574	-6.403626	0.717526	H	-1.598458	-2.657432	5.911580
H	-2.616860	-3.045919	3.697843				

**Table 1.5.** Optimized atomic coordinates of Ph<sub>2</sub>CP<sub>8</sub>Nb(OC[<sup>i</sup>Pr]Mes)<sub>3</sub>.

Atom	x	y	z	Atom	x	y	z
Nb	0.046329	-0.034886	0.040051	P	0.103366	0.046456	2.600645
P	2.089768	0.112568	1.641900	P	-0.343999	2.113948	3.230243
P	2.732915	2.225333	1.791064	P	1.081834	2.333525	4.939716
P	3.107402	2.386283	3.990386	P	2.009377	4.273094	4.413002
P	0.781105	3.226230	1.699671	C	1.219257	4.774260	2.696926
C	2.218689	5.583790	1.856724	C	1.740465	6.385650	0.811601
C	2.611019	7.072653	-0.023069	C	3.985783	6.990470	0.170980
C	4.473871	6.222247	1.217992	C	3.601320	5.529937	2.051220
H	0.672993	6.477634	0.647837	H	2.208290	7.679098	-0.830604
H	4.668188	7.527339	-0.483339	H	5.544259	6.152149	1.394388
H	4.019765	4.941018	2.857949	C	-0.004422	5.643230	3.010739
C	0.158401	6.788013	3.801937	C	-0.911678	7.629810	4.076417
C	-2.171614	7.362643	3.551754	C	-2.345253	6.242109	2.751892
C	-1.274564	5.394334	2.486990	H	-1.441308	4.541097	1.843639
H	-3.317729	6.023366	2.317772	H	-3.007275	8.026922	3.756561
H	-0.755720	8.507905	4.697395	H	1.138244	7.035152	4.195560
O	-1.887437	-0.054626	0.081748	C	-3.140152	-0.200634	0.601260
O	0.531846	-1.797110	-0.404413	C	1.208669	-2.950410	-0.711191
O	0.437340	1.259366	-1.291774	C	0.493903	2.014525	-2.435993
C	1.731850	-2.991330	-2.107487	C	0.970443	-3.597613	-3.123388
C	1.442187	-3.566179	-4.434335	C	2.645215	-2.954649	-4.771326
C	3.403626	-2.402319	-3.744696	C	2.976521	-2.414423	-2.418480
H	0.845832	-4.029527	-5.216389	H	4.360504	-1.943619	-3.980492
C	3.866756	-1.844781	-1.351142	H	4.078993	-2.590117	-0.577813
H	3.403474	-0.998003	-0.845788	H	4.817243	-1.507975	-1.774175
C	-0.322645	-4.305405	-2.824486	H	-0.845271	-4.563459	-3.750397
H	-0.989450	-3.698560	-2.210789	H	-0.137756	-5.234258	-2.272261
C	3.096302	-2.865642	-6.201693	H	2.767397	-3.734199	-6.780372
H	4.186037	-2.800283	-6.273397	H	2.676747	-1.969550	-6.677129
C	-0.809763	2.135592	-3.151276	C	-1.606280	3.283890	-3.007480
C	-2.820761	3.356698	-3.690040	C	-3.273391	2.325251	-4.505143
C	-2.456253	1.209237	-4.653531	C	-1.232497	1.095004	-3.999951
H	-2.776429	0.399916	-5.305440	H	-3.429997	4.250085	-3.576787



**Table 1.5.** Optimized atomic coordinates of  $\text{Ph}_2\text{CP}_8\text{Nb}(\text{OC}^i\text{Pr})\text{Mes}_3$ , continued.

C	-1.163806	4.456026	-2.177324	H	-0.481809	5.097328	-2.750049
H	-0.630458	4.142371	-1.280700	H	-2.021273	5.067032	-1.880209
C	-0.388502	-0.122513	-4.239516	H	-0.511741	-0.862809	-3.445441
H	0.674221	0.125112	-4.283964	H	-0.668741	-0.607212	-5.179187
C	-4.611395	2.394466	-5.186044	H	-4.925725	3.429410	-5.349759
H	-5.378171	1.904464	-4.572099	H	-4.589986	1.887140	-6.155749
C	-3.429814	-1.590365	1.055677	C	-3.584017	-2.602801	0.085530
C	-3.728555	-3.922406	0.498201	C	-3.733994	-4.276668	1.846595
C	-3.646413	-3.258174	2.784550	C	-3.503210	-1.917428	2.419468
C	-3.635219	-2.271121	-1.380296	H	-2.681307	-1.888304	-1.745048
H	-4.378124	-1.489687	-1.574542	H	-3.899414	-3.153141	-1.970077
C	-3.472189	-0.887350	3.514428	H	-3.140514	0.086326	3.162445
H	-4.479599	-0.764088	3.935761	H	-2.811634	-1.204523	4.327312
H	-3.680041	-3.505946	3.843084	H	-3.835652	-4.699617	-0.254764
C	-3.867337	-5.712857	2.267524	H	-3.352542	-6.378449	1.567463
H	-4.922585	-6.012356	2.300086	H	-3.442298	-5.873654	3.262714
C	1.339369	-3.922161	0.210846	C	0.737483	-3.813621	1.581520
C	-4.026639	0.815967	0.603105	C	-5.449535	0.625130	1.039244
C	-3.671735	2.189417	0.119405	C	1.653627	2.548995	-2.864854
C	1.724154	3.361927	-4.124653	C	2.947944	2.390644	-2.125270
H	3.790390	2.378264	-2.827728	H	3.109066	3.233292	-1.442536
H	2.980344	1.478647	-1.533629	H	2.122870	4.362633	-3.908293
H	2.422622	2.893149	-4.832504	H	0.759840	3.468495	-4.622780
H	-4.267897	2.945663	0.644614	H	-2.617885	2.419597	0.263337
H	-3.881699	2.289985	-0.954008	H	-6.131556	0.986583	0.255839
H	-5.695309	-0.417151	1.249213	H	-5.663573	1.221275	1.937978
H	0.600708	-4.809497	2.016902	H	1.392816	-3.250872	2.256114
H	-0.232813	-3.317511	1.568402	C	2.133649	-5.162083	-0.070096
H	1.500374	-6.053312	0.040580	H	2.577606	-5.170190	-1.066743
H	2.940537	-5.259240	0.670320				

**Table 1.6.** Optimized atomic coordinates of  $\text{Ph}_2\text{CP}_8\text{Nb}(\text{OC}^i\text{Pr})\text{Mes}_3(\text{ONC}_5\text{H}_5)$ .

Atom	x	y	z	Atom	x	y	z
C	-3.336538	-1.994729	2.961204	C	-3.405899	-1.741637	1.577077
C	-3.677116	-2.820777	0.707269	C	-3.805048	-4.107331	1.216957
C	-3.688193	-4.380537	2.576441	C	-3.472932	-3.306175	3.426045
C	-3.202892	-0.361372	1.024940	C	-4.076859	0.652957	1.230837
C	-3.813019	2.059994	0.786729	C	-3.856299	-2.622907	-0.767263
C	-3.833663	-5.784430	3.090433	C	-3.165088	-0.918306	3.996525
O	-2.114637	-0.208928	0.221103	Nb	-0.190591	-0.084215	-0.193148
O	0.152391	1.438540	-1.322538	C	0.484312	2.148103	-2.453894
C	1.756047	2.494207	-2.749681	C	2.948662	2.051713	-1.967417
P	0.051764	0.055661	2.358363	P	-0.406763	2.103268	3.076900
P	0.704180	3.323447	1.615313	C	1.197942	4.780116	2.713462
C	0.015900	5.679121	3.092967	C	0.256068	6.812680	3.880705
C	-0.769408	7.688037	4.213015	C	-2.062191	7.466313	3.750894
C	-2.313590	6.355458	2.957936	C	-1.287236	5.472913	2.636265

**Table 1.6.** Optimized atomic coordinates of Ph<sub>2</sub>CP<sub>8</sub>Nb(OC[<sup>i</sup>Pr]Mes)<sub>3</sub>(ONC<sub>5</sub>H<sub>5</sub>), continued.

P	1.968355	0.184062	1.333569	P	2.631635	2.279677	1.607712
P	3.043475	2.279623	3.813860	P	1.988491	4.150250	4.386268
P	1.028654	2.198037	4.783209	O	0.426942	-1.854731	-0.382167
C	1.166522	-2.970994	-0.664593	C	1.348473	-3.926391	0.267990
C	2.188438	-5.137500	-0.009888	C	2.215026	5.607829	1.912020
C	1.752404	6.447087	0.889307	C	2.634905	7.166500	0.095809
C	4.006594	7.079335	0.310593	C	4.479017	6.270818	1.334515
C	3.593814	5.545169	2.125380	C	1.714575	-3.004214	-2.053307
C	0.945920	-3.552684	-3.095824	C	1.436277	-3.503271	-4.398521
C	2.668992	-2.932543	-4.701943	C	3.438179	-2.452070	-3.648476
C	2.991714	-2.485713	-2.327472	C	-0.371870	-4.223567	-2.825799
C	3.138917	-2.815653	-6.124200	C	3.907041	-2.023515	-1.229563
C	-0.660646	2.511406	-3.348980	C	-1.560979	3.536132	-2.997894
C	-2.631523	3.826497	-3.841883	C	-2.833995	3.148718	-5.040844
C	-1.898915	2.186955	-5.401574	C	-0.814485	1.855046	-4.587620
C	-1.355648	4.376033	-1.769610	C	-4.026337	3.445861	-5.906000
C	0.156410	0.817541	-5.082698	C	0.767277	-3.832603	1.646550
C	-5.402755	0.456168	1.907960	C	2.084965	3.396035	-3.906440
H	0.687233	6.544210	0.713630	H	2.244645	7.803768	-0.694130
H	4.698691	7.643411	-0.309672	H	5.546405	6.195435	1.525857
H	3.998999	4.923015	2.913765	H	-1.514683	4.627696	2.001525
H	-3.313614	6.172655	2.572856	H	-2.862746	8.159272	3.997968
H	-0.552519	8.557995	4.827166	H	1.263712	7.024141	4.221530
H	0.835380	-3.922714	-5.201773	H	4.420202	-2.035043	-3.855630
H	4.259532	-2.879345	-0.640635	H	3.410863	-1.349773	-0.532249
H	4.783693	-1.515171	-1.640427	H	-0.822970	-4.583220	-3.755356
H	-1.069792	-3.543824	-2.338787	H	-0.243644	-5.084048	-2.160096
H	2.776652	-3.648141	-6.735407	H	4.231103	-2.798914	-6.183992
H	2.766010	-1.885287	-6.571360	H	-2.020824	1.658931	-6.343639
H	-3.323966	4.615004	-3.553901	H	-0.573086	5.122420	-1.955999
H	-1.026502	3.789673	-0.914711	H	-2.271983	4.910331	-1.502164
H	0.316983	0.024737	-4.351643	H	1.132768	1.260831	-5.298141
H	-0.209787	0.365103	-6.009324	H	-4.045448	4.499105	-6.209627
H	-4.958574	3.242076	-5.365984	H	-4.025618	2.830891	-6.810243
H	-2.890064	-2.491413	-1.249392	H	-4.461290	-1.737440	-0.978527
H	-4.346165	-3.491527	-1.216784	H	-2.798208	0.013625	3.577045
H	-4.129510	-0.710600	4.479924	H	-2.470583	-1.244454	4.776619
H	-3.405712	-3.482536	4.496782	H	-4.006309	-4.922578	0.525836
H	-3.302196	-6.494307	2.447191	H	-4.889997	-6.082334	3.110589
H	-3.436963	-5.883210	4.104887	H	3.728438	1.690186	-2.652275
H	3.378699	2.888196	-1.403109	H	2.716869	1.257916	-1.266172
H	2.621933	4.280010	-3.533686	H	2.767306	2.894890	-4.606786
H	1.208565	3.739874	-4.456714	H	-3.976004	2.750708	1.626225
H	-2.796924	2.208445	0.429911	H	-4.510599	2.368525	-0.006198
H	-6.204882	0.859187	1.271597	H	-5.629063	-0.592117	2.106559
H	-5.453832	1.011576	2.855204	H	0.552228	-4.834216	2.037785
H	1.482002	-3.360810	2.333820	H	-0.153824	-3.254011	1.675445

**Table 1.6.** Optimized atomic coordinates of Ph<sub>2</sub>CP<sub>8</sub>Nb(OC[<sup>i</sup>Pr]Mes)<sub>3</sub>(ONC<sub>5</sub>H<sub>5</sub>), continued.

H	1.588115	-6.050478	0.110775	H	2.621520	-5.139693	-1.011508
H	3.003863	-5.203010	0.724502	O	-1.307249	-0.768208	-2.471803
N	-2.463291	-0.523658	-2.989625	C	-2.923210	-1.336006	-3.987199
C	-4.173368	-1.157902	-4.536016	C	-4.998596	-0.131674	-4.088150
C	-4.505686	0.704160	-3.096371	C	-3.248391	0.506386	-2.567927
H	-2.231430	-2.114335	-4.275631	H	-4.495470	-1.843655	-5.313791
H	-5.993104	0.010673	-4.499774	H	-5.093266	1.529602	-2.708168
H	-2.823901	1.123591	-1.798260				

**Table 1.7.** Optimized atomic coordinates of ONb(OC[<sup>i</sup>Pr]Mes)<sub>3</sub>(ONC<sub>5</sub>H<sub>5</sub>).

Atom	x	y	z	Atom	x	y	z
C	-0.439640	-3.552329	0.919035	N	0.670699	-4.074399	0.315225
C	0.721672	-5.422676	0.090261	C	-0.328502	-6.245021	0.432701
C	-1.472072	-5.721802	1.026815	C	-1.505087	-4.352609	1.269921
O	1.640392	-3.313641	-0.037224	Nb	2.068099	-2.566736	-2.815369
O	3.551784	-1.796183	-1.837865	C	4.745885	-1.154222	-2.043437
C	5.542273	-1.695502	-3.181512	C	6.278221	-2.884114	-2.995144
C	6.941371	-3.446697	-4.079723	C	6.904870	-2.867499	-5.348104
C	6.209924	-1.676367	-5.498561	C	5.525358	-1.076018	-4.439172
C	6.373860	-3.529518	-1.639525	C	7.592878	-3.526403	-6.510064
C	4.811972	0.223641	-4.689591	O	0.343698	-1.774517	-2.395404
C	-0.578708	-0.938189	-2.972851	C	-0.503090	0.398276	-2.831842
C	0.594332	1.059209	-2.048553	C	-1.699748	-1.655593	-3.656929
C	-2.788341	-2.108600	-2.882494	C	-3.796581	-2.851606	-3.486143
C	-3.775700	-3.150823	-4.847532	C	-2.727555	-2.646869	-5.601784
C	-1.687052	-1.903462	-5.038205	C	-2.913303	-1.756325	-1.424935
C	-0.607021	-1.401277	-5.955043	C	-4.868869	-3.971015	-5.472553
C	-1.498541	1.324621	-3.468071	O	2.319678	-2.046445	-4.412481
O	2.142479	-4.510525	-2.899183	C	2.215523	-5.605731	-3.713083
C	2.877439	-6.719647	-3.335913	C	2.895919	-7.953902	-4.192750
C	1.498974	-5.486392	-5.016645	C	2.206697	-5.131332	-6.180874
C	1.511595	-5.009769	-7.380938	C	0.141214	-5.236306	-7.469452
C	-0.531791	-5.610024	-6.313963	C	0.118982	-5.736518	-5.086970
C	3.684542	-4.864825	-6.166562	C	-0.575237	-5.084833	-8.781756
C	-0.680908	-6.130468	-3.876723	C	3.658985	-6.819517	-2.058769
C	5.143103	-0.161069	-1.224908	C	6.446142	0.557839	-1.424773
C	4.293832	0.310825	-0.078186	H	8.682528	-3.510583	-6.383432
H	7.284725	-4.574034	-6.600895	H	7.496115	-4.370940	-3.934499
H	7.000017	-4.425476	-1.676698	H	7.354578	-3.023574	-7.451726
H	6.807346	-2.833730	-0.911959	H	4.200432	-5.477103	-5.425582
H	4.120461	-5.067143	-7.149791	H	5.390411	-3.813535	-1.257028
H	3.883980	-3.818144	-5.918963	H	6.173601	-1.201662	-6.476405
H	-0.082552	-6.713009	-3.173255	H	2.062507	-4.727046	-8.275372
H	-0.192290	-5.797894	-9.522084	H	-1.552820	-6.724945	-4.167636
H	-1.050964	-5.243285	-3.352051	H	-1.599471	-5.803813	-6.357213
H	-1.649956	-5.256693	-8.673597	H	-0.432133	-4.077224	-9.189836
H	5.527773	1.056820	-4.678149	H	4.323961	0.210681	-5.668814

**Table 1.7.** Optimized atomic coordinates of ONb(OC[<sup>i</sup>Pr]Mes)<sub>3</sub>(ONC<sub>5</sub>H<sub>5</sub>), continued.

H	4.054150	0.427442	-3.934374	H	0.005085	-2.234428	-6.315239
H	0.055853	-0.690120	-5.466243	H	-5.104555	-4.845953	-4.856609
H	-4.581725	-4.325214	-6.466762	H	-1.951675	-1.802234	-0.915170
H	-2.697313	-2.845353	-6.669579	H	-4.624880	-3.205659	-2.876394
H	-1.057537	-0.912880	-6.827793	H	-3.608134	-2.434411	-0.921188
H	-5.789142	-3.382919	-5.580256	H	-3.297123	-0.733748	-1.314298
H	1.627343	-5.757199	-0.388205	H	-0.239223	-7.306110	0.217651
H	-2.310176	-6.359857	1.288793	H	-2.369975	-3.884194	1.730033
H	-0.396943	-2.481952	1.066926	H	4.692573	-7.130230	-2.270921
H	3.700376	-5.875795	-1.516784	H	3.239047	-7.592316	-1.396933
H	2.535919	-8.821912	-3.620475	H	2.276575	-7.856424	-5.085256
H	3.920944	-8.195549	-4.510151	H	-0.975294	2.087657	-4.061474
H	-2.201316	0.806293	-4.123400	H	-2.075427	1.863559	-2.702210
H	0.215553	1.962435	-1.551872	H	1.010270	0.400673	-1.285212
H	1.417673	1.379346	-2.703374	H	4.926358	0.642216	0.755085
H	3.676911	1.172278	-0.372753	H	3.625369	-0.473443	0.283341
H	7.052418	0.517717	-0.508741	H	7.036693	0.141077	-2.242838
H	6.270537	1.623100	-1.636934				

**Table 1.8.** Optimized atomic coordinates of Ph<sub>2</sub>CP<sub>8</sub>ONb(OC[<sup>i</sup>Pr]Mes)<sub>3</sub> (metallacycle).

Atom	x	y	z	Atom	x	y	z
Nb	-0.117280	0.120239	-0.081958	P	0.149408	0.169503	2.547880
P	2.259841	0.322645	1.909985	O	1.821882	0.279210	0.324649
P	-0.355557	2.083810	3.440096	P	2.822506	2.421189	2.394741
P	0.936049	3.523022	2.387206	P	0.877126	1.832667	5.270430
P	2.994502	1.981849	4.556177	P	1.931494	3.750026	5.343953
C	1.387869	4.716781	3.771239	C	2.557636	5.555167	3.240416
C	2.314501	6.463758	2.203545	C	3.349523	7.189080	1.631466
C	4.654068	7.036247	2.090555	C	4.905144	6.162905	3.138531
C	3.867027	5.434157	3.709479	H	1.301661	6.598385	1.840269
H	3.134052	7.876400	0.817813	H	5.467273	7.595639	1.635797
H	5.915698	6.034330	3.518431	H	4.099959	4.756691	4.522714
C	0.226535	5.620559	4.187862	C	-1.088467	5.410856	3.771916
C	-2.114838	6.258893	4.169571	C	-1.849011	7.338858	4.999940
C	-0.543654	7.560166	5.426510	C	0.481675	6.715653	5.022020
H	-1.330343	4.585536	3.117457	H	-3.126533	6.068865	3.819182
H	-2.650002	8.006840	5.305721	H	-0.317568	8.405213	6.071214
H	1.497659	6.920999	5.341538	O	-0.189946	1.781781	-0.937144
C	-0.198686	2.927286	-1.691191	C	0.941845	3.571055	-2.004779
C	0.924349	4.831477	-2.817025	H	-0.073608	5.104393	-3.161388
H	1.337075	5.663642	-2.230090	H	1.574643	4.717041	-3.695086
C	2.297895	3.112135	-1.566419	H	2.715076	3.815699	-0.833672
H	2.987847	3.101391	-2.421359	H	2.290779	2.125482	-1.113692
C	-1.584902	3.311222	-2.069357	C	-2.277050	4.313367	-1.369111
C	-3.621920	4.532771	-1.665128	C	-4.297838	3.792419	-2.627312
C	-3.579199	2.836291	-3.338738	C	-2.237063	2.580782	-3.079505
C	-1.613877	5.168490	-0.328336	H	-2.343991	5.529408	0.401222

**Table 1.8.** Optimized atomic coordinates of Ph<sub>2</sub>CP<sub>8</sub>ONb(OC[<sup>t</sup>Pr]Mes)<sub>3</sub> (metallacycle), continued.

H	-1.148669	6.048839	-0.790726	H	-0.830960	4.631074	0.203304
H	-4.156516	5.300137	-1.110889	C	-5.766668	3.984835	-2.869805
H	-6.005751	3.915674	-3.935797	H	-6.341091	3.207754	-2.348933
H	-6.109438	4.956579	-2.503656	H	-4.079288	2.260964	-4.114236
C	-1.520568	1.528216	-3.874106	H	-0.461783	1.762038	-3.998790
H	-1.579246	0.552459	-3.384527	H	-1.968014	1.420642	-4.866594
O	0.266273	-1.448307	-1.095090	C	0.934590	-2.311235	-1.920014
C	1.287751	-3.540017	-1.498004	C	1.015003	-4.019194	-0.102715
H	0.118038	-3.569805	0.322513	H	0.883507	-5.107432	-0.091843
H	1.861274	-3.788436	0.559749	C	1.993132	-4.506246	-2.404028
H	1.376278	-5.405395	-2.547584	H	2.216324	-4.085717	-3.386116
H	2.934375	-4.842967	-1.947465	C	3.467297	-0.951170	-2.551397
H	4.227003	-0.236577	-2.880276	H	3.957228	-1.924280	-2.419190
H	3.102778	-0.640305	-1.572857	C	1.178709	-1.768065	-3.288635
C	2.361974	-1.058732	-3.564491	C	2.530741	-0.495062	-4.828500
C	1.573021	-0.622929	-5.830641	C	0.437565	-1.375847	-5.552305
C	0.221976	-1.953891	-4.301940	C	-0.999482	-2.805006	-4.090996
H	-0.754681	-3.863202	-4.252729	H	-1.789327	-2.535568	-4.798719
H	-1.395208	-2.721545	-3.079563	H	-0.310453	-1.514793	-6.329146
H	3.441368	0.062090	-5.033895	C	1.744656	0.056523	-7.159272
H	1.256721	-0.505284	-7.961966	H	1.297071	1.058809	-7.135153
H	2.801916	0.171299	-7.417285	O	-1.948922	-0.265649	0.339944
C	-3.028264	-0.752315	1.020268	C	-3.911549	0.072599	1.620307
C	-3.759793	1.561927	1.629810	H	-2.778975	1.891091	1.301222
H	-3.939769	1.958031	2.636996	H	-4.503720	2.019018	0.960855
C	-5.147430	-0.449174	2.292179	H	-5.306836	-1.515345	2.125310
H	-5.101179	-0.268412	3.375467	H	-6.029417	0.092769	1.923284
C	-3.176858	-2.235732	0.922930	C	-3.589849	-2.779535	-0.312438
C	-3.679839	-4.159526	-0.453796	C	-3.383589	-5.029344	0.594666
C	-3.023887	-4.472909	1.813512	C	-2.919280	-3.092522	2.006130
C	-2.579581	-2.603408	3.386804	H	-2.292358	-1.555353	3.402655
H	-3.446755	-2.727848	4.049854	H	-1.756505	-3.187557	3.812153
H	-2.812702	-5.129632	2.654550	C	-3.492951	-6.517270	0.418006
H	-4.525306	-6.851303	0.583648	H	-2.851624	-7.050216	1.126362
H	-3.204044	-6.817961	-0.594119	H	-3.993421	-4.569647	-1.410721
C	-3.977624	-1.888728	-1.459093	H	-4.382196	-2.475152	-2.288389
H	-3.127944	-1.314437	-1.830490	H	-4.735573	-1.162369	-1.145254

**Table 1.9.** Optimized atomic coordinates of Ph<sub>2</sub>CP<sub>8</sub>(C<sub>6</sub>H<sub>8</sub>).

Atom	x	y	z	Atom	x	y	z
H	3.495100	2.779720	-3.952985	H	3.269185	0.301394	-3.905796
C	3.085385	2.281630	-3.078178	C	2.956395	0.896860	-3.051647
H	-2.799046	-0.671970	-2.658016	H	2.794313	4.099668	-1.966129
H	-4.144152	1.299215	-2.103206	H	-6.076343	-0.131003	-1.840029
C	2.691820	3.017614	-1.970130	C	2.431024	0.262574	-1.935256
H	2.355773	-0.818859	-1.930003	C	-3.374730	-0.674020	-1.735104
C	-4.117986	0.539961	-1.313120	C	-5.558138	0.151345	-0.914869

**Table 1.9.** Optimized atomic coordinates of Ph<sub>2</sub>CP<sub>8</sub>(C<sub>6</sub>H<sub>8</sub>), continued.

H	-2.864277	-2.651935	-1.122221	C	-3.408297	-1.733574	-0.911163
H	-6.084004	1.020790	-0.502782	C	2.157248	2.381519	-0.853280
C	2.002896	0.995080	-0.819184	H	-6.170997	-1.855269	-0.350447
P	-1.235559	1.729610	-0.356608	C	-5.582146	-1.033174	0.075582
P	-0.356707	-0.300663	-0.261369	H	1.857881	2.990174	-0.008445
H	0.985246	-2.531817	0.038623	P	-3.350879	1.418072	0.210050
C	-4.165548	-1.588617	0.356915	H	2.537911	-4.331867	0.593318
C	1.357987	0.240535	0.356325	C	1.932563	-2.275581	0.497351
H	-6.066277	-0.747832	1.017297	H	-4.245630	-2.537889	0.899095
C	2.818487	-3.303666	0.808243	C	2.262535	-0.939995	0.737528
C	4.052357	-3.021373	1.377536	H	4.743897	-3.823927	1.620778
C	3.521823	-0.671151	1.289502	H	3.828173	0.355317	1.456721
C	4.398251	-1.696273	1.618563	P	-3.336093	-0.367243	1.586802
P	-1.205044	-1.001674	1.664159	P	-0.658403	2.503029	1.649705
H	5.363640	-1.453355	2.055188	P	1.230043	1.370165	1.935318
P	-0.597284	0.688286	2.980815				

**Table 1.10.** Optimized atomic coordinates of Ph<sub>2</sub>CP<sub>8</sub> (diphosphone).

Atom	x	y	z	Atom	x	y	z
P	0.000686	-0.023773	-0.003277	P	-0.008080	-0.009467	2.047628
P	2.138867	0.011141	-0.660928	P	2.124462	0.043908	2.730365
P	2.701300	2.124355	-0.095187	P	2.670937	2.145259	2.132525
P	4.565523	1.713505	1.039932	C	4.729807	-0.234927	1.044121
P	3.024276	-1.060008	1.051106	C	5.488240	-0.708373	2.295888
C	6.060386	-1.987254	2.311373	C	6.713504	-2.467062	3.438592
C	6.826339	-1.677662	4.577354	C	6.279765	-0.402606	4.571620
C	5.619014	0.074918	3.444852	H	5.208962	1.076970	3.477142
H	6.365926	0.234783	5.447969	H	7.342791	-2.051052	5.457705
H	7.140257	-3.466599	3.423163	H	6.004869	-2.617345	1.431775
C	5.537919	-0.587114	-0.216405	C	5.205426	-1.647557	-1.063648
C	5.972482	-1.942575	-2.186213	C	7.090872	-1.180751	-2.493295
C	7.451730	-0.138885	-1.647053	C	6.695511	0.143536	-0.517677
H	7.018143	0.944494	0.137455	H	8.332469	0.460376	-1.863382
H	7.683592	-1.402672	-3.377095	H	5.689653	-2.779133	-2.820028
H	4.347481	-2.272660	-0.846743				

**Table 1.11.** Crystallographic data for ONb(OC[<sup>2</sup>Ad]Mes)<sub>3</sub>(Et<sub>2</sub>O) and H<sub>2</sub>PP<sub>7</sub>Nb(OC[<sup>2</sup>Ad]Mes)<sub>3</sub>.

	ONb(OC[ <sup>2</sup> Ad]Mes) <sub>3</sub> (OEt <sub>2</sub> )	H <sub>2</sub> PP <sub>7</sub> Nb(OC[ <sup>2</sup> Ad]Mes) <sub>3</sub>
Empirical formula	C <sub>67</sub> H <sub>92.50</sub> NbO <sub>5.75</sub>	C <sub>66</sub> H <sub>81</sub> NbO <sub>3</sub> P <sub>8</sub>
Formula weight (g mol <sup>-1</sup> )	1082.82	1262.98
Temperature (K)	100(2)	100(2)
Wavelength (Å)	0.71073	0.71073
Crystal system	Triclinic	Rhombohedral
Space group	<i>P</i> $\bar{1}$	<i>R</i> $\bar{3}$
Unit cell dimensions (Å, °)	<i>a</i> = 12.592(3), $\alpha$ = 73.720(4) <i>b</i> = 14.592(3), $\beta$ = 78.872(4) <i>c</i> = 17.436(4), $\gamma$ = 80.224(4)	<i>a</i> = 17.393(4), $\alpha$ = 90 <i>b</i> = 17.393(4), $\beta$ = 90 <i>c</i> = 35.036(17), $\gamma$ = 120
Volume (Å <sup>3</sup> )	2983.1(12)	9179(5)
<i>Z</i>	2	6
Density (calculated) (Mg m <sup>-3</sup> )	1.206	1.371
Absorption coefficient (mm <sup>-1</sup> )	0.251	0.452
<i>F</i> (000)	1163	3972
Crystal size (mm <sup>3</sup> )	0.10 × 0.05 × 0.02	0.10 × 0.10 × 0.05
Theta range for collection (°)	1.66 to 23.36	1.74 to 27.63
Index ranges	-14 ≤ <i>h</i> ≤ 14, -16 ≤ <i>k</i> ≤ 16, -19 ≤ <i>l</i> ≤ 19	-22 ≤ <i>h</i> ≤ 22, -22 ≤ <i>k</i> ≤ 22, -45 ≤ <i>l</i> ≤ 45
Reflections collected	41641	56962
Independent reflections	8618 [R(int) = 0.1004]	4745 [R(int) = 0.1067]
Completeness to $\theta_{\max}$ (%)	99.3	100.0
Absorption correction	Semi-empirical from equivalents	Semi-empirical from equivalents
Max. and min. transmission	0.9950 and 0.9753	0.9777 and 0.9562
Refinement method	Full-matrix least-squares on <i>F</i> <sup>2</sup>	Full-matrix least-squares on <i>F</i> <sup>2</sup>
Data / restraints / parameters	8616 / 875 / 748	4745 / 489 / 376
Goodness-of-fit <sup>a</sup>	1.042	1.026
Final <i>R</i> indices [ <i>I</i> > 2 $\sigma$ ( <i>I</i> ) <sup>b</sup> [ <i>I</i> > 2 $\sigma$ ( <i>I</i> )]	<i>R</i> <sub>1</sub> = 0.0594, <i>wR</i> <sub>2</sub> = 0.1596	<i>R</i> <sub>1</sub> = 0.0602, <i>wR</i> <sub>2</sub> = 0.1437
<i>R</i> indices (all data) <sup>b</sup>	<i>R</i> <sub>1</sub> = 0.0934, <i>wR</i> <sub>2</sub> = 0.1830	<i>R</i> <sub>1</sub> = 0.0910, <i>wR</i> <sub>2</sub> = 0.1623
Largest diff. peak and hole (e Å <sup>-3</sup> )	0.912 and -0.772	0.590 and -0.841

*a*

$$\text{Goof} = \left[ \frac{\sum [w(F_o^2 - F_c^2)^2]}{(n-p)} \right]^{\frac{1}{2}}$$

*b*

$$R_1 = \frac{\sum ||F_o| - |F_c||}{\sum |F_o|}; wR_2 = \left[ \frac{\sum [w(F_o^2 - F_c^2)^2]}{\sum [w(F_o^2)^2]} \right]^{\frac{1}{2}}; w = \frac{1}{\sigma^2(F_o^2) + (aP)^2 + bP}; P = \frac{2F_c^2 + \max(F_o^2, 0)}{3}$$

**Table 1.12.** Crystallographic data for  $\text{Ph}_2\text{CP}_8\text{Nb}(\text{OC}[\text{}^2\text{Ad}]\text{Mes})_3$  and  $\text{Ph}_2\text{CP}_8(\text{C}_6\text{H}_8)$ .

	$\text{Ph}_2\text{CP}_8\text{Nb}(\text{OC}[\text{}^2\text{Ad}]\text{Mes})_3$	$\text{Ph}_2\text{CP}_8(\text{C}_6\text{H}_8)$
Empirical formula	$\text{C}_{73}\text{H}_{85}\text{NbO}_3\text{P}_8$	$\text{C}_{19}\text{H}_{18}\text{P}_8$
Formula weight ( $\text{g mol}^{-1}$ )	1351.08	494.09
Temperature (K)	100(2)	100(2)
Wavelength ( $\text{\AA}$ )	0.71073	1.54178
Crystal system	Triclinic	Triclinic
Space group	$P\bar{1}$	$P\bar{1}$
Unit cell dimensions ( $\text{\AA}$ , $^\circ$ )	$a = 12.7948(7)$ , $\alpha = 94.990(1)$ $b = 15.1999(8)$ , $\beta = 96.670(1)$ $c = 18.6193(10)$ , $\gamma = 110.899(1)$	$a = 8.2378(2)$ , $\alpha = 71.266(1)$ $b = 11.4022(2)$ , $\beta = 83.684(1)$ $c = 12.4717(3)$ , $\gamma = 74.020(1)$
Volume ( $\text{\AA}^3$ )	3327.6(3)	1066.22(4)
Z	2	2
Density (calculated) ( $\text{Mg m}^{-3}$ )	1.348	1.539
Absorption coefficient ( $\text{mm}^{-1}$ )	0.421	6.145
$F(000)$	1416	504
Crystal size ( $\text{mm}^3$ )	$0.20 \times 0.11 \times 0.03$	$0.25 \times 0.10 \times 0.05$
Theta range for collection ( $^\circ$ )	1.70 to 29.57	3.74 to 68.24
Index ranges	$-17 \leq h \leq 17$ , $-21 \leq k \leq 21$ , $-25 \leq l \leq 25$	$-9 \leq h \leq 9$ , $-13 \leq k \leq 13$ , $-15 \leq l \leq 14$
Reflections collected	74449	22396
Independent reflections	18607 [R(int) = 0.0786]	3883 [R(int) = 0.0194]
Completeness to $\theta_{\text{max}}$ (%)	99.7	99.5
Absorption correction	Semi-empirical from equivalents	Semi-empirical from equivalents
Max. and min. transmission	0.9875 and 0.9206	0.7487 and 0.3088
Refinement method	Full-matrix least-squares on $F^2$	Full-matrix least-squares on $F^2$
Data / restraints / parameters	18607 / 0 / 775	3883 / 32 / 244
Goodness-of-fit <sup>a</sup>	1.074	1.081
Final R indices [ $I > 2\sigma(I)$ ] <sup>b</sup>	$R_1 = 0.0569$ , $wR_2 = 0.0933$	$R_1 = 0.0276$ , $wR_2 = 0.0716$
R indices (all data) <sup>b</sup>	$R_1 = 0.0908$ , $wR_2 = 0.1034$	$R_1 = 0.0286$ , $wR_2 = 0.0722$
Largest diff. peak and hole ( $\text{e \AA}^{-3}$ )	0.464 and $-0.638$	0.404 and $-0.225$

a

$$\text{Goof} = \left[ \frac{\sum[w(F_o^2 - F_c^2)^2]}{(n-p)} \right]^{\frac{1}{2}}$$

b

$$R_1 = \frac{\sum||F_o| - |F_c||}{\sum|F_o|}; wR_2 = \left[ \frac{\sum[w(F_o^2 - F_c^2)^2]}{\sum[w(F_o^2)^2]} \right]^{\frac{1}{2}}; w = \frac{1}{\sigma^2(F_o^2) + (aP)^2 + bP}; P = \frac{2F_c^2 + \max(F_o^2, 0)}{3}$$



## 1.10 REFERENCES

- [1] Filippelli, G. *Elements* **2008**, 4, 89–95.
- [2] Oelkers, E.; Valsami-Jones, E. *Elements* **2008**, 4, 83–87.
- [3] Emsley, J. *The 13th Element: The Sordid Tale of Murder, Fire, and Phosphorus*; John Wiley & Sons, Inc.: New York, 2000.
- [4] Corbridge, D. *Phosphorus: An Outline of its Chemistry, Biochemistry, and Technology*, 5th ed.; Elsevier: New York, 1994.
- [5] Engel, R. *Synthesis of Carbon Phosphorus Bonds*, 2nd ed.; CRC Press: Boca Raton, 2004.
- [6] Quin, L. D. *A Guide to Organophosphorus Chemistry*; John Wiley & Sons, Inc.: New York, 2000; pp 314–317.
- [7] Cummins, C. *Prog. Inorg. Chem.* **1998**, 47, 685–847.
- [8] Dillon, K.; Mathey, F.; Nixon, J. *Phosphorus: The Carbon Copy: From Organophosphorus to Phospha-organic Chemistry*, 1st ed.; Wiley: West Sussex, 1998.
- [9] Hulley, E. B.; Wolczanski, P. T.; Lobkovsky, E. B. *Chem. Commun.* **2009**, 42, 6412–6414.
- [10] Scherer, O. J.; Swarowsky, H.; Wolmershäuser, G.; Kaim, W.; Kohlmann, S. *Angew. Chem., Int. Ed. Engl.* **1987**, 26, 1153–1155.
- [11] Scherer, O.; Werner, B.; Heckmann, G.; Wolmershäuser, G. *Angew. Chem., Int. Ed.* **1991**, 30, 553–555.
- [12] Scherer, O. J.; Schwalb, J.; Swarowsky, H.; Wolmershäuser, G.; Kaim, W.; Gross, R. *Chem. Ber.* **1988**, 121, 443–449.
- [13] Konchenko, S.; Pushkarevsky, N.; Gamer, M.; Koppe, R.; Schnockel, H.; Roesky, P. *J. Am. Chem. Soc.* **2009**, 131, 5740–5741.
- [14] Urnezzius, E.; Brennessel, W. W.; Cramer, C. J.; Ellis, J. E.; Schleyer, P. v. R. *Science* **2002**, 295, 832–834.
- [15] Scherer, O. J.; Sitzmann, H.; Wolmershäuser, G. *Angew. Chem., Int. Ed. Engl.* **1985**, 24, 351–353.
- [16] Herberhold, M.; Frohmader, G.; Milius, W. *Phosphorus, Sulfur Silicon Relat. Elem.* **1994**, 93, 205–208.
- [17] Reddy, A. C.; Jemmis, E. D.; Scherer, O. J.; Winter, R.; Heckmann, G.; Wolmershäuser, G. *Organometallics* **1992**, 11, 3894–3900.
- [18] Scherer, O. J.; Vondung, J.; Wolmershäuser, G. *Angew. Chem., Int. Ed. Engl.* **1989**, 28, 1355–1357.
- [19] Ehses, M.; Romerosa, A.; Peruzzini, M. *Metal-mediated degradation and reaggregation of white phosphorus*; Topics In Current Chemistry, Vol. 220; Springer: Berlin, 2002; pp 107–140.
- [20] Baudler, M. *Angew. Chem. Int. Ed.* **1987**, 26, 419–441.
- [21] Baudler, M.; Glinka, K. *Chem. Rev.* **1993**, 93, 1623–1667.
- [22] Ahlrichs, R.; Fenske, D.; Fromm, K.; Krautscheid, H.; Krautscheid, U.; Treutler, O. *Chem. Eur. J.* **1996**, 2, 238–244.
- [23] Charles, S.; Eichhorn, B. W.; Rheingold, A. L.; Bott, S. G. *J. Am. Chem. Soc.* **1994**, 116, 8077–8086.
- [24] Charles, S.; Fettingner, J. C.; Eichhorn, B. W. *Inorg. Chem.* **1996**, 35, 1540–1548.
- [25] Charles, S.; Danis, J. A. F.; Fettingner, J. C.; Eichhorn, B. W. *Inorg. Chem.* **1997**, 36, 3772–3778.
- [26] Figueroa, J. S.; Cummins, C. C. *J. Am. Chem. Soc.* **2003**, 125, 4020–4021.
- [27] Piro, N. A.; Figueroa, J. S.; McKellar, J. T.; Cummins, C. C. *Science* **2006**, 313, 1276–1279.
- [28] Piro, N. A.; Cummins, C. C. *Inorg. Chem.* **2007**, 46, 7387–7393.
- [29] Piro, N. A.; Cummins, C. C. *Angew. Chem., Int. Ed.* **2008**, 48, 934–938.
- [30] Bradley, D. C.; Mehrotra, R.; Rothwell, I.; Singh, A. *Alkoxo and Aryloxo Derivatives of Metals*; Academic Press: San Diego, 2001.
- [31] Rothwell, I. P. *Acc. Chem. Res.* **1988**, 21, 153–159.
- [32] Chamberlain, L. R.; Rothwell, A. P.; Rothwell, I. P. *J. Am. Chem. Soc.* **1984**, 106, 1847–1848.
- [33] Chamberlain, L. R.; Rothwell, I. P. *J. Am. Chem. Soc.* **1982**, 104, 7338–7340.

- [34] Chamberlain, L. R.; Rothwell, I. P.; Huffman, J. C. *J. Am. Chem. Soc.* **1986**, *108*, 1502–1509.
- [35] Laplaza, C. E.; Cummins, C. C. *Science* **1995**, *268*, 861–863.
- [36] Cummins, C. C. In *Progress In Inorganic Chemistry, Vol 47*; Progress In Inorganic Chemistry, Vol. 47, 1998; pp 685–836.
- [37] Cummins, C. C. *Angew. Chem., Int. Ed.* **2006**, *45*, 862–870.
- [38] Soo, H. S.; Diaconescu, P. L.; Cummins, C. C. *Organometallics* **2004**, *23*, 498–503.
- [39] Soo, H. S.; Figueroa, J. S.; Cummins, C. C. *J. Am. Chem. Soc.* **2004**, *126*, 11370–11376.
- [40] Figueroa, J. S.; Cummins, C. C. *J. Am. Chem. Soc.* **2004**, *126*, 13916–13917.
- [41] Piro, N. A.; Ph.D. thesis; Massachusetts Institute of Technology; 2009.
- [42] Soo, H. S.; Master's thesis; Massachusetts Institute of Technology; 2003.
- [43] Agapie, T.; Diaconescu, P. L.; Cummins, C. C. *J. Am. Chem. Soc.* **2002**, *124*, 2412–2413.
- [44] Kim, E.; Odom, A. L.; Cummins, C. C. *Inorg. Chim. Acta.* **1998**, *278*, 103–107.
- [45] Peters, J. C.; Johnson, A. R.; Odom, A. L.; Wanandi, P. W.; Davis, W. M.; Cummins, C. C. *J. Am. Chem. Soc.* **1996**, *118*, 10175–10188.
- [46] Agapie, T.; Diaconescu, P. L.; Mindiola, D. J.; Cummins, C. C. *Organometallics* **2002**, *21*, 1329–1340.
- [47] Chadeayne, A. R.; Wolczanski, P. T.; Lobkovsky, E. B. *Inorg. Chem.* **2004**, *43*, 3421–3432.
- [48] Figueroa, J. S.; Cummins, C. C. *Angew. Chem., Int. Ed.* **2004**, *43*, 984–988.
- [49] Ting Kwok Chan, W.; Garcia, F.; Hopkins, A. D.; Martin, L. C.; McPartlin, M.; Wright, D. S. *Angew. Chem. Int. Ed.* **2007**, *46*, 3084–3086.
- [50] Mathey, F.; Marinetti, A. *J. Am. Chem. Soc.* **1982**, *104*, 4484.
- [51] Mathey, F. *Dalton Trans.* **2007**, 1861–1868.
- [52] Le Floch, P.; Marinetti, A.; Ricard, L.; Mathey, F. *J. Am. Chem. Soc.* **1990**, *112*, 2407–2410.
- [53] Marinetti, A.; Ricard, L.; Mathey, F. *Organometallics* **1990**, *9*, 788–793.
- [54] Shah, S.; Protasiewicz, J. D. *Chem. Commun.* **1998**, 1585–1586.
- [55] Cummins, C. C.; Schrock, R. R.; Davis, W. M. *Angew. Chem., Int. Ed. Engl.* **1993**, *32*, 756–759.
- [56] Peruzzini, M.; Gonsalvi, L.; Romerosa, A. *Chem. Soc. Rev.* **2005**, *34*, 1038–1047.
- [57] Barbaro, P.; Peruzzini, M.; Ramirez, J. A.; Vizza, F. *Organometallics* **1999**, *18*, 4237–4240.
- [58] Masuda, J.; Schoeller, W. W.; Donnadiou, B.; Bertrand, G. *Angew. Chem., Int. Ed.* **2007**, *46*, 7052–7055.
- [59] Peruzzini, M.; Abdreimova, R. R.; Budnikova, Y.; Romerosa, A.; Scherer, O. J.; Sitzmann, H. *J. Organomet. Chem.* **2004**, *689*, 4319–4331.
- [60] Barbaro, P.; Ienco, A.; Mealli, C.; Peruzzini, M.; Scherer, O. J.; Schmitt, G.; Vizza, F.; Wolmershäuser, G. *Chem. Eur. J.* **2003**, *9*, 5195–5210.
- [61] Scherer, O. J.; Ehses, M.; Wolmershäuser, G. *Angew. Chem., Int. Ed.* **1998**, *37*, 507–510.
- [62] Ginsberg, A.; Lindsell, W. *J. Am. Chem. Soc.* **1971**, *93*, 2082–2084.
- [63] Yakhvarov, D.; Babaro, P.; Gonsalvi, L.; Carpio, S. M.; Midollini, S.; Orlandini, A.; Peruzzini, M.; Sinyashin, O.; Zanobini, F. *Angew. Chem., Int. Ed.* **2006**, *45*, 4182–4185.
- [64] Scherer, O. J. *Acc. Chem. Res.* **1999**, *32*, 751–762.
- [65] Figueroa, J. S.; Cummins, C. C. *Dalton Trans.* **2006**, 2161–2168.
- [66] Schrock, R. R. *J. Am. Chem. Soc.* **1976**, *98*, 5399–5400.
- [67] Regitz, M.; Scherer, O. J. *Multiple Bonds and Low Coordination in Phosphorus Chemistry*; Thieme: Stuttgart, 1990.
- [68] Appel, R.; Knoll, F.; I., R. *Angew. Chem., Int. Ed. Engl.* **1981**, *20*, 731–744.
- [69] Verkade, J. G.; Quin, L. D. *Phosphorus-31 NMR Spectroscopy in Spectrochemical Analysis*; Methods in Spectrochemical Analysis, Vol. 8; VCH Publishers, Inc.: Deerfield Beach, 1987.
- [70] Masuda, J. D.; Schoeller, W. W.; Donnadiou, B.; Bertrand, G. *J. Am. Chem. Soc.* **2007**, *129*, 14180–14181.
- [71] Phillips, I. G.; Ball, R.; Cavell, R. G. *Inorg. Chem.* **1992**, *31*, 1633–1641.

- [72] Vizi-Orosz, A.; Páalyi, G.; Markó, L. *J. Organomet. Chem.* **1973**, *60*, C25–C26.
- [73] Goh, L. Y.; Chu, C. K.; Wong, R. C. S.; Hambley, T. W. *J. Chem. Soc., Dalton Trans.* **1989**, 1951–1956.
- [74] Anslyn, E. V.; Dougherty, D. A. *Modern Physical Organic Chemistry*; University Science Books: Sausalito, 2006.
- [75] Bear, B. R.; Sparks, S. M.; Shea, K. J. *Angew. Chem. Int. Ed.* **2001**, *40*, 821–849.
- [76] Jaffe, H. H. *Chem. Rev.* **1953**, *51*, 191–261.
- [77] Ritchie, C. D.; Sager, W. F. In *Prog. Phys. Org. Chem.*; Interscience: New York; p 323.
- [78] Fenske, D.; Merzweiler, K. *Angew. Chem. Int. Ed.* **1986**, *25*, 338–339.
- [79] Huy, N.; Inubushi, Y.; Ricard, L.; Mathey, F. *Organometallics* **1997**, *16*, 2506–2508.
- [80] Huttner, G.; Borm, J.; Zsolnai, L. *J. Organomet. Chem.* **1986**, *304*, 309–321.
- [81] Amor, F.; Royo, P.; Spaniol, T. P.; Okuda, J. *J. Organomet. Chem.* **2000**, *604*, 126–131.
- [82] Carroll, R. L.; Carter, R. P. *Inorg. Chem.* **1967**, *6*, 401–403.
- [83] Pangborn, A. B.; Giardello, M. A.; Grubbs, R. H.; Rosen, R. K.; Timmers, F. J. *Organometallics* **1996**, *15*, 1518–1520.
- [84] Gibson, V. C.; Kee, T. P.; Shaw, A. *Polyhedron* **1988**, *7*, 2217–2219.
- [85] Hartung, J. B.; Pedersen, S. F. *Organometallics* **1990**, *9*, 1414–1417.
- [86] Enquist, P. A.; Nilsson, P.; Larhed, M. *Org. Lett.* **2003**, *5*, 4875–4878.
- [87] Williams, T.; Kelley, C.; *Gnuplot*; 2002. <http://www.gnuplot.info>.
- [88] Sheldrick, G. M.; (*SHELXTL*); 2005–2008.
- [89] Sheldrick, G. M. *Acta Crystallogr., Sect. A: Fundam. Crystallogr.* **1990**, *46*, 467–473.
- [90] Sheldrick, G. M. *Acta Crystallogr., Sect. A: Fundam. Crystallogr.* **2008**, *64*, 112–122.
- [91] Sheldrick, G. M.; (*SHELXL*)-97: *Program for crystal structure determination*; 1997.
- [92] Müller, P.; Herbst-Irmer, R.; Spek, A. L.; Schneider, T. R.; Sawaya, M. R. *Crystal Structure Refinement: A Crystallographer's Guide to (SHELXL)*; Müller, P., Ed.; IUCr Texts on Crystallography; Oxford University Press: Oxford, 2006.
- [93] The Reciprocal Net Site Network is a distributed database for crystallographic information, supported by the National Science Digital Library, and is run by participating crystallography labs across the world. Crystallographic data for complexes in this chapter are available under the identification codes listed in Tables 1.11 and 1.12 from the MIT Reciprocal Net site. <http://reciprocal.mit.edu/recipnet>.
- [94] These data can be obtained free of charge from The Cambridge Crystallographic Data Centre via [http://www.ccdc.cam.ac.uk/data\\_request/cif](http://www.ccdc.cam.ac.uk/data_request/cif).
- [95] te Velde, G.; Bickelhaupt, F. M.; Baerends, E. J.; Fonseca Guerra, C.; van Gisbergen, S. J. A.; Snijders, J. G.; Ziegler, T. *J. Comput. Chem.* **2001**, *22*, 931–967.
- [96] Fonseca Guerra, C.; Snijders, J. G.; te Velde, G.; Baerends, E. J. *Theo. Chem. Acc.* **1998**, *99*, 391–403.
- [97] Vosko, S. H.; Wilk, L.; Nusair, M. *Can. J. Phys.* **1980**, *58*, 1200–1211.
- [98] Baker, J.; Pulay, P. *J. Chem. Phys.* **2002**, *117*, 1441–1449.
- [99] van Lenthe, E.; Baerends, E. J.; Snijders, J. G. *J. Chem. Phys.* **1993**, *99*, 4597–4610.
- [100] van Lenthe, E.; Baerends, E. J.; Snijders, J. G. *J. Chem. Phys.* **1994**, *101*, 9783–9792.
- [101] van Lenthe, E.; Ehlers, A.; Baerends, E. J. *J. Chem. Phys.* **1999**, *110*, 8943–8953.
- [102] Schreckenbach, G.; Ziegler, T. *J. Phys. Chem.* **1995**, *99*, 606–611.
- [103] Schreckenbach, G.; Ziegler, T. *Int. J. Quantum Chem.* **1997**, *61*, 899–918.
- [104] Wolff, S. K.; Ziegler, T. *J. Chem. Phys.* **1998**, *109*, 895–905.
- [105] Wolff, S. K.; Ziegler, T.; van Lenthe, E.; Baerends, E. J. *J. Chem. Phys.* **1999**, *110*, 7689–7698.
- [106] van Wüllen, C. *Phys. Chem. Chem. Phys.* **2000**, *2*, 2137–2144.
- [107] Johnson, M. J. A.; Odom, A. L.; Cummins, C. C. *Chem. Commun.* **1997**, 1523–1524.



# CHAPTER 2

## Synthesis, Physical Properties, and Reactivity Patterns of $\text{AsP}_3$

### Contents

<b>2.1</b>	<b>Introduction</b>	<b>87</b>
2.1.1	Phosphorus and Arsenic Tetrahedra	87
2.1.2	A Brief History of <i>Cyclo</i> - $\text{P}_3$ Ligands	88
2.1.3	The Varied Reactivity of <i>Cyclo</i> - $\text{P}_3$ Anion Complexes	89
2.1.4	$\text{P}_4$ Activation by $[\text{Na}][\text{P}\equiv\text{Nb}(\text{N}[\text{CH}_2^t\text{Bu}]\text{Ar})_3]$	90
<b>2.2</b>	<b>Facile Synthesis of a <i>Cyclo</i>-<math>\text{P}_3</math> Anion Complex</b>	<b>91</b>
2.2.1	Two Strategies for the Reduction of $\text{Cl}_2\text{Nb}(\text{ODipp})_3$ in the Presence of $\text{P}_4$	91
2.2.2	Structural Aspects of $[\text{Na}(\text{THF})_3][\text{P}_3\text{Nb}(\text{ODipp})_3]$	92
<b>2.3</b>	<b>Synthesis of <math>\text{AsP}_3</math></b>	<b>93</b>
2.3.1	Reaction of $[\text{Na}(\text{THF})_3][\text{P}_3\text{Nb}(\text{ODipp})_3]$ with $\text{AsCl}_3$ in THF	93
2.3.2	Proposed Mechanism for $\text{AsP}_3$ Formation	95
<b>2.4</b>	<b>Physical and Electronic Properties of <math>\text{AsP}_3</math></b>	<b>98</b>
2.4.1	Gas Phase Electron Diffraction; Collaboration with Prof. Norbert Mitzel, Raphael Berger, and Stuart Hayes, University of Bielefeld	98
2.4.2	Photoelectron Spectroscopy; Collaboration with Prof. Dennis Lichtenberger and Ashley R. Head, University of Arizona	100
2.4.3	Solid-State NMR Spectroscopy; Collaboration with Prof. Gang Wu, Queen's University	103
2.4.4	Experimental and Computed Electronic Properties of $\text{AsP}_3$ and $\text{P}_4$	106
2.4.5	Computed Thermodynamic Properties of $\text{As}_n\text{P}_{4-n}$ Tetrahedra	113

Reproduced in part with permission from:

Cossairt, B. M.; Cummins, C. C. *Science*, **2009**, 323, 602, Copyright 2009 AAAS.

Cossairt, B. M.; Cummins, C. C. *J. Am. Chem. Soc.*, **2009**, 131, 15501–15511, Copyright 2009 American Chemical Society, License 2380430920657.

<b>2.5</b>	<b>Reactivity Patterns of AsP<sub>3</sub></b>	<b>114</b>
2.5.1	Thermal, and Photolytic Reactions of AsP <sub>3</sub>	114
2.5.2	Coordination of an Intact AsP <sub>3</sub> Tetrahedron	116
2.5.3	Cleavage of a Single As–P Bond	119
2.5.4	Reactivity with HNb( $\eta^2$ - <sup>t</sup> BuCH=NAr)(N[CH <sub>2</sub> <sup>t</sup> Bu]Ar) <sub>2</sub> and Mo(N[ <sup>t</sup> Bu]Ar) <sub>3</sub>	123
2.5.5	Selective Cleavage of Three As–P Bonds in AsP <sub>3</sub> : Reaction with [GaC(SiMe <sub>3</sub> ) <sub>3</sub> ] <sub>4</sub>	125
2.5.6	Bringing it Back: Sodium Amalgam Reduction of Cl <sub>2</sub> Nb(ODipp) <sub>3</sub> in the Presence of AsP <sub>3</sub>	129
<b>2.6</b>	<b>Reaction of the <i>Cyclo</i>-P<sub>3</sub> Anion Complex with Other Tripositive Electrophiles</b>	<b>133</b>
2.6.1	Halide Dependence of SbP <sub>3</sub> Synthesis	133
2.6.2	<i>In Situ</i> Reactivity of SbP <sub>3</sub>	134
<b>2.7</b>	<b>Towards Arsenic-Rich Tetrahedra</b>	<b>136</b>
2.7.1	Synthesis and Structure of [Na(THF) <sub>3</sub> ][As <sub>3</sub> Nb(ODipp) <sub>3</sub> ]	137
2.7.2	Reaction of [Na(THF) <sub>3</sub> ][As <sub>3</sub> Nb(ODipp) <sub>3</sub> ] with PCl <sub>3</sub>	138
<b>2.8</b>	<b>Conclusions</b>	<b>140</b>
<b>2.9</b>	<b>Experimental Details</b>	<b>140</b>
2.9.1	General Considerations	140
2.9.2	Preparation of [Na][P <sub>3</sub> Nb(N[CH <sub>2</sub> <sup>t</sup> Bu]Ar) <sub>3</sub> ] from [Na][P≡Nb(N[CH <sub>2</sub> <sup>t</sup> Bu]Ar) <sub>3</sub> ] and P <sub>4</sub>	141
2.9.3	Preparation of [Na(THF) <sub>3</sub> ][P <sub>3</sub> Nb(ODipp) <sub>3</sub> ], <b>25</b>	142
2.9.4	Preparation of [CoCp <sub>2</sub> ][P <sub>3</sub> Nb(ODipp) <sub>3</sub> ], <b>26</b>	142
2.9.5	Preparation of AsP <sub>3</sub> , <b>27</b>	143
2.9.6	Thermolysis of AsP <sub>3</sub>	143
2.9.7	Photolysis of AsP <sub>3</sub>	144
2.9.8	Preparation of (AsP <sub>3</sub> )Mo(CO) <sub>3</sub> (P <sup><i>i</i></sup> Pr) <sub>2</sub> , <b>28</b>	144
2.9.9	Preparation of [(AsP <sub>3</sub> )Fe(Cp*)(dppe)][BPh <sub>4</sub> ], <b>29</b>	145
2.9.10	Preparation of AsP <sub>3</sub> (P(N( <sup><i>i</i></sup> Pr) <sub>2</sub> )N(SiMe <sub>3</sub> ) <sub>2</sub> ) <sub>2</sub> , <b>30</b>	145
2.9.11	Synthesis and Equilibrium Study of (Ar[ <sup>t</sup> Bu]N) <sub>3</sub> Ti[P(P <sub>2</sub> )As]Ti(N[ <sup>t</sup> Bu]Ar) <sub>3</sub> , <b>31</b> , and (Ar[ <sup>t</sup> Bu]N) <sub>3</sub> Ti[P(P <sub>2</sub> )P]Ti(N[ <sup>t</sup> Bu]Ar) <sub>3</sub> , <b>32</b>	146
2.9.12	Preparation of (Ar[CH <sub>2</sub> <sup>t</sup> Bu]N) <sub>3</sub> Nb(PAs)Nb(N[CH <sub>2</sub> <sup>t</sup> Bu]Ar) <sub>3</sub> , <b>33</b> , and (Ar[CH <sub>2</sub> <sup>t</sup> Bu]N) <sub>3</sub> Nb(P <sub>2</sub> )Nb(N[CH <sub>2</sub> <sup>t</sup> Bu]Ar) <sub>3</sub> , <b>34</b>	146
2.9.13	Preparation of As≡Mo(N[ <sup>t</sup> Bu]Ar) <sub>3</sub> , <b>35-As</b> , and P≡Mo(N[ <sup>t</sup> Bu]Ar) <sub>3</sub> , <b>35-P</b>	147
2.9.14	Preparation of As[GaC(SiMe <sub>3</sub> ) <sub>3</sub> ] <sub>3</sub> P <sub>3</sub> , <b>36</b>	147
2.9.15	Preparation of [Na(THF) <sub>3</sub> ][P <sub>3</sub> Nb(ODipp) <sub>3</sub> ] ( <b>25</b> ), [Na(THF) <sub>3</sub> ][P <sub>2</sub> AsNb(ODipp) <sub>3</sub> ] ( <b>37</b> ), [Na(THF) <sub>3</sub> ][PA <sub>2</sub> Nb(ODipp) <sub>3</sub> ] ( <b>38</b> ), and [Na(THF) <sub>3</sub> ][As <sub>3</sub> Nb(ODipp) <sub>3</sub> ] ( <b>39</b> ) from AsP <sub>3</sub> and their conversion to AsP <sub>3</sub> ( <b>27</b> ), As <sub>2</sub> P <sub>2</sub> ( <b>40</b> ), As <sub>3</sub> P ( <b>41</b> ), and As <sub>4</sub> ( <b>42</b> )	148
2.9.16	Reaction of [Na(THF) <sub>3</sub> ][P <sub>3</sub> Nb(ODipp) <sub>3</sub> ] with SbCl <sub>3</sub>	149

2.9.17 <i>In situ</i> reaction of SbP <sub>3</sub> with ClFeCp*(dppe) and NaBPh <sub>4</sub> . . . . .	149
2.9.18 <i>In situ</i> reaction of SbP <sub>3</sub> with (OTf)Re(CO) <sub>2</sub> (triphos) and NaBPh <sub>4</sub> . . . . .	150
2.9.19 Preparation of [Na(THF) <sub>3</sub> ][As <sub>3</sub> Nb(ODipp) <sub>3</sub> ] . . . . .	150
2.9.20 Reaction of [Na(THF) <sub>3</sub> ][As <sub>3</sub> Nb(ODipp) <sub>3</sub> ] with PCl <sub>3</sub> . . . . .	151
2.9.21 X-Ray Structure Determinations . . . . .	151
2.9.22 Computational Studies . . . . .	152
2.9.23 Gas-Phase Electron Diffraction; University of Bielefeld . . . . .	157
2.9.24 Photoelectron Spectroscopy; University of Arizona . . . . .	158
2.9.25 Solid-State NMR Spectroscopy; Queen's University . . . . .	158
<b>2.10 References . . . . .</b>	<b>159</b>

## 2.1 INTRODUCTION

In the preceding chapter was described P<sub>4</sub> reductive coupling by a niobium trisenolate platform to give an unusual diniobium octaphosphorus cluster, from which both niobium metal centers were eventually eliminated to generate Ph<sub>2</sub>CP<sub>8</sub>(C<sub>6</sub>H<sub>8</sub>), an unusual phosphorus-rich organic molecule. In this chapter, the chemistry of a P<sub>4</sub>-derived *cyclo*-P<sub>3</sub> anion complex of niobium is developed. Most noteworthy, the remarkable P<sub>3</sub><sup>3-</sup> transfer chemistry of this complex leads to the synthesis of tetraatomic AsP<sub>3</sub>. The properties and reactivity of the phosphorus-rich cluster AsP<sub>3</sub> are then developed.

### 2.1.1 Phosphorus and Arsenic Tetrahedra

The stable molecular form of phosphorus, P<sub>4</sub>, is known as white phosphorus and is the key industrial intermediate for most phosphorus compounds of commercial importance.<sup>1</sup> In contrast, the corresponding arsenic molecule, As<sub>4</sub> (yellow arsenic), is both thermally and photochemically unstable such that it reverts readily to the stable grey allotrope with its infinite sheet structure.<sup>2</sup> As a result of this instability and the need to handle it both in the cold and in the dark, little chemistry has developed from As<sub>4</sub> as a starting point. Three binary molecules of intermediate composition As<sub>n</sub>P<sub>4-n</sub> (*n* = 1-3) may be considered; perhaps due to their phosphorus content, they may turn out to be more robust than As<sub>4</sub>, Figure 2.1. To date, essentially all that is known of the interpnictide molecules As<sub>n</sub>P<sub>4-n</sub> has come from gas-phase studies wherein hot (660 °C) vapors of phosphorus/arsenic mixtures under equilibrium reaction conditions were subjected to Raman spectroscopic analysis.<sup>3</sup>

In this chapter the chemistry of niobium-based P<sub>3</sub><sup>3-</sup> transfer agents is developed with an eye toward the synthesis of mixed arsenic-phosphorus tetrahedra.<sup>4,5</sup> With this chemistry I specifically

set out to generate  $\text{AsP}_3$  at temperatures close to ambient in order to determine its properties as a pure and isolated substance.

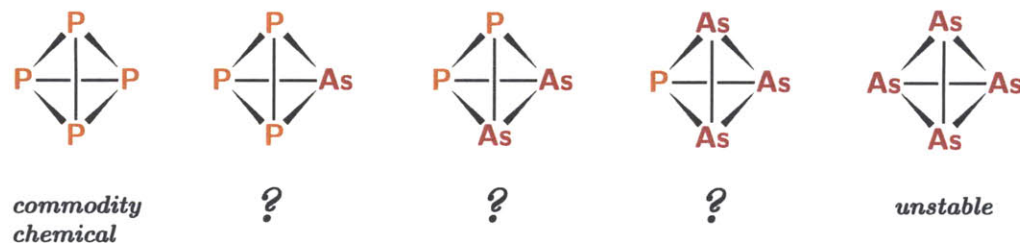


Figure 2.1. Group 15 elemental molecules:  $\text{As}_n\text{P}_{4-n}$  ( $n = 1-3$ ).

### 2.1.2 A Brief History of *Cyclo-P*<sub>3</sub> Ligands

Central to our goal of synthesizing molecular tetrahedra such as  $\text{AsP}_3$  is the use of *cyclo-P*<sub>3</sub> ligands complexed to transition metal fragments as precursors. The activation of  $\text{P}_4$  in the coordination sphere of a metal to give a triphosphorus ligand has been observed frequently, often as a pathway that competes with formation of a monophosphide complex.<sup>6</sup> Triphosphorus ligands derived from  $\text{P}_4$  appear generally as *cyclo-P*<sub>3</sub> units that bind to a metal in an  $\eta^3$  coordination mode. Sacconi and coworkers have provided the field with numerous examples of *cyclo-P*<sub>3</sub> ligands crowning various transition metal centers, including the first structurally characterized example in both a terminal disposition (in a cobalt system) and as a symmetrical  $\mu_2 : \eta^3, \eta^3$  ligand connecting two nickel centers.<sup>7</sup> Much of this seminal late-metal work has been reviewed.<sup>6,8-10</sup>

The earliest *cyclo-P*<sub>3</sub> complexes in an early-transition-metal context were isolated as products of  $\text{P}_4$  activation chemistry. For example, the complexes  $(\eta^3\text{-P}_3)\text{Mo}(\text{CO})_2\text{Cp}$  and  $(\eta^3\text{-P}_3)\text{Cr}(\text{CO})_2\text{Cp}$  were isolated from product mixtures that resulted when the parent dimer complexes  $[\text{Cp}(\text{CO})_2\text{Mo}]_2$  and  $[\text{Cp}(\text{CO})_3\text{Cr}]_2$  were treated with  $\text{P}_4$  in hot toluene solutions, Figure 2.2.<sup>11,12</sup> Similarly, Chisholm *et al.* found that treatment of the dimethylamine adduct of the tungsten dimer  $\text{W}_2(\text{OCH}_2^t\text{Bu})_6$  with  $\text{P}_4$  led to a trimetallic monophosphide cluster together with the *cyclo-P*<sub>3</sub> complex  $(\eta^3\text{-P}_3)\text{W}(\text{OCH}_2^t\text{Bu})_3$  as a minor product.<sup>13</sup>

Masked metal(III) ( $\text{M} = \text{Cr}, \text{Mo}, \text{W}$ ) derivatives have also been found to produce *cyclo-P*<sub>3</sub> complexes upon activation of white phosphorus. For instance,  $\text{Mo}(\text{H})(\eta^2\text{-Me}_2\text{C}=\text{NAr})(\text{N}^i\text{PrAr})_2$  (a tautomer of  $\text{Mo}(\text{N}^i\text{PrAr})_3$ ) reacts with  $\text{P}_4$  to provide the  $\mu$ -phosphide complex  $\text{P}[\text{Mo}(\text{N}^i\text{PrAr})_3]_2$  in high yield; this is the main reaction pathway when diethyl ether, in which  $\text{P}_4$  is not very soluble, is used as the solvent. However, addition of a toluene solution of the molybdaziridine hydride complex  $\text{Mo}(\text{H})(\eta^2\text{-Me}_2\text{C}=\text{NAr})(\text{N}^i\text{PrAr})_2$  to a toluene solution containing excess  $\text{P}_4$  results in formation of the *cyclo-P*<sub>3</sub> complex  $(\eta^3\text{-P}_3)\text{Mo}(\text{N}^i\text{PrAr})_3$  as the major reaction product.<sup>14</sup>



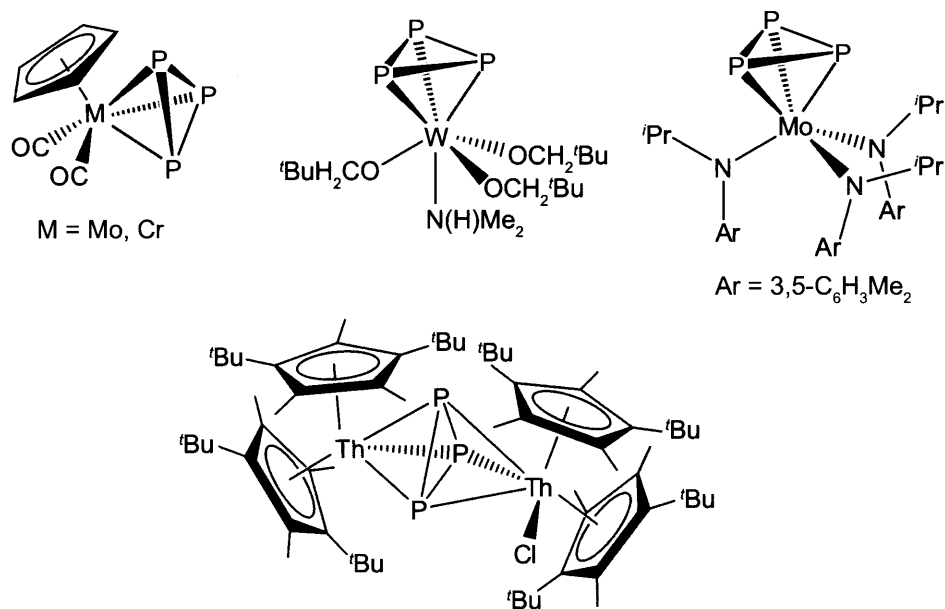


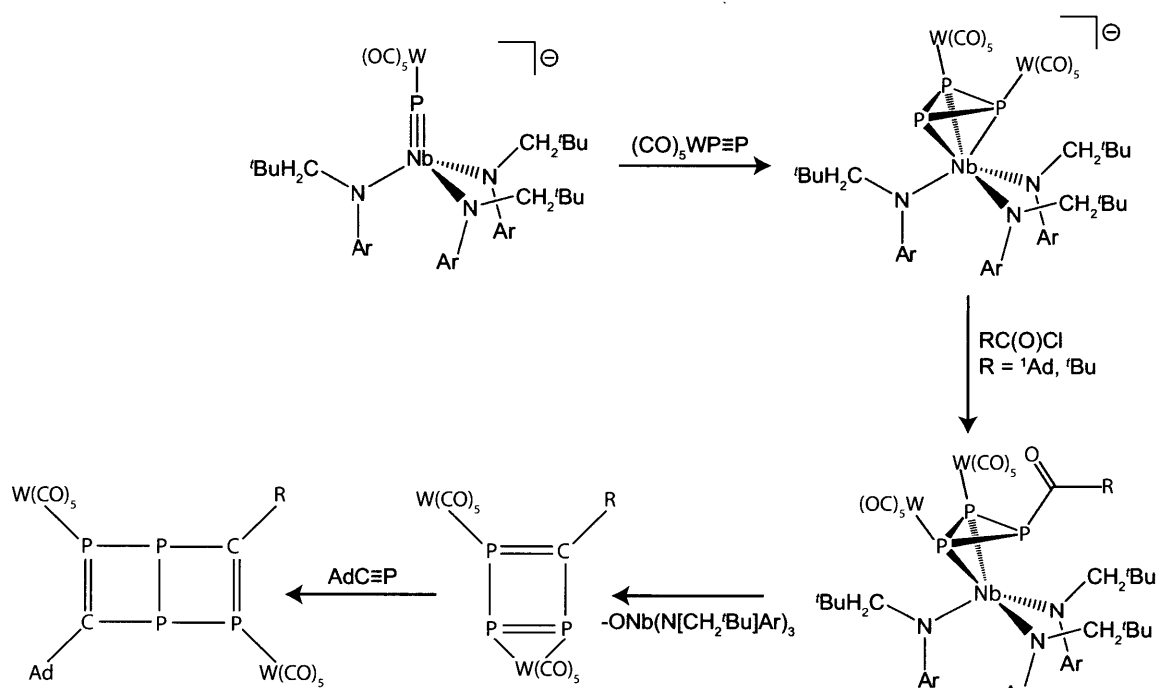
**Figure 2.2.** Previously reported *Cyclo-P<sub>3</sub>* complexes obtained by early-transition-metal-P<sub>4</sub> activation.

There are several unifying features to the small family of known early-transition-metal terminal *cyclo-P<sub>3</sub>* complexes. *Cyclo-P<sub>3</sub>* complexes display a characteristic <sup>31</sup>P resonance between –170 and –220 ppm. Such a high-field shift is characteristic of polyphosphorus units with small endocyclic bond angles, such as those found in a P<sub>3</sub> ring.<sup>15</sup> Structurally, each of the above-mentioned *cyclo-P<sub>3</sub>* complexes displays a symmetrical P<sub>3</sub> unit that can reasonably be viewed as a P<sub>3</sub><sup>3-</sup> ligand. It should be noted, however, that the P–P interatomic distances for structurally characterized P<sub>3</sub> complexes are not invariant. For instance, (η<sup>3</sup>-P<sub>3</sub>)Cr(CO)<sub>2</sub>Cp and (η<sup>3</sup>-P<sub>3</sub>)W(OCH<sub>2</sub>tBu)<sub>3</sub> both display somewhat short average P–P interatomic distances of 2.12 and 2.15 Å, respectively. Elongation of the P–P distances in a *cyclo-P<sub>3</sub>* ring is observed for bimetallic P<sub>3</sub> complexes. *Cyclo-P<sub>3</sub>* as a bridging ligand is rare within the early-transition-metal regime, though examples do exist. For example, treatment of Cp\*<sub>2</sub>Th(η<sup>4</sup>-C<sub>4</sub>H<sub>6</sub>) with P<sub>4</sub> in the presence of 0.5 equiv of MgCl<sub>2</sub>(OEt<sub>2</sub>) in toluene at 100 °C for 20 h was reported to give the asymmetric bimetallic complex Cp\*<sub>2</sub>Th(μ<sub>2</sub>:η<sup>3</sup>,η<sup>3</sup>-P<sub>3</sub>)Th(Cl)Cp\*<sub>2</sub>.<sup>16</sup> The average P–P distance in Cp\*<sub>2</sub>Th(μ<sub>2</sub>:η<sup>3</sup>,η<sup>3</sup>-P<sub>3</sub>)Th(Cl)Cp\*<sub>2</sub> was found to be 2.185 Å.

### 2.1.3 The Varied Reactivity of *Cyclo-P<sub>3</sub>* Anion Complexes

Functionalizations of *cyclo-P<sub>3</sub>* complexes were first reported for the series (P<sub>3</sub>)M(triphos) (M = Co, Rh, Ir) and required the highly electrophilic reagents [Me<sub>3</sub>O][BF<sub>4</sub>] or MeOTf to afford the methylated species.<sup>17</sup> It was shown by Piro and Cummins in 2008 that the anionic nature of the *cyclo-P<sub>3</sub>* complex [Na][{W(CO)<sub>5</sub>}<sub>2</sub>P<sub>3</sub>Nb(N[CH<sub>2</sub>tBu]Ar)<sub>3</sub>], derived from P<sub>2</sub>W(CO)<sub>5</sub> trapping by [Na][{W(CO)<sub>5</sub>}P≡Nb(N[CH<sub>2</sub>tBu]Ar)<sub>3</sub>], imparts the molecule with greater nucleophilic character, allowing for functionalization using milder reagents to give a variety of products.<sup>4,5</sup>

One exciting progression along these lines involved acylation of the  $W(CO)_5$ -coordinated *cyclo*- $P_3$  complex  $[Na][\{W(CO)_5\}_2P_3Nb(N[CH_2^tBu]Ar)_3]$  with either pivaloyl chloride or 1-adamantanecarbonyl chloride. These acylations afforded the triphosphirene complexes  $\{(OC)_5W\}_2RC(O)P_3Nb(N[CH_2^tBu]Ar)_3$ , ( $Ar = 3,5\text{-Me}_2C_6H_3$ ,  $R = 1\text{-adamantyl, } tert\text{-butyl}$ ), which were discovered to be thermally unstable toward deoxygenation of the acyl triphosphirene ligand to form  $ONb(N[CH_2^tBu]Ar)_3$  and red precipitate of empirical formula  $RCP_3(W(CO)_5)_2$ , Scheme 2.1. The nature of the transient  $RCP_3(W(CO)_5)_2$  species was explored through chemical trapping experiments, eventually leading to a preparation of a fascinating tetraphosphabenzene molecule, Scheme 2.1. With the goal of propelling forward the investigations of niobium *cyclo*- $P_3$  anion complexes, we sought to gain access to a more efficient synthesis for this family of complexes.

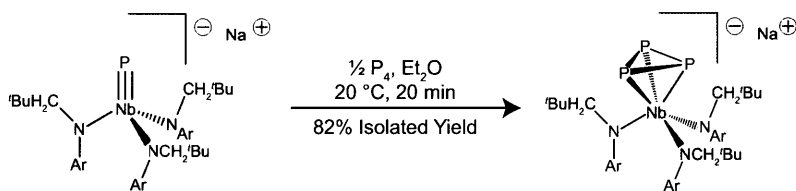


**Scheme 2.1.** Previously observed reactivity of a niobium *cyclo*- $P_3$  anion complex.

#### 2.1.4 $P_4$ Activation by $[Na][P\equiv Nb(N[CH_2^tBu]Ar)_3]$

As briefly discussed above, Nick Piro elegantly described the preparation of *cyclo*- $P_3$  anion complexes of niobium through trapping of  $P\equiv PW(CO)_5$ , or its synthetic equivalent, with  $[Na][\{W(CO)_5\}P\equiv Nb(N[CH_2^tBu]Ar)_3]$ . Seeking to improve our ability to access such interesting *cyclo*- $P_3$  anion complexes, we discovered that treatment of  $[Na][P\equiv Nb(N[CH_2^tBu]Ar)_3]$  with 0.5 equiv of  $P_4$  rapidly and quantitatively produces the desired  $[Na][P_3Nb(N[CH_2^tBu]Ar)_3]$  species; a rare example of  $P_4$  activation by a metal-ligand multiple bond. This reaction was found to proceed cleanly in  $Et_2O$ , benzene, toluene, and other non-polar solvents. The *cyclo*- $P_3$  anion complex  $[Na][P_3Nb(N[CH_2^tBu]Ar)_3]$  could be isolated from the reaction mixture in upwards of

82% yield and greatly facilitated our laboratory's access to this intriguing molecule. One drawback of this method, however, is that it requires the use of the exotic terminal phosphide anion species  $[\text{Na}][\text{P}\equiv\text{Nb}(\text{N}[\text{CH}_2^t\text{Bu}]\text{Ar})_3]$ . Terminal phosphide anion complexes are rare in the literature and so access to a range of *cyclo*- $\text{P}_3$  anion complexes would not be possible using this strategy. As such, we turned to look at other more general and direct methods for forming the *cyclo*- $\text{P}_3$  anion functional group.



**Scheme 2.2.**  $\text{P}_4$  addition to  $[\text{Na}][\text{P}\equiv\text{Nb}(\text{N}[\text{CH}_2^t\text{Bu}]\text{Ar})_3]$ .

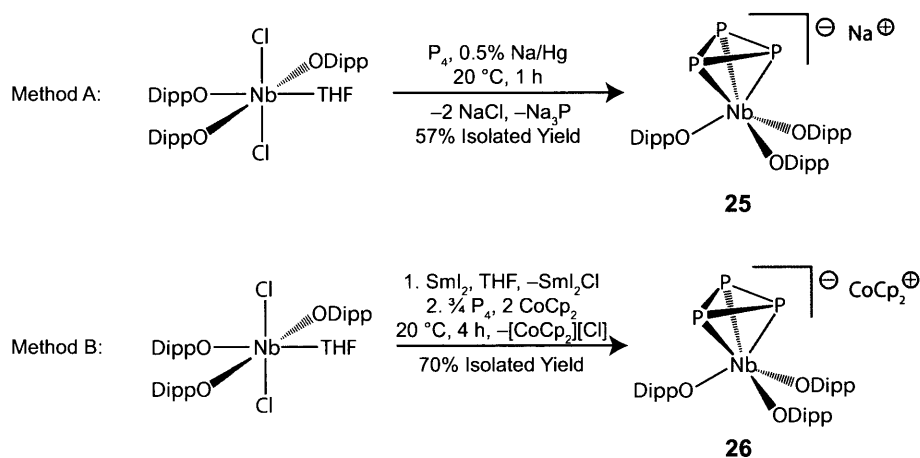
## 2.2 FACILE SYNTHESIS OF A *Cyclo*- $\text{P}_3$ ANION COMPLEX

### 2.2.1 Two Strategies for the Reduction of $\text{Cl}_2\text{Nb}(\text{ODipp})_3$ in the Presence of $\text{P}_4$

It was postulated that an *in situ* reduction of niobium(V) dihalide precursors (or niobium(IV) monohalide precursors) in the presence of  $\text{P}_4$  might allow direct access to the desired *cyclo*- $\text{P}_3$  anion functional group. Rothwell's  $\text{Cl}_2\text{Nb}(\text{ODipp})_3$ <sup>18,19</sup> (Dipp = 2,6-diisopropylphenyl) was identified as an intriguing literature compound for testing our hypothesis as this bishalide is accessible in large quantities from the reaction of commercially available  $\text{NbCl}_5$  and 2,6-diisopropylphenol.<sup>18</sup> Two strategies were explored for *in situ* reduction of  $\text{Cl}_2\text{Nb}(\text{ODipp})_3$ . The first strategy involved reduction of  $\text{Cl}_2\text{Nb}(\text{ODipp})_3$  with a 0.5% sodium amalgam in the presence of 1 equiv of  $\text{P}_4$  as a solution in THF; a reaction first carried out by Mariam Diawara, a visiting student in the Cummins lab.<sup>20</sup> After workup and crystallization this procedure gave  $[\text{Na}(\text{THF})_3][\text{P}_3\text{Nb}(\text{ODipp})_3]$ , **25**, in an optimized isolated yield of 57%, Scheme 2.3. An alternative path to an anionic *cyclo*- $\text{P}_3$  complex was desired because the sodium amalgam reductant is capable of short-circuiting the synthesis by reducing  $\text{P}_4$  to generate  $\text{Na}_3\text{P}$ , which was presumed to be hampering the yield of  $[\text{Na}(\text{THF})_3][\text{P}_3\text{Nb}(\text{ODipp})_3]$ .

An alternative method involves initial one-electron reduction of  $\text{Cl}_2\text{Nb}(\text{ODipp})_3$  with  $\text{SmI}_2$  (employed as a 0.1 M THF solution) to afford  $\text{ClNb}(\text{ODipp})_3(\text{THF})$  and  $\text{SmI}_2\text{Cl}$ , the latter being easily separated by filtration. White phosphorus (0.75 equiv) addition to the solution containing  $\text{ClNb}(\text{ODipp})_3(\text{THF})$ , followed by cobaltocene (2 equiv), and stirring for 4 h produced an orange solution containing the desired product. Concentration, filtration (to remove  $[\text{CoCp}_2]\text{Cl}$ ), and crystallization gave a 70% isolated yield of vibrant orange crystals of  $[\text{CoCp}_2][\text{P}_3\text{Nb}(\text{ODipp})_3]$ , **26**, Scheme 2.3. Both salts (sodium or cobaltocenium) are found to be efficient  $\text{P}_3^{3-}$  synthons. However,

due to cost and convenience, **25** is the preferred  $P_3^{3-}$  synthon. It is noteworthy, then, that **25** is readily available in *two steps* from commercially available starting materials. Characterization data for **25** and **26** obtained by elemental analysis and nuclear magnetic resonance (NMR) spectroscopy ( $^{31}P$ ,  $^{13}C$ ,  $^1H$ ) in benzene- $d_6$  solution are consistent with the structural assignment as terminal *cyclo*- $P_3$  units, with the  $^{31}P$  NMR data (singlets at a chemical shift,  $\delta$ , of  $-206$  ppm for **25** and  $-170$  ppm for **26**) serving as spectroscopic signatures for this system.



**Scheme 2.3.** Two methods for preparing  $P_3\text{Nb}(\text{ODipp})_3$  anion.

## 2.2.2 Structural Aspects of $[\text{Na}(\text{THF})_3][\text{P}_3\text{Nb}(\text{ODipp})_3]$

Two different crystalline forms of sodium salt **25** have been obtained and characterized by single-crystal X-ray crystallography. In the first, Figure 2.3 left, the sodium counter cation is bound in an  $\eta^3$  fashion to the *cyclo*- $P_3$  ring and its coordination sphere is completed by two molecules of  $\text{Et}_2\text{O}$  and one molecule of THF. The P–P interatomic distances in this structure are 2.194(4), 2.205(4), and 2.190(4) Å (one of the two independent molecules discussed). This gives an average P–P interatomic distance of 2.196 Å with a variation of 0.015 Å between the P–P distances. When we compare this to the structure in which the sodium counter cation has been fully sequestered by six molecules of THF, Figure 2.3 right, we have a slightly different structure. The P–P interatomic distances are 2.176(1), 2.179(1), and 2.179(1) Å giving an average of 2.178 Å and a variation of only 0.003 Å. The average P–P interatomic distance, then, is shortened by 0.02 Å between the two structures, suggesting that the interaction of the sodium counter cation in the first structure does cause a significant distortion of the *cyclo*- $P_3$  ring. No significant differences are observed in the other bond distances between these two structures. It is noteworthy that the average P–P interatomic distances reported here are significantly longer than those of neutral *cyclo*- $P_3$  metal complexes by approximately 0.05 Å.<sup>11–13</sup>

The Nb–P interatomic distances in both structures range from 2.494(4) to 2.525(2) Å, which is in the range of previously observed Nb–P single bonds.<sup>4,21,22</sup> There is quite substantial variation

between the Nb–O bond distances in both molecules with distances spanning 1.926(7) to 1.965(2) Å. The Na–P contacts in the first structure are on average 3.167 Å in length, which are quite long when compared to the distances observed for the Na–O bonds (2.2 to 2.4 Å) in the same molecule.

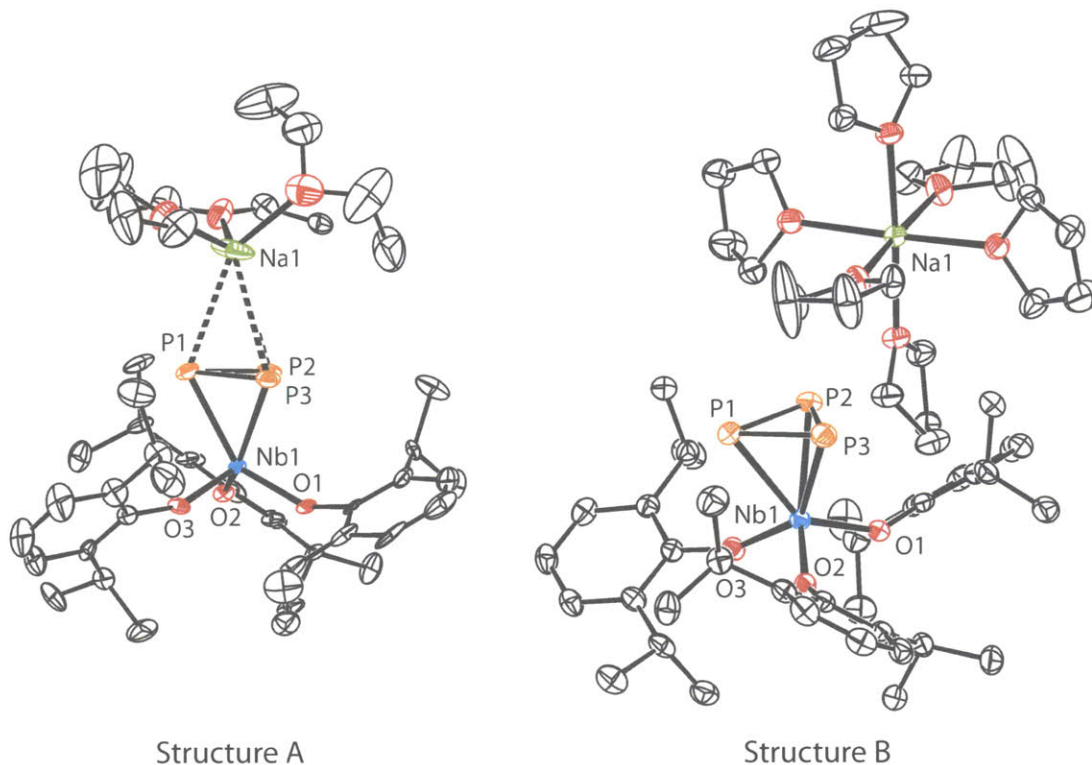


**Figure 2.3.** Thermal ellipsoid plots (50% probability) of  $[\text{Na}(\text{THF})_3][\text{P}_3\text{Nb}(\text{ODipp})_3]$  and  $[\text{Na}(\text{THF})_6][\text{P}_3\text{Nb}(\text{ODipp})_3]$  with hydrogen atoms omitted for clarity.

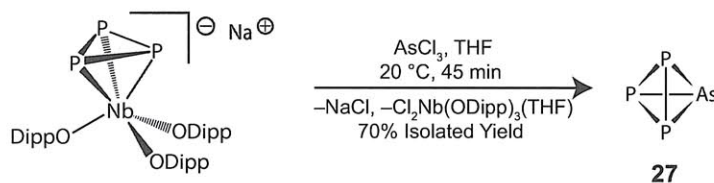
## 2.3 SYNTHESIS OF $\text{AsP}_3$

The discovery of an efficient synthesis for a *cyclo*- $\text{P}_3$  anion complex in two synthetic steps from commercially available  $\text{NbCl}_5$ , HODipp,  $\text{P}_4$ , and reducing agent opened up the door for in depth investigation of its reactivity properties. Complete transfer of the  $\text{P}_3^{3-}$  ligand to generate molecular  $\text{AsP}_3$  is now discussed.

### 2.3.1 Reaction of $[\text{Na}(\text{THF})_3][\text{P}_3\text{Nb}(\text{ODipp})_3]$ with $\text{AsCl}_3$ in THF

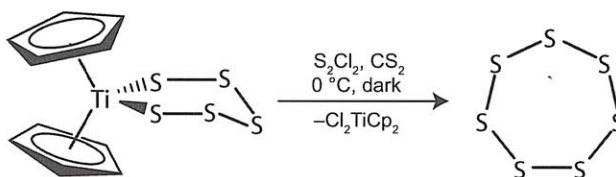
Treatment of a thawing 0.3 M THF solution of **25** with 1 equiv  $\text{AsCl}_3$ , Scheme 2.4, resulted rapidly in a brightening of the orange solution with concomitant precipitation of a fine, light-colored powder. After 30 minutes, filtration through a pad of Celite to remove the precipitated salt afforded a bright orange solution containing only  $\text{Cl}_2\text{Nb}(\text{ODipp})_3(\text{THF})$  and  $\text{AsP}_3$ , **27**. Removal

of the THF and sublimation of the solids afforded off-white  $\text{AsP}_3$  in 70% yield, leaving pure  $\text{Cl}_2\text{Nb}(\text{ODipp})_3(\text{THF})$  behind for recycling back into the synthesis.



**Scheme 2.4.** Preparation of  $\text{AsP}_3$ .

Transition-metal chalcogenide chemistry provides a family of reactions bearing close relation to our synthesis of  $\text{AsP}_3$ . Namely, treatment of  $\text{Y}_2\text{X}_2$  ( $\text{Y} = \text{S, Se, Te}$ ;  $\text{X} = \text{Cl}$  or  $\text{Br}$ ) with  $\text{S}_5\text{TiCp}_2$  results in formation of  $\text{Y}_2\text{S}_5$  and  $\text{X}_2\text{TiCp}_2$ .<sup>23–25</sup> The first example of such a reaction ( $\text{Y} = \text{S}$ ,  $\text{X} = \text{Cl}$ ) comes from a 1968 report by Schmidt and co-workers, Scheme 2.5.<sup>23</sup> When  $\text{Y} = \text{Se}$  or  $\text{Te}$ , this reaction is an illustrative example of the solution synthesis of a heteroatomic interchalcogenide using transfer of  $\text{S}_5^{2-}$  from an early transition metal center to an  $\text{Y}_2^{2+}$  fragment; this strategy is similar to our solution synthesis of a heteroatomic interpnictide using transfer of  $\text{P}_3^{3-}$  from an early transition metal center to an  $\text{As}^{3+}$  fragment.



**Scheme 2.5.** Preparation of  $\text{S}_7$  from  $\text{Cp}_2\text{Ti(S}_5)$  and  $\text{S}_2\text{Cl}_2$ .

The physical properties of  $\text{AsP}_3$  have been probed by a variety of methods.  $\text{AsP}_3$  readily sublimates under vacuum at  $60\text{ }^\circ\text{C}$  and melts without decomposition at  $70\text{ }^\circ\text{C}$ .<sup>26</sup>  $\text{AsP}_3$  has been shown to be thermally stable in refluxing toluene solution for more than one week. High-resolution, electron impact mass spectroscopy on a solid sample of  $\text{AsP}_3$  has provided a mass of  $167.8426\text{ m/z}$  (theoretical mass is  $167.8423\text{ m/z}$ ), Figure 2.4. A solution molecular weight determination of  $\text{AsP}_3$  gives a molecular weight of  $167(5)\text{ m/z}$  (95% confidence level), confirming that the molecule also exists in the monomeric form when in solution. Phosphorus NMR spectroscopy shows a single sharp resonance at  $-484\text{ ppm}$  in benzene solution. This shift is  $36\text{ ppm}$  downfield of that for elemental phosphorus in the form of  $\text{P}_4$  (*vide infra*).

Raman spectroscopy obtained on solid samples of  $\text{AsP}_3$  shows four resonances at  $313\text{ (e)}$ ,  $345\text{ (a}_1)$ ,  $428\text{ (e)}$ , and  $557\text{ (a}_1)\text{ cm}^{-1}$ , consistent with calculated stretching modes for this  $\text{C}_{3v}$  symmetric molecule, Figure 2.5.<sup>3</sup> The four bands observed in the Raman spectrum are readily assigned using

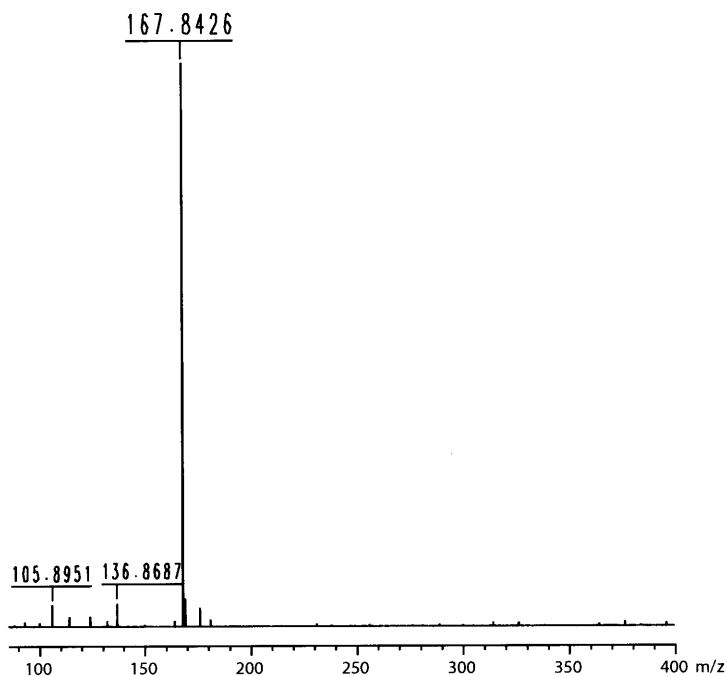


**Figure 2.4.** High-resolution electron-impact mass spectrum of  $\text{AsP}_3$ .

Raman polarization spectroscopy, Figure 2.6. The depolarization ratio,  $\rho$ , is defined as the ratio of the intensity of the perpendicular to the parallel components of the Stokes line. Those Raman lines for which  $\rho = 0.75$  are referred to as depolarized lines and correspond to vibrations of the molecule that are not totally symmetric. Those Raman lines for which  $0 < \rho < 0.75$  are referred to as polarized lines. The vibrations of the molecule must transform as  $A_1$  in order to be polarized. Figure 2.6 shows the response of the three most intense Raman bands to changing the polarization of the laser light. Both the band at  $557$  and  $345 \text{ cm}^{-1}$  respond dramatically to polarization, with  $\rho = 0.41$  and  $0.35$  respectively, identifying them as  $a_1$  vibrational modes.

### 2.3.2 Proposed Mechanism for $\text{AsP}_3$ Formation

While an experimental mechanistic investigation on the formation of  $\text{AsP}_3$  has not been possible, a reasonable mechanism for the process is shown in Scheme 2.6. Given the precedent for facile salt elimination on reaction of niobium *cyclo*- $\text{P}_3$  anion complexes with electrophiles, a logical first step involves reaction of **25** with  $\text{AsCl}_3$  to give  $\text{NaCl}$  and  $\text{Cl}_2\text{AsP}_3\text{Nb}(\text{ODipp})_3$ . While this  $\text{AsCl}_2$  substituted *cyclo*- $\text{P}_3$  complex has not been directly observed, related species have. For instance, it was found that when **25** is treated with 1 equiv  $\text{SbI}_3$  at  $-50 \text{ }^\circ\text{C}$ ,  $\text{I}_2\text{SbP}_3\text{Nb}(\text{ODipp})_3$  was persistent and readily identified by NMR spectroscopy (singlet  $-165$  ppm in the  $^{31}\text{P}$  NMR spectrum, *vide infra*). Once  $\text{Cl}_2\text{AsP}_3\text{Nb}(\text{ODipp})_3$  forms, it seems reasonable that the substituted P atom could invert, bringing the As–Cl bonds in close proximity to the niobium metal center. This inversion

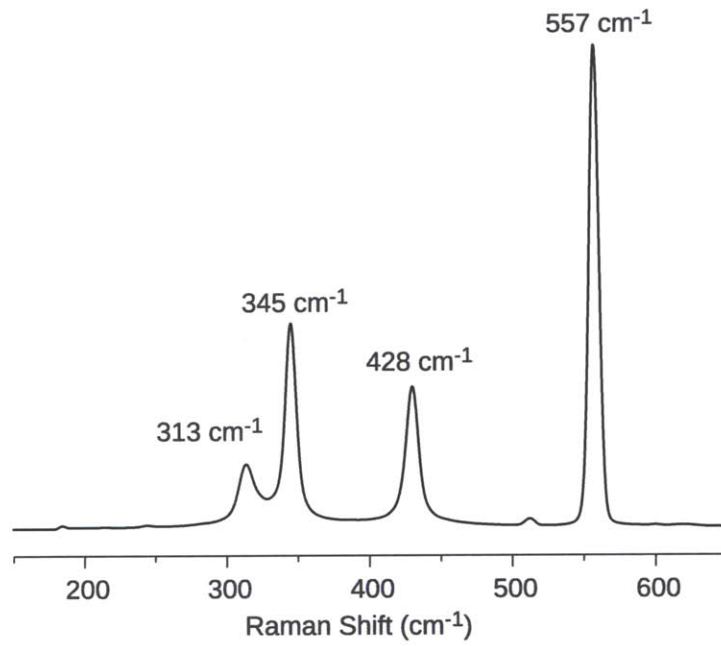


Figure 2.5. Raman spectrum of AsP<sub>3</sub>.

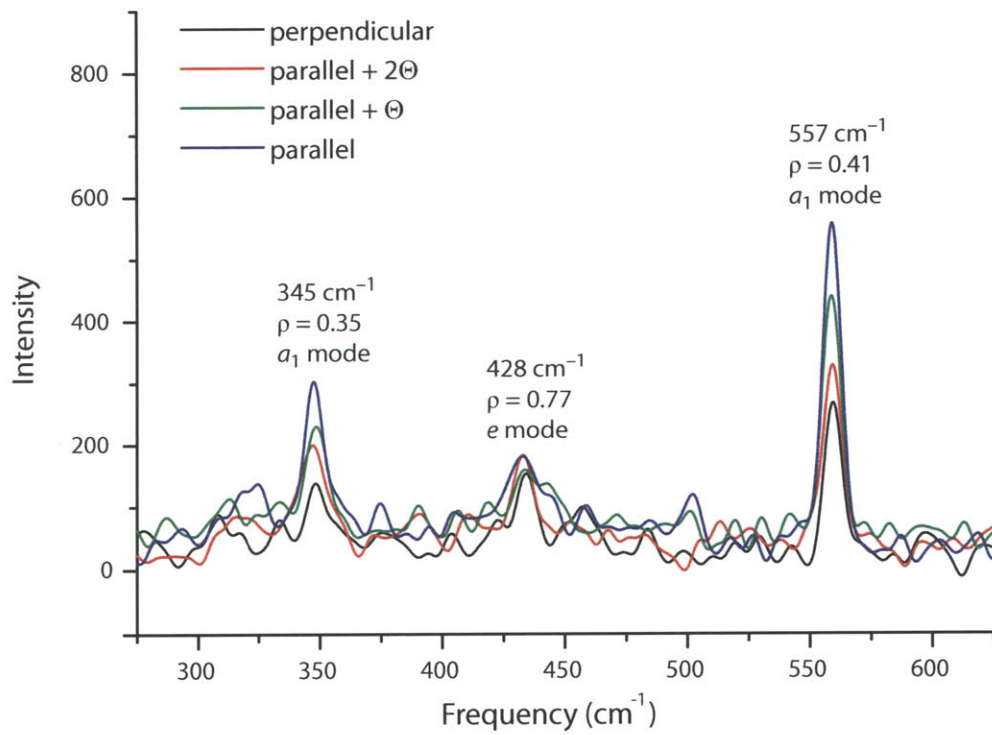
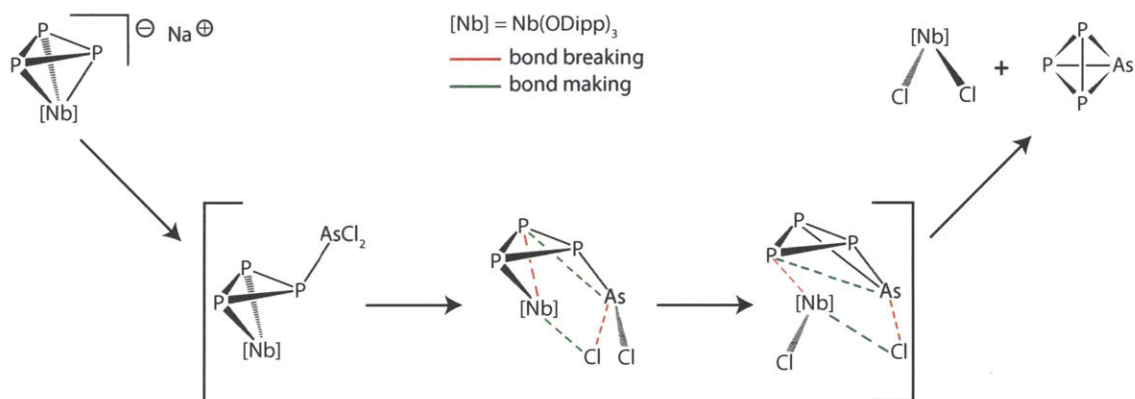


Figure 2.6. Raman polarization experiment for AsP<sub>3</sub>.



driven mechanism is analogous to that observed by Nick Piro in the mechanism for deoxygenation of the acyltriphosphirene complex  $\text{RC(O)P}_3\text{Nb}(\text{N}[\text{CH}_2^t\text{Bu}]\text{Ar})_3$ .<sup>27,28</sup> As–Cl bond cleavage and As–P bond formation would then be accompanied by simultaneous Nb–P bond rupture and Nb–Cl bond formation through a metallacyclic intermediate. Two such events would give rise to the observed products,  $\text{Cl}_2\text{Nb}(\text{ODipp})_3(\text{THF})$  and  $\text{AsP}_3$ . An alternative mechanism may involve ionization of the As–Cl bonds from  $\text{Cl}_2\text{AsP}_3\text{Nb}(\text{ODipp})_3$  following the initial salt elimination event.



**Scheme 2.6.** Proposed mechanism for the formation of  $\text{AsP}_3$  from  $[\text{Na}(\text{THF})_3][\text{P}_3\text{Nb}(\text{ODipp})_3]$  and  $\text{AsCl}_3$ .

One important point to address is whether or not the  $\text{P}_3$  source is important in the preparation of  $\text{AsP}_3$ . In order to address this issue we can refer to two cases:  $\text{P}_3\text{W}(\text{ODipp})_3$  (Jens Breunig, Cummins lab unpublished results) and  $[\text{Na}][\{\text{W}(\text{CO})_5\}_2\text{P}_3\text{Nb}(\text{N}[\text{CH}_2^t\text{Bu}]\text{Ar})_3]$  (Nicholas Piro).<sup>28</sup> In the case of tungsten, the potential product  $\text{Cl}_3\text{W}(\text{ODipp})_3$  is a well known molecule,<sup>29</sup> however, treatment of  $\text{P}_3\text{W}(\text{ODipp})_3$  with  $\text{AsCl}_3$  gives rise to ligand exchange, cleanly generating  $\text{P}_3\text{W}(\text{ODipp})_2\text{Cl}$  and  $\text{As}(\text{ODipp})\text{Cl}_2$ , even in the presence of an excess of  $\text{AsCl}_3$ ; transfer of the  $\text{P}_3$  ligand from the metal center was not observed. This suggests that the anionic charge on  $[\text{Na}(\text{THF})_3][\text{P}_3\text{Nb}(\text{ODipp})_3]$  is a necessary attribute, but as discussed below, not sufficient. Nick Piro has shown that  $[\text{Na}][\{\text{W}(\text{CO})_5\}_2\text{P}_3\text{Nb}(\text{N}[\text{CH}_2^t\text{Bu}]\text{Ar})_3]$  reacts with  $\text{PCl}_3$  to give small amounts of  $\text{P}_4$  with loss of  $\text{Cl}_2\text{Nb}(\text{N}[\text{CH}_2^t\text{Bu}]\text{Ar})_3$ ,  $\text{NaCl}$ , and  $\text{W}(\text{CO})_5$ , but that it does not generate  $\text{AsP}_3$  by treatment with  $\text{AsCl}_3$ . We have further shown that the more similar “naked” *cyclo*- $\text{P}_3$  anion  $[\text{Na}][\text{P}_3\text{Nb}(\text{N}[\text{CH}_2^t\text{Bu}]\text{Ar})_3]$  reacts with  $\text{AsCl}_3$  to generate very small quantities of  $\text{AsP}_3$  (less than 20% conversion); metallic arsenic and red phosphorus were identified as the insoluble components of the reaction mixture. This is an interesting case for comparison because, in the absence of these data, it would seem reasonable to assume that any *cyclo*- $\text{P}_3$  anion of niobium would be sufficient. In the case of the bis-tungsten capped *cyclo*- $\text{P}_3$  anion complex, it seems reasonable that the  $\text{W}(\text{CO})_5$  units might stabilize a  $\text{P}_3\text{As}$ -cyclobutadiene-like intermediate as has been seen in the acylation chemistry pursued by Nick Piro.<sup>30</sup> This species likely decomposes by a variety of methods, leading to insoluble and intractable product mixtures. The low-yield in the case of  $[\text{Na}][\text{P}_3\text{Nb}(\text{N}[\text{CH}_2^t\text{Bu}]\text{Ar})_3]$  may be a result of the different electronic properties provided by the

anilide ligand set, but it may also have to do with the steric hindrance at the metal center, precluding easy access to the transition state needed to cleanly form  $\text{AsP}_3$ .

## 2.4 PHYSICAL AND ELECTRONIC PROPERTIES OF $\text{AsP}_3$

Due to its structural simplicity, thermal stability, heavy-atom composition, and volatility,  $\text{AsP}_3$  is an ideal candidate for a wide variety of physical and electronic investigations including geometric structure determination by means of gas-phase electron diffraction (GED) and gas-phase electronic structure determination by photoelectron spectroscopy. The determination of the structure of free molecules of  $\text{AsP}_3$  in the gas phase, unbiased by solid state intermolecular interactions, as well as a reinvestigation of the gas-phase structure of elemental white phosphorus, i.e.  $\text{P}_4$  molecules, has been carried out for comparison. The electronic structures of neutral  $\text{AsP}_3$  and  $\text{P}_4$  and the energies associated with geometric distortion upon ionization are compared by photoelectron spectroscopy. Solid-state nuclear magnetic resonance investigations are provided to directly probe the electronic environments of the arsenic atom ( $^{75}\text{As}$  NMR) and the phosphorus atoms ( $^{31}\text{P}$  NMR). Finally, ADF calculations provide a more complete understanding of the electronic structure and thermodynamic properties of  $\text{AsP}_3$ .

### 2.4.1 Gas Phase Electron Diffraction; Collaboration with Prof. Norbert Mitzel, Raphael Berger, and Stuart Hayes, University of Bielefeld

Electron diffraction data were acquired for  $\text{AsP}_3$  at a compound temperature of about 110 °C and nozzle temperature of 115 °C. Figure 2.7 gives the reduced molecular scattering intensities and the radial distribution curve.  $C_{3v}$  symmetry was assumed for the structure refinement; hence the geometry can be expressed in terms of two independent coordinates, which were chosen to be the P–P and the As–P distances. The two structural parameters were refined together and independently (as an average value and a difference), while the two interatomic vibrational amplitudes were restrained to a fixed ratio relative to the values predicted by ab-initio calculations. The P–P and the As–P distances were determined to be 2.195(1) and 2.304(3) Å ( $r_g$  structure type, all experimental distances from this study are given with uncertainties of  $1\sigma$ ).

Examination of the P–P and P–As interatomic distances in the single crystal X-ray diffraction structures of transition metal- $\text{AsP}_3$  adducts (*vide infra*) give As–P bond lengths ranging from 2.306(6) to 2.336(2) Å (distances to the non-metal-bound P atom) and P–P bonds ranging from 2.165(8) to 2.231(3) Å (distances to the non metal-bound P atom). The values obtained from the gas-phase structure are in good agreement with these solid-state data. These data also compare favorably with the DFT optimized structure of  $\text{AsP}_3$  which gives an As–P interatomic distance of 2.328 Å and a P–P interatomic distance of 2.212 Å and with the computed single bond distances of 2.32 Å for As–P and 2.22 Å for P–P computed from single bond covalent radii.<sup>31</sup> The P–As–P and

the P–P–As angles, which are dependent parameters, were determined to be 56.9(1)° and 61.6(1)°. Calculations predict that both interatomic vibrational amplitudes (P–P and As–P) are equal within reasonable accuracy and they were refined to a value of 0.06(2) Å.

For comparison with the structure of AsP<sub>3</sub> it was desirable to have access to a precise gas-phase structure of free P<sub>4</sub> molecules. However, despite its structural simplicity, various and partly contradicting results about the molecular structure of free P<sub>4</sub> have been published, the most recent in 1999.<sup>32</sup> There is only one GED investigation of P<sub>4</sub> to be found in the literature which stems from 1935.<sup>33</sup> In this study, no rotating sector has been used.<sup>34</sup> Mitzel recently demonstrated that such investigations, despite all merits regarding the relative accuracy bearing in mind the archaic simplicity of employed techniques, yield in cases only very limited absolute accuracies.<sup>35</sup> For these reasons we undertook parallel to the study of AsP<sub>3</sub> also a re-investigation of the gas-phase structure of P<sub>4</sub> by means of electron diffraction. Molecular scattering intensities and the radial distribution curve are given in Figure 2.7. At a nozzle temperature of 100 °C, diffraction data were acquired which resulted by using a T<sub>d</sub>-symmetric one-parameter model in a  $r_g$  distance of 2.1994(3) Å between the P atoms and an interatomic vibrational amplitude of 0.0560(5) Å. It is also worthy to compare this new value to those obtained from structures of P<sub>4</sub> in other phases. For example, values extracted from X-ray diffraction experiments of P<sub>4</sub> in the liquid phase at 321 K and 499 K provide a P–P bond length of  $r_{av} = 2.25$  Å.<sup>36,36</sup> In the solid state, single crystal X-ray diffraction of the β-P<sub>4</sub> phase, crystallised from CS<sub>2</sub> solution, gives an average P–P interatomic distance of 2.182(5) Å (range 2.175(5) to 2.192(5) Å) as determined from 18 P–P bond lengths of three crystallographically independent molecules, which was further corrected for libration to a value of 2.204 Å (range 2.199 to 2.212 Å).<sup>37</sup>

In 1997, Persson et al. estimated the basis set limit at the non-relativistic CCSD(T) level of theory for the equilibrium P–P distance of 2.186(1) Å, while they achieved a value of 2.188 Å using an ANO type basis set of the contraction form [6s11p4d3f1g].<sup>38</sup> Now we could verify this estimation of the basis set limit at the explicitly correlated CCSD(T)-F12/aug-cc-pCVQZ level of theory including all electrons into the correlation space, yielding a value of 2.1860 Å for P–P in P<sub>4</sub>. Remarkably, core electron correlation affects the calculated P–P distance significantly by shortening it by approximately 1 pm compared to the result from taking only valence electrons into the correlation space (2.194 Å).

The experimental structures give  $r_g$  P–P bond lengths for AsP<sub>3</sub> and P<sub>4</sub> that are equal within three standard deviations: AsP<sub>3</sub> [2.192 - 2.198 Å], P<sub>4</sub> [2.198 - 2.200 Å]. The best theoretically obtained values for P–P interatomic distances are 2.186 Å for P<sub>4</sub><sup>38</sup> and 2.212 Å for AsP<sub>3</sub>, while a value of 2.328 Å has been predicted for the As–P interatomic distances. In order to allow a comparison of these equilibrium distances ( $r_e$ ) with our experimental ( $r_g$ ) values, one would have to estimate distance correction for ro-vibrational effects at the experimental temperature. In principle this can be attempted using calculated anharmonic force fields, leading in our case to corrections of the magnitude 0.003 Å (to be subtracted from the  $r_g$  values). However, great care is suggested

using such corrections, as the literature discussing the earlier gas phase structure determination of  $P_4$  by means of high-resolution IR spectroscopy<sup>32</sup> in comparison with the calculated re values mentions problems with highly excited rotational states and difficulties in estimating reliable distance corrections. As this problem has not been resolved thus far, we abstain from such a direct comparison using corrections of unknown reliability in these particular cases.

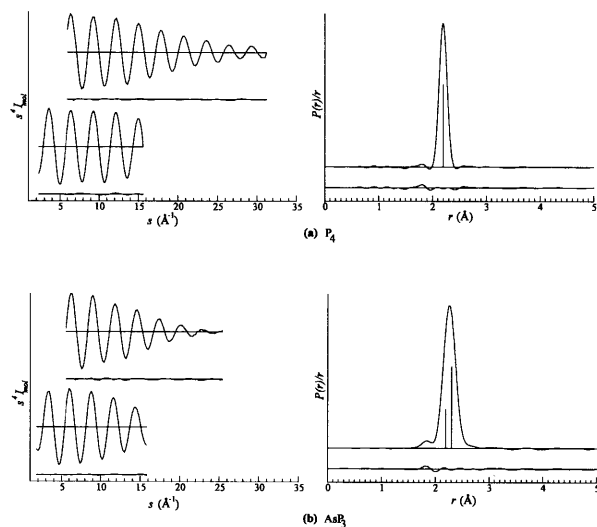


**Figure 2.7.** Molecular scattering intensities and radial distribution curves for  $P_4$  (top) and  $AsP_3$  (bottom).

#### 2.4.2 Photoelectron Spectroscopy; Collaboration with Prof. Dennis Lichtenberger and Ashley R. Head, University of Arizona

Gas-phase photoelectron spectroscopy directly probes the electronic structure of molecules. In order to understand the photoelectron spectrum and the electronic structure of  $AsP_3$ , it is useful to start with a summary of  $P_4$ , previously reported by Wang et al.<sup>39</sup> The valence photoelectron spectra of  $AsP_3$  and  $P_4$  are compared in Figure 2.8. The highest occupied orbitals of  $P_4$  are  $(2a_1)^2(2t_2)^6(e)^4$ . When an electron is ionized from the HOMO  $e$  orbital, a  ${}^2E$  state is formed which couples with the  $\nu_2(e)$  vibration, causing a Jahn-Teller distortion in the cation. The  ${}^2E$  state can also be split by spin-orbit coupling. The first two peaks, labeled A in the photoelectron spectrum in the bottom of Figure 2.8, are a result of this ionization, and they have an observed splitting energy of 0.38 eV. This splitting is primarily the result of the Jahn-Teller reduction in symmetry since the spin-orbit coupling of the valence ionizations of the P atom is on the order of only 0.04 eV. The next band in the spectrum, labeled B in the figure, contains three components that begin as the  $t_2$  set in the neutral molecule. Upon ionization, the two different effects again combine to remove the triple degeneracy of the  ${}^2T_2$  state. The Jahn-Teller distortion, due to mostly the  $\nu_3(t_2)$  vibration, splits the  $t_2$  orbitals into three components in the cation. Since the splitting energies are larger than 0.04 eV, Jahn-Teller effects are the dominant reason for the splitting. The last peak at 11.9 eV (labeled C) corresponds to

formation of the  $^2A_1$  cationic state and shows vibrational fine structure due to the  $\nu_1(a)$  symmetric vibration with a frequency spacing of  $554(11) \text{ cm}^{-1}$ .

The photoelectron spectrum of  $\text{AsP}_3$  is shown on the top of Figure 2.8. It contains similar features to those seen for  $\text{P}_4$ , though most of the peaks are shifted to lower ionization energies, as seen in Table 2.1, and there is a greater spread of ionizations in band B. With the replacement of one P atom with a more electron rich, less electronegative As atom, the molecular orbitals should be easier to ionize. The vibrational structure is not as resolved as in the  $\text{P}_4$  spectrum except for peak C. This is largely due to lower frequency vibrations that result in smaller spacings which cannot be seen with our instrument resolution. The  $T_d$  symmetry is lowered to  $C_{3v}$  and the symmetries of the highest occupied molecular orbitals of the neutral molecule change to  $(3a_1)^2(4a_1)^2(2e)^4(3e)^4$ . The doublet in the A ionization band arises again from the Jahn-Teller distortion with the same splitting energy as in the  $\text{P}_4$  spectrum.

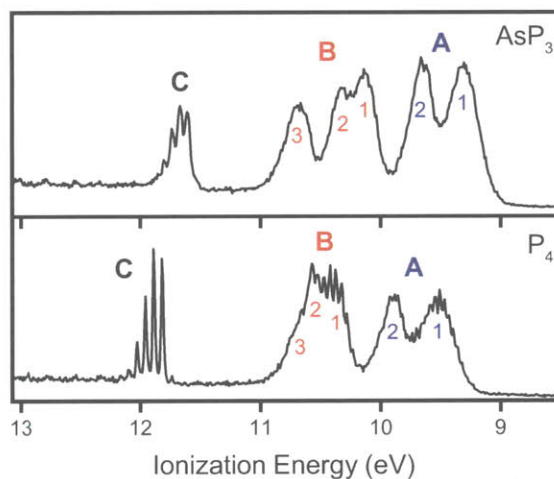


**Figure 2.8.** Photoelectron spectra of  $\text{AsP}_3$  (top) and  $\text{P}_4$  (bottom).

The major difference in appearance between the two spectra occurs in band B. In the  $\text{AsP}_3$  spectrum, the highest energy component is a distinct peak instead of a shoulder. A lowering of molecular symmetry to  $C_{3v}$  splits the  $2t_2$  triple degeneracy that occurs in  $\text{P}_4$  into the  $4a_1$  and  $2e$  orbitals in the neutral molecule of  $\text{AsP}_3$ . This removal of degeneracy in the neutral molecule and before ionization is in contrast to that of  $\text{P}_4$  where the lifting of the degeneracy occurs in the cation. The peaks labeled B(1) and B(2) are a result of a Jahn-Teller distortion and spin-orbit coupling, but the spin-orbit coupling is slightly larger in this system. The spin-orbit coupling constant of the As neutral atom and monovalent ion is 0.20 eV.<sup>40</sup> This increase from about 0.04 eV for the P atom results in a spin-orbit coupling constant of about 0.08 eV on average for the molecule, assuming completely delocalized orbitals for  $\text{AsP}_3$ , and is reflected in the increase of the splitting between the two lower energy components from 0.19 to 0.22 eV.

**Table 2.1.** Vertical ionization energies of  $P_4$  and  $AsP_3$ . The peak positions move to a lower ionization energy from  $P_4$  to  $AsP_3$ .

Peak	$P_4$	$AsP_3$
A(1)	9.52	9.30
A(2)	9.90	9.66
B(1)	10.35	10.13
B(2)	10.54	10.35
B(3)	10.86	10.68
C	11.89	11.67

<sup>a</sup> Values are in units of eV.

Clear vibrational structure outlines the peak at 11.75 eV and is analyzed with a Poisson distribution in Figure 2.9. The spacing of the vibrational progression indicates a vibrational frequency of  $523(3) \text{ cm}^{-1}$ , corresponding to a symmetric stretch of the atoms. This frequency is smaller than that of  $P_4$ , but the Huang-Rhys distortion factor of  $1.15(2)$  is the same. The strong correlations in this vibrational structure between the two molecules further illustrate similarities in electronic structure.

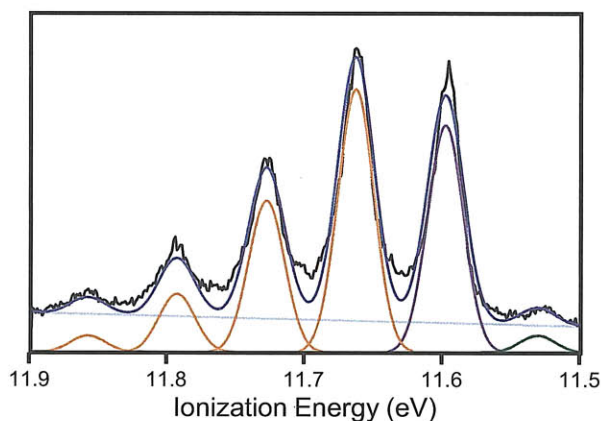


**Figure 2.9.** The vibrational progression of the symmetric stretch in the He I photoelectron spectrum of  $AsP_3$ . The leading green band corresponds to a hot band transition. The purple band is the reference peak; the progression in yellow was generated by a Poisson distribution with a frequency of  $523 \pm 3 \text{ cm}^{-1}$  and a Huang-Rhys factor of 1.15.

Our DFT calculations agree well with the photoelectron spectra of  $P_4$  and  $AsP_3$  (*vide infra*). Comparison of the separation of Kohn-Sham orbitals with the separation of the peaks in the photoelectron spectra shows that the DFT calculations accurately model the electronic structure of the molecules. For peaks affected by the cationic Jahn-Teller distortion and spin-orbit coupling,

an average peak position is used for comparison to the calculated values. Figure 2.10 compares the experimental and calculated orbital separations in an energy level diagram.

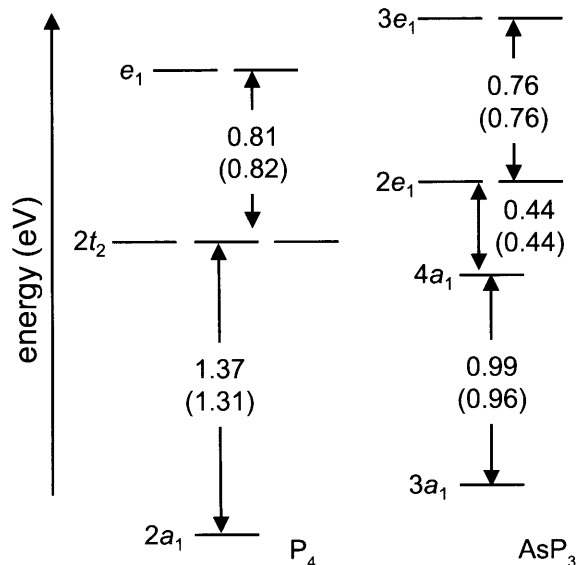


**Figure 2.10.** Energy level diagram of both P<sub>4</sub> and AsP<sub>3</sub>. The top number is the experimental splitting (averaged for the split ionization bands) obtained from the photoelectron spectroscopy data and the bottom number in parentheses is the splitting of Kohn-Sham orbital energies as obtained from DFT calculations.

By changing the photon source of the experiment from He I (21.22 eV) to He II (40.81 eV), insight into the atomic character of molecular orbitals can be obtained. The areas of the peaks change as a result of the photoionization cross-section of each atomic orbital. Because the change in photoionization cross-section from He I to He II for As 4*p* is about double that of P 3*p*,<sup>41</sup> it is expected that the He II intensity of AsP<sub>3</sub> should decrease more than P<sub>4</sub>. However, as illustrated by the spectra in Figure 2.11, the relative decrease in the He II intensity is fairly similar for AsP<sub>3</sub> and P<sub>4</sub>. Table 2.2 lists the ratios of the He II to He I peak areas for each ionization band of both molecules with the area of band A being the reference, and the change in area is the same for both molecules. This consistent area change demonstrates that the photoionization cross-section of the molecules is not dependent on atomic orbital character, indicating that the electrons are extremely delocalized in these molecules.

### 2.4.3 Solid-State NMR Spectroscopy; Collaboration with Prof. Gang Wu, Queen's University

Figure 2.12 shows the solid-state <sup>75</sup>As and <sup>31</sup>P NMR spectra obtained at 14.09 T for a stationary powder sample of AsP<sub>3</sub> at 298 K. The fact that a single sharp peak was observed in each of these

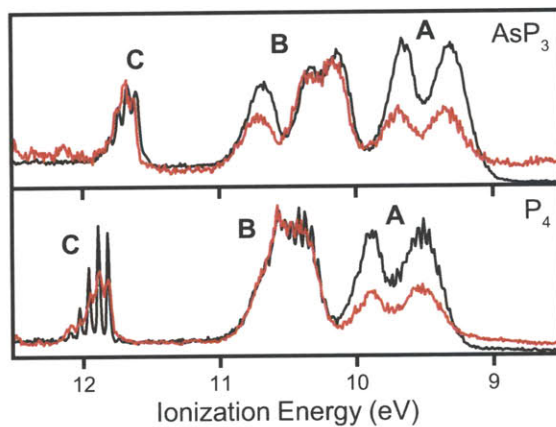


**Figure 2.11.** The comparison between the He I (black) and He II (red) photoelectron spectra show that the changes in peak intensity from He I to He II are very similar, indicating that the electrons are extremely delocalized in these molecules.

**Table 2.2.** The ratios of the peak areas from the He I and the He II photoelectron spectra of  $\text{AsP}_3$  and  $\text{P}_4$  normalized to the area of peak A. The similar area ratios indicate that the molecular orbitals are very delocalized across all four atoms in both molecules.

Ionization Peak	He II/He I $\text{P}_4^a$	He II/He I $\text{AsP}_3$
A	1	1
B	1.90	1.93
C	2.60	2.40

<sup>a</sup> Values are unitless and normalized to peak A.



**Table 2.3.** A comparison of the isotropic  $^{31}\text{P}$  chemical shifts between  $\text{P}_4$  and  $\text{AsP}_3$  in different environments.

Molecule	$\delta_{iso}(^{31}\text{P})$ (ppm)	Molecule	$\delta_{iso}(^{31}\text{P})$ (ppm)
$\text{P}_4$ (g) <sub>exptl</sub>	-551.5	$\text{AsP}_3$ (g) <sub>exptl</sub>	—
$\text{P}_4$ (g) <sub>calc</sub> <sup>a</sup>	-530	$\text{AsP}_3$ (g) <sub>calc</sub>	-492
$\text{P}_4$ (benzene)	-520	$\text{AsP}_4$ (benzene)	-484
$\text{P}_4$ (l)	-460	$\text{AsP}_3$ (l)	—
$\text{P}_4$ (s)	—	$\text{AsP}_3$ (s)	-413

<sup>a</sup> The  $^{31}\text{P}$  chemical shift ( $\delta$ ) was converted from the computed shielding constant ( $\sigma$ ) using the absolute  $^{31}\text{P}$  shielding scale:  $\delta = 328.35 - \sigma$ .

NMR spectra immediately suggests that  $\text{AsP}_3$  molecules undergo rapid reorientation (or jumps) in the solid state at this temperature. This plastic crystal phase behavior of  $\text{AsP}_3$  was observed at temperatures above 213 K. It is well known that above 196.3 K  $\text{P}_4$  is also in a plastic crystal phase.<sup>42</sup> The observed  $^{31}\text{P}$  chemical shift for solid  $\text{AsP}_3$ , -413 ppm, is quite different from that measured in benzene solution, -484 ppm. In fact, as seen from Table 2.3, the  $^{31}\text{P}$  chemical shifts of  $\text{P}_4$  and  $\text{AsP}_3$  exhibit strong dependence on the chemical environment of the molecules. The  $^{75}\text{As}$  chemical shift observed for solid  $\text{AsP}_3$ , -962 ppm, is the most negative value (corresponding to the most shielded environment at the  $^{75}\text{As}$  nucleus) observed among all known arsenic compounds.

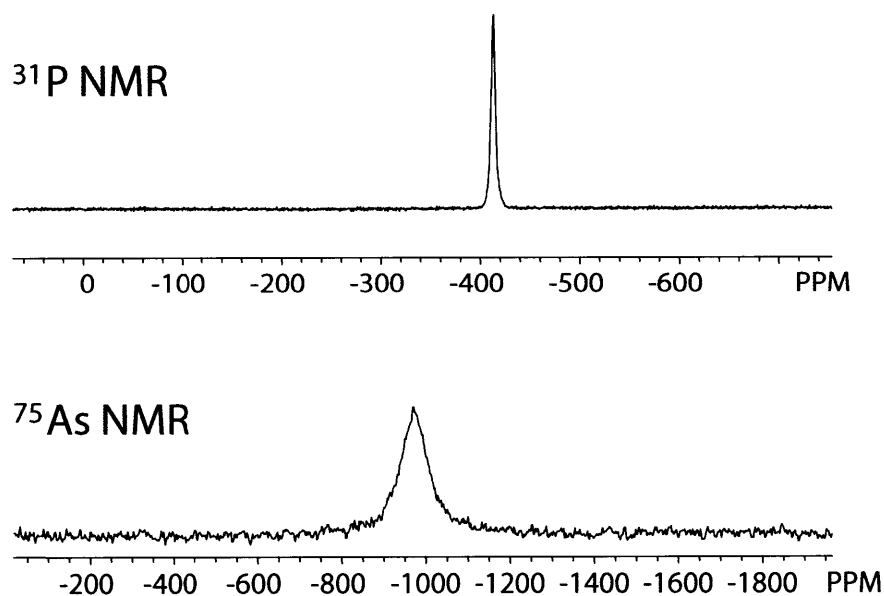


**Figure 2.12.** Solid-state  $^{75}\text{As}$  and  $^{31}\text{P}$  NMR data for  $\text{AsP}_3$  obtained at 14.09 T at 298 K on stationary samples.

To learn more about the molecular dynamics of  $\text{AsP}_3$  in the solid state, spin-lattice relaxation times ( $T_1$ ) were determined for both the  $^{75}\text{As}$  and  $^{31}\text{P}$  nuclei at temperatures between 213 and 313

K. At 14.09 T, the relaxation mechanism for  $^{31}\text{P}$  is predominantly the chemical shift anisotropy. On the other hand, the relaxation mechanism for  $^{75}\text{As}$  ( $I = 3/2$ ) is the quadrupolar interaction. Similar to the case of  $\text{P}_4$ , the molecular jumps of  $\text{AsP}_3$  in the plastic crystal phase satisfy the extreme narrowing condition, i.e.,  $\omega_0\tau \ll 1$  where  $\omega_0$  is the Larmor angular frequency of the nucleus under observation and  $\tau$  is the correlation time for molecular reorientation. It was possible to analyze simultaneously the  $^{75}\text{As}$  and  $^{31}\text{P}$   $T_1$  data shown in Figure 2.13. This analysis yields the following parameters for  $\text{AsP}_3$  reorientation dynamics:  $\tau = \tau_0 \exp(E_a/RT)$  where  $\tau_0 = 3.1 \times 10^{-13}$  s and  $E_a = 5.8$  kJ mol $^{-1}$ . These parameters compare well with those reported for  $\text{P}_4$  ( $\tau_0 = 4.7 \times 10^{-13}$  s and  $E_a = 5.7$  kJ mol $^{-1}$ ).<sup>42</sup> The same  $T_1$  analysis also yields two important NMR parameters:  $\Delta\sigma(^{31}\text{P}) = \sigma_{33} - \sigma_{11} = 400 \pm 10$  ppm, and  $C_Q(^{75}\text{As}) = 42 \pm 2$  MHz, assuming that both the  $^{31}\text{P}$  shielding tensor and the  $^{75}\text{As}$  quadrupole coupling tensor are axially symmetric. The observed  $^{31}\text{P}$  shielding anisotropy for solid  $\text{AsP}_3$  is in excellent agreement with that measured for  $\text{P}_4$ ,  $\Delta\sigma(^{31}\text{P}) = 405$  ppm.<sup>43</sup>

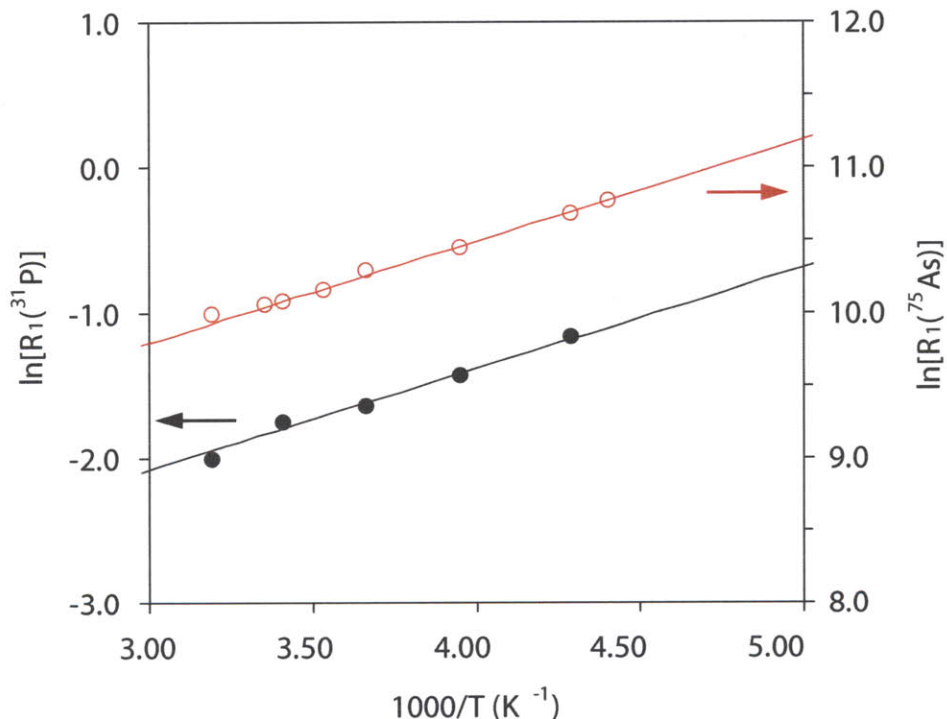


**Figure 2.13.** Variable-temperature  $^{75}\text{As}$  and  $^{31}\text{P}$  spin-lattice relaxation data obtained for solid  $\text{AsP}_3$ .

#### 2.4.4 Experimental and Computed Electronic Properties of $\text{AsP}_3$ and $\text{P}_4$

##### Electrochemistry

The electrochemical profiles of  $\text{AsP}_3$  and  $\text{P}_4$  have been compared using cyclic voltammetry in THF solution Figure 2.14.  $\text{P}_4$  has a single broad reduction event with onset at  $-1.3$  V (peak at  $-1.85$  V) vs  $\text{Fc}/\text{Fc}^+$ , Figure 2.14. This is the only observable reduction feature in the  $\text{P}_4$

cyclic voltammogram (CV) and possibly indicates formation of the  $P_4$  radical anion followed by irreversible bond rupture.<sup>44</sup> Scanning cathodically, the CV of  $AsP_3$  displays a similarly broad irreversible reduction event with onset at  $-1.0$  V (peak at  $-1.6$  V) vs  $Fc/Fc^+$ , which likely is a result of the more easily generated  $AsP_3$  radical anion followed by bond rupture. The earlier onset of reduction for  $AsP_3$  suggests that the LUMO of  $AsP_3$  is lower in energy than the LUMO of  $P_4$  by approximately  $10$  kcal mol<sup>-1</sup>. The calculated molecular orbitals for  $P_4$  and  $AsP_3$  show that the LUMO of  $AsP_3$  is lower in energy by  $4.9$  kcal mol<sup>-1</sup>, Figure 2.15. Scanning anodically from the rest potential, no observable oxidation events are initially observable in the solvent window of the experiment. Upon reduction however, both the  $AsP_3$  and  $P_4$  solutions show a single oxidation wave. Repeated scanning causes the oxidation events to grow in intensity and shift slightly in potential, suggesting that they are a result of electropolymerization or some other complicating process. The observed stabilization of the  $AsP_3$  LUMO relative to that of  $P_4$  renders reduction chemistry more facile and is certainly a contributor to the enhanced reactivity of  $AsP_3$  as compared to  $P_4$ . This result is consistent with information from DFT calculations, as well as with the photoelectron spectroscopy and the solution NMR behavior (*vide infra*).

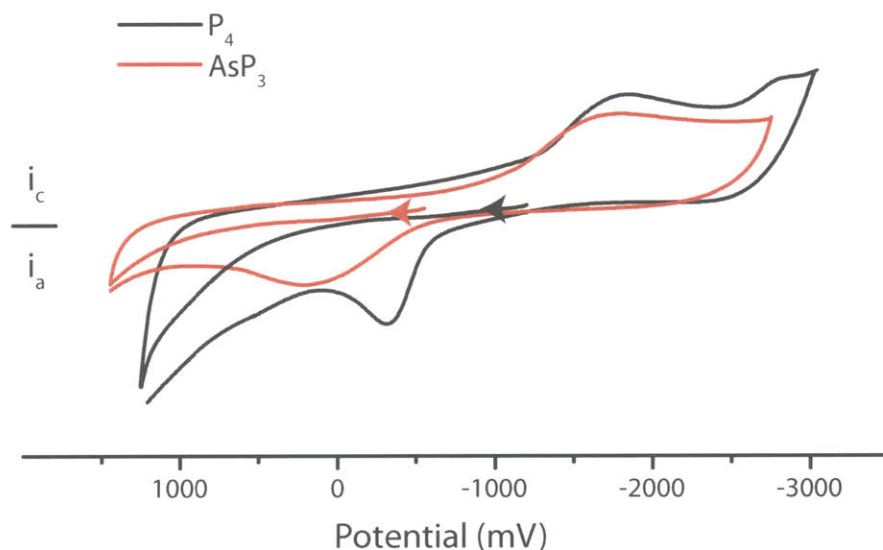


**Figure 2.14.** Cyclic voltammogram of  $AsP_3$  and  $P_4$  obtained in THF with  $0.2$  M  $[TBA][PF_6]$  at a scan rate of  $300$  mV s<sup>-1</sup>.

### Electronic Structure and NMR Chemical Shift

Closer scrutiny of the molecular orbital diagrams of  $AsP_3$  and  $P_4$  gives additional insight into the differences of these two related molecules, Figure 2.15. We find that the HOMO-LUMO energy gap of  $AsP_3$  is smaller in magnitude by roughly  $0.40$  eV compared to that for  $P_4$ . The lower-energy HOMO-LUMO gap of  $AsP_3$  is manifest spectroscopically in the  $^{31}P$  NMR spectrum. It might be expected, on the basis of the electron density distribution in  $AsP_3$ , that the presence of the more

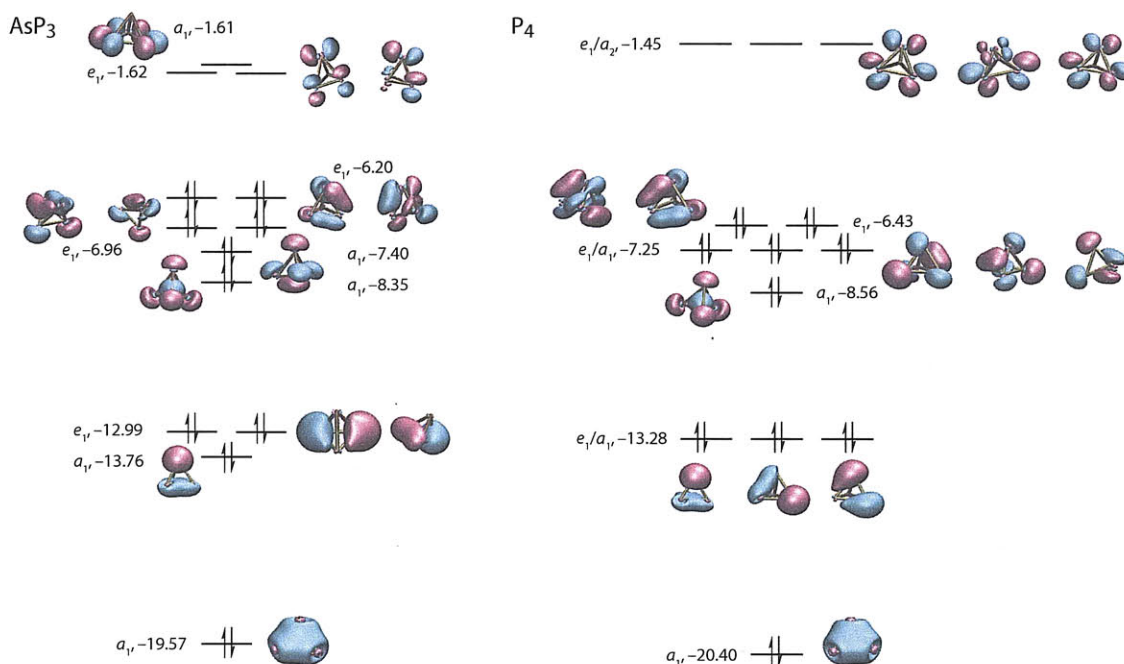


**Figure 2.15.** Molecular orbital diagram of AsP<sub>3</sub> and P<sub>4</sub>.

**Table 2.4.** Computed NMR Chemical Shifts for AsP<sub>3</sub> and P<sub>4</sub>.

Molecule	$\sigma_{dia}$	$\sigma_{para}$	$\sigma_{SO}$	HLG (eV)
AsP <sub>3</sub>	954.694	-151.744	17.372	4.58
P <sub>4</sub>	953.301	-111.418	16.116	4.98

electropositive As atom would increase the electron density at the phosphorus nuclei, causing the remaining three phosphorus atoms to be more shielded and resonate at higher field relative to P<sub>4</sub>. This, however, is not the case. In benzene solution, P<sub>4</sub> resonates at -520 ppm in the <sup>31</sup>P NMR spectrum, while the phosphorus nuclei of AsP<sub>3</sub> resonate at -484 ppm. A decomposition of the NMR shielding terms, as calculated with ADF,<sup>45,46</sup> reveals that the paramagnetic shielding term is the dominant contributor to the chemical shift difference when comparing AsP<sub>3</sub> and P<sub>4</sub>, Table 2.4. The paramagnetic shielding term of AsP<sub>3</sub> is more negative by approximately 40 ppm. This decrease in the paramagnetic term arises from greater coupling of the virtual and occupied orbitals due to the decrease in the HOMO-LUMO gap.<sup>47</sup> Thus, it is the HOMO-LUMO gap, not the electron density at P, that is responsible for the observed chemical shift difference between P<sub>4</sub> and AsP<sub>3</sub>.

### UV-Vis Absorption Spectroscopy

As a complement to the MO description above, the UV-Vis absorption spectrum of AsP<sub>3</sub> was collected in acetonitrile solution to obtain an experimental energy for the HOMO-LUMO gap of AsP<sub>3</sub>. This spectrum shows one distinct absorption maximum at 229 nm with an extinction

coefficient of approximately  $2470 \text{ M}^{-1} \text{ cm}^{-1}$ , Figure 2.16. This feature compares favorably with the lowest energy electronic transition of  $\text{P}_4$  which is reported to have an absorption maximum at 224 nm with an extinction coefficient of  $2550 \text{ M}^{-1} \text{ cm}^{-1}$ . This lowest energy transition in the two tetrahedra corresponds to the HOMO to LUMO transition and indicates that indeed, the HOMO-LUMO gap of  $\text{AsP}_3$  is significantly smaller than that found for  $\text{P}_4$  by 0.12 eV.

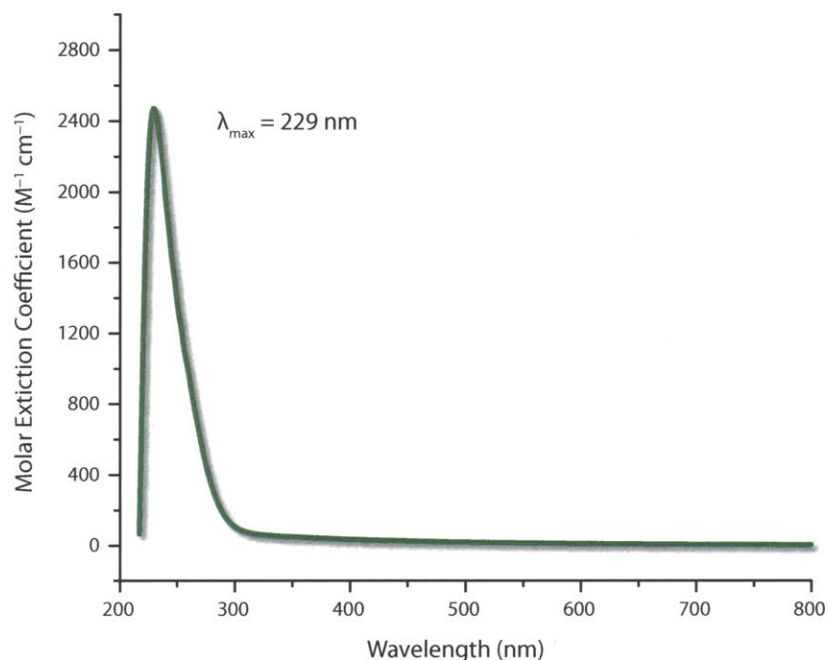


**Figure 2.16.** UV-Vis absorption spectrum of  $\text{AsP}_3$ .

**Two Views of Spherical Aromaticity in  $\text{AsP}_3$  and  $\text{P}_4$ ; Collaboration with Prof. Norbert Mitzel, Raphael Berger, and Stuart Hayes, University of Bielefeld**

An additional electronic property of note for comparison between  $\text{P}_4$  and  $\text{AsP}_3$  is the degree of spherical aromaticity harbored by these clusters. Hirsch and co-workers have previously applied the concept of spherical aromaticity to a variety of  $T_d$  cage molecules including  $\text{P}_4$  by calculating the nucleus-independent chemical shift (NICS) at the cage critical point.<sup>48,49</sup> The NICS value for  $\text{P}_4$  is known by this method to be large and negative, indicative of spherical aromaticity and large diamagnetic ring currents in the cluster. Following location of the cage critical points in  $\text{P}_4$  and  $\text{AsP}_3$ , we find that the NICS value calculated for  $\text{P}_4$ ,  $-59.444$ , is only one unit more negative than that found for  $\text{AsP}_3$ ,  $-58.230$ . This indicates that despite the lowering in molecular symmetry upon going from  $\text{P}_4$  to  $\text{AsP}_3$ , a great deal of spherical aromaticity is retained. The retention of spherical aromaticity is partially due to the fact that  $\text{AsP}_3$ , like  $\text{P}_4$ , maintains closed shell  $\sigma$  and  $\pi$  subsystems, resulting in symmetrically distributed angular momenta and thereby fulfills the  $2(N+1)^2$  rule for spherical aromaticity of cage molecules.<sup>49</sup>

Comparing  $P_4$  and  $AsP_3$  in the above NICS calculations is a bit ambiguous, unfortunately, because using the cage critical point as the reference does not provide a direct comparison due to the symmetry difference in the two molecules. Thus, further investigations were carried out to quantify and compare the degree of aromaticity of  $P_4$  and  $AsP_3$ . GIMIC<sup>50,51</sup> calculations have been performed using electron densities calculated at the DFT level of theory in order to calculate a magnetically induced current density field for  $P_4$  and  $AsP_3$ . The magnetic field was oriented parallel to the center of the gravity-apex atom vector as shown in Figure 2.17. Some representative current density vectors in a plane orthogonal to the magnetic field vector and slightly below the  $P_3$  ring plane are shown in Figure 2.17. The larger current density vectors in this plane outside the molecule describe a strong diamagnetic circular ring current. In order to determine the strength of the total current density induced, the current density vectors were integrated through planes (dark and light gray areas in Figure 2.17) extending from 10 Å below the  $P_3$  ring plane up to 3 Å above the apex atom. The total current densities per magnetic field strength ( $dI/dB$ ) are 49 nA/T for  $P_4$  and 81 nA/T for  $AsP_3$ .

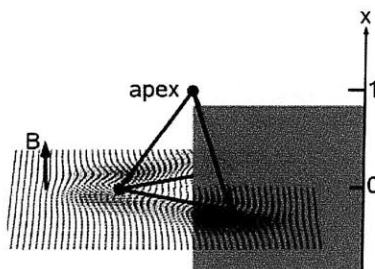


**Figure 2.17.** Relative orientation of the magnetic field ( $B$ ) and the molecules used in the GIMIC calculations.

Since the integration plane passes through half the apex atoms a large contribution to the total current density is given by their closed sub-shells (each closed shell is equivalent to a spherical aromatic system).<sup>50,51</sup> In order to estimate the amount of ring current which does not stem from the apex atoms, the  $x$  derivative of the integrated currents was numerically formed, yielding a local density contribution function. The local minima of these functions  $X_{min}$  (marked in Figure 2.18 with the base of bold vectors) correspond in a sense to a region where the apex-atoms contributions to the current just balance the contribution from the rest of the molecule. Hence the total currents integrated from  $-\infty$  (here numerically approximated by  $-10$  Å) up to  $X_{min}$  can be taken as the apex atom independent ring current. These values are 29 and 17 nA/T for  $P_4$  and  $AsP_3$ . Hence the situation is the reverse of that compared to complete induced ring current values. Our calculations suggest that both compounds can be regarded as strongly aromatic (benzene shows approximate values between 10 and 11 nA/T weakly depending on the level of theory employed to calculate the electron density),<sup>50,51</sup> however,  $AsP_3$  shows distinctly lower magnetically induced current densities flowing through the bond cage than  $P_4$ .

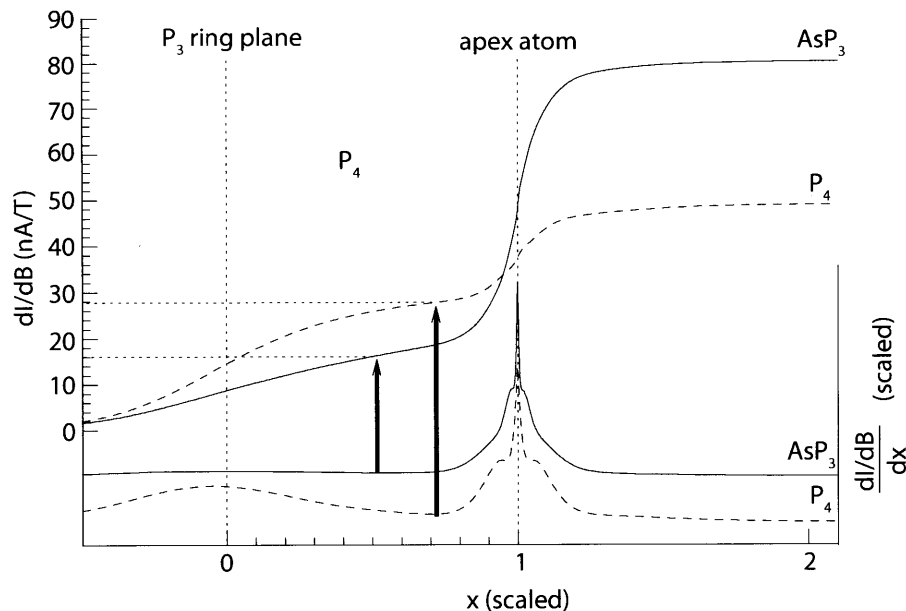


**Figure 2.18.** The two upper curves show the current densities integrated over rectangular regions from 10 Å below the  $P_3$  ring plane to  $x$  for  $P_4$  (dotted line) and  $AsP_3$  (full line). In order to determine the local current contributions from a certain  $x$  level in the molecule, the numerical derivatives of the current density integral curves over  $x$  are determined (two lower curves). The integrated current densities up to the local minima of the derivatives (origins of bold vectors) may be taken as an estimate of the fraction of the total spherical current originating only from the  $P_3$  ring.

### Charge Distribution in $AsP_3$

That the degree of spherical aromaticity in  $AsP_3$  is not diminished relative to that of  $P_4$  implies that the presence of the single As atom does not greatly perturb the charge distribution. There are two limiting views of the charge distribution in  $AsP_3$ : one view is that  $AsP_3$  contains an  $As^{3+}$  ion supported by a  $P_3^{3-}$  unit, while an alternative view is that  $AsP_3$  contains neutral P atoms and a neutral As atom. Calculations using the AIM method have suggested that the phosphorus atoms of  $AsP_3$  harbor a very slight negative charge of  $-0.04 e$  and the arsenic atom makes up the balance, having a slight positive charge of  $+0.12 e$ . Table 2.5 compiles the charge descriptions given by the AIM method, as well as the Hirshfeld and Voroni Deformation Density methods.<sup>52,53</sup> All three methods give generally good agreement of the assigned charges and support the description that  $AsP_3$  contains a neutral As atom and three neutral P atoms. This charge distribution informs our description of  $AsP_3$  as a soluble, molecular combination of these two elements. This analysis is in agreement with more simple interpretations based on Pauling electronegativities (P, 2.19 and As, 2.18), as well as with more complicated theoretical descriptions.<sup>54</sup>

### Atoms in Molecules Analysis of $AsP_3$

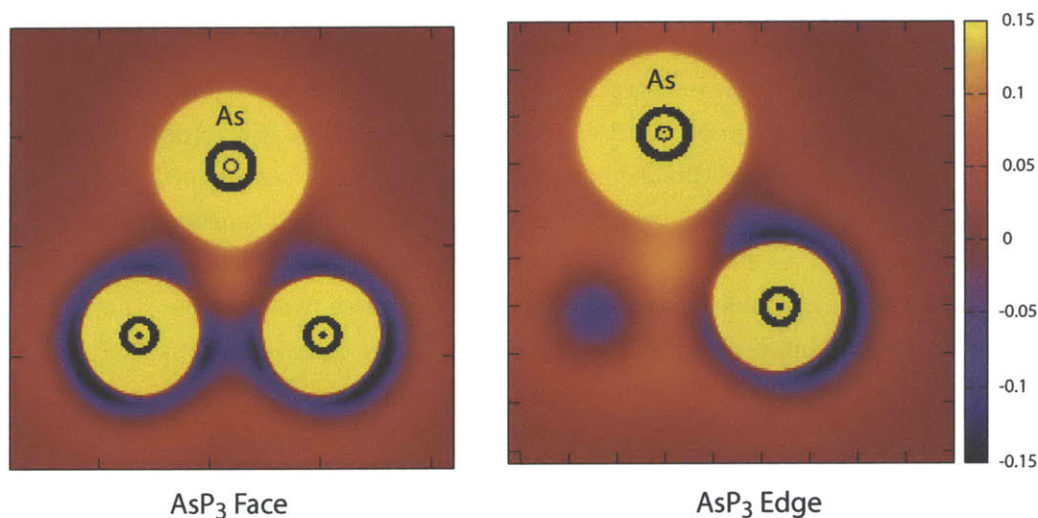
One potentially useful way to visualize the electronic surfaces in these molecules is to plot the Laplacian of the electron density  $\nabla^2(\rho)$ . This function is the scalar derivative of the gradient vector

**Table 2.5.** Calculated Atomic Charges for AsP<sub>3</sub>.

Atom	AIM <sup>a</sup>	Hirschfeld	Voronoi
As	+0.126	+0.046	+0.051
P	-0.042	-0.015	-0.018

<sup>a</sup> Values are in units of *e*

field of the electron density, and it determines where electronic charge is locally concentrated,  $\nabla^2(\rho) < 0$ , and depleted,  $\nabla^2(\rho) > 0$ , with the local charge concentrations providing a mapping of the electron pairs of the Lewis and VSEPR models.<sup>55</sup> A plot of  $\nabla^2(\rho)$  clearly reveals a striking difference in the electronic properties of phosphorus atoms in AsP<sub>3</sub> on the one hand, and the arsenic atom on the other, Figure 2.19. From this, it is evident that the As atom region is associated with diffuse electron density, with a  $\nabla^2(\rho)$  value of  $-0.015$  at the 3,  $-1$  critical point (CP) between the As and P nuclei. This feature observed for the arsenic atom is typical for AIM studies of electropositive metallic elements.<sup>56,57</sup> The P atoms are much more effective at giving rise to regions of valence shell charge concentration (VSCC), in particular between adjacent P atoms with a  $\nabla^2(\rho)$  value of  $-0.0721$  found at the 3,  $-1$  CP, and especially in the spatial regions where VSEPR theory would place a lone pair.<sup>58</sup> These data suggest that in the interaction of AsP<sub>3</sub> with a Lewis acid, one expects binding to occur preferentially at a single phosphorus vertex, and a general ordering of the strength of Lewis basic sites in AsP<sub>3</sub> are as follows: P vertex  $>$  P-P edge  $>$  As-P edge  $>$  As vertex. Furthermore, the diminished concentration of electron density along the As-P bond path ( $\rho = 0.0909$  at the 3,  $-1$  CP) as compared with the P-P bond path ( $\rho = 0.1058$  at the 3,  $-1$  CP) would suggest that As-P bonds will be more susceptible to cleavage than P-P bonds, as has already been suggested by our electrochemistry data.

**Figure 2.19.** Two views of the Laplacian of electron density in AsP<sub>3</sub>.



**Table 2.6.** Calculated heats of atomization, bond energies, and standard heats of formation for  $\text{As}_n\text{P}_{4-n}$ .

Molecule	Heat of Atomization <sup>a,b</sup>	Bond Energy <sup>c</sup>	$\Delta_f H^\circ_0$ <sup>d</sup>
$\text{P}_4$	284	P–P 47	17
$\text{AsP}_3$	266	P–P 47; As–P 41	32
$\text{As}_2\text{P}_2$	250	P–P 47; As–P 41; As–As 36	45
$\text{As}_3\text{P}$	234	As–P 41; As–As 36	57
$\text{As}_4$	220	As–As 36	68

<sup>a</sup> Values are in units of  $\text{kcal mol}^{-1}$  <sup>b</sup> Heat of atomization =  $|\text{total bonding energy } \text{As}_n\text{P}_{4-n}| - |n(\text{energy } ^4\text{S As atoms}) + (4-n)(\text{energy } ^4\text{S P atom})| - |\text{zero-point energy}|$ . <sup>c</sup> Heat of atomization/6. <sup>d</sup>  $\Delta_f H^\circ_0 = \sum(\Delta_f H^\circ_0 \text{ constituent atoms})^{61} - \text{heat of atomization}$ .

#### 2.4.5 Computed Thermodynamic Properties of $\text{As}_n\text{P}_{4-n}$ Tetrahedra

To obtain a more quantitative depiction of the As–P and P–P bond energies in  $\text{AsP}_3$ , the heats of atomization of  $\text{AsP}_3$ ,  $\text{As}_2\text{P}_2$ ,  $\text{As}_3\text{P}$ ,  $\text{P}_4$ , and  $\text{As}_4$  were investigated, which allows for the calculation of average bond energies for these species.<sup>54</sup> Bond energies were computed as an energy difference between the molecule and the single atoms, and the individual atoms were treated as spherically symmetric and spin-restricted.<sup>59</sup> To accurately represent the true atomic ground state, the fragment energy of a single P atom with three  $\alpha$  spins ( $^4\text{S}$  ground state) was used.<sup>59</sup> After correction for the true atomic ground state and for the zero-point energy of the molecule, reliable and accurate heats of atomization were obtained as shown in Table 2.6. These data permit estimation of the bond dissociation energies; for example, the  $\text{P}_4$  molecule is composed of six P–P bonds, so division of the heat of atomization of  $\text{P}_4$  by six gives an estimate of the P–P bond energy. These calculations put the P–P bond energy of  $\text{P}_4$  at  $47 \text{ kcal mol}^{-1}$ , which compares favorably with the  $47 \text{ kcal mol}^{-1}$  obtained from experimental values.<sup>58</sup> Using this energy for the P–P bonds, the As–P bond strength in  $\text{AsP}_3$  can be determined. Following subtraction of 3 P–P single bond energies from the heat of atomization we computed for  $\text{AsP}_3$ , there remain 3 As–P bonds; with an estimated bond dissociation energy of  $41 \text{ kcal mol}^{-1}$  each. Similarly, the As–As bonds of  $\text{As}_4$  were found to have bond dissociation energies of  $36 \text{ kcal mol}^{-1}$ . Keeping the P–P and As–As bond energies constant, extraction of P–As bond energies from the heats of atomization of  $\text{As}_2\text{P}_2$  and  $\text{As}_3\text{P}$  give the same value of  $41 \text{ kcal mol}^{-1}$ , Table 2.6. In summary, these calculations indicate that the As–P bonds of  $\text{AsP}_3$  are  $6 \text{ kcal mol}^{-1}$  weaker than the P–P bonds of  $\text{P}_4$  (and  $5 \text{ kcal mol}^{-1}$  stronger than the As–As bonds of  $\text{As}_4$ ). This is in agreement with the observation of enhanced reactivity of  $\text{AsP}_3$  (*vide infra*) relative to  $\text{P}_4$ , as well as with the reported values for typical P–P, P–As, and As–As single bond strengths.<sup>60</sup>

From the calculated values for heats of atomization and the known heats of formation of the As and P atoms at 0 K, it is possible to extract estimated heats of formation at 0 K for  $\text{As}_n\text{P}_{4-n}$  by summation of the experimental heats of formation of the constituent atoms followed by subtraction of the calculated heats of atomization, Table 2.6. As would be expected, there is a monotonic

increase in the standard heats of formation with increasing  $n$ , Figure 2.20. This trend in heats of formation begins to shed light on the thermodynamic stability of these tetrahedral pnictogen molecules and shows that upon increasing the arsenic content there is a significant price to pay for formation of  $\text{As}_n\text{P}_{4-n}$  from the elements in their standard states.

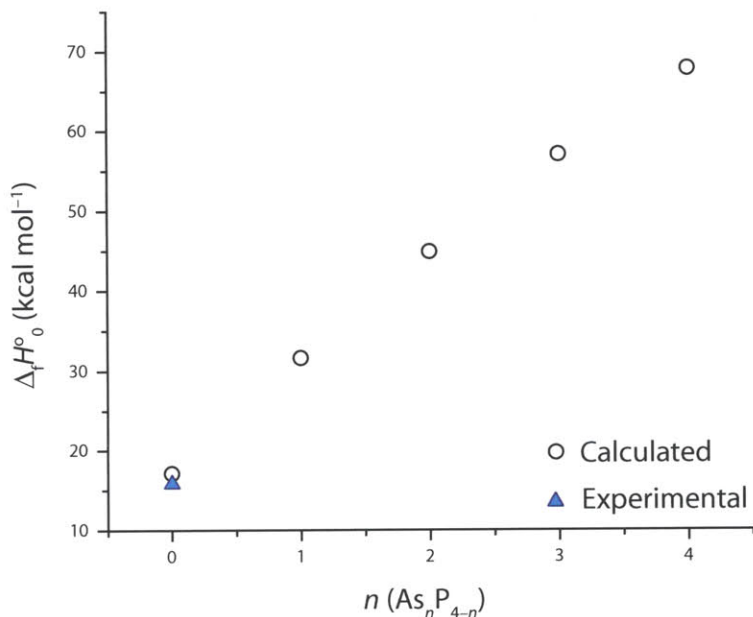


Figure 2.20. Plot of  $\Delta_f H^\circ$  vs  $n$  for  $\text{As}_n\text{P}_{4-n}$ .

## 2.5 REACTIVITY PATTERNS OF $\text{AsP}_3$

A series of reactivity studies have been carried out with  $\text{AsP}_3$ . The reactions chosen have previously been successfully carried out with  $\text{P}_4$  and include thermolysis, adduct formation, single bond cleavage reactions by transition metal and organic radicals, and molecule activation with  $\text{Nb}(\text{H})(\eta^2\text{-}^i\text{Bu}(\text{H})\text{CNAr})(\text{N}[\text{CH}_2^i\text{Bu}]\text{Ar})_2$  ( $\text{Ar} = 3,5\text{-Me}_2\text{C}_6\text{H}_3$ ),  $\text{Mo}(\text{N}[^i\text{Bu}]\text{Ar})_3$ ,  $[\text{GaC}(\text{SiMe}_3)_3]_4$ , and  $\text{Cl}_2\text{Nb}(\text{ODipp})_3$  under reducing conditions. Looking at such a class of reactions would allow for a comparison of the reactivity patterns of  $\text{P}_4$  and  $\text{AsP}_3$  in light of their contrasting physical and electronic properties as elucidated in the preceding studies.

### 2.5.1 Thermal, and Photolytic Reactions of $\text{AsP}_3$

Amorphous red phosphorus was first obtained in 1848 by heating  $\text{P}_4$  in the absence of air for several days at high temperatures, and is now made on a commercial scale of 7000 tons per year by a similar thermal conversion process.<sup>2</sup> Red phosphorus is much less toxic and much less reactive than monomeric white phosphorus and it is extensively used in the production of matches, flame retardants, and phosphide materials for semiconductor applications.<sup>2</sup> Semiconductor applications

account for a majority of red phosphorus consumption, with aluminum phosphide production accounting for over 24% of the total consumption. Much of this aluminum phosphide is further alloyed with species such as gallium arsenide to tune the semiconductor band gap.<sup>2,62</sup> Polymeric forms of P/As alloys are exceedingly rare.<sup>63,64</sup>

## Thermolysis

Intrigued by the possibility of a “red  $\text{AsP}_3$ ” phase wherein one out of every four sites in red P would be occupied by an As atom, we subjected  $\text{AsP}_3$  to the same conditions under which  $\text{P}_4$  converts to red P. Heating a sealed tube containing white  $\text{AsP}_3$  to 300 °C for 36 h resulted in apparent segregation of the elements, producing amorphous metallic arsenic and amorphous red phosphorus, as determined by Raman spectroscopy (diagnostic for red P),<sup>65</sup> powder XRD analysis (diagnostic for amorphous metallic As),<sup>66</sup> and EDS elemental analysis of the bulk material, Figure 2.21. The EDS elemental map shown in Figure 2.21 shows distinct regions where only phosphorus (red) and only arsenic (green) are sequestered; however, there are some regions (yellow) where the two species may be found together, suggestive of incomplete separation. Repetition of this experiment on a variety of scales gave reproducible results.

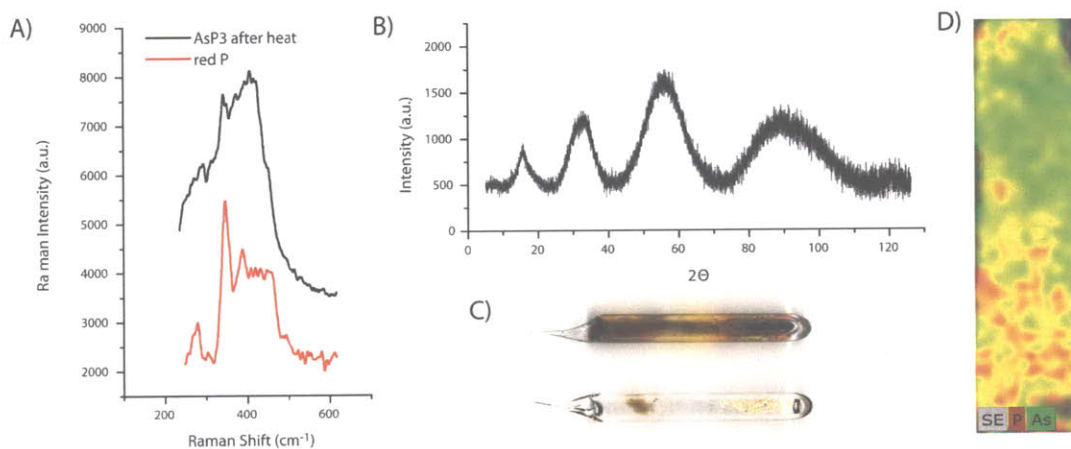


**Figure 2.21.**  $\text{AsP}_3$  thermolysis. (A) Raman spectrum of thermolyzed material and genuine red P; (B) Powder XRD spectrum of the thermolyzed material clearly showing the characteristic pattern for amorphous arsenic; (C) Before and after images of the reaction tube; (D) EDS elemental map of the thermolyzed material showing areas of arsenic and phosphorus separation.

Thermal decomposition of  $\text{AsP}_3$  to the elements was unexpected and the mechanism by which this occurs is not known. One possibility is that under thermal conditions four molecules of  $\text{AsP}_3$  disproportionate to give rise to three molecules of  $\text{P}_4$  and one molecule of  $\text{As}_4$ , which themselves then revert to red phosphorus and metallic arsenic. From our calculated heats of formation, Figure 2.20, we can get an estimate for the heat of disproportionation of four molecules of  $\text{AsP}_3$  to give three molecules of  $\text{P}_4$  and one molecule of  $\text{As}_4$ . In so doing we find that the process is downhill by 7.42 kcal mol<sup>-1</sup>, suggesting that the kinetic stability of  $\text{AsP}_3$  is quite important in its isolability, as

thermodynamically it is only metastable. An alternative mechanism might involve the formation of “red  $\text{AsP}_3$ ”, which is not itself thermally robust, reverting to red phosphorus and metallic arsenic. A final possibility involves direct homolysis of the As–P bonds, resulting in unstable fragments that would readily polymerize to As metal and red P.

### Photolysis

UV-photolysis of  $\text{AsP}_3$  represents, perhaps, a gentler alternative to accessing a polymeric form of  $\text{AsP}_3$  when compared to high temperature thermolysis procedures. It is known that  $\text{P}_4$  can give rise to red P under suitable photolysis conditions, however it is thought that the polymerization process is preceded by fragmentation of  $\text{P}_4$  to 2 units of  $\text{P}_2$  or to  $\text{P}_1$  and  $\text{P}_3$ , depending on the energies applied.<sup>67</sup> Given the similarity in the absorption spectra of  $\text{AsP}_3$  and the slight red shift of the HOMO to LUMO transition, Figure 2.16, it seemed likely that  $\text{AsP}_3$  would behave similarly and that photolysis would potentially allow access to polymeric  $\text{AsP}_3$ .  $\text{AsP}_3$  was subjected to UV radiation in the range from 190 to 250 nm as a solution in THF. After just 20 minutes, the homogeneous colorless solution became turbid with a brick-red precipitate, Figure 2.22.



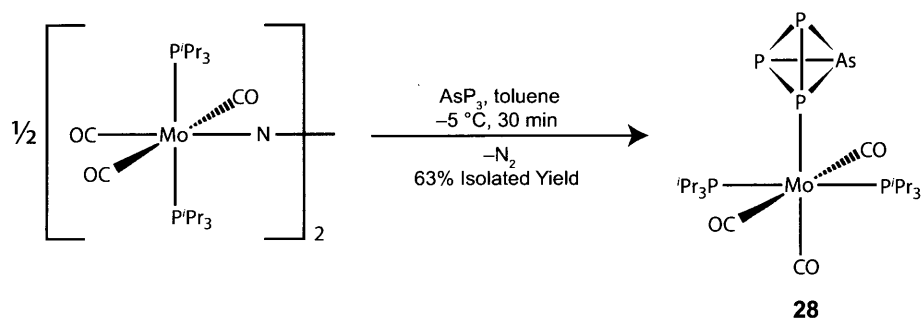
**Figure 2.22.**  $\text{AsP}_3$  photolysis; before and after.

It was found that 4 h of photolysis was sufficient to consume all of the  $\text{AsP}_3$  starting material. Isolation of the precipitated solids that formed upon photolysis and analysis by Raman spectroscopy, powder diffraction studies, and EDS spectroscopy led again to the conclusion that element segregation had ensued, resulting in amorphous metallic arsenic (clearly observable by powder diffraction) and amorphous red phosphorus (clearly observable by Raman spectroscopy). The mechanism for  $\text{AsP}_3$  degradation under UV photolysis likely proceeds by a similar mechanism to  $\text{P}_4$  with fragmentation of the  $\text{AsP}_3$  tetrahedron into  $\text{As}\equiv\text{P}$  and  $\text{P}\equiv\text{P}$  or As and  $\text{P}_3$  being the first step. This result in conjunction with the thermolysis studies strongly suggests that  $\text{AsP}_3$  can be thought of as a metastable species, readily reverting to its constituent elements.

### 2.5.2 Coordination of an Intact $\text{AsP}_3$ Tetrahedron

In order to crystallographically characterize and begin exploring the reactivity properties of  $\text{AsP}_3$ , we sought to complex it to a metal fragment. Scheer and coworkers have shown that the electronically and coordinatively unsaturated complexes  $[\text{M}(\text{CO})_3(\text{PR}_3)_2]$  ( $\text{M} = \text{Mo}, \text{W}$  and  $\text{R} = ^i\text{Pr}$ ,

Cy) are capable of binding  $P_4$  at a vertex.<sup>68,69</sup> Treatment of 1 equiv of  $(N_2)[Mo(CO)_3(P^iPr_3)_2]_2$  with 2 equiv of  $AsP_3$  in toluene at  $-5\text{ }^\circ\text{C}$  resulted in rapid displacement of the bridging  $N_2$  ligand to give a deep orange solution. After 30 minutes of reaction time, concentration of the toluene solution at  $0\text{ }^\circ\text{C}$  and subsequent storage at  $-35\text{ }^\circ\text{C}$  yielded orange crystals of  $(AsP_3)Mo(CO)_3(P^iPr_3)_2$ , **28**, in 63% yield (Scheme 2.7). Solid samples of **28** are stable at room temperature, but solutions of complex **28** must be kept cold to avoid degradation.<sup>68</sup> Complex **28** has been characterized by single-crystal X-ray crystallography, Figure 2.23. The  $AsP_3$  tetrahedron is bound to the metal center by a single phosphorus vertex at a distance of  $2.487(1)\text{ \AA}$  (for comparison the Mo-phosphine distances average to  $2.530\text{ \AA}$ ). The three P–P bonds in the tetrahedron average to  $2.177\text{ \AA}$  while the three As–P bonds are longer at an average of  $2.305\text{ \AA}$ . The NMR data ( $^{31}\text{P}$ ,  $^{13}\text{C}$ ,  $^1\text{H}$ ) for this complex were initially collected at  $-10\text{ }^\circ\text{C}$  with the  $^{31}\text{P}$  NMR spectrum showing three broadened features in a 2:1:2 ratio at 58 ( $P^iPr_3$ ),  $-361$  (Mo– $PP_2As$ ), and  $-448$  (Mo– $PP_2As$ ) ppm, respectively. Upon further cooling to  $-55\text{ }^\circ\text{C}$ , the  $AsP_3$  derived resonances sharpen into a doublet and a triplet with  $^1J_{P/P} = 218\text{ Hz}$ . At this temperature is also observed the growth in of a proposed coordination isomer assigned as the P–P edge-bound form of complex **28** with resonances at approximately  $-330$  (Mo– $P_2PAs$ ), and  $-440$  (Mo– $P_2PAs$ ) ppm for the edge-bound tetrahedron and  $K_{eq} = 0.38$  at  $-55\text{ }^\circ\text{C}$ , where  $K_{eq} = [\text{edge bound}]/[\text{vertex bound}]$ , Figure 2.24. It is noteworthy that most  $\eta^1$ -monohapto  $P_4$  complexes and all of the known edge-bound  $P_4$  complexes are thermally unstable, and that it is relatively rare to isolate a complex with an intact  $P_4$  tetrahedron.<sup>68,70–76</sup> The observation of  $AsP_3$  coordination to Mo through a P rather than an As vertex is consistent with frontier orbital considerations for  $AsP_3$ .



**Scheme 2.7.** Preparation of  $(AsP_3)Mo(CO)_3(P^iPr_3)_2$ .

Isolation of **28** left us somewhat unsatisfied as the complex was difficult to work with in solution due to its thermal instability, and the single crystal X-ray structure showed the arsenic atom disordered over two positions. We therefore sought to synthesize a thermally stable adduct of  $AsP_3$  and hoped to obtain accurate metrical parameters from an ordered crystal structure. Use of the precursor complex  $FeCp^*(dppe)Cl$ , which had been reported to form a stable  $P_4$  adduct,<sup>73</sup> allowed us to realize this goal. Treatment of dark-green  $FeCp^*(dppe)Cl$  with 1 equiv of  $AsP_3$  in THF resulted in a gradual color change to brown over 20 min. Subsequent treatment of the

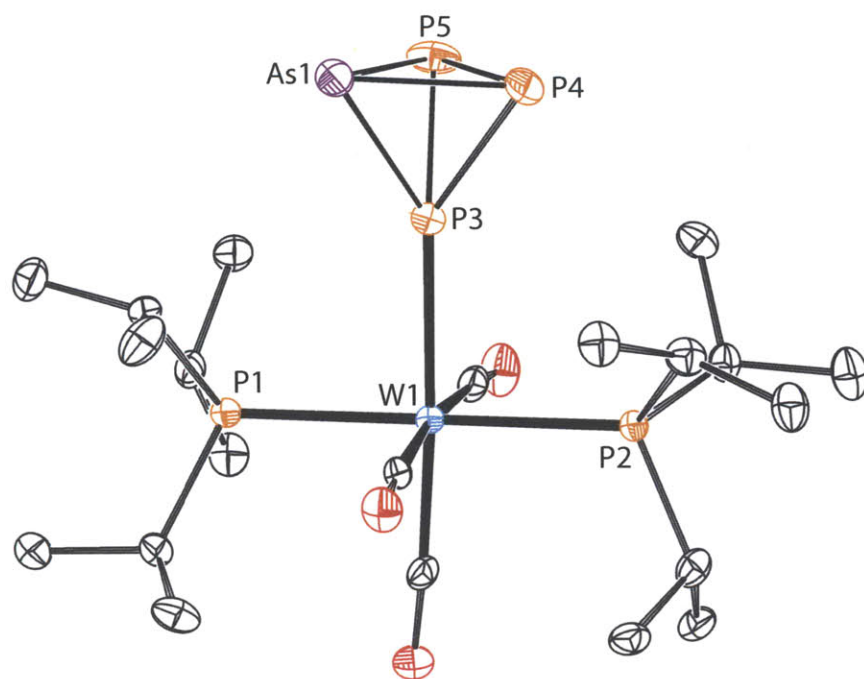


**Figure 2.23.** Thermal ellipsoid plot (50% probability) of  $(AsP_3)Mo(CO)_3(P^iPr_3)_2$  with hydrogen atoms omitted for clarity.

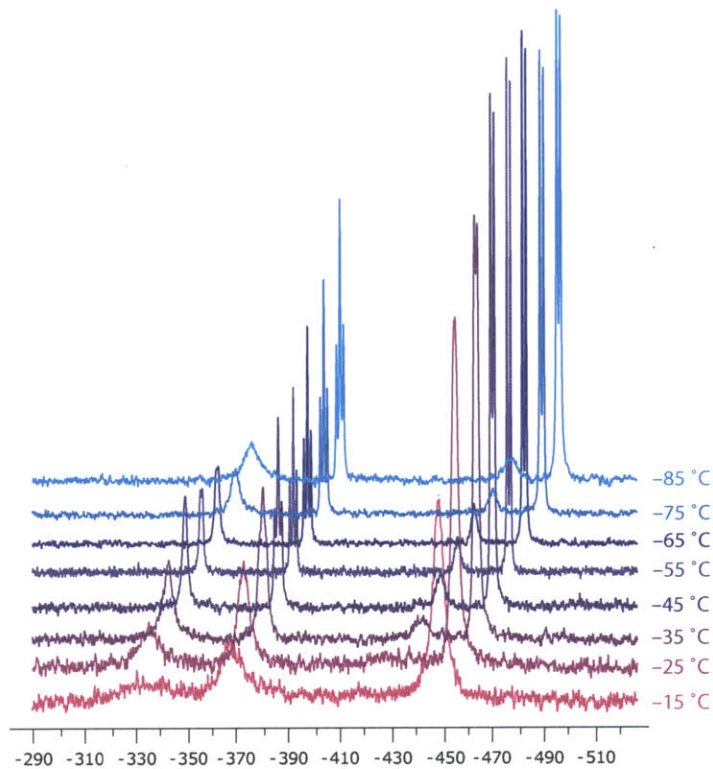
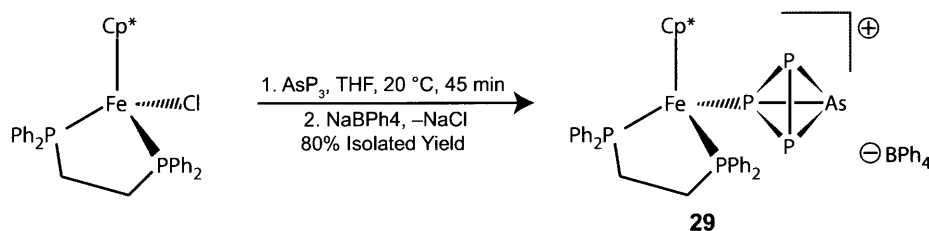


**Figure 2.24.** Variable temperature  $^{31}P$  NMR spectrum of  $(AsP_3)Mo(CO)_3(P^iPr_3)_2$  showing an equilibrium between the P vertex-bound form and the P-P edge-bound form.

reaction mixture with 1 equiv of Na[BPh<sub>4</sub>] to fully displace the coordinated chloride ion resulted in an immediate color change to bright magenta. Following removal of the NaCl byproduct, [(AsP<sub>3</sub>)Fe(Cp\*)(dppe)][BPh<sub>4</sub>], **29**, was isolated in 80% yield by recrystallization of the crude solids from 1:1 Et<sub>2</sub>O/THF, Scheme 2.8. X-ray diffraction quality crystals of **29** were grown from a mixture of THF and CH<sub>2</sub>Cl<sub>2</sub> at -35 °C over the course of several days. The X-ray crystal structure of **29**, Figure 2.25, displays a fully ordered AsP<sub>3</sub> tetrahedron in an η<sup>1</sup> binding mode at a phosphorus vertex. The solid-state structure of **29** is consistent with the solution-phase configuration of the AsP<sub>3</sub> unit as assigned by NMR spectroscopy, Figure 2.26. The P3-As1 and P3-P4,5 distances in **29** are 2.283(2) Å and 2.183(3) Å, respectively, and are noticeably shorter than typical P-As and P-P single bonds. The other As-P and P-P bonds are noticeably longer with As1-P4 at 2.334(2) Å, As1-P5 at 2.336(2) Å, and P4-P5 at 2.231(3) Å. The shortened bond lengths to P3 are likely a direct effect of coordination of the Lewis acidic iron fragment to the P atom, removing electron density from that atom and causing it to bond more strongly to the AsP<sub>2</sub> ring, Figure 2.27. It is noteworthy that the Fe1-P3 interatomic distance of 2.172(2) Å is significantly shorter than the Fe-phosphine bond distances at 2.233(2) Å and 2.242(2) Å.



**Scheme 2.8.** Preparation of [(AsP<sub>3</sub>)Fe(Cp\*)(dppe)][BPh<sub>4</sub>].

### 2.5.3 Cleavage of a Single As-P Bond

The estimated 6 kcal mol<sup>-1</sup> difference in energy between the As-P bonds and the P-P bonds in AsP<sub>3</sub> suggests that reactions resulting in selective As-P bond cleavage may be possible. Several systems are known to promote radical opening of the P<sub>4</sub> tetrahedron to produce substituted tetraphosphabicyclobutane structures. A noteworthy example of this reaction type was reported by Lappert and coworkers and uses (P(N(<sup>*i*</sup>Pr)<sub>2</sub>)N(SiMe<sub>3</sub>)<sub>2</sub>)<sub>2</sub> as a source of the phosphorus radical P(N(<sup>*i*</sup>Pr)<sub>2</sub>)N(SiMe<sub>3</sub>)<sub>2</sub>, which was shown to activate P<sub>4</sub> to produce the corresponding 1,4-bis(phosphido)tetraphosphabicyclobutane.<sup>77</sup> Whereas activation of P<sub>4</sub> by (P(N(<sup>*i*</sup>Pr)<sub>2</sub>)N(SiMe<sub>3</sub>)<sub>2</sub>)<sub>2</sub> requires somewhat harsh conditions (refluxing in toluene for 1.5 h), the corresponding reaction with AsP<sub>3</sub> is rapid at room temperature. Upon mixing (P(N(<sup>*i*</sup>Pr)<sub>2</sub>)N(SiMe<sub>3</sub>)<sub>2</sub>)<sub>2</sub> with 1 equiv of AsP<sub>3</sub> in toluene the initially colorless reaction mixture turns bright yellow. NMR spectroscopic analysis of the crude reaction mixture shows clean and

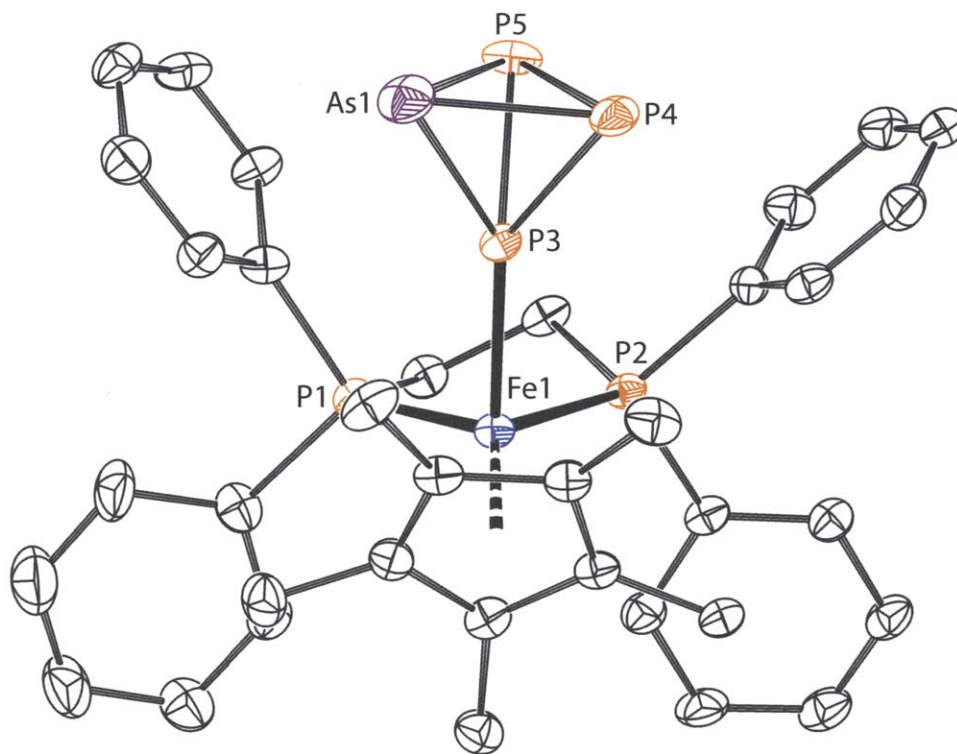


**Figure 2.25.** Thermal ellipsoid plot (50% probability) of  $[(AsP_3)Fe(Cp^*)(dppe)][BPh_4]$  with hydrogen atoms and BPh<sub>4</sub> counter-ion omitted for clarity. The major component of the disordered tetrahedron is shown.

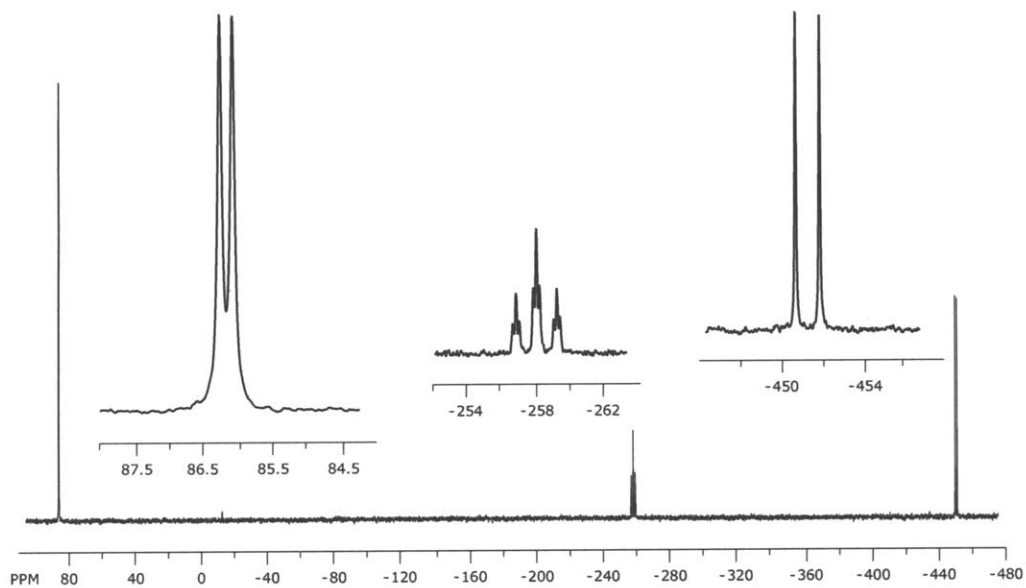


**Figure 2.26.** <sup>31</sup>P NMR spectrum of  $[(AsP_3)Fe(Cp^*)(dppe)][BPh_4]$ .



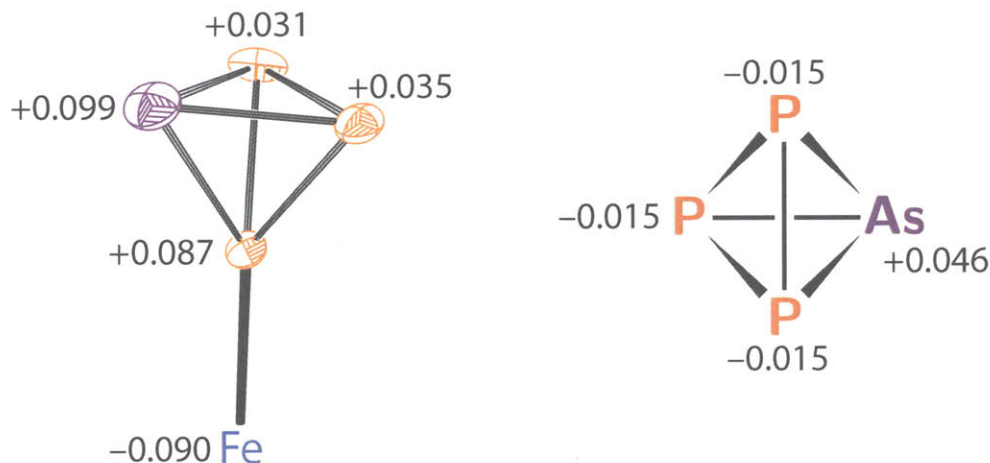
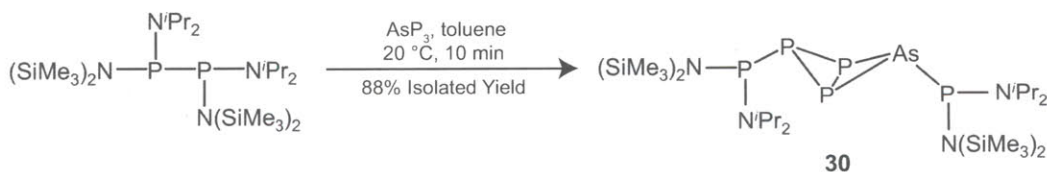


**Figure 2.27.** Charge analysis of  $[(\text{AsP}_3)\text{Fe}(\text{Cp}^*)(\text{dppe})][\text{BPh}_4]$  and comparison with free  $\text{AsP}_3$ .

quantitative conversion to  $[\text{P}(\text{N}^i\text{Pr}_2)(\text{N}(\text{SiMe}_3)_2)]_2(\text{AsP}_3)$ , **61**, in which a single As–P bond has been selectively cleaved, as assigned by  $^{31}\text{P}$  NMR spectroscopy, Scheme 2.9 and Figure 2.28. Recrystallization of the crude reaction mixture from *n*-hexane/ $\text{Et}_2\text{O}$  gave crystalline **30** in 88% yield. X-ray crystallographic analysis on a single crystal of **30** confirmed the selective As–P bond cleavage as shown in Figure 2.29. The geometrical parameters of the arsatriphosphabicyclobutane core of **30** are nearly isomorphous with the all-phosphorus analogue as reported by Lappert and co-workers.<sup>77</sup> A discussion of accurate P–P and As–P bond lengths is precluded by disorder in the crystal structure of **30**. Notably, there is a positional disorder of As1 and P4, but there is no As component to the P3 or P5 positions.



**Scheme 2.9.** Preparation of  $[\text{P}(\text{N}^i\text{Pr}_2)(\text{N}(\text{SiMe}_3)_2)]_2(\text{AsP}_3)$ .

The bright green Ti(III) reagent  $\text{Ti}(\text{N}^t\text{BuAr})_3$  ( $\text{Ar} = 3,5\text{-Me}_2\text{C}_6\text{H}_3$ ) has proven to be a potent metalloradical and one electron reductant since its first synthesis by reduction of the corresponding  $\text{ClTi}(\text{N}^t\text{BuAr})_3$  complex in 1995.<sup>78–82</sup> Given the facile radical opening of the  $\text{AsP}_3$  tetrahedron with  $(\text{P}(\text{N}^i\text{Pr}_2)\text{N}(\text{SiMe}_3)_2)_2$ , we hypothesized that  $\text{Ti}(\text{N}^t\text{BuAr})_3$  would be a good candidate for forming a 1,4-bis(metallo)arsatriphosphabicyclobutane. In fact,  $\text{Ti}(\text{N}^t\text{BuAr})_3$  does react with  $\text{AsP}_3$  to generate the desired 1,4-bis(metallo)arsatriphosphabicyclobutane,  $(\text{Ar}^t\text{BuN})_3\text{Ti}[\text{P}(\text{P}_2)\text{As}]\text{Ti}(\text{N}^t\text{BuAr})_3$ , **31**, in which a single As–P bond has been cleaved selectively; however, the reaction does not go to completion. Instead, an equilibrium is

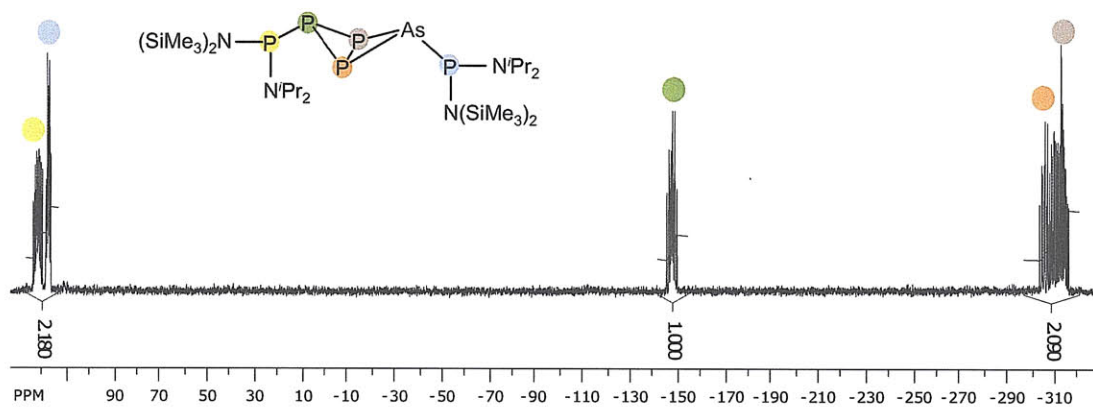


**Figure 2.28.**  $^{31}\text{P}$  NMR spectrum of  $[\text{P}(\text{N}^i\text{Pr}_2)(\text{N}(\text{SiMe}_3)_2)]_2(\text{AsP}_3)$ .

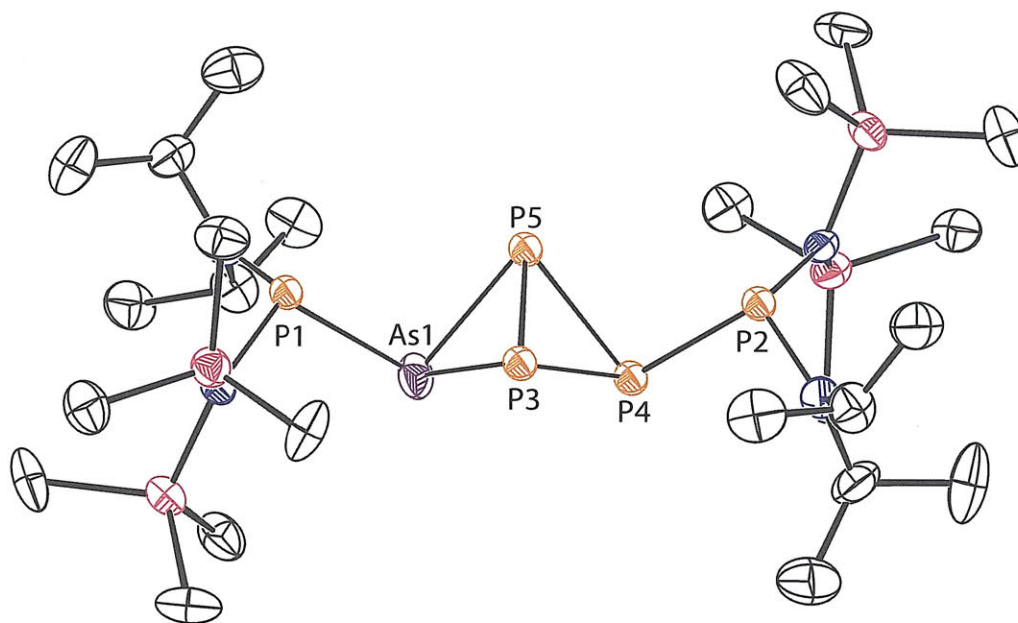
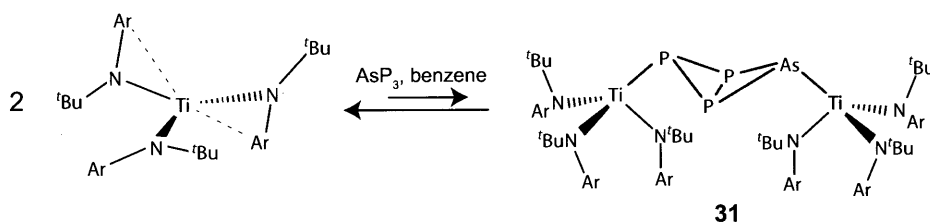


**Figure 2.29.** Thermal ellipsoid plot (50% probability) of  $[\text{P}(\text{N}^i\text{Pr}_2)(\text{N}(\text{SiMe}_3)_2)]_2(\text{AsP}_3)$  with hydrogen atoms omitted for clarity. The major component of the disordered arsenatrichosphabicyclobutane unit is shown.

established between  $\text{AsP}_3$ ,  $\text{Ti}(\text{N}[\text{tBu}]\text{Ar})_3$ , and **31**, Scheme 2.10. This equilibrium was studied by  $^{31}\text{P}$  NMR spectroscopy at a variety of concentrations and temperatures. In all cases the equilibrium favored the reactants, with **31** never accounting for more than 30% of the reaction mixture.<sup>83</sup> The analogous reaction with  $\text{P}_4$  likewise gave an equilibrium mixture, but the 1,4-bis(metallo)tetraphosphabicyclobutane product,  $(\text{Ar}[\text{tBu}]\text{N})_3\text{Ti}[\text{P}(\text{P}_2)\text{P}]\text{Ti}(\text{N}[\text{tBu}]\text{Ar})_3$ , **32**, never accounted for more than 5% of the reaction mixture under identical conditions. Although no intermediates were detected in these equilibria, the systems did not conform to the simple equilibrium expression,  $K_{eq} = 3/[\text{Ti}(\text{N}[\text{tBu}]\text{Ar})_3]_2[\text{EP}_3]$  ( $\text{E} = \text{As}, \text{P}$ ), suggesting that more complicated processes are at work. It should be noted that the concentration of  $\text{Ti}(\text{N}[\text{tBu}]\text{Ar})_3$  was obtained by subtraction of **31** (or **32**) from  $[\text{Ti}(\text{N}[\text{tBu}]\text{Ar})_3]_0$ . As a confirmation that more complicated equilibria processes were involved, it was found that when concentrated solutions of  $\text{Ti}(\text{N}[\text{tBu}]\text{Ar})_3$  and  $\text{AsP}_3$  were allowed to sit, the presence of  $\text{P}_4$  and  $\text{As}_2\text{P}_2$  could be confirmed after 24 h by  $^{31}\text{P}$  NMR spectroscopy (singlets at  $-520$  and  $-452$ , respectively), suggestive of multimolecular degradation pathways being accessible.



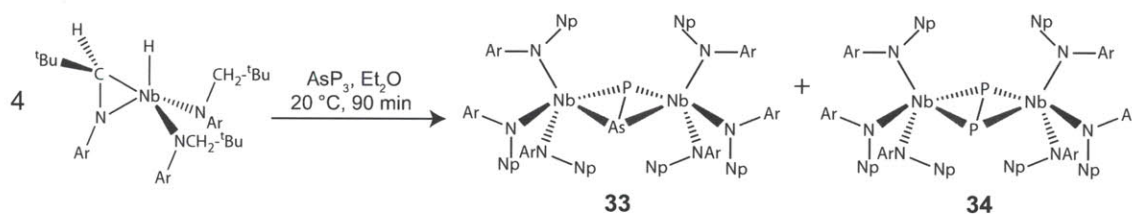
**Scheme 2.10.** Preparation of  $(\text{Ar}[\text{tBu}]\text{N})_3\text{Ti}[\text{P}(\text{P}_2)\text{As}]\text{Ti}(\text{N}[\text{tBu}]\text{Ar})_3$ .

In direct competition reactions, the tendency of  $\text{Ti}(\text{N}[\text{tBu}]\text{Ar})_3$  to react with  $\text{EP}_3$  ( $\text{E} = \text{P}, \text{As}$ ) to form the radical-opened bicyclobutane derivatives, **31** and **32**, revealed a measurable preference for edge-opening of  $\text{AsP}_3$ , consistent with heightened reactivity for  $\text{AsP}_3$  over  $\text{P}_4$  (*vide supra*). One hypothesis for why  $\text{Ti}(\text{N}[\text{tBu}]\text{Ar})_3$  is unsuccessful at driving the radical cleavage of either  $\text{P}_4$  or  $\text{AsP}_3$  fully to the edge-opened products is centered upon the unfavorable loss in entropy inherent in forming a single product molecule from three reactant molecules. The interaction between the hard titanium(IV) metal center and the soft phosphorus (or arsenic) center does not provide a large enough enthalpic contribution to counterbalance the entropic losses incurred.

#### 2.5.4 Reactivity with $\text{HNb}(\eta^2\text{-tBuCH=NAr})(\text{N}[\text{CH}_2\text{tBu}]\text{Ar})_2$ and $\text{Mo}(\text{N}[\text{tBu}]\text{Ar})_3$

The activation of white phosphorus by early transition-metal complexes has been a prolific area of investigation in recent years.<sup>10,84–86</sup> Included among these are niobium complexes bearing three monoanionic ligands. This class of complexes has given rise to a wide array of  $\text{P}_n$  ligands ( $n = 1-8$ ).<sup>84</sup> The metallaziridine-hydride derivative,  $\text{HNb}(\eta^2\text{-tBuCH=NAr})(\text{N}[\text{CH}_2\text{tBu}]\text{Ar})_2$ , was found to react with 0.25 equiv of white phosphorus to quantitatively give rise to the corresponding butterfly complex,  $(\mu_2\text{:}\eta^2, \eta^2\text{-P}_2)[\text{Nb}(\text{N}[\text{CH}_2\text{tBu}]\text{Ar})_3]_2$ , which has a diagnostic phosphorus NMR resonance

at 399 ppm in C<sub>6</sub>D<sub>6</sub>. Because of the high efficiency of this reaction it seemed to be an ideal candidate for reactivity tests with AsP<sub>3</sub>, with an eye toward formation of ( $\mu_2$ : $\eta^2$ , $\eta^2$ -P<sub>2</sub>)[Nb(N[CH<sub>2</sub><sup>t</sup>Bu]Ar)<sub>3</sub>]<sub>2</sub> and ( $\mu_2$ : $\eta^2$ , $\eta^2$ -AsP)[Nb(N[CH<sub>2</sub><sup>t</sup>Bu]Ar)<sub>3</sub>]<sub>2</sub> in a 1:1 ratio. In fact, treatment of bright yellow HNb( $\eta^2$ -<sup>t</sup>BuCH=NAr)(N[CH<sub>2</sub><sup>t</sup>Bu]Ar)<sub>2</sub> with a slight excess (0.35 equiv) of AsP<sub>3</sub> results in conversion to the expected 1:1 green mixture of products, ( $\mu_2$ : $\eta^2$ , $\eta^2$ -P<sub>2</sub>)[Nb(N[CH<sub>2</sub><sup>t</sup>Bu]Ar)<sub>3</sub>]<sub>2</sub>, **34**, and ( $\mu_2$ : $\eta^2$ , $\eta^2$ -AsP)[Nb(N[CH<sub>2</sub><sup>t</sup>Bu]Ar)<sub>3</sub>]<sub>2</sub>, **33**, over the course of 90 min, Scheme 2.11. <sup>31</sup>P NMR spectroscopic analysis of the crude reaction mixture shows exclusively two resonances in a 2:1 ratio at 399 and 438 ppm, respectively, Figure 2.30. Assignment of the resonance at 438 ppm to **33** was corroborated by DFT NMR shielding calculations. This reaction provides access to a rare AsP ligand bridging two niobium metal centers.<sup>87–89</sup>



**Scheme 2.11.** Preparation of (Ar[CH<sub>2</sub><sup>t</sup>Bu]N)<sub>3</sub>Nb(PE)Nb(N[CH<sub>2</sub><sup>t</sup>Bu]Ar)<sub>3</sub> (E = P, As).

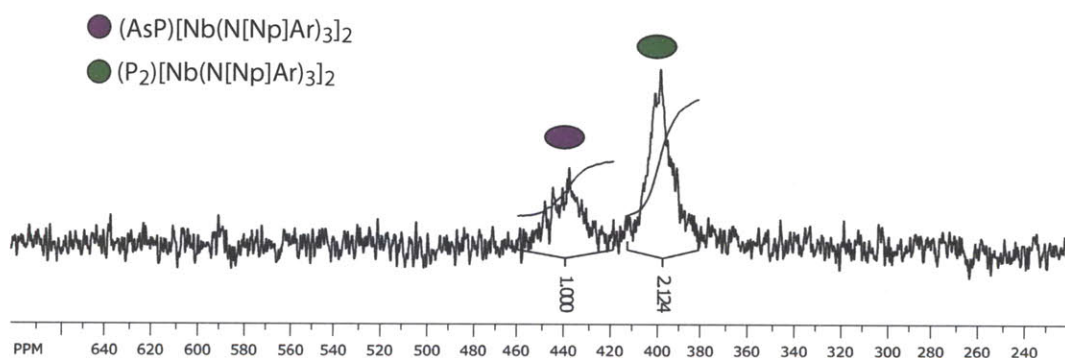
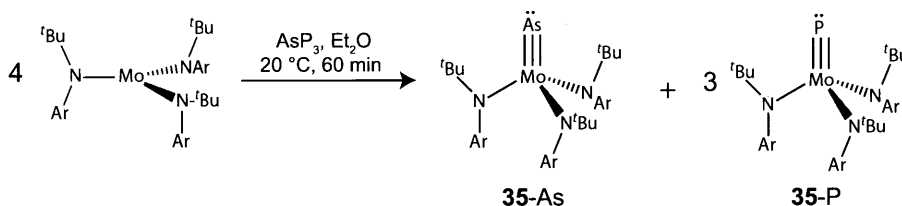


**Figure 2.30.** <sup>31</sup>P NMR spectrum of (Ar[CH<sub>2</sub><sup>t</sup>Bu]N)<sub>3</sub>Nb(PE)Nb(N[CH<sub>2</sub><sup>t</sup>Bu]Ar)<sub>3</sub> (E = P, As).

P<sub>4</sub> degradation to monophosphorus units has been previously observed in the treatment of the reactive Mo(III) precursor Mo(N[<sup>t</sup>Bu]Ar)<sub>3</sub> with 0.25 equiv of P<sub>4</sub> to give the P≡Mo(N[<sup>t</sup>Bu]Ar)<sub>3</sub> complex.<sup>90</sup> A thorough review on the topic of M≡E triple bonds (E = P, As, Sb) has been provided by Scheer.<sup>91,92</sup> Access to the arsenide congener of P≡Mo(N[<sup>t</sup>Bu]Ar)<sub>3</sub> is also afforded by the corresponding reaction with As<sub>4</sub>; however, this experiment is challenging because As<sub>4</sub> is thermally and photochemically unstable.<sup>93</sup> A thermally stable, molecular source of As<sup>0</sup> would be preferable to obtain a stoichiometric transformation to the terminal arsenide complex, and AsP<sub>3</sub> proved to be an effective source of a single As<sup>0</sup> equivalent. Treatment of Mo(N[<sup>t</sup>Bu]Ar)<sub>3</sub> with a slight excess of AsP<sub>3</sub> (0.29 equiv) resulted in formation of a 1:3 mixture of As≡Mo(N[<sup>t</sup>Bu]Ar)<sub>3</sub>, **35-As**, and P≡Mo(N[<sup>t</sup>Bu]Ar)<sub>3</sub>, **35-P**, over the course of 1 h, Scheme 2.12. The <sup>1</sup>H NMR spectroscopic features

for **35-As** and **35-P** are coincident, but the corresponding  $^{13}\text{C}$  NMR spectroscopic features are distinct and revealed that the reaction cleanly formed **35-As** and **35-P** in a 1:3 ratio. Interestingly, it was found that in 1:1 competition experiments of  $\text{AsP}_3$  and  $\text{P}_4$  with  $\text{Mo}(\text{N}[\text{tBu}]\text{Ar})_3$ , there is no selectivity for reaction with  $\text{AsP}_3$  over  $\text{P}_4$ , which may be the result of the reaction being under kinetic control. This is a striking example of a reaction in which  $\text{AsP}_3$  does not give enhanced reactivity over  $\text{P}_4$ , and is an interesting case. The reaction of  $\text{AsP}_3$  with  $\text{Mo}(\text{N}[\text{tBu}]\text{Ar})_3$  gives us clear proof that  $\text{AsP}_3$  functions experimentally as a soluble source of  $\text{As}^0$  and  $\text{P}^0$  and also provides motivation for future studies in the synthesis of precise 3:1 mixtures of metal phosphides and metal arsenides for materials applications.<sup>94–96</sup>



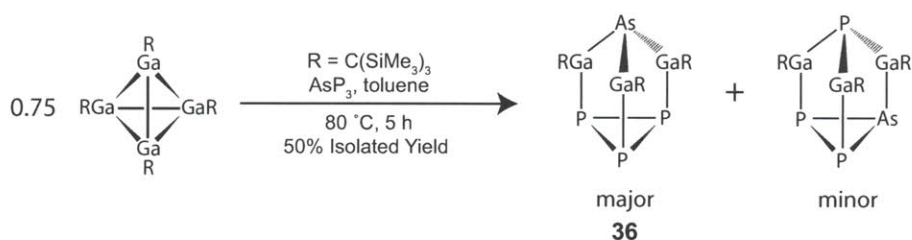
**Scheme 2.12.** Preparation of  $\text{As}\equiv\text{Mo}(\text{N}[\text{tBu}]\text{Ar})_3$  and  $\text{P}\equiv\text{Mo}(\text{N}[\text{tBu}]\text{Ar})_3$ .

### 2.5.5 Selective Cleavage of Three As–P Bonds in $\text{AsP}_3$ : Reaction with $[\text{GaC}(\text{SiMe}_3)_3]_4$

Uhl and coworkers have reported the synthesis of a novel tetragallane compound  $[\text{GaC}(\text{SiMe}_3)_3]_4$ , which exists as a tetramer in the solid state, but dissociates into monomeric  $\text{GaC}(\text{SiMe}_3)_3$  fragments in dilute solutions and at elevated temperatures.<sup>97</sup>  $[\text{GaC}(\text{SiMe}_3)_3]_4$  is synthetically available in good yield by the reduction of the corresponding alkyltrichlorogallate with Rieke magnesium,<sup>98</sup> and shows remarkable chemical reactivity similar to the, up to now, more intensively investigated indium analogue  $[\text{InC}(\text{SiMe}_3)_3]_4$ .<sup>99</sup> Uhl and coworkers found that  $[\text{GaC}(\text{SiMe}_3)_3]_4$  and  $\text{P}_4$  reacted slowly in boiling *n*-hexane to give yellow crystals of the novel trigallium tetraphosphorus compound  $\text{P}[\text{GaC}(\text{SiMe}_3)_3]_3\text{P}_3$  in moderate (52%) yield.<sup>100</sup> The structure of  $\text{P}[\text{GaC}(\text{SiMe}_3)_3]_3\text{P}_3$  shows the insertion of three monomeric  $\text{GaC}(\text{SiMe}_3)_3$  fragments into three of the six P–P bonds of the  $\text{P}_4$  tetrahedron with a *cyclo*- $\text{P}_3$  ring intact and a lone gallium-bound P atom at the molecule's apex. Because this reaction is a rare example of  $\text{P}_4$  activation in which all three P–P bonds of a single P atom are cleaved, this reaction seemed ideally suited to treatment with  $\text{AsP}_3$ , in which case cleavage of all three As–P bonds would be expected due to the diminished bond dissociation energy of an As–P bond in comparison to a P–P bond.

With this target in mind, it was discovered that treatment of 1 equiv of  $\text{AsP}_3$  with 0.75 equiv of  $[\text{GaC}(\text{SiMe}_3)_3]_4$  in toluene at  $80\text{ }^\circ\text{C}$  over 5 h results in a lightening of the solution from red-orange to yellow and, upon cooling, precipitation of fibrous yellow needles. This yellow material was obtained in 50% yield upon isolation and analysis clearly identified the product as the desired triple insertion product, Scheme 2.13. Although  $\text{As}[\text{GaC}(\text{SiMe}_3)_3]_3\text{P}_3$ , **36**, is the major species (80%) there is some formation of the the alternative triple insertion product  $\text{P}[\text{GaC}(\text{SiMe}_3)_3]_3\text{AsP}_2$  as can clearly

be seen by  $^{31}\text{P}$  NMR spectroscopy, Figure 2.31. The  $^{31}\text{P}$  NMR spectrum of  $\text{As}[\text{GaC}(\text{SiMe}_3)_3]_3\text{P}_3$  is simple, as expected, with only a singlet resonance at  $-192$  ppm. The alternative structure  $\text{P}[\text{GaC}(\text{SiMe}_3)_3]_3\text{AsP}_2$  shows a doublet at  $-174$  ppm (2P) and a triplet at  $-495$  ppm (1P) with  $^2J_{\text{P/P}}$  at 34 Hz, which is quite similar to the reported values of  $-202$  (d, 3P) and  $-522$  (q, 1P) with  $^2J_{\text{P/P}}$  at 31 Hz for the all phosphorus congener provided by Uhl and coworkers.<sup>100</sup> Perhaps the most exciting feature of this reaction of  $[\text{GaC}(\text{SiMe}_3)_3]_4$  with  $\text{AsP}_3$  is that the insertion isomers are not statistical and there is a strong preference for selective cleavage of the As–P bonds versus the P–P bonds.



**Scheme 2.13.** Preparation of  $\text{As}[\text{GaC}(\text{SiMe}_3)_3]_3\text{P}_3$  and  $\text{P}[\text{GaC}(\text{SiMe}_3)_3]_3\text{AsP}_2$  from the triple insertion of “ $\text{GaC}(\text{SiMe}_3)_3$ ” into  $\text{AsP}_3$ .

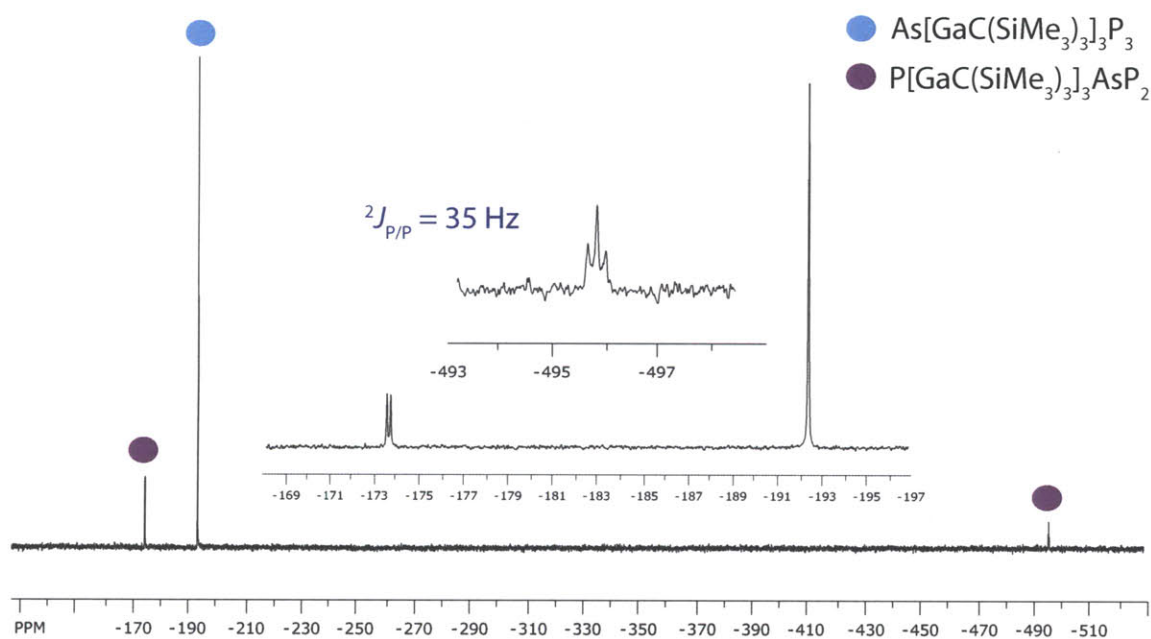


**Figure 2.31.**  $^{31}\text{P}$  NMR spectrum of  $\text{As}[\text{GaC}(\text{SiMe}_3)_3]_3\text{P}_3$  and  $\text{P}[\text{GaC}(\text{SiMe}_3)_3]_3\text{AsP}_2$ .

$\text{As}[\text{GaC}(\text{SiMe}_3)_3]_3\text{P}_3$  was selectively crystallized as yellow needles from diffusion of pentane into a toluene solution at  $-35^\circ\text{C}$  and the thermal ellipsoid plot is shown in Figure 2.32. Compound **36** crystallized in the hexagonal space group  $P6_3$ . The crystal structure of **36** shows clearly three  $\text{GaC}(\text{SiMe}_3)_3$  fragments inserted into the three As–P bonds of  $\text{AsP}_3$  with an intact *cyclo*- $\text{P}_3$  ring and

no disorder of the arsenic and phosphorus positions. The Ga1–As1 interatomic distance is 2.426(1) Å, the Ga1–P1 interatomic distance is 2.397(2) Å. There are three equivalent P–P bonds in the molecule which have an interatomic distance of 2.213(3) Å. The Ga atoms are in approximately a trigonal planar conformation with a P1–Ga1–As1 angle of 115.08(5)°, a C1–Ga1–P1 angle of 120.08°, and a C1–Ga1–As1 angle of 124.6(2)°. This structure is not isostructural with the all phosphorus analogue P[GaC(SiMe<sub>3</sub>)<sub>3</sub>]<sub>3</sub>P<sub>3</sub> prepared by Uhl and coworkers, which crystallized in the orthorhombic space group *Pnma*.<sup>100</sup>

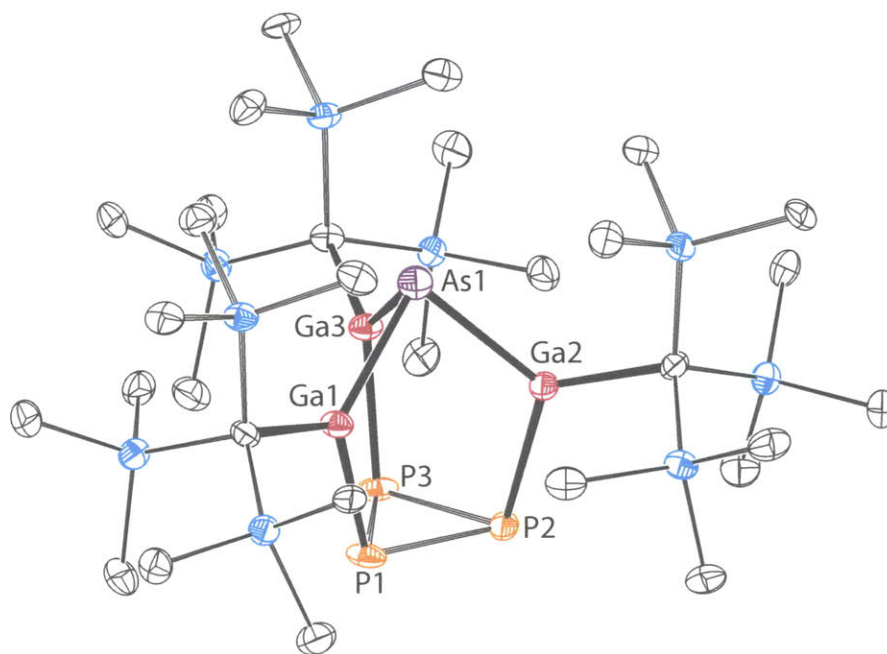


**Figure 2.32.** Thermal ellipsoid plot (50% probability) of As[GaC(SiMe<sub>3</sub>)<sub>3</sub>]<sub>3</sub>P<sub>3</sub> with hydrogen atoms omitted for clarity.

Interestingly, when AsP<sub>3</sub> is treated with 1 equiv of [GaC(SiMe<sub>3</sub>)<sub>3</sub>]<sub>4</sub> instead of 0.75 equiv, a different reaction product is obtained. The <sup>31</sup>P NMR spectrum of this new species shows a triplet at –155 ppm and a doublet at 182 ppm in a 1:2 ratio. This pattern would seem to suggest that the P<sub>3</sub> ring has ruptured, giving a quadruple insertion product. DFT calculations have confirmed that the observed <sup>31</sup>P chemical shifts are consistent with such a structure and surprisingly, it was found that this reaction is not unique to AsP<sub>3</sub>. In fact, when P<sub>4</sub> is treated with 1 equiv [GaC(SiMe<sub>3</sub>)<sub>3</sub>]<sub>4</sub>, an analogous species is obtained. Work is ongoing to further characterize these unusual species.

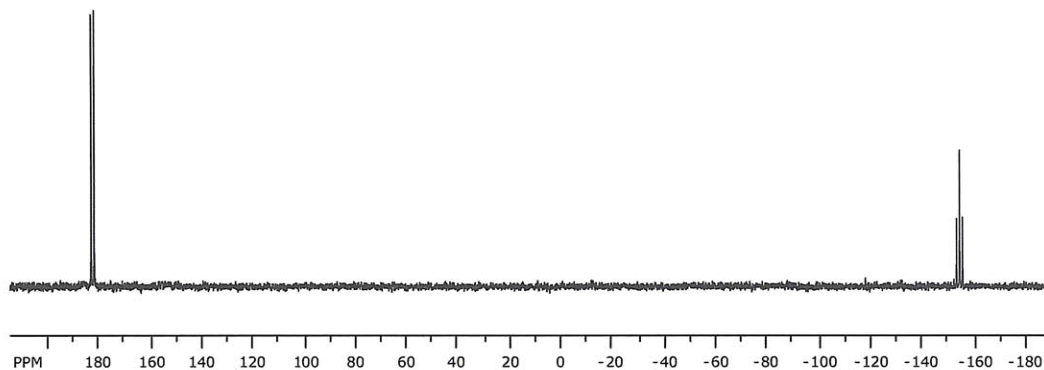


**Figure 2.33.**  $^{31}\text{P}$  NMR spectrum of  $\text{AsP}_3[\text{GaC}(\text{SiMe}_3)_3]_4$ , a quadruple insertion product.

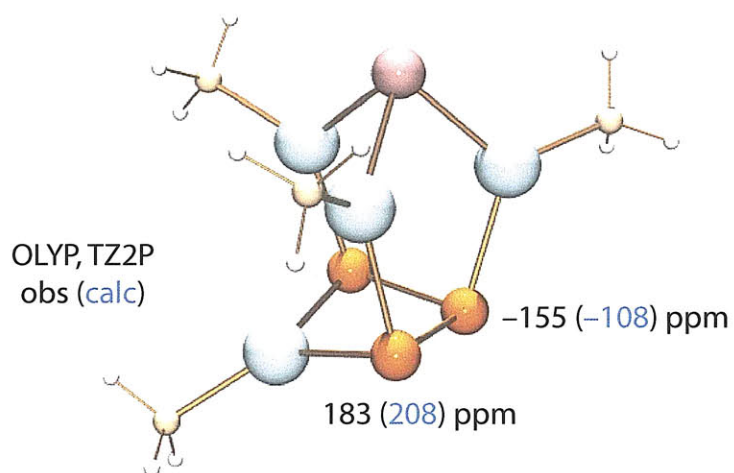


**Figure 2.34.** DFT geometry optimization of a model complex ( $\text{AsP}_3[\text{GaCH}_3]_4$ ) of the quadruple insertion product.



### 2.5.6 Bringing it Back: Sodium Amalgam Reduction of $\text{Cl}_2\text{Nb}(\text{ODipp})_3$ in the Presence of $\text{AsP}_3$

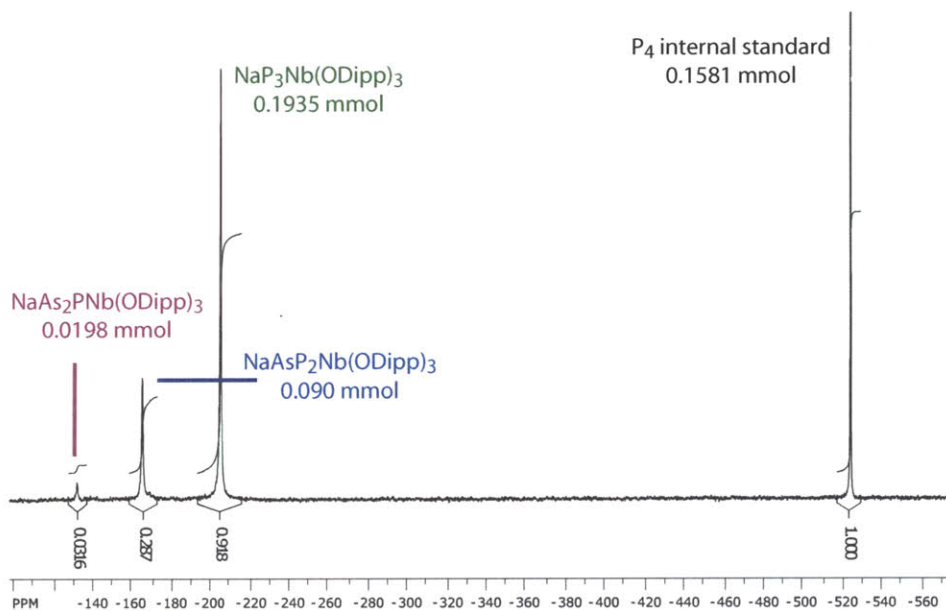
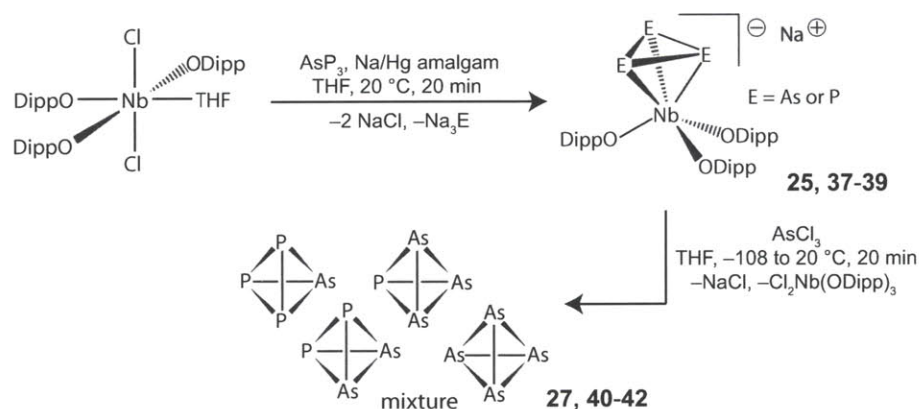
The original synthesis of  $\text{AsP}_3$  involved treatment of an anionic niobium *cyclo*- $\text{P}_3$  complex with  $\text{AsCl}_3$  to obtain the tetraatomic tetrahedron. Since that discovery, we have been interested in preparing other anionic *cyclo*- $\text{E}_3$  compounds, in particular an anionic *cyclo*- $\text{As}_2\text{P}$  complex. Such a species could, in principle, be used to synthesize the previously unexplored tetraatomic interpnictides  $\text{As}_2\text{P}_2$  and  $\text{As}_3\text{P}$  by treatment of the *cyclo*- $\text{As}_2\text{P}$  derivative with the appropriate  $\text{ECl}_3$  reagent ( $\text{E} = \text{P}, \text{As}$ ). Strides in this direction have been made by investigating the reaction between  $\text{AsP}_3$  and  $\text{Cl}_2\text{Nb}(\text{ODipp})_3$  in the presence of a reducing agent.<sup>18</sup> Combining  $\text{AsP}_3$  with  $\text{Cl}_2\text{Nb}(\text{ODipp})_3$  in a 1:1 ratio in THF followed by treatment with Na/Hg amalgam gives rise to a mixture of  $[\text{Na}][\text{P}_3\text{Nb}(\text{ODipp})_3]$ , **25**,  $[\text{Na}][\text{AsP}_2\text{Nb}(\text{ODipp})_3]$ , **37**,  $[\text{Na}][\text{As}_2\text{PNb}(\text{ODipp})_3]$ , **38**, and presumably,  $[\text{Na}][\text{As}_3\text{Nb}(\text{ODipp})_3]$ , **39**, over the course of 30 min, Scheme 2.14. Evidence for formation of **25**, **37**, and **38** in a 10:5:1 molar ratio (76% yield from  $\text{Cl}_2\text{Nb}(\text{ODipp})_3$ ) is provided by the clean appearance of three singlets in the  $^{31}\text{P}$  NMR spectrum of the crude reaction mixture, spaced as expected for sequential As-doping of the *cyclo*- $\text{P}_3$  complex at  $-206$  (**25**),  $-167$  (**37**), and  $-132$  ppm (**38**), Figure 2.35. From the considerable concentration of the unexpected **38** (and from subsequent analysis, *vide infra*), we propose that **39** is also present in low concentration. Treatment of this crude reaction mixture with  $\text{AsCl}_3$  with the exclusion of light rapidly generated a reaction mixture containing  $\text{Cl}_2\text{Nb}(\text{ODipp})_3(\text{THF})$  and the tetraatomic interpnictides  $\text{AsP}_3$ ,  $\text{As}_2\text{P}_2$ , and  $\text{As}_3\text{P}$ , as well as  $\text{As}_4$ , Scheme 2.14.<sup>101</sup> The presence of the four tetrahedral molecules is confirmed by  $^{31}\text{P}$  NMR spectroscopy and by GC-MS, Table 2.7, Figure 2.37, Figure 2.38. It is of note that the ratio of As to P atoms in the final product mixture is 1 to 1.6, which is very near the 1 to 1.3 ratio that we would expect ( $3/4 \text{AsP}_3 + \text{AsCl}_3$ ) over the course of the two reactions. This is an important observation that implies that there is no selective loss of As or P atoms during the synthesis.

We are currently investigating alternative syntheses of  $\text{As}_2\text{P}_2$  and  $\text{As}_3\text{P}$  for exploration of these molecules as pure substances. One exciting recent development toward this end has been the selective synthesis of  $[\text{Na}][\text{P}_3\text{Nb}(\text{ODipp})_3]$  and  $[\text{Na}][\text{AsP}_2\text{Nb}(\text{ODipp})_3]$  using in situ reduction of  $\text{ClNb}(\text{ODipp})_3(\text{THF})$  with  $\text{CoCp}_2$  in the presence of  $\text{AsP}_3$ . Treatment of this mixture with  $\text{AsCl}_3$  then provides access to mixtures of only  $\text{AsP}_3$  and  $\text{As}_2\text{P}_2$ ! It is hoped that running this reaction on a preparative scale and sublimation will afford a clean mixture of  $\text{AsP}_3$  and  $\text{As}_2\text{P}_2$  for study.

**Table 2.7.** NMR and GC-MS Data for the generation of AsP<sub>3</sub>, As<sub>2</sub>P<sub>2</sub>, As<sub>3</sub>P, and As<sub>4</sub>.

	P <sub>4</sub> (int. std.)	AsP <sub>3</sub>	As <sub>2</sub> P <sub>2</sub>	As <sub>3</sub> P	As <sub>4</sub>
<sup>31</sup> P chemical shift (ppm)	-520	-484	-452	-432	N/A
calculated <sup>31</sup> P chemical shift (ppm)	-520	-482	-451	-424	N/A
retention time (min) <sup>a</sup>	7.8	8.9	9.8	10.6	11.2
mass (m/z)	124	168	212	256	300
area (au)	50994	30475	11348	3176	1977
yield <sup>b</sup>	N/A	49%	39%	50%	2%

<sup>a</sup> GC-MS data were collected using an Agilent 6890N network GC system with an Agilent 5973 Network mass selective detector and an Rtx-1 column from Restek. <sup>b</sup> Yields of AsP<sub>3</sub>, As<sub>2</sub>P<sub>2</sub>, and As<sub>3</sub>P are calculated from the corresponding starting concentration of [Na(THF)<sub>3</sub>][E<sub>3</sub>Nb(ODipp)<sub>3</sub>]; in each case the theoretical yield is 100%; for As<sub>4</sub> the yield is calculated from the starting concentration of Cl<sub>2</sub>Nb(ODipp)<sub>3</sub> making the theoretical yield >> 100%.

**Figure 2.35.** <sup>31</sup>P NMR spectrum of [Na(THF)<sub>3</sub>][E<sub>3</sub>Nb(ODipp)<sub>3</sub>]. P<sub>4</sub> added as an internal standard.

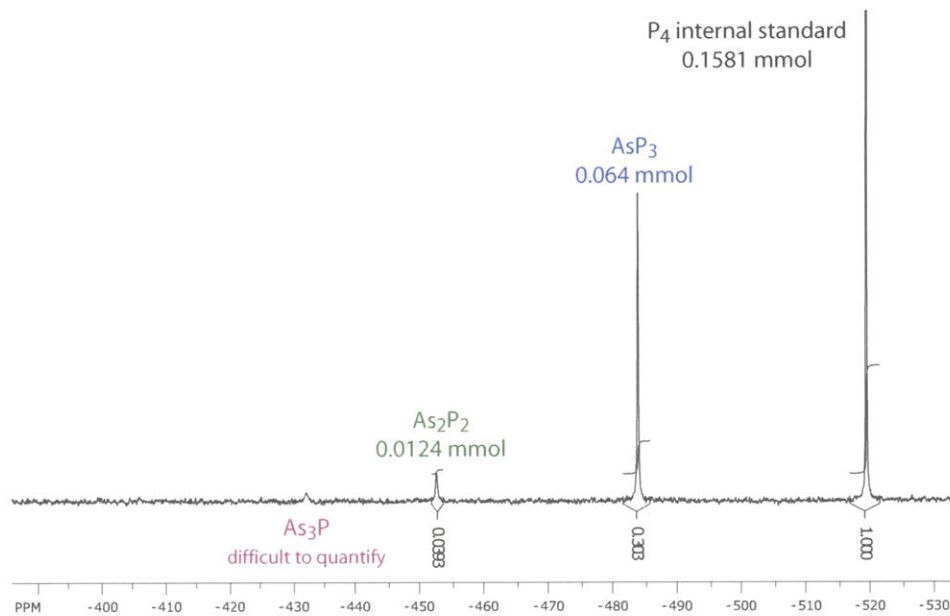


Figure 2.36.  $^{31}\text{P}$  NMR spectrum of  $\text{AsP}_3$ ,  $\text{As}_2\text{P}_2$ ,  $\text{As}_3\text{P}$ .

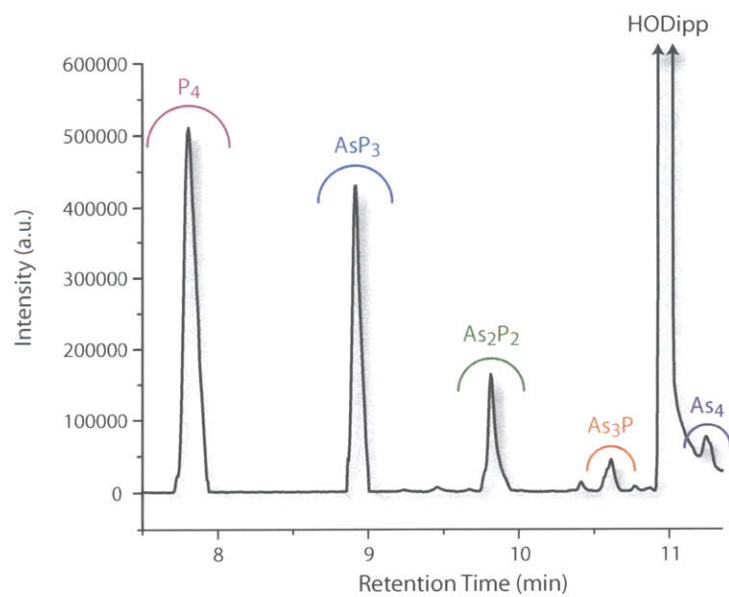


Figure 2.37. GC chromatograph of tetrahedra mixture.

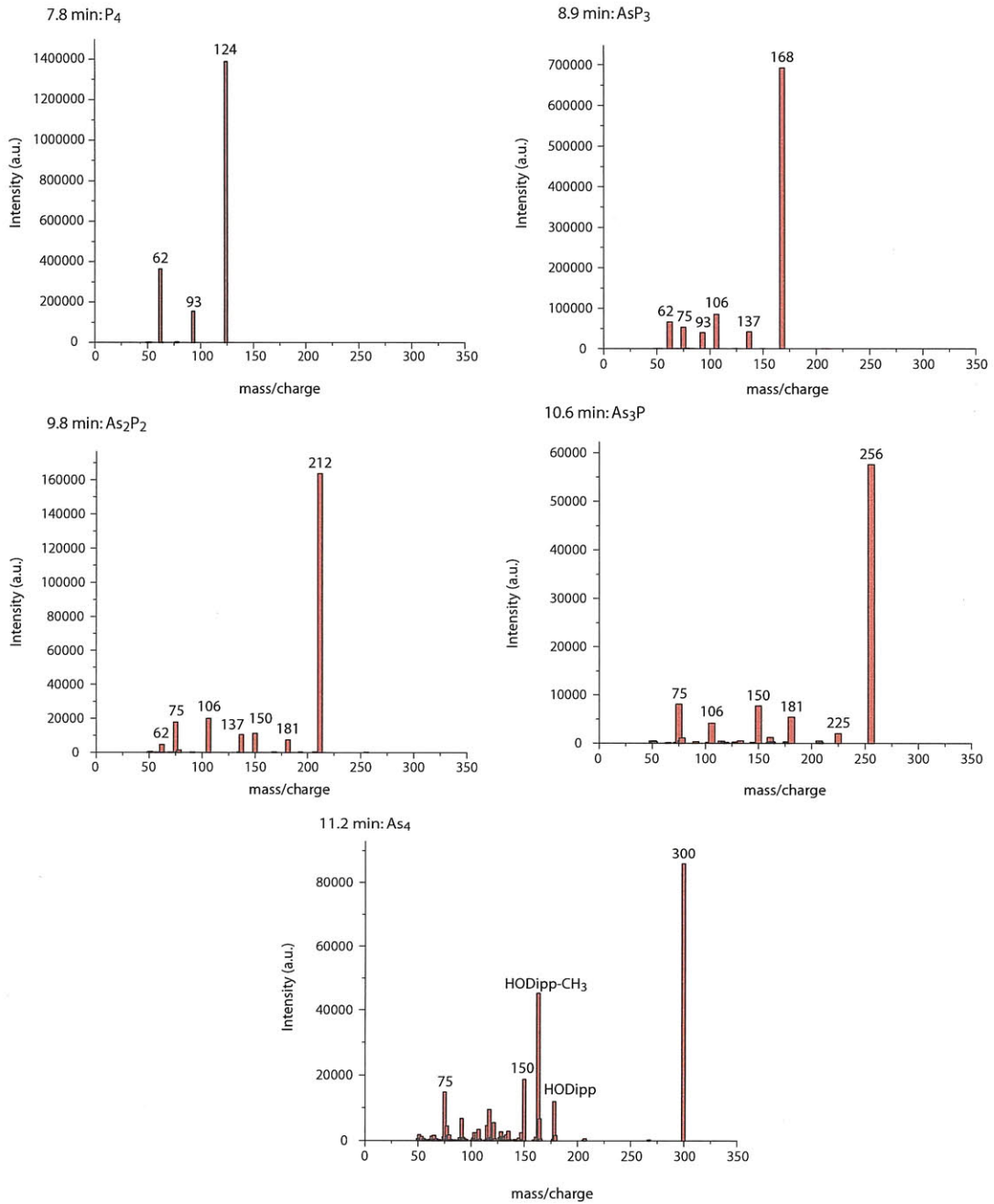


Figure 2.38. Fragmentation patterns for the tetrahedra.

## 2.6 REACTION OF THE *Cyclo*-P<sub>3</sub> ANION COMPLEX WITH OTHER TRIPOSITIVE ELECTROPHILES

The use of [Na(THF)<sub>3</sub>][P<sub>3</sub>Nb(ODipp)<sub>3</sub>] as a P<sub>3</sub><sup>3-</sup> transfer agent to ECl<sub>3</sub> sources was found not to be limited to E = As. In fact, when E = P, a high (81%) yielding synthesis of P<sub>4</sub> could be devised. We were curious whether the heavier group 15 trihalides could be used to access more exotic tetrahedra. Interestingly, SbCl<sub>3</sub> is competent in these transformations. Treatment of [Na(THF)<sub>3</sub>][P<sub>3</sub>Nb(ODipp)<sub>3</sub>] with SbCl<sub>3</sub> in THF at -50 °C gave rise to SbP<sub>3</sub> with 11% conversion by NMR spectroscopy, Figure 2.39. SbP<sub>3</sub> appears in the <sup>31</sup>P NMR spectrum at -462 ppm, which compares favorably with the calculated value of -462 ppm and trends nicely with the further decrease in HOMO-LUMO gap when compared to AsP<sub>3</sub> and P<sub>4</sub>, Table 2.8. The low yield of SbP<sub>3</sub> seems to be due, in part, to the reducing power of [Na(THF)<sub>3</sub>][P<sub>3</sub>Nb(ODipp)<sub>3</sub>], which is hypothesized to be effecting direct reduction of SbCl<sub>3</sub>. [Na(THF)<sub>3</sub>][P<sub>3</sub>Nb(ODipp)<sub>3</sub>] shows a single broad and irreversible oxidation event which peaks at approximately -100 mV vs Fc/Fc<sup>+</sup> in THF.

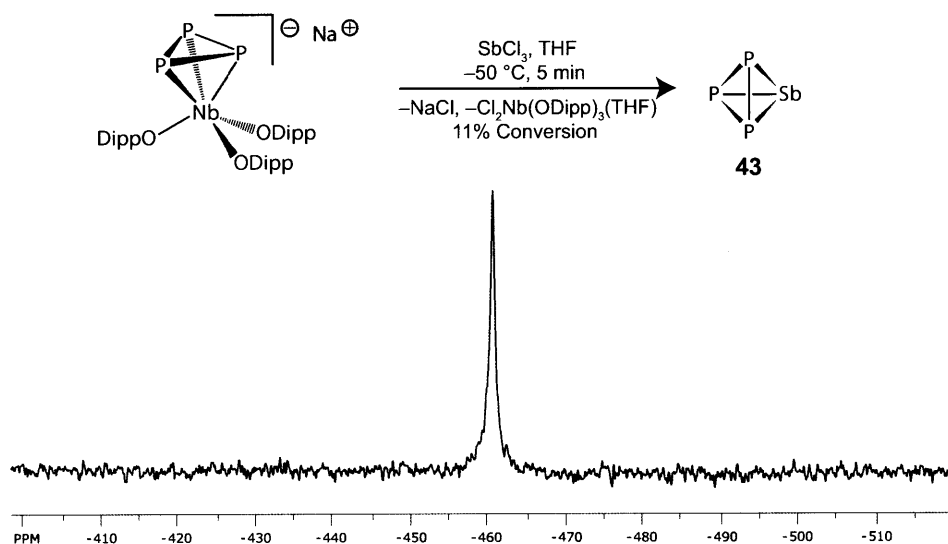


Figure 2.39. Generation and <sup>31</sup>P NMR spectrum of SbP<sub>3</sub>.

### 2.6.1 Halide Dependence of SbP<sub>3</sub> Synthesis

Different SbX<sub>3</sub> precursors were used to try and find an optimized protocol for SbP<sub>3</sub> synthesis. It was found that when prepared at -50 °C, SbBr<sub>3</sub> gave the highest average yield of 19% over three separate runs. SbCl<sub>3</sub>, on the other hand, gave an average conversion of only 11%. It was expected, then, that SbI<sub>3</sub> might be an even better candidate for the synthesis of SbP<sub>3</sub>. Interestingly, SbI<sub>3</sub> behaved differently altogether, with no appreciable reaction taking place between

**Table 2.8.** Comparison of chemical shift and HOMO-LUMO gaps in EP<sub>3</sub> tetrahedra (E = P, As, Sb).

	P <sub>4</sub>	AsP <sub>3</sub>	SbP <sub>3</sub>
<sup>31</sup> P chemical shift (ppm)	-520	-484	-462
calculated <sup>31</sup> P chemical shift (ppm)	-520	-482	-462
HOMO-LUMO gap (eV) <sup>a</sup>	4.937	4.514	3.692

<sup>a</sup> HOMO-LUMO gaps were calculated in ADF using the OLYP functional with the QZ4P basis sets on all atoms and spin-orbit effects accounted for using the relativistic spin-orbit ZORA.

[Na(THF)<sub>3</sub>][P<sub>3</sub>Nb(ODipp)<sub>3</sub>] and SbI<sub>3</sub> at -50 °C. Warming the reaction mixture slowly to -20 °C resulted in slow conversion of the [Na(THF)<sub>3</sub>][P<sub>3</sub>Nb(ODipp)<sub>3</sub>] starting material to a new species with a broad singlet in the <sup>31</sup>P NMR spectrum of -165 ppm. This species has been assigned as the salt elimination product I<sub>2</sub>SbP<sub>3</sub>Nb(ODipp)<sub>3</sub> based on its spectroscopic signatures. This species was found to persist at -20 °C for several hours never giving rise to any observable SbP<sub>3</sub>. It was found that I<sub>2</sub>SbP<sub>3</sub>Nb(ODipp)<sub>3</sub> slowly decomposed to I<sub>2</sub>Nb(ODipp)<sub>3</sub>, Sb<sup>0</sup>, and red phosphorus over the course of 12 h at -15 °C. This process was nearly instantaneous at room temperature.

### 2.6.2 *In Situ* Reactivity of SbP<sub>3</sub>

It was hypothesized that it might be possible to stabilize SbP<sub>3</sub> in the coordination sphere of a metal center. To address this possibility, two strategies were investigated. The first strategy involved targeting the complex [(SbP<sub>3</sub>)Fe(Cp\*)(dppe)][BPh<sub>4</sub>], **44**, as the [FeCp\*(dppe)]<sup>+</sup> unit had been shown previously to make unusually stable complexes with P<sub>4</sub>,<sup>102</sup> and as demonstrated above, with AsP<sub>3</sub>. Generation of SbP<sub>3</sub> was carried out by treatment of a THF solution of [Na(THF)<sub>3</sub>][P<sub>3</sub>Nb(ODipp)<sub>3</sub>] at -50 °C in the dark with a solution of SbCl<sub>3</sub> in THF. After allowing this solution to stir for 20 minutes at -50 °C, a THF solution of ClFeCp\*(dppe) was added, followed by a THF solution of Na[BPh<sub>4</sub>]. NMR analysis of this crude reaction mixture after 15 minutes shows conclusive evidence for the formation of the desired [(SbP<sub>3</sub>)Fe(Cp\*)(dppe)][BPh<sub>4</sub>] as the only diamagnetic, phosphorus-containing product, Figure 2.40. Unfortunately, [(SbP<sub>3</sub>)Fe(Cp\*)(dppe)][BPh<sub>4</sub>] was found itself to rapidly degrade in solution and was never isolated as a pure material. DFT calculations on an optimized structure of [(SbP<sub>3</sub>)Fe(Cp\*)(dppe)]<sup>+</sup> corroborate our assignment of the <sup>31</sup>P NMR spectrum, Figure 2.41.

From the DFT calculations shown below, it was thought that the FeCp\*(dppe) unit did not provide sufficient steric protection to the SbP<sub>3</sub> tetrahedron, leaving the SbP<sub>3</sub> unit susceptible to degradation through bimolecular pathways. It was thought that complexation by two metal centers might be an ideal strategy for accessing a stable complex of SbP<sub>3</sub>. Fortunately, there exists literature precedent for coordination of an intact P<sub>4</sub> tetrahedron by two rhenium metal centers.<sup>103</sup> In order to

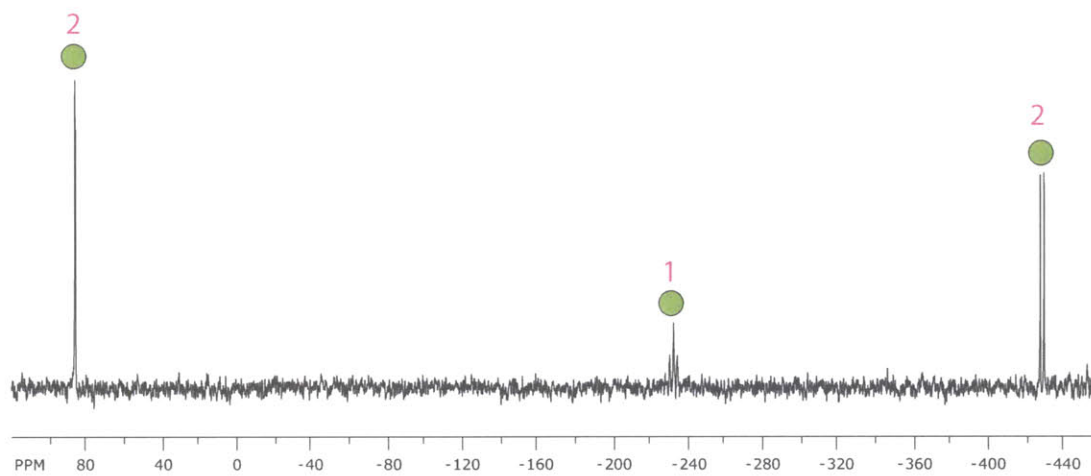


Figure 2.40.  $^{31}\text{P}$  NMR spectrum of  $[(\text{SbP}_3)\text{Fe}(\text{Cp}^*)(\text{dppe})][\text{BPh}_4]$ .

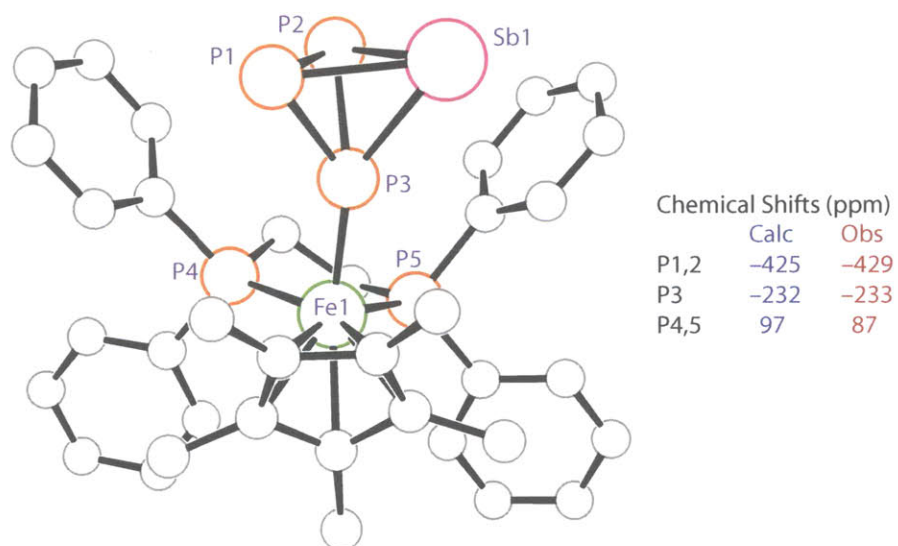
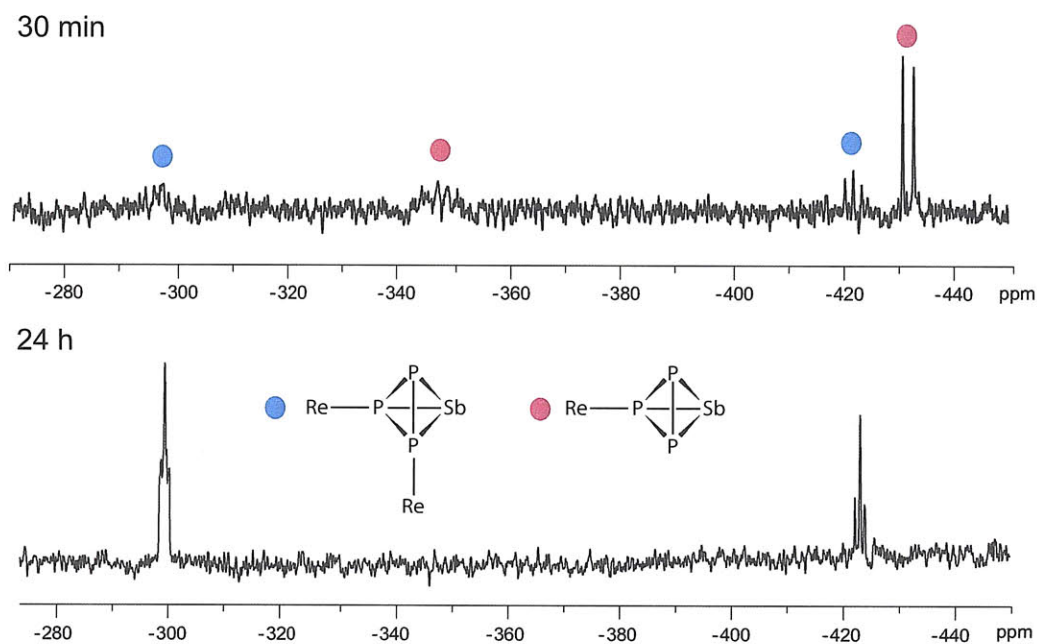


Figure 2.41. Optimized geometry and  $^{31}\text{P}$  chemical shift calculations for  $[(\text{SbP}_3)\text{Fe}(\text{Cp}^*)(\text{dppe})][\text{BPh}_4]$ .

attempt this bimetallic complexation strategy with *in situ* prepared  $\text{SbP}_3$ , a solution of  $\text{SbP}_3$  in THF was prepared as described above at  $-50\text{ }^\circ\text{C}$  in the dark. To this solution was added two equivalents of the  $(\text{OTf})\text{Re}(\text{CO})_2(\text{triphos})$  complex, followed by one equivalent of  $\text{Na}[\text{BPh}_4]$  (used to displace the OTf ligand from the Re metal center). After stirring for 30 minutes in the dark, analysis of the crude reaction mixture showed the presence of both the monometallic complex and the bimetallic complex in a 4:1 ratio, Figure 2.42. Monitoring this reaction mixture at room temperature over 24 h in ambient light showed complete degradation of the monometallic species with the solution becoming more enriched in the more stable bimetallic complex. Surprisingly,  $\text{P}_4$  formation was accompanied by the decomposition of the monometallic species, suggestive of bimolecular decomposition pathways being accessible. Unfortunately the bimetallic complex was itself never able to be isolated due to the low yield in which it formed and due to the fact that the complex decomposed slowly during attempted crystallizations.



**Figure 2.42.**  $^{31}\text{P}$  NMR spectrum of  $(\text{SbP}_3)[\text{Re}(\text{CO})_2(\text{triphos})]_2$  and  $(\text{SbP}_3)\text{Re}(\text{CO})_2(\text{triphos})$ .

## 2.7 TOWARDS ARSENIC-RICH TETRAHEDRA

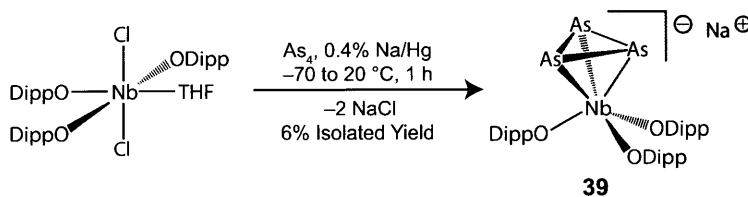
A major goal in the further development of syntheses of the group 15 tetrahedra would be to have access to a complete series of arsenic-phosphorus interpnictogen molecules. While  $\text{P}_3^{3-}$  transfer has allowed access to  $\text{AsP}_3$  in pure form, it does not provide an obvious method for synthesis of more arsenic-rich tetrahedra. Access to an analogous  $\text{As}_3^{3-}$  transfer agent, however, could allow for access to  $\text{As}_3\text{P}$ , the elemental complement of  $\text{AsP}_3$ . With the initial goal of developing a synthesis of  $\text{As}_3\text{P}$ , I set out to synthesize  $[\text{Na}(\text{THF})_3][\text{As}_3\text{Nb}(\text{ODipp})_3]$ . The hypothesis was that the same



protocol for  $[\text{Na}(\text{THF})_3][\text{P}_3\text{Nb}(\text{ODipp})_3]$  synthesis might translate to  $[\text{Na}(\text{THF})_3][\text{As}_3\text{Nb}(\text{ODipp})_3]$  production if  $\text{As}_4$  is substituted for  $\text{P}_4$ . Access to  $\text{As}_4$ , however, is not facile because, as previously mentioned,  $\text{As}_4$  is unstable in the solid state and photolytically unstable in the solution or gas phase. A procedure for relatively large scale production of  $\text{As}_4$  that uses a custom built tube furnace has been developed in our lab. This apparatus is based on one described in early reports of  $\text{As}_4$  generation by Erdmann and the modern version has been described recently by Spinney et al.<sup>104,105</sup> It is noteworthy that there do exist a few known examples of neutral *cyclo*- $\text{As}_3$  or mixed *cyclo*- $\text{P}_n\text{As}_{3-n}$  ligands, however, no ionic *cyclo*- $\text{E}_3$  ligands of the heavier group 15 elements have been observed to date.<sup>10,87,105</sup>

### 2.7.1 Synthesis and Structure of $[\text{Na}(\text{THF})_3][\text{As}_3\text{Nb}(\text{ODipp})_3]$

It was found that treatment of an  $\text{As}_4$  saturated solution of THF with  $\text{Cl}_2\text{Nb}(\text{ODipp})_3$  and a 0.4% Na/Hg amalgam, with the exclusion of light, from  $-70\text{ }^\circ\text{C}$  to  $20\text{ }^\circ\text{C}$ , resulted in the formation of a murky orange suspension. Cannula filtration of the reaction mixture into a dry Schlenk flask, THF evaporation, extraction with  $\text{Et}_2\text{O}$ , and a second filtration resulted in a bright orange solution. Concentration, addition of THF, and cooling to  $-35\text{ }^\circ\text{C}$  for 16 h does result in formation of X-ray quality bright orange crystals of  $[\text{Na}(\text{THF})_3][\text{As}_3\text{Nb}(\text{ODipp})_3]$ , **39**, in 6% yield based on  $\text{Cl}_2\text{Nb}(\text{ODipp})_3$ , Scheme 2.15. Several strategies were pursued to try to optimize the yield of  $[\text{Na}(\text{THF})_3][\text{As}_3\text{Nb}(\text{ODipp})_3]$  such as varying solvent volume, concentration, reaction temperature, reducing agent, and amount of  $\text{Cl}_2\text{Nb}(\text{ODipp})_3$ , but greater than a 6% yield was never realized. Nevertheless,  $[\text{Na}(\text{THF})_3][\text{As}_3\text{Nb}(\text{ODipp})_3]$  is available through this procedure in pure form.



**Scheme 2.15.** Preparation of  $[\text{Na}(\text{THF})_3][\text{As}_3\text{Nb}(\text{ODipp})_3]$  from  $\text{As}_4$ .

The single crystal X-ray structure of  $[\text{Na}(\text{THF})_6][\text{As}_3\text{Nb}(\text{ODipp})_3]$  is shown in Figure 2.43. The As–As interatomic distances in this structure are 2.4024(6), 2.4124(7), and 2.4082(6) Å, which gives an average As–As distance of 2.4076 Å. This is 0.23 Å longer than the average P–P interatomic distances in the analogous  $[\text{Na}(\text{THF})_6][\text{P}_3\text{Nb}(\text{ODipp})_3]$  structure. The Nb–As distances are similarly lengthened at 2.6262(5), 2.6245(5), and 2.6262(5) Å for an average of 2.6256 Å. Again, this is 0.115 Å longer than the average Nb–P distances in  $[\text{Na}(\text{THF})_6][\text{P}_3\text{Nb}(\text{ODipp})_3]$ .

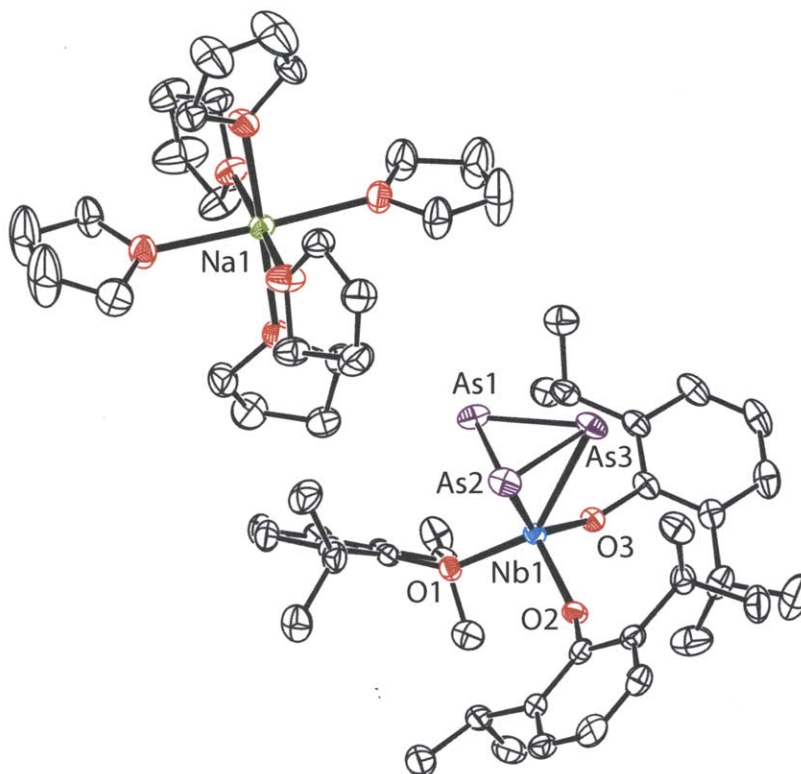


**Figure 2.43.** Thermal ellipsoid plot (50% probability) of  $[\text{Na}(\text{THF})_6][\text{As}_3\text{Nb}(\text{ODipp})_3]$  with hydrogen atoms omitted for clarity.

### 2.7.2 Reaction of $[\text{Na}(\text{THF})_3][\text{As}_3\text{Nb}(\text{ODipp})_3]$ with $\text{PCl}_3$

With  $[\text{Na}(\text{THF})_3][\text{As}_3\text{Nb}(\text{ODipp})_3]$  available in pure form, attempts to make  $\text{As}_3\text{P}$  were made. Treatment of a thawing THF solution of  $[\text{Na}(\text{THF})_3][\text{As}_3\text{Nb}(\text{ODipp})_3]$  with  $\text{PCl}_3$  in the dark resulted in formation of some insoluble materials after 20 minutes. Filtration and NMR analysis of the crude reaction mixture showed 63% conversion to  $\text{As}_3\text{P}$  which appears as a singlet in the  $^{31}\text{P}$  NMR spectrum at  $-432$  ppm, Scheme 2.16, Figure 2.44. The computed chemical shift using ADF was  $-424$  ppm. GC-MS analysis of the crude reaction mixture showed the intact  $\text{As}_3\text{P}$  tetrahedron with a retention time of 10.6 minutes and molecular weight of 256 m/z. Monitoring a solution of the reaction mixture at  $20$  °C over time showed complete decomposition of the tetrahedron after 175 minutes. It is not known whether this is due to inherent instability of  $\text{As}_3\text{P}$  or due to chemical decomposition with other components of the reaction mixture. Nevertheless, it is exciting to get our first hints that  $\text{As}_3\text{P}$  can be accessed in solution and improved syntheses of *cyclo*- $\text{As}_3$  anion complexes will greatly facilitate exploration of this arsenic-rich tetrahedron further.

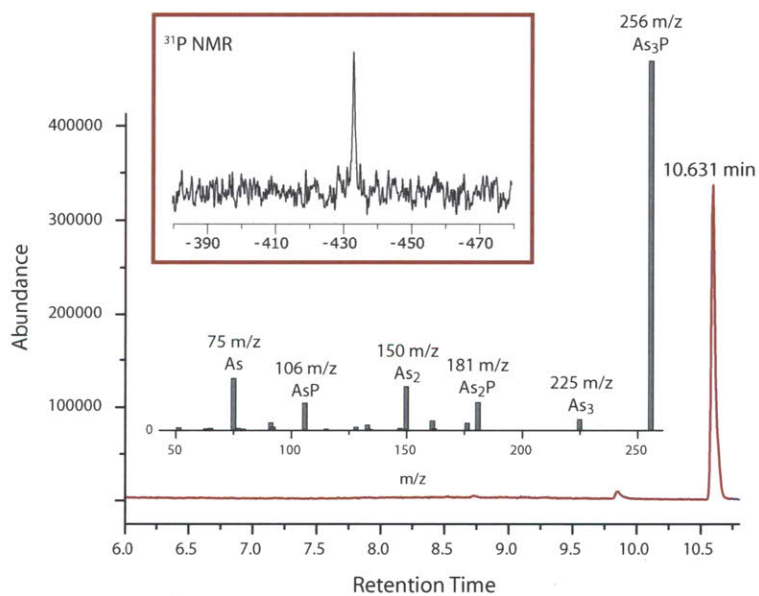
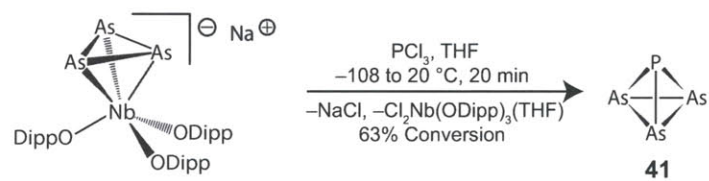


**Figure 2.44.**  $^{31}\text{P}$  NMR spectrum and GC-mass spectrum of  $\text{As}_3\text{P}$ .

## 2.8 CONCLUSIONS

The availability of a *cyclo*-P<sub>3</sub> anion complex of niobium in two synthetic steps from commercially available reagents has provided access to AsP<sub>3</sub> as a pure substance for the first time. This tetraatomic interpnictogen molecule has been studied by several physical techniques including gas-phase electron diffraction to investigate its molecular structure (in collaboration with Prof. Norbert Mitzel at University of Bielefeld), photoelectron spectroscopy to study its electronic structure (in collaboration with Ashley R. Head and Prof. Dennis Lichtenberger at University of Arizona), solid-state <sup>75</sup>As and <sup>31</sup>P NMR spectroscopies (in collaboration with Prof. Gang Wu at Queen's University), microwave spectroscopy to obtain a dipole moment and rotational constants (in collaboration with Adam Daly and Prof. Stephen Kukolich at University of Arizona; ongoing studies), as well as by more conventional mass spectrometry, Raman spectroscopy, and solution NMR spectroscopy. AsP<sub>3</sub> has been shown to be susceptible to decomposition to the elements (red P and As metal) under thermal and UV photolysis conditions, however despite this metastability, AsP<sub>3</sub> has also been shown to undergo a rich reaction chemistry including selective As–P bond cleavage events to yield a variety of new main-group and transition-metal containing products. The doors are wide open for further synthetic explorations with this small molecule substrate. Furthermore, we have just begun to scratch the surface in developing robust syntheses of other exotic group 15 tetrahedra including SbP<sub>3</sub> and As<sub>3</sub>P. In particular, a more efficient synthesis of [Na(THF)<sub>3</sub>][As<sub>3</sub>Nb(ODipp)<sub>3</sub>] is greatly needed. Access to this potential As<sub>3</sub><sup>3-</sup> transfer agent could unlock a lot of new chemistry in this direction. The use of As<sub>5</sub>Me<sub>5</sub> or other cyclic arsines to this end has been suggested by Prof. Arnie Rheingold and is an avenue worthy of investigation.<sup>106</sup> Nevertheless, the development of a highly optimized procedure for the synthesis of [Na(THF)<sub>3</sub>][P<sub>3</sub>Nb(ODipp)<sub>3</sub>] has set the stage for additional P-ligand transfer chemistry such as will be discussed in the next chapter.

## 2.9 EXPERIMENTAL DETAILS

### 2.9.1 General Considerations

All manipulations were performed in a Vacuum Atmospheres model MO-40M glove box under an atmosphere of purified dinitrogen. Solvents were obtained anhydrous and oxygen-free from a Contour Glass Solvent Purification System, or by analogous methods.<sup>107</sup> Celite 435 (EM Science), 4 Å molecular sieves (Aldrich), and alumina (EM Science) were dried by heating at 200 °C under dynamic vacuum for at least 24 hours prior to use. All glassware was oven-dried at temperatures greater than 170 °C prior to use. Deuterated solvents for NMR spectroscopy were purchased from Cambridge Isotope Labs. Benzene-*d*<sub>6</sub>, pyridine-*d*<sub>5</sub>, and toluene-*d*<sub>8</sub> were degassed and stored over molecular sieves for at least 2 days prior to use. CDCl<sub>3</sub> was distilled off of CaH<sub>2</sub> and

stored over molecular sieves. The compounds  $[\text{Na}][\text{P}\equiv\text{Nb}(\text{N}[\text{CH}_2^t\text{Bu}]\text{Ar})_3]$ ,<sup>108</sup>  $\text{Cl}_2\text{Nb}(\text{ODipp})_3$ ,<sup>18</sup>  $\text{N}_2[\text{Mo}(\text{CO})_3(\text{P}^i\text{Pr}_3)_2]_2$ ,<sup>69</sup>  $\text{Mo}(\text{N}[\text{tBu}]\text{Ar})_3$ ,<sup>109</sup>  $\text{Ti}(\text{N}[\text{tBu}]\text{Ar})_3$ ,<sup>80</sup>  $\text{Nb}(\text{H})(\eta^2\text{-}^t\text{Bu}(\text{H})\text{C}=\text{NAr})(\text{N}[\text{CH}_2^t\text{Bu}]\text{Ar})_2$ ,<sup>22</sup>  $(\text{PN}(^i\text{Pr})_2\text{N}(\text{SiMe}_3)_2)_2$ ,<sup>77,110</sup>  $[\text{GaC}(\text{SiMe}_3)_3]_4$ ,<sup>97,98,100</sup>  $\text{FeCp}^*(\text{dppe})\text{Cl}$ ,<sup>111</sup> and  $(\text{OTf})\text{Re}(\text{CO})_2(\text{triphos})$ <sup>112</sup> were synthesized according to reported methods.  $\text{AsCl}_3$  and  $\text{NaBPh}_4$  were purchased from Aldrich chemical company and used as received.  $\text{CoCp}_2$  was purchased from STREM chemical company and used as received. NMR spectra were obtained on Varian Mercury 300 or Varian Inova 500 instruments equipped with Oxford Instruments superconducting magnets or on Bruker Avance 400 instruments equipped with Magnex Scientific superconducting magnets.  $^1\text{H}$  NMR spectra were referenced to residual  $\text{C}_6\text{D}_5\text{H}$  (7.16 ppm),  $\text{CHCl}_3$  (7.27 ppm) or  $\text{C}_5\text{D}_4\text{HN}$  (8.74 ppm).  $^{13}\text{C}$  NMR spectra were referenced to  $\text{C}_6\text{D}_6$  (128.39 ppm),  $\text{CDCl}_3$  (77.23 ppm), or  $\text{C}_5\text{D}_5\text{N}$  (150.35 ppm).  $^{31}\text{P}$  NMR spectra were referenced externally to 85%  $\text{H}_3\text{PO}_4$  (0 ppm). Elemental analyses were performed by Midwest Microlab, LLC (Indianapolis, Indiana). GC-MS data were collected using an Agilent 6890N network GC system with an Agilent 5973 Network mass selective detector and an Rtx-1 column from Restek. MALDI-TOF MS data were collected on a Bruker OmniFlex instrument, and data were processed using the Bruker FlexControl software package. For Raman studies, an Invictus solid-state laser at 785 nm, manufactured by Kaiser Optics, was routed through fiber-optic cables to a Hololab series 5000 Raman Microscope. The Raman scattering was observed *via* 180 ° reflectance through the objective of the Raman microscope. Each spectrum was corrected for dark current and cosmic ray interference using the Hololab software. For the Raman polarization experiments, a 514.5 nm laser was used with 2 mW power at the sample. Powder diffraction data were collected on a PANalytical X'Pert Pro multipurpose diffractometer equipped with a 1.8 kW sealed tube X-ray source using Mo  $\text{K}\alpha$  radiation ( $\lambda = 0.71073 \text{ \AA}$ ) and equipped with high-speed Bragg-Brentano optics. Scanning electron microscopy was performed on a JEOL JSM-5910 instrument using a JEOL BEI detector and a Rontec EDX system for elemental analysis and mapping. Bulk photolysis experiments were performed using a Rayonet RPR-200 photo-reactor supplied by Southern New England Ultraviolet Company. UV-vis spectra were obtained on a Cary 14 spectrophotometer, running the OLIS Globalworks software suite, in 1 cm quartz cells manufactured by Starna.

### 2.9.2 Preparation of $[\text{Na}][\text{P}_3\text{Nb}(\text{N}[\text{CH}_2^t\text{Bu}]\text{Ar})_3]$ from $[\text{Na}][\text{P}\equiv\text{Nb}(\text{N}[\text{CH}_2^t\text{Bu}]\text{Ar})_3]$ and $\text{P}_4$

$[\text{Na}][\text{P}\equiv\text{Nb}(\text{N}[\text{CH}_2^t\text{Bu}]\text{Ar})_3]$  (300 mg, 0.378 mmol) was dissolved in 40 mL of  $\text{Et}_2\text{O}$  and was combined with  $\text{P}_4$  (24 mg, 0.189 mmol, 0.5 equiv) as a stock solution in  $\text{C}_6\text{D}_6$ . The reaction mixture was allowed to stir for 20 minutes after which time the reaction mixture was concentrated under reduced pressure to a total of 7 mL. The reaction mixture was placed in the glove box freezer at  $-35^\circ$  for crystallization. After 24 h, a copious orange precipitate formed and was isolated atop a frit resulting in 292 mg (90% yield) of pure  $[\text{Na}][\text{P}_3\text{Nb}(\text{N}[\text{CH}_2^t\text{Bu}]\text{Ar})_3]$ .  $^1\text{H}$  NMR ( $\text{C}_6\text{D}_6$ , 500

MHz, 20 °C): 0.985 (s, 27 H, <sup>t</sup>Bu); 2.280 (s, 18 H, ArCH<sub>3</sub>); 3.942 (s, 6 H, NCH<sub>2</sub>); 6.556 (s, 3 H, *p*-Ar); 6.946 (s, 6 H, *o*-Ar) ppm; <sup>31</sup>P NMR (C<sub>6</sub>D<sub>6</sub>, 202 MHz, 20 °C): -223 ppm (s, 3 P).

### 2.9.3 Preparation of [Na(THF)<sub>3</sub>][P<sub>3</sub>Nb(ODipp)<sub>3</sub>], 25

Caution: Na<sub>3</sub>P is formed during the course of this reaction. Proper care must be taken with its disposal as it is highly pyrophoric.

P<sub>4</sub> (1.3 g, 10.5 mmol) was added as a solid to a 500 mL round bottom flask equipped with a teflon coated stir-bar and THF (400 mL) was added. Note: It is important that all of the P<sub>4</sub> be dissolved prior to beginning the reduction. In a separate vessel, a 0.5% Na/Hg amalgam was prepared by carefully adding 1.4 g of Na (62.4 mmol) to 250 g of Hg. This was set aside to cool. Once the P<sub>4</sub> was dissolved, Cl<sub>2</sub>Nb(ODipp)<sub>3</sub> (7.2 g, 10.4 mmol) was added as a solid to the stirring solution of P<sub>4</sub>. Following dissolution of the Cl<sub>2</sub>Nb(ODipp)<sub>3</sub>, the cooled Na/Hg amalgam was added with stirring. The reaction mixture was stirred vigorously for 1 h. Note: It is important to ensure that the amalgam stirs well for the entire reaction time. Once the reaction time had elapsed, the black-brown reaction mixture was decanted away from the amalgam and was filtered through a pad of Celite and the resulting solution was taken to dryness under reduced pressure. Note: It is important that the residue be dried to constant mass under reduced pressure before moving on with the work up in order to facilitate removal of the NaCl formed during the reaction. To the fully dried residue was added 75 mL of Et<sub>2</sub>O. The resulting mixture was filtered through a pad of Celite resulting in an orange filtrate and a black residue left on the Celite pad. The orange solution was taken to dryness and the resulting orange residue was dissolved in 7 mL of Et<sub>2</sub>O and 7 mL of THF and is cooled for 16 h at -35 °C. The resulting orange crystals were isolated atop a frit, washed with a minimal amount (3 mL) of *n*-pentane and dried to constant mass under reduced pressure. Yield after recrystallization: 5.65 g, 57%. <sup>1</sup>H NMR (C<sub>6</sub>D<sub>6</sub>, 500 MHz, 20 °C): 1.33 (THF, m, 12 H); 1.43 (Me, d, 36 H); 3.32 (THF, m, 12 H); 4.06 (<sup>i</sup>Pr, sep, 6 H); 6.99 (Ar, t, 3 H); 7.20 (Ar, d, 6 H) ppm; <sup>13</sup>C{<sup>1</sup>H} NMR (C<sub>6</sub>D<sub>6</sub>, 126 MHz, 20 °C): 24.55 (Me), 25.59 (THF), 27.28 (<sup>i</sup>Pr), 68.13 (THF), 121.48 (Ar), 123.32 (Ar), 138.81 (Ar), 161.09 (Ar) ppm; <sup>31</sup>P NMR (C<sub>6</sub>D<sub>6</sub>, 202 MHz, 20 °C): -206 ppm (s, 3 P). Electrochemistry: Single irreversible reduction at -78 mV vs. Fc/Fc<sup>+</sup>. Elemental analysis calculated for C<sub>48</sub>H<sub>74</sub>NaNbO<sub>6</sub>P<sub>3</sub>: C 60.24, H 7.90, P 9.71; Found: C 60.08, H 7.20, P 9.26.

### 2.9.4 Preparation of [CoCp<sub>2</sub>][P<sub>3</sub>Nb(ODipp)<sub>3</sub>], 26

SmI<sub>2</sub> (26.56 g of 0.1 M solution in THF, 2.9 mmol) was added to a solution of Cl<sub>2</sub>Nb(ODipp)<sub>3</sub> (2.0 g, 2.88 mmol, 1 equiv) in 25 mL of THF. Immediately upon addition the solution assumed a bright yellow color. The reaction mixture was allowed to stir for 20 minutes and the bright yellow SmI<sub>2</sub>Cl which had precipitated during the reaction was then filtered away. An aliquot of the bright yellow filtrate was taken to dryness and the residue was then dissolved in C<sub>6</sub>D<sub>6</sub> and taken for NMR and EPR analysis indicating complete conversion to ClNb(ODipp)<sub>3</sub>(THF). At this time P<sub>4</sub> (268 mg, 2.16

mmol, 0.75 equiv) was added. Following dissolution of the P<sub>4</sub>, CoCp<sub>2</sub> (1.09 g, 5.76 mmol, 2 equiv) was added to the reaction mixture which was then allowed to stir for 3 h. At this time the reaction mixture was concentrated to half the original volume and 20 mL of hexane were added. The reaction mixture was then filtered through Celite to remove yellow [CoCp<sub>2</sub>][Cl]. The filtrate was taken to dryness and was slurried in 25 mL of Et<sub>2</sub>O and placed in a liquid nitrogen cooled cold well for 15 minutes. The resulting bright orange precipitate was collected atop a frit and dried to constant mass giving 1.82 g (70% yield) of [CoCp<sub>2</sub>][P<sub>3</sub>Nb(ODipp)<sub>3</sub>]. <sup>1</sup>H NMR (C<sub>6</sub>D<sub>6</sub>, 500 MHz, 20 °C): 1.17 (Me, d, 36 H); 3.71 (<sup>i</sup>Pr, sep, 6 H); 5.58 (CoCp<sub>2</sub>, s, 10 H); 6.86 (Ar, t, 3 H); 7.06 (Ar, d, 6 H) ppm; <sup>13</sup>C{<sup>1</sup>H} NMR (C<sub>6</sub>D<sub>6</sub>, 126 MHz, 20 °C): 24.49 (Me); 27.04 (<sup>i</sup>Pr); 85.99 (CoCp<sub>2</sub>); 120.48 (Ar); 123.13 (Ar); 124.0 (Ar); 139.17 (Ar) ppm; <sup>31</sup>P{<sup>1</sup>H} NMR (C<sub>6</sub>D<sub>6</sub>, 202 MHz, 20 °C): -170.41 ppm. Elemental analysis calculated for C<sub>46</sub>H<sub>61</sub>CoNbO<sub>3</sub>P<sub>3</sub>:C 60.93, H 6.78, P 10.25; Found: C 60.23, H 6.82, P 9.88.

### 2.9.5 Preparation of AsP<sub>3</sub>, 27

Caution: AsCl<sub>3</sub> is toxic and should be handled with the utmost care. AsP<sub>3</sub> is highly pyrophoric and should be handled in the absence of oxygen.

[Na(THF)<sub>3</sub>][P<sub>3</sub>Nb(ODipp)<sub>3</sub>] (2.91 g, 3.04 mmol) was dissolved in 50 mL of THF in a 100 mL round bottom flask equipped with a Teflon coated stir bar. This solution was frozen in the glove box cold well along with a vial containing AsCl<sub>3</sub> (547 mg, 3.04 mmol) in 5 mL of THF. Upon thawing the AsCl<sub>3</sub> solution was added to the THF solution of [Na(THF)<sub>3</sub>][P<sub>3</sub>Nb(ODipp)<sub>3</sub>]. The reaction mixture was allowed warm to room temperature and was allowed to stir for 45 minutes. After the reaction time had elapsed, the reaction mixture was filtered through a pad of Celite and the volatile components were removed under reduced pressure. The resulting residue was isolated and placed into a sublimation apparatus. The residue was sublimed with the exclusion of light at 65 °C under dynamic vacuum for 6 h. A constant stream of cold water was kept running through the cold finger during the sublimation to ensure no loss of AsP<sub>3</sub>. After cooling, the sublimation apparatus was returned to the glove box and the crystalline AsP<sub>3</sub> was isolated from the cold finger, with pure orange Cl<sub>2</sub>Nb(ODipp)<sub>3</sub>(THF) remaining in the bottom of the sublimation apparatus. Yield after sublimation: 332 mg, 65%. <sup>31</sup>P NMR (C<sub>6</sub>D<sub>6</sub>, 202 MHz, 20 °C): -484 ppm (s, 3 P); Raman Spectrum: 313 (*e*), 345 (*a*<sub>1</sub>), 428 (*e*), 557 (*a*<sub>1</sub>) cm<sup>-1</sup>; GC-MS: 9.1 min retention time with parent ion at 168 m/z; EI-MS: 167.8426 m/z; MP: 71–73 °C; Decomposition Point: 230 °C (DSC); UV-Vis λ<sub>max</sub> = 229 nm with ε = 2470 M<sup>-1</sup> cm<sup>-1</sup>.

### 2.9.6 Thermolysis of AsP<sub>3</sub>

AsP<sub>3</sub> (100 mg, 0.596 mmol) was loaded into a thick-walled glass tube. The tube was sealed under vacuum. The tube was wired to a thermocouple probe, and the probe and tube were wrapped completely with heating tape. The heating tape was set to heat at 290-300 °C for 40 h. After this

time the apparatus was cooled, and the heating tape was removed. The white-yellow  $\text{AsP}_3$  had been converted to a red-black material as well as a metallic shiny material which had sublimed partially up the tube. Raman spectroscopy of the bulk material through the tube revealed complete consumption of the  $\text{AsP}_3$  tetrahedron. The tube was scored and broken open. The contents of the tube were removed and placed on a zero background silicon 510 surface for powder diffraction. Powder diffraction data: broad peaks centered around  $18^\circ$ ,  $32^\circ$ ,  $58^\circ$ , and  $90^\circ$   $2\theta$ . The product mixture was then also analyzed by Raman spectroscopy and EDS using a JEOL SEM microscope. Raman spectroscopy results: broad and weak resonance at  $280\text{ cm}^{-1}$ , sharp and intense resonance at  $320\text{ cm}^{-1}$ , broad and intense resonances extending from  $340$  to  $500\text{ cm}^{-1}$ . SEM data: in a  $50\text{ }\mu\text{m} \times 50\text{ }\mu\text{m}$  region, elemental composition analysis gave phosphorus 74.01% (error 0.66%) and arsenic 25.98% (error 0.76%).

### 2.9.7 Photolysis of $\text{AsP}_3$

$\text{AsP}_3$  (56 mg, 0.33 mmol) was dissolved in 10 mL of THF and was placed into a 100 mL quartz reaction vessel equipped with a stir bar. This vessel was sealed and was placed into the UV photoreactor (Rayonet by New England Ultraviolet Company) equipped with 8 lamps (4 RPR-4190 with  $\lambda_{\text{max}}$  419 nm and 4 RPR 2537 with  $\lambda_{\text{max}}$  254 nm) with a fan blowing to cool the system. The reaction mixture was allowed to sit in the UV reactor with stirring for 3 h 15 min with stirring, during which time a copious red precipitate formed. This precipitate was spun down into a pellet under nitrogen in a centrifuge and then was isolated and dried to a constant mass of 48 mg. This material was analyzed by Raman spectroscopy, which clearly showed the presence of red P (as described above), powder diffraction, which clearly showed the appearance of amorphous metallic arsenic (as described above), and by SEM microscopy which showed clear regions of only P and only As (as described above).

### 2.9.8 Preparation of $(\text{AsP}_3)\text{Mo}(\text{CO})_3(\text{P}^i\text{Pr}_3)_2$ , 28

Yellow  $(\text{N}_2)[\text{Mo}(\text{CO})_3(\text{P}^i\text{Pr}_3)_2]_2$  (142 mg, 0.137 mmol, 1 equiv) was dissolved in toluene (5 mL) forming a green solution. This solution was placed in a thick walled glass reactor and was frozen in the cold well.  $\text{AsP}_3$  (45 mg, 0.268 mmol, 2 equiv) was separately dissolved in toluene (5 mL) and this solution was layered atop the frozen solution of  $(\text{N}_2)[\text{Mo}(\text{CO})_3(\text{P}^i\text{Pr}_3)_2]_2$ . The reactor was then returned to the cold well and the  $\text{AsP}_3$  solution was frozen. The reaction vessel was removed from the glove box and was placed in a salt water and ice bath at  $-5^\circ\text{C}$ . Upon mixing of the two layers, the green solution assumed a vibrant orange color. The reactor was then placed under reduced pressure to remove the toluene while maintaining the  $-5^\circ\text{C}$  temperature conditions. The reaction mixture took about 5 h to come to dryness. The vessel was returned to the glove box where cold toluene (5 mL at approximately  $-35^\circ\text{C}$ ) was used to dissolve the residue. This solution was placed in the glove box freezer to crystallize. After 4 h a significant amount of red-orange precipitate had



formed. This precipitate was isolated and washed with diethyl ether resulting in 112 mg of material (63% yield). IR was collected on the solids as a KBr pellet. The NMR shifts reported below were collected at  $-10\text{ }^{\circ}\text{C}$  on a toluene solution of the solids making sure to never let the solution get above  $0\text{ }^{\circ}\text{C}$ .  $^1\text{H}$  NMR ( $\text{C}_6\text{D}_6$ , 400 MHz,  $-10\text{ }^{\circ}\text{C}$ ): 1.18 (Me, br, 36 H); 2.16 ( $i$ Pr, br, 6 H) ppm;  $^{13}\text{C}\{^1\text{H}\}$  NMR ( $\text{C}_6\text{D}_6$ , 101 MHz,  $-10\text{ }^{\circ}\text{C}$ ): 20.09 (Me); 27.63 (br,  $i$ Pr) ppm;  $^{31}\text{P}\{^1\text{H}\}$  NMR ( $\text{C}_6\text{D}_6$ , 162 MHz,  $-10\text{ }^{\circ}\text{C}$ ):  $-448.82$  (Mo-PP<sub>2</sub>As, br, 2 P; sharpens to d with  $^1J_{\text{P/P}} = 218\text{ Hz}$  at  $-55\text{ }^{\circ}\text{C}$ );  $-366.87$  (Mo-PP<sub>2</sub>As, br, 1 P, sharpens to t with  $^1J_{\text{P/P}} = 218\text{ Hz}$  at  $-55\text{ }^{\circ}\text{C}$ ); 58.39 ( $P^i$ Pr, s, 2 P) ppm; IR: 1846, 1880, 1954  $\text{cm}^{-1}$  for  $\nu\text{CO}$ . Elemental analysis: calculated for  $\text{C}_{28}\text{H}_{50}\text{AsMoO}_3\text{P}_5$  (complex + 1 toluene, as crystallized): C 44.22, H 6.63; Found C44.15, H 6.90.

### 2.9.9 Preparation of $[(\text{AsP}_3)\text{Fe}(\text{Cp}^*)(\text{dppe})][\text{BPh}_4]$ , 29

$\text{FeCp}^*(\text{dppe})\text{Cl}$  (144 mg, 0.230 mmol, 1 equiv) was dissolved in 8 mL of THF and was transferred to a vial containing solid  $\text{AsP}_3$  (43 mg, 0.256 mmol, 1.1 equiv) and a stir bar. The reaction mixture was allowed to stir for 30 min during which time the originally green reaction mixture went slightly orange (subtle change). At this point  $\text{NaBPh}_4$  (79 mg, 0.230 mmol, 1 equiv) was added, resulting in immediate formation of a bright magenta-purple color. The reaction mixture was allowed to stir an additional 10 min. At this point the reaction mixture was concentrated, and  $n$ -pentane was added to help precipitate the salt. The reaction mixture was filtered through a plug of Celite, and the volatile components were concentrated to 5 mL.  $\text{Et}_2\text{O}$  (3 mL) was added, and the purple solution was placed in the freezer to induce precipitation. After 30 min, a copious magenta precipitate had formed. This precipitate was isolated atop a frit, resulting in 198 mg (0.183 mmol) of material (80% yield). X-ray diffraction-quality crystals were grown from an  $\text{Et}_2\text{O}/\text{CH}_2\text{Cl}_2$  (1:1) solution at  $-35\text{ }^{\circ}\text{C}$ .  $^1\text{H}$  NMR (20  $^{\circ}\text{C}$ , acetone- $d_6$ , 500 MHz):  $\delta = 1.48$  (15 H, s,  $\text{Cp}^*\text{Me}$ ), 2.61 (2 H, m,  $\text{dppe-CH}_2$ ), 2.75 (2 H, m,  $\text{dppe-CH}_2$ ), 6.77 (m, 8 H, Ar), 6.91 (m, 12 H, Ar), 7.34 (br, 8 H, Ar), 7.50 (br, 4 H, Ar), 7.61 (br, 8 H, Ar).  $^{31}\text{P}\{^1\text{H}\}$  NMR (20  $^{\circ}\text{C}$ , acetone- $d_6$ , 202.5 MHz):  $\delta = -450$  (2 P, d,  $^1J_{\text{P/P}} = 245\text{ Hz}$ , non-Fe bound P),  $-261$  (1 P, tt,  $^1J_{\text{P/P}} = 245\text{ Hz}$ ,  $^2J_{\text{P/P}} = 37\text{ Hz}$ , Fe-bound P), 89 (2 P, d,  $^2J_{\text{P/P}} = 37\text{ Hz}$ ,  $\text{dppe-P}$ ).  $^{13}\text{C}\{^1\text{H}\}$  NMR (20  $^{\circ}\text{C}$ , acetone- $d_6$ , 125.8 MHz):  $\delta = 10.6$  (s,  $\text{Cp}^*\text{-Me}$ ), 29.5 (t,  $\text{dppe-CH}_2$ ), 90.7 (s,  $\text{Cp}^*\text{-ring}$ ), 122.8 (Ar), 126.6 (Ar), 129.6 (Ar), 131.7 (Ar), 133.2 (Ar), 137.6 (Ar), 164.9 (Ar), 165.7 (Ar). UV-vis: 494 nm ( $\epsilon = 590\text{ M}^{-1}\text{ cm}^{-1}$ ), 543 nm ( $\epsilon = 480\text{ M}^{-1}\text{ cm}^{-1}$ ). MALDI-TOF MS: 757.0318  $m/z$  ( $[\text{AsP}_3\text{FeCp}^*(\text{dppe})]^+$ ), 589.2216  $m/z$  ( $[\text{FeCp}^*(\text{dppe})]^+$ ), 319.1650  $m/z$  ( $[\text{BPh}_4]^-$ ). Elem. Anal. Calcd for  $\text{C}_{60}\text{H}_{59}\text{AsBFeP}_5$ : C 66.94, H 5.52, P 14.39; Found: C 66.87, H 5.61, P 13.98.

### 2.9.10 Preparation of $\text{AsP}_3(\text{P}(\text{N}(i\text{Pr})_2)\text{N}(\text{SiMe}_3)_2)_2$ , 30

$(\text{P}(\text{N}(i\text{Pr})_2)\text{N}(\text{SiMe}_3)_2)_2$  (190 mg, 0.295 mmol) was dissolved in 10 mL of toluene and was added slowly to a vial containing a solution of  $\text{AsP}_3$  (54 mg, 0.321 mmol) in 5 mL of toluene. Upon mixing the two colorless reagents, the reaction mixture took on a vibrant yellow color. The mixture

was stirred for an additional 20 min, and an aliquot was withdrawn for NMR analysis which showed clean and complete conversion of the starting materials to  $\text{AsP}_3(\text{P}(\text{N}(\text{iPr})_2)\text{N}(\text{SiMe}_3)_2)_2$ . The reaction mixture was taken to dryness under reduced pressure, and the resulting residue was dissolved in *n*-hexane/Et<sub>2</sub>O (2:1) and recrystallized, affording 196 mg (0.261 mmol, 88% yield) of pale-yellow crystals of  $\text{AsP}_3(\text{P}(\text{N}(\text{iPr})_2)\text{N}(\text{SiMe}_3)_2)_2$  (mixture of isomers). <sup>1</sup>H NMR (20 °C, benzene-d<sub>6</sub>, 500 MHz): δ = 0.43 (36 H, br, SiMe<sub>3</sub>), 1.03 (12H, m, <sup>i</sup>Pr-Me), 1.20 (6 H, m, <sup>i</sup>Pr-Me), 1.26 (6 H, m, <sup>i</sup>Pr-Me), 3.34 (2 H, m, <sup>i</sup>Pr-CH), 3.48 (2 H, m, <sup>i</sup>Pr-CH). <sup>31</sup>P{<sup>1</sup>H} NMR (20 °C, benzene-d<sub>6</sub>, 202.5 MHz): δ = -311 (2 P, m, P(*PP*)As), -148.5 (1 P, m, P(*PP*)As), 118.5 (1 P, m, As bound phosphine), 123 (1 P, m, P bound phosphine). <sup>13</sup>C{<sup>1</sup>H} NMR (20 °C, benzene-d<sub>6</sub>, 125.8 MHz): δ = 5.1 (br, SiMe<sub>3</sub>), 6.53 (br, SiMe<sub>3</sub>), 23.6 (m, <sup>i</sup>Pr-Me), 24.7 (m, <sup>i</sup>Pr-Me), 48.2 (m, <sup>i</sup>Pr-CH). Elem. Anal. Calcd for C<sub>24</sub>H<sub>64</sub>AsN<sub>4</sub>P<sub>5</sub>Si<sub>4</sub>: C 38.39, H 8.59, N 7.46, P 20.62; Found: C 39.42, H 8.78, N 8.26, P 19.27.

### 2.9.11 Synthesis and Equilibrium Study of $(\text{Ar}[\text{iBu}]\text{N})_3\text{Ti}[\text{P}(\text{P}_2)\text{As}]\text{Ti}(\text{N}[\text{iBu}]\text{Ar})_3$ , **31**, and $(\text{Ar}[\text{iBu}]\text{N})_3\text{Ti}[\text{P}(\text{P}_2)\text{P}]\text{Ti}(\text{N}[\text{iBu}]\text{Ar})_3$ , **32**

To begin the measurements, AsP<sub>3</sub> (15 mg, 0.09 mmol), P<sub>4</sub> (11 mg, 0.09 mmol), PPh<sub>3</sub> (12 mg, 0.045 mmol), Ti(N[<sup>i</sup>Bu]Ar)<sub>3</sub> (68 mg, 0.118 mmol), and toluene (872 mg) were combined and placed in a J-Young-style NMR tube. The temperature was varied between 5 and 35 °C, allowing the tube to fully equilibrate before taking the final concentration readings. The simplest equilibrium expression was not obeyed, but the product concentration for **31** was always higher than for **32**. For example, at 20 °C **31** and **32** were present in a 7:1 ratio. These results show that in a 1:1 mixture of AsP<sub>3</sub> and P<sub>4</sub>, a greater percentage of AsP<sub>3</sub> undergoes reaction. This experiment was repeated with only AsP<sub>3</sub> in the reaction mixture and alternatively with only P<sub>4</sub> present to obtain clean NMR spectral data for both **31** and **32**. <sup>31</sup>P{<sup>1</sup>H} NMR (AsP<sub>3</sub>[Ti(N[<sup>i</sup>Bu]Ar)<sub>3</sub>], 20 °C, benzene-d<sub>6</sub>, 202.5 MHz): δ = -275 (2 P, d, <sup>1</sup>J<sub>P/P</sub> = 200 Hz, P(*PP*)As), -9.6 (1 P, t, <sup>1</sup>J<sub>P/P</sub> = 200 Hz, P(*PP*)As). <sup>31</sup>P{<sup>1</sup>H} NMR (P<sub>4</sub>[Ti(N[<sup>i</sup>Bu]Ar)<sub>3</sub>], 20 °C, benzene-d<sub>6</sub>, 202.5 MHz): δ = -284 (2 P, t, <sup>1</sup>J<sub>P/P</sub> = 188 Hz, P(*PP*)P), 12.9 (2 P, t, <sup>1</sup>J<sub>P/P</sub> = 188 Hz, P(*PP*)P).

### 2.9.12 Preparation of $(\text{Ar}[\text{CH}_2\text{iBu}]\text{N})_3\text{Nb}(\text{PAs})\text{Nb}(\text{N}[\text{CH}_2\text{iBu}]\text{Ar})_3$ , **33**, and $(\text{Ar}[\text{CH}_2\text{iBu}]\text{N})_3\text{Nb}(\text{P}_2)\text{Nb}(\text{N}[\text{CH}_2\text{iBu}]\text{Ar})_3$ , **34**

Nb(H)(η<sup>2</sup>-<sup>i</sup>Bu(H)C=NAr)(N[CH<sub>2</sub><sup>i</sup>Bu]Ar)<sub>2</sub> (113 mg, 0.17 mmol) was dissolved in 5 mL of Et<sub>2</sub>O and was added to a vial containing AsP<sub>3</sub> (10 mg, 0.06 mmol) and a stir bar. The reaction mixture was vigorously stirred for 90 min during which time the originally yellow solution took on a deep-green color. The volatile components of the reaction mixture were removed under reduced pressure. The resulting green powder was taken up in C<sub>6</sub>D<sub>6</sub> for NMR analysis. Recrystallization from Et<sub>2</sub>O/pentane (1:2) afforded 98 mg (82% yield) of a 1:1 mixture of (μ<sub>2</sub>:η<sup>2</sup>, η<sup>2</sup>-P<sub>2</sub>)[Nb(N[CH<sub>2</sub><sup>i</sup>Bu]Ar)<sub>3</sub>]<sub>2</sub> and (μ<sub>2</sub>:η<sup>2</sup>, η<sup>2</sup>-AsP)[Nb(N[CH<sub>2</sub><sup>i</sup>Bu]Ar)<sub>3</sub>]<sub>2</sub>. <sup>1</sup>H NMR (20 °C, benzene-d<sub>6</sub>,

500 MHz):  $\delta = 6.98$  (24 H, br, *o*-Ar), 6.59 (12 H, s, *p*-Ar), 4.23 (24 H, br, N-CH<sub>2</sub>), 2.25 (36 H, s, Ar-CH<sub>3</sub>,  $\mu$ -P<sub>2</sub>), 2.23 (36 H, s, Ar-CH<sub>3</sub>,  $\mu$ -AsP), 0.97 (54 H, s, <sup>*t*</sup>Bu,  $\mu$ -P<sub>2</sub>), 0.95 (54 H, s, <sup>*t*</sup>Bu,  $\mu$ -AsP). <sup>31</sup>P{<sup>1</sup>H} NMR (20 °C, benzene-d<sub>6</sub>, 202.5 MHz):  $\delta = 399$  (2 P, br,  $\mu$ -P<sub>2</sub>), 438 (1 P, br,  $\mu$ -AsP). <sup>13</sup>C{<sup>1</sup>H} NMR (20 °C, benzene-d<sub>6</sub>, 125.7 MHz):  $\delta = 154.2$  (Ar), 138.1 (Ar), 126.6 (Ar), 124.4 (Ar), 73 (N-CH<sub>2</sub>), 37.3 (C(CH<sub>3</sub>)), 30.3 (C(CH<sub>3</sub>),  $\mu$ -P<sub>2</sub>), 30.1 (C(CH<sub>3</sub>),  $\mu$ -AsP), 22.1 (Ar-CH<sub>3</sub>).

### 2.9.13 Preparation of As≡Mo(N[<sup>*t*</sup>Bu]Ar)<sub>3</sub>, 35-As, and P≡Mo(N[<sup>*t*</sup>Bu]Ar)<sub>3</sub>, 35-P

Mo(N[<sup>*t*</sup>Bu]Ar)<sub>3</sub> (100 mg, 0.16 mmol) was dissolved in 5 mL of Et<sub>2</sub>O and was added to a vial containing solid AsP<sub>3</sub> (8 mg, 0.047 mmol). The mixture was stirred for 60 min during which time the reaction mixture assumed a dark orange color. The volatile components of the reaction mixture were removed under reduced pressure. The resulting residue was dissolved in C<sub>6</sub>D<sub>6</sub> and was taken for NMR analysis. Recrystallization from Et<sub>2</sub>O/*n*-pentane (1:2) afforded 75 mg (70% yield) of 3:1 PMo(N[<sup>*t*</sup>Bu]Ar)<sub>3</sub> and AsMo(N[<sup>*t*</sup>Bu]Ar)<sub>3</sub>. <sup>1</sup>H NMR (20 °C, benzene-d<sub>6</sub>, 500 MHz):  $\delta = 6.61$  (6 H, s, *o*-Ar), 5.81 (3 H, br, *p*-Ar), 2.04 (18 H, s, Ar-Me), 1.66 (27 H, s, <sup>*t*</sup>Bu). <sup>31</sup>P{<sup>1</sup>H} NMR (20 °C, benzene-d<sub>6</sub>, 202.5 MHz):  $\delta = 1216$  (1 P, br, P≡Mo). <sup>13</sup>C{<sup>1</sup>H} NMR (20 °C, benzene-d<sub>6</sub>, 125.7 MHz):  $\delta = 150.6$  (Ar, P≡Mo), 150.0 (Ar, As≡Mo), 136.85 (Ar, P≡Mo), 136.80 (Ar, As≡Mo), 130.6 (Ar, As≡Mo), 130.4 (Ar, P≡Mo), 127.7 (Ar), 60.6 (C(CH<sub>3</sub>), P≡Mo), 59.8 (C(CH<sub>3</sub>), As≡Mo), 34.1 (C(CH<sub>3</sub>), As≡Mo), 33.9 (C(CH<sub>3</sub>), P≡Mo), 21.5 (Ar-CH<sub>3</sub>).

### 2.9.14 Preparation of As[GaC(SiMe<sub>3</sub>)<sub>3</sub>]<sub>3</sub>P<sub>3</sub>, 36

AsP<sub>3</sub> (78 mg, 0.467 mmol) was dissolved in 10 mL of toluene (freshly distilled off of Na/benzophenone). [GaC(SiMe<sub>3</sub>)<sub>3</sub>]<sub>4</sub> (422 mg, 0.350 mmol) was also dissolved in 10 mL of toluene. The two solutions were combined in a thick-walled glass reactor along with an additional 5 mL of toluene to effect quantitative transfer of the reagents. The reaction mixture was heated with stirring for 5 h at 80 °C. During this time the solution lightened from a red-orange color to a yellow-orange color. On cooling, a copious amount of fibrous-yellow precipitate formed in the reaction flask. The solution was concentrated to 15 mL and 5 mL of cold pentane were added. The resulting yellow microcrystalline solids were isolated atop a frit and were dried to constant mass giving 251 mg of cotton-like yellow solids. The filtrate was dried under reduced pressure and the residue was dissolved in 5 mL of toluene and placed in the freezer in order to obtain a second crop containing an additional 28 mg for a total of 279 mg (0.260 mmol, 56% yield) of a 4:1 mixture of As[GaC(SiMe<sub>3</sub>)<sub>3</sub>]<sub>3</sub>P<sub>3</sub> to P[GaC(SiMe<sub>3</sub>)<sub>3</sub>]<sub>3</sub>AsP<sub>2</sub>. <sup>1</sup>H NMR (20 °C, benzene-d<sub>6</sub>, 500 MHz): 0.418 (27 H, s, As[GaC(SiMe<sub>3</sub>)<sub>3</sub>]<sub>3</sub>P<sub>3</sub>), 0.428 (roughly 7 H (20% of total), s, P[GaC(SiMe<sub>3</sub>)<sub>3</sub>]<sub>3</sub>AsP<sub>2</sub>) ppm. <sup>31</sup>P{<sup>1</sup>H} NMR (20 °C, benzene-d<sub>6</sub>, 202.5 MHz): -192.39 (3 P, s, As[GaC(SiMe<sub>3</sub>)<sub>3</sub>]<sub>3</sub>P<sub>3</sub>), -173.61 (roughly 0.75 P (20% of total), d, <sup>2</sup>J<sub>P/P</sub> = 34 Hz, P[GaC(SiMe<sub>3</sub>)<sub>3</sub>]<sub>3</sub>AsP<sub>2</sub>), -495.84 (roughly 0.25 P (20% of total), t, <sup>2</sup>J<sub>P/P</sub> = 34 Hz, P[GaC(SiMe<sub>3</sub>)<sub>3</sub>]<sub>3</sub>AsP<sub>2</sub>) ppm. <sup>13</sup>C{<sup>1</sup>H} NMR (20 °C, benzene-d<sub>6</sub>, 125.7 MHz): 6.615 (s, As[GaC(SiMe<sub>3</sub>)<sub>3</sub>]<sub>3</sub>P<sub>3</sub>), 6.736 (s, P[GaC(SiMe<sub>3</sub>)<sub>3</sub>]<sub>3</sub>AsP<sub>2</sub>), 27.62

(s, As[GaC(SiMe<sub>3</sub>)<sub>3</sub>]<sub>3</sub>P<sub>3</sub>), 27.78 (s, P[GaC(SiMe<sub>3</sub>)<sub>3</sub>]<sub>3</sub>AsP<sub>2</sub>). UV-vis: 294 nm ( $\epsilon = 2866 \text{ M}^{-1} \text{ cm}^{-1}$ ), 382 nm ( $\epsilon = 1412 \text{ M}^{-1} \text{ cm}^{-1}$ ). Elem. Anal. Calcd for C<sub>30</sub>H<sub>81</sub>AsGa<sub>3</sub>P<sub>3</sub>Si<sub>9</sub>: C 33.62, H 7.62, P 8.67; Found: C 33.53, H 7.24, P 9.07.

### 2.9.15 Preparation of [Na(THF)<sub>3</sub>][P<sub>3</sub>Nb(ODipp)<sub>3</sub>] (**25**), [Na(THF)<sub>3</sub>][P<sub>2</sub>AsNb(ODipp)<sub>3</sub>] (**37**), [Na(THF)<sub>3</sub>][PAs<sub>2</sub>Nb(ODipp)<sub>3</sub>] (**38**), and [Na(THF)<sub>3</sub>][As<sub>3</sub>Nb(ODipp)<sub>3</sub>] (**39**) from AsP<sub>3</sub> and their conversion to AsP<sub>3</sub> (**27**), As<sub>2</sub>P<sub>2</sub> (**40**), As<sub>3</sub>P (**41**), and As<sub>4</sub> (**42**)

Cl<sub>2</sub>Nb(ODipp)<sub>3</sub> (278 mg, 0.40 mmol) was combined with solid AsP<sub>3</sub> (67 mg, 0.40 mmol) and then dissolved in 10 mL of THF. After all the AsP<sub>3</sub> was dissolved a 0.5% Na/Hg amalgam was added. The reaction mixture was allowed to stir for 20 min during which time it assumed a dark orange-brown color. The reaction mixture was taken to dryness. To the residue was added 5 mL of Et<sub>2</sub>O. The resulting residue was filtered to remove any insoluble material. The filtrate was taken to dryness under reduced pressure. The resulting residue was dissolved in a stock solution of P<sub>4</sub> (0.158 mmol total as an internal standard) in C<sub>6</sub>D<sub>6</sub> for NMR analysis. <sup>31</sup>P{<sup>1</sup>H} NMR (20 °C, benzene-d<sub>6</sub>, 202.5 MHz):  $\delta = -520$  (P<sub>4</sub>, s, 0.1581 mmol),  $-206$  ([Na][P<sub>3</sub>Nb(ODipp)<sub>3</sub>], s, 0.1935 mmol, 48% yield),  $-167$  ([Na][P<sub>2</sub>AsNb(ODipp)<sub>3</sub>], s, 0.090 mmol, 23% yield),  $-132$  ([Na][PAs<sub>2</sub>Nb(ODipp)<sub>3</sub>], s, 0.0198 mmol, 5% yield). The total yield of **25**, **37**, and **38** is 76% based on Cl<sub>2</sub>Nb(ODipp)<sub>3</sub>, which is consistent with the yields obtained for the synthesis of **25** from P<sub>4</sub>. The NMR tube was returned to the glovebox, and its contents were taken to dryness. The resulting residue was dissolved in 5 mL of THF, and the solution was frozen in the cold well. AsCl<sub>3</sub> (72 mg) was added to this thawing solution as a stock solution in toluene. The resulting mixture was allowed to stir for 20 min after which time it was filtered through a pad of Celite and concentrated to 1 mL. This sample was placed in an NMR tube (wrapped in Al foil) for analysis. <sup>31</sup>P{<sup>1</sup>H} NMR (20 °C, benzene-d<sub>6</sub>, 202.5 MHz):  $\delta = -520$  (P<sub>4</sub>, s),  $-484$  (AsP<sub>3</sub>, s),  $-452$  (As<sub>2</sub>P<sub>2</sub>, s),  $-432$  (AsP<sub>3</sub>, s). A portion of the sample was diluted 100-fold with C<sub>6</sub>H<sub>6</sub> and was analyzed by GC-MS. GC-MS: P<sub>4</sub> [retention time 7.8 min, parent ion 124 m/z with fragments at 93 (P<sub>3</sub>) and 62 (P<sub>2</sub>), total area 50994], AsP<sub>3</sub> [retention time 8.9 min, parent ion 168 m/z with fragments at 137 (AsP<sub>2</sub>), 106 (AsP), 93 (P<sub>3</sub>), 75 (As), and 62 (P<sub>2</sub>), total area 30475, 49% yield from **25**], As<sub>2</sub>P<sub>2</sub> [retention time 9.8 min, parent ion 212 m/z with fragments at 181 (As<sub>2</sub>P), 150 (As<sub>2</sub>), 137 (AsP<sub>2</sub>), 106 (AsP), 75 (As), and 62 (P<sub>2</sub>), total area 11348, 39% yield from **37**], As<sub>3</sub>P [retention time 10.6 min, parent ion 256 m/z with fragments at 225 (As<sub>3</sub>), 181 (As<sub>2</sub>P), 150 (As<sub>2</sub>), 106 (AsP), and 75 (As), total area 3176, 50% yield from **38**], As<sub>4</sub> [retention time 11.2 min, parent ion 300 m/z with fragments at 150 (As<sub>2</sub>) and 75 (As); peaks from neighboring HODipp signal also present, approximate total area 1977, 2% yield from Cl<sub>2</sub>Nb(ODipp)<sub>3</sub>].

### 2.9.16 Reaction of $[\text{Na}(\text{THF})_3][\text{P}_3\text{Nb}(\text{ODipp})_3]$ with $\text{SbCl}_3$

THF (2 mL) was placed in a thick walled glass tube with a 14/20 joint and was degassed by three cycles of the freeze-pump-thaw method.  $\text{SbCl}_3$  (18 mg, 0.79 mmol) and  $[\text{Na}(\text{THF})_3][\text{P}_3\text{Nb}(\text{ODipp})_3]$  (75 mg, 0.79 mmol) were placed in a NMR tube equipped with a 14/20 joint and gas inlet adapter. The tube was then evacuated. The two solids were not allowed to come in contact as it was found that they react upon contact in the solid state. The vessels were removed from the glove box and the THF tube was attached to the vacuum line and the NMR tube was placed in a liquid nitrogen cooled bath after a spinner for the NMR probe was fit on the tube. Approximately 1.5 mL of THF was vacuum transferred to the NMR tube. The NMR tube was flame sealed and brought down to the DCIF. The NMR probe was cooled to  $-50\text{ }^\circ\text{C}$  and the temperature was measured with an NMR thermometer ( $-50.43\text{ }^\circ\text{C}$ ). The NMR tube was then put into the probe, spinning was turned on, and the probe was tuned to phosphorus while the temperature of the tube was allowed to equilibrate (10 min). The initial scan of the tube showed only  $\text{SbP}_3$  present with all of the starting *cyclo*- $\text{P}_3$  complex already consumed (singlet  $-462\text{ ppm}$ , calculated shift  $-462\text{ ppm}$ ). A kinetic run was set up to take scans every 2 min for 3.5 h. Over this time period very little change in signal strength was observed. After this time, the probe was warmed to  $-30\text{ }^\circ\text{C}$  (NMR thermometer at  $-29.87\text{ }^\circ\text{C}$  (taken after experiment)). Upon warming, a significant amount of the  $\text{SbP}_3$  species decomposed to some insoluble material, and over the next 60 minutes at  $-30\text{ }^\circ\text{C}$  the remaining signal decayed into the baseline. This experiment demonstrates that  $\text{SbP}_3$  is obtainable at low temperatures when maintained in the dark. The NMR yield of  $\text{SbP}_3$  was determined to be 11% depending on the run.  $\text{SbBr}_3$  was found to give modest increases in yield to 19% averaged over 3 runs.

### 2.9.17 *In situ* reaction of $\text{SbP}_3$ with $\text{Cp}^*\text{Fe}(\text{dppe})\text{Cl}$ and $\text{NaBPh}_4$

$[\text{Na}(\text{THF})_3][\text{P}_3\text{Nb}(\text{ODipp})_3]$  (918 mg, 0.96 mmol) was dissolved in 50 mL of THF and was frozen in the cold well in a flask wrapped in aluminum foil to exclude light.  $\text{SbCl}_3$  (219 mg, 0.96 mmol) was dissolved in 10 mL of THF and was also frozen. The thawing  $\text{SbCl}_3$  solution was added to the thawing solution of  $[\text{Na}(\text{THF})_3][\text{P}_3\text{Nb}(\text{ODipp})_3]$ . The reaction mixture was allowed to stir for 20 minutes, after which time,  $\text{Cp}^*\text{Fe}(\text{dppe})\text{Cl}$  (500 mg, 0.80 mmol) was added. After an additional 2 minutes,  $\text{NaBPh}_4$  (274 mg, 0.80 mmol) was added to the solution. The reaction mixture was allowed to stir for 45 minutes, after which time, the reaction mixture was filtered through a plug of Celite, and an aliquot was removed for NMR analysis (the only P-containing diamagnetic species present was the desired  $\text{SbP}_3$  complex). The volatile components were then removed from the bulk of the resulting filtrate. The dry residue was extracted with  $\text{CH}_2\text{Cl}_2$  and filtered to remove any salts. The filtrate was again taken to dryness, and to the dry solids were added 45 mL of pentane. The solids were vigorously stirred until a free flowing powder and an orange filtrate were obtained. Filtration of this material resulted in isolation of 1.36 g of chocolate brown, fluffy powder. The orange filtrate was taken to dryness and NMR analysis revealed it to contain only  $\text{Cl}_2\text{Nb}(\text{ODipp})_3(\text{THF})$ . The

brown powder contained the desired  $[(\text{SbP}_3)\text{Fe}(\text{Cp}^*)(\text{dppe})][\text{BPh}_4]$  complex, but paramagnetic Fe-containing material represented the bulk of the sample.  $^{31}\text{P}\{^1\text{H}\}$  NMR (20 °C, THF, 202.5 MHz):  $\delta = -429$  (2P, d,  $^1J_{\text{P/P}} = 247$  Hz),  $-233$  (1P, td,  $^1J_{\text{P/P}} = 245$  Hz,  $^2J_{\text{P/P}} = 34$  Hz),  $-87$  (2P, d,  $^2J_{\text{P/P}} = 34$  Hz).

### 2.9.18 *In situ* reaction of $\text{SbP}_3$ with (OTf)Re(CO)<sub>2</sub>(triphos) and NaBPh<sub>4</sub>

(OTf)Re(CO)<sub>2</sub>(triphos) (86 mg, 0.088 mmol) was dissolved in 3 mL of THF to which was added NaBPh<sub>4</sub> (30 mg, 0.088 mmol). This reaction mixture was allowed to stir for 30 minutes during which time a fine white precipitate formed. The reaction mixture was filtered and was set aside. Separately,  $[\text{Na}(\text{THF})_3][\text{P}_3\text{Nb}(\text{ODipp})_3]$  (42 mg, 0.044 mmol) was dissolved in 1 mL of THF and was frozen in the cold well in a vial that was covered in black electrical tape. SbCl<sub>3</sub> (10 mg, 0.044 mmol) was likewise dissolved in 1 mL of THF and was frozen. Upon thawing the solution of SbCl<sub>3</sub> was added with stirring to the solution of  $[\text{Na}(\text{THF})_3][\text{P}_3\text{Nb}(\text{ODipp})_3]$ . The reaction mixture was allowed to stir for 7 minutes in the dark, after which time the  $[\text{BPh}_4][\text{Re}(\text{CO})_2(\text{triphos})]$  solution was added with stirring. The reaction mixture was allowed to further stir for 30 minutes in the dark and was then taken to dryness under reduced pressure. The resulting residue was dissolved in 1 mL of THF and filtered through a plug of Celite for  $^{31}\text{P}$  NMR analysis. The phosphorus NMR spectrum was monitored for 24 h over which time the monometallic complex was observed to decompose.  $^{31}\text{P}\{^1\text{H}\}$  NMR (20 °C, THF, 202.5 MHz):  $\delta = -422$  (1P, t,  $^1J_{\text{P/P}} = 205$  Hz, bimetallic),  $-297$  (2P, m, bimetallic),  $-10$  (6P, m, triphos, bimetallic) ppm;  $-431$  (2P, t,  $^1J_{\text{P/P}} = 228$  Hz, monometallic),  $-347$  (1P, m, monometallic),  $-13$  (6P, m, triphos, monometallic) ppm.

### 2.9.19 Preparation of $[\text{Na}(\text{THF})_3][\text{As}_3\text{Nb}(\text{ODipp})_3]$

The As<sub>4</sub> generator was set up,<sup>105</sup> using 8 g of metallic arsenic and was run for 2 h at 600 °C. A THF-filled Schlenk flask was kept cold at  $-70$  °C during the entire run by cooling in an isopropanol-liquid nitrogen bath. The flask was wrapped in aluminum foil to keep the light out. No grey arsenic was observed in any of the bleach bubblers, suggesting that all of the sublimed arsenic was being trapped in the reaction flask. After the apparatus cooled back to room temperature, Cl<sub>2</sub>Nb(ODipp)<sub>3</sub> (3 g, 4.32 mmol) and the 0.4% Na/Hg amalgam was added under a flow of argon. The reaction mixture was stirred for 1 h under argon during which time the mixture assumed a dark brown color. After the reaction time had elapsed the supernatant was cannula filtered off of the amalgam into a clean, dry round bottom flask that was under argon. After the transfer was complete the volatile components of the reaction mixture were removed and the vessel was returned to the glove box. Extracting the brown residue with Et<sub>2</sub>O and filtration through a pad of Celite gave a bright orange filtrate. The filtrate was taken to dryness and the residue was dissolved in 3:1 Et<sub>2</sub>O/THF mixture (10 mL). After 16 h, bright red-orange needles had crystallized cleanly from the reaction mixture. The crystals were isolated atop a frit and were dried to constant mass giving 300 mg (0.275 mmol)

of  $[\text{Na}(\text{THF})_3][\text{As}_3\text{Nb}(\text{ODipp})_3]$ , 6% isolated yield based on  $\text{Cl}_2\text{Nb}(\text{ODipp})_3$ .  $^1\text{H}$  NMR (20 °C, benzene- $d_6$ , 500 MHz):  $\delta = 1.339$  (m, 12 H, THF), 1.428 (d, 36 H,  $^1J_{\text{H}/\text{H}} = 7$  Hz), 3.354 (m, 12 H, THF), 4.057 (sep, 6 H,  $^1J_{\text{H}/\text{H}} = 7$  Hz), 7.008 (t, 3 H,  $^1J_{\text{H}/\text{H}} = 8$  Hz), 7.209 (d, 6 H,  $^1J_{\text{H}/\text{H}} = 8$  Hz).  $^{13}\text{C}\{^1\text{H}\}$  NMR (20 °C, benzene- $d_6$ , 125.8 MHz):  $\delta = 24.639$  ( $^i\text{Pr-Me}$ ), 25.630 (THF), 27.282 ( $^i\text{Pr-CH}$ ), 68.087 (THF), 121.778 (Ar), 123.429 (Ar), 138.959 (Ar), 161.922 (Ar). Elem. Anal. Calcd for  $\text{C}_{48}\text{H}_{75}\text{As}_3\text{NaNbO}_6$ : C 52.95, H 6.94; Found: C 53.26, H 6.96.

### 2.9.20 Reaction of $[\text{Na}(\text{THF})_3][\text{As}_3\text{Nb}(\text{ODipp})_3]$ with $\text{PCl}_3$

$[\text{Na}(\text{THF})_3][\text{As}_3\text{Nb}(\text{ODipp})_3]$  (15 mg of bright orange-red crystals) was dissolved in 1 mL of THF and frozen in the cold well.  $\text{PCl}_3$  (1.9 mg, as a stock solution in toluene) was added to the frozen solution. The mixture was allowed to warm to room temperature and was then filtered into an NMR tube through a plug of Celite. The tube was spiked with  $\text{C}_6\text{D}_6$  and was taken for  $^{31}\text{P}$  NMR analysis showing a clean singlet in the spectrum at  $-432$  ppm as the only species (calculated shift for  $\text{As}_3\text{P}$  is  $-424$ ). The conversion to  $\text{As}_3\text{P}$  under these conditions was found to be 63%. The NMR tube was returned to the glovebox and its contents were filtered through alumina into a fresh vial. The solution was diluted with 15 mL of toluene and the vial was wrapped in electrical tape and equipped with a septum for GC-MS analysis. The parent molecular ion for  $\text{As}_3\text{P}$  showed a retention time of 10.63 minutes with mass 256  $m/z$ . The fragments from the parent molecular ion came at 225  $m/z$  ( $\text{As}_3$ ), 181  $m/z$  ( $\text{As}_2\text{P}$ ), 150  $m/z$  ( $\text{As}_2$ ), 106  $m/z$  ( $\text{AsP}$ ), and 75  $m/z$  ( $\text{As}$ ). In order to determine the 20°C stability of  $\text{As}_3\text{P}$  in solution, a spectrum of 512 scans was acquired every 20 minutes for 4 h on a freshly prepared sample. The  $\text{As}_3\text{P}$  signal slowly decayed over the course of 175 minutes with no visible signal after that time. This experiment suggests that  $\text{As}_3\text{P}$  is likely not stable in solution at room temperature. However, since this experiment could not be run on pure material, chemical degradation pathways cannot be ruled out.

### 2.9.21 X-Ray Structure Determinations

Diffraction quality crystals of  $[\text{Na}(\text{THF})_3][\text{P}_3\text{Nb}(\text{ODipp})_3]$  were grown from  $\text{Et}_2\text{O}/n$ -hexane at  $-35$  °C. Crystals of  $[\text{Na}(\text{THF})_6][\text{P}_3\text{Nb}(\text{ODipp})_3]$  were grown from THF at  $-35$  °C over 1 week. Crystals of  $(\text{AsP}_3)\text{Mo}(\text{CO})_3(\text{P}^i\text{Pr}_3)_2$  were grown from toluene at  $-35$  °C for two days. Crystals of  $[(\text{AsP}_3)\text{Fe}(\text{Cp}^*)(\text{dppe})][\text{BPh}_4]$  were grown from  $\text{CH}_2\text{Cl}_2$  over the course of 10 days at  $-35$  °C. Crystals of  $[\text{P}(\text{N}^i\text{Pr}_2)(\text{N}(\text{SiMe}_3)_2)_2](\text{AsP}_3)$  were grown from  $\text{Et}_2\text{O}/\text{hexane}$  at  $-35$  °C over 2 days. Crystals of  $[\text{Na}(\text{THF})_6][\text{As}_3\text{Nb}(\text{ODipp})_3]$  were grown from  $\text{Et}_2\text{O}/\text{THF}$  (3:1) at  $-35$  °C for two days. Crystals of  $\text{As}[\text{GaC}(\text{SiMe}_3)_3]_3\text{P}_3$  were grown from pentane diffusion into a toluene solution at  $-35$  °C. All crystals were mounted in hydrocarbon oil on a nylon loop or a glass fiber. Low-temperature (100 K) data were collected on a Siemens Platform three-circle diffractometer coupled to a Bruker-AXS Smart Apex CCD detector with graphite-monochromated Mo  $\text{K}\alpha$  radiation ( $\lambda = 0.71073$  Å) performing  $\phi$ - and  $\omega$ -scans. A semi-empirical absorption correction was applied

to the diffraction data using SADABS.<sup>113</sup> All structures were solved by direct or Patterson methods using SHELXS<sup>114,115</sup> and refined against  $F^2$  on all data by full-matrix least squares with SHELXL-97.<sup>115,116</sup> All non-hydrogen atoms were refined anisotropically. All hydrogen atoms were included in the model at geometrically calculated positions and refined using a riding model. The isotropic displacement parameters of all hydrogen atoms were fixed to 1.2 times the  $U_{eq}$  value of the atoms they are linked to (1.5 times for methyl groups). In structures where disorders were present, the disorders were refined within SHELXL with the help of rigid bond restraints as well as similarity restraints on the anisotropic displacement parameters for neighboring atoms and on 1,2- and 1,3-distances throughout the disordered components.<sup>117</sup> The relative occupancies of disordered components were refined freely within SHELXL. Further details are provided in Tables 2.19 – 2.22, on Reciprocal Net,<sup>118</sup> and in the form of cif files available from the CCDC.<sup>119</sup>

## 2.9.22 Computational Studies

All calculations were carried out using ADF 2007.01 or ADF 2008.01 from Scientific Computing and Modeling (<http://www.scm.com>) on an eight or 32-processor Quantum Cube workstation from Parallel Quantum Solutions (<http://www.pqschem.com>).<sup>45,46</sup> In all cases, the LDA functional employed was that of Vosko, Wilk, and Nusair (VWN),<sup>120</sup> while the GGA part was handled using the functionals of Baker and Pulay (OLYP).<sup>121</sup> In addition, all calculations were carried out using the zero-order regular approximation (ZORA) for relativistic effects.<sup>122–124</sup> For phosphorus and arsenic, the basis sets were quadruple- $\zeta$  with four polarization functions (QZ4P) as supplied with ADF and frozen-core approximations were not made. In all other cases, the basis sets were triple- $\zeta$  with two polarization functions (TZ2P) as supplied with ADF and again, frozen-core approximations were not made. Chemical shielding tensors were calculated for the  $^{31}\text{P}$  nuclei in the optimized structures by the GIAO method using the ADF package.<sup>125–128</sup> The functionals, basis sets, and relativistic approximations used were the same as those described above. The isotropic value of the absolute chemical shielding was converted to a chemical shift downfield of 85% phosphoric acid using  $\text{PH}_3$  or  $\text{P}_4$  as a computational reference; its computed absolute shielding value was associated with a chemical shift equal to its experimental value in the gas phase.<sup>129,130</sup> Geometries were optimized to default convergence criteria and energies are uncorrected for zero-point energies.

**Table 2.9.** Optimized atomic coordinates of  $\text{AsP}_3$ .

Atom	x	y	z	Atom	x	y	z
As	0.000000	0.000000	0.000000	P	0.000000	0.000000	2.328433
P	1.946660	0.000000	1.277315	P	0.689257	-1.820654	1.277546

**Table 2.10.** Optimized atomic coordinates of  $\text{P}_4$ .

Atom	x	y	z	Atom	x	y	z
P	0.000000	0.000000	0.000000	P	0.000000	0.000000	2.328433
P	1.946660	0.000000	1.277315	P	0.689257	-1.820654	1.277546



**Table 2.11.** Optimized atomic coordinates of As<sub>2</sub>P<sub>2</sub>.

Atom	x	y	z	Atom	x	y	z
As	8.032434	-4.108725	-0.081378	As	6.333900	-5.842816	0.018593
P	8.600965	-6.360917	0.052807	P	7.715693	-5.391198	1.834149

**Table 2.12.** Optimized atomic coordinates of As<sub>3</sub>P.

Atom	x	y	z	Atom	x	y	z
P	7.981905	-4.193700	-0.059303	As	6.297425	-5.799947	-0.021879
As	8.653340	-6.423434	-0.024693	As	7.677581	-5.357089	1.932513

**Table 2.13.** Optimized atomic coordinates of [(AsP<sub>3</sub>)Fe(Cp\*)(dppe)]<sup>+</sup>.

Atom	x	y	z	Atom	x	y	z
H	-3.172660	-3.371932	-3.905621	H	-1.985850	-1.332907	-3.345354
H	1.254163	0.480557	-3.164083	H	-1.315743	0.478781	-3.150351
C	-3.140899	-3.047227	-2.868895	H	4.555116	-2.990006	-2.890524
H	2.567100	-1.593519	-2.795788	C	-2.455865	-1.881601	-2.539918
H	0.576368	-1.021638	-2.500182	H	5.079171	3.609433	-2.054612
H	-4.338909	-4.683668	-2.147515	C	0.667616	0.054920	-2.346189
H	-0.620750	1.772413	-2.230522	C	-0.709652	0.687848	-2.268595
H	3.576958	5.582445	-1.931044	C	-3.792570	-3.781888	-1.885888
C	4.043501	3.486981	-1.752559	C	4.396083	-2.354844	-2.025173
C	3.203432	4.593494	-1.684265	C	3.253410	-1.559290	-1.960889
H	4.251754	1.376891	-1.519467	C	3.569920	2.213857	-1.439028
H	-3.653937	4.642452	-1.008543	C	1.878927	4.418542	-1.291908
H	1.212964	5.274548	-1.231267	H	-1.794513	3.083228	-1.071847
C	-3.842030	3.585450	-0.841551	C	-2.387978	-1.434697	-1.213968
C	2.240891	2.023784	-1.039006	C	-2.781257	2.686151	-0.877925
C	1.410261	3.149279	-0.967712	H	6.220602	-2.947045	-1.049657
H	-5.963597	3.838225	-0.561375	C	5.330798	-2.328347	-0.995980
C	-5.135462	3.136240	-0.596920	P	0.587916	-3.940081	-0.573572
C	3.018514	-0.729673	-0.855959	H	0.390017	3.041766	-0.633100
C	-2.983429	1.312367	-0.675375	P	1.525984	0.339841	-0.723026
C	-3.741601	-3.349200	-0.564393	P	-1.549656	0.134359	-0.713377
C	-5.357133	1.775680	-0.415903	C	-4.296672	0.873648	-0.460243
H	-6.363658	1.404271	-0.247421	H	-4.514876	-0.179137	-0.347085
C	-3.032330	-2.199381	-0.229537	H	-4.254023	-3.910304	0.211247
C	5.120016	-1.491724	0.096669	C	3.976194	-0.707296	0.164832
H	-2.993969	-1.888108	0.806354	P	0.298229	-2.229466	0.760632
H	5.851907	-1.447953	0.898385	P	1.709723	-3.805851	1.336129
H	-0.062721	3.773611	1.389689	H	3.850346	-0.046433	1.010618
Fe	0.025701	-0.017812	0.929687	As	-0.602905	-4.268853	1.409714
H	3.114717	1.686651	2.172016	H	-1.759694	3.271651	1.457068
H	2.117329	3.026108	1.622428	C	-0.787629	3.171169	1.933278
C	-0.362873	1.746838	2.095011	C	2.177835	2.213475	2.343106
H	-3.191696	1.510374	2.071622	H	-3.229169	-0.145761	2.672070
C	0.983713	1.314959	2.325967	H	-0.873109	3.609725	2.937216
C	-1.240096	0.684158	2.513112	H	3.024219	-0.601035	2.928506

**Table 2.13.** Optimized atomic coordinates of [(AsP<sub>3</sub>)Fe(Cp\*)(dppe)]<sup>+</sup>, continued.

C	-2.709577	0.809218	2.748046	C	0.948346	-0.003146	2.865537
H	2.240514	2.661046	3.344437	C	-0.436825	-0.379826	3.000013
H	-1.889910	-1.931612	3.381122	C	2.104078	-0.704016	3.500016
H	-2.862131	1.178243	3.771187	H	1.922105	-1.768504	3.635603
C	-0.957775	-1.537089	3.785431	H	-0.243727	-2.355681	3.856983
H	2.279716	-0.269494	4.492910	H	-1.162381	-1.190704	4.807149

**Table 2.14.** Optimized atomic coordinates of (Ph[Me]N)<sub>3</sub>Ti[P(P<sub>2</sub>)As]Ti(N[Me]Ph)<sub>3</sub>.

Atom	x	y	z	Atom	x	y	z
Ti	-2.306523	-0.007509	0.029322	As	0.225503	0.837180	-0.390807
N	-2.411735	-1.887075	0.449375	N	-2.883503	1.264808	1.343429
P	1.130593	-0.716497	-1.909868	P	1.668413	-0.946331	0.197025
P	3.086888	0.081541	-1.206783	C	-3.742243	1.085000	2.445634
C	-2.274366	2.599204	1.242306	C	-3.272390	-2.396211	1.459155
Ti	4.888593	-1.597763	-1.947815	C	-1.841386	-2.942737	-0.392449
N	6.367101	-0.795093	-1.044828	N	4.691470	-1.529006	-3.861737
N	-3.033851	0.452497	-1.727585	C	-3.668078	1.641842	-2.126398
C	-2.712219	-0.447946	-2.838680	C	-4.985259	0.459389	2.278021
C	-5.850205	0.286514	3.349753	C	-5.506925	0.743902	4.616011
C	-4.439495	-3.102693	1.130246	C	-5.263957	-3.614315	2.123193
C	-4.950249	-3.423051	3.465088	C	-3.397426	2.262223	-3.359057
C	-4.043484	3.434243	-3.730141	C	-4.982533	4.026702	-2.894258
C	-4.279101	1.371984	4.796924	C	-3.406476	1.541713	3.730707
C	-3.799385	-2.722154	3.802388	C	-2.960781	-2.225006	2.811424
C	-5.270397	3.417784	-1.677676	C	-4.632541	2.245099	-1.303404
C	7.564034	-0.219959	-1.513347	C	6.290075	-1.030415	0.403844
C	5.611151	-0.927269	-4.753005	C	3.510098	-2.079796	-4.528311
N	4.731903	-3.460753	-1.339077	C	3.377824	-4.004612	-1.327218
C	5.724950	-4.308132	-0.853988	C	8.821783	-0.685356	-1.094981
C	9.987560	-0.124232	-1.597886	C	9.932209	0.914001	-2.522058
C	5.243471	0.150016	-5.574106	C	6.153320	0.703739	-6.464270
C	7.451743	0.209193	-6.548065	C	5.451029	-5.421746	-0.034388
C	6.470881	-6.246629	0.424917	C	7.796423	-6.003180	0.088298
C	8.083380	-4.916579	-0.733784	C	7.073024	-4.094093	-1.202637
C	7.827267	-0.854615	-5.738887	C	6.913888	-1.427178	-4.862364
C	8.692835	1.395418	-2.925794	C	7.522158	0.845082	-2.421350
H	-1.910855	2.772802	0.226735	H	-3.025110	3.370666	1.456720
H	-1.422249	2.727606	1.922546	H	-1.054390	-2.541074	-1.031791
H	-1.383657	-3.715161	0.241375	H	-2.594903	-3.432675	-1.027841
H	-3.583183	-0.567697	-3.498625	H	-2.444239	-1.435357	-2.466081
H	-1.865242	-0.090948	-3.437912	H	-5.281978	0.110319	1.295636
H	-6.803992	-0.207572	3.187032	H	-6.187959	0.612433	5.452398
H	-4.703796	-3.246493	0.086855	H	-6.162766	-4.159946	1.845338
H	-5.602493	-3.813669	4.241530	H	-2.664661	1.838091	-4.034998
H	-3.801761	3.889874	-4.686800	H	-5.488100	4.941430	-3.189735
H	-3.990413	1.730693	5.781930	H	-2.449006	2.023317	3.898947
H	-3.549301	-2.556833	4.846514	H	-2.052369	-1.695133	3.079013

**Table 2.14.** Optimized atomic coordinates of (Ph[Me]N)<sub>3</sub>Ti[P(P<sub>2</sub>)As]Ti(N[Me]Ph)<sub>3</sub>, continued.

H	-6.015355	3.847794	-1.013223	H	-4.891085	1.777967	-0.363594
H	5.268355	-1.303598	0.684360	H	6.945239	-1.844268	0.737032
H	6.543991	-0.108662	0.943543	H	2.834481	-1.290605	-4.884549
H	3.808895	-2.699467	-5.385875	H	2.938301	-2.706547	-3.842667
H	3.000257	-4.158109	-0.307479	H	3.327976	-4.957981	-1.874087
H	2.679708	-3.306741	-1.794127	H	8.887675	-1.498152	-0.381211
H	10.949143	-0.506025	-1.263071	H	10.847362	1.348626	-2.915103
H	4.239120	0.556864	-5.508334	H	5.845157	1.532298	-7.097685
H	8.162266	0.647508	-7.243793	H	4.433828	-5.647568	0.259470
H	6.217948	-7.091961	1.060148	H	8.589298	-6.651994	0.448261
H	9.109446	-4.715069	-1.031440	H	7.326827	-3.274234	-1.860795
H	8.837270	-1.251239	-5.790226	H	7.202387	-2.284187	-4.264197
H	8.630834	2.213878	-3.637006	H	6.561239	1.247576	-2.723107

**Table 2.15.** Optimized atomic coordinates of AsP<sub>3</sub>(GaCH<sub>3</sub>)<sub>4</sub>.

Atom	x	y	z	Atom	x	y	z
P	-2.014886	-0.114238	-0.085671	P	-1.195178	-2.175505	-0.524859
P	-0.741423	-1.978968	-2.748617	As	2.186234	0.109668	-0.554501
Ga	0.010109	1.146071	-0.061242	Ga	1.114366	-2.025827	0.039791
Ga	1.135880	-0.499890	-2.702248	Ga	-2.182520	-0.137029	-2.427200
C	2.001546	0.126791	-4.386426	C	0.013323	3.031902	0.596834
C	-3.437674	0.698677	-3.718776	C	2.106314	-3.634104	0.667084
H	3.047495	-0.200477	-4.409454	H	1.488932	-0.250028	-5.277374
H	1.998574	1.223539	-4.407661	H	0.434891	3.689571	-0.172340
H	-0.991019	3.380478	0.856981	H	0.656607	3.104981	1.481438
H	-2.896681	1.231393	-4.510242	H	-4.024516	-0.098911	-4.190464
H	-4.120613	1.393745	-3.218837	H	1.839586	-3.837906	1.711563
H	1.805100	-4.503635	0.070642	H	3.189799	-3.501694	0.597302

**Table 2.16.** Optimized atomic coordinates of [(SbP<sub>3</sub>)Fe(Cp\*)(dppe)]<sup>+</sup>.

Atom	x	y	z	Atom	x	y	z
H	-3.039598	-3.483257	-3.818061	H	-1.908484	-1.400329	-3.301597
H	1.245297	0.466872	-3.174681	H	-1.331105	0.467176	-3.157036
C	-3.060013	-3.110316	-2.799652	H	4.494357	-3.131017	-2.748468
H	2.574544	-1.633412	-2.762124	C	-2.405143	-1.920272	-2.494010
H	0.566107	-1.029102	-2.499610	H	5.084343	3.592229	-2.078350
H	-4.265968	-4.729683	-2.055856	C	0.658645	0.048706	-2.353306
H	-0.623358	1.771361	-2.260876	C	-0.719201	0.687128	-2.281485
H	3.593059	5.573559	-1.944236	C	-3.744148	-3.809530	-1.812535
C	4.050345	3.477036	-1.773133	C	4.341246	-2.459005	-1.910122
C	3.216871	4.584798	-1.702561	C	3.236692	-1.608349	-1.907074
H	4.250509	1.361833	-1.539722	C	3.570398	2.204642	-1.459596
H	-3.650452	4.670346	-1.062698	C	1.888447	4.414956	-1.311594
H	1.225424	5.278756	-1.248659	H	-1.805861	3.096523	-1.177463
C	-3.833377	3.621078	-0.847498	C	-2.393349	-1.416252	-1.185427
C	2.240086	2.021788	-1.058049	C	-2.781684	2.712581	-0.914043

**Table 2.16.** Optimized atomic coordinates of  $[(\text{SbP}_3)\text{Fe}(\text{Cp}^*)(\text{dppe})]^+$ , continued.

C	1.412989	3.149532	-0.989097	H	6.088421	-3.128510	-0.845513
H	-5.932788	3.899151	-0.451142	C	5.237556	-2.454063	-0.848200
C	-5.114188	3.190187	-0.515061	P	0.739399	-3.796031	-0.669776
C	3.001709	-0.741983	-0.830148	H	0.392730	3.040673	-0.662931
C	-2.981258	1.346634	-0.659814	P	1.518964	0.345014	-0.731805
C	-3.753218	-3.318331	-0.510345	P	-1.553036	0.161782	-0.713616
C	-5.333107	1.836799	-0.281906	C	-4.283547	0.925526	-0.362534
H	-6.330456	1.480132	-0.039797	H	-4.505271	-0.121038	-0.206028
C	-3.065189	-2.150542	-0.196684	H	-4.294635	-3.849107	0.265785
C	5.039203	-1.570526	0.208922	C	3.934619	-0.727069	0.215876
H	-3.061152	-1.805430	0.828129	P	0.262407	-2.202082	0.758694
H	5.744643	-1.539769	1.033936	P	1.808576	-3.681048	1.277169
H	-0.209585	3.765629	1.182612	H	3.813960	-0.036892	1.037020
Fe	0.005262	0.017156	0.918419	Sb	-0.626309	-4.485452	1.347157
H	3.052881	1.818918	1.889891	H	-1.865890	3.291261	1.583681
H	1.975716	3.200528	1.744122	C	-0.826640	3.211511	1.893867
C	-0.392825	1.790130	2.075690	C	2.151067	2.275251	2.300483
H	-3.200900	1.615233	2.178247	H	-3.255035	-0.111767	2.539121
C	0.960553	1.373740	2.300374	H	-0.726777	3.722095	2.865055
C	-1.256584	0.723139	2.501035	H	2.987578	-0.654006	2.863641
C	-2.725625	0.820582	2.753569	C	0.938062	0.060148	2.855855
H	2.367374	2.548290	3.342485	C	-0.438124	-0.329795	2.995914
H	-1.833683	-1.950253	3.312263	C	2.103917	-0.620138	3.504597
H	-2.878332	1.042098	3.819823	H	1.874140	-1.639764	3.796851
C	-0.959831	-1.483961	3.784277	H	-0.212771	-2.255393	3.949578
H	2.374247	-0.065708	4.413588	H	-1.279610	-1.110964	4.767165

### Computational Details for the GIMIC Calculations

The DFT calculations were carried out using the TURBOMOLE program package<sup>131</sup> version 5.10. The geometries of  $\text{P}_4$  and  $\text{AsP}_3$  were optimized using the RI-DFT program deck which utilizes the “RI two electron integral evaluation routine”. All-electron def2-SV(P) basis sets for both P and As were employed. The electron densities were calculated in terms of gauge independent atomic orbitals (GIAO) using TURBOMOLE’s mpshift routine. Non-standard computation criteria used were \$denconv 1.0D-7 and \$scfconv 6, and an integration grid of m4 quality. The GIMIC input files were generated using TURBOMOLE’s (hidden) \$gimic flag. GIMIC version 2.1<sup>50</sup> was used for the calculation of the current density vectors and their numerical integration.

The closed shell coupled-clusters calculation was performed with MOLPRO version 2008.114 at the CCSD(T) level of theory using the explicitly correlated F12b method<sup>40</sup> together with the quadruple- $\zeta$  type aug-cc-pCVQZ basis set<sup>132</sup> suitable for including core electron correlation. All electrons were taken into the correlation space. The employed auxiliary basis set for the F12b method was of aug-cc-pwCVQZ/mp2fit18 type. The geometry was optimized with MOLPRO’s numerical gradient method.

**Table 2.17.** Refinement Details for the Gas-Phase Electron Diffraction Structure Determination of P<sub>4</sub>.

Dataset	1	2
R[G] (%)	5.60	5.96
R[D] (%)	3.98	4.51
Scale Factor	0.831(5)	0.807(6)
Correlation Parameter	0.49	0.49
del -s (nm <sup>-1</sup> )	1.00	2.00
s (min) (nm <sup>-1</sup> )	23.00	60.00
sw (1) (nm <sup>-1</sup> )	43.00	80.00
sw (2) (nm <sup>-1</sup> )	133.00	266.00
s (max) (nm <sup>-1</sup> )	155.00	310.00
Camera Distance (mm)	500.00	250.00
Electron Wavelength (pm)	4.8100	4.8300

<sup>a</sup> r-factors: R[G] 5.84%, R[D] 4.15%.

### 2.9.23 Gas-Phase Electron Diffraction; University of Bielefeld

Electron scattering intensities for P<sub>4</sub> and AsP<sub>3</sub> were recorded at 100 °C and 110 °C sample temperature and about 110 and 115 °C nozzle temperature using a newly constructed high temperature nozzle and reusable Fuji imaging plates on a Balzers KD-G2 Gas-Eldigraph in Bielefeld<sup>133</sup> (formerly operated in Tübingen by H. Oberhammer), equipped with a new electron source (STAIB Instruments), operating at ca. 60 kV and with a beam current of ca. 200 nA. During data acquisition the background pressure rose from  $1.3 \times 10^{-6}$  to  $2.5 \times 10^{-5}$  mbar and the optimal exposure time was 15-20 s. Exposed imaging plates were scanned using a commercially available Fuji FLA 3000 scanner, yielding digital 16-bit grey-scale image data. The image data were reduced to total intensities using T. G. Strand's program PIMAG<sup>134</sup> (version 040827) in connection with a sector curve, which is based on experimental xenon diffraction data and tabulated scattering factors of xenon. Further data reduction (yielding molecular-intensity curves), the molecular structure refinement, and the electron wavelength determination (from benzene data) were performed using version 2.4 of the ed@ed program.<sup>135</sup> The scattering factors employed were those of Ross et al.<sup>136</sup> Further details about the Bielefeld GED apparatus and methods were published previously.<sup>133</sup> Data analysis parameters for each compound and each data set including R-factors (R<sub>d</sub> and R<sub>g</sub>), scale factors, correlation parameter values, data ranges, weighting points, nozzle-to-plate distances and electron wavelengths are given below in Tables 2.17 and 2.18.

**Table 2.18.** Refinement Details for the Gas-Phase Electron Diffraction Structure Determination of AsP<sub>3</sub>.

Dataset	1	2
R[G] (%)	3.14	10.20
R[D] (%)	2.21	7.28
Scale Factor	0.867(6)	0.760(9)
Correlation Parameter	0.4808	0.4808
del -s (nm <sup>-1</sup> )	2.00	2.00
s (min) (nm <sup>-1</sup> )	18.00	56.00
sw (1) (nm <sup>-1</sup> )	38.00	76.00
sw (2) (nm <sup>-1</sup> )	138.00	218.00
s (max) (nm <sup>-1</sup> )	160.00	254.00
Camera Distance (mm)	501.20	250.00
Electron Wavelength (pm)	4.8100	4.8100

<sup>a</sup> r-factors: R[G] 6.50%, R[D] 4.66%.

### 2.9.24 Photoelectron Spectroscopy; University of Arizona

Gas-phase photoelectron spectra (He I and He II) were recorded on an instrument built around a 36 cm radius, 8 cm gap hemispherical analyzer<sup>137</sup> (McPherson) using a custom-designed photon source and collection methods.<sup>138,139</sup> Instrument control and electron counting were interfaced to a National Instruments USB-6251 multifunction DAQ board and custom software. Samples sublimed cleanly at room temperature from a Young's tube with no evidence of decomposition. The argon <sup>2</sup>P<sub>3/2</sub> ionization at 15.759 eV was used as an internal calibration lock of the absolute ionization energy, and its difference with the CH<sub>3</sub>I <sup>2</sup>E<sub>1/2</sub> ionization at 9.538 eV provided an external calibration of the energy scale. The instrument resolution (measured as the full width at half maximum (FWHM) of the argon <sup>2</sup>P<sub>3/2</sub> ionization) was 0.020-0.028 eV during data collection. The intensity of the ionizations was corrected for the He Iβ line (1.866 eV higher in energy and 3% the intensity of the He Iα line) and for an experimentally determined analyzer sensitivity function versus electron kinetic energy.

### 2.9.25 Solid-State NMR Spectroscopy; Queen's University

Solid-state NMR experiments were performed on a Bruker Avance-600 spectrometer (14.09 T) operating at 102.76 and 242.95 MHz for <sup>75</sup>As and <sup>31</sup>P nuclei, respectively. Approximately 10 mg of AsP<sub>3</sub> powder samples were sealed in a glass tube (4 mm o.d.). All <sup>31</sup>P and <sup>75</sup>As chemical shifts were referenced to 85% H<sub>3</sub>PO<sub>4</sub>(aq) and 0.5 M NaAsF<sub>6</sub> (in CH<sub>3</sub>CN), respectively. The spin-lattice relaxation time (*T*<sub>1</sub>) measurements for <sup>31</sup>P were carried out using the inversion recovery method with a recycle delay of 30 s. For <sup>75</sup>As, *T*<sub>1</sub> was determined from the full width at half height (FWHH,

$\Delta_{1/2}$ ), using  $T_1 = T_2 = 1/(\pi\Delta_{1/2})$ . This assumption was verified by measuring  $T_1$  directly at several temperatures using the saturation recovery method.

## 2.10 REFERENCES

- [1] Emsley, J. *The 13th element : the sordid tale of murder, fire and phosphorus*; John Wiley & Sons, Inc.: New York, 2000.
- [2] Greenwood, N. N.; Earnshaw, A. *Chemistry of the Elements*, 2nd ed.; Butterworth-Heinemann: Oxford, 1997.
- [3] Ozin, G. A. *J. Chem. Soc. A* **1970**, 2307–2310.
- [4] Piro, N. A.; Cummins, C. C. *J. Am. Chem. Soc.* **2008**, *130*, 9524–9535.
- [5] Piro, N. A.; Cummins, C. C. *Angew. Chem., Int. Ed.* **2008**, *48*, 934–938.
- [6] Ehses, M.; Romerosa, A.; Peruzzini, M. *Metal-mediated degradation and reaggregation of white phosphorus*; Topics In Current Chemistry, Vol. 220; Springer: Berlin, 2002; pp 107–140.
- [7] Di Vaira, M.; Ghilardi, C. A.; Midollini, S.; Sacconi, L. *J. Am. Chem. Soc.* **1978**, *100*, 2550–2551.
- [8] Vaira, M. D.; Stoppioni, P.; Peruzzini, M. *Polyhedron* **1987**, *6*, 351 – 382.
- [9] Di Vaira, M.; Sacconi, L. *Angew. Chem., Int. Ed. Engl.* **1982**, *21*, 330–342.
- [10] Scherer, O. J. *Acc. Chem. Res.* **1999**, *32*, 751–762.
- [11] Scherer, O. J.; Sitzmann, H.; Wolmershäuser, G. *J. Organomet. Chem.* **1984**, *268*, C9–C12.
- [12] Goh, L. Y.; Chu, C. K.; Wong, R. C. S.; Hambley, T. W. *J. Chem. Soc., Dalton Trans.* **1989**, 1951–1956.
- [13] Chisholm, M. H.; Huffman, J. C.; Pasterczyk, J. W. *Inorg. Chim. Acta.* **1987**, *133*, 17–18.
- [14] Stephens, F. H.; Johnson, M. J. A.; Cummins, C. C.; Kryatova, O. P.; Kryatov, S. V.; Rybak-Akimova, E. V.; McDonough, J. E.; Hoff, C. D. *J. Am. Chem. Soc.* **2005**, *127*, 15191–15200.
- [15] Verkade, J. G.; Quin, L. D. *Phosphorus-31 NMR Spectroscopy in Spectrochemical Analysis*; Methods in Spectrochemical Analysis, Vol. 8; VCH Publishers, Inc.: Deerfield Beach, 1987.
- [16] Scherer, O.; Werner, B.; Heckmann, G.; Wolmershäuser, G. *Angew. Chem., Int. Ed.* **1991**, *30*, 553–555.
- [17] Capozzi, G.; Chiti, L.; Di Vaira, M.; Peruzzini, M.; Stoppioni, P. *J. Chem. Soc., Chem. Commun.* **1986**, 1799–1800.
- [18] Clark, J. R.; Pulvirenti, A. L.; Fanwick, P. E.; Sigalas, M.; Eisenstein, O.; Rothwell, I. P. *Inorg. Chem.* **1997**, *36*, 3623–3631.
- [19] Yu, J. S.; Fanwick, P. E.; Rothwell, I. P. *J. Am. Chem. Soc.* **1990**, *112*, 8171–8172.
- [20] Mariam Celine Diawara was a visiting graduate student from France that helped greatly in the early stages of the development of this procedure. She was the first to observe the *cyclo*-P<sub>3</sub> anion complex in solution following in situ reduction with Na/Hg amalgam. Her work contributed greatly to the development of this optimized protocol.
- [21] Figueroa, J. S.; Cummins, C. C. *Angew. Chem., Int. Ed.* **2005**, *44*, 4592–4596.
- [22] Figueroa, J. S.; Cummins, C. C. *J. Am. Chem. Soc.* **2003**, *125*, 4020–4021.
- [23] Schmidt, M.; Block, B.; Block, H. D.; Kopf, H.; Wilhelm, E. *Angew. Chem. Int. Ed.* **1968**, *7*, 632–633.
- [24] Steudel, R.; Papavassiliou, M.; Strauss, E.; Laitinen, R. *Angew. Chem. Int. Ed.* **1986**, *25*, 99–101.
- [25] Steudel, R.; Jensen, D.; Baumgart, F. *Polyhedron* **1990**, *9*, 1199–1208.
- [26] This value was obtained using a calibrated melting point apparatus and was confirmed using differential scanning calorimetry (DSC).
- [27] Piro, N.; Cummins, C. *Angew. Chem., Int. Ed.* **2009**, *48*, 934–938.
- [28] Piro, N. A.; Ph.D. thesis; Massachusetts Institute of Technology; 2009.

**Table 2.19.** Crystallographic data for [Na][P<sub>3</sub>Nb(ODipp)<sub>3</sub>] and [Na][P<sub>3</sub>Nb(ODipp)<sub>3</sub>].

	[Na(THF)(Et <sub>2</sub> O) <sub>2</sub> ][P <sub>3</sub> Nb(ODipp) <sub>3</sub> ]	[Na(THF) <sub>6</sub> ][P <sub>3</sub> Nb(ODipp) <sub>3</sub> ]
Empirical formula	C <sub>48</sub> H <sub>78.50</sub> NaNbO <sub>6</sub> P <sub>3</sub>	C <sub>68</sub> H <sub>115</sub> NaNO <sub>11</sub> P <sub>3</sub>
Formula weight (g mol <sup>-1</sup> )	960.42	1317.41
Temperature (K)	100(2)	100(2)
Wavelength (Å)	0.71073	1.54178
Crystal system	Monoclinic	Monoclinic
Space group	<i>P</i> <sub>n</sub>	<i>C</i> <sub>c</sub>
Unit cell dimensions (Å, °)	<i>a</i> = 13.3389(13), α = 90 <i>b</i> = 27.098(3), β = 101.835(2) <i>c</i> = 15.0367(15), γ = 90	<i>a</i> = 21.792(3), α = 90 <i>b</i> = 15.3669(18), β = 109.634(2) <i>c</i> = 22.695(3), γ = 90
Volume (Å <sup>3</sup> )	5319.7(9)	7158.2(15)
<i>Z</i>	4	4
Density (calculated) (Mg m <sup>-3</sup> )	1.199	1.222
Absorption coefficient (mm <sup>-1</sup> )	0.366	0.295
<i>F</i> (000)	2046	2832
Crystal size (mm <sup>3</sup> )	0.50 × 0.15 × 0.15	0.50 × 0.40 × 0.12
Theta range for collection (°)	1.50 to 25.35	1.66 to 27.10
Index ranges	-16 ≤ <i>h</i> ≤ 16, -32 ≤ <i>k</i> ≤ 32, -18 ≤ <i>l</i> ≤ 18	-27 ≤ <i>h</i> ≤ 27, -19 ≤ <i>k</i> ≤ 19, -29 ≤ <i>l</i> ≤ 29
Reflections collected	85190	67184
Independent reflections	19440 [R(int) = 0.0713]	15693 [R(int) = 0.0408]
Completeness to θ <sub>max</sub> (%)	99.9	100.0
Absorption correction	Semi-empirical from equivalents	Semi-empirical from equivalents
Max. and min. transmission	0.9471 and 0.8380	0.9654 and 0.8663
Refinement method	Full-matrix least-squares on <i>F</i> <sup>2</sup>	Full-matrix least-squares on <i>F</i> <sup>2</sup>
Data / restraints / parameters	19440 / 1488 / 1086	15693 / 48 / 770
Goodness-of-fit <sup>a</sup>	1.044	1.024
Final <i>R</i> indices [ <i>I</i> > 2σ( <i>I</i> ) <sup>b</sup> [ <i>I</i> > 2σ( <i>I</i> )]	<i>R</i> <sub>1</sub> = 0.0602, <i>wR</i> <sub>2</sub> = 0.1300	<i>R</i> <sub>1</sub> = 0.0378, <i>wR</i> <sub>2</sub> = 0.0917
<i>R</i> indices (all data) <sup>b</sup>	<i>R</i> <sub>1</sub> = 0.0882, <i>wR</i> <sub>2</sub> = 0.1470	<i>R</i> <sub>1</sub> = 0.0429, <i>wR</i> <sub>2</sub> = 0.0961
Largest diff. peak and hole (e Å <sup>-3</sup> )	1.087 and -1.158	0.910 and -0.443

$$^a \text{Goof} = \left[ \frac{\sum [w(F_o^2 - F_c^2)]}{(n-p)} \right]^{\frac{1}{2}}$$

$$^b R_1 = \frac{\sum ||F_o| - |F_c||}{\sum |F_o|}; wR_2 = \left[ \frac{\sum [w(F_o^2 - F_c^2)^2]}{\sum [w(F_o^2)]} \right]^{\frac{1}{2}}; w = \frac{1}{\sigma^2(F_o^2) + (aP)^2 + bP}; P = \frac{2F_c^2 + \max(F_o^2, 0)}{3}$$



**Table 2.20.** Crystallographic data for (AsP<sub>3</sub>)Mo(CO)<sub>3</sub>(P<sup>i</sup>Pr<sub>3</sub>)<sub>2</sub> and [(AsP<sub>3</sub>)Fe(Cp\*)(dppe)][BPh<sub>4</sub>].

	(AsP <sub>3</sub> )Mo(CO) <sub>3</sub> (P <sup>i</sup> Pr <sub>3</sub> ) <sub>2</sub>	[(AsP <sub>3</sub> )Fe(Cp*)(dppe)][BPh <sub>4</sub> ]
Empirical formula	C <sub>28</sub> H <sub>66</sub> AsMoO <sub>3</sub> P <sub>5</sub>	C <sub>60</sub> H <sub>59</sub> AsBCl <sub>0.75</sub> FeP <sub>5</sub>
Formula weight (g mol <sup>-1</sup> )	776.52	1103.09
Temperature (K)	100(2)	100(2)
Wavelength (Å)	0.71073	1.54178
Crystal system	Triclinic	Triclinic
Space group	<i>P</i> $\bar{1}$	<i>P</i> $\bar{1}$
Unit cell dimensions (Å, °)	<i>a</i> = <i>a</i> = 8.6993(13), $\alpha$ = 82.121(3) <i>b</i> = 8.9742(13), $\beta$ = 89.990(3) <i>c</i> = 21.272(3), $\gamma$ = 72.935(3)	<i>a</i> = 22.7716(5), $\alpha$ = 101.5880(10) <i>b</i> = 22.7817(4), $\beta$ = 101.5520(10) <i>c</i> = 24.3610(8), $\gamma$ = 113.0980(10)
Volume (Å <sup>3</sup> )	1571.2(4)	10828.0(5)
<i>Z</i>	2	8
Density (calculated) (Mg m <sup>-3</sup> )	1.641	1.353
Absorption coefficient (mm <sup>-1</sup> )	1.748	4.939
<i>F</i> (000)	816	4566
Crystal size (mm <sup>3</sup> )	0.20 × 0.10 × 0.05	0.15 × 0.15 × 0.05
Theta range for collection (°)	0.97 to 27.88	1.95 to 68.96
Index ranges	-11 ≤ <i>h</i> ≤ 11, -11 ≤ <i>k</i> ≤ 11, -27 ≤ <i>l</i> ≤ 26	-27 ≤ <i>h</i> ≤ 26, -27 ≤ <i>k</i> ≤ 27, -26 ≤ <i>l</i> ≤ 28
Reflections collected	27751	162122
Independent reflections	7485 [R(int) = 0.0835]	38291 [R(int) = 0.0681]
Completeness to $\theta_{\max}$ (%)	99.8	95.1
Absorption correction	Semi-empirical from equivalents	Semi-empirical from equivalents
Max. and min. transmission	0.9177 and 0.7213	0.7903 and 0.5246
Refinement method	Full-matrix least-squares on <i>F</i> <sup>2</sup>	Full-matrix least-squares on <i>F</i> <sup>2</sup>
Data / restraints / parameters	7485 / 14 / 358	38291 / 2508 / 2570
Goodness-of-fit <sup>a</sup>	1.008	1.052
Final <i>R</i> indices [ <i>I</i> > 2σ( <i>I</i> ) <sup>b</sup> [ <i>I</i> > 2σ( <i>I</i> )]	<i>R</i> <sub>1</sub> = 0.0464, <i>wR</i> <sub>2</sub> = 0.0874	<i>R</i> <sub>1</sub> = 0.0668, <i>wR</i> <sub>2</sub> = 0.1771
<i>R</i> indices (all data) <sup>b</sup>	<i>R</i> <sub>1</sub> = 0.0856, <i>wR</i> <sub>2</sub> = 0.1002	<i>R</i> <sub>1</sub> = 0.0806, <i>wR</i> <sub>2</sub> = 0.1871
Largest diff. peak and hole (e Å <sup>-3</sup> )	0.748 and -0.632	2.216 and -1.699

<sup>a</sup>

$$\text{Goof} = \left[ \frac{\sum [w(F_o^2 - F_c^2)]^2}{(n-p)} \right]^{\frac{1}{2}}$$

<sup>b</sup>

$$R_1 = \frac{\sum ||F_o| - |F_c||}{\sum |F_o|}; wR_2 = \left[ \frac{\sum [w(F_o^2 - F_c^2)]^2}{\sum [w(F_o^2)]^2} \right]^{\frac{1}{2}}; w = \frac{1}{\sigma^2(F_o^2) + (aP)^2 + bP}; P = \frac{2F_c^2 + \max(F_o^2, 0)}{3}$$

**Table 2.21.** Crystallographic data for  $[P(N^iPr_2)(N(SiMe_3)_2)]_2(AsP_3)$  and  $[Na][As_3Nb(ODipp)_3]$ .

	$[P(N^iPr_2)(N(SiMe_3)_2)]_2(AsP_3)$	$[Na(THF)_6][As_3Nb(ODipp)_3]$
Empirical formula	$C_{24}H_{64}AsN_4P_5Si_4$	$C_{68}H_{115}As_3NaNbO_{11}$
Formula weight (g mol <sup>-1</sup> )	750.92	1449.26
Temperature (K)	100(2)	100(2)
Wavelength (Å)	0.71073	1.54178
Crystal system	Monoclinic	Monoclinic
Space group	$P_c$	$C_c$
Unit cell dimensions (Å, °)	$a = 14.7891(15)$ , $\alpha = 90$ $b = 10.9697(11)$ , $\beta = 111.807(2)$ $c = 13.8057(15)$ , $\gamma = 90$	$a = 21.9189(15)$ , $\alpha = 90$ $b = 15.4751(10)$ , $\beta = 109.4900(10)$ $c = 22.7586(15)$ , $\gamma = 90$
Volume (Å <sup>3</sup> )	2079.5(4)	7277.3(8)
Z	2	4
Density (calculated) (Mg m <sup>-3</sup> )	1.199	1.323
Absorption coefficient (mm <sup>-1</sup> )	1.145	1.578
$F(000)$	800	3048
Crystal size (mm <sup>3</sup> )	$0.10 \times 0.10 \times 0.02$	$0.20 \times 0.20 \times 0.10$
Theta range for collection (°)	1.48 to 25.35	1.64 to 28.14
Index ranges	$-17 \leq h \leq 17$ , $-13 \leq k \leq 13$ , $-16 \leq l \leq 16$	$-28 \leq h \leq 28$ , $-20 \leq k \leq 20$ , $-30 \leq l \leq 30$
Reflections collected	33538	72102
Independent reflections	7555 [R(int) = 0.0740]	17595 [R(int) = 0.0458]
Completeness to $\theta_{max}$ (%)	100.0	99.7
Absorption correction	Semi-empirical from equivalents	Semi-empirical from equivalents
Max. and min. transmission	0.9775 and 0.8941	0.8581 and 0.7431
Refinement method	Full-matrix least-squares on $F^2$	Full-matrix least-squares on $F^2$
Data / restraints / parameters	7555 / 334 / 379	17595 / 765 / 786
Goodness-of-fit <sup>a</sup>	1.032	1.038
Final R indices [ $I > 2\sigma(I)$ ] <sup>b</sup> [ $I > 2\sigma(I)$ ]	$R_1 = 0.0513$ , $wR_2 = 0.1123$	$R_1 = 0.0438$ , $wR_2 = 0.1075$
R indices (all data) <sup>b</sup>	$R_1 = 0.0741$ , $wR_2 = 0.1258$	$R_1 = 0.0563$ , $wR_2 = 0.1145$
Largest diff. peak and hole (e Å <sup>-3</sup> )	0.775 and -0.479	1.875 and -0.568

<sup>a</sup>

$$\text{Goof} = \left[ \frac{\sum [w(F_o^2 - F_c^2)]^2}{(n-p)} \right]^{\frac{1}{2}}$$

<sup>b</sup>

$$R_1 = \frac{\sum ||F_o| - |F_c||}{\sum |F_o|}; wR_2 = \left[ \frac{\sum [w(F_o^2 - F_c^2)]^2}{\sum [w(F_o^2)]^2} \right]^{\frac{1}{2}}; w = \frac{1}{\sigma^2(F_o^2) + (aP)^2 + bP}; P = \frac{2F_c^2 + \max(F_o^2, 0)}{3}$$

**Table 2.22.** Crystallographic data for As[GaC(SiMe<sub>3</sub>)<sub>3</sub>]<sub>3</sub>P<sub>3</sub>.

As[GaC(SiMe <sub>3</sub> ) <sub>3</sub> ] <sub>3</sub> P <sub>3</sub>	
Empirical formula	C <sub>23.33</sub> H <sub>62</sub> As <sub>0.67</sub> Ga <sub>2</sub> P <sub>2</sub> Si <sub>6</sub>
Formula weight (g mol <sup>-1</sup> )	762.60
Temperature (K)	100(2)
Wavelength (Å)	0.71073
Crystal system	Hexagonal
Space group	<i>P</i> 6(3)
Unit cell dimensions (Å, °)	<i>a</i> = 19.361(2), α = 90 <i>b</i> = 19.361(2), β = 90 <i>c</i> = 9.0004(9), γ = 120
Volume (Å <sup>3</sup> )	2921.7(5)
<i>Z</i>	3
Density (calculated) (Mg m <sup>-3</sup> )	1.300
Absorption coefficient (mm <sup>-1</sup> )	2.225
<i>F</i> (000)	1200
Crystal size (mm <sup>3</sup> )	0.35 × 0.05 × 0.05
Theta range for collection (°)	1.21 to 25.42
Index ranges	-23 ≤ <i>h</i> ≤ 23, -21 ≤ <i>k</i> ≤ 23, -10 ≤ <i>l</i> ≤ 10
Reflections collected	40161
Independent reflections	3580 [R(int) = 0.1230]
Completeness to θ <sub>max</sub> (%)	99.9
Absorption correction	Semi-empirical from equivalents
Max. and min. transmission	0.8969 and 0.5098
Refinement method	Full-matrix least-squares on <i>F</i> <sup>2</sup>
Data / restraints / parameters	3580 / 168 / 232
Goodness-of-fit <sup>a</sup>	1.059
Final <i>R</i> indices [ <i>I</i> > 2σ( <i>I</i> ) <sup>b</sup> [ <i>I</i> > 2σ( <i>I</i> )]	<i>R</i> <sub>1</sub> = 0.0447, <i>wR</i> <sub>2</sub> = 0.0957
<i>R</i> indices (all data) <sup>b</sup>	<i>R</i> <sub>1</sub> = 0.0611, <i>wR</i> <sub>2</sub> = 0.1036
Absolute Structure Parameter	0.471(17)
Largest diff. peak and hole (e Å <sup>-3</sup> )	0.529 and -0.885

<sup>a</sup> 
$$\text{Goof} = \left[ \frac{\sum [w(F_o^2 - F_c^2)^2]}{(n-p)} \right]^{\frac{1}{2}}$$

<sup>b</sup> 
$$R_1 = \frac{\sum ||F_o| - |F_c||}{\sum |F_o|}; wR_2 = \left[ \frac{\sum [w(F_o^2 - F_c^2)^2]}{\sum [w(F_o^2)^2]} \right]^{\frac{1}{2}}; w = \frac{1}{\sigma^2(F_o^2) + (aP)^2 + bP}; P = \frac{2F_c^2 + \max(F_o^2, 0)}{3}$$

- [29] Quignard, F.; Leconte, M.; Basset, J. M.; Hsu, L. Y.; Alexander, J. J.; Shore, S. G. *Inorg. Chem.* **1987**, *26*, 4272–4277.
- [30] Piro, N. A.; Cummins, C. C. *Angew. Chem. Int. Ed.* **2009**, *48*, 934–938.
- [31] Pyykkö, P.; Atsumi, M. *Chem. Eur. J.* **2009**, *15*, 186–197.
- [32] Boudon, V.; Mkadmi, E. B.; Burger, H.; Pierre, G. *Chem. Phys. Lett.* **1999**, *305*, 21–27.
- [33] Maxwell, L. R.; Hendricks, S. B.; Mosley, V. M. *J. Chem. Phys.* **1935**, *3*, 699–709.
- [34] Tremmel, J.; Hargittai, I. *Stereochemical Applications of Gas-Phase Electron Diffraction*; Hargittai, I.; Hargittai, M., Eds.; VCH Publishers Inc., 1988; Chapter Part A: The Electron Diffraction Technique, p 198.
- [35] Berger, R. J. F.; Mitzel, N. W. *J. Mol. Struct.* **2010**, *Submitted*.
- [36] Thomasand, C. D.; Gingrich, N. S. *J. Chem. Phys.* **1938**, *6*, 659.
- [37] Simon, A.; Borrmann, H.; Horkah, J. *Chem. Ber.* **1997**, *130*, 1235.
- [38] Persson, B. J.; Taylor, P. R.; Lee, T. J. *J. Chem. Phys.* **1997**, *107*, 5051–5057.
- [39] Wang, L. S.; Niu, B.; Lee, Y. T.; Shirley, D. A.; Ghelichkhani, E.; Grant, E. R. *J. Chem. Phys.* **1990**, *93*, 6318–6326.
- [40] Ishiguro, E.; Kobori, M. *J. Phys. Soc. Japan* **1967**, *22*, 263–270.
- [41] Yeh, J. J. *Atomic Calculation of Photoionization Cross-Sections and Asymmetry Parameters*; Gordon & Breach: Langhorne, PA, 1993.
- [42] Boden, N.; Folland, R. *Mol. Phys.* **1971**, *21*, 1123.
- [43] Spiess, H. W.; Grosecu, R.; Haeberle, U. *Chem. Phys.* **1974**, *6*, 226–234.
- [44] The electrochemistry data were collected in 0.25 M [TBA][PF<sub>6</sub>] at a scan rate of 300 mV s<sup>-1</sup>. A 1 mm diameter Pt disk working electrode, curly Pt wire counter electrode, and Ag wire pseudo-reference electrode were used for all measurements. All measurements are corrected to Cp<sub>2</sub>Fe<sup>0/+</sup> by the addition of Cp<sub>2</sub>Fe as an internal standard.
- [45] te Velde, G.; Bickelhaupt, F. M.; Baerends, E. J.; Fonseca Guerra, C.; van Gisbergen, S. J. A.; Snijders, J. G.; Ziegler, T. *J. Comput. Chem.* **2001**, *22*, 931–967.
- [46] Fonseca Guerra, C.; Snijders, J. G.; te Velde, G.; Baerends, E. J. *Theo. Chem. Acc.* **1998**, *99*, 391–403.
- [47] Widdifield, C. M.; Schurko, R. *Concept. Magn. Reson. A* **2009**, *34A*, 91–123.
- [48] Schleyer, P. V.; Maerker, C.; Dransfeld, A.; Jiao, H.; Hommes, N. *J. Am. Chem. Soc.* **1996**, *118*, 6317–6318.
- [49] Hirsch, A.; Chen, Z.; Jiao, H. *Angew. Chem. Int. Ed.* **2001**, *40*, 2834–2838.
- [50] Juselius, J.; Sundholm, D.; Gauss, J. *J. Chem. Phys.* **2004**, *121*, 3952–3963.
- [51] Johansson, M. P.; Juselius, J.; Sundholm, D. *Angew. Chem. Int. Ed.* **2005**, *44*, 1843–1846.
- [52] Nalewajski, R. F. *Phys. Chem. Chem. Phys.* **2002**, *4*, 1710–1721.
- [53] Fonseca Guerra, C.; Handgraaf, J. W.; Baerends, E. J.; Bickelhaupt, F. M. *J. Comput. Chem.* **2003**, *25*, 189–210.
- [54] Pauling, L. *The Nature of the Chemical Bond*, 3rd ed.; Cornell University Press: Ithaca, 1960.
- [55] Popelier, P. *Atoms in Molecules: An Introduction*; Pearson Education, Ltd.: Essex, 2000.
- [56] Alcami, M.; Mo, O.; Yanez, M. *J. Chem. Phys.* **1998**, *108*, 8957–8963.
- [57] Gibbs, G. V.; Tamada, O.; Boisen, M. B.; Hill, F. C. *Am. Mineral.* **1999**, *84*, 435–446.
- [58] Tsirelson, V. G.; Tarasova, N. P.; Bobrov, M. F.; Smetannikov, Y. V. *Heteroatom Chem.* **2006**, *17*, 572–578.
- [59] Baerends, E. J.; Branchadell, V.; Sodupe, M. *Chem. Phys. Lett.* **1997**, *265*, 481–489.
- [60] Norman, N. C. *Chemistry of Arsenic, Antimony, and Bismuth*; Springer: New York, 1998.
- [61] Chase, M. *NIST-JANAF Thermodynamic Tables*, 1988.
- [62] Emsley, J. *The 13th Element: The Sordid Tale of Murder, Fire, and Phosphorus*; John Wiley & Sons, Inc.: New York, 2000.
- [63] Jayasekera, B.; Somaskandan, K.; Brock, S. L. *Inorg. Chem.* **2004**, *43*, 6902–6904.
- [64] Von Schnering, H. G.; Honle, W. *Chem. Rev.* **1988**, *88*, 243–273.
- [65] Fasol, G.; Cardona, M.; Honle, W.; Von Schnering, H. G. *Solid State Commun.* **1984**, *52*, 307–310.
- [66] Breitling, G. *Mat. Res. Bull.* **1969**, *4*, 19–32.

- [67] Rathenau, G. *Physica* **1937**, *4*, 503–514.
- [68] Gröer, T.; Baum, G.; Scheer, M. *Organometallics* **1998**, *17*, 5916–5919.
- [69] Wasserman, H. J.; Kubas, G. J.; Ryan, R. R. *J. Am. Chem. Soc.* **1986**, *108*, 2294–2301.
- [70] Ginsberg, A.; Lindsell, W.; McCullough, K.; Sprinkle, C.; Welch, A. *J. Am. Chem. Soc.* **1986**, *108*, 403–416.
- [71] Lindsell, W. E. *J. Chem. Soc., Chem. Commun.* **1982**, 1422–1424.
- [72] Lindsell, W. E.; McCullough, K. J.; Welch, A. J. *J. Am. Chem. Soc.* **1983**, *105*, 4487–4489.
- [73] de los Rios, I.; Hamon, J.; Hamon, P.; Lapinte, C.; Toupet, L.; Romerosa, A.; Peruzzini, M. *Angew. Chem., Int. Ed.* **2001**, *40*, 3910–3912.
- [74] Krossing, I.; van Wüllen, L. *Chem. Eur. J.* **2002**, *8*, 700–711.
- [75] Krossing, I. *J. Am. Chem. Soc.* **2001**, *123*, 4603–4604.
- [76] Dapporto, P.; Midollini, S.; Sacconi, L. *Angew. Chem., Int. Ed. Engl.* **1979**, *18*, 469–469.
- [77] Bezombes, J. P.; Hitchcock, P. B.; Lappert, M. F.; Nycz, J. E. *Dalton Trans.* **2004**, 499–501.
- [78] Wanandi, P. W.; Davis, W. M.; Cummins, C. C.; Russell, M. A.; Wilcox, D. E. *J. Am. Chem. Soc.* **1995**, *117*, 2110–2111.
- [79] Agarwal, P.; Piro, N. A.; Meyer, K.; Müller, P.; Cummins, C. C. *Angew. Chem., Int. Ed.* **2007**, *46*, 3111–3114.
- [80] Peters, J. C.; Johnson, A. R.; Odom, A. L.; Wanandi, P. W.; Davis, W. M.; Cummins, C. C. *J. Am. Chem. Soc.* **1996**, *118*, 10175–10188.
- [81] Agapie, T.; Diaconescu, P. L.; Cummins, C. C. *J. Am. Chem. Soc.* **2002**, *124*, 2412–2413.
- [82] Kim, E.; Odom, A. L.; Cummins, C. C. *Inorg. Chim. Acta.* **1998**, *278*, 103–107.
- [83] Concentrations of AsP<sub>3</sub> and **31** were determined by integration against an internal standard (PPh<sub>3</sub>). The concentration of Ti(N[<sup>t</sup>Bu]Ar)<sub>3</sub> was inferred using the equation  $[\text{Ti}(\text{N}[\text{tBu}]\text{Ar})_3]_f = [\text{Ti}(\text{N}[\text{tBu}]\text{Ar})_3]_i - 2[\mathbf{31}]_f$ . This assumes no other degradation pathways are operative during the course of the reaction.
- [84] Figueroa, J. S.; Cummins, C. C. *Dalton Trans.* **2006**, 2161–2168.
- [85] Ehses, M. P.; Romerosa, A.; Peruzzini, M. *Top. Curr. Chem.* **2002**, *220*, 107–140.
- [86] Peruzzini, M.; Gonsalvi, L.; Romerosa, A. *Chem. Soc. Rev.* **2005**, *34*, 1038–1047.
- [87] Umbarkar, S.; Sekar, P.; Scheer, M. *J. Chem. Soc., Dalton Trans.* **2000**, 1135–1137.
- [88] Davies, J. E.; Mays, M. J.; Raithby, P. R.; Shields, G. P.; Tompkin, P. K.; Woods, A. D. *J. Chem. Soc., Dalton Trans.* **2000**, 1925–1930.
- [89] Davies, J.; Kerr, L.; Mays, M.; Raithby, P.; Tompkin, P.; Woods, A. *Angew. Chem. Int. Ed.* **1998**, *37*, 1428–1429.
- [90] Laplaza, C. E.; Davis, W. M.; Cummins, C. C. *Angew. Chem., Int. Ed. Engl.* **1995**, *34*, 2042–2044.
- [91] Johnson, B. P.; Bal(a)zs, G.; Scheer, M. *Complexes with a metal-phosphorus triple bond*; Topics In Current Chemistry, Vol. 232; Springer: Berlin, 2004; pp 1–23.
- [92] Bal(a)zs, G.; Gregoriades, L. J.; Scheer, M. *Organometallics* **2007**, *26*, 3058–3075.
- [93] Curley, J. C.; Piro, N. A.; Cummins, C. C. *Inorg. Chem.* **2009**, *48*, 9599–9601.
- [94] Carencio, S.; Resa, I.; LeGoff, X.; LeFloch, P.; Mezailles, N. *Chem. Commun.* **2008**, 2568–2570.
- [95] Yan, P.; Xie, Y.; Wang, W.; Liu, F.; Qian, Y. *J. Mater. Chem.* **1999**, *9*, 1831–1833.
- [96] Li, B.; Xie, Y.; Jiaying, H.; Liu, Y.; Qian, Y. *Ultrason. Sono.* **2001**, *8*, 331–334.
- [97] Uhl, W.; Hiller, W.; Layh, M.; Schwarz, W. *Angew. Chem. Int. Ed.* **1992**, *31*, 1364.
- [98] Uhl, W.; Jantschak, A. *J. Organomet. Chem.* **1998**, *555*, 263.
- [99] Uhl, W.; Graupner, R.; Layh, M.; Schuz, U. *J. Organomet. Chem.* **1995**, *493*, C1.
- [100] Uhl, W.; Benter, M. *Chem. Commun.* **1999**, 771–772.
- [101] P<sub>4</sub> was used as an internal standard for monitoring purposes. No P<sub>4</sub> was present in the reaction mixture prior to its addition.
- [102] de los Rios, I.; Hamon, J. R.; Hamon, P.; Lapinte, C.; Toupet, L.; Romerosa, A.; Peruzzini, M. *Angew. Chem., Int. Ed.* **2001**, *40*, 3910–3912.
- [103] Peruzzini, M.; Marvelli, L.; Romerosa, A.; Rossi, R.; Vizza, F.; Zanobini, F. *Eur. J. Inorg. Chem.* **1999**, 931–933.

- [104] Erdmann, H.; von Unruh, M. Z. *Z. Anorg. Chem.* **1902**, *32*, 437–452.
- [105] Spinney, H. A.; Piro, N. A.; Cummins, C. C. *J. Am. Chem. Soc.* **2009**, *131*, 16233–16243.
- [106] DiMaio, A. J.; Rheingold, A. L. *Chem. Rev.* **1990**, *90*, 169–190.
- [107] Pangborn, A. B.; Giardello, M. A.; Grubbs, R. H.; Rosen, R. K.; Timmers, F. J. *Organometallics* **1996**, *15*, 1518–1520.
- [108] Figueroa, J. S.; Cummins, C. C. *J. Am. Chem. Soc.* **2004**, *126*, 13916–13917.
- [109] Laplaza, C. E.; Cummins, C. C. *Science* **1995**, *268*, 861–863.
- [110] Bezombes, J. P.; Borisenko, K. B.; Hitchcock, P. B.; Lappert, M. F.; Nycz, J. E.; Rankin, D. W. H.; Robertson, H. E. *Dalton Trans.* **2004**, 1980–1988.
- [111] Roger, C.; Hamon, P.; Toupet, L.; Rabaa, H.; Saillard, J. Y.; Hamon, J. R.; Lapinte, C. *Organometallics* **1991**, *10*, 1045–1054.
- [112] Bergamini, P.; DeBiani, F. F.; Marvelli, L.; Mascellani, N.; Peruzzini, M.; Rossi, R.; Zanello, P. *New J. Chem.* **1999**, 207–217.
- [113] Sheldrick, G. M.; (*SHELXTL*); 2005–2008.
- [114] Sheldrick, G. M. *Acta Crystallogr., Sect. A: Fundam. Crystallogr.* **1990**, *46*, 467–473.
- [115] Sheldrick, G. M. *Acta Crystallogr., Sect. A: Fundam. Crystallogr.* **2008**, *64*, 112–122.
- [116] Sheldrick, G. M.; (*SHELXL*)-97: *Program for crystal structure determination*; 1997.
- [117] Müller, P.; Herbst-Irmer, R.; Spek, A. L.; Schneider, T. R.; Sawaya, M. R. *Crystal Structure Refinement: A Crystallographer's Guide to (SHELXL)*; Müller, P., Ed.; IUCr Texts on Crystallography; Oxford University Press: Oxford, 2006.
- [118] The Reciprocal Net Site Network is a distributed database for crystallographic information, supported by the National Science Digital Library, and is run by participating crystallography labs across the world. Crystallographic data for complexes in this chapter are available under the identification codes listed in Tables 2.19 – 2.22 from the MIT Reciprocal Net site. <http://reciprocal.mit.edu/recipnet>.
- [119] These data can be obtained free of charge from The Cambridge Crystallographic Data Centre via [http://www.ccdc.cam.ac.uk/data\\_request/cif](http://www.ccdc.cam.ac.uk/data_request/cif).
- [120] Vosko, S. H.; Wilk, L.; Nusair, M. *Can. J. Phys.* **1980**, *58*, 1200–1211.
- [121] Baker, J.; Pulay, P. *J. Chem. Phys.* **2002**, *117*, 1441–1449.
- [122] van Lenthe, E.; Baerends, E. J.; Snijders, J. G. *J. Chem. Phys.* **1993**, *99*, 4597–4610.
- [123] van Lenthe, E.; Baerends, E. J.; Snijders, J. G. *J. Chem. Phys.* **1994**, *101*, 9783–9792.
- [124] van Lenthe, E.; Ehlers, A.; Baerends, E. J. *J. Chem. Phys.* **1999**, *110*, 8943–8953.
- [125] Schreckenbach, G.; Ziegler, T. *J. Phys. Chem.* **1995**, *99*, 606–611.
- [126] Schreckenbach, G.; Ziegler, T. *Int. J. Quantum Chem.* **1997**, *61*, 899–918.
- [127] Wolff, S. K.; Ziegler, T. *J. Chem. Phys.* **1998**, *109*, 895–905.
- [128] Wolff, S. K.; Ziegler, T.; van Lenthe, E.; Baerends, E. J. *J. Chem. Phys.* **1999**, *110*, 7689–7698.
- [129] van Wüllen, C. *Phys. Chem. Chem. Phys.* **2000**, *2*, 2137–2144.
- [130] Johnson, M. J. A.; Odom, A. L.; Cummins, C. C. *Chem. Commun.* **1997**, 1523–1524.
- [131] Ahlrichs, R.; Bar, M.; Haser, M.; Horn, H.; Kolmel, C. *Chem. Phys. Lett.* **1989**, *162*, 165–169.
- [132] DeYonker, N. J.; Peterson, K. A.; Wilson, A. K. *J. Phys. Chem. A* **2007**, *111*, 11383–11393.
- [133] Berger, R. J. F.; Hoffmann, M.; Hayes, S. A.; Mitzel, N. W. *Z. Naturforsch. B* **2009**, *64*, 11–12.
- [134] Gundersen, S.; Samdal, S.; Strand, T. G.; Volden, H. V. *J. Mol. Struct.* **2007**, *832*, 164–171.
- [135] Hinchley, S. L.; Robertson, H. E.; Borisenko, K. B.; Turner, A. R.; Johnston, B. F.; Rankin, D. W. H.; Ahmadian, M.; Jones, J. N.; Cowley, A. H. *Dalton Trans.* **2004**, 2469–2476.
- [136] Ross, A. W.; Fink, M.; Hilderbrandt, R. *International Tables for Crystallography, Vol. C*; Wilson, A. J. C., Ed.; Kluwer, 1992.

- [137] Siegbahn, K.; Nordling, C.; Fahlman, A.; Nordberg, R.; Hamrin, K.; Hedman, J.; Johansson, G.; Bergmark, T.; Karlsson, S. E.; Lindgren, I.; Lindberg, B. *Nova Acta Regiae Societatis Scientiarum Upsaliensis* **1967**, *20*, 282.
- [138] Cranswick, M. A.; Dawson, A.; Cooney, J. J. A.; Gruhn, N. E.; Lichtenberger, D. L.; Enemark, J. H. *Inorg. Chem.* **2007**, *46*, 10639–10646.
- [139] Lichtenberger, D. L.; Kellogg, G. E.; Kristofski, J. G.; Page, D.; Turner, S.; Klinger, G.; Lorenzen, J. *Rev. Sci. Inst.* **1986**, *57*, 2366.





# CHAPTER 3

## The Development of New P<sub>3</sub> Transfer Reagents: Ph<sub>3</sub>SnP<sub>3</sub>(C<sub>6</sub>H<sub>8</sub>) and Related Compounds

### Contents

<b>3.1</b>	<b>Introduction</b> . . . . .	<b>170</b>
<b>3.2</b>	<b>Synthesis of Substituted <i>Cyclo</i>-P<sub>3</sub> Complexes</b> . . . . .	<b>171</b>
<b>3.3</b>	<b>P<sub>3</sub> Transfer Chemistry of a Triphosphirene Complex</b> . . . . .	<b>172</b>
3.3.1	Synthesis of Ph <sub>3</sub> SnP <sub>3</sub> (C <sub>6</sub> H <sub>8</sub> ) . . . . .	173
<b>3.4</b>	<b>The Diverse Reactivity of Ph<sub>3</sub>SnP<sub>3</sub>(C<sub>6</sub>H<sub>8</sub>)</b> . . . . .	<b>176</b>
3.4.1	Retro-Diels-Alder Reactivity . . . . .	177
3.4.2	Reactivity of the Olefinic Unit . . . . .	177
3.4.3	P <sub>3</sub> Transfer with Ph <sub>3</sub> SnP <sub>3</sub> (C <sub>6</sub> H <sub>8</sub> ) . . . . .	179
<b>3.5</b>	<b>Preparation and Reaction Chemistry of LiP<sub>3</sub>(C<sub>6</sub>H<sub>8</sub>)</b> . . . . .	<b>182</b>
3.5.1	Reaction with [H <sub>5</sub> C <sub>5</sub> NH][Cl]: Synthesis of HP <sub>3</sub> (C <sub>6</sub> H <sub>8</sub> ) . . . . .	183
3.5.2	Spectroscopic Identification of P <sub>3</sub> H <sub>3</sub> . . . . .	184
<b>3.6</b>	<b>Conclusions</b> . . . . .	<b>189</b>
<b>3.7</b>	<b>Experimental Details</b> . . . . .	<b>189</b>
3.7.1	General Considerations . . . . .	189
3.7.2	Preparation of Ph <sub>3</sub> SnP <sub>3</sub> Nb(ODipp) <sub>3</sub> , <b>45</b> . . . . .	190
3.7.3	Preparation of Me <sub>3</sub> SiP <sub>3</sub> Nb(ODipp) <sub>3</sub> , <b>47</b> . . . . .	190
3.7.4	Preparation of Ph <sub>3</sub> SiP <sub>3</sub> Nb(ODipp) <sub>3</sub> , <b>48</b> . . . . .	191
3.7.5	Preparation of Ph <sub>3</sub> CP <sub>3</sub> Nb(ODipp) <sub>3</sub> , <b>49</b> . . . . .	191
3.7.6	Preparation of Cp <sub>2</sub> ClZrP <sub>3</sub> Nb(ODipp) <sub>3</sub> , <b>51</b> . . . . .	191
3.7.7	Preparation of (Ar[ <sup>t</sup> Bu]N) <sub>3</sub> TiP <sub>3</sub> Nb(ODipp) <sub>3</sub> , <b>50</b> . . . . .	192

Reproduced in part with permission from:  
Cossairt, B. M.; Cummins, C. C. *Angew. Chem. Int. Ed.*, **2010**, *49*, 1595–1598; Copyright 2010 Wiley-VCH.

3.7.8	Monitoring the reaction between $\text{Ph}_3\text{SnP}_3\text{Nb}(\text{ODipp})_3$ and $\text{ONC}_5\text{H}_5$ in the presence of 20 equiv 1,3-cyclohexadiene . . . . .	192
3.7.9	Preparation of $\text{Ph}_3\text{SnP}_3(\text{C}_6\text{H}_8)$ , <b>52</b> : One pot procedure . . . . .	193
3.7.10	Treatment of $\text{Ph}_3\text{SnP}_3\text{Nb}(\text{ODipp})_3$ with 1 equiv of $\text{ONC}_5\text{H}_5$ in the Absence of Added Trapping Agent . . . . .	193
3.7.11	Diene Exchange with $\text{Ph}_3\text{SnP}_3(\text{C}_6\text{H}_8)$ , Generation of $\text{Ph}_3\text{SnP}_3(\text{C}_6\text{H}_{10})$ , <b>54</b>	194
3.7.12	Preparation of $\text{Ph}_3\text{SnP}_3(\text{C}_6\text{H}_8)(\text{C}_2\text{N}_2(\text{NC}_5\text{H}_4)_2)$ , <b>55</b> . . . . .	194
3.7.13	Preparation of $\text{P}_3\text{Rh}(\text{PPh}_3)_3$ , <b>56</b> . . . . .	195
3.7.14	Reaction of $[\text{Na}(\text{THF})_3][\text{P}_3\text{Nb}(\text{ODipp})_3]$ with $\text{ClRh}(\text{PPh}_3)_3$ followed by $\text{ONC}_5\text{H}_5$ . . . . .	195
3.7.15	Preparation of solvate-free $\text{LiP}_3(\text{C}_6\text{H}_8)$ , <b>57</b> . . . . .	196
3.7.16	Reaction of $\text{LiP}_3(\text{C}_6\text{H}_8)$ with $\text{Ph}_3\text{SnCl}$ . . . . .	196
3.7.17	Treatment of $\text{LiP}_3(\text{C}_6\text{H}_8)$ with $[\text{HNC}_5\text{H}_5][\text{Cl}]$ , observation of $\text{HP}_3(\text{C}_6\text{H}_8)$ , <b>58</b> . . . . .	197
3.7.18	Treatment of $[\text{Na}(\text{THF})_3][\text{P}_3\text{Nb}(\text{ODipp})_3]$ with $\text{HOC}_6\text{F}_5$ ; observation of $\text{P}_3\text{H}_3$ , <b>59</b> . . . . .	197
3.7.19	X-Ray Structure Determinations . . . . .	197
3.7.20	Computational Studies . . . . .	198
<b>3.8</b>	<b>References</b> . . . . .	<b>203</b>

### 3.1 INTRODUCTION

The previous chapter focused on the use of  $[\text{Na}(\text{THF})_3][\text{P}_3\text{Nb}(\text{ODipp})_3]$  as a  $\text{P}_3^{3-}$  transfer agent which ultimately found use in the direct synthesis of tetraatomic  $\text{AsP}_3$ . In this chapter, the focus is shifted to elaboration of the anionic  $\text{P}_3\text{Nb}(\text{ODipp})_3$  platform by reaction with electrophiles to generate substituted triphosphirene ligands. Given the exceptional chemical stability of neutral *cyclo*- $\text{P}_3$  metal complexes, this facile substitution chemistry with an anionic variant is of great interest. Functionalizations of *cyclo*- $\text{P}_3$  complexes were first reported for  $\text{P}_3\text{M}(\text{triphos})$  ( $\text{M} = \text{Co}, \text{Rh}, \text{Ir}$ ;  $\text{triphos} = \text{PhC}(\text{CH}_2\text{CH}_2\text{PPh}_2)_3$ ), and required the use of the highly potent electrophiles  $[\text{Me}_3\text{O}][\text{BF}_4]$  or  $\text{MeOTf}$  to afford the methylated species.<sup>1</sup> Such substituted *cyclo*- $\text{P}_3$  complexes are possibly best described as coordinated diphosphene species by virtue of their  $\eta^2$  coordination mode, and several of these have been reported.<sup>2-8</sup> When the bound diphosphene is part of an all-phosphorus, three-membered ring, the ligand can also be described as a coordinated triphosphirene. Such  $\eta^2$ -bound triphosphirene ligands have been described by Peruzzini and coworkers.<sup>9,10</sup> As alluded to previously, Piro and Cummins demonstrated that the anionic nature of the *cyclo*- $\text{P}_3$  complex  $[\text{Na}][\{\text{W}(\text{CO})_5\}_2\text{P}_3\text{Nb}(\text{N}[\text{CH}_2^t\text{Bu}]\text{Ar})_3]$ , derived from  $\text{P}_2\text{W}(\text{CO})_5$  trapping by  $[\text{Na}][\{\text{W}(\text{CO})_5\}\text{P}\equiv\text{Nb}(\text{N}[\text{CH}_2^t\text{Bu}]\text{Ar})_3]$ , imparts the molecule with greater

nucleophilic character, allowing for functionalization using mild reagents to give a variety of products.<sup>11,12</sup> Thus, it was expected that the anionic nature of  $[P_3Nb(ODipp)_3]$  would impart the  $P_3$  ring with greater nucleophilic character, allowing for functionalization with a wide array of electrophiles. Of particular interest in this section is the  $Ph_3Sn$ -substituted *cyclo*- $P_3$  complex, which has been studied in detail as a  $P_3$  transfer agent.

### 3.2 SYNTHESIS OF SUBSTITUTED *Cyclo*- $P_3$ COMPLEXES

Our initial studies in functionalizing *cyclo*- $P_3$  complexes focused on the formation of new main-group and transition-metal substituted triphosphirene ligands. Upon treatment with a variety of electrophiles, salt elimination from  $[Na(THF)_3][P_3Nb(ODipp)_3]$  allows access to a wide array of substituted *cyclo*- $P_3$  ligands bound to niobium. For instance it was found that  $Ph_3SnCl$ ,  $nBu_3SnCl$ ,  $Ph_3SiCl$ ,  $tPr_3SiCl$ ,  $Me_3SiCl$ ,  $Ph_3CCl$ ,  $Cl_2ZrCp_2$ , and  $ClTi(N[{}^tBu]Ar)_3$  all served as precursors for the synthesis of substituted triphosphirenes, Figure 3.1.

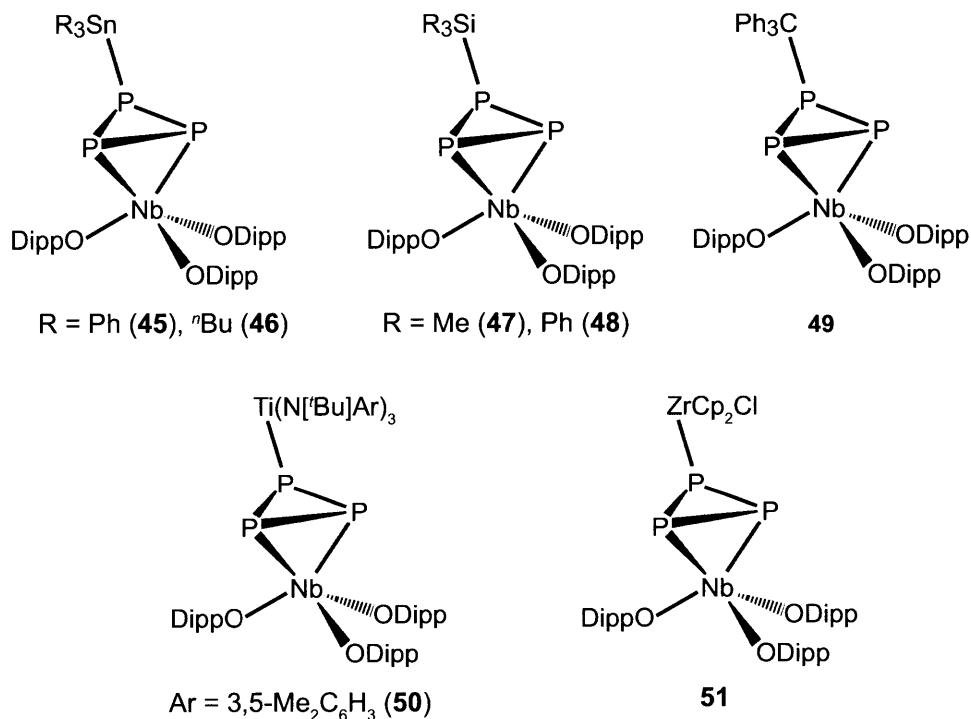
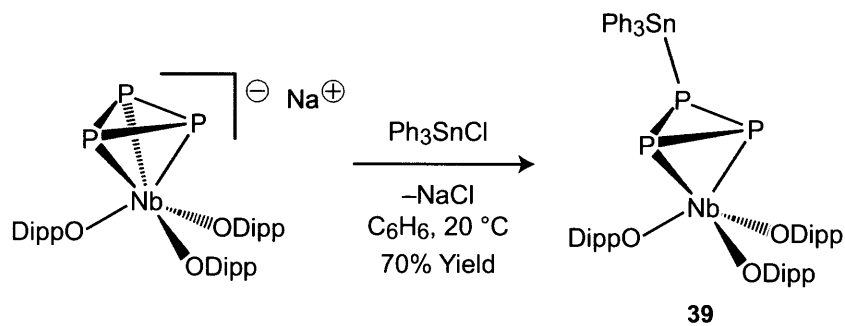


**Figure 3.1.** Substituted niobium *cyclo*- $P_3$  complexes.

As a specific and useful example, it was found that treatment of  $[Na(THF)_3][P_3Nb(ODipp)_3]$  with  $Ph_3SnCl$  results in loss of  $NaCl$  and formation of  $Ph_3SnP_3Nb(ODipp)_3$ , **45**, Scheme 3.1. The  $^{31}P$  NMR spectrum of **45** consists of a single sharp singlet at  $-235$  ppm with visible  $^{117/119}Sn$  satellites ( $^1J_{119Sn/P} = 336$  Hz,  $^1J_{117Sn/P} = 321$  Hz), Figure 3.2. This sharp singlet is indicative of

whizzing of the  $\text{Ph}_3\text{Sn}$  moiety about the *cyclo*- $\text{P}_3$  ring.<sup>13–16</sup> Variable temperature NMR spectra obtained as low as  $-90\text{ }^\circ\text{C}$  reveal no locking out of this movement on the NMR timescale, Figure 3.3.



**Scheme 3.1.** Synthesis of  $\text{Ph}_3\text{SnP}_3\text{Nb}(\text{ODipp})_3$ .

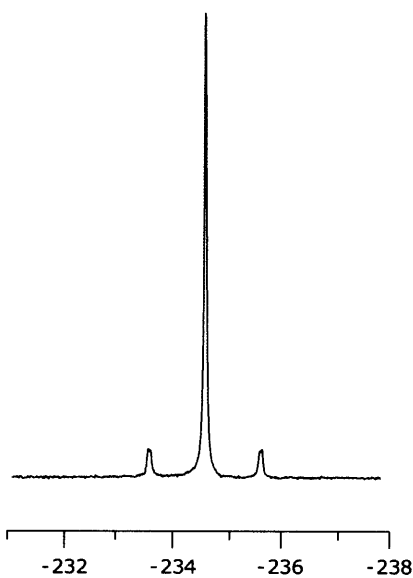


**Figure 3.2.**  $^{31}\text{P}$  NMR spectrum of  $\text{Ph}_3\text{SnP}_3\text{Nb}(\text{ODipp})_3$ .

### 3.3 $\text{P}_3$ TRANSFER CHEMISTRY OF A TRIPHOSPHIRENE COMPLEX

The niobium-phosphorus interaction in  $\text{Ph}_3\text{SnP}_3\text{Nb}(\text{ODipp})_3$  (and the other  $\text{RP}_3\text{Nb}(\text{ODipp})_3$  complexes) may be regarded as side-on coordination of a diphosphene ( $\text{RP}=\text{PR}$ ) to a strongly  $\pi$ -donating  $d^2$   $\text{Nb}(\text{ODipp})_3$  fragment, a situation encountered before in the compound  $\text{Ph}_2\text{CP}_8\text{Nb}(\text{OC}[\text{}^2\text{Ad}]\text{Mes})_3$ , **10** (Chapter 1). This structural similarity suggested that it may be possible to liberate the triphosphirene unit in **45** with the use of an O-atom transfer reagent such as pyridine-*N*-oxide to

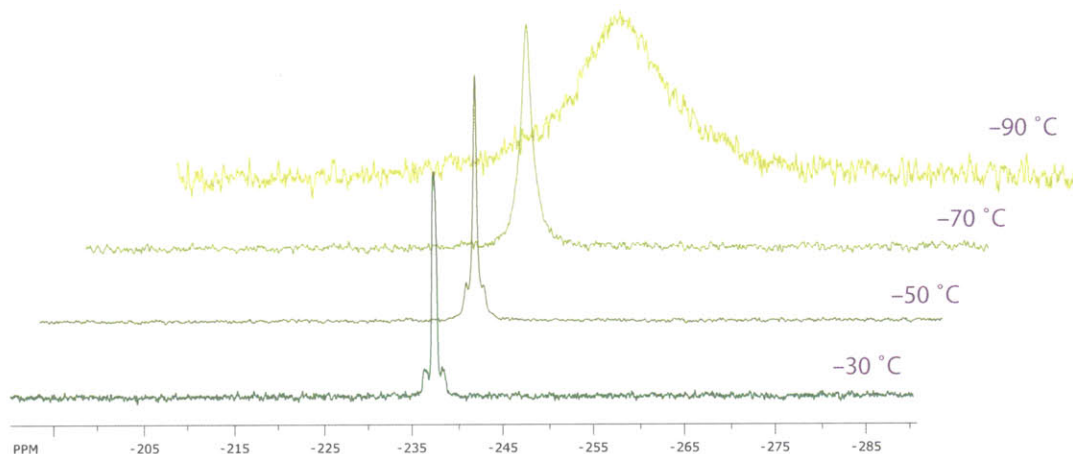
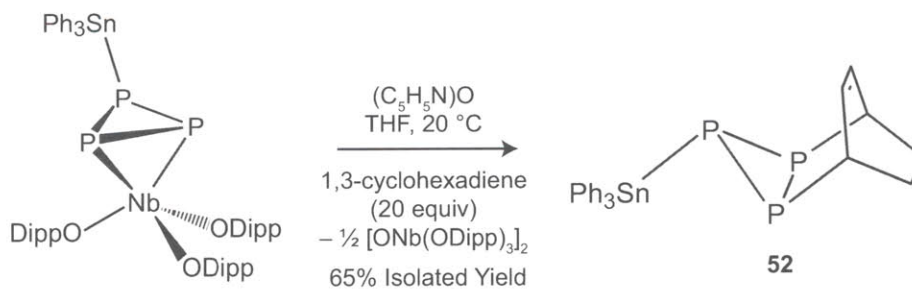


**Figure 3.3.** Variable temperature  $^{31}\text{P}$  NMR spectra of  $\text{Ph}_3\text{SnP}_3\text{Nb}(\text{ODipp})_3$ .

release the niobium oxo fragment. With this thought in mind, such triphosphirene transfer chemistry was pursued.

### 3.3.1 Synthesis of $\text{Ph}_3\text{SnP}_3(\text{C}_6\text{H}_8)$

To liberate the triphosphirene molecule  $\text{P}_3\text{SnPh}_3$  from niobium, complex **45** was treated with a stoichiometric amount of pyridine-*N*-oxide in the presence of excess 1,3-cyclohexadiene, the latter to serve as a trapping agent; this protocol resulted in formation of the desired Diels-Alder cycloaddition product  $\text{Ph}_3\text{SnP}_3(\text{C}_6\text{H}_8)$ , **52**, together with 0.5 equiv of the known niobium oxo dimer  $[\text{ONb}(\text{ODipp})_3]_2$  (via  $\text{ONb}(\text{ODipp})_3(\text{NC}_5\text{H}_5)$ ), Scheme 3.2.<sup>17</sup> Compound **52** was isolated in 65% yield by filtration after it selectively precipitated upon concentration of the ethereal reaction mixture. Conveniently, compound **52** could also be prepared directly in a single pot, without isolation of complex **45**, in an overall yield of 65% over the two steps.



**Scheme 3.2.** Synthesis of  $\text{Ph}_3\text{SnP}_3(\text{C}_6\text{H}_8)$ .

The phosphorus NMR spectrum of **52** features a sharp doublet and a sharp triplet flanked by  $^{117/119}\text{Sn}$  satellites centered at  $-234$  ppm ( $^2J_{^{117/119}\text{Sn}-\text{P}} = 105$  Hz) and  $-231$  ppm ( $^1J_{^{117/119}\text{Sn}-\text{P}} = 736$  Hz), respectively, Figure 3.4.<sup>12</sup> This coupling is mirrored nicely in the  $^{119}\text{Sn}$  NMR spectrum of **52**, Figure 3.5. X-ray quality crystals of **52** were grown from a saturated THF solution at  $-35$

°C, Figure 3.6. The Sn1–P3 interatomic distance is 2.528(1) Å, which is typical for a Sn–P single bond, and the olefin double bond is found between C44 and C45 with a distance of 1.330(6) Å as compared with the C41 to C42 interatomic distance which is found to be 1.549(6) Å. As can be seen in both the phosphorus NMR spectrum and the crystal structure for compound **52**, only a single isomer is observed due to the endo effect stemming from secondary orbital interactions with P3 during the cycloaddition reaction. This appears to be a general feature of this class of cycloaddition products.

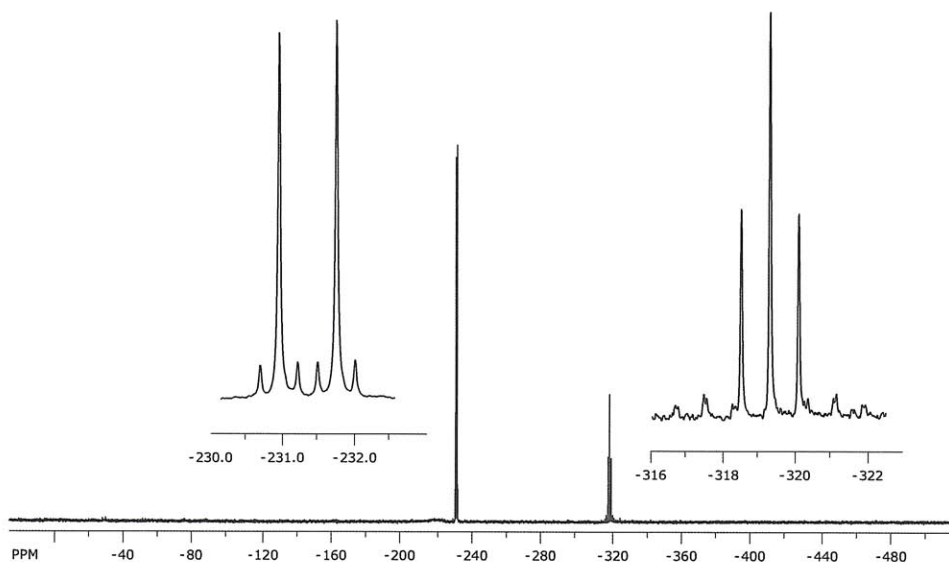


Figure 3.4.  $^{31}\text{P}$  NMR spectrum of  $\text{Ph}_3\text{SnP}_3(\text{C}_6\text{H}_8)$ .

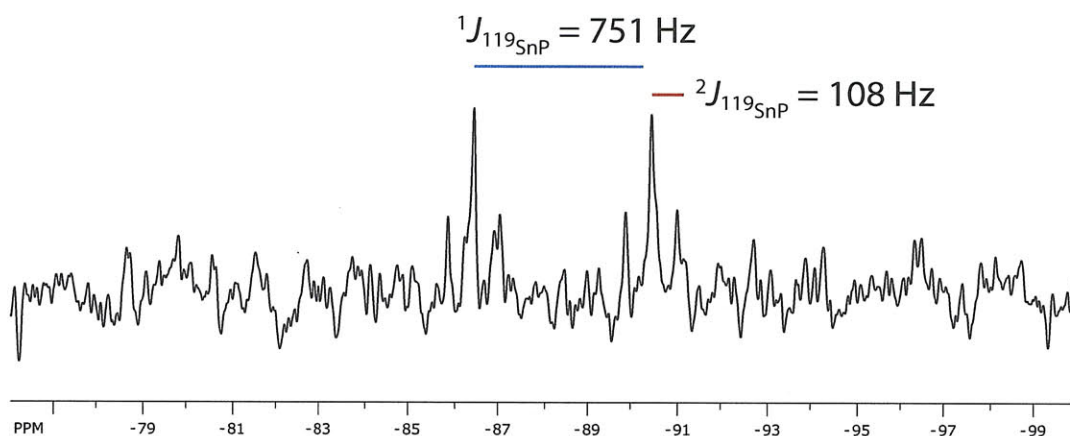
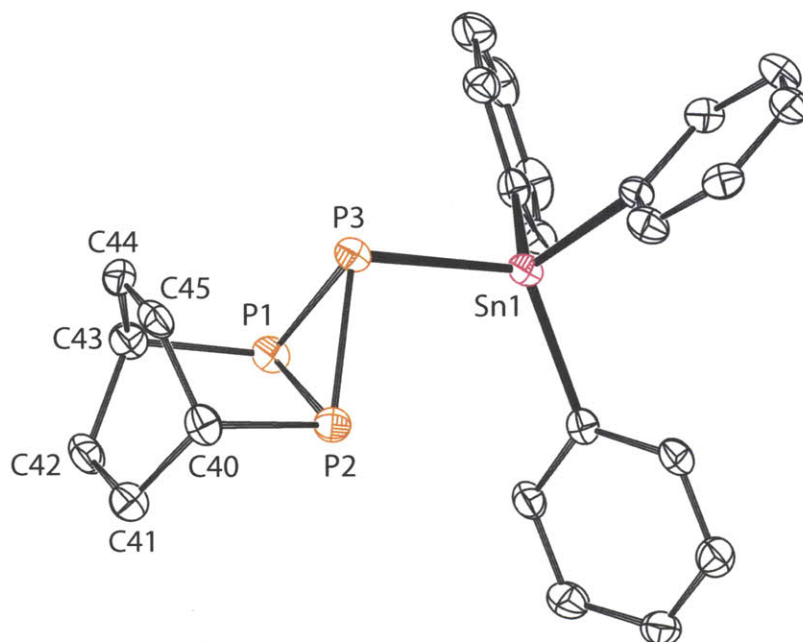


Figure 3.5.  $^{119}\text{Sn}$  NMR spectrum of  $\text{Ph}_3\text{SnP}_3(\text{C}_6\text{H}_8)$ .

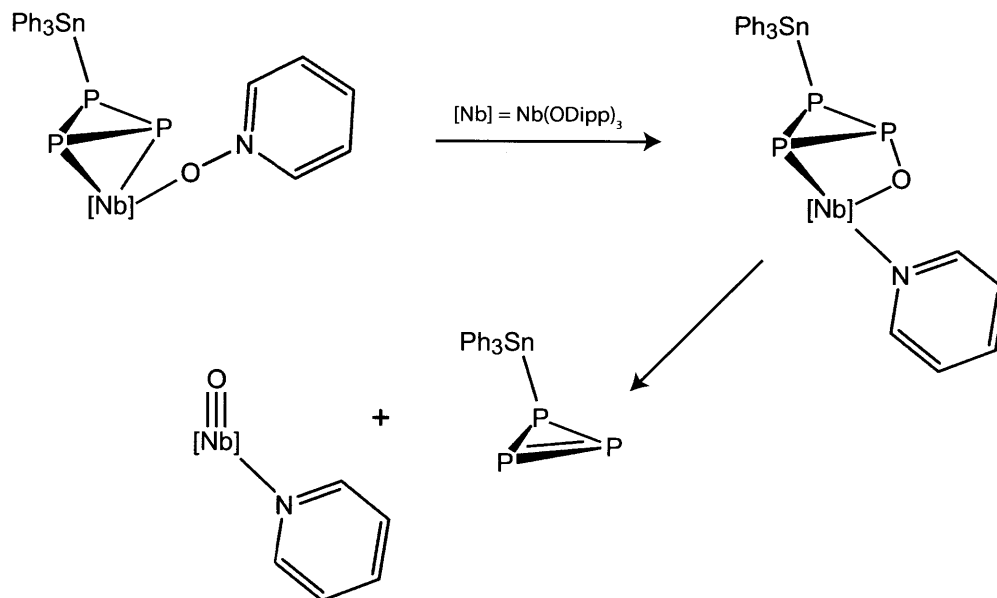
The reaction between complex **45** and  $\text{ONC}_5\text{H}_5$  in the presence of 20 equiv 1,3-cyclohexadiene was monitored by  $^{31}\text{P}$  and  $^1\text{H}$  NMR spectroscopy in toluene. At room temperature, the reaction



**Figure 3.6.** Thermal ellipsoid plot (50% probability) of  $\text{Ph}_3\text{SnP}_3(\text{C}_6\text{H}_8)$  with hydrogen atoms omitted for clarity.

was found to proceed rapidly with no observable intermediates; the disappearance of  $^{31}\text{P}$  NMR resonances for **45** was concomitant with appearance of those assigned to **2**. However, when the reaction was monitored at  $-10\text{ }^\circ\text{C}$ , complex **45** was consumed giving rise to a single new species with a phosphorus NMR resonance at  $-170\text{ ppm}$ . This species appeared stable at  $-10\text{ }^\circ\text{C}$  for several hours and was identified by  $^1\text{H}$  and  $^{31}\text{P}$  NMR spectroscopy as the  $\text{ONC}_5\text{H}_5$  adduct of  $\text{Ph}_3\text{SnP}_3\text{Nb}(\text{ODipp})_3$ , **45-ONC}\_5\text{H}\_5. Complex **45-ONC}\_5\text{H}\_5 precipitated from toluene solution as a pink powder when held at  $-10\text{ }^\circ\text{C}$  for several minutes and it was necessary to gently warm the reaction mixture to resolubilize the complex and monitor its conversion to **52**. Accordingly, upon warming to  $30\text{ }^\circ\text{C}$ , conversion of **45-ONC}\_5\text{H}\_5 to compound **52** was observed with no other major species growing in. These observations suggest that breakup of the pyridine-*N*-oxide adduct, **45-ONC}\_5\text{H}\_5, is the rate-determining step in the formation of compound **52** at  $20\text{ }^\circ\text{C}$ . A proposed mechanism for this reaction is shown in Scheme 3.3; this process is currently being investigated computationally by Glenn Morello and Prof. Thomas Cundari.********

The outcome of the reaction of **45** with  $\text{ONC}_5\text{H}_5$  in the presence of 1,3-cyclohexadiene is rationalized by loss of a free triphosphirene, that is, a species with a *cyclo*- $\text{P}_3$  unit bound in an  $\eta^1$  fashion to the  $\text{Ph}_3\text{Sn}$  fragment.<sup>18–20</sup> In order to study the feasibility of such a hypothesis we turned to calculations to investigate the possible conformations of the proposed  $\text{Ph}_3\text{SnP}_3$  intermediate. Both  $(\eta^1\text{-P}_3)\text{SnPh}_3$  and  $(\eta^3\text{-P}_3)\text{SnPh}_3$  structures were considered. Despite the fact that six-coordinate tin is relatively common,<sup>21</sup> all attempts to optimize the  $(\eta^3\text{-P}_3)\text{SnPh}_3$  structure resulted in convergence to the  $(\eta^1\text{-P}_3)\text{SnPh}_3$  form, which is structurally very similar to **52 sans diene**. The  $\text{P}=\text{P}$  distance in this intermediate was calculated to be  $2.019\text{ \AA}$  whereas the  $\text{P}-\text{P}$  distances averaged to  $2.250\text{ \AA}$  in



**Scheme 3.3.** Proposed mechanism for formation of  $\text{Ph}_3\text{SnP}_3$  from  $\text{Ph}_3\text{SnP}_3\text{Nb}(\text{ODipp})_3$  and  $\text{ONC}_5\text{H}_5$ .

length. The one short Sn–P interaction falls at 2.622 Å while the distances from the Sn center to the phosphorus atoms of the diphosphene average 3.884 Å. This outcome suggests that the reactive ( $\eta^1\text{-P}_3$ ) $\text{SnPh}_3$  intermediate does indeed harbor a free diphosphene unit and that this P=P moiety does not interact appreciably with the Sn center. To get a further sense of the chemical nature of the transient ( $\eta^1\text{-P}_3$ ) $\text{SnPh}_3$  intermediate, we sought to investigate its fate in the absence of an added chemical trap. In this effort, phosphorus NMR spectroscopic analyses and elemental analyses suggest that ( $\eta^1\text{-P}_3$ ) $\text{SnPh}_3$  cleanly oligomerizes to  $(\text{Ph}_3\text{SnP}_3)_x$ , however both the value of  $x$  and the connectivity of this oligomer remains unknown.

### 3.4 THE DIVERSE REACTIVITY OF $\text{Ph}_3\text{SnP}_3(\text{C}_6\text{H}_8)$

The cyclohexadiene trapping product  $\text{Ph}_3\text{SnP}_3(\text{C}_6\text{H}_8)$  has several different potentially reactive functional groups. To begin, **52** has a cyclic olefin that could engage in a variety of transformations that result in reduction of the C=C double bond or simple cycloaddition chemistry. Secondly, this cyclic olefin serves to protect a diphosphene unit which may be revealed by a retro-cycloaddition reaction. Lastly, the Sn–P bond is potentially cleavable by a variety of substrates. Taken separately, these features suggest many reactions that would lead to elaboration of **52** into various derivatives of interest. There also exists the possibility to simultaneously cleave the Sn–P bond and undergo retro-cycloaddition to effect  $\text{P}_3^{1-}$  transfer to a platform of interest. All of these modes of reactivity are explored in the following subsections.



### 3.4.1 Retro-Diels-Alder Reactivity

It is often found in the chemistry of diphosphenes (RP=PR) that Diels-Alder cycloaddition reactions can be reversible.<sup>2</sup> With this thought in mind, I sought to free the triphosphirene unit, Ph<sub>3</sub>SnP<sub>3</sub>, from **52** via a retro Diels-Alder reaction. The heating of **52** with an excess (20 equiv) of 2,3-dimethylbutadiene in THF between 75 and 80 °C was monitored by <sup>31</sup>P NMR spectroscopy. It was found that **52** slowly but cleanly converts to the corresponding 2,3-dimethylbutadiene trapping product, Ph<sub>3</sub>SnP<sub>3</sub>(C<sub>6</sub>H<sub>10</sub>), **54**, by a diene-exchange reaction with a half life of 70 h, Figure 3.7. This slow conversion is consistent with the rates seen for retro-cycloadditions of other unstable diphosphenes, Figure 3.8.<sup>22</sup> This observation of reversible cycloaddition by the putative triphosphirene Ph<sub>3</sub>SnP<sub>3</sub> bolsters support for the intermediacy of this intriguing species.

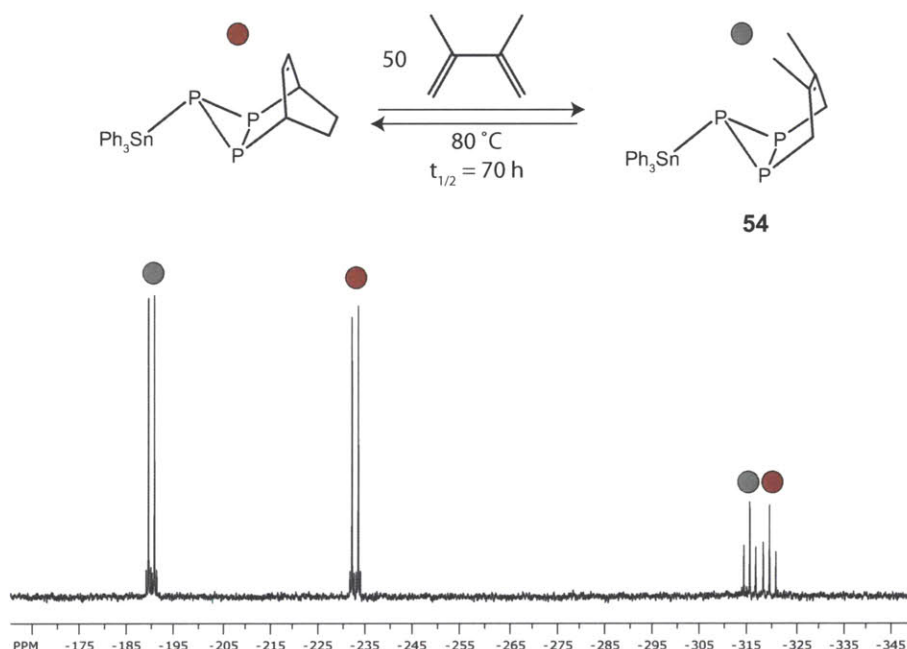
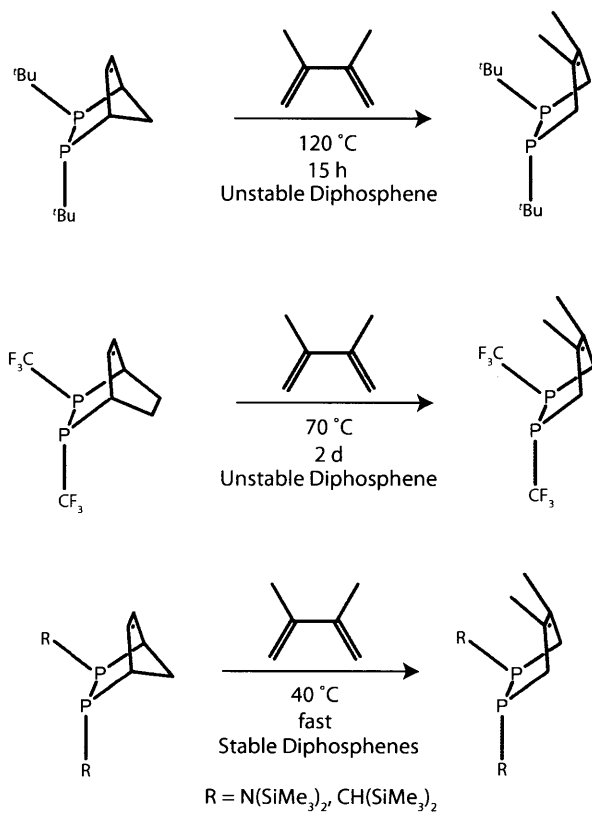


**Figure 3.7.** Conversion of Ph<sub>3</sub>SnP<sub>3</sub>(C<sub>6</sub>H<sub>8</sub>) to Ph<sub>3</sub>SnP<sub>3</sub>(C<sub>6</sub>H<sub>10</sub>) by a retro-Diels-Alder reaction. <sup>31</sup>P NMR spectrum shown after 50% conversion.

### 3.4.2 Reactivity of the Olefinic Unit

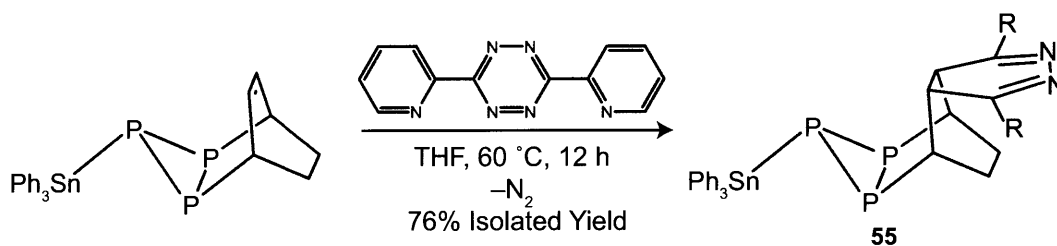
Seeking to exploit other modes for reactivity of **52**, a selective reaction of the olefinic unit was sought. Tetrazines were identified as a class of compounds that react efficiently and selectively with alkenes and it was thought that this type of reactivity would be selective in our case due to the sluggish rate of the retro-cycloaddition reaction of the diene and the diphosphene. Carboni and Lindsey were the first to carry out a detailed examination of the reaction of alkenes with tetrazines,<sup>23</sup> however they did not investigate the mechanism of the reaction, but noted that electron-



Weber. *Chem. Rev.*, **1992**, *92*, 1839.

**Figure 3.8.** Literature examples of diene-exchange reactions of substituted diphosphenes.

donor substituents in the dienophile and electron-acceptor substituents in the tetrazine facilitated the reaction. In this regard, they expressed the assumption that the olefin initially attacks the tetrazine at the para carbon atoms. The small values of the activation enthalpies and the high absolute values of the activation entropies indicate the ease with which this reaction occurs. Along with the high degree of order of the transition state,<sup>24</sup> this may serve as a satisfactory argument in favor of a concerted mechanism for the cycloaddition. With this precedent in mind, **52** was treated with 3,6-di-2-pyridyl-tetrazine in THF at 60 °C for 12 h, during which time the reaction mixture proceeded from magenta to yellow with effervescence of N<sub>2</sub>. This procedure afforded, after work up, Ph<sub>3</sub>SnP<sub>3</sub>(C<sub>6</sub>H<sub>8</sub>)(C<sub>2</sub>N<sub>2</sub>(NC<sub>5</sub>H<sub>4</sub>)<sub>2</sub>), **55**, in 47% isolated yield, Scheme 3.4.



**Scheme 3.4.** Treatment of Ph<sub>3</sub>SnP<sub>3</sub>(C<sub>6</sub>H<sub>8</sub>) with 2,6-di-4-pyridyl tetrazine.

Single crystals of **55** were grown by diffusion of pentane into toluene at –35 °C over 3 days. Yellow crystals of **55** crystallized in the space group  $P\bar{1}$ . The average P–P distance in the crystal structure is 2.2126 Å and the P<sub>3</sub>–Sn1 interatomic distance is 2.515(1) Å. The C–C bonds in the C<sub>6</sub>H<sub>8</sub> unit are consistent for C–C single bond lengths with C6–C5 at 1.562(5) Å and C2–C3 at 1.539(6) Å. The C6–C7 interatomic distance is slightly shortened at 1.505(5) Å and the C7–N1 bond length registers at 1.284(5) Å, indicating a clear C=N double bond. The N1–N2 distance is 1.438(4) Å, consistent with an N–N single bond.

### 3.4.3 P<sub>3</sub> Transfer with Ph<sub>3</sub>SnP<sub>3</sub>(C<sub>6</sub>H<sub>8</sub>)

Not only can Ph<sub>3</sub>SnP<sub>3</sub>(C<sub>6</sub>H<sub>8</sub>) undergo retro-cycloaddition chemistry, it also has a potentially reactive P–Sn bond, making it a possible P<sub>3</sub><sup>–</sup> transfer agent.<sup>25–27</sup> As proof of principle that **52** would be able to serve as a source of P<sub>3</sub><sup>–</sup> in reaction chemistry, **52** was treated with 1 equiv of ClRh(PPh<sub>3</sub>)<sub>3</sub>, Wilkinson’s catalyst, Scheme 3.5. <sup>1</sup>H, <sup>31</sup>P, and <sup>119</sup>Sn NMR spectroscopy and GC-MS gave evidence for loss of Ph<sub>3</sub>SnCl and 1,3-cyclohexadiene in a 1:1 ratio. Following diethyl ether extraction of the crude reaction mixture, the tan-colored P<sub>3</sub>Rh(PPh<sub>3</sub>)<sub>3</sub>, **56**, was isolated in pure form.

The phosphorus NMR spectrum of **56** displays a doublet of quartets for the phosphine P atoms (31 ppm, <sup>1</sup>J<sub>103Rh/P</sub> = 150 Hz, <sup>2</sup>J<sub>P/P</sub> = 16 Hz) and an overlapping pair of quartets for the *cyclo*-P<sub>3</sub> moiety (–191 ppm, <sup>1</sup>J<sub>103Rh/P</sub> = 32 Hz, <sup>2</sup>J<sub>P/P</sub> = 16 Hz), Figure 3.10, which is quite similar to the spectral properties reported for P<sub>3</sub>Rh(triphos) (triphos = CH<sub>3</sub>C(CH<sub>2</sub>PPh<sub>2</sub>)<sub>3</sub>), which was obtained

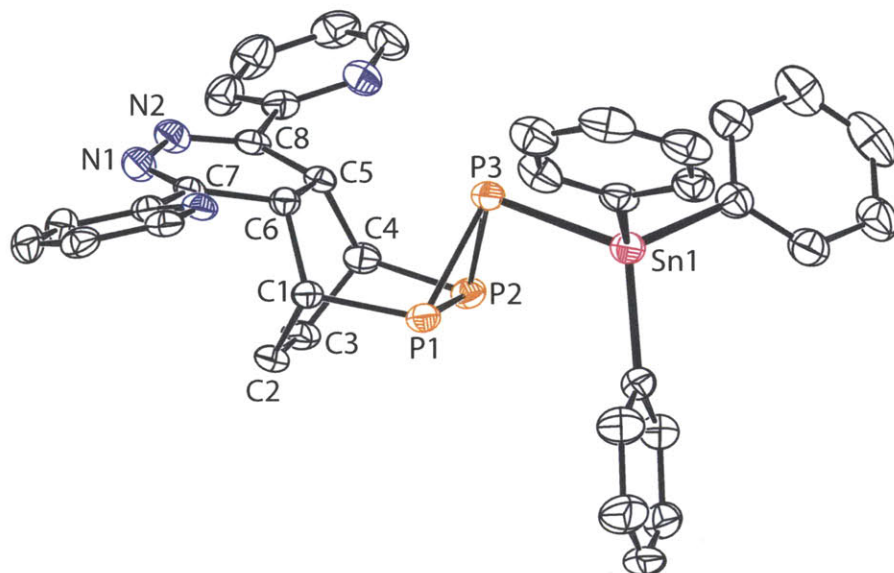
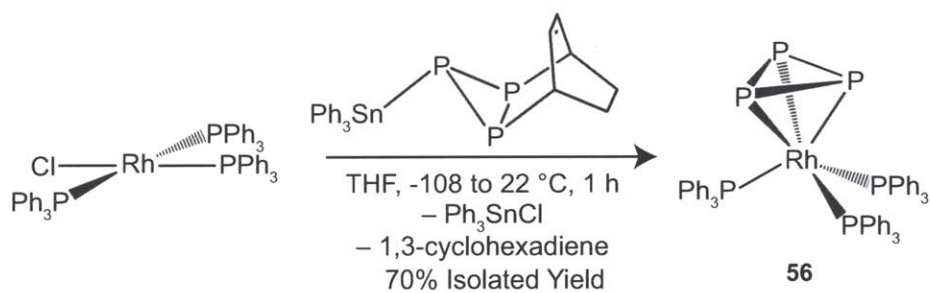


**Figure 3.9.** Thermal ellipsoid plot (50% probability) of  $\text{Ph}_3\text{SnP}_3(\text{C}_6\text{H}_8)(\text{C}_2\text{N}_2(\text{NC}_5\text{H}_4)_2)$  with hydrogen atoms omitted for clarity.



**Scheme 3.5.** Synthesis of  $\text{P}_3\text{Rh}(\text{PPh}_3)_3$ .

via  $P_4$  activation as described by Di Vaira and Sacconi.<sup>28</sup> X-ray quality crystals of **56** were grown by vapor diffusion of  $Et_2O$  into a concentrated  $CH_2Cl_2$  solution at  $-35\text{ }^\circ\text{C}$ , Figure 3.11. Complex **56** displays a symmetric *cyclo*- $P_3$  unit where the Rh-P4,P5,P6 interatomic distances average to 2.374 Å and the Rh-P1,P2,P3 interatomic distances average to 2.420 Å.

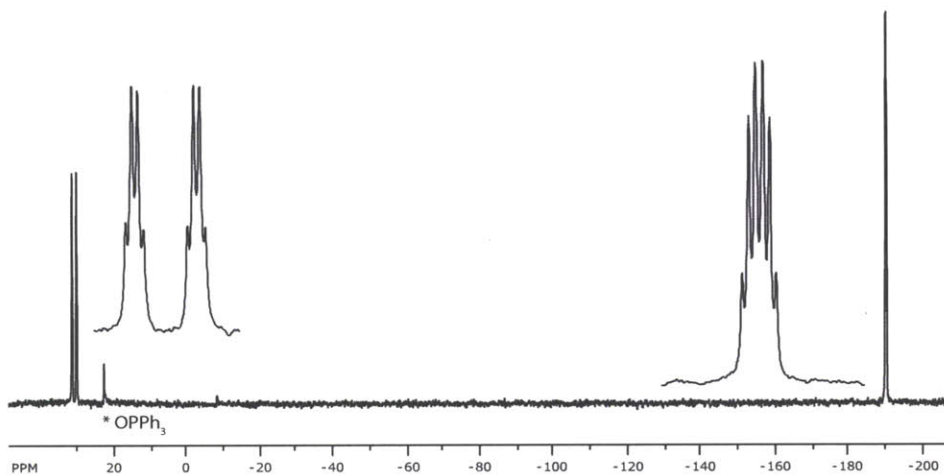


**Figure 3.10.**  $^{31}\text{P}$  NMR spectrum of  $P_3\text{Rh}(\text{PPh}_3)_3$ .  $\text{OPPh}_3$  (\*) is present as an impurity.

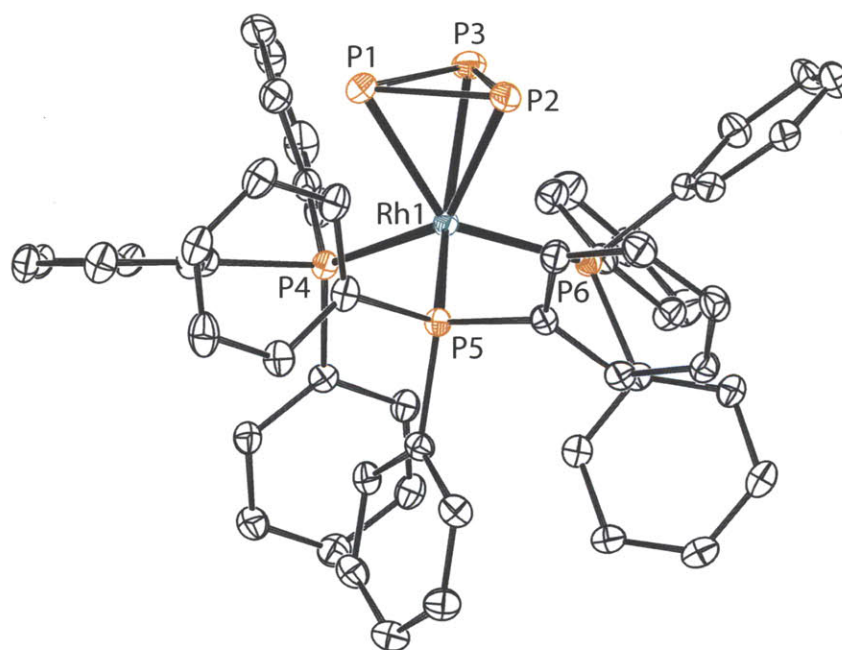


**Figure 3.11.** Thermal ellipsoid plot (50% probability) of  $P_3\text{Rh}(\text{PPh}_3)_3$  with hydrogen atoms omitted for clarity.

It was found additionally in the course of this study that  $[\text{Na}(\text{THF})_3][\text{P}_3\text{Nb}(\text{ODipp})_3]$  on its own can transfer a triphosphorus unit to Wilkinson's catalyst *via* the bimetallic complex  $(\text{Ph}_3\text{P})_3\text{Rh}(\mu_2:\eta^1, \eta^2\text{-P}_3)\text{Nb}(\text{ODipp})_3$  with loss of  $\text{NaCl}$ . However the subsequent elimination of

**56** and formation of niobium oxo using  $\text{ONC}_5\text{H}_5$  is neither as efficient nor as clean as is the  $\text{P}_3^-$  transfer with compound **52**. The use of compound **52** as a source of  $\text{P}_3^-$  represents a new methodology for accessing phosphorus-containing molecules. This method for the synthesis of **56** bears close relation to the installation of a nitrido functional group using deprotonated 2,3:5,6-dibenzo-7-azabicyclo[2.2.1]hepta-2,5-diene (dbabh) as an  $\text{N}^-$  source with loss of anthracene.<sup>29</sup> A defining feature of the  $\text{P}_3^-$  transfer reaction yielding **56** is the oxidation of rhodium from the +1 to the +3 oxidation state.<sup>30</sup>

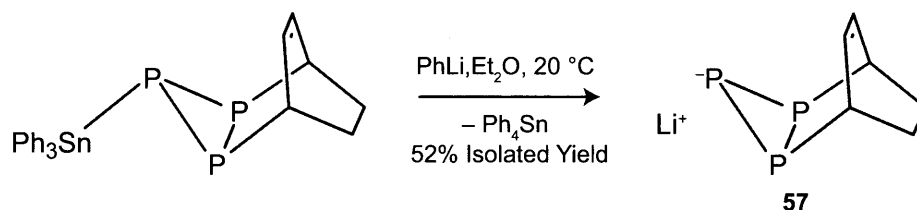
Recently, somewhat related phosphorus transfer chemistry was reported by Miluykov and coworkers through reaction of a  $\text{Me}_3\text{Sn}$  derivative of 1,2,4-triphosphacyclopentadienide with  $\text{BrMn}(\text{CO})_5$ .<sup>31</sup> Intrigued by this result, **52** was exposed to both  $\text{BrMn}(\text{CO})_5$  and  $\text{BrRe}(\text{CO})_5$  in refluxing THF under reduced pressure for 16 h. A color change from pale yellow to orange and effervescence was observed in both cases.  $\text{Ph}_3\text{SnBr}$  and 1,3-cyclohexadiene were also clearly identified in both cases. The metal containing reaction products gave very similar IR spectra with two broad absorbances at 1950 and 2004  $\text{cm}^{-1}$  (Mn) and at 1939 and 1995  $\text{cm}^{-1}$  (Re), consistent with a  $C_{3v}$  symmetric  $\text{P}_3\text{M}(\text{CO})_3$  product. Both compounds were high spin  $d^4$  as determined by Evans' method magnetism and it is our hope to obtain further conclusive characterization on the identity of these intriguing species in the near term. To the best of our knowledge these tricarbonyl species have not been previously synthesized, but are closely related to the known  $\text{P}_3\text{Co}(\text{CO})_3$  molecule.<sup>32</sup>

### 3.5 PREPARATION AND REACTION CHEMISTRY OF $\text{LiP}_3(\text{C}_6\text{H}_8)$

While  $\text{Ph}_3\text{SnP}_3(\text{C}_6\text{H}_8)$  was found to be a viable  $\text{P}_3^-$  transfer agent in the synthesis of  $\text{P}_3\text{Rh}(\text{PPh}_3)_3$ , this type of reactivity was found not to be completely general. In cases where the E–X bond of the substrate was stronger than the desired Sn–X bond, no reaction was observed ( $\text{Mes}^*\text{N}=\text{PCl}$ ,  $\text{Cl}_2\text{Nb}(\text{ODipp})_3$ ,  $\text{ClMo}(\text{N}[\text{tPr}]\text{Ar})_3$ ,  $\text{FeCl}_2(\text{dppe})$ ,  $\text{SnCl}_2$ ). It was thus the goal to generate a more reactive source of  $\text{P}_3^-$  and  $\text{LiP}_3(\text{C}_6\text{H}_8)$  seemed like a promising target molecule in this direction because  $\text{LiX}$  salt elimination should be more energetically favorable than  $\text{Ph}_3\text{SnX}$  loss.

Several lithiating reagents were screened and it was ultimately found that  $\text{PhLi}$  was the ideal reagent for  $\text{Ph}_3\text{Sn}^+$  abstraction from **52**. Treatment of a suspension of **52** in  $\text{Et}_2\text{O}$  with one equivalent of  $\text{PhLi}$  resulted in rapid homogenization and yellowing of the solution followed by slow formation of a white colored precipitate. The white precipitate was identified as  $\text{Ph}_4\text{Sn}$  and was removed by filtration. Subsequent drying of the filtrate and extraction of the residue with benzene resulted in a yellow powder which was isolated by filtration in 52% yield. On drying, the yellow powder took on a deep orange-black color and was readily identified by  $^1\text{H}$ ,  $^{13}\text{C}$ ,  $^{31}\text{P}$ , and  $^7\text{Li}$  NMR analysis as the desired solvate-free  $\text{LiP}_3(\text{C}_6\text{H}_8)$ , **57**, Scheme 3.6. The  $^{31}\text{P}$  NMR spectrum of compound **57** shows a doublet at  $-216$  ppm and a triplet at  $-256$  ppm with no Sn-satellites present, Figure 3.12. The lithium cation in this salt is readily sequestered without decomposition of

the material by addition of 2 equivalents of 12-crown-4. It was found that **57** is stable at room temperature, however, gentle heating in THF or pyridine above 40 °C resulted in loss of 1,3-cyclohexadiene and decomposition to an intractable mixture of phosphorus-containing products. As a first simple test of reactivity, **57** was treated with 1 equiv of  $\text{Ph}_3\text{SnCl}$  in THF. This reaction was found to cleanly and quantitatively give rise to the  $\text{Ph}_3\text{SnP}_3(\text{C}_6\text{H}_8)$  starting material. Thus far few reactivity studies have been pursued with  $\text{LiP}_3(\text{C}_6\text{H}_8)$  and this area is ripe for exploration. One interesting first result has been the observation of clean formation of  $\text{HP}_3(\text{C}_6\text{H}_8)$  upon quenching  $\text{LiP}_3(\text{C}_6\text{H}_8)$  with acids.



**Scheme 3.6.** Synthesis of  $\text{LiP}_3(\text{C}_6\text{H}_8)$ .

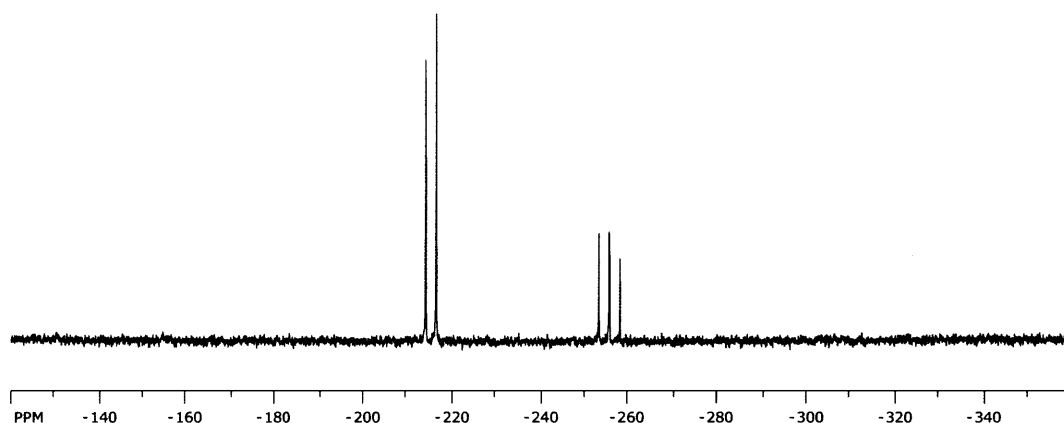


**Figure 3.12.**  $^{31}\text{P}$  NMR spectrum of  $\text{LiP}_3(\text{C}_6\text{H}_8)$ .

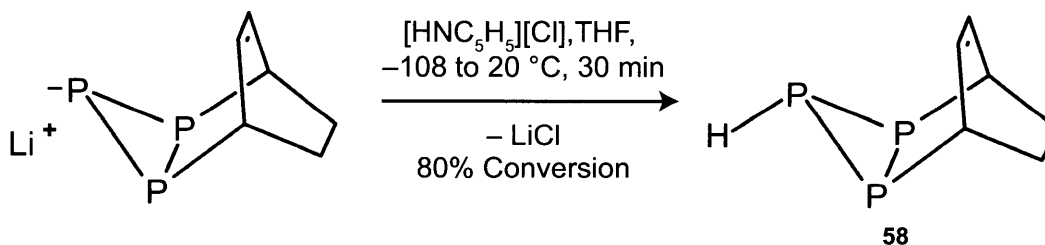
### 3.5.1 Reaction with $[\text{H}_5\text{C}_5\text{NH}][\text{Cl}]$ : Synthesis of $\text{HP}_3(\text{C}_6\text{H}_8)$

The number of known hydrides of phosphorus is only exceeded by that of carbon.<sup>33</sup> The simplest cyclic polyphosphane,  $\text{P}_3\text{H}_3$ , was first detected by mass spectrometric techniques in 1972.<sup>34</sup> Since then, many substituent-stabilized three-membered phosphorus homocycles (triphosphiranes or cyclotriphosphanes) have been synthesized,<sup>34–36</sup> however, no synthesis of  $\text{P}_3\text{H}_3$  in pure form has been devised and no information on the molecular structure of  $\text{P}_3\text{H}_3$  exists. This makes  $\text{P}_3\text{H}_3$  and other lightly substituted cyclotriphosphane species of considerable interest. These species are likely also to have great applicability in the synthesis of both phosphorus-rich molecules and materials.

### Preparation of $\text{HP}_3(\text{C}_6\text{H}_8)$

There has been some success in moving toward the goal of identifying a reproducible synthesis of  $\text{P}_3\text{H}_3$  and related phosphorus hydrides. Being able to obtain **57** in pure form, several acids were screened for effecting selective protonation of a single phosphorus atom. It was found that treatment of **57** with 1 equiv of  $[\text{HNC}_5\text{H}_5][\text{Cl}]$  in thawing THF solution gave 80% conversion by NMR spectroscopy to the desired phosphorus hydride  $\text{HP}_3(\text{C}_6\text{H}_8)$ , **58**, Scheme 3.7. The proton-decoupled phosphorus NMR spectrum of **58** appears as a sharp doublet and a triplet at  $-325$  and  $-223$  ppm, respectively. Proton coupling results in a dramatic splitting of these resonances as shown in Figure 3.13. The  $^1\text{H}$  NMR spectrum of **58** shows the phosphorus-bound hydride at  $-1.1$  ppm with a large P–H one bond coupling constant of 160 Hz and a small P–H two bond coupling constant of 20 Hz.

A geometry optimization of **58** performed using the OLYP functional in ADF, with the TZ2P basis set on all atoms, gave the structure shown in Figure 3.14.  $^{31}\text{P}$  NMR chemical shielding calculations performed on this geometry optimized structure gave  $^{31}\text{P}$  resonances at  $-305$  ppm (2P) and  $-240$  ppm, in excellent agreement with the observed chemical shifts. Furthermore, the calculated P–H proton chemical shift was  $-1.3$  ppm, again, in good agreement with the experimental data. The limitation of this preparation at the moment is the reaction scale; namely, we are limited by the amount of  $\text{LiP}_3(\text{C}_6\text{H}_8)$  that can be isolated at one time, which has thus far precluded isolation of **58** as a pure substance.



Scheme 3.7. Synthesis of  $\text{HP}_3(\text{C}_6\text{H}_8)$ .

### 3.5.2 Spectroscopic Identification of $\text{P}_3\text{H}_3$

Encouraged by the above result, we were intrigued by the possibility of gaining entry to a solution synthesis of  $\text{P}_3\text{H}_3$  in pure form. The *cyclo*- $\text{P}_3$  anion complex **25** would appear to be an ideal precursor to  $\text{P}_3\text{H}_3$  and it was hoped that a simple quench with an appropriate acid would lead to this interesting phosphorus hydride. The difficulty here arises in the ease with which the aryloxy ligands on niobium are protonated in the presence of acids. With this complication in mind, it was thought that treatment of  $[\text{Na}(\text{THF})_3][\text{P}_3\text{Nb}(\text{ODipp})_3]$  with 6 equivalents of an alcohol would result



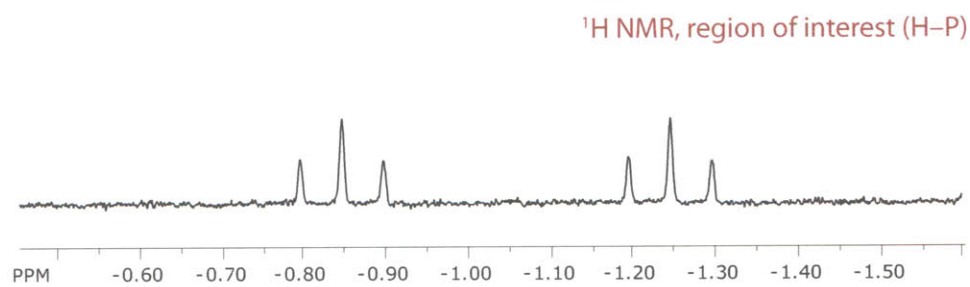
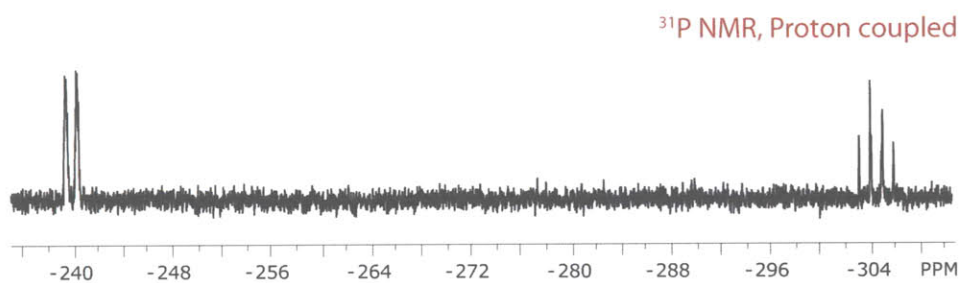
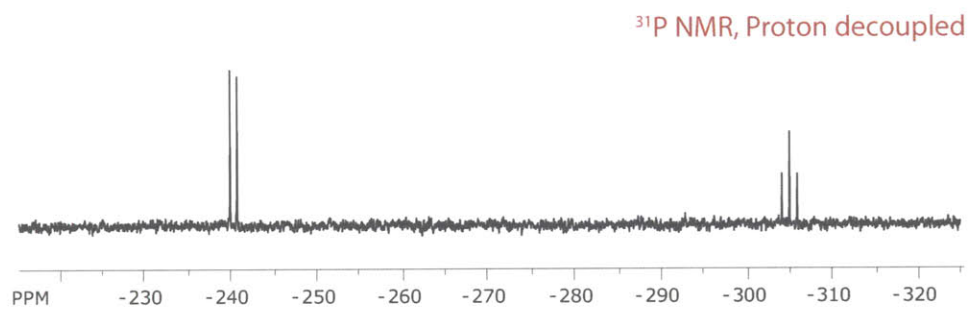


**Figure 3.13.** Proton-coupled and proton-decoupled <sup>31</sup>P NMR spectra and <sup>1</sup>H NMR spectrum of HP<sub>3</sub>(C<sub>6</sub>H<sub>8</sub>).

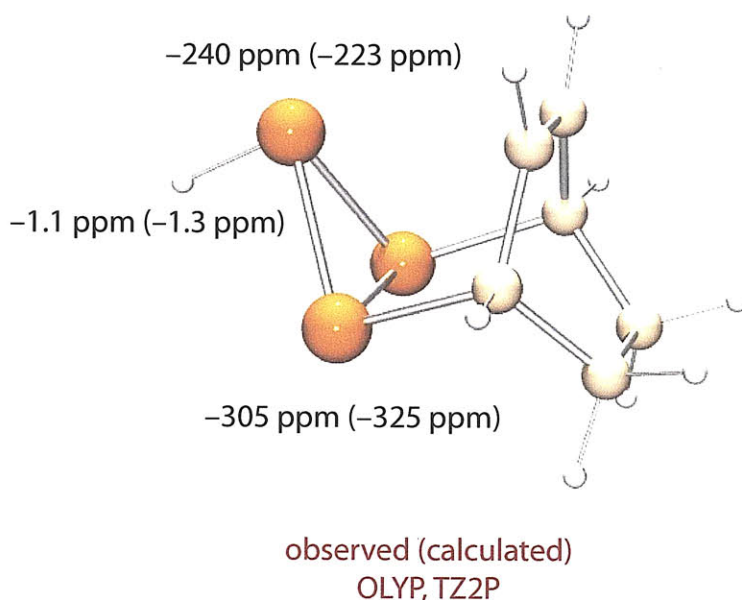


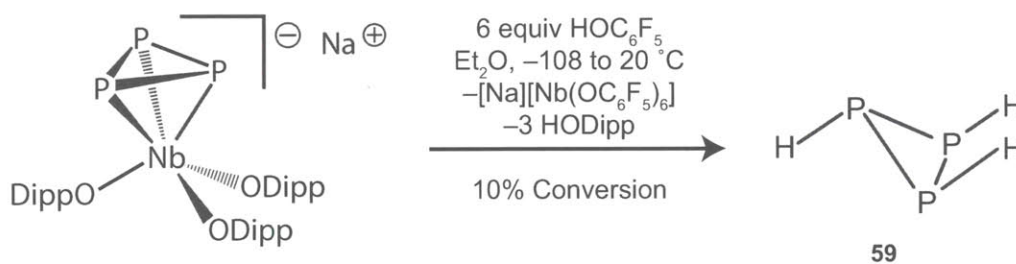
**Figure 3.14.** Geometry optimization and calculated chemical shifts of  $\text{HP}_3(\text{C}_6\text{H}_8)$ .

in formation of the niobate  $[\text{Na}][\text{Nb}(\text{OR})_6]$  and  $\text{P}_3\text{H}_3$ . Looking to the literature for a niobate to target,  $[\text{Na}][\text{Nb}(\text{OC}_6\text{F}_5)_6]$  presented itself as a suitable candidate.<sup>37</sup>

Treatment of  $[\text{Na}(\text{THF})_3][\text{P}_3\text{Nb}(\text{ODipp})_3]$  with 6 equivalents of  $\text{HOC}_6\text{F}_5$  resulted in incremental protonation of the 2,6-diisopropylphenoxide ligands followed by protonation of the *cyclo*- $\text{P}_3$  ligand. Formation of  $[\text{Na}][\text{Nb}(\text{OC}_6\text{F}_5)_6]$  was confirmed by  $^{93}\text{Nb}$  and  $^{19}\text{F}$  NMR spectroscopy as well as by elemental analysis on the isolated material, Scheme 3.8. In the proton decoupled  $^{31}\text{P}$  NMR spectrum, the singlet at  $-242$  ppm corresponds to  $\text{PH}_3$  and the doublet and triplet pair at  $-295$  ppm and  $-267$  ppm correspond to  $\text{P}_3\text{H}_3$  as confirmed by the proton-coupled spectrum and by DFT NMR chemical shielding calculations, Figure 3.16. The proton coupled  $^{31}\text{P}$  NMR spectrum is quite complicated due to strong one bond and two bond P–H coupling, Figure 3.15. This represents the first NMR spectroscopic observation of this cyclic phosphorus hydride.

Unfortunately, the reaction does not always proceed to completion, and in stoichiometric experiments run under mild conditions,  $[\text{Na}][\text{P}_3\text{Nb}(\text{ODipp})(\text{OC}_6\text{F}_5)_2]$  was the predominant species isolated and has been characterized as the bis-12-crown-4 solvate by single crystal X-ray diffraction, Figure 3.17.  $[\text{Na}(\text{12-crown-4})_2][\text{P}_3\text{Nb}(\text{ODipp})(\text{OC}_6\text{F}_5)_2]$ , **60**, crystallizes in the monoclinic space group  $C2/c$ . The P–P interatomic distances are 2.1575(13), 2.1689(12), and 2.1693(13) Å, which are approximately 0.1 Å shorter than the analogous P–P distances in the structure of  $[\text{Na}(\text{THF})_6][\text{P}_3\text{Nb}(\text{ODipp})_3]$ . The Nb–ODipp interatomic distance is short at 1.968(2) Å compared with 2.020(2) and 2.023(2) Å for the Nb– $\text{OC}_6\text{F}_5$  bond distances. There is a long Nb–O(THF) interaction at 2.305(2) Å, which, while long compared to the other Nb–O distances in this structure is quite short compared to typical Nb–O(solvent) interactions seen previously in these studies. This

is suggestive of greater Lewis acidity at the niobium center due to the presence of the two  $\text{OC}_6\text{F}_5$  ligands. Replacement of the final ODipp ligand and phosphorus ligand protonation occurs under more forcing conditions (a combination of longer reaction times, excess  $\text{HOC}_6\text{F}_5$ , and/or higher temperatures). To date only 5 to 10 % conversion to  $\text{P}_3\text{H}_3$  has been realized and future work will focus more heavily on identifying the ideal alcoholysis reagent (or alternative proton source) to effect efficiently this transformation.



**Scheme 3.8.** Synthesis of  $\text{P}_3\text{H}_3$ .

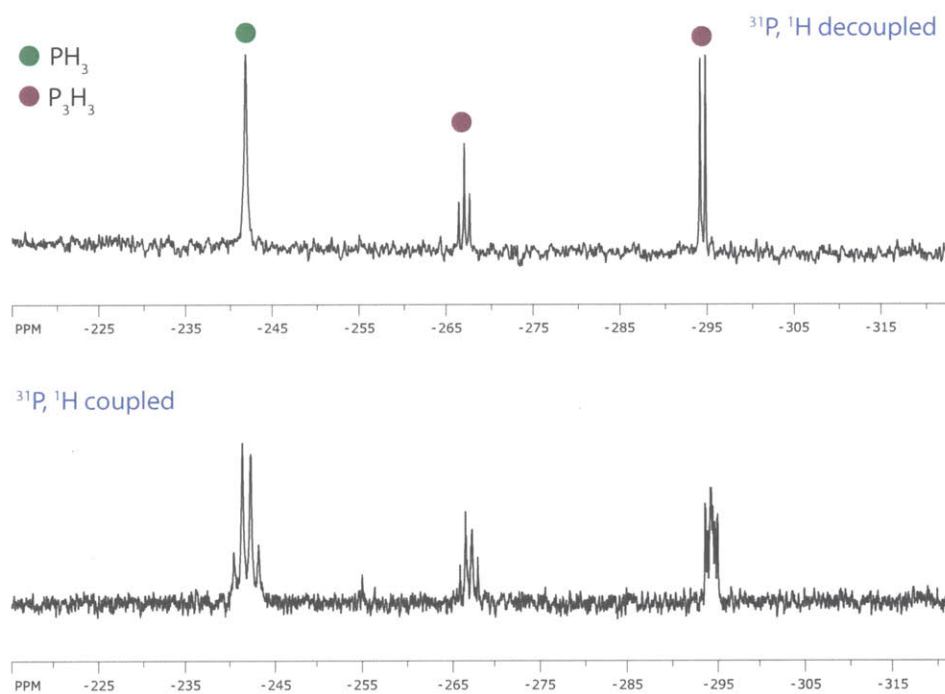


**Figure 3.15.** Proton-coupled and proton-decoupled  $^{31}\text{P}$  NMR spectra of  $\text{P}_3\text{H}_3$ .

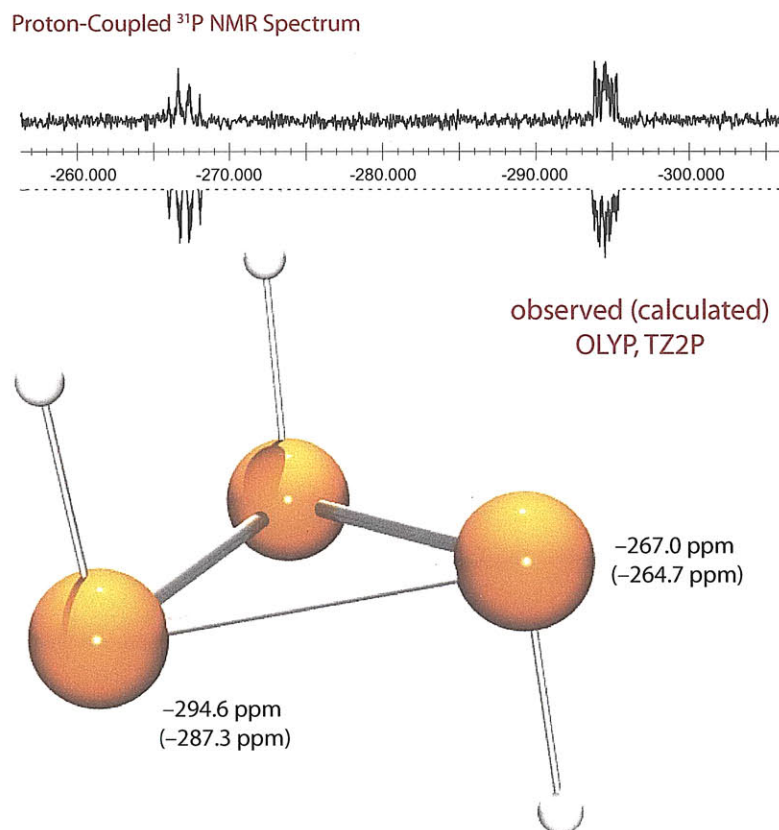


**Figure 3.16.** Geometry optimization and calculated/observed chemical shifts of  $\text{P}_3\text{H}_3$ .

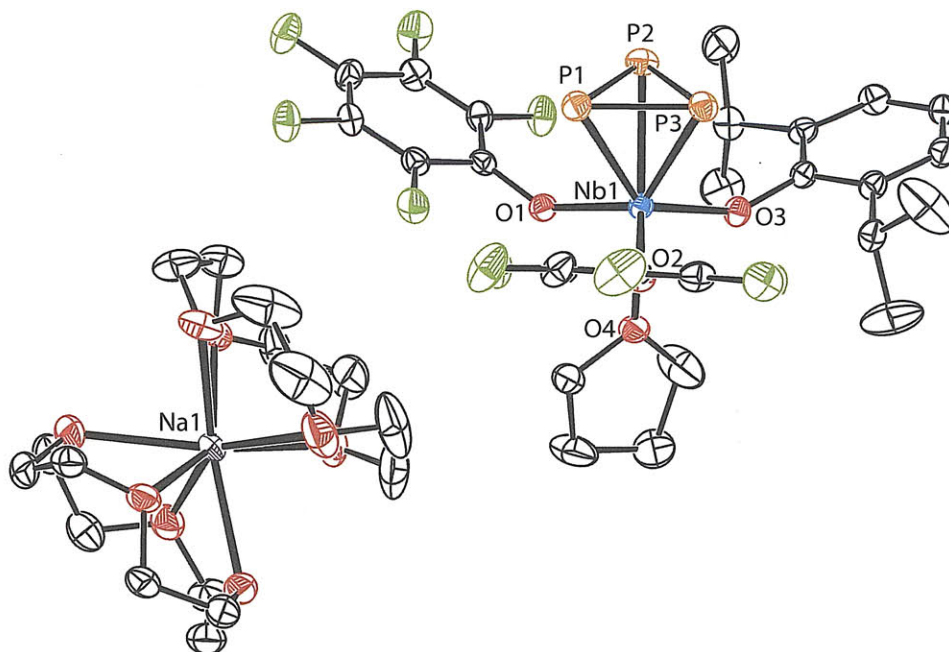


**Figure 3.17.** Thermal ellipsoid plot (50% probability) of  $[\text{Na}][\text{Nb}(\text{OC}_6\text{F}_5)_2(\text{ODipp})]$  with hydrogen atoms omitted for clarity.

## 3.6 CONCLUSIONS

Several new modes of *cyclo*-P<sub>3</sub> functionalization and transfer have been explored in this chapter. A highlight of this chemistry has been the synthesis of Ph<sub>3</sub>SnP<sub>3</sub>(C<sub>6</sub>H<sub>8</sub>), a product of diene trapping of a liberated triphosphirene unit. The reaction that forms Ph<sub>3</sub>SnP<sub>3</sub>(C<sub>6</sub>H<sub>8</sub>) involves treatment of Ph<sub>3</sub>SnP<sub>3</sub>Nb(ODipp)<sub>3</sub> with an equivalent of pyridine-*N*-oxide in the presence of an excess of 1,3-cyclohexadiene. This reaction is quite similar to that observed in Chapter 1 where treatment of Ph<sub>2</sub>CP<sub>8</sub>Nb(OC[<sup>2</sup>Ad]Mes)<sub>3</sub> with pyridine-*N*-oxide in the presence of excess 1,3-cyclohexadiene resulted in the synthesis of Ph<sub>2</sub>CP<sub>8</sub>(C<sub>6</sub>H<sub>8</sub>) by diphosphene trapping. This suggests that the ability of pyridine-*N*-oxide to extrude a niobium-bound diphosphene might be a general feature of such niobium complexes.

The varied chemistry of Ph<sub>3</sub>SnP<sub>3</sub>(C<sub>6</sub>H<sub>8</sub>) has been explored. It was revealed that the diphosphene can be reaccessed by retro-Diels Alder cycloaddition chemistry, that the cyclic olefin itself can undergo cycloaddition with a pyridyl-substituted tetrazine, and most interestingly, that Ph<sub>3</sub>SnP<sub>3</sub>(C<sub>6</sub>H<sub>8</sub>) can act as a source of P<sub>3</sub><sup>-</sup> in reactions that liberate 1,3-cyclohexadiene and Ph<sub>3</sub>Sn<sup>+</sup>. This strategy has allowed for the synthesis of new *cyclo*-P<sub>3</sub> complexes and is an area wide open for further exploration. Treatment of Ph<sub>3</sub>SnP<sub>3</sub>(C<sub>6</sub>H<sub>8</sub>) with PhLi was revealed to produce Ph<sub>4</sub>Sn and LiP<sub>3</sub>(C<sub>6</sub>H<sub>8</sub>), a phosphorus-rich salt that merits an in depth exploration. Not only could LiP<sub>3</sub>(C<sub>6</sub>H<sub>8</sub>) be used as a more reactive source of P<sub>3</sub><sup>-</sup>, it has the potential to serve as a monoanionic ligand for a variety of transition metal complexes. Furthermore, the first spectroscopic observations of the phosphorus hydrides P<sub>3</sub>H<sub>3</sub> and HP<sub>3</sub>(C<sub>6</sub>H<sub>8</sub>) have been made and these molecules represent interesting targets for further optimization and exploration.

## 3.7 EXPERIMENTAL DETAILS

### 3.7.1 General Considerations

All manipulations were performed in a Vacuum Atmospheres model MO-40M glove box under an atmosphere of purified dinitrogen. Solvents were obtained anhydrous and oxygen-free from a Contour Glass Solvent Purification System, or by analogous methods.<sup>38</sup> Celite 435 (EM Science), 4 Å molecular sieves (Aldrich), and alumina (EM Science) were dried by heating at 200 °C under dynamic vacuum for at least 24 hours prior to use. All glassware was oven-dried at temperatures greater than 170 °C prior to use. Deuterated solvents for NMR spectroscopy were purchased from Cambridge Isotope Labs. Benzene-*d*<sub>6</sub>, pyridine-*d*<sub>5</sub>, and toluene-*d*<sub>8</sub> were degassed and stored over molecular sieves for at least 2 days prior to use. CDCl<sub>3</sub> was distilled off of CaH<sub>2</sub> and stored over molecular sieves. ITi(N[<sup>*t*</sup>Bu]Ar)<sub>3</sub> and ClV(N[CH<sub>2</sub><sup>*t*</sup>Bu]Ar)<sub>3</sub> were prepared according to literature procedures.<sup>39-41</sup> Pyridine-*N*-oxide was purchased from Aldrich chemical company and was sublimed prior to use. Ph<sub>3</sub>SnCl was purchased from Aldrich chemical company and

was recrystallized from Et<sub>2</sub>O prior to use. 3,6-di-2-pyridyl tetrazine, Me<sub>3</sub>SiCl, PhLi, Ph<sub>3</sub>CCl, Ph<sub>3</sub>SiCl, and <sup>n</sup>Bu<sub>3</sub>SnCl were purchased from Aldrich chemical company and were used without further purification. ClRh(PPh<sub>3</sub>)<sub>3</sub> was purchased from STREM chemical company and was used without further purification. NMR spectra were obtained on Varian Mercury 300 or Varian Inova 500 instruments equipped with Oxford Instruments superconducting magnets or on Bruker Avance 400 instruments equipped with Magnex Scientific superconducting magnets. <sup>1</sup>H NMR spectra were referenced to residual C<sub>6</sub>D<sub>5</sub>H (7.16 ppm), CHCl<sub>3</sub> (7.27 ppm) or C<sub>5</sub>D<sub>4</sub>HN (8.74 ppm). <sup>13</sup>C NMR spectra were referenced to C<sub>6</sub>D<sub>6</sub> (128.39 ppm), CDCl<sub>3</sub> (77.23 ppm), or C<sub>5</sub>D<sub>5</sub>N (150.35 ppm). <sup>31</sup>P NMR spectra were referenced externally to 85% H<sub>3</sub>PO<sub>4</sub> (0 ppm). <sup>119</sup>Sn NMR were referenced externally to SnMe<sub>4</sub> (5% in CH<sub>2</sub>Cl<sub>2</sub>, 0 ppm). Elemental analyses were performed by Midwest Microlab, LLC (Indianapolis, Indiana).

### 3.7.2 Preparation of Ph<sub>3</sub>SnP<sub>3</sub>Nb(ODipp)<sub>3</sub>, 45

[Na(THF)<sub>3</sub>][P<sub>3</sub>Nb(ODipp)<sub>3</sub>] (1.02 g, 1.07 mmol, 1 equiv) was dissolved in 30 mL of Et<sub>2</sub>O. To this solution was added Ph<sub>3</sub>SnCl (411 mg, 1.07 mmol, 1 equiv). The reaction mixture was allowed to stir for 2 h during which time there was no appreciable color change. The reaction mixture was filtered through a plug of Celite to remove the precipitated salt. The resulting solution was then taken to dryness under reduced pressure. The resulting residue was dissolved in 4 mL of pentane and was placed in the freezer at -35 °C for 36 h during which time a golden colored precipitate formed. This precipitate was isolated atop a frit and dried to constant mass giving pure (η<sup>2</sup>-Ph<sub>3</sub>SnP<sub>3</sub>)Nb(ODipp)<sub>3</sub> (756 mg, 0.71 mmol, 66% yield). Elemental Analysis calculated for C<sub>54</sub>H<sub>66</sub>Nb<sub>1</sub>O<sub>3</sub>P<sub>3</sub>Sn<sub>1</sub>: C 60.74, H 6.23, P 8.70; Found C 60.40, H 6.10, P 8.79. <sup>1</sup>H NMR (C<sub>6</sub>D<sub>6</sub>): 1.24 (d, 36 H, <sup>1</sup>J<sub>H/H</sub> = 6.8 Hz), 3.78 (sep, 6 H, <sup>1</sup>J<sub>H/H</sub> = 6.8 Hz), 7.00 (t, 3 H, <sup>1</sup>J<sub>H/H</sub> = 7.5 Hz), 7.06 (m, 6 H), 7.10 (d, 6 H, <sup>1</sup>J<sub>H/H</sub> = 7.5 Hz), 7.27 (m, 6 H), 7.55 (m, 3 H) ppm. <sup>13</sup>C NMR (C<sub>6</sub>D<sub>6</sub>): 24.3 (s), 27.5 (s), 123.6 (s), 123.8 (s), 129.2 (s), 130.1 (s), 136.5 (s), 137.0 (s), 138.3 (s), 160.7 (s) ppm. <sup>31</sup>P NMR (C<sub>6</sub>D<sub>6</sub>): -235 (s, Sn satellites, <sup>1</sup>J<sub>117Sn/P</sub> = 322 Hz, <sup>1</sup>J<sub>119Sn/P</sub> = 337 Hz) ppm.

### 3.7.3 Preparation of Me<sub>3</sub>SiP<sub>3</sub>Nb(ODipp)<sub>3</sub>, 47

[Na(THF)<sub>3</sub>][P<sub>3</sub>Nb(ODipp)<sub>3</sub>] (1.6 g, 1.67 mmol, 1 equiv) was dissolved in benzene (50 mL) and was placed in a thick-walled glass reactor equipped with a stir bar along with Me<sub>3</sub>SiCl (1.82 g, 1.67 mmol, 1 equiv). The reactor was sealed, shaken, removed from the glove box, and placed into an oil bath preheated to 60 °C. The reaction mixture was heated for 2 h during which time a fine white precipitate formed. The reaction mixture was filtered to remove NaCl and then the volatile components of the reaction mixture were removed under reduced pressure. The resulting red-orange oil was stirred in hexane, which was subsequently removed under reduced pressure giving, again, a red-orange oil (1.30 g, 98% yield), which was shown to be pure by NMR spectroscopic analysis. <sup>1</sup>H NMR (C<sub>6</sub>D<sub>6</sub>): 0.04 (s, 9 H), 1.31 (d, 36 H, <sup>1</sup>J<sub>H/H</sub> = 6.8 Hz), 3.76 (sep, 6 H, <sup>1</sup>J<sub>H/H</sub> = 6.8 Hz),

6.99 (t, 3 H,  $^1J_{\text{H}/\text{H}} = 7.5$  Hz), 7.11 (d, 6 H,  $^1J_{\text{H}/\text{H}} = 7.5$  Hz) ppm.  $^{31}\text{P}$  NMR ( $\text{C}_6\text{D}_6$ ):  $-191$  (d, 2 P,  $^1J_{\text{P}/\text{P}} = 242$  Hz),  $-180$  (t, 1 P,  $^1J_{\text{P}/\text{P}} = 242$  Hz) ppm.

### 3.7.4 Preparation of $\text{Ph}_3\text{SiP}_3\text{Nb}(\text{ODipp})_3$ , 48

$[\text{Na}(\text{THF})_3][\text{P}_3\text{Nb}(\text{ODipp})_3]$  (600 mg, 0.627 mmol, 1 equiv) was dissolved in 25 mL of  $\text{Et}_2\text{O}$ . To this solution was added  $\text{Ph}_3\text{SiCl}$  (185 mg, 0.627 mmol, 1 equiv). The reaction mixture was allowed to stir for 48 h during which time there was no appreciable color change. The reaction mixture was filtered through a plug of Celite to remove the precipitated NaCl. The remaining solution was placed in the freezer at  $-35$  °C to induce crystallization. After 36 h, a copious orange precipitate had formed. Isolation gave 349 mg of spectroscopically pure material (349 mg, 0.36 mmol, 57% yield). Elemental Analysis calculated for  $\text{C}_{54}\text{H}_{66}\text{Nb}_1\text{O}_3\text{P}_3\text{Si}_1$ : C 66.38, H 6.81, P 9.51; Found C 67.10, H 6.75, P 9.72.  $^1\text{H}$  NMR ( $\text{C}_6\text{D}_6$ ): 1.27 (d, 36 H,  $^1J_{\text{H}/\text{H}} = 6.8$  Hz), 3.71 (sep, 6 H,  $^1J_{\text{H}/\text{H}} = 6.8$  Hz), 6.94 (t, 3 H,  $^1J_{\text{H}/\text{H}} = 7.6$  Hz), 7.06 (d, 6H,  $^1J_{\text{H}/\text{H}} = 7.6$  Hz), 7.1–7.2 (multiple overlapping resonances, 12 H), 7.65 (m, 3H) ppm.  $^{13}\text{C}\{^1\text{H}\}$  NMR ( $\text{C}_6\text{D}_6$ ): 24.6 (s), 28.0 (s), 124.2 (s), 124.4 (s), 130.7 (s), 135.1 (s), 136.2 (s), 138.6 (s), 139.2 (s), 161.2 (s) ppm.  $^{31}\text{P}\{^1\text{H}\}$  NMR ( $\text{C}_6\text{D}_6$ ):  $-192$  (d, 2 P,  $^1J_{\text{P}/\text{P}} = 238$  Hz),  $-180$  (t, 1 P,  $^1J_{\text{P}/\text{P}} = 238$  Hz) ppm.

### 3.7.5 Preparation of $\text{Ph}_3\text{CP}_3\text{Nb}(\text{ODipp})_3$ , 49

$[\text{Na}(\text{THF})_3][\text{P}_3\text{Nb}(\text{ODipp})_3]$  (324 mg, 0.338 mmol, 1 equiv) was dissolved in 15 mL of  $\text{Et}_2\text{O}$ . To this solution was added  $[\text{Ph}_3\text{C}][\text{B}(\text{C}_6\text{F}_5)_4]$  (308 mg, 0.338 mmol, 1 equiv). The reaction mixture was allowed to stir for 1.5 h during which time there was no appreciable color change. The volume of the reaction mixture was taken to 5 mL under reduced pressure and hexane (10 mL) was added. The mixture so obtained was placed in the freezer at  $-35$  °C for 30 minutes during which time a copious light-colored precipitate formed. This precipitate was removed by filtration and  $^{19}\text{F}$  NMR analysis proved it to be the  $[\text{Na}][\text{B}(\text{C}_6\text{F}_5)_4]$  byproduct. The remaining solution was returned to the freezer to induce crystallization. After 36 h a significant amount of dark orange blocks had formed. These were isolated atop a frit giving 210 mg of product (210 mg, 0.22 mmol, 65% yield). Elemental Analysis calculated for  $\text{C}_{55}\text{H}_{66}\text{Nb}_1\text{O}_3\text{P}_3$ : C 68.74, H 6.92, P 9.67; Found C 68.59, H 7.13, P 9.51.  $^1\text{H}$  NMR ( $\text{C}_6\text{D}_6$ ): 1.22 (d, 36 H,  $^1J_{\text{H}/\text{H}} = 6.8$  Hz), 3.69 (sep, 6 H,  $^1J_{\text{H}/\text{H}} = 6.8$  Hz), 6.8–7.2 (multiple overlapping resonances, 24 H) ppm.  $^{13}\text{C}\{^1\text{H}\}$  NMR ( $\text{C}_6\text{D}_6$ ): 23.9 (s), 28.0 (s), 57.6 (d,  $^1J_{\text{C}/\text{P}} = 7$  Hz), 123.8 (s), 124.0 (s), 126.6 (s), 128.6 (s), 129.9 (s), 138.1 (s), 144.4 (s), 161.3 (s) ppm.  $^{31}\text{P}\{^1\text{H}\}$  NMR ( $\text{C}_6\text{D}_6$ ):  $-170$  (d, 2 P,  $^1J_{\text{P}/\text{P}} = 256$  Hz),  $-129$  (t, 1 P,  $^1J_{\text{P}/\text{P}} = 256$  Hz) ppm.

### 3.7.6 Preparation of $\text{Cp}_2\text{ClZrP}_3\text{Nb}(\text{ODipp})_3$ , 51

$[\text{Na}(\text{THF})_3][\text{P}_3\text{Nb}(\text{ODipp})_3]$  (500 mg, 0.522 mmol) was dissolved in 30 mL of  $\text{Et}_2\text{O}$  and was chilled to thawing in the cold well. To the thawing solution of  $[\text{Na}(\text{THF})_3][\text{P}_3\text{Nb}(\text{ODipp})_3]$  was added

$\text{Cp}_2\text{ZrCl}_2$  (153 mg, 0.52 mmol) with stirring. The reaction mixture was allowed to stir for 1 h during which time it took on a red-orange color. The reaction mixture was filtered through a plug of Celite to remove the precipitated salt and was then taken to dryness under reduced pressure. The resulting residue was stirred in 20 mL of hexane and then dried again. To the resulting residue was added 25 mL of pentane and the residue was stirred for 20 minutes during which time a fine orange powder formed. The orange powder was isolated atop a frit and was washed with 10 mL of cold pentane and dried to constant mass (205 mg). The filtrate was concentrated to 10 mL and was placed in the freezer for isolation of a second crop. Overnight fine needle like crystals formed and these were isolated adding an additional 92 mg of material when dried to constant mass. (Total: 297 mg, 0.31 mmol, 59% yield). Elemental Analysis calculated for  $\text{C}_{46}\text{H}_{61}\text{ClNbO}_3\text{P}_3\text{Zr}$ : C 56.70, H 6.31, P 9.54; Found C 56.11, H 6.18, P 10.19.  $^1\text{H}$  NMR ( $\text{C}_6\text{D}_6$ ): 1.42 (d, 36 H,  $^1J_{\text{H}/\text{H}} = 6.6$  Hz), 3.93 (sep, 6 H,  $^1J_{\text{H}/\text{H}} = 6.9$  Hz), 5.53 (s, 10 H), 7.02 (t, 3H,  $^1J_{\text{H}/\text{H}} = 7.9$  Hz), 7.17 (d, 6 H,  $^1J_{\text{H}/\text{H}} = 8.0$  Hz) ppm.  $^{13}\text{C}\{^1\text{H}\}$  NMR ( $\text{C}_6\text{D}_6$ ): 24.3 (s,  $i\text{Pr}$ ), 27.5 (s,  $i\text{Pr}$ ), 114.2 (s, Cp), 123.5 (s, Ar), 124.0 (s, Ar), 138.4 (s, Ar), 160.5 (s, Ar) ppm.  $^{31}\text{P}\{^1\text{H}\}$  NMR ( $\text{C}_6\text{D}_6$ ):  $-168$  (s) ppm.

### 3.7.7 Preparation of $(\text{Ar}[^i\text{Bu}]\text{N})_3\text{TiP}_3\text{Nb}(\text{ODipp})_3$ , 50

$[\text{Na}(\text{THF})_3][\text{P}_3\text{Nb}(\text{ODipp})_3]$  (500 mg, 0.52 mmol) was dissolved in 30 mL of  $\text{Et}_2\text{O}$ . In a separate vial  $\text{ITi}(\text{N}[^i\text{Bu}]\text{Ar})_3$  (370 mg, 0.52 mmol) was dissolved in 20 mL of  $\text{Et}_2\text{O}$ . The  $[\text{Na}(\text{THF})_3][\text{P}_3\text{Nb}(\text{ODipp})_3]$  was added to the titanium solution. The reaction mixture was allowed to stir for 30 minutes during which time there was a reddening of the solution. An aliquot taken from the reaction mixture revealed incomplete consumption of the starting materials so the reaction was allowed to stir for a total of 12 h (monitoring every 3 h). During the 12 h a white precipitate formed. After the reaction was complete, the reaction mixture was filtered through a pad of Celite and the volatile components of the filtrate were removed under reduced pressure. The resulting orange residue was dissolved in 1:1 pentane: $\text{Et}_2\text{O}$  and was allowed to crystallize at  $-35$  °C. After 24 h, an orange powder formed and was isolated atop a frit, washed with 5 mL of cold pentane, and was dried to a constant mass of 424 mg (0.35 mmol, 68% yield).  $^1\text{H}$  NMR ( $\text{C}_6\text{D}_6$ ): 1.274 (s, 27 H), 1.332 (d, 36 H,  $^1J_{\text{H}/\text{H}} = 6.7$  Hz), 2.237 (s, 18 H), 3.771 (sep, 6 H,  $^1J_{\text{H}/\text{H}} = 6.7$  Hz), 6.119 (br s, 6 H), 6.914 (s, 3H), 7.009 (t, 3H,  $^1J_{\text{H}/\text{H}} = 7.5$  Hz), 7.122 (d, 6 H,  $^1J_{\text{H}/\text{H}} = 7.5$  Hz) ppm.  $^{31}\text{P}\{^1\text{H}\}$  NMR ( $\text{C}_6\text{D}_6$ ):  $-192$  (d, 2 P,  $^1J_{\text{P}/\text{P}} = 239$  Hz),  $-181$  (t, 1 P,  $^1J_{\text{P}/\text{P}} = 239$  Hz) ppm.

### 3.7.8 Monitoring the reaction between $\text{Ph}_3\text{SnP}_3\text{Nb}(\text{ODipp})_3$ and $\text{ONC}_5\text{H}_5$ in the presence of 20 equiv 1,3-cyclohexadiene

$\text{Ph}_3\text{SnP}_3\text{Nb}(\text{ODipp})_3$  was freshly prepared in diethyl ether by combining  $[\text{Na}(\text{THF})_3][\text{P}_3\text{Nb}(\text{ODipp})_3]$  (75 mg, 0.078 mmol) and  $\text{Ph}_3\text{SnCl}$  (30 mg, 0.078 mmol) and allowing them to stir for 1.5 h. The purity of the so prepared  $\text{Ph}_3\text{SnP}_3\text{Nb}(\text{ODipp})_3$  was assessed by  $^1\text{H}$  and  $^{31}\text{P}$  NMR spectroscopy prior to continuation of the experiment. The  $\text{Ph}_3\text{SnP}_3\text{Nb}(\text{ODipp})_3$  was combined with 125 mg



of 1,3-cyclohexadiene in 0.5 mL of toluene- $d_8$  and was frozen in the bottom of a sealable NMR tube. Separately  $\text{ONC}_5\text{H}_5$  was dissolved in 0.5 mL of toluene- $d_8$  and was layered atop the frozen solid  $\text{Ph}_3\text{SnP}_3\text{Nb}(\text{ODipp})_3/\text{diene}$  layer and was itself frozen. The NMR tube was removed from the glovebox and was placed in liquid nitrogen and brought to the NMR for analysis. The NMR probe was pre-cooled to  $-10\text{ }^\circ\text{C}$  and the experiment was begun upon mixing of the two thawing layers. This reaction was repeated two additional times to assess its reproducibility and the observations were the same each time. In the absence of 1,3-cyclohexadiene, the intermediate species at  $-170$  ppm is observed at  $-10\text{ }^\circ\text{C}$ . With these observations, it is likely that breakup of the pyridine-*N*-oxide adduct is the rate determining step in the reaction pathway to form  $\text{Ph}_3\text{SnP}_3(\text{C}_6\text{H}_8)$ . It would appear that when the intermediate is allowed to build up in the reaction mixture that some alternate degradation pathways are accessible leading to small amounts of impurities in the final reaction mixture. The build up of no other species that could be classified as an intermediate was observed when the tube was held at  $-10\text{ }^\circ\text{C}$ .

### 3.7.9 Preparation of $\text{Ph}_3\text{SnP}_3(\text{C}_6\text{H}_8)$ , 52: One pot procedure

$[\text{Na}(\text{THF})_3][\text{P}_3\text{Nb}(\text{ODipp})_3]$  (1.5 g, 1.57 mmol) was dissolved in 50 mL of  $\text{Et}_2\text{O}$ . To this solution was added  $\text{Ph}_3\text{SnCl}$  (604 mg, 1.57 mmol) with stirring. The reaction mixture was allowed to stir for 1 h after which time the reaction mixture was filtered through a plug of Celite into a fresh reaction flask. To the filtrate was added 1,3-cyclohexadiene (2.5 g, 31.3 mmol). With vigorous stirring, solid  $\text{ONC}_5\text{H}_5$  (149 mg, 1.57 mmol) was added. The reaction mixture was stirred for 1.5 h during which time the reaction mixture took on a golden yellow color. Following the reaction time the reaction mixture was concentrated to half the original volume under reduced pressure resulting in precipitation of an off-white powder. This powder was isolated atop a glass frit and was washed three times with 10 mL of  $\text{Et}_2\text{O}$  and dried to constant mass resulting in pure  $\text{Ph}_3\text{SnP}_3(\text{C}_6\text{H}_8)$  in 64% yield (529 mg, 1.01 mmol). X-ray quality crystals of this material were afforded by recrystallization using 1:1 toluene:THF at  $-35\text{ }^\circ\text{C}$ . Elemental Analysis calculated for  $\text{C}_{24}\text{H}_{23}\text{P}_3\text{Sn}$ : C 55.11, H 4.47, P 17.36; Found C 54.91, H 4.47, P 17.76.  $^1\text{H}$  NMR ( $\text{C}_6\text{D}_6$ ): 1.25 (m, 4 H), 2.43 (m, 2 H), 5.27 (m, 2 H), 7.18 (m, 9 H), 7.77 (m, 6 H) ppm.  $^{13}\text{C}\{^1\text{H}\}$  NMR ( $\text{C}_6\text{D}_6$ ): 22.8 (s), 29.2 (m), 118.4 (m), 128.1 (s), 129.0 (s), 129.4 (s), 137.7 (s) ppm.  $^{31}\text{P}\{^1\text{H}\}$  NMR ( $\text{C}_6\text{D}_6$ ):  $-235$  (d, 2P,  $^1J_{\text{P}/\text{P}} = 163$  Hz,  $^2J_{117/119\text{Sn}/\text{P}} = 105$  Hz),  $-321$  (t, 1 P,  $^1J_{\text{P}/\text{P}} = 163$  Hz,  $^1J_{117/119\text{Sn}/\text{P}} = 736$  Hz) ppm.  $^{119}\text{Sn}\{^1\text{H}\}$  NMR ( $\text{C}_6\text{D}_6$ ):  $-88$  ppm (dt,  $^1J_{119\text{Sn}/\text{P}} = 739$  Hz,  $^2J_{119\text{Sn}/\text{P}} = 107$  Hz).

### 3.7.10 Treatment of $\text{Ph}_3\text{SnP}_3\text{Nb}(\text{ODipp})_3$ with 1 equiv of $\text{ONC}_5\text{H}_5$ in the Absence of Added Trapping Agent

$\text{Ph}_3\text{SnP}_3\text{Nb}(\text{ODipp})_3$  (250 mg, 0.234 mmol) was dissolved in toluene (5 mL). To this reaction mixture was added solid pyridine-*N*-oxide (23 mg, 0.24 mmol). The reaction mixture was stirred for 1.5 h during which time the reaction mixture took on a golden yellow color. Following the reaction

time the reaction mixture was dried under reduced pressure. The resulting residue was stirred in 15 mL of Et<sub>2</sub>O for 20 minutes. The reaction mixture was filtered removing yellow [ONb(ODipp)<sub>3</sub>]<sub>2</sub>. The resulting solution was concentrated to 3 mL and cooled to -35 °C. After 5 h a pale precipitate formed resulting in 50 mg of solids when dried to constant mass. The phosphorus NMR spectrum of these solids is shown below, Figure 3.18. Work is now in progress to further characterize and study this interesting molecule which is tentatively assigned as [Ph<sub>3</sub>SnP<sub>3</sub>]<sub>2</sub>. Elemental Analysis calculated for C<sub>18</sub>H<sub>15</sub>Sn<sub>1</sub>P<sub>3</sub>: C 48.81, H 3.41, P 20.98; Found C 50.12, H 3.44, P 21.58.

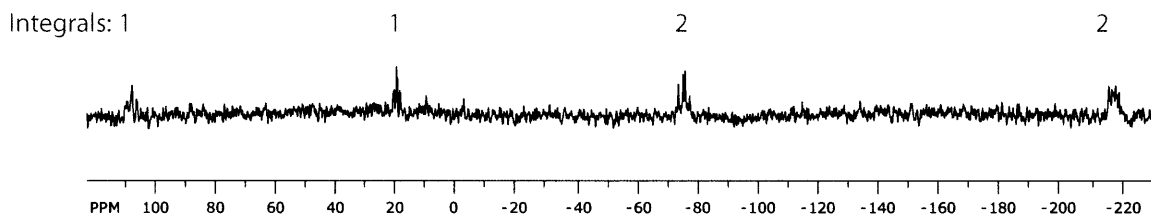


**Figure 3.18.** <sup>31</sup>P NMR spectrum of of putative [Ph<sub>3</sub>SnP<sub>3</sub>]<sub>x</sub>.

### 3.7.11 Diene Exchange with Ph<sub>3</sub>SnP<sub>3</sub>(C<sub>6</sub>H<sub>8</sub>), Generation of Ph<sub>3</sub>SnP<sub>3</sub>(C<sub>6</sub>H<sub>10</sub>), 54

Ph<sub>3</sub>SnP<sub>3</sub>(C<sub>6</sub>H<sub>8</sub>) (20 mg, 0.038 mmol) was dissolved in a 1:1 mixture of 2,3-dimethylbutadiene and THF (for solubility) and was placed into an NMR tube which was then put under vacuum and sealed. The NMR tube was heated between 75 and 80 °C and the reaction was monitored by <sup>31</sup>P NMR spectroscopy. The reaction proceeds to 50% in roughly 72 hours and is complete (with greater than 95% conversion) after 7 days. <sup>31</sup>P{<sup>1</sup>H} NMR (C<sub>6</sub>D<sub>6</sub>): -190 (d, 2P, <sup>1</sup>J<sub>P/P</sub> = 152 Hz, <sup>2</sup>J<sub>117/119</sub>Sn/P = 114 Hz), -316 (t, 1 P, <sup>1</sup>J<sub>P/P</sub> = 154 Hz, <sup>1</sup>J<sub>117/119</sub>Sn/P = 738 Hz) ppm.

### 3.7.12 Preparation of Ph<sub>3</sub>SnP<sub>3</sub>(C<sub>6</sub>H<sub>8</sub>)(C<sub>2</sub>N<sub>2</sub>(NC<sub>5</sub>H<sub>4</sub>)<sub>2</sub>), 55

Ph<sub>3</sub>SnP<sub>3</sub>(C<sub>6</sub>H<sub>8</sub>) (186 mg, 0.354 mmol) was dissolved in 30 mL of THF along with 3,6-di-2-pyridyl-tetrazine (84 mg, 0.354 mmol) producing a magenta colored solution. This reaction mixture was placed into a thick-walled glass reactor and was sealed and removed from the glove box. The mixture was placed into a pre-heated oil bath at 70 °C, and heated for 12 h during which time the reaction mixture took on a orange-yellow hue. The reaction vessel was returned to the glove box and the solution was filtered through a pad of Celite and the filtrate was taken to dryness. The resulting orange residue was dissolved in 5 mL of toluene and 15 mL of Et<sub>2</sub>O and the solution was filtered again, removing a small amount of pink solid. The resulting yellow filtrate was taken to dryness and was dissolved in Et<sub>2</sub>O and toluene (8 mL and 3 mL) and was placed in the glove box freezer at -35 °C to encourage precipitation. After 12 h, the reaction mixture was filtered through a frit and the collected solids dried to constant mass giving 121 mg (0.165 mmol, 47% yield) of yellow powder which was shown to be pure by NMR spectroscopy. Elemental Analysis calculated

for  $C_{36}H_{31}N_4Sn_1P_3$ : C 59.12, H 4.27, N 7.66, P 12.70; Found C 58.37, H 4.42, N 6.54, P 11.60.  $^1H$  NMR ( $C_6D_6$ ): 1.30 (m, 4 H), 2.59 (m, 2 H), 3.88 (m, 2 H), 6.55 (m, 2 H, py-Ar), 7.01 (m, 2 H, py-Ar), 7.15 (m, 9 H, Sn-Ar), 7.63 (m, 6 H, Sn-Ar), 8.27 (m, 2 H, py-Ar), 8.41 (m, 2 H, py-Ar) ppm.  $^{13}C\{^1H\}$  NMR ( $C_6D_6$ ): 18.90 (s), 23.50 (s), 32.04 (d,  $^1J_{C/P} = 16$  Hz), 123.26 (s), 124.75 (s), 129.25 (s), 129.82 (s), 136.53 (s), 128.06 (s), 138.27 (s), 149.28 (s), 155.63 (s), 161.32 (s) ppm.  $^{31}P\{^1H\}$  NMR ( $C_6D_6$ ): -271 (t, 1 P,  $^1J_{P/P} = 180$  Hz,  $^1J_{117/119Sn/P} = 745$  Hz), -182 (d, 2 P,  $^1J_{P/P} = 180$  Hz,  $^2J_{117/119Sn/P} = 84$  Hz) ppm.

### 3.7.13 Preparation of $P_3Rh(PPh_3)_3$ , 56

$Ph_3SnP_3(C_6H_8)$  (120 mg, 0.229 mmol) was dissolved in 7 mL of THF and the solution was frozen. Wilkinson's catalyst (212 mg, 0.23 mmol) was likewise dissolved in 7 mL of THF and the solution was frozen solid. Upon thawing, the solution of  $Ph_3SnP_3(C_6H_8)$  was added to the solution of Wilkinson's catalyst with stirring. The reaction mixture was allowed to stir at 20 °C for 2 h, after which time the reaction mixture was taken to dryness under reduced pressure. The resulting brown residue was stirred in hexane (10 mL) for 20 minutes and then was dried again under reduced pressure. The resulting brown powder was stirred vigorously in  $Et_2O$  for 30 minutes after which time it was collected by filtration as a sand-colored solid and a colorless filtrate. The colorless filtrate was taken to dryness resulting in a white powder which was a mixture of  $Ph_3SnCl$  and a small quantity of  $PPh_3$ . The sand-colored solid was dried to a constant mass of 157 mg (70% crude yield). The solids were dissolved in 2 mL of  $CH_2Cl_2$  into which  $Et_2O$  was slowly diffused at -35 °C resulting 60% yield (135 mg, 0.137 mmol) of X-ray quality crystals of  $P_3Rh(PPh_3)_3$ . Elemental Analysis calculated for  $C_{54}H_{45}P_6Rh$ : C 66.00, H 4.61, P 18.91; Found C 65.63, H 4.41, P 18.38.  $^1H$  NMR (THF- $d_8$ ): 5.14 (t, 6 H,  $^1J_{H/H} = 7$  Hz), 5.23 (br m, 6 H), 5.36 (t, 3 H,  $^1J_{H/H} = 7$  Hz) ppm.  $^{13}C\{^1H\}$  NMR (THF- $d_8$ ): 129.3 (s), 129.4 (s), 133.1 (s), 135.3 (m) ppm.  $^{31}P\{^1H\}$  NMR (THF- $d_8$ ): 34 (dq, 3 P,  $^1J_{103Rh/P} = 150$  Hz,  $^2J_{P/P} = 16$  Hz), -187 (dq, 3 P,  $^1J_{103Rh/P} = 32$  Hz,  $^2J_{P/P} = 16$  Hz) ppm. MALDI-TOF MS: 982.1004 m/z.

### 3.7.14 Reaction of $[Na(THF)_3][P_3Nb(ODipp)_3]$ with $ClRh(PPh_3)_3$ followed by $ONC_5H_5$

$[Na(THF)_3][P_3Nb(ODipp)_3]$  (40 mg, 0.042 mmol, 1 equiv) was dissolved in 1 mL of  $C_6D_6$ . To this solution was added  $ClRh(PPh_3)_3$  (39 mg, 0.042 mmol, 1 equiv) with stirring. The reaction mixture was allowed to stir for 30 minutes during which time the reaction mixture darkened to red-brown. The reaction mixture was filtered through a plug of Celite to remove the precipitated salt and was then taken for NMR analysis showing clean and quantitative formation of  $(Ph_3P)_3Rh(\mu_2:\eta^1, \eta^2-P_3)Nb(ODipp)_3$  as the only product.  $^1H$  NMR ( $C_6D_6$ ): 1.29 (d, 36 H,  $^1J_{H/H} = 6.5$  Hz), 3.89 (sep, 6 H,  $^1J_{H/H} = 6.5$  Hz), 6.86 (t, 3 H,  $^1J_{H/H} = 7.7$  Hz), 7.04 (m, 6 H), 7.14 (d, 6 H,  $^1J_{H/H} = 7.7$  Hz), 7.33 (m, 6 H), 7.39 (m, 3 H) ppm.  $^{31}P\{^1H\}$  NMR ( $C_6D_6$ ): -63 (m, 3 P), 47 (dq, 3 P,  $^1J_{103Rh/P} = 195$  Hz,  $^2J_{P/P} = 21$  Hz) ppm. At this point  $ONC_5H_5$  (5 mg, 0.042 mmol) was added to the

reaction mixture. The reaction mixture was allowed to stir for 28 h (with monitoring every 2 to 4 h) until all of the starting materials had been consumed. The final reaction mixture contained  $\text{P}_3\text{Rh}(\text{PPh}_3)_3$ , (56% spectroscopic yield) as well as  $\text{PPh}_3$ ,  $\text{OPPh}_3$ , and  $[\text{ONb}(\text{ODipp})_3]_2$ . The oxo complex  $[\text{ONb}(\text{ODipp})_3]_2$  has been previously reported in the literature.<sup>17</sup>

### 3.7.15 Preparation of solvate-free $\text{LiP}_3(\text{C}_6\text{H}_8)$ , 57

$\text{Ph}_3\text{SnP}_3(\text{C}_6\text{H}_8)$  (750 mg, 1.431 mmol) was suspended in 60 mL of  $\text{Et}_2\text{O}$  to which was added  $\text{PhLi}$  (795  $\mu\text{L}$  solution, 1.431 mmol) dropwise with stirring. The reaction mixture quickly became homogeneous and then a light-colored precipitate began to form. The reaction mixture was allowed to stir for 1 h after which time it was filtered through a glass frit, removing 290 mg of  $\text{Ph}_4\text{Sn}$ . The ethereal filtrate was taken to dryness under reduced pressure. To the resulting residue was added 30 mL of hexane which was then taken to dryness. To this final residue was added toluene (70 mL). The resulting suspension was stirred vigorously for 10 minutes and then the reaction mixture was filtered through a frit. As the filtration proceeded, a yellow precipitate was collected. When taken to dryness, this formerly yellow solid turned a dark red-black color and constituted 133 mg of material (0.74 mmol, 52% yield). The filtrate contained predominantly  $\text{Ph}_4\text{Sn}$  by NMR spectroscopy and it was not isolated. The isolated red-black material was easily dissolved in THF or pyridine to give yellow-orange solutions. Elemental Analysis calculated for  $\text{C}_6\text{H}_8\text{LiP}_3$ : C 40.03, H 4.48, P 51.62; Found C 39.12, H 4.09, P 52.27.  $^1\text{H}$  NMR (pyridine- $d_5$ ): 1.57 (m, 4 H), 2.60 (m, 2 H), 5.73 (m, 2 H) ppm.  $^{13}\text{C}\{^1\text{H}\}$  NMR (pyridine- $d_5$ ): 25.26 (s), 37.28 (m), 117.39 (s) ppm.  $^{31}\text{P}\{^1\text{H}\}$  NMR (pyridine- $d_5$ ): -216 (d, 2 P,  $^1J_{\text{P/P}} = 287$  Hz), -256 (t, 1 P,  $^1J_{\text{P/P}} = 285$  Hz) ppm.  $^7\text{Li}$  NMR (pyridine- $d_5$ ): -4.22 ppm.

### 3.7.16 Reaction of $\text{LiP}_3(\text{C}_6\text{H}_8)$ with $\text{Ph}_3\text{SnCl}$

$\text{LiP}_3(\text{C}_6\text{H}_8)$  (10 mg, 0.055 mmol) and  $\text{Ph}_3\text{SnCl}$  (21 mg, 0.055 mmol) were each separately dissolved in 1 mL of THF and the solutions were frozen in the cold well. Upon thawing, the reagents were combined forming a yellow solution. Upon warming to room temperature (with stirring), the yellow color of the reaction mixture gradually faded to colorless. After 30 minutes of stirring at room temperature, the reaction mixture was taken to dryness under reduced pressure. The resulting colorless powder was stirred in  $\text{C}_6\text{D}_6$  and then filtered through Celite and the filtrate was taken for NMR analysis.  $^1\text{H}$  NMR ( $\text{C}_6\text{D}_6$ ): 1.25 (m, 4 H), 2.43 (m, 2 H), 5.27 (m, 2 H), 7.18 (m, 9 H), 7.77 (m, 6 H) ppm.  $^{13}\text{C}\{^1\text{H}\}$  NMR ( $\text{C}_6\text{D}_6$ ): 22.8 (s), 29.2 (m), 118.4 (m), 128.1 (s), 129.0 (s), 129.4 (s), 137.7 (s) ppm.  $^{31}\text{P}$  NMR ( $\text{C}_6\text{D}_6$ ): -235 (d, 2P,  $^1J_{\text{P/P}} = 163$  Hz,  $^2J_{^{117/119}\text{Sn/P}} = 105$  Hz), -321 (t, 1 P,  $^1J_{\text{P/P}} = 163$  Hz,  $^1J_{^{117/119}\text{Sn/P}} = 736$  Hz) ppm.  $^{119}\text{Sn}$  NMR ( $\text{C}_6\text{D}_6$ ): -88 ppm (dt,  $^1J_{^{119}\text{Sn/P}} = 739$  Hz,  $^2J_{^{119}\text{Sn/P}} = 107$  Hz).

### 3.7.17 Treatment of $\text{LiP}_3(\text{C}_6\text{H}_8)$ with $[\text{HNC}_5\text{H}_5][\text{Cl}]$ , observation of $\text{HP}_3(\text{C}_6\text{H}_8)$ , 58

$\text{LiP}_3(\text{C}_6\text{H}_8)$  (10 mg, 0.055 mmol) and  $[\text{HNC}_5\text{H}_5][\text{Cl}]$  (6 mg, 0.055 mmol) were each separately dissolved in 1 mL of THF and the solutions were frozen in the cold well. Upon thawing the solutions were combined forming a yellow reaction mixture. Upon warming to room temperature (with stirring) the yellow color of the reaction mixture gradually faded to colorless. After 30 minutes of stirring at room temperature, the reaction mixture was taken to dryness under reduced pressure. The resulting colorless powder was stirred in  $\text{Et}_2\text{O}$  and then filtered through Celite and dried again. The resulting colorless residue was dissolved in  $d_5$ -pyridine and was taken for NMR analysis.  $^1\text{H}$  NMR (pyridine- $d_5$ ): -1.05 (dt,  $^1J_{\text{P}/\text{H}} = 160$  Hz,  $^2J_{\text{P}/\text{H}} = 21$  Hz, 1 H, PH), 1.05 (m, 4 H), 2.82 (m, 2 H), 5.37 (m, 2 H) ppm.  $^{31}\text{P}\{^1\text{H}\}$  NMR (pyridine- $d_5$ ): -240 (d, 2 P,  $^1J_{\text{P}/\text{P}} = 145$  Hz), -305 (t, 1 P,  $^1J_{\text{P}/\text{P}} = 145$  Hz) ppm.  $^{31}\text{P}$  NMR (pyridine- $d_5$ ): -240 (m, 2 P,  $^1J_{\text{P}-\text{P}} = 145$  Hz,  $^2J_{\text{P}/\text{H}} = 21$  Hz), -305 (m, 1 P,  $^1J_{\text{P}/\text{P}} = 145$  Hz,  $^1J_{\text{P}/\text{H}} = 160$  Hz) ppm.

### 3.7.18 Treatment of $[\text{Na}(\text{THF})_3][\text{P}_3\text{Nb}(\text{ODipp})_3]$ with $\text{HOC}_6\text{F}_5$ ; observation of $\text{P}_3\text{H}_3$ , 59

$[\text{Na}(\text{THF})_3][\text{P}_3\text{Nb}(\text{ODipp})_3]$  (233 mg, 0.244 mmol) was dissolved in 2 mL of  $\text{Et}_2\text{O}$  and was frozen solid in a Schlenk flask in the cold well. A cold solution of  $\text{HOC}_6\text{F}_5$  (269 mg, 1.46 mmol) in 1 mL of  $\text{Et}_2\text{O}$  was layered on top of the frozen  $[\text{Na}(\text{THF})_3][\text{P}_3\text{Nb}(\text{ODipp})_3]$  solution and the entire mixture was then frozen solid. The reaction vessel was sealed and allowed to warm to room temperature with stirring. After stirring for 10 minutes, the flask was removed from the glove box, and the contents were again frozen solid. The vessel was connected to a vacuum transfer bridge, which was connected to a medium walled NMR tube fitted with a 14/20 joint on the other side. The reaction mixture was allowed to warm to room temperature, and the NMR tube was placed in a liquid nitrogen bath. The volatile components of the reaction mixture were vacuum transferred to the NMR tube, leaving an oily material behind in the reaction flask. The tube was subsequently flame sealed and taken for NMR analysis. The oily contents of the reaction mixture that remained after the transfer were dissolved in  $\text{C}_6\text{D}_6$  for NMR analysis as well. NMR analysis of the volatiles showed only a small amount of  $\text{PH}_3$  present. Analysis of the non-volatile material in  $\text{C}_6\text{D}_6$  showed  $[\text{Na}(\text{THF})_3][\text{P}_3\text{Nb}(\text{ODipp})(\text{OC}_6\text{F}_5)_2]$  as the major phosphorus-containing product, but  $\text{P}_3\text{H}_3$  was also present as approximately 10% of the total material.  $^{31}\text{P}\{^1\text{H}\}$  NMR ( $\text{C}_6\text{D}_6$ ): -294 (d, 2 P,  $^1J_{\text{P}/\text{P}} = 132$  Hz), -267 (t, 1 P,  $^1J_{\text{P}/\text{P}} = 132$  Hz) ppm.  $^{31}\text{P}$  NMR ( $\text{C}_6\text{D}_6$ ): -294 (m, 2 P), -267 (m, 1 P) ppm.

### 3.7.19 X-Ray Structure Determinations

Diffraction quality crystals of  $\text{Ph}_3\text{SnP}_3(\text{C}_6\text{H}_8)$  were grown from toluene/pentane at  $-35$  °C. Crystals of  $\text{Ph}_3\text{SnP}_3(\text{C}_6\text{H}_8)(\text{C}_2\text{N}_2(\text{NC}_5\text{H}_4)_2)$  were grown by slow evaporation of a benzene solution at  $20$  °C over 1 week. Crystals of  $\text{P}_3\text{Rh}(\text{PPh}_3)_3$  were grown from an  $\text{Et}_2\text{O}/\text{CH}_2\text{Cl}_2$  solution at

–35 °C over 10 days. Crystals of [Na][Nb(OC<sub>6</sub>F<sub>5</sub>)<sub>2</sub>ODipp] were grown from a 1:1 mixture of toluene and THF at –35 °C. All crystals were mounted in hydrocarbon oil on a nylon loop or a glass fiber. Low-temperature (100 K) data were collected on a Siemens Platform three-circle diffractometer coupled to a Bruker-AXS Smart Apex CCD detector with graphite-monochromated Mo K $\alpha$  radiation ( $\lambda = 0.71073$  Å) performing  $\phi$ - and  $\omega$ -scans. A semi-empirical absorption correction was applied to the diffraction data using SADABS.<sup>42</sup> All structures were solved by direct or Patterson methods using SHELXS<sup>43,44</sup> and refined against  $F^2$  on all data by full-matrix least squares with SHELXL-97.<sup>44,45</sup> All non-hydrogen atoms were refined anisotropically. All hydrogen atoms were included in the model at geometrically calculated positions and refined using a riding model. The isotropic displacement parameters of all hydrogen atoms were fixed to 1.2 times the  $U_{eq}$  value of the atoms they are linked to (1.5 times for methyl groups). In structures where disorders were present, the disorders were refined within SHELXL with the help of rigid bond restraints as well as similarity restraints on the anisotropic displacement parameters for neighboring atoms and on 1,2- and 1,3-distances throughout the disordered components.<sup>46</sup> The relative occupancies of disordered components were refined freely within SHELXL. Further details are provided in Tables 3.3 and 3.4, on Reciprocal Net,<sup>47</sup> and in the form of cif files available from the CCDC.<sup>48</sup>

### 3.7.20 Computational Studies

All calculations were carried out using ADF 2007.01 or ADF 2008.01 from Scientific Computing and Modeling (<http://www.scm.com>) on an 8- or 32-processor Quantum Cube workstation from Parallel Quantum Solutions (<http://www.pqschem.com>).<sup>49,50</sup> In all cases, the LDA functional employed was that of Vosko, Wilk, and Nusair (VWN),<sup>51</sup> while the GGA part was handled using the functionals of Baker and Pulay (OLYP).<sup>52</sup> In addition, all calculations were carried out using the zero-order regular approximation (ZORA) for relativistic effects.<sup>53–55</sup> For phosphorus, the basis sets were quadruple- $\zeta$  with four polarization functions (QZ4P) as supplied with ADF and frozen-core approximations were not made. In all other cases, the basis sets were triple- $\zeta$  with two polarization functions (TZ2P) as supplied with ADF and again, frozen-core approximations were not made. Chemical-shielding tensors were calculated for the <sup>31</sup>P nuclei in the optimized structures by the GIAO method using the ADF package.<sup>56–59</sup> The functionals, basis sets, and relativistic approximations used were the same as those described above. The isotropic value of the absolute chemical shielding was converted to a chemical shift downfield of 85% phosphoric acid using PH<sub>3</sub> or P<sub>4</sub> as a computational reference; its computed absolute shielding value was associated with a chemical shift equal to its experimental value in the gas phase.<sup>60,61</sup> Geometries were optimized to default convergence criteria and energies are uncorrected for zero-point energies.

**Table 3.1.** Optimized atomic coordinates of P<sub>3</sub>Rh(PPh<sub>3</sub>)<sub>3</sub>.

Atom	x	y	z	Atom	x	y	z
C	1.359756	1.750389	–5.539873	C	1.427168	3.134202	–5.423078
C	0.727868	0.985648	–4.561604	C	0.864154	3.747567	–4.307885
C	–1.224370	–2.824963	–4.385540	C	–0.210662	–3.664714	–3.930125

**Table 3.1.** Optimized atomic coordinates of  $P_3Rh(PPh_3)_3$ , continued.

C	-1.381226	-1.551445	-3.846633	C	0.148753	1.589488	-3.436499
C	0.240102	2.984875	-3.327028	C	-4.276582	2.421122	-3.098057
C	4.444255	1.446724	-2.690818	C	0.647911	-3.216960	-2.932106
C	-2.915554	2.178045	-2.922484	C	5.766993	1.294175	-2.293391
C	-5.215834	1.447667	-2.775293	C	-0.536199	-1.097004	-2.823486
C	-2.458830	0.958722	-2.405731	C	0.479811	-1.947153	-2.385963
C	-4.776222	0.226420	-2.274317	C	-3.418303	-0.011493	-2.084931
C	3.408051	1.109946	-1.822369	C	6.045040	0.805872	-1.017968
C	3.669322	0.616500	-0.544821	C	-3.805636	-3.757237	-0.119167
C	-2.427885	-3.618282	-0.259720	C	5.009512	0.474907	-0.150608
C	3.552352	-3.775630	-0.152615	C	3.429925	-2.388351	-0.204597
C	-1.784564	-2.496286	0.251358	C	-4.525609	-2.771410	0.550089
C	2.765708	-4.523747	0.717155	C	2.513277	-1.715885	0.616017
C	-2.496704	-1.491155	0.916642	C	-3.879366	-1.650365	1.068553
C	-3.741791	1.655249	1.239061	C	-4.789602	2.477774	1.633617
C	1.844686	-3.870128	1.530552	C	1.715382	-2.486709	1.472345
C	-2.902010	1.047313	2.182509	C	3.091205	0.628387	2.180430
C	3.435603	1.979496	2.340961	C	-5.011516	2.731648	2.984044
C	3.414554	-0.257792	3.212392	C	4.056485	2.429786	3.499703
C	-0.991332	-0.781937	3.200787	C	-3.135412	1.308902	3.537343
C	-4.176898	2.147329	3.931288	C	-1.560557	-1.950751	3.726616
C	-0.028911	-0.115691	3.966630	C	4.042603	0.195144	4.372465
C	4.358948	1.539147	4.527393	C	-1.180786	-2.429420	4.978172
C	0.338889	-0.586205	5.223931	C	-0.235278	-1.745770	5.736140
H	1.802216	1.251379	-6.397333	H	1.918806	3.728636	-6.187794
H	-1.897053	-3.158204	-5.169734	H	0.703522	-0.088727	-4.685371
H	0.915568	4.826131	-4.190566	H	-0.090444	-4.659212	-4.351588
H	-2.169287	-0.915332	-4.231803	H	4.204073	1.834999	-3.674391
H	6.576943	1.558313	-2.968221	H	-4.596825	3.378233	-3.498601
H	-2.220916	2.950981	-3.218539	H	-6.276344	1.634201	-2.920235
H	-0.168233	3.492801	-2.465177	H	1.445352	-3.852817	-2.560683
H	2.391843	1.252563	-2.147657	H	-5.488176	-0.553643	-2.021566
H	-3.117966	-0.975779	-1.701344	H	1.148340	-1.628050	-1.602960
H	7.073782	0.682035	-0.692279	H	-4.312827	-4.625977	-0.529608
H	-1.849362	-4.369425	-0.785164	H	4.273805	-4.269114	-0.797754
H	4.054776	-1.839803	-0.897164	H	-0.715012	-2.408839	0.121702
H	-5.601108	-2.872424	0.675895	H	-3.596558	1.474899	0.185015
H	2.868442	-5.604552	0.761584	H	5.255947	0.102329	0.836343
H	-5.427851	2.923419	0.876971	H	-4.464734	-0.904967	1.591126
H	3.247819	2.689221	1.546888	H	1.218991	-4.432024	2.217289
H	0.994666	-2.011969	2.121547	H	-5.827104	3.378641	3.294879
H	3.203037	-1.314654	3.122522	H	4.311424	3.481239	3.592300
H	-2.309349	-2.499329	3.168187	H	0.437733	0.781944	3.586079
H	-2.517763	0.858277	4.302444	H	-4.337815	2.334337	4.989500
H	4.289858	-0.518213	5.153989	H	4.849440	1.889097	5.431373
H	-1.640995	-3.333758	5.363754	H	1.084683	-0.042331	5.795640
H	0.051655	-2.113343	6.717615	P	-0.658883	0.601604	-2.082231

**Table 3.1.** Optimized atomic coordinates of  $P_3Rh(PPh_3)_3$ , continued.

P	1.042617	3.332668	-0.095601	P	-1.087767	3.260994	0.221219
P	2.277538	0.127755	0.584375	P	-1.535280	-0.050545	1.579921
P	0.246548	2.906982	1.854029	Rh	0.064599	1.112467	0.204329

**Table 3.2.** Optimized atomic coordinates of  $Ph_3SnP_3$  (free triphosphirene).

Atom	x	y	z	Atom	x	y	z
C	2.802447	0.117724	-4.005220	C	1.506022	-0.396439	-3.994333
C	3.278001	0.813224	-2.892935	C	0.691269	-0.223334	-2.872278
C	-4.130379	0.102305	-1.663370	C	2.459637	0.989912	-1.775521
C	1.155630	0.469908	-1.743557	C	-2.851317	0.567136	-1.353146
C	-4.647187	-1.016723	-1.009585	C	-2.062621	-0.081173	-0.388932
C	-3.877302	-1.670889	-0.049306	C	-2.595310	-1.207022	0.257191
C	1.999577	-1.445253	1.181114	C	0.848157	-0.721402	1.529631
C	2.592445	-2.329983	2.084827	C	0.308121	-0.912577	2.812414
C	2.048024	-2.502894	3.356759	C	0.902818	-1.793773	3.718135
H	3.441604	-0.027311	-4.873507	H	1.129644	-0.942229	-4.856878
H	4.289701	1.213003	-2.892234	H	-0.310173	-0.646680	-2.885116
H	-4.724629	0.615016	-2.416675	H	-2.471562	1.440327	-1.881540
H	-5.646045	-1.375817	-1.247910	H	2.858421	1.530465	-0.918065
H	-4.272031	-2.546305	0.462367	H	2.441111	-1.334571	0.194461
H	-2.010420	-1.744368	0.999552	H	3.482363	-2.884010	1.792841
H	-0.590224	-0.382828	3.120396	H	2.514042	-3.186120	4.063417
H	0.471029	-1.925890	4.707918	P	-0.085796	3.157250	0.704301
P	-1.170598	3.267469	2.668760	P	0.846607	3.271135	2.751440
Sn	-0.050927	0.614967	0.063345				



**Table 3.3.** Crystallographic data for  $\text{Ph}_3\text{SnP}_3(\text{C}_6\text{H}_8)$  and  $\text{Ph}_3\text{SnP}_3(\text{C}_6\text{H}_8)(\text{C}_2\text{N}_2(\text{NC}_5\text{H}_4)_2)$ .

	$\text{Ph}_3\text{SnP}_3(\text{C}_6\text{H}_8)$	$\text{Ph}_3\text{SnP}_3(\text{C}_6\text{H}_8)(\text{C}_2\text{N}_2(\text{NC}_5\text{H}_4)_2)$
Empirical formula	$\text{C}_{24}\text{H}_{23}\text{P}_3\text{Sn}$	$\text{C}_{43}\text{H}_{39}\text{N}_4\text{P}_3\text{Sn}$
Formula weight ( $\text{g mol}^{-1}$ )	523.02	823.38
Temperature (K)	100(2)	100(2)
Wavelength ( $\text{\AA}$ )	0.71073	0.71073
Crystal system	Monoclinic	Triclinic
Space group	$P21/c$	$P\bar{1}$
Unit cell dimensions ( $\text{\AA}$ , $^\circ$ )	$a = 11.541(3)$ , $\alpha = 90$ $b = 16.844(4)$ , $\beta = 105.124(4)$ $c = 11.660(3)$ , $\gamma = 90$	$a = 9.5383(8)$ , $\alpha = 69.473(2)$ $b = 14.7391(13)$ , $\beta = 78.5150(10)$ $c = 16.3039(14)$ , $\gamma = 79.749(2)$
Volume ( $\text{\AA}^3$ )	2188.1(9)	2088.9(3)
Z	4	2
Density (calculated) ( $\text{Mg m}^{-3}$ )	1.588	1.309
Absorption coefficient ( $\text{mm}^{-1}$ )	1.395	0.760
$F(000)$	1048	840
Crystal size ( $\text{mm}^3$ )	$0.10 \times 0.07 \times 0.03$	$0.16 \times 0.11 \times 0.08$
Theta range for collection ( $^\circ$ )	1.83 to 28.57	1.35 to 27.37
Index ranges	$-15 \leq h \leq 15$ , $-22 \leq k \leq 22$ , $-15 \leq l \leq 15$	$-12 \leq h \leq 12$ , $-19 \leq k \leq 19$ , $-21 \leq l \leq 21$
Reflections collected	35245	39816
Independent reflections	5568 [R(int) = 0.1085]	9412 [R(int) = 0.0742]
Completeness to $\theta_{\text{max}}$ (%)	99.6	99.2
Absorption correction	Semi-empirical from equivalents	Semi-empirical from equivalents
Max. and min. transmission	0.9594 and 0.8731	0.9417 and 0.8881
Refinement method	Full-matrix least-squares on $F^2$	Full-matrix least-squares on $F^2$
Data / restraints / parameters	5568 / 0 / 253	9412 / 57 / 498
Goodness-of-fit <sup>a</sup>	1.016	1.026
Final R indices [ $I > 2\sigma(I)$ ] <sup>b</sup> [ $I > 2\sigma(I)$ ]	$R_1 = 0.0459$ , $wR_2 = 0.0819$	$R_1 = 0.0498$ , $wR_2 = 0.1086$
R indices (all data) <sup>b</sup>	$R_1 = 0.0808$ , $wR_2 = 0.0957$	$R_1 = 0.0806$ , $wR_2 = 0.1236$
Largest diff. peak and hole ( $\text{e \AA}^{-3}$ )	0.894 and $-0.677$	0.932 and $-0.681$

a

$$\text{GooF} = \left[ \frac{\sum [w(F_o^2 - F_c^2)^2]}{(n-p)} \right]^{\frac{1}{2}}$$

b

$$R_1 = \frac{\sum ||F_o| - |F_c||}{\sum |F_o|}; wR_2 = \left[ \frac{\sum [w(F_o^2 - F_c^2)^2]}{\sum [w(F_o^2)^2]} \right]^{\frac{1}{2}}; w = \frac{1}{\sigma^2(F_o^2) + (aP)^2 + bP}; P = \frac{2F_c^2 + \max(F_o^2, 0)}{3}$$

**Table 3.4.** Crystallographic data for P<sub>3</sub>Rh(PPh<sub>3</sub>)<sub>3</sub> and [Na][P<sub>3</sub>Nb(ODipp)(OC<sub>6</sub>F<sub>5</sub>)<sub>2</sub>].

	P <sub>3</sub> Rh(PPh <sub>3</sub> ) <sub>3</sub>	[Na(12c4) <sub>2</sub> ][P <sub>3</sub> Nb(ODipp)(OC <sub>6</sub> F <sub>5</sub> ) <sub>2</sub> ]
Empirical formula	C <sub>56</sub> H <sub>49</sub> Cl <sub>14</sub> P <sub>6</sub> Rh	C <sub>58</sub> H <sub>73</sub> F <sub>10</sub> NaNbO <sub>12</sub> P <sub>3</sub>
Formula weight (g mol <sup>-1</sup> )	1152.48	1360.97
Temperature (K)	100(2)	100(2)
Wavelength (Å)	0.71073	0.71073
Crystal system	Triclinic	Monoclinic
Space group	<i>P</i> $\bar{1}$	<i>C</i> 2/ <i>c</i>
Unit cell dimensions (Å, °)	<i>a</i> = 13.2449(11), $\alpha$ = 74.1830(10) <i>b</i> = 14.2057(11), $\beta$ = 84.6070(10) <i>c</i> = 15.1004(12), $\gamma$ = 82.2850(10)	<i>a</i> = 22.304(2), $\alpha$ = 90 <i>b</i> = 18.657(2), $\beta$ = 108.484(2) <i>c</i> = 31.657(4), $\gamma$ = 90
Volume (Å <sup>3</sup> )	2704.0(4)	12494(2)
<i>Z</i>	2	8
Density (calculated) (Mg m <sup>-3</sup> )	1.416	1.447
Absorption coefficient (mm <sup>-1</sup> )	0.728	0.365
<i>F</i> (000)	1176	5832
Crystal size (mm <sup>3</sup> )	0.40 × 0.25 × 0.10	0.10 × 0.10 × 0.10
Theta range for collection (°)	1.40 to 29.64	1.36 to 27.47
Index ranges	-18 ≤ <i>h</i> ≤ 18, -19 ≤ <i>k</i> ≤ 19, -20 ≤ <i>l</i> ≤ 20	-28 ≤ <i>h</i> ≤ 28, -24 ≤ <i>k</i> ≤ 24, -40 ≤ <i>l</i> ≤ 41
Reflections collected	59044	120631
Independent reflections	15065 [R(int) = 0.0495]	14287 [R(int) = 0.0725]
Completeness to $\theta_{\max}$ (%)	98.7	99.9
Absorption correction	Semi-empirical from equivalents	Semi-empirical from equivalents
Max. and min. transmission	0.9308 and 0.7596	0.9645 and 0.9645
Refinement method	Full-matrix least-squares on <i>F</i> <sup>2</sup>	Full-matrix least-squares on <i>F</i> <sup>2</sup>
Data / restraints / parameters	15065 / 203 / 647	14287 / 0 / 768
Goodness-of-fit <sup>a</sup>	1.029	1.035
Final <i>R</i> indices [ <i>I</i> > 2σ( <i>I</i> ) <sup>b</sup> [ <i>I</i> > 2σ( <i>I</i> )]	<i>R</i> <sub>1</sub> = 0.0479, <i>wR</i> <sub>2</sub> = 0.1122	<i>R</i> <sub>1</sub> = 0.0530, <i>wR</i> <sub>2</sub> = 0.1222
<i>R</i> indices (all data) <sup>b</sup>	<i>R</i> <sub>1</sub> = 0.0659, <i>wR</i> <sub>2</sub> = 0.1239	<i>R</i> <sub>1</sub> = 0.0823, <i>wR</i> <sub>2</sub> = 0.1419
Largest diff. peak and hole (e Å <sup>-3</sup> )	1.395 and -1.597	1.322 and -0.734

<sup>a</sup>

$$\text{Goof} = \left[ \frac{\sum [w(F_o^2 - F_c^2)^2]}{(n-p)} \right]^{\frac{1}{2}}$$

<sup>b</sup>

$$R_1 = \frac{\sum ||F_o| - |F_c||}{\sum |F_o|}; wR_2 = \left[ \frac{\sum [w(F_o^2 - F_c^2)^2]}{\sum [w(F_o^2)^2]} \right]^{\frac{1}{2}}; w = \frac{1}{\sigma^2(F_o^2) + (aP)^2 + bP}; P = \frac{2F_c^2 + \max(F_o^2, 0)}{3}$$

### 3.8 REFERENCES

- [1] Capozzi, G.; Chiti, L.; Di Vaira, M.; Peruzzini, M.; Stoppioni, P. *J. Chem. Soc., Chem. Commun.* **1986**, 1799–1800.
- [2] Weber, L. *Chem. Rev.* **1992**, *92*, 1839–1906.
- [3] Chatt, J.; Hitchcock, P. B.; Pidcock, A.; Warrens, C. P.; Dixon, D. A. *J. Chem. Soc., Chem. Commun.* **1982**, 932–933.
- [4] Dillon, K.; Mathey, F.; Nixon, J. *Phosphorus: The Carbon Copy: From Organophosphorus to Phospha-organic Chemistry*, 1st ed.; Wiley: West Sussex, 1998.
- [5] Schäfer, H.; Binder, D.; Fenske, D. *Angew. Chem., Int. Ed. Engl.* **1985**, *24*, 522–524.
- [6] Schäfer, H.; Binder, D. *Z. Anorg. Allg. Chem.* **1988**, *560*, 65–79.
- [7] Regitz, M.; Scherer, O. J. *Multiple Bonds and Low Coordination in Phosphorus Chemistry*; Thieme: Stuttgart, 1990.
- [8] Phillips, I. G.; Ball, R.; Cavell, R. G. *Inorg. Chem.* **1992**, *31*, 1633–1641.
- [9] Barbaro, P.; Ienco, A.; Mealli, C.; Peruzzini, M.; Scherer, O. J.; Schmitt, G.; Vizza, F.; Wolmershäuser, G. *Chem. Eur. J.* **2003**, *9*, 5195–5210.
- [10] Yakhvarov, D.; Babaro, P.; Gonsalvi, L.; Carpio, S. M.; Midollini, S.; Orlandini, A.; Peruzzini, M.; Sinyashin, O.; Zanobini, F. *Angew. Chem., Int. Ed.* **2006**, *45*, 4182–4185.
- [11] Piro, N. A.; Cummins, C. C. *Angew. Chem. Int. Ed.* **2009**, *48*, 934–938.
- [12] Piro, N. A.; Cummins, C. C. *J. Am. Chem. Soc.* **2008**, *130*, 9524–9535.
- [13] Piro, N. A.; Cummins, C. C. *J. Am. Chem. Soc.* **2008**, *130*, 9524–9535.
- [14] Kocak, F. S.; Zavalij, P. Y.; Lam, Y. F.; Eichhorn, B. W. *Chem. Commun.* **2009**, 4197–4199.
- [15] Whitesides, T. H.; Lichtenberger, D. L.; Budnik, R. A. *Inorg. Chem.* **1975**, *14*, 68–73.
- [16] Cotton, F. A. *Inorg. Chem.* **2002**, *41*, 643–658.
- [17] Visciglio, V. M.; Fanwick, P. E.; Rothwell, I. P. *Acta. Cryst. C.* **1994**, *50*, 900–902.
- [18] Masuda, J. D.; Schoeller, W. W.; Donnadiou, B.; Bertrand, G. *J. Am. Chem. Soc.* **2007**, *129*, 14180–14181.
- [19] Masuda, J. D.; Schoeller, W. W.; Donnadiou, B.; Bertrand, G. *Angew. Chem. Int. Ed.* **2007**, *46*, 7052–7055.
- [20] Masuda, J. D.; Schoeller, W. W.; Donnadiou, B.; Bertrand, G. *J. Am. Chem. Soc.* **2007**, *129*, 14180–14181.
- [21] Cotton, F. A.; Wilkinson, G.; Murillo, C. A.; Bochmann, M. *Advanced Inorganic Chemistry*, 6th ed.; John Wiley & Sons, 1999.
- [22] Weber, L. *Chem. Rev.* **1992**, *92*, 1839–1906.
- [23] Carboni, R. A.; Lindsey, R. V. *J. Am. Chem. Soc.* **1959**, *81*, 4342.
- [24] Shegal, I. L.; Matveeva, N. A.; Shegal, L. M. *Uspekhi Khim.* **1980**, *49*, 637.
- [25] Schumann, H.; Von Deuster, E. *J. Organomet. Chem.* **1972**, *40*, C27–C28.
- [26] Schumann, H. *Angew. Chem. Int. Ed.* **1969**, *8*, 937–950.
- [27] Weber, L. *Chemical Reviews* **1992**, *92*, 1839–1906.
- [28] DiVaira, M.; Sacconi, L. *Angew. Chem. Int. Ed.* **1982**, *21*, 330–342.
- [29] Mendiola, D. J.; Cummins, C. C. *Angew. Chem. Int. Ed.* **1998**, *37*, 945–947.
- [30] Bennett, M. A.; Bhargava, S. K.; Ke, M.; Willis, A. C. *J. Chem. Soc., Dalton Trans.* **2000**, 3537–3545.
- [31] Miluykov, V.; Bezkishko, I.; Krivolapov, D.; Kataeva, O.; Sinyashin, O.; Hey-Hawkins, E.; Parameswaran, A.; Krupskaya, Y.; Kataev, V.; Klingeler, R.; Büchner, B. *Organometallics* **2010**, *29*, 1339–1342.
- [32] Vizi-Orosz, A. *J. Organomet. Chem.* **1976**, *111*, 61–64.
- [33] Baudler, M. *Angew. Chem. Int. Ed.* **1987**, *26*, 419–441.
- [34] Baudler, M.; Standeke, H.; Kemper, M. *Z. Anorg. Allg. Chem.* **1972**, *388*, 125.
- [35] Baudler, M.; Hahn, J.; Clef, E. *Z. Naturforsch.* **1984**, *39b*, 438.

- [36] Wiberg, N.; Worner, A.; Lerner, H. W.; Karaghiosoff, K.; Fenske, D.; Baum, G.; Dransfeld, P.; Schleyer, R. *Eur. J. Inorg. Chem.* **1998**, *1*, 833.
- [37] Sun, Y.; Metz, M. V.; Stern, C. L.; Marks, T. J. *Organometallics* **2000**, *19*, 1625–1627.
- [38] Pangborn, A. B.; Giardello, M. A.; Grubbs, R. H.; Rosen, R. K.; Timmers, F. J. *Organometallics* **1996**, *15*, 1518–1520.
- [39] Johnson, A. R.; Wanandi, P. W.; Cummins, C. C.; Davis, W. M. *Organometallics* **1994**, *13*, 2907–2909.
- [40] Peters, J. C.; Ph.D. thesis; Massachusetts Institute of Technology, Chemistry; Cambridge; 1998.
- [41] Agarwal, P.; Piro, N. A.; Meyer, K.; Müller, P.; Cummins, C. C. *Angew. Chem., Int. Ed.* **2007**, *46*, 3111–3114.
- [42] Sheldrick, G. M.; (*SHELXTL*); 2005–2008.
- [43] Sheldrick, G. M. *Acta Crystallogr., Sect. A: Fundam. Crystallogr.* **1990**, *46*, 467–473.
- [44] Sheldrick, G. M. *Acta Crystallogr., Sect. A: Fundam. Crystallogr.* **2008**, *64*, 112–122.
- [45] Sheldrick, G. M.; (*SHELXL*)-97: *Program for crystal structure determination*; 1997.
- [46] Müller, P.; Herbst-Irmer, R.; Spek, A. L.; Schneider, T. R.; Sawaya, M. R. *Crystal Structure Refinement: A Crystallographer's Guide to (SHELXL)*; Müller, P., Ed.; IUCr Texts on Crystallography; Oxford University Press: Oxford, 2006.
- [47] The Reciprocal Net Site Network is a distributed database for crystallographic information, supported by the National Science Digital Library, and is run by participating crystallography labs across the world. Crystallographic data for complexes in this chapter are available under the identification codes listed in Tables 1.11 and 1.12 from the MIT Reciprocal Net site. <http://reciprocal.mit.edu/recipnet>.
- [48] These data can be obtained free of charge from The Cambridge Crystallographic Data Centre via [http://www.ccdc.cam.ac.uk/data\\_request/cif](http://www.ccdc.cam.ac.uk/data_request/cif).
- [49] te Velde, G.; Bickelhaupt, F. M.; Baerends, E. J.; Fonseca Guerra, C.; van Gisbergen, S. J. A.; Snijders, J. G.; Ziegler, T. *J. Comput. Chem.* **2001**, *22*, 931–967.
- [50] Fonseca Guerra, C.; Snijders, J. G.; te Velde, G.; Baerends, E. J. *Theo. Chem. Acc.* **1998**, *99*, 391–403.
- [51] Vosko, S. H.; Wilk, L.; Nusair, M. *Can. J. Phys.* **1980**, *58*, 1200–1211.
- [52] Baker, J.; Pulay, P. *J. Chem. Phys.* **2002**, *117*, 1441–1449.
- [53] van Lenthe, E.; Baerends, E. J.; Snijders, J. G. *J. Chem. Phys.* **1993**, *99*, 4597–4610.
- [54] van Lenthe, E.; Baerends, E. J.; Snijders, J. G. *J. Chem. Phys.* **1994**, *101*, 9783–9792.
- [55] van Lenthe, E.; Ehlers, A.; Baerends, E. J. *J. Chem. Phys.* **1999**, *110*, 8943–8953.
- [56] Schreckenbach, G.; Ziegler, T. *J. Phys. Chem.* **1995**, *99*, 606–611.
- [57] Schreckenbach, G.; Ziegler, T. *Int. J. Quantum Chem.* **1997**, *61*, 899–918.
- [58] Wolff, S. K.; Ziegler, T. *J. Chem. Phys.* **1998**, *109*, 895–905.
- [59] Wolff, S. K.; Ziegler, T.; van Lenthe, E.; Baerends, E. J. *J. Chem. Phys.* **1999**, *110*, 7689–7698.
- [60] van Wüllen, C. *Phys. Chem. Chem. Phys.* **2000**, *2*, 2137–2144.
- [61] Johnson, M. J. A.; Odom, A. L.; Cummins, C. C. *Chem. Commun.* **1997**, 1523–1524.

# APPENDIX A

## Radical Synthesis of Trisubstituted Phosphines from P<sub>4</sub>

### Contents

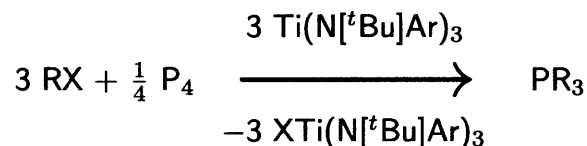
<b>A.1 Introduction</b> . . . . .	<b>205</b>
A.1.1 Halogen Atom Abstraction and Ti(N[ <sup>t</sup> Bu]Ar) <sub>3</sub> . . . . .	206
<b>A.2 Synthesis of Homoleptic Trisubstituted Phosphines</b> . . . . .	<b>207</b>
<b>A.3 Synthesis of Heteroleptic Trisubstituted Phosphines</b> . . . . .	<b>209</b>
A.3.1 Targeting Intermediate Structures in the Degradation of the P <sub>4</sub> Tetrahedron	209
<b>A.4 Conclusions</b> . . . . .	<b>209</b>
<b>A.5 Experimental Details</b> . . . . .	<b>210</b>
A.5.1 General Experimental Considerations . . . . .	210
A.5.2 Representative Protocol for Reaction Between Ti(N[ <sup>t</sup> Bu]Ar) <sub>3</sub> , RX (RX = PhBr, MesBr, DmpI, CyBr, Me <sub>3</sub> SiI, and Ph <sub>3</sub> SnCl), and P <sub>4</sub> : Synthesis of PPh <sub>3</sub> . . . . .	211
A.5.3 Characterization Data . . . . .	212
A.5.4 Screening other Potential Halogen Atom Abstractors for PR <sub>3</sub> Synthesis . . . . .	215
<b>A.6 References</b> . . . . .	<b>217</b>

### A.1 INTRODUCTION

It is known that P<sub>4</sub>, white phosphorus, has excellent properties as a trap for carbon-centered radicals in solution and under the mild conditions that are typical for organic synthesis.<sup>1</sup> The most

---

Reproduced in part with permission from:  
Cossairt, B. M.; Cummins, C. C. *New J. Chem.* **2010**, DOI: 10.1039/c0nj00124d, Copyright 2010 RSC Publishing.



**Scheme A.1.** Idealized scheme for the synthesis of phosphines from P<sub>4</sub> using Ti(N<sup>t</sup>Bu)Ar<sub>3</sub>.

prominent example of this was the demonstration that phosphonic acids may be prepared from corresponding carboxylic acids by way of *O*-acyl derivatives of *N*-hydroxy-2-thiopyridone (Barton PTOC esters).<sup>2</sup> The latter provide carbon centered radicals in an oxygen-initiated chain reaction, and these are consumed upon combination with P<sub>4</sub> as the critical P–C bond-forming event; upon oxidative workup, any remaining P–P bonds are cleaved and the phosphonic acid RP(O)(OH)<sub>2</sub> is the end product.<sup>2</sup> It is also known that P–P bonds *other* than those in P<sub>4</sub> may serve as traps for organic radicals. This has been shown by Sato et al. in a scheme for radical phosphination of organic halides wherein ArX serves as a source of Ar· which in turn attacks Ph<sub>2</sub>P–PPh<sub>2</sub>, yielding ArPPh<sub>2</sub>.<sup>3</sup>

Such a vision for phosphine synthesis *via* homolytic substitution at a phosphorus center has also been developed by Vaillard et al., who employed Me<sub>3</sub>MPPH<sub>2</sub> (M = Si or Sn) as the phosphorus substrate and RX as the carbon-radical source, together with a radical initiator, to produce RP(O)Ph<sub>2</sub> efficiently after an oxidative workup.<sup>4</sup> For our part, we have previously shown that the three-coordinate titanium(III) complex Ti(N<sup>t</sup>Bu)Ar<sub>3</sub> (Ar = 3,5-Me<sub>2</sub>C<sub>6</sub>H<sub>3</sub>), is a potent halogen-atom abstractor, capable of abstracting X· (X = Cl, Br, or I) from various donor molecules at room temperature or below, in aprotic organic media. With the present work, we sought to develop a high-yield synthesis of phosphines PR<sub>3</sub> from 3 RX and 0.25 P<sub>4</sub>, using Ti(N<sup>t</sup>Bu)Ar<sub>3</sub> as a halogen atom sink, Scheme A.1. Success in this arena would demonstrate that it is possible to synthesize valuable tertiary phosphanes PR<sub>3</sub> through direct functionalization and complete consumption of P<sub>4</sub> by a radical mechanism.

### A.1.1 Halogen Atom Abstraction and Ti(N<sup>t</sup>Bu)Ar<sub>3</sub>

In the course of a prior study of radical cleavage of symmetrical 1,4-dicarbonyl compounds by Ti(N<sup>t</sup>Bu)Ar<sub>3</sub>, the propensity of Ti(N<sup>t</sup>Bu)Ar<sub>3</sub> to abstract X· from halobenzenes was examined.<sup>5</sup> This study revealed that treatment of Ti(N<sup>t</sup>Bu)Ar<sub>3</sub> with a stoichiometric amount of PhBr or PhI effected conversion to XTi(N<sup>t</sup>Bu)Ar<sub>3</sub> rapidly at room temperature, while conversion to ClTi(N<sup>t</sup>Bu)Ar<sub>3</sub> upon treatment with PhCl was considerably slower. Dissolution of Ti(N<sup>t</sup>Bu)Ar<sub>3</sub> in *neat* chlorobenzene and stirring overnight at room temperature did effect complete conversion to ClTi(N<sup>t</sup>Bu)Ar<sub>3</sub>, however. A radical cyclization experiment using *o*-bromophenyl allyl ether as the RX substrate for Ti(N<sup>t</sup>Bu)Ar<sub>3</sub> has been used to substantiate the hypothesis that phenyl radicals are indeed generated upon halogen atom abstraction from PhX by Ti(N<sup>t</sup>Bu)Ar<sub>3</sub>.<sup>5,6</sup> On

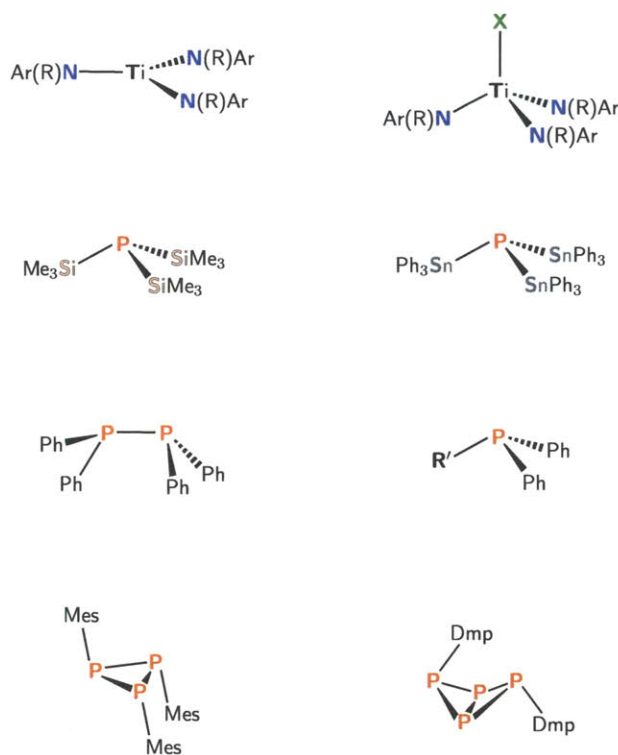


**Figure A.1.**  $\text{Ti}(\text{N}[\text{ᵗBu}]\text{Ar})_3$  together with various  $\text{P}_4$ -derived phosphanes and polyphosphorus products.  $\text{R} = \text{ᵗBu}$ ;  $\text{X} = \text{Cl, Br, I}$ ;  $\text{R}' = \text{Ph, Mes, Cy, Ph}_3\text{Sn}$ ;  $\text{Mes} = 2,4,6\text{-Me}_3\text{C}_6\text{H}_2$ ;  $\text{Dmp} = 2,6\text{-Mes}_2\text{C}_6\text{H}_3$ .

the basis of this information, together with the knowledge from recent independent work that  $\text{Ti}(\text{N}[\text{ᵗBu}]\text{Ar})_3$  engages in negligible reaction with  $\text{P}_4$ ,<sup>7</sup> we realized that  $\text{Ti}(\text{N}[\text{ᵗBu}]\text{Ar})_3$  is an unusual reducing agent in that it could be selective for  $\text{RX}$  activation in the presence of  $\text{P}_4$ . This is unusual because most chemical reducing agents capable of  $\text{X}\cdot$  abstraction from  $\text{RX}$  would not be expected to be selective for this reactivity channel in the presence of  $\text{P}_4$ . An aspect of this type of special selectivity in reactions of  $\text{Ti}(\text{N}[\text{ᵗBu}]\text{Ar})_3$  has been demonstrated previously wherein 7-chloronorborene was treated with a 1:1 mixture of  $\text{Ti}(\text{N}[\text{ᵗBu}]\text{Ar})_3$  and  $\text{Mo}(\text{N}[\text{ᵗBu}]\text{Ar})_3$ ; in this instance  $\text{Ti}(\text{N}[\text{ᵗBu}]\text{Ar})_3$  was entirely selective for Cl-atom abstraction giving  $\text{ClTi}(\text{N}[\text{ᵗBu}]\text{Ar})_3$ , while exhibiting no propensity for trapping the 7-norborenyl radical which was seen to interact selectively with the molybdenum complex.<sup>8</sup> In addition, typical one-electron reducing agents that might be used for effecting  $\text{X}\cdot$  abstraction, e.g.  $\text{ClCo}(\text{PPh}_3)_3$ ,  $\text{SmI}_2$ ,<sup>9</sup> or  $\text{Cp}_2\text{TiCl}$ , simply give no reaction with a substrate such as  $\text{PhBr}$ .

## A.2 SYNTHESIS OF HOMOLEPTIC TRISUBSTITUTED PHOSPHINES

In a first reaction targeted at generating  $\text{PPh}_3$ , it was found that addition of 3 equiv of  $\text{PhBr}$  by microsyringe to a 0.04 M solution of 0.25 equiv  $\text{P}_4$  containing 3 equiv of  $\text{Ti}(\text{N}[\text{ᵗBu}]\text{Ar})_3$  in benzene results in immediate formation of a bright orange solution containing  $\text{BrTi}(\text{N}[\text{ᵗBu}]\text{Ar})_3$ ,  $\text{PPh}_3$  (71%

**Table A.1.** Synthesis of  $\text{PR}_3$  from  $n(\text{RX} + \text{Ti}(\text{N}[\text{tBu}]\text{Ar})_3)$  and 0.25  $\text{P}_4$  in benzene solvent at 20 °C.

Entry	$n^a$	R	X	$\delta \text{PR}_3^b$	% yield <sup>c</sup>
1	3	Ph	Br	-4.9	71
2	3.75	Ph	Br	-4.9	82
3	5	Ph	Br	-4.9	95
4	3	Ph	I	-4.9	65
5	3	Ph	Cl	n/a	0
6	3	$\text{Ph}_3\text{Sn}$	Cl	-325 <sup>d</sup>	96
7	3	$\text{Me}_3\text{Si}$	I	-252	97
8	3	Cy	Br	10.5	64
9	3.75	Cy	Br	10.5	77
10	5	Cy	Br	10.5	95

<sup>a</sup> Number of equivalents per phosphorus atom.

<sup>b</sup>  $^{31}\text{P}$  NMR chemical shift for the  $\text{PR}_3$  product referenced to external 85%  $\text{H}_3\text{PO}_4$ .

<sup>c</sup> Phosphorus-based yield of  $\text{PR}_3$  as determined by  $^{31}\text{P}$  NMR spectroscopy *via* integration with respect to an internal standard using a single-pulse experiment.

<sup>d</sup>  $^1J_{^{119}\text{Sn}/\text{P}} = 442 \text{ Hz}$ ,  $^1J_{^{117}\text{Sn}/\text{P}} = 425 \text{ Hz}$ .

of the P-containing product), and  $\text{P}_2\text{Ph}_4$  (29% of the P-containing product, Table A.1).  $\text{P}_2\text{Ph}_4$  is one of the four possible stable intermediates en route to complete  $\text{P}_4$  degradation by  $\text{P}_4$  to give  $\text{PPh}_3$  and is present in this stoichiometric treatment because the trapping of the highly reactive phenyl radicals is not completely efficient in this system. In order to convert the full equivalent of  $\text{P}_4$  to  $\text{PPh}_3$ , 5 equiv of  $\text{PhBr}$  and  $\text{Ti}(\text{N}[\text{tBu}]\text{Ar})_3$  are used, giving 95% conversion and an isolated yield of 72% (Table A.1). We could also selectively target  $\text{P}_2\text{Ph}_4$  by treatment of 0.25 equiv of 0.04 M  $\text{P}_4$  in benzene with 2 equiv of  $\text{Ti}(\text{N}[\text{tBu}]\text{Ar})_3$  followed by 2 equiv of  $\text{PhBr}$ , which gives  $\text{P}_2\text{Ph}_4$  in 80% yield with small amounts of  $\text{PPh}_3$  and  $\text{P}_4\text{Ph}_4$  being observed as well. Evidence for the intermediacy of  $\text{P}_2\text{Ph}_4$  along the reaction pathway was provided by the use of  $\text{P}_2\text{Ph}_4$  itself as a starting material for  $\text{PPh}_3$  synthesis. Also, it was found that  $\text{PhI}$  can be used in place of  $\text{PhBr}$  with similar results, however  $\text{PhCl}$  does not lead to any  $\text{PPh}_3$  or  $\text{P}_2\text{Ph}_4$  formation as  $\text{Ti}(\text{N}[\text{tBu}]\text{Ar})_3$  reacts very slowly with  $\text{PhCl}$  under these conditions.<sup>5</sup>

This synthesis of phosphines from  $\text{P}_4$  and a burst of radicals was found not to be limited to aryl substituents. Treatment of a 0.04 M solution of 0.25 equiv  $\text{P}_4$  with 5 equiv of  $\text{Ti}(\text{N}[\text{tBu}]\text{Ar})_3$  and 5 equiv of  $\text{CyBr}$  results in formation of  $\text{PCy}_3$  as the exclusive P-containing product (Table A.1). The use of less than 5 equiv of  $\text{CyBr}$  resulted in mixtures of  $\text{P}_2\text{Cy}_4$  and  $\text{PCy}_3$ , much like what was seen for  $\text{PhBr}$ . When the radicals produced were longer lived, it was possible to obtain stoichiometric conversion of  $\text{P}_4$  to the trisubstituted phosphine. For instance, treatment of a 0.04 M solution of 0.25 equiv  $\text{P}_4$  with 3 equiv of  $\text{Ti}(\text{N}[\text{tBu}]\text{Ar})_3$  and 3 equiv of  $\text{Me}_3\text{SiI}$  or  $\text{Ph}_3\text{SnCl}$  results in clean



and quantitative formation of the known phosphines  $P(\text{SiMe}_3)_3$  or  $P(\text{SnPh}_3)_3$ , respectively, as the sole products (Table A.1, Figure A.1).<sup>10,11</sup> The  $P(\text{SiMe}_3)_3$  produced here is easily separated from the reaction coproducts by vacuum transfer from the crude reaction mixture in 86% yield, while the highly crystalline  $P(\text{SnPh}_3)_3$  can be isolated in 75% yield.

### A.3 SYNTHESIS OF HETEROLEPTIC TRISUBSTITUTED PHOSPHINES

The ability of  $P_4$  to act as a radical trap in combination with the work of Sato and coworkers on the radical phosphination of aryl halides suggests that P–P bonds, generally, may be competent radical traps.<sup>3</sup> This was found to be the case using our radical method, opening up the potential for the synthesis of asymmetric phosphines. Treatment of 0.5 equiv of  $P_2\text{Ph}_4$  with 1 equiv of PhBr, MesBr, CyBr, or  $\text{Ph}_3\text{SnCl}$  and 1 equiv of  $\text{Ti}(\text{N}[\text{tBu}]\text{Ar})_3$  quantitatively produced 1 equiv of  $\text{PPh}_3$  ( $\delta$  4.9 ppm),  $\text{P}(\text{Ph}_2)\text{Mes}$  ( $\delta$  16.0 ppm),<sup>12</sup>  $\text{P}(\text{Ph}_2)\text{Cy}$  ( $\delta$  3.4 ppm),<sup>13</sup> or  $\text{P}(\text{Ph}_2)\text{SnPh}_3$  ( $\delta$  56.2 ppm,  $^1J_{119\text{Sn}/\text{P}} = 715$  Hz,  $^1J_{117\text{Sn}/\text{P}} = 682$  Hz),<sup>14</sup> respectively (Figure A.1). This striking attribute of P–P single bond chemistry has great potential for further synthetic development.

#### A.3.1 Targeting Intermediate Structures in the Degradation of the $P_4$ Tetrahedron

Based on our hypothesis that the radical-degradation of the  $P_4$  tetrahedron occurs in a stepwise manner, we thought that it might be possible to target intermediate structures by tuning the steric properties of the RX substrate. It was found that treatment of 0.25 equiv of 0.04 M  $P_4$  in benzene with 1.5 equiv  $\text{Ti}(\text{N}[\text{tBu}]\text{Ar})_3$  followed by 1.5 equiv of MesBr gives  $\text{P}_3\text{Mes}_3$  as the major product and small amounts of  $\text{P}_2\text{Mes}_4$ .<sup>15–17</sup>  $\text{P}_3\text{Mes}_3$  could be isolated from the reaction mixture in 61% yield. Increasing the steric pressure further, we found that treatment of 0.25 equiv of 0.04 M  $P_4$  with 1.5 equiv of  $\text{Ti}(\text{N}[\text{tBu}]\text{Ar})_3$  and 1.5 equiv of DmpI (Dmp = 2,6-Mes<sub>2</sub>C<sub>6</sub>H<sub>3</sub>) gives *cis,trans*-Dmp $P_4$ Dmp as the exclusive product and isolated in 78% yield.<sup>18</sup> This latter reaction represents a facile approach for the synthesis of novel substituted tetraphosphabicyclobutane molecules directly from  $P_4$  in a single step. Many of the previously reported syntheses of stable tetraphosphabicyclobutanes involve coupling of two substituted diphosphanes,<sup>19</sup> or activation of  $P_4$  by some highly designed substrate.<sup>18,20–22</sup> The present synthesis is unique in that a large number of sterically hindered aryl or alkyl halides could be employed in a general synthesis.

### A.4 CONCLUSIONS

In terms of recycling the titanium byproducts from these syntheses, it is worth noting that X- $\text{Ti}(\text{N}[\text{tBu}]\text{Ar})_3$  (X = I, Br, Cl) are cleanly reduced back to  $\text{Ti}(\text{N}[\text{tBu}]\text{Ar})_3$  by reduction with Na/Hg amalgam.<sup>23,24</sup> This ability to easily recycle the titanium byproducts generates a closed cycle for the synthesis of trisubstituted phosphines from  $P_4$ . One might begin to contemplate a catalytic cycle

using this system, however, the reduction of  $\text{XTi}(\text{N}[\text{tBu}]\text{Ar})_3$  is slow and  $\text{P}_4$  is itself susceptible to reduction to  $\text{Na}_3\text{P}$  by  $\text{Na}/\text{Hg}$  amalgam under such conditions. As such, other halogen atom abstractors are currently being screened as potential entry points into the catalytic generation of trisubstituted phosphines from  $\text{P}_4$  by this radical trapping method.

The present day synthesis of organophosphorus compounds is a multistep process in which  $\text{P}_4$  is first chlorinated to generate  $\text{PCl}_3$ .<sup>25</sup>  $\text{PCl}_3$  is then functionalized *via* salt elimination reactions with appropriate Grignard or organolithium reagents, or with the organohalide and a harsh reducing agent.<sup>25</sup> For example, the industrial method for triphenylphosphine preparation is based on the high temperature reaction of chlorobenzene with phosphorus trichloride in the presence of molten sodium.<sup>1</sup> Manufacturers of organophosphorus compounds have recognized that the direct functionalization of white phosphorus is one of the major challenges in this field.<sup>1,26</sup> New studies are needed to work out alternative direct routes to organophosphorus compounds avoiding chlorination of white phosphorus. Strides have been made with regard to the electrosynthesis of trisubstituted phosphines directly from  $\text{P}_4$ ,<sup>27</sup> but facile solution methods are lacking. It is our hope that this work will inspire a renewed interest in the use of P–P bonds as efficient radical traps and will eventually lead to a robust catalytic system for the synthesis of organophosphorus compounds directly from white phosphorus. Meanwhile, the syntheses reported herein represent novel methodologies for the direct functionalization of  $\text{P}_4$  and will themselves be the subject of further investigation.

## A.5 EXPERIMENTAL DETAILS

### A.5.1 General Experimental Considerations

All manipulations were performed in a Vacuum Atmospheres model MO-40M glovebox under an inert atmosphere of purified  $\text{N}_2$ . All solvents were obtained anhydrous and oxygen-free by bubble degassing ( $\text{N}_2$ ) and purification using a Glass Contours Solvent Purification System built by SG Water. Deuterated solvents were purchased from Cambridge Isotope Labs. Benzene- $d_6$  was degassed and stored over molecular sieves for at least 2 d prior to use. Celite 435 (EM Science) were dried by heating above  $200\text{ }^\circ\text{C}$  under a dynamic vacuum for at least 24 h prior to use.  $\text{Ti}(\text{N}[\text{tBu}]\text{Ar})_3$  ( $\text{Ar} = 3,5\text{-Me}_2\text{C}_6\text{H}_3$ ),<sup>28</sup>  $\text{V}(\text{N}[\text{Np}]\text{Ar})_3$  ( $\text{Np} = \text{CH}_2\text{tBu}$ ) (*vide infra*),<sup>29</sup>  $\text{Cp}^*\text{Sm}$ ,<sup>30</sup> and  $\text{Cp}_2\text{TiCl}$ <sup>31</sup> were prepared by literature methods. All other reagents were purchased from Aldrich chemical company and were used without further purification. All glassware was oven-dried at temperatures greater than  $170\text{ }^\circ\text{C}$  prior to use. NMR spectra were obtained on Varian Inova 500 instruments equipped with Oxford Instruments superconducting magnets and referenced to residual  $\text{C}_6\text{H}_5\text{D}$  ( $^1\text{H} = 7.16\text{ ppm}$ ,  $^{13}\text{C} = 128.06\text{ ppm}$ ).  $^{31}\text{P}$  NMR spectra were referenced externally to 85%  $\text{H}_3\text{PO}_4$  (0 ppm). GC-MS data were collected using an Agilent 6890N network GC system with an Agilent 5973 Network mass selective detector and an RTX-1 column from Restek.

### A.5.2 Representative Protocol for Reaction Between $\text{Ti}(\text{N}^t\text{BuAr})_3$ , RX (RX = PhBr, MesBr, DmpI, CyBr, $\text{Me}_3\text{SiI}$ , and $\text{Ph}_3\text{SnCl}$ ), and $\text{P}_4$ : Synthesis of $\text{PPh}_3$

$\text{Ti}(\text{N}^t\text{BuAr})_3$  (279 mg, 0.484 mmol) was added to a 0.04 M solution of  $\text{P}_4$  in benzene (5 mg total  $\text{P}_4$ , 0.040 mmol). PhBr (76 mg, 0.484 mmol) was then added to the reaction mixture at room temperature by microliter syringe. Over the course of about a minute, the originally green reaction mixture took on a bright orange color. The reaction mixture was analyzed by  $^1\text{H}$ ,  $^{13}\text{C}$ , and  $^{31}\text{P}$  NMR spectroscopies. Using  $\text{OPPh}_3$  (26 ppm) as an internal standard, a single pulse  $^{31}\text{P}$  NMR experiment showed 71% conversion to  $\text{PPh}_3$  (s,  $-4.9$  ppm) with the balance made up by  $\text{P}_2\text{Ph}_4$  ( $-14$  ppm). GC-MS analysis confirmed that assignment. A solvent screening (benzene, toluene, THF,  $\text{Et}_2\text{O}$ , *n*-hexane) and concentration screening (0.01 M  $\text{P}_4$ , 0.02 M  $\text{P}_4$ , 0.03 M  $\text{P}_4$ , 0.04 M  $\text{P}_4$ , and 0.05 M  $\text{P}_4$ ) indicated these conditions as optimal for conversion of 0.25 equiv  $\text{P}_4$  to 1 equiv  $\text{PPh}_3$  using 3 equiv  $\text{Ti}(\text{N}^t\text{BuAr})_3$  and 3 equiv PhBr.

In order to convert all of the  $\text{P}_4$  to  $\text{PPh}_3$ , the reaction was repeated using a 0.04 M solution of  $\text{P}_4$  (5 mg total  $\text{P}_4$ , 0.040 mmol, 0.25 equiv), 5 equiv (465 mg, 0.807 mmol) of  $\text{Ti}(\text{N}^t\text{BuAr})_3$  and 5 equiv (126 mg, 0.807 mmol) of  $\text{BrC}_6\text{H}_5$ . Again, over the course of a minute, the originally green reaction mixture took on a bright orange color. The reaction mixture was analyzed by  $^1\text{H}$ ,  $^{13}\text{C}$ , and  $^{31}\text{P}$  NMR spectroscopies. Using  $\text{OPPh}_3$  (26 ppm) as an internal standard, a single pulse  $^{31}\text{P}$  NMR experiment showed 98% conversion to  $\text{PPh}_3$  (s,  $-4.9$  ppm). GC-MS analysis confirmed that assignment. A screening of reaction stoichiometry showed 5 equiv of  $\text{Ti}(\text{N}^t\text{BuAr})_3$  and 5 equiv  $\text{BrC}_6\text{H}_5$  was necessary for the complete conversion of  $\text{P}_4$  to  $\text{PPh}_3$ ; when fewer equivalents were used, small amounts of  $\text{P}_2\text{Ph}_4$  were still observed. When the optimized conditions are scaled up 10-fold,  $\text{PPh}_3$  was isolated by repeated crystallizations at  $-35$  °C in  $\text{Et}_2\text{O}$  in 72% yield (304 mg).

These optimized conditions of 0.04 M  $\text{P}_4$  (0.25 equiv), benzene, and 5 equiv of RX/ $\text{Ti}(\text{N}^t\text{BuAr})_3$  are effective for both  $\text{PPh}_3$  and  $\text{PCy}_3$  syntheses. For  $\text{P}(\text{SiMe}_3)_3$  and  $\text{P}(\text{SnPh}_3)_3$  the same conditions are used but with only 3 equiv (stoichiometric) RX/ $\text{Ti}(\text{N}^t\text{BuAr})_3$ . Starting with 50 mg of  $\text{P}_4$ ,  $\text{P}(\text{SiMe}_3)_3$  was isolated by vacuum transfer in 86% yield (348 mg as a solution in benzene) and  $\text{P}(\text{SnPh}_3)_3$  was isolated in 75% yield (1.30 g) by repeated recrystallization from  $\text{Et}_2\text{O}$ . For the synthesis of  $\text{P}_3\text{Mes}_3$  and *cis,trans*- $\text{DmpP}_4\text{Dmp}$ , the same conditions are used but with only 1.5 equiv of RX/ $\text{Ti}(\text{N}^t\text{BuAr})_3$ .  $\text{P}_3\text{Mes}_3$  was isolated by repeated crystallization from  $\text{Et}_2\text{O}$  in 61% yield starting with 50 mg of  $\text{P}_4$ . *cis,trans*- $\text{DmpP}_4\text{Dmp}$  was isolated by repeated crystallization from  $\text{Et}_2\text{O}$  in 78% yield starting with 50 mg of  $\text{P}_4$ .

In using  $\text{P}_2\text{Ph}_4$  as the starting material for  $\text{PPh}_3$  synthesis, the same reaction protocol and conditions can be used. Treatment of a 0.04 M solution of  $\text{P}_2\text{Ph}_4$  (5 mg, 0.014 mmol, 0.5 equiv) with  $\text{Ti}(\text{N}^t\text{BuAr})_3$  (93 mg, 0.16 mmol, 1 equiv) followed by BrPh (60 mg, 0.16 mmol, 1 equiv) resulted in a rapid color change from green to orange upon stirring. The reaction mixture was analyzed by  $^1\text{H}$ ,  $^{13}\text{C}$ , and  $^{31}\text{P}$  NMR spectroscopies. Using  $\text{OPPh}_3$  (26 ppm) as an internal standard, a single pulse  $^{31}\text{P}$  NMR experiment showed 97% conversion to  $\text{PPh}_3$  (s,  $-4.9$  ppm). Similar results were found when 0.5 equiv  $\text{P}_2\text{Ph}_4$  was treated with 1 equiv of MesBr, CyBr, or  $\text{Ph}_3\text{SnCl}$ , which produced

1 equiv of P(Ph<sub>2</sub>)Mes (−16.0 ppm), P(Ph<sub>2</sub>)Cy (−3.4 ppm), or P(Ph<sub>2</sub>)SnPh<sub>3</sub> (−56.2 ppm, <sup>1</sup>J<sub>119Sn/P</sub> = 715 Hz, <sup>1</sup>J<sub>117Sn/P</sub> = 682 Hz), respectively, each in greater than 95% spectroscopic yield.

### A.5.3 Characterization Data

#### **PPh<sub>3</sub>**

<sup>31</sup>P{<sup>1</sup>H} NMR (202 MHz, C<sub>6</sub>D<sub>6</sub>, 20 °C): δ = −4.9 ppm (s, 1P). GC-MS = 262 m/z.

#### **P<sub>2</sub>Ph<sub>4</sub>**

<sup>31</sup>P{<sup>1</sup>H} NMR (202 MHz, C<sub>6</sub>D<sub>6</sub>, 20 °C): δ = −14.4 ppm (s, 1P). GC-MS = 370 m/z.

#### **PCy<sub>3</sub>**

<sup>31</sup>P{<sup>1</sup>H} NMR (202 MHz, C<sub>6</sub>D<sub>6</sub>, 20 °C): δ = 10.5 ppm (s, 1P). GC-MS = 280 m/z.

#### **P(Ph<sub>2</sub>)Mes**

<sup>31</sup>P{<sup>1</sup>H} NMR (202 MHz, C<sub>6</sub>D<sub>6</sub>, 20 °C): δ = −16.0 ppm (s, 1P). GC-MS = 304 m/z.

#### **P(Ph<sub>2</sub>)Cy**

<sup>31</sup>P{<sup>1</sup>H} NMR (202 MHz, C<sub>6</sub>D<sub>6</sub>, 20 °C): δ = −3.4 ppm (s, 1P). GC-MS = 268 m/z.

#### **P(Ph)<sub>2</sub>SnPh<sub>3</sub>**

<sup>31</sup>P{<sup>1</sup>H} NMR (202 MHz, C<sub>6</sub>D<sub>6</sub>, 20 °C): δ = −56.2 ppm (s, 1P, <sup>1</sup>J<sub>119Sn/P</sub> = 715 Hz, <sup>1</sup>J<sub>117Sn/P</sub> = 682 Hz).

#### **P(SiMe<sub>3</sub>)<sub>3</sub>**

<sup>1</sup>H NMR (500 MHz, C<sub>6</sub>D<sub>6</sub>, 20 °C): δ = 0.27 ppm (d, <sup>3</sup>J<sub>P/H</sub> = 4 Hz, 27H, SiMe<sub>3</sub>); <sup>31</sup>P{<sup>1</sup>H} NMR (202 MHz, C<sub>6</sub>D<sub>6</sub>, 20 °C): δ = −251.9 ppm.

#### **P(SnPh<sub>3</sub>)<sub>3</sub>**

<sup>31</sup>P{<sup>1</sup>H} NMR (202 MHz, C<sub>6</sub>D<sub>6</sub>, 20 °C): δ = −324.7 ppm (<sup>1</sup>J<sub>119Sn/P</sub> = 442 Hz, <sup>1</sup>J<sub>117Sn/P</sub> = 425 Hz).

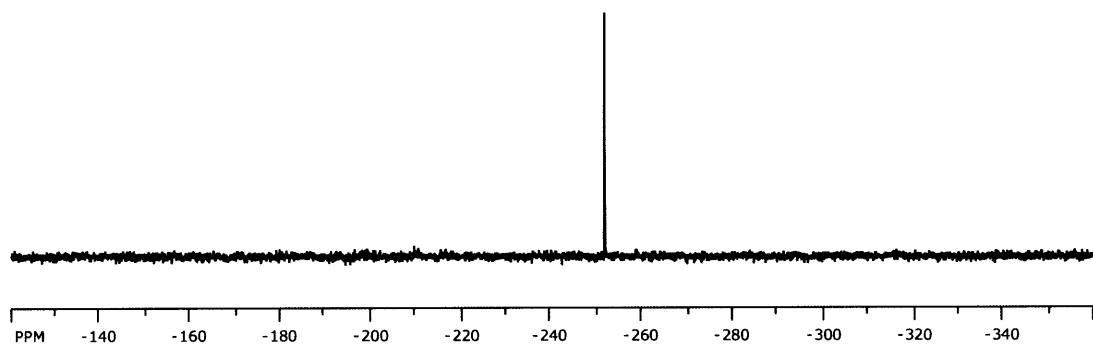


**Figure A.2.**  $^{31}\text{P}\{^1\text{H}\}$  NMR spectrum of  $\text{P}(\text{SiMe}_3)_3$ .

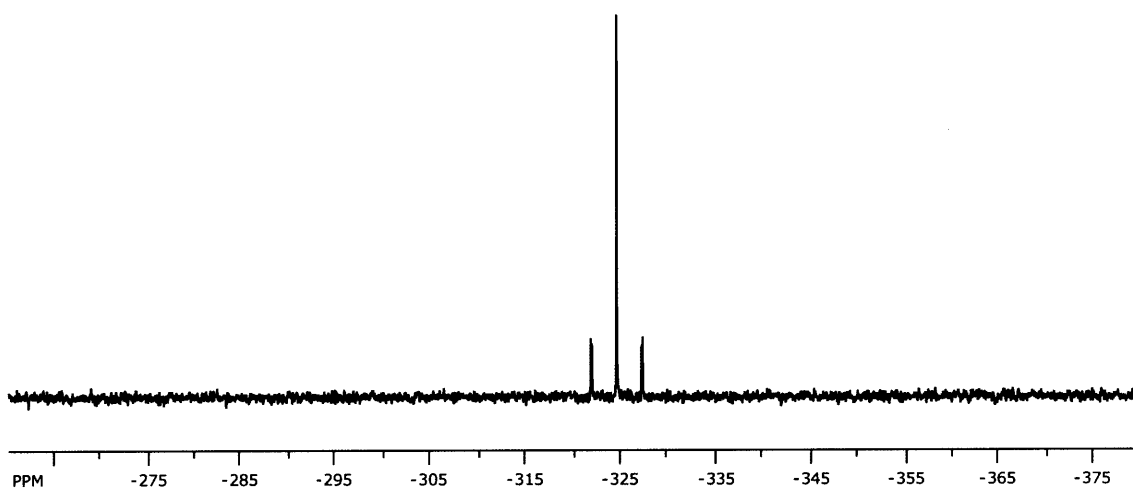


**Figure A.3.**  $^{31}\text{P}\{^1\text{H}\}$  NMR spectrum of  $\text{P}(\text{SnPh}_3)_3$ .

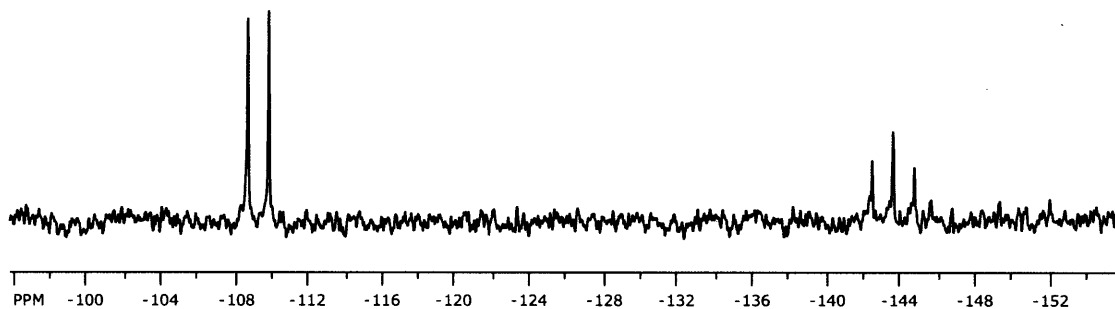


Figure A.4.  $^{31}\text{P}\{^1\text{H}\}$  NMR spectrum of  $\text{P}_3\text{Mes}_3$ .

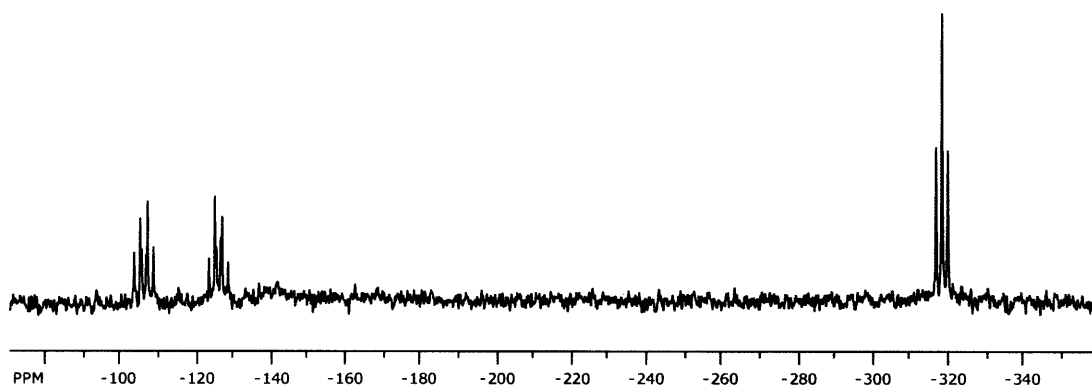


Figure A.5.  $^{31}\text{P}\{^1\text{H}\}$  NMR spectrum of *cis,trans*-DmpP<sub>4</sub>Dmp.

### $\text{P}_3\text{Mes}_3$

$^1\text{H}$  NMR (500 MHz,  $\text{C}_6\text{D}_6$ , 20 °C):  $\delta$  = 1.92 (s, 6 H, *p*-CH<sub>3</sub> of *cis*-oriented 2,4,6-Me<sub>3</sub>C<sub>6</sub>H<sub>2</sub>), 2.07 (s, 3 H, *p*-CH<sub>3</sub>, of *trans*-oriented 2,4,6-Me<sub>3</sub>C<sub>6</sub>H<sub>2</sub>), 2.49 (s, 12 H, *o*-CH<sub>3</sub> of *cis*-oriented 2,4,6-Me<sub>3</sub>C<sub>6</sub>H<sub>2</sub>), 2.79 (s, 6 H, *o*-CH<sub>3</sub> of *trans*-oriented 2,4,6-Me<sub>3</sub>C<sub>6</sub>H<sub>2</sub> group), 6.5 (s, 4 H, *m*-H of *cis*-oriented 2,4,6-Me<sub>3</sub>C<sub>6</sub>H<sub>2</sub> groups), 6.69 (s, 2 H, *m*-H of *trans*-oriented 2,4,6-Me<sub>3</sub>C<sub>6</sub>H<sub>2</sub> group).  $^{31}\text{P}\{^1\text{H}\}$  NMR (202 MHz,  $\text{C}_6\text{D}_6$ , 20 °C):  $\delta$  = -109.3 (d, 2 P,  $^1J_{\text{P/P}} = 185$  Hz), -143.8 (t, 1 P,  $^1J_{\text{P/P}} = 185$  Hz).

### *cis,trans*-DmpP<sub>4</sub>Dmp

$^1\text{H}$  NMR (500 MHz,  $\text{C}_6\text{D}_6$ , 20 °C):  $\delta$  = 2.216 (s, 12 H, *o*-CH<sub>3</sub>), 2.222 (s, 12 H, *o*-CH<sub>3</sub>), 2.303 (s, 6 H, *p*-CH<sub>3</sub>), 2.335 (s, 6 H, *p*-CH<sub>3</sub>), 6.8–7.2 (multiple overlapping signals, 14 H);  $^{31}\text{P}\{^1\text{H}\}$  NMR (202 MHz,  $\text{C}_6\text{D}_6$ , 20 °C):  $\delta$  = -104 ppm (apparent q, 1 P,  $^1J_{\text{P/P}} = 193$  Hz), -123 ppm (apparent q, 1 P,  $^1J_{\text{P/P}} = 191$  Hz), -318 ppm (t, 2 P,  $^1J_{\text{P/P}} = 190$  Hz).

**CITi(N<sup>t</sup>Bu)Ar)<sub>3</sub>**

<sup>1</sup>H NMR (500 MHz, C<sub>6</sub>D<sub>6</sub>, 20 °C): δ = 1.3973 (s, 27 H, <sup>t</sup>Bu), 2.2103 (s, 18 H, Ar-Me), 6.3219 (br s, 6 H, *m*-Ar), 6.7259 (s, 3 H, *p*-Ar) ppm.

**BrTi(N<sup>t</sup>Bu)Ar)<sub>3</sub>**

<sup>1</sup>H NMR (500 MHz, C<sub>6</sub>D<sub>6</sub>, 20 °C): δ = 1.3772 (s, 27 H, <sup>t</sup>Bu), 2.2285 (s, 18 H, Ar-Me), 6.6045 (br s, 6 H, *m*-Ar), 6.7379 (s, 3 H, *p*-Ar) ppm.

**ITi(N<sup>t</sup>Bu)Ar)<sub>3</sub>**

<sup>1</sup>H NMR (500 MHz, C<sub>6</sub>D<sub>6</sub>, 20 °C): δ = 1.3789 (s, 27 H, <sup>t</sup>Bu), 2.2530 (s, 18 H, Ar-Me), 6.8146 (s, 6 H, *m*-Ar), 6.9121 (s, 3 H, *p*-Ar) ppm.

**A.5.4 Screening other Potential Halogen Atom Abstractors for PR<sub>3</sub> Synthesis**

Using the same protocol as outlined above for the generation of PPh<sub>3</sub> and PCy<sub>3</sub>, other halogen atom abstractors were tested for competency. The first experiments performed here were with 12 equiv of reagent (halogen atom abstractors include: SmI<sub>2</sub>, Fe<sup>0</sup> at 100 °C, Zn<sup>0</sup> at 100 °C, Cp<sub>2</sub>TiCl, ClCo(PPh<sub>3</sub>)<sub>3</sub>, Cp\*<sub>2</sub>Sm, CrCl<sub>2</sub>, and V(N[Np]Ar)<sub>3</sub>) with 1 equiv of P<sub>4</sub> to ensure that no reaction takes place. All reactions were carried out at 20 °C except for the reactions with Fe and Zn, which were carried out at 100 °C. All experiments were analyzed by <sup>31</sup>P NMR spectroscopy.

Following the control runs with P<sub>4</sub> only, the reactions with the two different RBr sources (PhBr, CyBr) were carried out as follows: For SmI<sub>2</sub>, ClCo(PPh<sub>3</sub>)<sub>3</sub>, and Cp\*<sub>2</sub>Sm, 12 equiv of reagent were combined with 3.7 mg of P<sub>4</sub> as a stock solution in benzene. For ClCo(PPh<sub>3</sub>)<sub>3</sub>, 1 additional mL of benzene was added and for the Cp\*<sub>2</sub>Sm and SmI<sub>2</sub> reactions, THF was used as the solvent. Upon mixing, 12 equiv of the RBr source was added. The reaction mixtures were allowed to stir for 5 h during which time no observable change took place for the SmX<sub>2</sub> reactions (Cp\*<sub>2</sub>Sm reacts directly with P<sub>4</sub> and that product does not react further with RX), however the ClCo(PPh<sub>3</sub>)<sub>3</sub> reaction mixture darkened from light green to a dark green-brown. Following the reaction time the <sup>31</sup>P NMR spectra of all samples were obtained. It is of note that SmI<sub>2</sub> is known to be competent for abstracting halogen atoms from aryl iodides and aryl bromides, however in these cases HMPA is necessary as an additive to produce SmI<sub>2</sub> with maximum reducing power. It is therefore quite conceivable that using SmI<sub>2</sub> in a mixture of HMPA/THF would allow for a synthesis of trisubstituted phosphines from P<sub>4</sub>. As a first test of this possibility, 5 mg of P<sub>4</sub> (0.04 mmol) were combined with SmI<sub>2</sub> (4.46 g of 0.1 M solution in THF, 0.484 mmol, 12 equiv) and HMPA (867 mg, 4.84 mmol, 120 equiv). When the P<sub>4</sub> had fully dissolved, PhI (54 μL, 0.484 mmol, 12 equiv) was added to the reaction mixture. No immediate color change was observed. Over the next 17 h the PhI was consumed and SmI<sub>3</sub> was formed, but no PPh<sub>3</sub> was generated during the process. It is possible that other RX

**Table A.2.** Attempt to generate PR<sub>3</sub> from P<sub>4</sub> using other halogen atom abstractors.

Reagent	Rxn P <sub>4</sub> ?	PPh <sub>3</sub> ?	Rxn BrPh?	PCy <sub>3</sub> ?	Rxn BrCy?
Ti(N[ <sup>t</sup> Bu]Ar) <sub>3</sub>	weak eq.	yes	yes	yes	yes
SmI <sub>2</sub>	no	no	no	no	no
Fe <sup>0</sup>	no	no	no	no	no
Zn <sup>0</sup>	no	no	no	no	no
Cp <sub>2</sub> TiCl	no	no	no	no	no
ClCo(PPh <sub>3</sub> ) <sub>3</sub>	yes	no	no	no	no
Cp* <sub>2</sub> Sm	yes	no	no	no	no
CrCl <sub>2</sub>	no	no	no	no	no
V(N[Np]Ar) <sub>3</sub>	no	no	no	yes	yes

**Table A.3.** Effect of stoichiometry on reaction of V(N[Np]Ar)<sub>3</sub> with P<sub>4</sub> and CyBr.

Equiv CyBr and V(N[Np]Ar) <sub>3</sub>	[P <sub>4</sub> ]	Yield PCy <sub>3</sub>	PCy <sub>3</sub> :P <sub>2</sub> Cy <sub>4</sub>
12	0.02 M	40%	2.5:1
15	0.02 M	61%	3.2:1
15	0.04 M	75%	5:1
20	0.04 M	90%	10.2:1

substrates might be more amenable here. For Fe powder, Zn dust, and CrCl<sub>2</sub>, 12 equiv of reagent were placed in thick walled tubes along with 3.7 mg of P<sub>4</sub> and 12 equiv of RBr in THF. The reaction mixtures were refluxed for 5 h with stirring during which time no consumption of the respective metals was observed. After the reaction time had elapsed, the solutions were taken for <sup>31</sup>P NMR analysis. Cp<sub>2</sub>TiCl was first prepared by treatment of 89 mg of Cp<sub>2</sub>TiCl<sub>2</sub> with 30 mg of Zn (1.2 equiv) in benzene. The bright red reaction mixtures were allowed to stir for 1.5 h during which time the color slowly progressed to bright emerald-turquoise green. Following the reaction time, 3.7 mg of P<sub>4</sub> was added followed by 12 equiv of RBr. The reaction mixtures were allowed to stir 4 h during which time there was no observable color change. Following the reaction time the reaction mixtures were assessed by <sup>31</sup>P NMR spectroscopy. The results of all experiments are summarized in Table A.2 above (along with the Ti(N[<sup>t</sup>Bu]Ar)<sub>3</sub> results).



## A.6 REFERENCES

- [1] Engel, R. *Synthesis of Carbon Phosphorus Bonds*, 2nd ed.; CRC Press: Boca Raton, 2004.
- [2] Barton, D. H. R.; Zhu, J. *J. Am. Chem. Soc.* **1993**, *115*, 2071–2072.
- [3] Sato, A.; Yorimitsu, H.; Oshima, K. *J. Am. Chem. Soc.* **2006**, *128*, 4240–4241.
- [4] Vaillard, S.; Mck-Lichtenfeld, C.; Grimme, S.; Studer, A. *Angew. Chem. Int. Ed.* **2007**, *46*, 6533–6536.
- [5] Agapie, T.; Diaconescu, P. L.; Mindiola, D. J.; Cummins, C. C. *Organometallics* **2002**, *21*, 1329–1340.
- [6] Curran, D. P.; Tottleben, M. J. *J. Am. Chem. Soc.* **1992**, *114*, 6050–6058.
- [7] Cossairt, B. M.; Cummins, C. C. *J. Am. Chem. Soc.* **2009**, *131*, 15501–15511.
- [8] Agapie, T.; Diaconescu, P. L.; Cummins, C. C. *J. Am. Chem. Soc.* **2002**, *124*, 2412–2413.
- [9] It has been well documented that  $\text{SmI}_2$  is capable of slowly reducing aryl halides in the presence of HMPA, however the slow rate of this transformation did not allow for a radical-synthesis of trisubstituted phosphines.
- [10] Karsch, H. H.; Bienlein, F.; Rupprich, T.; Uhlig, F.; Herrmann, E.; Scheer, M. *Phosphorus, Antimony, Arsenic, and Bismuth*; Karsch, H. H., Ed.; Verlag, 1996; pp 58–64.
- [11] Engelhardt, V. G. *Z. Anorg. Allg. Chem.* **1972**, *387*, 52–60.
- [12] Blount, J. F.; Camp, D.; Hart, R. D.; Healy, P. C.; Skelton, B. W.; White, A. H. *Austr. J. Chem.* **1994**, *47*, 1631–1639.
- [13] Grim, S. O.; McFarlan, W. *Nature* **1965**, *208*, 995–996.
- [14] Engelhardt, G.; Reich, P.; Schumann, H. *Z. Nat. B* **1967**, *22*, 352–353.
- [15] Frenzel, C.; Hey-Hawkins, E. *Phosphorus, Sulfur, Silicon Relat. Elem.* **1998**, *143*, 1–17.
- [16] Li, X.; Lei, D.; Chiang, M. Y.; Gaspar, P. P. *J. Am. Chem. Soc.* **1992**, *114*, 8526–8531.
- [17] Li, X.; Weissman, S. I.; Lin, T.-S.; Gaspar, P. P.; Cowley, A. H.; Smirnov, A. I. *J. Am. Chem. Soc.* **1994**, *116*, 7899–7900.
- [18] Fox, A. R.; Wight, R. J.; Rivard, E.; Power, P. P. *Angew. Chem. Int. Ed.* **2005**, *44*, 7729–7733.
- [19] Niecke, E.; Rger, R.; Krebs, B. *Angew. Chem. Int. Ed.* **1982**, *21*, 544–545.
- [20] Power, M. B.; Barron, A. R. *Angew. Chem. Int. Ed.* **1991**, *30*, 1353–1354.
- [21] Bezombes, J. P.; Hitchcock, P. B.; Lappert, M. F.; Nycz, J. E. *Dalton Trans.* **2004**, 499–501.
- [22] Scherer, O. J.; Hilt, T.; Wolmershäuser *Organometallics* **1998**, *17*, 4110–4112.
- [23] Peters, J. C.; Ph.D. thesis; Massachusetts Institute of Technology, Chemistry; Cambridge; 1998.
- [24] Wanandi, P. W.; Davis, W. M.; Cummins, C. C.; Russell, M. A.; Wilcox, D. E. *J. Am. Chem. Soc.* **1995**, *117*, 2110–2111.
- [25] Emsley, J. *The 13th Element: The Sordid Tale of Murder, Fire, and Phosphorus*; John Wiley & Sons, Inc.: New York, 2000.
- [26] Emsley, J.; Hall, D. *The Chemistry of Phosphorus: Environmental, Organic, Inorganic, Biochemical, and Spectroscopic Aspects*; Harper and Row: London, 1976.
- [27] Budnikova, Y. H.; Yakhvarov, D. G.; Sinyashin, O. G. *J. Organomet. Chem.* **2005**, *690*, 2416–2425.
- [28] Peters, J. C.; Johnson, A. R.; Odom, A. L.; Wanandi, P. W.; Davis, W. M.; Cummins, C. C. *J. Am. Chem. Soc.* **1996**, *118*, 10175–10188.
- [29] Agarwal, P.; Piro, N. A.; Meyer, K.; Müller, P.; Cummins, C. C. *Angew. Chem., Int. Ed.* **2007**, *46*, 3111–3114.
- [30] Berg, D.; Burns, C.; Andersen, R.; Zalkin, A. *Organometallics* **1989**, *8*, 1865–1870.
- [31] Spencer, R.; Schwartz, J. *J. Org. Chem.* **1997**, *62*, 4204–4205.



## Acknowledgments

The four years that have passed while I pursued my PhD research were made not only possible, but enjoyable by a number of important people. Firstly, I would like to thank Kit. Never a week went by when Kit didn't come down to 6-332 to make sure I was having fun with my molecules. That constant reminder that exploratory chemistry is an adventure was greatly appreciated and made coming into work on Saturday morning something I wanted to do, not just something I should do; a more supportive mentor does not exist. Furthermore, Kit always welcomed me into his office to discuss ideas and to provide helpful suggestions on all aspects of the chemistry I chose to pursue.

Secondly, I would like to thank my parents who were always there on the other end of the phone line to listen and ask, "Oooh. What color is it?" and "Did you get crystals?"... their excitement at something they could barely grasp kept me motivated to keep reaching further. My parents have supported me in all of my crazy endeavors over the years and even when I went, what some might consider, a little too far in my quest for the truth, they were there to hold my hand at the end of the day. They allowed me to be my own person and allowed me to follow my own path and they loved me no matter what.

Next, I need to thank several of my lab mates. Nick Piro was my mentor, my office mate, and my friend, and I will always stick by my statement that much of what I was able to accomplish would not have been possible without his patience with my questions and his daily input, for which I am forever grateful. John Curley always reminded me that my own ideas and opinions were important and that no matter how much the man upstairs wanted me to go down certain paths, I should always find a way to pursue my own ideas as well. John also is one of the most helpful people I have ever met (I'm not joking!). Whenever I needed a resource he knew where to find it. Glen Alliger has been a constant in an ever changing lab. Glen is without a doubt the most dedicated and thoughtful researcher I have met while at MIT. I am also grateful to Glen for dating Sam who became a really great friend and someone I always hoped to see after work. Manis rejoined the lab my second year, entering as a senior student. Manis was always willing to go out of his way to help his lab mates whenever asked and his giving nature was sometimes overlooked because of his extreme sense of humor. I think people that get to know him well know that no better friend can be found. Heather was my female partner in crime in the lab for the majority of my graduate career. It was refreshing to have a strong female force to balance out what could sometimes be quite a male dominated environment. Heather is a friend that I am sad to leave, but that I know will stay in touch. Alex Fox has sort of been the emotional barometer for the lab and when times got tough you could always look to him to go bananas, which kept me calm for some weird reason. He is an incredible chemist, a great conversationalist, and has had a lot of shared history which we enjoyed reminiscing about in the group room. If I ever get a neurotic cat, I will name him Arfox and love him to death. Matt Rankin has been, perhaps, the most welcome addition to 6-332 for me. His knowledge of chemistry and the literature are unmatched and he is just an incredible person that I will never forget. Daniel Tofan was the first student younger than me to join the lab and its been a lot of fun to try and be a mentor for his research in phosphorus chemistry. I knew Tofan as an undergraduate at Caltech and I am thankful that I have had the chance to become his friend in graduate school. Alexandra is

the newest Cummins' group graduate student and she too I knew as an undergraduate at Caltech. Perhaps my best memory of her was her dancing with me in my hoop to some funky electronic beats. Those were the good old days for sure. Now, I share an office with Alexandra and have the pleasure of seeing her mature into an amazing scientist. It's pretty awesome. There have been numerous other post-docs and visiting students and undergraduates passing through the lab during my time at MIT and I know my experience has been greatly shaped by all of them as well, for which I am thankful. One visiting student in particular I must thank by name, and that is Mariam. Mariam visited us for a short time from France and her arrival brought the  $-ODipp$  ligand to our lab and her contributions changed the trajectory of my PhD project in a great way.

I have three very close friends from my Caltech days that have remained by my side during these past four years. Mo, Ashok, and Michael Rule... it is reassuring to know that they are out there in the world and are still always willing to talk and be fun.

Without the guidance of several professors over the years, I would not be here. Mr. Jarrell was my junior high science teacher and was the reason I initially became interested in chemistry at all. Mr. Zawodny, Mr. Garcia, and Dr. Hood were my high school chemistry, biology, and physics teachers, respectively; they kept me safe, healthy, sane, and interested in science during some very tumultuous years of my life. Tony Hynes is a Professor at the University of Miami Rosenstiel School of Marine and Atmospheric Science, and he gave me my first lab position as a high school student. While many people of my age and experience level were washing glass ware and filing papers, he trusted me to take on my own research and allowed me to participate in many of his graduate students projects. The experiences he provided me are without a doubt the reason I got into Caltech. Jonas Peters is a Professor at Caltech and he offered me my first position in a synthetic lab. The seeds of an inorganic chemist were definitely sown in his lab. Jonas also gave me the sage advice to join Kit's lab in grad school, which I think worked out well! I also want to thank Professors Schrock, Nocera, and Lippard for providing an enriching graduate experience; as well as Dr. Peter Müller and Dr. Jeff Simpson for all of their help over the years obtaining characterization on my wacky molecules.

Last, but most important of all, I need to thank Jared. Jared is my lab mate, my friend, and my reason for waking up in the morning. So much of what I have accomplished in lab has developed as the results of our chemistry discussions and his general brilliance. So much of what I have become as a person is owed to his care and love. If I had to point to a single reason that I am glad I came to MIT, it would have to be that it gave me the opportunity to meet Jared, whom I love and appreciate more than words can express.

# Brandi M. Cossairt

Phone: (626) 622-0243  
E-mail: brandi@mit.edu  
brandibear@gmail.com

Massachusetts Institute of Technology  
Department of Chemistry  
77 Massachusetts Avenue, Room 6-332  
Cambridge, MA 02139

---

## EDUCATION

Ph.D. in Inorganic Chemistry, Massachusetts Institute of Technology, Cambridge, MA, 2010.

B.S. with Honors in Chemistry, California Institute of Technology, Pasadena, CA, 2006.

## RESEARCH EXPERIENCE

- 2006–2010 Niobium-Mediated Synthesis of Phosphorus-Rich Molecules  
Advisor: Prof. Christopher C. Cummins, Massachusetts Institute of Technology
- 2004–2006 Electrocatalytic Hydrogen Evolution by Cobalt and Nickel Diglyoximate Complexes  
Advisor: Prof. Jonas C. Peters, California Institute of Technology
- 2002–2004 MALDI-LIF Studies of Dye-Labelled Proteins  
Advisor: Prof. Jesse L. Beauchamp, California Institute of Technology
- 2000–2003 LIF Kinetic Studies on  $\cdot\text{OH}$  and  $\cdot\text{X}$  Radical Reactions  
Advisor: Prof. Anthony J. Hynes, University of Miami RSMAS

## AWARDS

- American Chemical Society Division of Inorganic Chemistry Young Investigator Award, 2009
- MIT Department of Chemistry Award for Outstanding Teaching, 2006–2007
- Strem Summer Graduate Fellowship, Massachusetts Institute of Technology, 2007
- Richard P. Schuster Memorial Prize in Chemistry, California Institute of Technology, 2006
- McLean Brothers Scholarship, California Institute of Technology, 2006
- Summer Undergraduate Research Fellowship, California Institute of Technology, 2003 and 2005
- Wasserman Foundation Scholarship, California Institute of Technology, 2004–2005
- Kanel Foundation Scholarship, California Institute of Technology, 2004–2005
- Noland Summer Research Internship, California Institute of Technology, 2004
- Robert C. Byrd Honors Scholarship, California Institute of Technology, 2002–2006
- Elks National Foundation Scholarship, California Institute of Technology, 2002–2006
- US Navy and Marine Corps Scholarship, California Institute of Technology, 2002–2006

- Intel Foundation Achievement Award, Intel International Science Fair, 2002
- NASA Achievement Award in Chemistry, Intel International Science Fair, 2002
- US Air Force First Prize in Chemistry, Intel International Science Fair, 2002
- Siemens Westinghouse Competition Finalist, 2001

## PUBLICATIONS

**B. M. Cossairt**, C. C. Cummins, A. R. Head, D. L. Lichtenberger, R. J. F. Berger, S. A. Hayes, N. W. Mitzel, G. Wu. On the Molecular and Electronic Structures of  $\text{AsP}_3$  and  $\text{P}_4$ . *J. Am. Chem. Soc.* **2010**, *In Press*.

**B. M. Cossairt**, C. C. Cummins. Radical Synthesis of Trialkyl, Triaryl, Trisilyl, and Tristannyl Phosphines from  $\text{P}_4$ . *New J. Chem.* **2010**, DOI 10.1039/c0nj00124d.

**B. M. Cossairt**, N. A. Piro, C. C. Cummins. Early-Transition-Metal Mediated Activation of White Phosphorus. *Chem. Rev.* **2010**, DOI 10.1021/cr9003709.

**B. M. Cossairt**, C. C. Cummins. Shuttling  $\text{P}_3$  from Nb to Rh: The Synthesis and Use of  $\text{Ph}_3\text{SnP}_3(\text{C}_6\text{H}_8)$  as a  $\text{P}_3^{1-}$  Synthone. *Angew. Chem., Int. Ed.* **2010**, *49*, 1595–1598.

**B. M. Cossairt**, C. C. Cummins. Properties and Reactivity Patterns of  $\text{AsP}_3$ : An Experimental and Computational Study of Group 15 Elemental Molecules. *J. Am. Chem. Soc.* **2009**, *131*, 15501–15511.

**B. M. Cossairt**, M. C. Diawara, C. C. Cummins. Facile Synthesis of  $\text{AsP}_3$ . *Science* **2009**, *323*, 602.

**B. M. Cossairt**, C. C. Cummins. A Niobium-Mediated Cycle Producing Phosphorus-Rich Organic Molecules from White Phosphorus ( $\text{P}_4$ ) via Activation, Functionalization, and Transfer Reactions. *Angew. Chem., Int. Ed.* **2008**, *47*, 8863–8866.

**B. M. Cossairt**, C. C. Cummins. Phosphaalkenes as Long-Lived Phosphorus Cluster Surface Functional Groups: Intramolecular  $\text{P}=\text{C}$  Addition to a Niobium-Supported  $\text{P}_7$  Cage. *Inorg. Chem.* **2008**, *47*, 9363–9371.

**B. M. Cossairt**, C. C. Cummins. A Reactive Niobium Phosphinidene  $\text{P}_8$  Cluster Obtained by White Phosphorus Reductive Coupling. *Angew. Chem., Int. Ed.* **2008**, *47*, 169–172.

X. Hu, **B. M. Cossairt**, B. S. Brunshwig, N. S. Lewis, J. C. Peters. Electrocatalytic Hydrogen Evolution by Cobalt Difluoroboryldiglyoximate Complexes. *Chem. Commun.* **2005**, *37*, 4723–4725.

M. B. Williams, P. Campuzano-Jost, **B. M. Cossairt**, A. J. Hynes. Experimental and Theoretical Studies of the Reaction of the OH Radical with Alkyl Sulfides: 1. Direct Observations of the Formation of the OHDMS Adduct - Pressure Dependence of the Forward Rate of Addition and Development of a Predictive Expression at Low Temperature. *J. Phys. Chem. A* **2007**, *111*, 89–104.

D. L. Donohue, D. Bauer, **B. M. Cossairt**, A. J. Hynes. Temperature and Pressure Dependent Rate Coefficients for the Reaction of Hg with Br and the Reaction of Br with Br: A Pulsed Laser Photolysis-Pulsed Laser Induced Fluorescence Study. *J. Phys. Chem. A* **2006**, *110*, 6623–6632.

## PRESENTATIONS

- American Chemical Society, San Francisco, March 2010. Oral Presentation. “P<sub>3</sub> transfer chemistry of *cyclo*-P<sub>3</sub> anion complexes: New methods for the synthesis of exotic main-group molecules from P<sub>4</sub>”.
- Massachusetts Institute of Technology Inorganic Chemistry Departmental Seminar, January 2010. Oral Presentation. “Niobium-Mediated Synthesis of Phosphorus-Rich Molecules”.
- American Chemical Society, Washington DC, August 2009. Oral Presentation, DIC Young Investigator Symposium. “Properties and Reactivity Patterns of AsP<sub>3</sub> and Related Tetrahedra”.
- Organometallic Gordon Research Conference 2009. Poster. “Properties and Reactivity Patterns of AsP<sub>3</sub>”.
- American Chemical Society, New Orleans, April 2008. Oral Presentation. “Synthesis and Reactivity of Dinuclear and Mononuclear Niobium Octaphosphorus Complexes and Free Organo-P<sub>8</sub> Clusters”.
- American Chemical Society, Boston, August 2007. Oral Presentation. “Architectures Incorporating a Niobium Trisenolate Framework”.
- Gordon Inorganic and Organometallic Research Conferences 2007. Poster. “A Niobium Trisenolate Platform for White Phosphorus Activation”.

## TEACHING EXPERIENCE

- 2006–2010 Mentoring of two undergraduate and three visiting graduate students
- 2006 5.111—Principles of Chemical Science  
Teaching Assistant with Profs. Christopher C. Cummins and Sylvia T. Ceyer
- 2007 5.111—Principles of Chemical Science  
Teaching Assistant with Dr. Janet Schrenk
- 2008 5.04—Principles of Inorganic Chemistry II  
Teaching Assistant with Prof. Daniel G. Nocera
- 2009 5.05—Principles of Inorganic Chemistry III  
Teaching Assistant with Prof. Christopher C. Cummins

